



Transient and accident analysis of a BN-800 type LMFR with near zero void effect

*Final report on an international benchmark programme
supported by the
International Atomic Energy Agency
and the
European Commission
1994–1998*



INTERNATIONAL ATOMIC ENERGY AGENCY

IAEA

May 2000

The originating Section of this publication in the IAEA was:

Nuclear Power Technology Development Section
International Atomic Energy Agency
Wagramer Strasse 5
P.O. Box 100
A-1400 Vienna, Austria

The IAEA does not normally maintain stocks of reports in this series. However, electronic copies of these reports can be obtained from:

INIS Clearinghouse
International Atomic Energy Agency
Wagramer Strasse 5
P.O. Box 100
A-1400 Vienna, Austria

Telephone: (43) 1 2600-22880 or 22866
Fax: (43) 1 2600-29882
E-mail: CHOUSE@IAEA.ORG
Web site: <http://www.iaea.org/programmes/inis/inis.htm>

Orders should be accompanied by prepayment of 100 Austrian Schillings in the form of a cheque or credit card (MasterCard, VISA).

TRANSIENT AND ACCIDENT ANALYSIS OF A BN-800 TYPE LMFR WITH
NEAR ZERO VOID EFFECT
IAEA, VIENNA, 2000
IAEA-TECDOC-1139
ISSN 1011-4289

© IAEA, 2000

Printed by the IAEA in Austria
May 2000

FOREWORD

Large conventional liquid metal cooled fast reactor (LMFR) cores show a significant reactivity increase if a coolant loss occurs by boiling or gas intrusion. Since this positive reactivity effect is very important for the overall behaviour of LMFRs from a safety point of view, a lot of attempts have been undertaken worldwide to reduce the sodium void reactivity effect (SVRE).

One proposal has been made by the Institute of Physics and Power Engineering (IPPE), Obninsk, Russian Federation, in which the core upper axial blanket is replaced by a sodium plenum consisting of sodium filled wrapper tubes. In this case the enhanced axial neutron leakage would result in a strong negative reactivity effect in case of sodium voiding which would compensate a large fraction of the positive SVRE in the core region. The International Atomic Energy Agency (IAEA) and the European Commission (EC) Joint Benchmark Programme have assessed the capability of reducing the SVRE of such innovative core design. The analysis (IAEA-TECDOC-731, 1994) showed that overall SVRE for the reference 2100 MW(th) MOX fuel core might be close to zero.

This method of reducing the SVRE has been adopted in the BN-800 reactor design in the Russian Federation. However, investigations were needed to determine differences in severe accident responses in order to estimate the feedback to overall safety that could be achieved by a reduction in the SVRE value for MOX fuel reactor core.

Therefore, recognizing the importance of such an innovative LMFR core design, a comparative exercise of severe accidents for BN-800 type reactors with reduced sodium void coefficient was jointly initiated by the IAEA and the EC in 1994. The Russian specialists took over the task to prepare the benchmark input data, a revised draft of which was distributed by the IAEA to the participants at the end of June 1995. The specifications of the benchmark were finally fixed in a meeting at the IAEA in Vienna on 11–13 December 1995.

The main findings resulted from intensive discussions through eight IAEA/EC joint meetings held in turn in Vienna and Brussels. The final meeting was held at IPPE, Obninsk, Russian Federation, on 2–6 June 1998. The benchmark programme resulted in an effective information exchange among the Member States sharing requirements as well as experience in advanced reactor design and computer codes for transient calculations.

This report, which describes the results of the benchmark programme, was coordinated by J. Kupitz, IAEA and G. van Goethem, European Commission. The IAEA officer responsible for this publication was A. Rineiskii, of the Division of Nuclear Power.

The IAEA wishes to express its appreciation to all those who participated in the benchmark programme which is a good example of the joint IAEA/EC research activities for LMFR development. Valuable contributions to the benchmark exercise have been made, in particular, by D. Struwe (FZK, Karlsruhe, Germany), I.A. Kuznetsov (IPPE, Obninsk, Russian Federation), J.M. Frizonnet (IPSN, Cadarache, France), H. Niwa (JNC, O-arai, Japan) and Om Pal Singh (IGCAR, Kalpakam, India). D. Struwe acted as Chairman throughout the joint meetings.

EDITORIAL NOTE

The use of particular designations of countries or territories does not imply any judgement by the publisher, the IAEA, as to the legal status of such countries or territories, of their authorities and institutions or of the delimitation of their boundaries.

The mention of names of specific companies or products (whether or not indicated as registered) does not imply any intention to infringe proprietary rights, nor should it be construed as an endorsement or recommendation on the part of the IAEA

CONTENTS

| | |
|---|-----|
| Summary | 1 |
| CHAPTER 1. SYNTHESIS OF NEUTRON PHYSICS CALCULATIONS | 15 |
| 1.1. Russian calculations | 15 |
| 1.1.1. Methods and calculational models | 15 |
| 1.1.2. Results of calculations | 21 |
| 1.2. Italian calculations | 25 |
| 1.2.1. Introduction | 25 |
| 1.2.2. Results of calculations | 28 |
| 1.3. Japanese calculations | 51 |
| 1.3.1. Introduction | 51 |
| 1.3.2. Results of calculations | 52 |
| 1.4. Comparative analysis of neutronics calculations | 56 |
| 1.5. Conclusions | 60 |
| References to Chapter 1 | 70 |
| CHAPTER 2. EVALUATION OF STEADY STATE CALCULATIONS OF THE FUEL PIN BEHAVIOUR DURING POWER OPERATION IN A BN-800 LIKE REACTOR CORE | 71 |
| 2.1. Introduction | 71 |
| 2.2. Basis of the calculations | 71 |
| 2.2.1. Case set-up | 71 |
| 2.2.2. Characterization of the applied fuel pin mechanics code packages | 78 |
| 2.3. Summary of results | 80 |
| 2.3.1. Fuels thermal behaviour | 80 |
| 2.3.2. Fuel to clad heat transfer | 84 |
| 2.3.3. Fission gas release during power operation | 88 |
| 2.4. Conclusions and recommendations | 88 |
| References to Chapter 2 | 91 |
| CHAPTER 3. PREBOILING ANALYSES OF ULOF ACCIDENTS | 93 |
| 3.1. Introduction | 93 |
| 3.2. Computer codes used | 93 |
| 3.3. Results | 95 |
| 3.3.1. Base case | 95 |
| 3.3.2. Parametric case | 99 |
| 3.3.3. Uncertainties in core physics data | 100 |
| 3.4. Conclusions | 104 |
| References to Chapter 3 | 104 |
| CHAPTER 4. BOILING AND POST FAILURE ANALYSIS RESULTS OF ULOF ACCIDENTS | 109 |
| 4.1. Boiling and post-failure phase transients | 109 |
| 4.1.1. Base case results | 110 |

| | |
|--|---------|
| 4.1.2. Parametric case results | 122 |
| 4.2. Core configuration at the end of the initiating phase | 143 |
| 4.3. Conclusions | 148 |
| | |
| CHAPTER 5. TRANSIENT ANALYSIS RESULTS OF UTOP AND UTOP/ULOF ACCIDENTS | 151 |
| 5.1. Introduction | 151 |
| 5.2. Basis of the calculations | 151 |
| 5.2.1. Case set-up | 151 |
| 5.2.2. Codes applied | 152 |
| 5.3. Transient results for the fast UTOP (0.5\$/S) | 153 |
| 5.4. Transient results for the slow UTOP (0.05\$/S) | 162 |
| 5.5. Transient results for the UTOP-ULOF accident | 170 |
| 5.6. Conclusions and recommendations | 190 |
| References to Chapter 5 | 191 |
| | |
| CHAPTER 6. PHYSICS PARAMETERS OF PARTIALLY DESTROYED CORE CONFIGURATION | 193 |
| 6.1. Calculation model and analysis methods | 193 |
| 6.2. Integral reactivity effects | 197 |
| 6.3. Doppler effect | 203 |
| 6.4. Reactivity of materials (2100 K) | 203 |
| 6.4.1. Sodium integrals of reactivity and space distribution | 203 |
| 6.4.2. Steel worth | 216 |
| 6.4.3. Fuel worth | 228 |
| 6.5. Reactivity effects caused by material expansion | 228 |
| 6.6. Neutron kinetics functionals | 229 |
| 6.7. Conclusions | 241 |
| List of participating organizations and participants | 243 |

SUMMARY

1. INTRODUCTION

Research on liquid metal fast reactors (LMFRs) during the last decade has significantly improved the understanding of the fast reactor issues. This forms the basis for the development of safety analysis methods and codes which are necessary to evaluate the safety characteristics of existing and new fast reactor core and plant designs and to optimize safety and operational procedures. In spite of all the progress made on the safety issues, the quest for excellence calls for further work. One of these issues is the positive sodium void reactivity effect of large size reactors. There is a strong incentive to search for core designs, which have a considerably reduced positive sodium void reactivity effect.

One idea followed by Russian scientists has been to investigate the suitability of reducing the integral sodium void reactivity by an axially heterogeneous core design with a sodium plenum region just above the fissile core region instead of the upper axial blanket. A first benchmark exercise on this subject was jointly organized by IAEA and EC. It was mainly devoted to the involved reactor physics issues under normal operation conditions. It could be demonstrated that the integral sodium void effect of a MOX fueled LMFR of the 2100 MWth class could be reduced to a value of nearly zero (IAEA-TECDOC-731). After finalization of this benchmark exercise it was clear that further investigations are needed to determine the transient response of such a design to severe accidents including those which could lead to core destruction. Such investigations form the basis for estimations to what extent a reduction of the positive void worth could contribute to a further reduction of the residual risk of LMFRs.

At the meeting of the IAEA's IWGFR in May 1994, a comparative exercise for a severe accident in a BN-800 type reactor with a near zero void innovative core was proposed by the Russian Federation. This proposal was endorsed by all the countries and the EC. The organizations participating in the comparative exercise are: FZK from Germany, IPSN from France, AEA-T from the UK, ENEA from Italy, PNC and HITACHI from Japan, IGCAR from India and IPPE from the Russian Federation. A variety of specialists from the participating organizations contributed to the comparative exercise.

The comparative exercise was organized on different stages. These different stages covered the following items:

Stage I: Case set-up covering core and plant design characteristics, the preparation of the neutron physics input data, the specification of thermal-hydraulic design values and the specification of the fuel loading scheme during power operation.

Stage II: Determination of the fuel pin state at the end-of-equilibrium-cycle (EOEC)-conditions taking into account the power operation history appropriately.

Stage III: Analysis of preboiling transients of the ULOF-accident by considering or not reactivity feedback related to the structures heat-up. Effects of load pad expansion and control rod drive line expansion were considered in detail.

Stage IV: Analysis of boiling transients up to fuel pin failure either due to clad melting onset or fuel pin break-up, i.e. due to sudden loss of the fuels structure geometry.

Stage V: Analysis of post-failure transients up to a core state at which larger parts of the core were destroyed and at which hexcan failures are to be expected.

Stage VI: Analysis of other initiators for core destruction as unprotected reactivity accidents leading to a transient overpower accident (UTOP). Three types of initiators were considered : an 0.5 \$/s reactivity ramp rate, an 0.05 \$/s reactivity ramp rate and a structured reactivity ramp rate superimposed by a loss of flow. These kind of accidents have some importance in residual risk studies performed for the BN-800 type reactor.

Different tools were applied by the different participants to the exercise. However, not all participants contributed to each stage. Main results of the different stages of the exercise are presented here in a concise manner. The main findings resulted from intensive discussions between the partners at eight Consultants Meetings organized by the IAEA.

2. RESULTS OF ANALYSES

2.1. Case set-up

The Institute of Physics and Power Engineering (IPPE) from Obninsk provided the necessary information on the case set-up. The given data are representative of a 1500 MW(th) reactor design with above core sodium plenum, as in BN-800 reactor core design. The central part of the reactor comprises the core, the primary shielding and the spent fuel assembly storage. The core and the blanket hexagonal fuel assemblies are inserted into the inlet header collector hole which is located at the reference height of 0.1 m. The radial blanket height is 1.84m and it comprises one row of 84 subassemblies surrounding the core. The primary shielding steel hexagonal are arranged with the same spacing as the one of core fuel elements. The core consists of 511 cells, 481 of which are filled with fuel subassemblies and 30 are intended for control, safety and shutdown rods. For radial flattening of the power production the core is divided into three different enrichment zones: the central low enrichment zone (LEZ) consisting of 181 subassemblies, the intermediate medium enrichment zone (MEZ), consisting of 138 subassemblies and the peripheral high enriched zone (HEZ) consisting of 162 subassemblies.

The fuel pin height consists of a 0.67 m long lower fission gas plenum followed by a 0.35 m long lower axial breeder zone. Fissile core height amounts to 0.84 m only followed by a 0.05 m long end cap region which acts as an upper axial reflector. Above this there is a sodium plenum of 0.35 m length followed by a B₄C shield of 0.25 m length. Fissile pellets are hollow pellets with chamfered edges. Fertile pellets are without chamfers. The total mass of fuel in the core amounts to 11668 kg. The cylindrical equivalent fissile core radius amounts to 1.1869 m. Fertile pellets of the radial blanket assemblies are fat solid pellets of depleted uranium oxide.

Coolant entering the inlet header of the reactor is distributed in between the following main areas: the core, the radial blanket, control absorber rods, the inner and outer radial shield and the spent fuel storage. Besides, some part of the coolant through subassembly foot penetrates into the inter-subassembly space and is discharged into the upper outlet plenum of the reactor. For flattening of the coolant outlet temperature distribution, hydraulic shaping is performed by means of appropriate choices of the hydraulic resistance of subassembly inlet devices. The total coolant mass flow through the core is 6027 kg/s. With a core inlet temperature of 627.15 K (354°C) this results in an average coolant heat-up along the core by about 190 K. The coolant pressure difference between the feeding header inlet and the argon

gas plenum amounts to 0.59 MPa with a pressure drop along the highest powered fuel pin bundle length of 0.302 MPa and along the lower subassembly tail and the pin bundle inlet of 0.11 MPa. If the plant's power supply gets lost and one assumes that the diesels of the emergency power supply system do not start as expected, the primary pumps begin to reduce their rotation speed by the law of free coast down. The halving time amounts to 5.5 s, i.e., the coolant mass flow gets reduced rather rapidly. The secondary sodium flow rate changes in time accordingly. However, the sodium inlet temperature will start rising smoothly only after 180 s into the transient.

The reactor is designed to operate on a three batch reloading scheme, with a total residence time for a particular subassembly of 420 equivalent full power days (i.e. three cycles, each of length 140 days). Subassemblies in the radial breeder zone have a residence time of 490 days. For determination of the local variation of the power and the reactivity feedback effects in the different enrichment zones, these are subdivided into representative subassembly groups (SAGs), four groups for the LEZ and three each for MEZ and HEZ, respectively. Each of the SAGs are subdivided into one third portions representing the three batch loading scheme. The radial breeder is represented by one SAG. In axial direction 12 zones have been chosen to simulate the axial profiles of power and reactivity feedback coefficients appropriately. As a consequence of this core representation, the reactor core is simulated with 30 SAGs and 10 radial zones for representation of neutron physics parameters in the fissile core region.

Evaluation of the neutron physics parameter of the core set-up was performed by IPPE from Obninsk, by ENEA from Italy and by HITACHI from Japan. The Russian evaluation of reactivity coefficients was based on tools using first order perturbation theory in 26-group diffusion theory. The calculations have been made using the standard version of the BNAB-78 data base applying the ARAMAKO-S system for preparation of the cross sections. In order to evaluate the effect of the use of different cross section libraries, some calculations were performed using a modified version of the RHEIN set developed in the framework of the former USSR — GDR bilateral co-operation. All these calculations were done in R-Z geometry. To evaluate the validity of the use of the first order perturbation theory, complementary calculations were performed with the 26-group SYNTEZ code and the 3D TRIGEX code with an 11-group representation. The ENEA calculations covered 2D and 3D representations of the core geometry. Due to the heterogeneous character of the core design, it was felt that a 3D representation was essential. The CITATION code was applied using a 22-group cross section library originating from the ENDF/B - V.II file. In addition, transport theory in a 3D hexagonal full core representation was provided for evaluation of the sodium void effect. The MCNP4A Monte Carlo Transport code was used. HITACHI performed both diffusion and Monte Carlo transport calculations in R-Z and Hex-Z configurations using the latest Japanese nuclear data library JENDL-3.2.

Comparison of the results of neutron physics calculations performed by the participants to this part of the exercise led to the following conclusions:

- The power distributions were in good agreement with each other with maximum deviations in integral results of only 2% and up to 4.1% deviations if local values of linear ratings were considered.
- The kinetics parameters were in satisfactory agreement with each other.
- Integral values of the Doppler coefficients were rather close in all calculations. However, differences were observed when evaluating the sums over the different enrichment zones.

These differences became larger for the voided core configurations. They were attributed to differences in cross-section libraries and more importantly to the selected range of temperatures forming the basis for the evaluation. In addition, it turned out that the amount of changes of the Doppler coefficient in case of voiding depends in a non negligible manner on the local void pattern along core cross section.

- The sodium void reactivity effect was calculated rather close to each other by the different participants. The largest differences in integral values amount to about 20%. However, each of the calculations has demonstrated that integral results are rather dependent on the local pattern of voiding and it is difficult to argue on the conservatism of an approach without detailed evaluations. An important impact of the use of higher order methods has been observed consistently by all participants to this part of the exercise. Similarly coherent were the results that appropriate consideration of fission products becomes essential when calculating the sodium void effect dependent on the residence time of subassemblies. Common to all results was that the sodium void effect amounts to 4.5 \$ if all positive contributions are summed up. The void effect of the fissile core region amounts to 2.7 \$ and the one of the upper sodium layer to -3.3 \$. The integral sodium void effect sums up to a considerably negative value of -0.6 \$.
- The steel reactivity feedback effect of the core region amounts to 5.2 \$ which included the clad and hexcan material.

In addition to the neutron physics parameters of the as designed core geometry, analyses were performed by IPPE on the influence of the core materials relocation on the neutron physics parameters. In this regard, core configurations considered are: sodium void inner the two enrichment zones, clad material accumulated partly at the upper end of fissile core height and dominantly around the lower end of fissile core height, i.e. at the boundary of the lower axial blanket. Such a configuration can only be achieved when the clad material and the fuel is heated up considerably. The analyses indicated a relatively little impact of distorted core configuration on the sodium void worth distribution but a large effect on Doppler reactivity feedback. The influence of these findings on transient analyses results could not be evaluated.

Common conclusions of this part of the exercise are that higher order methods have a considerable effect on sodium void worth effect, local patterns of voiding have a different effect on the integral value than determined from differences of unvoided and fully voided core configuration and core materials relocation seem to influence the Doppler feedback considerably. All these findings indicate that it might become necessary to apply space time neutronics methods for the transient analyses when aiming at a considerably higher precision in the transient analyses than the one achieved with currently available methods and data base.

2.2. Fuel pin characterisation at EOEC-conditions

Five countries participated to this stage of the exercise with different code systems: The Russian Federation with their KONDOR code package, France with the GERMINAL code, United Kingdom with the TRAFFIC code, Germany with the DEFORM-4C code package as part of the SAS4A code and India with the PINCH code package. The different codes applied in this comparative exercise cover the whole spectrum of currently available model capabilities ranging from detailed deterministic model approaches realised in codes such as GERMINAL and TRAFFIC up to simplified parametric approaches as DEFORM-4C and PINCH, KONDOR being somewhere in between the two modelling approaches.

Comparison of results provided by the participants to the exercise up to the 5th Consultants Meeting, December 1996 in Vienna led to the following conclusions:

- Results of the PINCH calculations for gap conductance compare well with other code predictions. Calculated values of the fractional fission gas releases are high and relatively low fuel temperatures are calculated. Review and refinement of the chosen approach is strongly recommended.
- Results of the TRAFFIC code calculations are difficult to compare to the results of the other participants because differences are mainly determined by the power history differently simulated for the 420 days power operation time and the simulation of a clad material which leads to a low clad swelling even for high doses. However, differences of the results to the ones of the other calculations are clearly explained by the different assumptions taken in the case set-up which were agreed upon at an early stage of the exercise.
- Results of the KONDOR, GERMINAL and DEFORM-4C calculations are relatively close to each other. However, differences in between the calculations become more pronounced when medium burnup levels of about 5 at% are exceeded. It appears as if more refined modelling approaches need to be developed for the KONDOR code system for an improved description of the fuel pin mechanics behaviour approaching high burnup levels of 8 to 10% at% and low linear ratings. Differences between DEFORM-4C and GERMINAL calculations evolve partly from different approaches to simulate JOG-formation and the respective behaviour during power operation. This is a topic of the current research and development activities in this field, which needs more refined analyses and model development and most importantly a broader experimental data base.

For evaluation of the reliability of the provided code predictions about the performance of the BN-800 fuel pins under power operation, it would be necessary to compare calculated results with experimental results for the specific BN-800 fuel pins considered in this exercise. This holds especially for results provided on the basis of parametric modelling approaches of DEFORM 4C. Impact of fuel fabrication and clad material properties variation with burnup can only be evaluated based on detailed experimental results. This was not the objective of this comparative exercise. However, it is strongly recommended that results should be compared in more depth with the experimental data base available in the Russian Federation from power operation of respective fuel pins in the BN-350 and the BN-600 reactors.

For the purpose of this exercise, comparison of results has shown that the calculated fuel pin states at the EOEC are rather close together. Therefore transient calculations start from initial conditions sufficiently close to each other so that possible differences in the transient calculations should not be dominated by differences in the state fuel pin characterisation after power operation. However, differences are to be expected between the transient calculations of the Russian Federation and India on the one side and the ones of France, Japan and Germany on the other side. This is due to the fact that fuel pin mechanics code packages are not applied during the transient calculations by the Russian Federation and India but they are consistently used in the calculations by the other three participants in the further stages of the exercise. This results in an important difference in the simulation of the further accident progression. The first two participants assume the heat transfer coefficient between fuel and clad is constant in time at a level evaluated at the end of the power operation in steady state. The other three participants calculate the change in time of the heat transfer coefficient consistently with the transient variation of the gap size and the contact pressure build-up.

Some differences in transient calculations are to be expected between the contributions from France and Japan on the one side and Germany on the other side because Germany applied a code version of DEFORM-4C for transient calculations which has been improved since December 1996 as compared to the one used by France and Japan.

2.3. Analyses of preboiling transients of the ULOF-accident

Five countries contributed to this stage of the exercise namely the Russian Federation, India, Japan, France and Germany. The Russian Federation applied their GRIF-SM code system, which calculated in great detail the thermal-hydraulics core behaviour and simulates the primary and secondary circuit behaviour of the BN-800 type reactor appropriately. Interwrapper sodium flow is simulated. However, the fuel pin behaviour considers the thermal behaviour appropriately but it does not calculate the transient fuel pin mechanics behaviour and hence applies axially variable but transiently constant gap heat transfer coefficients. India applied their PINCHTRAN code package, which accounts reactivity feedback effects in single phase comprehensively and sodium boiling is simulated similarly to the SAS1A model. Such a representation is felt too simplified for the simulation of two phase flow conditions. The transient fuel pin mechanics behaviour is not modelled. The primary and secondary circuit behaviour is simulated in a simplified manner. Japan, France and Germany applied slightly different code versions of the SAS4A-code being very close to the REF96.Rel1.0 code version. The French participant improved the sodium EOS in the post failure module and introduced mechanical properties of 15/15 Ti stabilized cladding. The German participant modified and improved the fuel pin mechanics model and the two-phase flow boiling model. The Japanese participant modified clad motion model to avoid the formation of the steel accumulation at the fissile top and thus extended the applicability of the model. They contributed to the exercise with the actually available most recent code versions to introduce the newest state of knowledge into the discussion of results. The representation of the BN-800 subassemblies is rather detailed. The primary and secondary circuits are simulated only approximately in the framework of a scaled-down LSPB plant design.

The calculations performed can be subdivided into three classes: (A) Base case calculations neglecting reactivity feedback effects as a consequence of the core structures heat-up and applying the reference neutron physics data. (B) Uncertainty analyses of the neutron physics input data. and (C) Consideration of different reactivity feedback effects due to core structures heat-up as radial core expansion and control rod drive line expansion. However, it seems appropriate to mention here that intensive discussions took place on the question whether there is sufficient evidence from theoretical and/or experimental investigations to argue that the efficiency of radial core expansion under the given conditions can be regarded as verified. On the background of experiences gained with respective analyses for FFTF, Phenix and Super-Phenix, it was decided to neglect this reactivity feedback effect totally. However, it was not possible to arrive at a uniquely accepted position. Therefore, it was agreed to consider the respective calculations as optimistic parametric cases.

On the basis of the results, the following conclusions can be drawn:

- The heat-up of the upper sodium layer leads to a negative reactivity feedback contributions related to the sodium heat-up in the fissile core region. The normalised power therefore decreases continuously after onset of the coolant mass flow decrease. However, boiling onset cannot be prevented neither in the class (A) nor in the class (C) calculations. The results are not very sensitive to uncertainties of the core physics parameters class (B) results.

- In the class (A) calculations, all participants predict boiling onset in the highest powered MEZ core region about 16.7 up to 18.9s into the transient. The normalised power level has decreased down to 71% to 63% of its nominal value. Up to this time into the transient, reactivity feedback effects remain quite small but differences in between the different calculations are observed which are related to different model assumptions on the calculation of fuel pin axial expansion.
- In the class (C) calculations, boiling onset is calculated in the highest powered MEZ core region as well but only at 28.9s to 33.2 into the transient when the normalised power has been reduced to a value of about 44% to 39% of its nominal value. Up to this time, the radial core expansion reactivity feedback amounts to about -0.43 \$.

These results indicate that the negative value of the sodium void reactivity is well suited to be identified as a passively activated safety measure which compensates potential difficulties which might arrive from the design feature of a quite rapid coolant mass flow reduction curve in the case of loss of offsite power and delayed availability of the emergency power supply.

2.4. Boiling and post-failure transients as a consequence of a ULOF-accident initiator

Five countries participated to this stage of the exercise namely the Russian Federation, India, Japan, France and Germany. The Russian Federation and India contributed with their GRIF-SM and PINCHTRAN code packages providing the capability to follow the transient behaviour up to peak cladding temperatures of 1500 K. For later phases of the accident the code packages cannot be applied because it does not provide models to describe consequences of clad and fuel relocation after clad melting onset. France, Germany and Japan used the SAS4A code, which was developed by these countries in the last 10 years in close co-operation starting from the code version provided by the US/DOE in 1986/88. The code versions used by these three partners are based on the identical version SAS4A REF96 Rel1.0, but each participant performed some modifications independently in order to apply it to this reactor successfully.

In principle, calculations can be grouped into two classes again:

- continuation of the class (A) calculations of stage III of the exercise (base case evaluations). Evaluations of these cases were complemented by analyses of consequences of an early loss of fission gases from the upper fission gas plena by Japan. As it turned out that this effect does not modify the integral event sequence drastically, it was agreed to neglect this effect in the bulk of the analyses. However, it is felt reasonable and necessary to re-evaluate the case when more reliable results than here are to be provided, i.e. if it would come to licensing of the reactor design.
- continuation of the class (C) calculations of stage III of the exercise, again neglecting the effect of an early fission gas release from the upper fission gas plena (parametric case evaluations).

Both kinds of analyses were performed using nominal reactivity feedback coefficients for Doppler, sodium void, fuel pin expansion, clad motion and fuel motion. In most of the considered cases the reactivity feedback effect of the expansion of the control rod drive lines are neglected.

Base case results: The negative reactivity feedback contribution due to the voiding of the upper sodium layer is a quite efficient measure to mitigate the impact of the positive reactivity feedback contribution when the coolant along fissile core height is voided. Along the first 2 s of the boiling transient, the normalised power decreases to a value of about 0.4 to 0.5. However, during the next 4 s, the net reactivity increases again to about delayed critical and the power increases to a value of about 0.6 to 0.7 nominal. The subsequent boiling development releases negative reactivity but this is partially compensated for by positive contributions related to clad material relocation. During the next 2 s, the sodium reactivity feedback becomes again positive being considerably enhanced by an increasingly positive reactivity feedback due to clad material relocation. The net reactivity becomes positive, driving the normalised power to nominal values and beyond. This mild power transient leads to fuel pin breakup in the high powered subassembly group of the medium enrichment zone. The subsequently calculated fuel relocation initiates a slow but gradually proceeding reactor shut down. Most of the fissile core channels are voided and the void reactivity has reached or exceeded its saturation value of about -0.6\$. Clad relocation continues but heat-up of the hexcan wrapper structure melts. Further core material phenomena will deviate considerably from the quasi-one-dimensional behaviour in the initiation phase. It can be concluded that the accident will enter into the transition phase. The ULOF-transient is not at all finished at the end of the calculations. Achievement of permanent subcriticality or in-place coolability of the partially destroyed core could not be demonstrated.

Parametric case results: The event sequence calculated for the case where radial core expansion is considered are generically very close to the results of the base case. However, time scales of the crucial events are longer and the respective power levels smaller during the boiling transient time period. Clad relocation cannot be prevented and it is this positive reactivity feedback together with some contribution from sodium boiling which drives the normalised power back to nominal values and above which then initiates a mild power transient leading to fuel pin breakup and a post-failure transient which is only little different from the one calculated for the base case. This accident enters similarly well into a transition phase which needs to be analysed carefully.

The Russian Federation analysed one further parametric case in which radial core expansion and control rod drive line expansion were considered. As a consequence of these two structure reactivity feedback effects, boiling onset is delayed and clad dry out is not predicted up to 100s of the transient. On the basis of this calculation, it was concluded by the Russian participant that long term coolability could be established if the structure feedback is sufficiently strong and becomes activated in due time. The other participants did not agree to this conclusion. First of all, it was felt necessary to continue the calculation beyond times at which the reactor coolant inlet temperature starts rising. Secondly it was felt overly optimistic to superimpose the reactivity feedback due to radial core expansion and control rod drive line expansion. Thirdly it was felt necessary to evaluate consequences of the transient, by considering variation of the fuel to clad heat transfer coefficient. This last item could have been evaluated only if calculations with a SAS4A-type of code would have been performed. The other participants were not in a position to do so because it would have needed a thorough review of the approach to simulate the primary and secondary circuit behaviour for these long lasting transients within the SAS4A code frame. However, this was not the purpose of the comparative exercise and the effort to do so was too large to be covered within the scope of this exercise.

The results have shown that the upper sodium layer is a quite efficient design measure to prevent the net reactivity to approach or exceed prompt criticality in the initiation phase. Within the framework of the exercise no analysis was performed for the transition. In this sense, it is

not yet demonstrated that this innovative core design leads only to benign consequences in terms of thermal and mechanical loading of structures of the primary system.

2.5. Consequence and analyses of other initiators for core destruction (UTOP, UTOP/ULOF)

Four countries participated to this state of the exercise namely the Russian Federation, India, France and Germany. However, contributions from the first two participants were only of limited value because their code systems do not provide information on the transient fuel pins behaviour. They do not provide the capability to calculate fuel pin failure conditions mechanistically and they do not provide information on consequences of core materials relocation after fuel pin failure other than to impose a pre-specified materials relocation behaviour which is not adequately representing the reality and which does not represent the current state of knowledge and technology. Therefore, discussion of results hereafter is mainly based on calculated results provided by the last two participants. At this stage of the exercise two classes of accident initiators were considered:

- Consequences of unprotected reactivity ramp rate accidents leading to a UTOP-accident. Two types of reactivity ramp rates were considered in detail: an $0.5\$/s$ reactivity ramp rate and an $0.05\$/s$ reactivity ramp rate. For both cases, impact of the reactivity feedback of radial core expansion on the event sequence was neglected and nominal values of the other reactivity feedback coefficients were used.
- Consequences of an accident scenario with unprotected withdrawal of 6 compensator rods from the core accompanied by failure of all scram system absorber rods and initiation of a loss-of flow. The externally supplied reactivity was limited to a maximum value of $3.9 \$$. This accident initiator leads to a so called UTOP/ULOF accident. It is of some interest for the evaluation of the residual risk associated with the operation of a BN-800 type reactor. Boundary conditions of the calculations are the same as for the previously mentioned analyses.

Calculated results of the pure UTOP analyses

To perform these calculations it was necessary to get access to experimental data of the BN-800 clad material properties. These should give insight into the relations between temperatures and strain rate on the one side and ultimate tensile strength and yield stress on the other side. Most importantly, experimental data on the respective failure strain values are necessary. In addition variation of these data with accumulated doses are necessary. The information could be provided only partially. The strain rate dependency could not be given as well as the failure strain dependencies of the irradiated clad material. Analyses were therefore performed with material property functions deduced in the framework of the CABRI experimental programme for a 20% coldworked 15/15 Ti stabilised clad material. This was done under the assumption that the BN-800 clad material behaves similarly. However, this is a quite risky procedure because extrapolation of clad material properties for irradiated clad represents a very difficult subject and definitely needs experimental backup. Thus, the results presented and discussed here can only be of a preliminary nature. This concern is to be taken seriously because information on material properties for the BN-800 clad material at high dose loads revealed that the material properties are considerably different than the ones assumed in these analyses. This information was provided only at the end of the exercise and could not be taken into account appropriately.

Results of the slow reactivity ramp rate calculations are sensitively dependent on the transient variation of contact pressures at the fuel to clad interface and on the balance of fuel melt cavity pressure buildup and the transient radial expansion of the still solid fuel. It is due to this fact that the calculation presented by France, calculates firstly boiling onset though the calculation presented by Germany predicts fuel pin failure prior to boiling onset. In both cases fuel pin failure is calculated in one subassembly group (SAG) at 36s to 41s of the transient, at 67% to 79% of the core height and when a failure strain of 1.7% or 0.5% becomes exceeded. At this point in time, the normalised power has reached about 3.1 times the nominal value which corresponds to a peak linear rating in the concerned SAG of about 1050 to 1100 W/cm. The two reliable calculations for this case have shown that failure conditions depend strongly on details of the fuel pin mechanics simulation and most pronouncedly on the actual established strain rate.

In the calculation presented by Germany, first fuel pin failure occurs at a time of the transient when heat-up of the fuel pins and clad straining in several SAGs results in liquid sodium displacement from central core regions. Therefore, it leads to a transient increase of the integral sodium reactivity feedback just prior to failure prediction. After failure, sodium is displaced additionally at the failure site by the ejected fuel. The cumulative effect of these reactivity feedbacks result in a slight increase of the power which is considerably reduced, with a time delay of about 170 ms, when dispersal initiates a rapid reactor shutdown.

When sodium boiling takes place before pin failure the post failure transient looks slightly different, but at the end of the calculations partial blockage formation in the concerned SAG leads to a core configuration which can hardly be cooled in-place on a long time scale. The accident most probably will enter into a slow core melt down with a progressive core destruction by a thermally induced subassembly to subassembly propagation.

Results of the rapid reactivity ramp rate calculations reveal a similar sensitivity against details of the simulation of the fuel pins mechanical behaviour and against actual strain rate dependencies of the clad material properties. These details influence the coolant heat-up considerably thus establishing transient conditions where fuel pin failure is calculated to occur either prior to boiling onset or only afterward with some time delay. If fuel pin failure occurs prior to boiling onset it is at 3.7s or 5.25s into the transient depending on assumptions about the actually established strain rate. The calculated failure location is between 62 % and 75% of the fissile core height. As a consequence of the quick voiding of the upper sodium plenum, reactor shut down is initiated due to a rapid reduction of the sodium void reactivity and an initially benign fuel dispersal. When a more massive fuel pin destruction takes place about 400ms after the first fuel pin failure, the net reactivity increases again due to the superimposed effects of sodium voiding and fuel relocation. However, 20ms to 30ms later reactor shut down is initiated by a rather massive dispersal and relocation.

Results of the pure UTOP-simulations are strongly dependent on the reliability of the calculated failure time and more importantly on the calculated failure position. The most recently developed modelling approaches with SAS4A have been qualified successfully on the experimental observations of the different CABRI-programmes. These results demonstrate a large margin to failure for hollow pellet fuel pin design under transient loading. However, the success of calculations depend to a large degree on the reliability of assumptions of the dose and strain rate dependence of clad material properties. The data of these assumptions need to be strengthened to defend the reliability of the presented calculations. It is strongly recommended to evaluate strain rate dependencies and temperature dependence of mechanical properties of

the irradiated BN-800 clad material up to dose values of 70 to 100 dpa NRT experimentally and to cover the strain rate dependency from 10^{-4} up to 1/s to 5/s in small steps.

UTOP/ULOF analyses

Four countries contributed to this part of the exercise namely the Russian Federation, India, France and Germany. Calculations were performed with the same code systems applied to states IV and V of the exercise. However, the Russian Federation used their newly developed CANDLE code package in addition to their GRIF-SM code. Nominal values of the reactivity feedback coefficients were used. reactivity feedback effects due to radial core expansion were neglected. Results of the calculations can be summarized as follows:

The UTOP/LOF-accident leads to coolant boiling firstly at the level of the upper sodium layer. This calculated to occur between 9.8s to 11.1s of the transient depending on the tool applied. The negative reactivity feedback due to the initial voiding of the upper sodium layer mitigates efficiently the positive reactivity feedback due to the further voiding of fissile core height. Initially the event sequence is quite similar to the one calculated at state IV of this exercise when the radial core expansion is neglected. However, the net reactivity and the normalised power level stays higher due to the super imposed external reactivity ramp rate and thus time scales of the event sequence become smaller. It is already at about 2.1s into the boiling sequence that clad relocation starts in the SAS4A type calculations. In the GRIF-SM/CANDLE calculations this time period is considerably delayed up to 5.1s which seems to be related to the fact that GRIF-SM does not calculate actually established gap conditions, i.e. the variation of the heat transfer coefficient between fuel clad is not taken into account appropriately. As a consequence of the clad material relocation, a positive reactivity feedback is built up which accelerates the one due to the rapidly progressing void evolution in the core region. Another 2s to 3s later fuel pin breakup conditions are met in the high powered SAG of the MEZ. Rapidly after about half of the other SAGs enter into breakup conditions as a consequence of a rather energetic power transient which develops due to a positive reactivity ramp rate resulting from the superimposed effect of sodium boiling and clad material relocation.

At the same time of the first fuel pin break up the net reactivity stays close to prompt critical, i.e., it amounts to 0.95\$ or 0.85\$ respectively, depending on the model used. After first fuel pin breakup, the net reactivity rises only gradually exceeding prompt criticality only for a very limited time period of a few milliseconds (in the French calculation) because a more or less continuous dispersive fuel relocation initiates reactor shutdown after a few 100ms. However, fuel relocation seems not sufficient to lead to permanent subcriticality of the establishing core configuration.

3. GENERAL CONCLUSIONS

Transient response of an innovative BN-800 type core design to severe accidents

Evaluated consequences of the accidents considered in this comparative exercise depend on the design details given in the case set-up and on the level of detail of theoretical analyses. In so far conclusions can only be drawn related to the specific cases considered in this exercise and deducted from results of the specific calculations. These conclusions are as follows:

Main advantages of the as specified innovative BN-800 type core design are to be seen in providing an additional inherently activated safety margin of preventing fuel pin failure or local boiling in the domain of operational and severe transients to be considered in the design basis. These features complement well the large margin to fuel pin failure achieved already with the hollow pellet fuel pin design and a clad material providing ductility even under high dose loads. Evaluation of the impact of the as specified core design features on the core behaviour during operational transients was not part of this exercise as well as stability analyses. This would have needed other theoretical approaches to evaluate the potentially involved problems.

In the beyond design basis accident¹ domain some clear advantages of the innovative core design have been identified:

Unprotected reactivity initiated accidents most probably lead to an early reactor shutdown either due to pre-failure in-pin fuel relocation and/or due to a rapid fuel dispersal after fuel pin failure in a few subassembly groups. Linear ratings at failure conditions most probably are high, i.e., at about 1000 W/cm and more. Evaluations of the long term coolability of the established core configuration after reactivity initiated accidents were not part of this comparative exercise. They need careful consideration to evaluate potential consequences of a thermally induced subassembly to subassembly propagation.

In case of unprotected loss-of-flow accidents the main advantage of the as specified innovative core design is that it is hardly possible to approach or exceed prompt criticality in the initiating phase of the transient. At the end of most of the calculated event sequences, core configurations were established that needed transition phase analyses. This type of analyses were not part of this comparative exercise. However, they will become complicated because it remains unclear in what way permanent reactor shut down might be achieved. Release of thermal and/or mechanical energy cannot be predicted without performing appropriate analyses taking representative results of the initiation phase as initial conditions. This still needs to be done.

Conclusions from this comparative exercise hold for the specified case set-up. They need to be reviewed when some of the design features change or when more detailed evaluations lead to different input data like

- magnitude and/or spatial distributions of reactivity feedback coefficients of core materials,
- reactivity feedback effects due to radial core expansion,
- fuel pin mechanical properties, and
- if more rapidly developing consequences of control rod drive line expansion could be demonstrated.

It is felt that there are possibilities for improvement of the analyses and/or for optimisation, especially when a more realistic core design would be considered. However the comparative exercise has shown as well that consequences of these type of modifications need to be analysed carefully and in detail on a case to case basis. The use of more sophisticated and experimentally validated theoretical models would be helpful to improve the reliability of results.

¹ The considered accidents have extremely low probability and should be categorized to residual risk.

Methods and codes for transient analysis

Results of this comparative exercise have shown as well that theoretical approaches chosen by India with their PINCHTRAN code package provides comprehensive results for single phase analyses but they use simplified approaches for two-phase flow. Fuel pin mechanics is not yet modeled.

The Russian GRIF-SM code package with the complementary CANDLE-code package provides results for ULOF-type transients up to molten clad relocation. However, it is strongly recommended to couple a transient fuel pin mechanics code package to the system, to develop fuel pin failure criteria considering special features of the BN-800 fuel pin design and to extend the capabilities of the code system to describe core material relocation phenomena after fuel pin failure or breakup.

The different code versions of the SAS4A-code family available in Japan, France and Germany allow to evaluate consequences of accident initiators leading to core destruction along all stages of the initiation phase up to hexcan melting on the basis of experimentally qualified models. Even these code systems undergo continuous improvement.

In France, the pre-failure in-pin fuel relocation model EJECT is approaching completion with qualification and in Japan coupling to space time kinetics methods is far advanced. Thus, more improved analysis tools will become available in future which provide the possibility of re-evaluating the current results and to follow continuously the impact of new and/or optimised design features of innovative core designs on the results of accident analyses to be considered in the beyond design basis accident domain.

**NEXT PAGE(S)
left BLANK**

Chapter 1

SYNTHESIS OF NEUTRON PHYSICS CALCULATIONS

1.1. RUSSIAN CALCULATIONS

1.1.1. Methods and calculational models

Evaluation of the reactivity coefficients used in the subsequent analysis was made mainly on the basis of tools of the first order perturbation theory in 26-group diffusion approach. The calculations have been made using standard version of BNAB -78 data base with ARAMAKO-S system preparation of the cross section applied for justification of the BN-800 reactor design with near zero SVRE value [1.1, 1.2]. In this connection, in spite of the changes in methodology and data base which have taken place by now in Russia, standard conservative methods of applied calculation of reactivity coefficient were used as well as their models in the form which was used earlier (in 1991-1992) for their realization conformably to the design justification. In order to estimate the effect of using the different cross-section libraries some calculations were also performed with the modified version of RHEIN set developed in the framework of the former USSR-GDR bilateral cooperation [1.3, 1.4]. So for the analysis code sets realizing the above calculational method in R,Z geometry were used, namely : RADAR code using standard version of BNAB -78 data base with ARAMAKO-S system preparation of the cross section and RHEIN set with ZEMO constant preparation system for the BNAB-90 data base.

In order to evaluate criticality parameters and to make tests of the results obtained using the perturbation theory, 26-group SYNTEZ code (standard 26-group presentation with BNAB-78 data base) and 3D (GEX-Z) TRIGEX code (6 points per SA in 11-group approach[1.5]) were used. Macro data (delay neutron yield and spectra) from BNAB-78 and standard TATL libraries were used for calculation of the neutron kinetics parameters. The main reactivity coefficients were calculated using the following assumptions:

Doppler reactivity effect: Doppler constants have been evaluated

$$(T\partial K / \partial T)_i = \frac{K_{\text{eff}}(T) - K_{\text{eff}}(T_0)}{K_{\text{eff}}(T)K_{\text{eff}}(T_0)} \frac{1}{\ln\{T / T_0\}_i}$$

These values were calculated using both well known perturbation theory relationships and direct computational methods in 26-group approach in order to make corrections for scale in case of large size of temperature perturbation zone and Doppler constant correction for the sodium content change in physical and geometrical zones under consideration.

Sodium density component: Sodium density component was also evaluated using the first order perturbation theory and presented as follows:

$$[RE]_{\text{Na}} = \sum_n (\rho_{\text{Na}}^* - \rho_{\text{Na}}^0)_n \delta K_{\text{Na}}^n$$

taking into account correction for the relieving of resonance cross sections (for instance [1.6, 1.7])

Components of thermal expansion: Components of thermal expansion of the core for the evaluated neutronics functionals in the diffusion approach were determined using similarity theory expressions in [1.7, 1.8]. In the framework of the diffusion approach in case of “i”

material thermal expansion in "k" zone, the following relationships between the linear dimension L, content $\rho(i,k)$ and reactivity RE are true:

$$RE = \sum_i \sum_k \left\{ \frac{(\rho^* L^* - \rho^0 L^0)}{\rho^0 L^0} \right\}_{i,k} \delta K_{i,k}^N$$

In this relationship, reactivity component values determined by the perturbation theory equations are as follows:

$$\delta K_1 = \frac{1}{S} \left\{ \int \sum_{k=1}^m 3\sigma_{tr}^{ki} j_k(r) j_k^+(r) 2\pi r dr \right\} \quad \text{- leakage in R-direction}$$

$$\delta K_2 = \frac{1}{S} \left\{ \int_0^H \sum_{k=1}^m 3\sigma_{tr}^{ki} j_k(z) j_k^+(z) dz \right\} \quad \text{-- leakage in Z-direction}$$

$$\delta K_3 = \frac{1}{S} \left\{ \int \left[- \sum_k \sigma_{c,f,d}^{ik} \Phi_k(r) \Phi_k^+(r) + \sum_{j=1}^{k-1} \sigma_{in}^{j \rightarrow k} \Phi_j(r) \Phi_k^+(r) + \frac{1}{K_{eff}} \nu_f^k \sigma_f^k \Phi_k(r) \sum_k \chi_k \Phi_k^+(r) \right] dV \right\}$$

-worth of main reactions

$$S = \int \sum_k \nu_f^k \sum_f \Phi_k(r) \sum_k \chi_k \Phi_k^*(r) dr$$

-perturbation denominator.

In such representation, reactivity effects caused by thermal expansion of the materials in axial and radial directions are evaluated using the following relationship:

$$[\Delta K / K]_H = -2 \frac{\Delta H}{H} \sum_n \sum_i \rho_{i,n} \delta K_1^{i,n} \quad \text{and}$$

$$[\Delta K / K]_R = - \frac{\Delta R}{R} \sum_n \sum_i \rho_{i,n} (\delta K_1 + 3\delta K_2 + \delta K_3)^{i,n}$$

Here the sodium is excluded from summation, since its expansion has already been taken into account by the sodium density components. On the other hand, the expansion model can take into account sodium displacement by the core materials expanded in radial direction.

It should be taken into consideration that the above presented model of the uniform radial expansion of the core was realized as that of an entity: «truncated cone model» with the support points in the core diagrid structure and on the SA spacer pads.

The main characteristics of the considered reactor are presented in table 1.1 and figs 1.1, 1.2 and 1.3. A core cartogram is shown in fig. 1.4.

For neutronic calculation the reactor calculational model in R-Z geometry was prepared. End of the run of equilibrium state was adopted. So all control rods were withdrawn from the core and placed at their upper positions. The calculational model is given in fig. 1.1. Each sub-zone is described by two figures. The upper one is the sub-zone temperature, K; the lower one is the sub-zone number. The following designation of sub-zones is adopted: 1,2,3 - Upper part of LEZ, MEZ and HEZ, respectively; 4 - Lower axial breeder blanket; 5 - Radial breeder blanket; 6 - Sodium layer; 7 - Upper axial boron carbide shield; 9 - Control rod follower; 10,13 - These numbers are not needed in the calculations; 11 - Compensating system rod; 12 - Safety system rod; 14 - Pin gas volumes; 15 - Radial steel shield; 16 - Upper, lower and radial reflector; 17 - Subassembly heads; 18,19,20 - Middle part of LEZ, MEZ and

TABLE 1.1. MAIN PARAMETERS OF THE BN-800/1500 MWTB BENCHMARK CORE

| Core concept | Heterogeneous / 3 Enrichments | |
|--|-------------------------------|-----------------|
| | Fissile | Fertile |
| Total thermal power (MW) | 1500 | |
| ISadiationtime(e.f.p.d./cycles) | 140x3 | |
| Pitch (m) | 0.1006 | |
| Unit cell area (m ²) | 0.008764 | |
| Coolant flow area (m ²) | 0.002403 | 0.001438 |
| Active core height (m) | 0.851 | 1.58 |
| Axial blanket height (m) | 0.355 | |
| Fuel assemblies | 181/138/162 | 84 |
| Pins/assemMy | 127 | 37 |
| Fuel | (U,Pu)O ₁₉₈ | UO ₂ |
| Fuel theoretical density (gr/cm ³) | 10.97 | 10.69 |
| Fresh fuel enrichment Pu/(Pu+U) | | |
| - Lower: | 20.08% | |
| - Midle: | 23.17% | |
| - Higher: | 27.35% | |
| Fuel-isotopic composition (%): | | |
| Pu238/Pu239/Pu240/Pu241 /Pu242 | 0.0/60.0/25.0/1 0.9/ 4.1 | |
| U235/U236/U238 | 0.4/0.0/99.6 | |
| Pellet shape | Chamferred edges | |
| - dimensions (m) | 0.00025x0.00025 | |
| - Pellet height (m) | 0.008 | |
| - Inner radius (m) | 0.000825 | 0.0 |
| - Outer radius (m) | 0.0028 | 0.0068 |
| Axial blanket | | |
| - Inner radius (m) | 0.0 | |
| - Outer radius (m) | 0.002825 | |
| Clad | | |
| - inner radius (m) | 0.0029 | 0.0066 |
| - outer radius (m) | 0.0033 | 0.0070 |
| Central pins wire diameter (m) | 0.00115 | |
| Near-wall pins wire diameter (m) | 0.0006 x 0.0013 | |
| Steel slug diameter (m) | 0.0016 | 0.0035 |
| Number of slugs | 36 | 18 |

| | | | | | | | | | | | | | | | | | |
|---------------|------------|-----------|------------|-----------|------------|-----------|------------|-----------|------------|------------|------------|-----------|-----------|-----------|-----------|---------------------|-----|
| DH\DR (sm) | 25.05 | 3.14 | 17.00 | 1.82 | 5.43 | 1.58 | 15.21 | 2.38 | 5.11 | 21.95 | 20.73 | 9.44 | 9.40 | 18.70 | 30.00 | | |
| 70.00 | 900 16 | 900 16 | 900 16 | 900 16 | 900 16 | 900 16 | 900 16 | | |
| 31.18 | 900 17 | 900 11 | 900 17 | 900 12 | 900 17 | 900 12 | 900 17 | 900 11 | 900 17 | 900 17 | 900 17 | 900 17 | 900 17 | 900 17 | 900 16 | | |
| 25.15 | 900 7 | 900 11 | 900 7 | 900 12 | 900 7 | 900 12 | 900 7 | 900 11 | 900 7 | 900 7 | 900 7 | 1200 5 | 900 15 | 900 8 | 900 16 | | |
| 35.21 | 900 6 | 900 11 | 900 6 | 900 12 | 900 6 | 900 12 | 900 6 | 900 11 | 900 6 | 900 6 | 900 6 | 1200 5 | 900 15 | 900 8 | 900 16 | | |
| 5.00 | 900 24 | 900 11 | 900 24 | 900 12 | 900 24 | 900 12 | 900 24 | 900 11 | 900 24 | 900 24 | 900 24 | 1200 5 | 900 15 | 900 8 | 900 16 | | |
| 28.00 | 1500 1 | 1500 9 | 1500 1 | 1500 9 | 1500 1 | 1500 9 | 1500 1 | 1500 9 | 1500 1 | 1500 2 | 1500 3 | 1200 5 | 900 15 | 900 8 | 900 16 | | |
| 28.00 | 1500 18 | 1500 9 | 1500 18 | 1500 9 | 1500 18 | 1500 9 | 1500 18 | 1500 9 | 1500 18 | 1500 19 | 1500 20 | 1200 5 | 900 15 | 900 8 | 900 16 | | |
| 29.10 | 1500 21 | 1500 9 | 1500 21 | 1500 9 | 1500 21 | 1500 9 | 1500 21 | 1500 9 | 1500 21 | 1500 22 | 1500 23 | 1200 5 | 900 15 | 900 8 | 900 16 | | |
| 35.50 | 1200 4 | 1200 9 | 1200 4 | 1200 9 | 1200 4 | 1200 9 | 1200 4 | 1200 9 | 1200 4 | 1200 4 | 1200 4 | 1200 4 | 900 15 | 900 8 | 900 16 | | |
| 67.00 | 900 14 | 900 9 | 900 14 | 900 9 | 900 14 | 900 9 | 900 14 | 900 9 | 900 14 | 900 14 | 900 14 | 900 14 | 900 14 | 900 14 | 900 16 | | |
| 70.00 | 900 16 | 900 16 | 900 16 | 900 16 | 900 16 | 900 16 | 900 16 | | |
| | | | | | | | | | | | | | | | | Radial shielding | |
| | | | | | | | | | | | | | | | | | LEZ |
| | | | | | | | | | | | | | | | | | MEZ |
| | | | | | | | | | | | | | | | | | HEZ |
| | | | | | | | | | | | | | | | | | RB |

FIG. 1.1. Reactor model for neutronics calculations.

HEZ, respectively; 21,22,23 - Lower part of LEZ, MEZ and HEZ, respectively; 24 - Pin steel plugs.

Nuclear concentrations in 10^{24} nucl/cm³ for subzones are listed in table1. A1 Appendix.

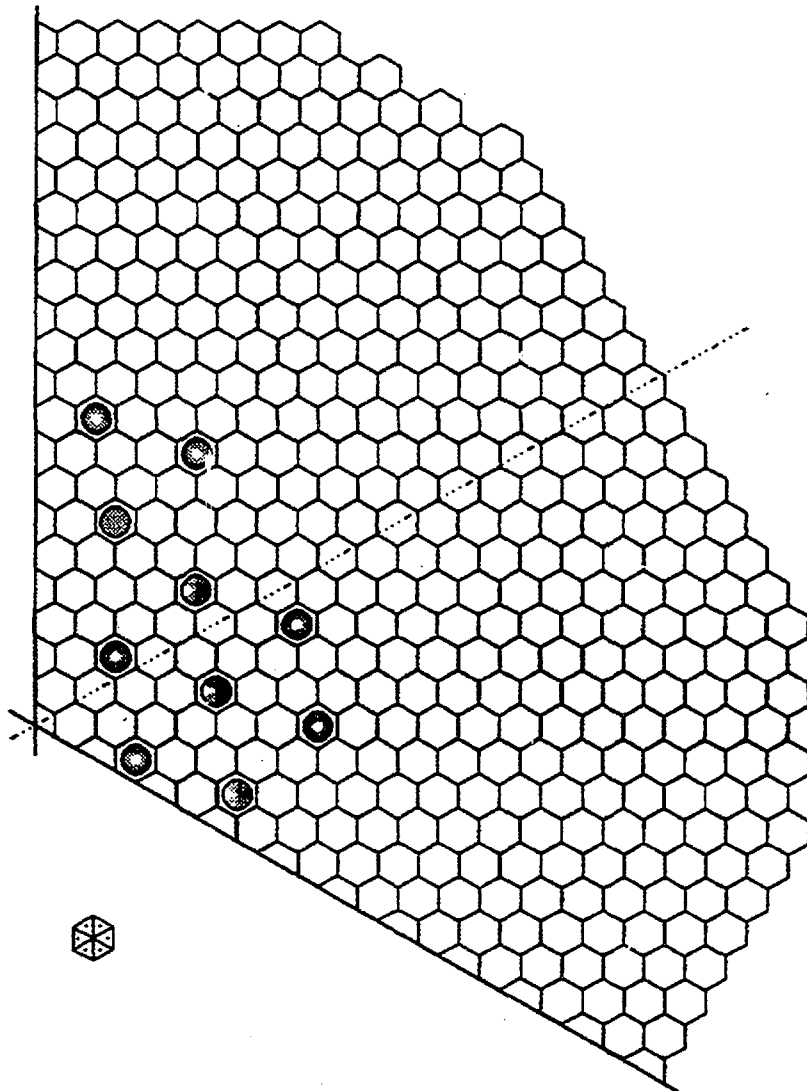


FIG. 1.2. Two 60° - sectors core layout for the BN-800 / 1500 MWth reactor. Six mesh points/plane per assembly.

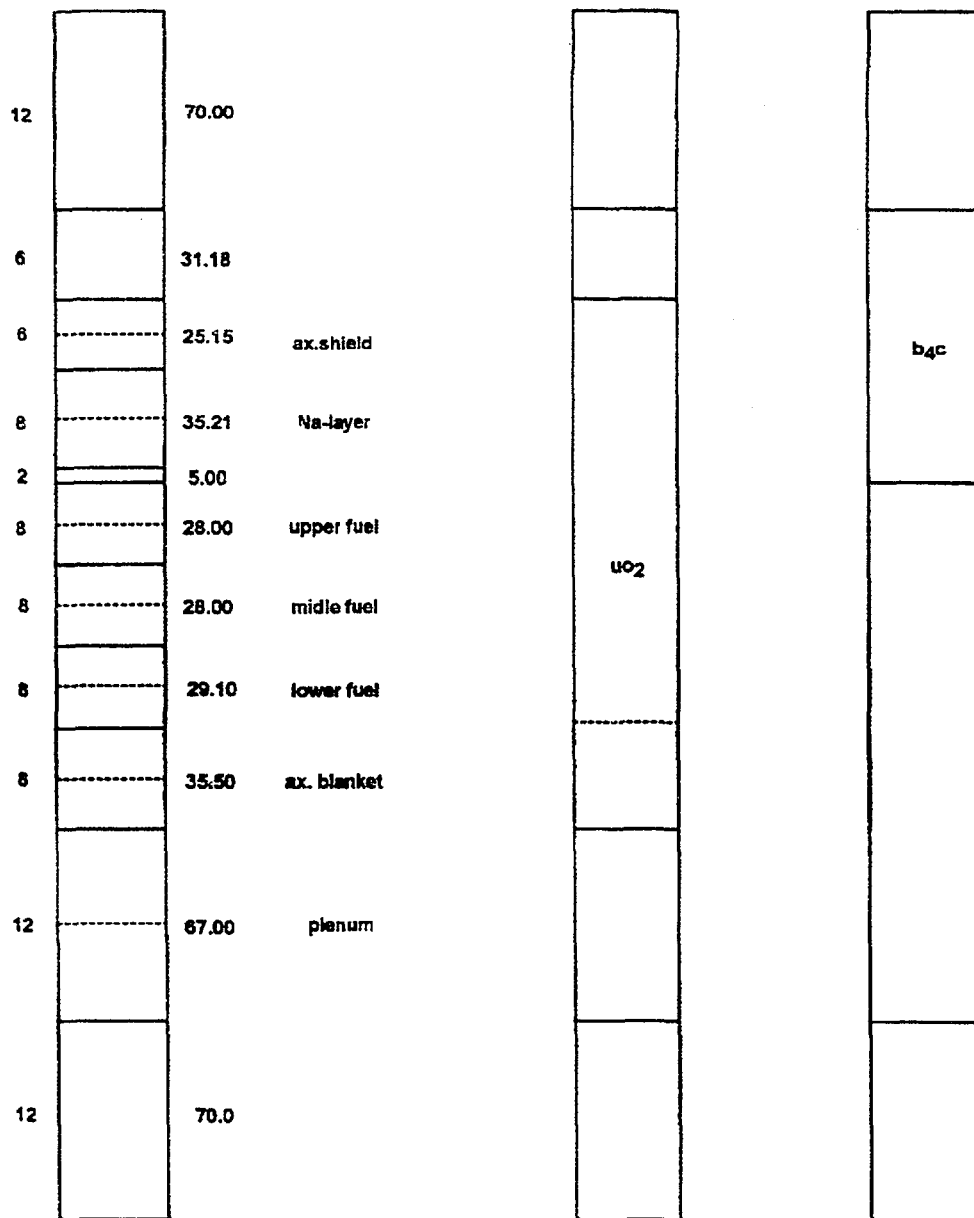


FIG. 1.3. Axial structure and geometry for fissile, fertile and c.r. assemblies for the neutronic calculations.

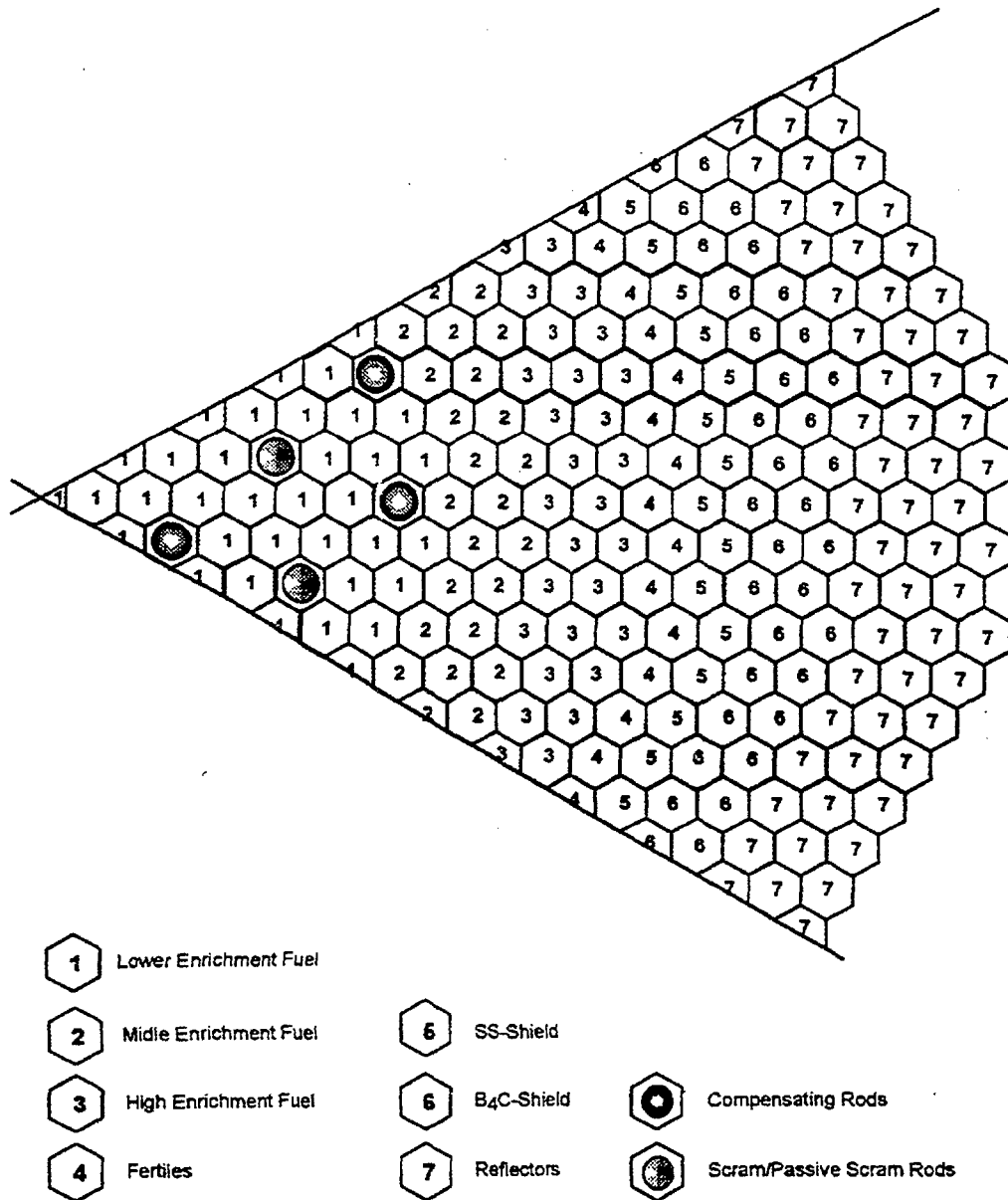


FIG. 1.4. One 60°- sector cross-section layout for the BN-800 / 1500 MWth benchmark core.

1.1.2. Results of calculations

Criticality parameters: Three different approaches that were used for calculations gave the following values of effective multiplication factor:

- 2D(RZ) geometry (finite diff. method): $K_{\text{eff}}=1.00445$
- 2D(RZ) geometry (synthetic method): $K_{\text{eff}}=1.006282$
- 3D(Z-HEX) geometry (finite diff. method): $K_{\text{eff}}=1.006762$

Neutron components in the reactor (finite difference method) for the first method are presented below:

| | |
|--|-----------|
| capture | 0.3028E+8 |
| fission | 0.1603E+8 |
| multiplication | 0.4651E+8 |
| N-2N | 0.5850E+5 |
| leakage | 0.2609E+6 |
| capture fraction | 0.9944 |
| leakage fraction | 0.0056 |
| fission neutron worth in the reactor, including | 0.3800E+9 |
| LEZ | 1.69E+8 |
| MEZ | 1.19E+8 |
| HEZ | 8.40E+7 |
| radial blanket | 4.06E+6 |

Neutron kinetics functionals: The main neutron kinetics functionals are given in table 1. 2 using delay neutron parameters based on BNAB and TATL data libraries in the framework of one computation code (RHEIN). The diversity of group values $\Sigma\beta$ and total value β_{eff} is caused mainly by the applied version of delay neutron parameters. Maximum difference is determined for the 6-th group, first of all owing to the high plutonium isotopes. In this case, it is to be noted that the absolute values of the delay neutron yield for ^{241}Pu and ^{242}Pu in the BNAB library corrected with account of the results of measurement of the plutonium critical assemblies.

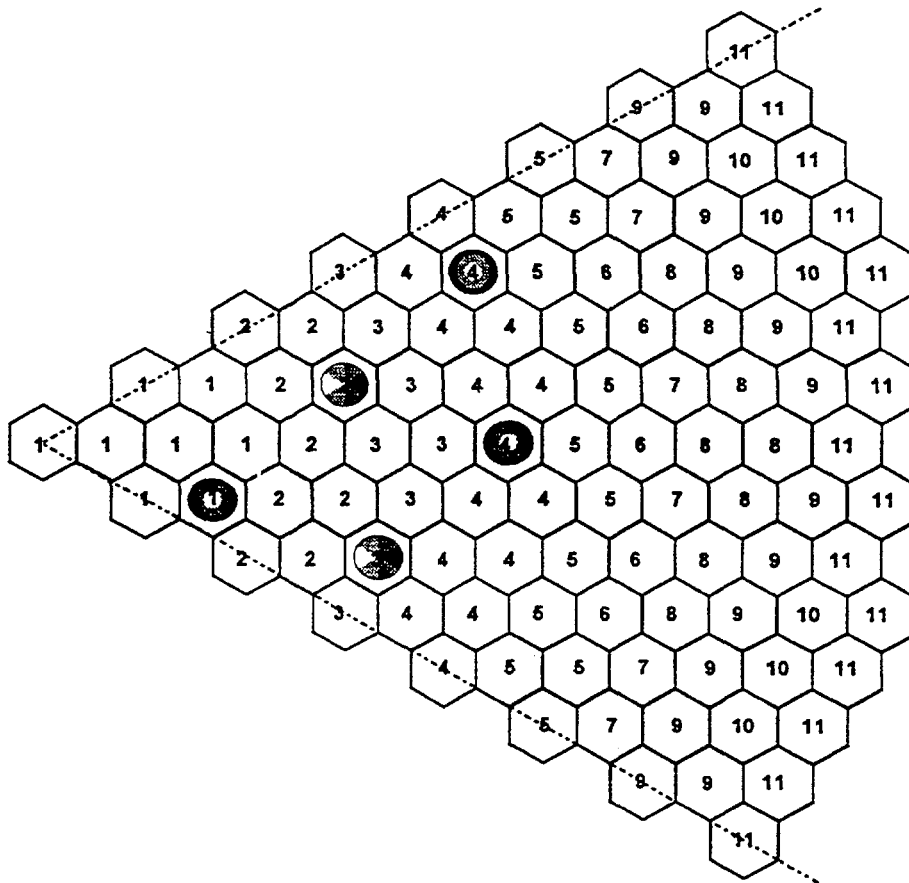


FIG. 1.5. Channels composition for one 60° - sector cross-section for the BN-800 / 1500 MWe benchmark core.

TABLE 1.2. NEUTRONICS PARAMETERS

| BNAB Library (Russia) | | | | | | |
|-----------------------|-------------------|-----------------|-----------------|-----------------|-----------------|-----------------|
| Group | β_1^{eff} | β_2^{eff} | β_3^{eff} | β_4^{eff} | β_5^{eff} | β_6^{eff} |
| U-235 | 0.281E-5 | 0.166E-4 | 0.145E-4 | 0.3158E-4 | 0.983E-5 | 0.2011E-5 |
| U-238 | 0.172E-4 | 0.1904E-3 | 0.222E-3 | 0.5342E-3 | 0.3073E-3 | 0.1033E-3 |
| Pu-239 | 0.4559E-4 | 0.3539E-3 | 0.2686E-3 | 0.4098E-3 | 0.1274E-3 | 0.4386E-4 |
| Pu-240 | 0.4936E-5 | 0.5060E-4 | 0.3501E-4 | 0.6422E-4 | 0.2323E-4 | 0.5360E-5 |
| Pu-241 | 0.6013E-5 | 0.1469E-3 | 0.1088E-3 | 0.2461E-3 | 0.1145E-3 | 0.1013E-4 |
| Pu-242 | 0.1839E-6 | 0.9257E-5 | 0.7516E-5 | 0.1933E-4 | 0.1015E-4 | 0.4682E-6 |
| $\Sigma\beta$ | 7.67E-5 | 7.68E-4 | 6.56E-4 | 1.31E-3 | 5.92E-4 | 1.65E-4 |
| β_{eff} | 0.3563E-2 | | | | | |
| L_p , sec | 0.4418E-6 (RADAR) | | | | | |
| λ_i , 1/sec | 0,0129 | 0,0311 | 0,134 | 0,331 | 1,260 | 3,210 |
| TATL Library (Russia) | | | | | | |
| U-235 | 0.2784E-5 | 0.1460E-4 | 0.1387E-4 | 0.3176E-4 | 0.1291E-4 | 0.5413E-5 |
| U-238 | 0.1932E-4 | 0.1585E-3 | 0.1813E-3 | 0.5444E-3 | 0.3558E-3 | 0.1452E-3 |
| Pu-239 | 0.4525E-4 | 0.3019E-3 | 0.2234E-3 | 0.4145E-3 | 0.2146E-3 | 0.6522E-4 |
| Pu-240 | 0.5281E-5 | 0.4271E-4 | 0.2487E-4 | 0.5525E-4 | 0.2990E- | 0.9155E-5 |
| Pu-241 | 0.1193E-4 | 0.1506E-3 | 0.9309E-4 | 0.2317E-3 | 0.1304E-3 | 0.4526E-4 |
| Pu-242 | 0.7824E-6 | 0.9349E-5 | 0.4943E-5 | 0.1304E-4 | 0.8984E-5 | 0.2869E-5 |
| $\Sigma\beta$ | 8.5343E-5 | 6.7765E-4 | 5.4146E-4 | 1.2906E-3 | 7.5260E-4 | 2.7316E-4 |
| β_{eff} | 3.6208E-3 | | | | | |
| L_p , sec | 4.4776E-7 (RHEIN) | | | | | |
| λ_i , 1/sec | 0.01340 | 0.030781 | 0.11742 | 0.30824 | 1.2418 | 2.9500 |

Sodium void and density reactivity effects: The results of calculations of SVRE as a function of sodium fraction in the different zones using SYNTEZ code are presented in the table1. 3. One can see from table1. 3 that the effect depends on temperature, changing non-linearly with sodium fraction.

As far as "interaction effect" between single voided fuel zones is concern it turns out that the simple sum of the single fuel zone reactivity worths under-estimates the positive actual value for the case of fully voided core by $\approx 5\%$, and the simple sum of the reactivity worths for all fuel zones and sodium layer zone differs from directly calculated value by 26% for $T=900K$ and almost by 3 times for $T=2100K$.

To complete the sodium void effect analysis it is necessary to make some comments with respect to the results presented in the "Input data" (table1. A.2, appendix). These data are the result of normalization of sodium efficiency spatial distribution obtained using perturbation theory on the directly calculated results. Sodium efficiency values in the bottom axial blanket and in the core have been normalized to the SVRE value in the core while the sodium efficiency in the above core area has been normalized to the sodium plenum efficiency. It is to be noted that SVRE for "Input Data.." was calculated under the condition that sodium was not removed from control rod channel but only from subassemblies.

Doppler reactivity: As it follows from table1.4 1-st order perturbation theory calculations gives overestimated absolute value of Doppler reactivity coefficients approximately by factor 1.5 as compare to the results of direct diffusion calculations and it is true both for voided an unvoided cases. In table1. 4 one can also observe the influence of application of different

TABLE 1.3. SODIUM VOID REACTIVITY AS A FUNCTION OF SODIUM FRACTION FOR DIFFERENT TEMPERATURE, % $\Delta K/K$

| Fissile zones only | | | | | |
|-------------------------------|-------|----------------------------|--------|--------|--------|
| Zone | T, °K | Na fraction in the zone, % | | | |
| | | 75 | 50 | 25 | 0 |
| L E Z | 900 | 0,193 | 0,396 | 0,602 | 0,800 |
| | 2100 | 0,213 | 0,433 | 0,658 | 0,882 |
| M E Z | 900 | 0,103 | 0,209 | 0,315 | 0,416 |
| | 2100 | 0,112 | 0,228 | 0,344 | 0,466 |
| H E Z | 900 | -0,040 | -0,082 | -0,131 | -0,195 |
| | 2100 | -0,035 | -0,075 | -0,119 | -0,175 |
| Whole core | 900 | 0,259 | 0,534 | 0,812 | 1,068 |
| | 2100 | 0,293 | 0,605 | 0,927 | 1,232 |
| Fissile zone "+" sodium layer | | | | | |
| L E Z | 900 | 0,137 | 0,242 | 0,292 | 0,165 |
| | 2100 | 0,156 | 0,287 | 0,360 | 0,267 |
| M E Z | 900 | -0,064 | 0,083 | 0,073 | 0,024 |
| | 2100 | 0,078 | 0,105 | 0,103 | -0,022 |
| H E Z | 900 | -0,160 | -0,269 | -0,421 | -0,664 |
| | 2100 | -0,028 | -0,151 | -0,307 | -0,558 |
| Whole core | 900 | -0,087 | -0,058 | -0,056 | -0,377 |
| | 2100 | 0,116 | 0,214 | 0,152 | -0,110 |

Note: Calculation has been made in diffusion approach.

TABLE 1.4. DOPPLER REACTIVITY FOR VARIOUS REACTOR ZONES IN THE TEMPERATURE RANGE 900-2100°K (DIFFUSION THEORY, BNAB-78 DATABASE), $\Delta K/K$

| Heated reactor part | SYNTEZ(direct calculation) | | 1-order perturbation theory RADAR (RHEIN) | |
|--------------------------------|----------------------------|-----------|--|----------------------------|
| | Fuel | Steel | Fuel | Steel |
| Unvoided core (100% of sodium) | | | | |
| LEZ | -0.0030 | -0.00029 | -0.00372 (-0.00405) | -0.000434 (-0.000466) |
| MEZ | -0.00147 | -0.00016 | -0.00158 (-0.00131) | -0.000181 (-0.000165) |
| HEZ | -0.000745 | | -0.000834 (-0.000801) | -0.000087 (-0.0000402) |
| Whole core | -0.00521 | -0.000482 | -0.00613 (-0.00616) | -0.00702 (-0.00671) |
| BAB | -0.0007 | | -0.000754 (-0.000906) | -0.00075 (-0.000482) |
| RB | -0.000311 | | -0.0005175 (-0.000575) | -0.0000168 (-0.0000166) |
| Voided core (0% sodium) | | | | |
| LEZ | -0.0019 | | (-0.00245) | (-0.000305) |
| MEZ | -0.00081 | | (-0.00096) | (-0.000106) |
| HEZ | -0.000535 | | (-0.000572) | (-0.000428) |
| Whole core | -0.00337 | | (-0.00398) | (-0.000839) |
| BAB | -0.000575 | | (-0.00093) | (-0.0000501) |
| RB | -0.00029 | | (-0.000605*) (-0.000439) (-0.00039*) | (-0.0000158) |

Note: "*" - the whole reactor is voided.

cross-section libraries used in RADAR and RHEIN codes. As regards fuel, the most effect (18%) is seen for the medium enrichment zone but for whole core the effect in the results provided is negligible. As regards steel, the most difference is observed for high enrichment zone but for the whole core as well as for fuel using of different cross-section libraries gives very similar values of Doppler reactivity coefficients. The data presented in two last rows of table 1. 4 shows that Doppler constant values for the separate reactor parts depends on the adopted drying model, which can include the whole reactor or the core only. Thus Doppler constant for bottom axial blanket decreases by factor of ~ 1.5 when the whole reactor is voided.

The same procedure as for sodium density reactivity was applied for evaluation of Doppler reactivity coefficients that were presented as input data for ULOF accident calculations (table 1 A.3, Appendix). In order to diminish the error the space distributions calculated by RHEIN were normalized to directly calculated (SYNTEZ -code) values of Doppler effect for different reactor zones (table 1. 5). The reduction factor of Doppler coefficients (table 1A.4, Appendix). was also calculated on the base of direct diffusion calculations that are presented in the table 1. 6.

Reactivity caused by material thermal expansion: Reactivity components due to the thermal core expansion were calculated using 1-st order perturbation theory in diffusion approach. The results in brief condensed form are presented in table 1. 7.

The results of these calculations were used for specification of axial and radial expansion coefficients (tables 1. A.4 and 1. A.5, respectively) in the "Input data..."

Material density coefficients for fuel and steel: Fuel and steel displacement reactivity coefficients as they presented in the "Input Data..." (table 1. A.6, 1. A.7) were calculated using 1-st order perturbation theory, diffusion approach (code RADAR).

1.2. ITALIEN CALCULATIONS

1.2.1. Introduction

Models of calculation: This analysis is based on the mixed oxide fuelled BN-800 heterogeneous type reactor design [1.2], in the variant of 1500 MWth (total power) proposed by IPPE, characterized by three enrichment zones. Details of the core layout, physical zones, physical properties, atomic densities at EoC and operative conditions for the benchmark core are given in [1.2]. Some parameters of the above input data are collected in table 1.1, while fig. 1. 2 shows two 60°- sectors cross-section of the benchmark core. This choice is related to the fact that the physical and geometrical period of the benchmark core is one 120°- sector. Similarly fig. 1. 3 shows the axial structure for the fissile, fertile and control rod assemblies. In this analysis, at the EoC-configuration, the compensating control rods are considered entirely withdrawal, fig. 1. 3. When the rods are inserted their B4C lower boundary is at the active core (fissile region) lower boundary while their B4C upper boundary is at the pin steel plugs upper boundary.

It has to be noted that from the atomic densities provided input data [1.2] the following can be obtained:

- End of Cycle (EoC) fuel enrichments: Pu/(Pu+U)
 - LEZ: 20.02%
 - MEZ: 22.65%

TABLE 1.5. DOPPLER REACTIVITY COEFFICIENT DISTRIBUTION IN THE CORE, $\Delta K/K\%$. (2D-DIFFUSION CALCULATIONS)

| B ₄ C | | | | |
|------------------|-----------|----------|----------|----------|
| Sodium layer | | | | |
| 1/3 Core | 0.0006137 | 0.000382 | 0.000206 | RB |
| 1/3 Core | 0.001348 | 0.000615 | 0.000301 | |
| 1/3 Core | 0.000997 | 0.000440 | 0.000239 | 0.000311 |
| BAB | 0.000698 | | | |
| | LEZ | MEZ | HEZ | |

TABLE 1.6. DOPPLER REACTIVITY COEFFICIENTS AS A FUNCTION OF SODIUM FRACTION, $\Delta K/K\%$. (2D-DIFFUSION CALCULATIONS)

| | Sodium fraction, % | | | |
|--------------------------------------|--------------------|--------|--------|--------|
| | 100 | 50 | 25 | 0 |
| LEZ | 0.299 | 0.249 | 0.238 | 0.232 |
| MEZ | 0.107 | 0.106 | 0.1055 | 0.105 |
| HEZ | 0.0745 | 0.0652 | 0.0649 | 0.0647 |
| Core | 0.593 | 0.538 | 0.529 | 0.522 |
| Core + Sodium layer + Shield + Plugs | 0.590 | 0.539 | 0.529 | 0.522 |
| BAB | 0.070 | 0.0707 | 0.0648 | 0.0575 |
| Ragial Blanket | 0.0311 | 0.0380 | 0.0367 | 0.0290 |

TABLE 1.7. REACTIVITY COMPONENTS DUE TO THERMAL EXPANSION OF CORE STRUCTURES, $\Delta K/K$ (DIFFUSION APPROACH, 1-ST ORDER PERTURBATION THEORY).

| Zone | Radial expansion | | Axial expansion | |
|--------------------------|------------------|----------|-----------------|----------|
| | steel | fuel | steel | fuel |
| Unvoided state (100% Na) | | | | |
| LEZ | 3.43E-3 | -2.88E-1 | -2.35E-3 | -4.20E-3 |
| MEZ | -3.49E-3 | -1.48E-1 | -9.44E-3 | -1.70E-2 |
| HEZ | -4.85E-3 | -5.11E-2 | -1.13E-2 | -2.06E-2 |
| RB (UO ₂) | -3.57E-3 | -1.01E-2 | -8.58E-3 | -3.17E-2 |
| BAB | -1.31E-2 | -2.03E-2 | -1.07E-3 | -2.01E-3 |
| Whole core | | -0.4919 | | -0.0649 |
| Whole reactor | | -0.5396 | | -0.1082 |
| Voided state (0% Na) | | | | |
| LEZ | -2.30E-3 | -3.09E-1 | -3.18E-3 | -5.87E-3 |
| MEZ | -6.22E-3 | -1.60E-1 | -1.15E-2 | -2.14E-2 |
| HEZ | -6.18E-3 | -5.91E-2 | -1.30E-2 | -2.44E-2 |
| RB (UO ₂) | -3.85E-3 | -1.13E-2 | -9.68E-3 | -3.66E-2 |
| BAB | -1.5(E-2 | -2.45E-2 | -1.17E-3 | -2.23E-3 |

Note: All values are given for conditional magnitude of the the linear thermal expansion coefficient $\alpha_i = 1 / \text{degree}$

- HEZ: 26.60%
- O/Met: 2.0
- Average Burnup: 4.124%,
distributed over the three enrichment zones as following: 4.274%, 4.376% and 3.743%.

Methods of calculation: For the benchmark exercise calculations the following methodology was adopted: a first evaluation of some integral neutronic parameters was performed in 2D(R,Z) frame, as in [1.2]; nevertheless because the heterogeneous character of the benchmark core, a correct neutronic description of the problem need a 3-dimensions geometry scheme. Because the scram and passive scram control rod assemblies have identical atomic composition and are under the same "benchmark-operative conditions" [1.2], the 120°- sector period may be reduced at one 60°-sector period. This allows to adopt this last configuration for the diffusion theory analysis of the benchmark core, saving both computing memory and time For a detailed radial description of the neutron fluxes and power distributions per assembly was adopted the 3-dimensions Triangular-Z scheme, using six mesh-points per plane and assembly with axial meshes structure as in fig.1. 3.

In this 3-dim, description the benchmark core is subdivided in 930 homogeneous cells whose 830 are fuel cells. fig.1. 4 shows the 60°-sector cross-section used in the diffusion theory calculations [1.9]. The CITATION code (Finite Differences Diffusion Code [1.10]) was used for the different eigenvalue calculations, where integral and local results and information are carried out using a 22-energy groups cross-section library originated from ENDF/B-V.11 file at 3 different temperatures: 700,1000 and 1500 K. On the other hand, for the sodium void effect analysis in transport theory a 3- dimensions Hexagonal-Z full core configuration was adopted. It means to a 3- dim, complete description of 1027 assemblies [1.11], using homogeneous cells. In this analysis a voided state is equivalent to a zero sodium atomic density. The MCNP4A code (Monte Carlo Transport Code [1.12]) was used for the transport eigenvalue calculations, with continuous energy cross-section library originated from JEF-1 file. For a significant reduction of the statistical 1σ -error (standard deviation) to less than 1‰ Δk , one up two millions neutron histories (5000 neutron histories per generation) are involved for each keff calculation. This choice is strongly related to the core voided configuration under study.

Computing conditions: This analysis was conducted running on the IBM/RISC-6000 machine with the following computing conditions, for each calculation:

| | | |
|---|----------------------------|-------------------------|
| - diffusion code: 22 energy groups: | | |
| | 2D(R,Z) | 3D(Triang,Z) |
| - Symmetry | / | 1/6 |
| - Axial nodes | 75 | 90 |
| - Radial nodes | 43 | 62*31 |
| - Accuracy | $\Delta k_{eff} < 1e-6$ | |
| - Convergence: | ≈ 35 iterations | ≈ 50 iterations |
| - CPU (min): | ≈ 55 | ≈ 112 |
| - Memory (MB): | ≈ 2.6 | ≈ 5.9 |
| - transport code: continuous energy cross-sections library: | | |
| | 2D(R,Z) | 3D(Hex,Z) |
| - neutron histories | 1.000.000 | |
| - Accuracy(1σ -error): | $< 0.8\%$ Δk_{eff} | |
| - CPU(min): | ≈ 235 | ≈ 360 |
| - Memory (MB): | ≈ 0.9 | |
| | 2D(R,Z) | 3D(Hex,Z) |

- neutron histories 2.000.000
- Accuracy (1 σ -error): <0.5% Δk_{eff}
- CPU(min): ≈ 450 ≈ 750
- Memory (MB): ≈ 0.9

Tasks to be performed :as was defined in [1.9] the neutron physics parameters to be calculated, and compared with the IPPE provided data, are subdivided in two groups:

- *Diffusion theory*: Integral and local neutronic parameters and performances of the benchmark core and their distribution over the different channels, stated for the ULOF transient analysis.

- *Transport theory*: Effective multiplication factors k_{eff} and statistical uncertainties for the steps with and without sodium for single zones and whole core.

Reactivity burnup swing and power swing, throughout a cycle, were not performed because the input data about refueling and/or shuffling strategy and fuel atomic densities at BoC have not been provided by IPPE. For the same reason control rods reactivity worth was performed only for the EOC-configuration.

1.2.2. Results of calculations

The obtained results, performed at EOC-configuration of the benchmark core for the BN-800/1500 MWth reactor, are subordinated to the benchmark exercise purpose, covering a great part of the neutronic design activities, i.e. criticality levels (eigenvalues), fluxes, powers, reactivity worths, kinetics parameters were investigated. Detailed results about: distributions per assembly, zone and channel (channels composition defined in with a 60°-sector cross-section representation in fig1..5) are given for: thermal power, power density, linear power, power peaking factors, Doppler coefficients, density reactivity coefficients. Also kinetics parameters, C.R. reactivity worth's, sodium void worth and other neutronic parameters are presented.

Eigenvalues: In the withdrawal control rods configuration (EOC), for the effective multiplication factor in the sodium unvoided case, was obtained:

- diffusion theory:
 - 2D(R,Z)geometry: $k_{\text{eff}}=1.00835$
 - 3D(T,Z) geometry: $k_{\text{eff}}=1.00882$;
- transport theory
 - 1.000.000 neutron histories:
 - 2D(R,Z) geometry: $k_{\text{eff}} = 1.00183 \pm 68\text{pcm}$
 - 3D(H,Z) geometry: $k_{\text{eff}} = 1.00323 \pm 74\text{pcm}$;
 - 2.000.000 neutron histories:
 - 2D(R,Z) geometry: $k_{\text{eff}} = 1.00215 \pm 48\text{pcm}$
 - 3D(H,Z) geometry: $k_{\text{eff}} = 1.00299 \pm 48\text{pcm}$.

It is worth to be observed that:

- in both diffusion and transport theory the 2D results are slightly lower than the 3D ones;
- the diffusion theory results appear very close but their comparison is meaningless because the different meshes number and different cells number;
- doubling the neutron histories in transport theory, the k_{eff} results do not change significantly, while the standard deviation improves of about 30% - 35%, but the computing time worsens by a factor of about 2.

Neutronic performances: The benchmark core, with neutron fluxes normalized to 1500 MWth of total power, is characterized by the following values:

- Neutron fluxes:
 - peak total flux: $7.12 \cdot 10^{15}$ n/cm² sec,
 - peak fast flux: $4.04 \cdot 10^{15}$ n/cm² sec,
 - peak fast dose: $1.46 \cdot 10^{23}$ n/cm²,

where the dose figure, important for the strain-analysis, was obtained assuming the peak fast flux constant during the assembly life (420 EFPD); nevertheless the obtained value is to consider underestimated, since the peak fast flux is greater in the B0C than in E0C.

- Thermal power.
- fractional distribution of the total power:
 - active core: 0.9251,
 - ax. blanket: 0.0312,
 - rd. blanket: 0.0338,
 - other zones: 0.0099.
- peak values:
 - linear power: 385.5 W/cm,
 - power density: 558.7 W/cm³.

In tab1..8 the power distribution per zone and channel is given; fig.1. 6 shows the total and active core power distribution per fuel assembly. fig.1.7 shows the average (active core)

TABLE 1.8.THERMAL POWER (MW) DISTRIBUTION PER ZONE AND CHANNEL.

| | Upper | Midle | Lower | Total | $\Delta\%(^*)$ |
|--------------|---------|---------|---------|---------|----------------|
| L.E.Z | 151.205 | 220.741 | 188.575 | 560.521 | +1.79 |
| M.E.Z | 116.545 | 166.402 | 138.217 | 421.164 | +0.39 |
| H.E.Z | 114.935 | 159.920 | 131.063 | 405.918 | +0.002 |
| B.A.B | | | | 46.792 | -1.49 |
| Rad. Blanket | | | | 50.742 | -1.41 |
| GasVol.Zones | | | | 1.324 | |
| Na-Layer | | | | 0.756 | |
| Ax. Shield | | | | 1.843 | |
| Heads Zone | | | | 0.032 | |
| C.Rods | | | | 2.959 | |
| Others | | | | 7.949 | |
| Total | | | | 1500.00 | |

Peak Power Density 558.7 (w/cm³)
 Peak Linear Power 385.5 (w/cm) $\Delta\%(^*)=+4.13$

| channel: | Power | $\Delta\%(^{**})$ |
|----------|---------|-------------------|
| 01 | 104.255 | + 7.40 |
| 02 | 138.340 | + 7.35 |
| 03 | 116.651 | + 6.81 |
| 04 | 228.870 | + 6.16 |
| 05 | 237.788 | + 4.36 |
| 06 | 93.405 | + 4.06 |
| 07 | 104.826 | + 2.84 |
| 08 | 143.536 | + 0.92 |
| 09 | 198.886 | + 2.98 |
| 10 | 75.375 | + 6.84 |
| 11 | 50.857 | - 1.48 |
| 12 | 7.211 | -43.97 |

(*) $\Delta=(\text{enea-ippe})/\text{ippe}$

(**) enea values: total power per channel.

and peak values distribution of the linear power per fuel assembly, while fig.1. 8 shows the same distribution of the power density. Similarly fig.1. 9 shows the power peaking factors (axial and radial) distribution per fuel assembly, while fig.1. 10 shows the axial distribution of the smeared relative power density rating (1/m3) for the first 10 (fuel) channels.

About the power distribution we observe a good agreement about the fuel zones, (discrepancies less than 2% for the integral results and 4.1% for the peak linear power) but not for the absorber and other structural zones. This may be attributed to the capture energy-yield of the B10 in the B4C, as well as to the slowing-down energy-loss evaluation for the Na23 in the sodium layer zone. Moreover the axial power density rating distributions per channel, provided by IPPE, in the central zone are greater than the ENEA ones with an "almost-systematic" difference of about 10%.

- Breeding properties:

Conversion factors and breeding ratios, defined for the z-zone as:

$$C.F (z) = \sum_n R_{c,n}^{fert} (n \in z) / \sum_m R_{a,m}^{fiss} (m \in z)$$

$$B.R (z) = \sum_n R_{c,n}^{fert} (n \in z) / \sum_m R_{a,m}^{fiss} (m \in Core)$$

with:

- $R_{c,n}^{fert}$ the capture rate for the n-fertile nuclide;

- $R_{a,m}^{fiss}$ the absorption (capture and fission) rate for the m-fissile nuclide, were

calculated:

| | C.F | B.R |
|-------------------|--------|--------|
| - active core: | 0.6891 | 0.6581 |
| - axial blanket: | 6.8168 | 0.1344 |
| - radial blanket: | 5.0986 | 0.1288 |
| - total reader | | 0.9213 |

The breeding ratio results show that the BN-800/1500 MWth benchmark core shows moderated "burner core" properties, at least in E0C-state.

- Kinetics parameters:

The BN-800/1500 MWth benchmark core is characterized by the following integral kinetics parameters:

- delayed fraction of source neutrons: $\beta = 4.0960 \cdot 10^{-3}$
- effective delayed neutrons fraction: $\beta_{eff} = 3.3769 \cdot 10^{-3}$
- prompt-neutrons life time: $L_p = 4.2435 \cdot 10^{-7} \text{sec}$
- mean decay constant: $\lambda = 9.6601 \cdot 10^{-2} \text{sec}^{-1}$
- mean-neutrons life time: $\tau = 3.4958 \cdot 10^{-2} \text{sec}$

where:

$$1/\lambda = [\sum_g \beta_{eff,g} / \lambda_g] / \beta_{eff}$$

$$\tau = (1 - \beta_{eff}) L_p + \sum_g \beta_{eff,g} / \lambda_g$$

- Control Rods Efficiency:

Compensating and scram control rods worth was calculated as total:

$$\Delta\rho = -31.626\text{\$}; \quad 1\$ = 3.3769 \cdot 10^{-3}$$

as well as separated systems:

- compensating rods:

- inner rings: (6 assemblies) $\Delta\rho = 6.194\text{\$}$
- outer rings: (12 assemblies) $\Delta\rho = -15.181\text{\$}$
- scram/passive scram: (12 assemblies) $\Delta\rho = -17.016\text{\$}$.

Defining "shadow effect" as:

$$[\Delta\rho - \sum_g \Delta\rho(g)] / \sum_g \Delta\rho(g)$$

the BN-800 benchmark core it is characterized by a "shadow effect" value of the -0.176 or 17.6% loss in efficiency for the whole control rods system.

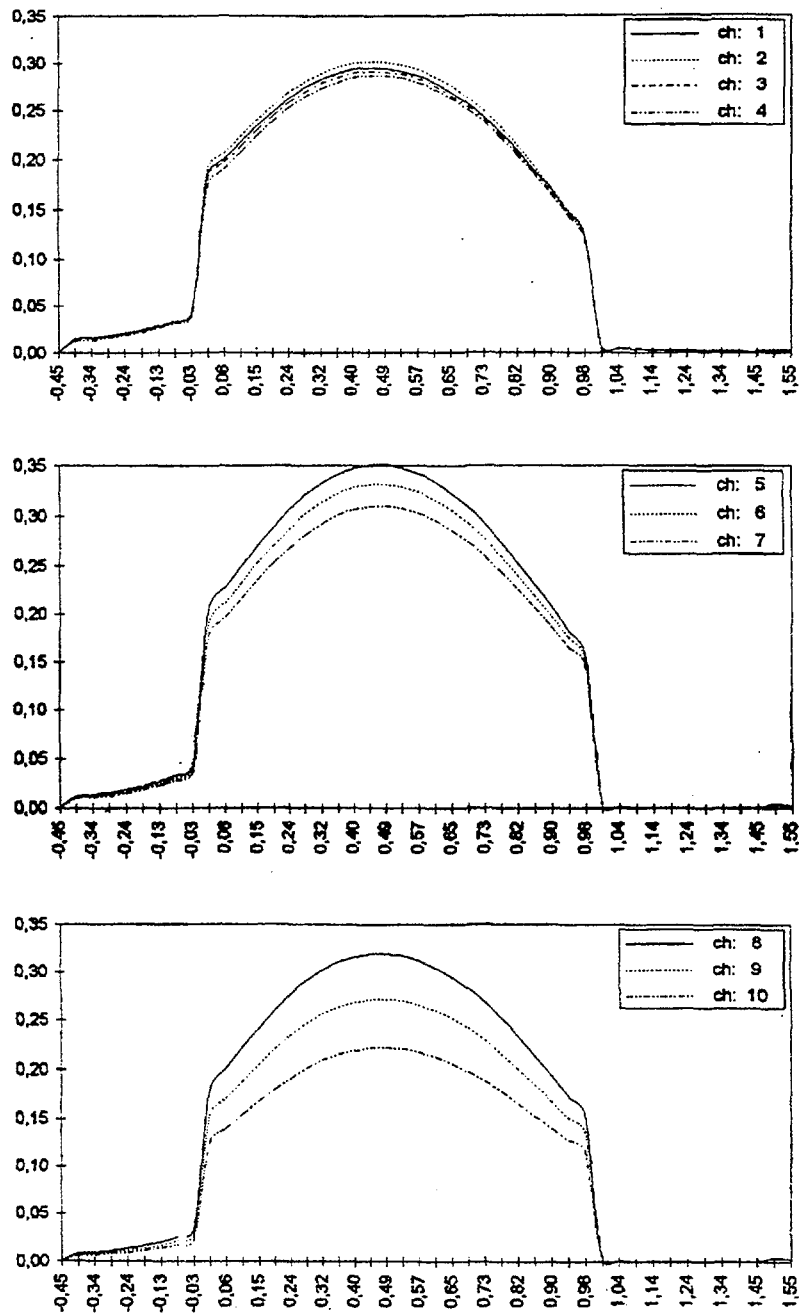


FIG. 1.10. Smeared relative power density rating ($1/m^3$) axial distribution per fuel channel for the BN-800 / 1500 MWth benchmark core. (Active core length normalized distance: origin in bottom)

Reactivity coefficients: Diffusion theory results about Doppler coefficients, uniform expansion coefficients, density reactivity coefficients (fuel, sodium, steel and absorber) are given, both as integral and local figures.

Doppler coefficients: The Doppler coefficients were calculated, both with and without sodium, in the range (1000 - 1500) K, for the different fuel zones. The integral values:

- unvoided case: $TdK(T)/dT = -811\text{pcm}$
- voided case: $TdK(T)/dT = -584\text{pcm}$

are distributed over the different zones and channels as in tab1..9, while fig.1.11 shows their distribution per fuel assembly with and without sodium; fig.1. 12 and Fig.1. 13 show the axial distribution of the smeared Doppler coefficients rating (pcm/m) for each average assembly of the first 10 (fuel) channels.

Uniform expansion coefficients: the coefficient of uniform expansion are calculated in to steps:

- changes in geometry (radially and axially) without varying the densities of the materials - “geometry effect”;
- changes in geometry (radially and axially) without varying the total mass (by an appropriate change in the density of all materials, Na is included) - “net effect”.

Both axial and radial uniform expansion coefficients were calculated as:

$$\delta k/k/\delta \xi/\xi; \xi=H; R$$

calculating separately geometry effect and net effect and combining these for the density effect value, i.e.:

$$\delta k/k/\delta \rho/\rho = C(\xi)[(\delta k/k/\delta \xi/\xi)_{geo} - (\delta k/k/\delta \xi/\xi)_{net}]$$

with:

$$C(\xi) = 1/(1 + \delta \xi, R); \delta \xi, R = \text{Kronecker delta.}$$

In this analysis because the total mass of the core is kept constant:

geometry effect mean:

$$\delta \xi/\xi \neq 0 \text{ and } \delta \rho/\rho = 0$$

and net effect mean:

$$\delta \xi/\xi \neq 0 \text{ and } \delta \rho/\rho = -\delta \xi/\xi$$

- **Axial expansion:** $\delta R/R = 0$

- Geometry effect:

$$\delta H/H = +0.05; \delta \rho/\rho = 0 \quad (\delta k/k/\delta H/H)_{geo} = 0.22519$$

- Net effect:

$$\delta H/H = +0.05 ; \delta \rho/\rho = -0.05 \quad (\delta k/k/\delta H/H)_{net} = -0.13804$$

TABLE 1.9. DOPPLER COEFFICIENTS TDK*/DT, WITH AND WITHOUT NA, AND THEIR DISTRIION PER CHANNEL.

| | 100% Na | 0%Na | ratio (0 to 100)% Na |
|--------------|----------|----------|-------------------------|
| L.E.Z | 3.746E-3 | 2.570E-3 | 0.6861 |
| M.E.Z | 1.916E-3 | 1.374E-3 | 0.7171 |
| H.E.Z | 1.075E-3 | 7.670E-4 | 0.7135 |
| B.A.B | 8.607E-4 | 6.881E-4 | 0.7995 |
| Rad. Blanket | 5.155E-4 | 4.415E-4 | 0.8565 |

| nominal doppler coeff's | | voided doppler coeff's | | |
|-------------------------|--------|------------------------|---------|--------|
| channel | (pcm) | $\Delta\%(*)$ | channel | (pcm) |
| 01 | 77.68 | 50.17 | 01 | 54.35 |
| 02 | 100.51 | 37.62 | 02 | 70.36 |
| 03 | 83.54 | 25.97 | 03 | 58.44 |
| 04 | 162.74 | 17.86 | 04 | 113.68 |
| 05 | 121.40 | 44.86 | 05 | 88.23 |
| 06 | 45.42 | 30.58 | 06 | 32.98 |
| 07 | 47.76 | 13.19 | 07 | 34.66 |
| 08 | 47.52 | 89.98 | 08 | 34.30 |
| 09 | 55.55 | 37.95 | 09 | 40.08 |
| 10 | 16.54 | -12.30 | 10 | 11.94 |
| 11 | 51.55 | 27.44 | 11 | 44.15 |

(*) $\Delta = (\text{enea-ippe})/\text{ippe}$

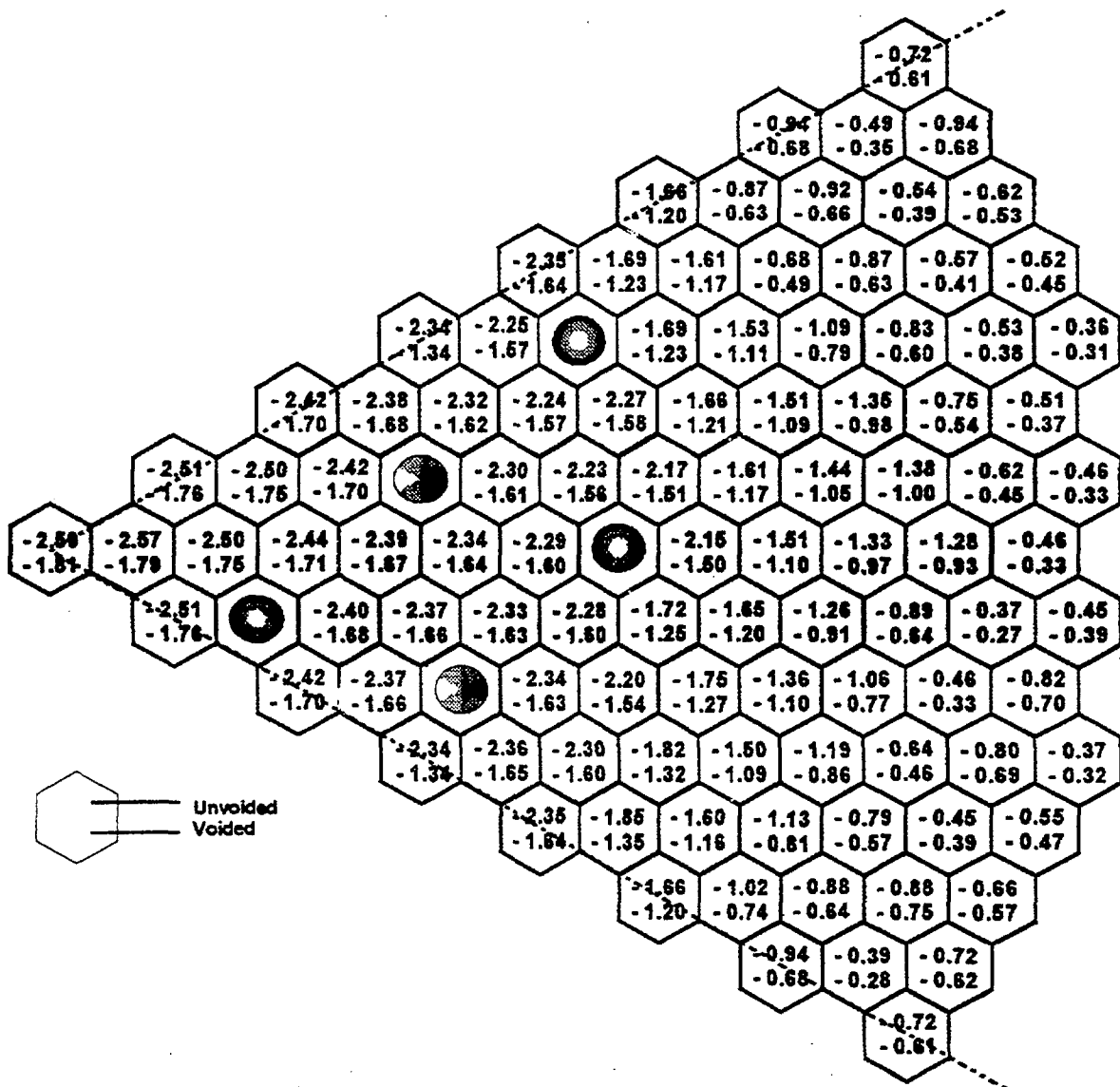


FIG. 1.11. Nominal and voided Doppler coefficients Tdk/dT (pcm) per fuel assembly for the BN-800 / 1500 MWth benchmark core.

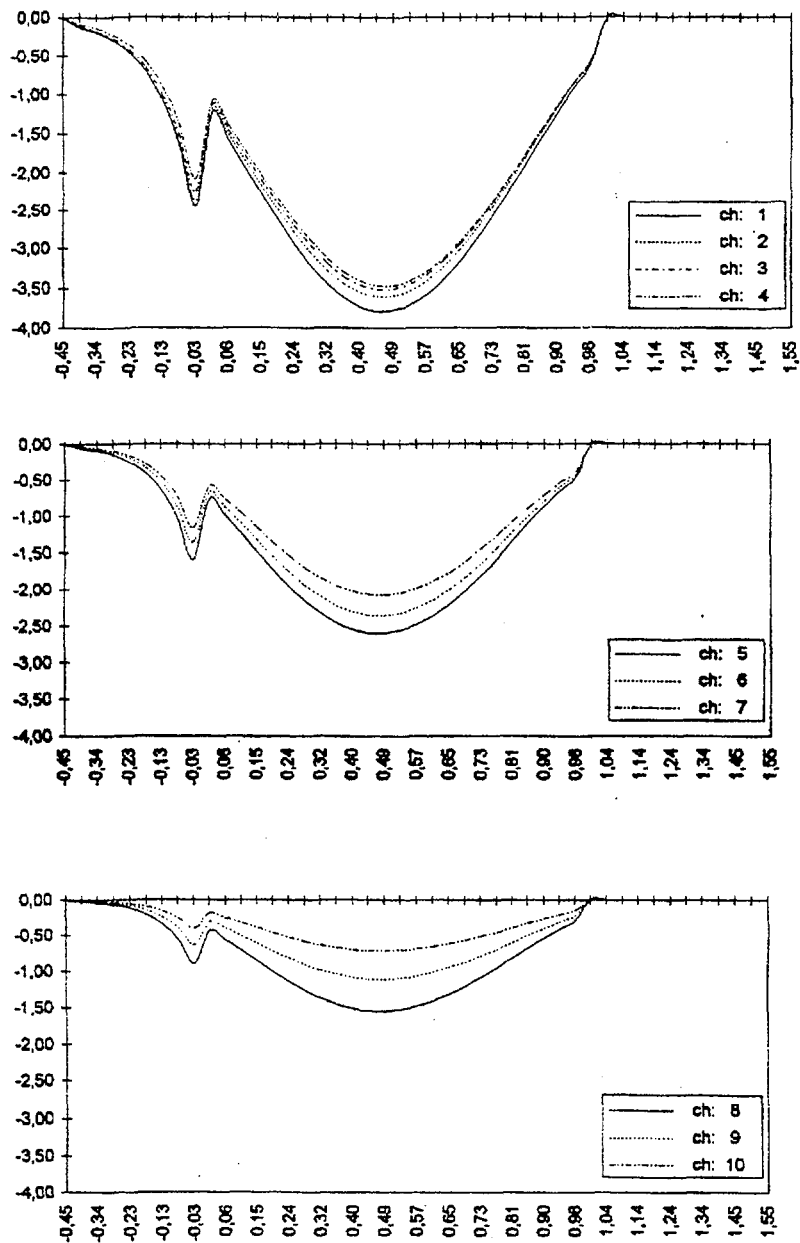


FIG. 1.12. Smeared nominal Doppler coefficients (pcm/m) axial distribution per fuel channel for the BN-800 / 1500 MWth reactor. (Active core length normalized distance; origin in bottom).

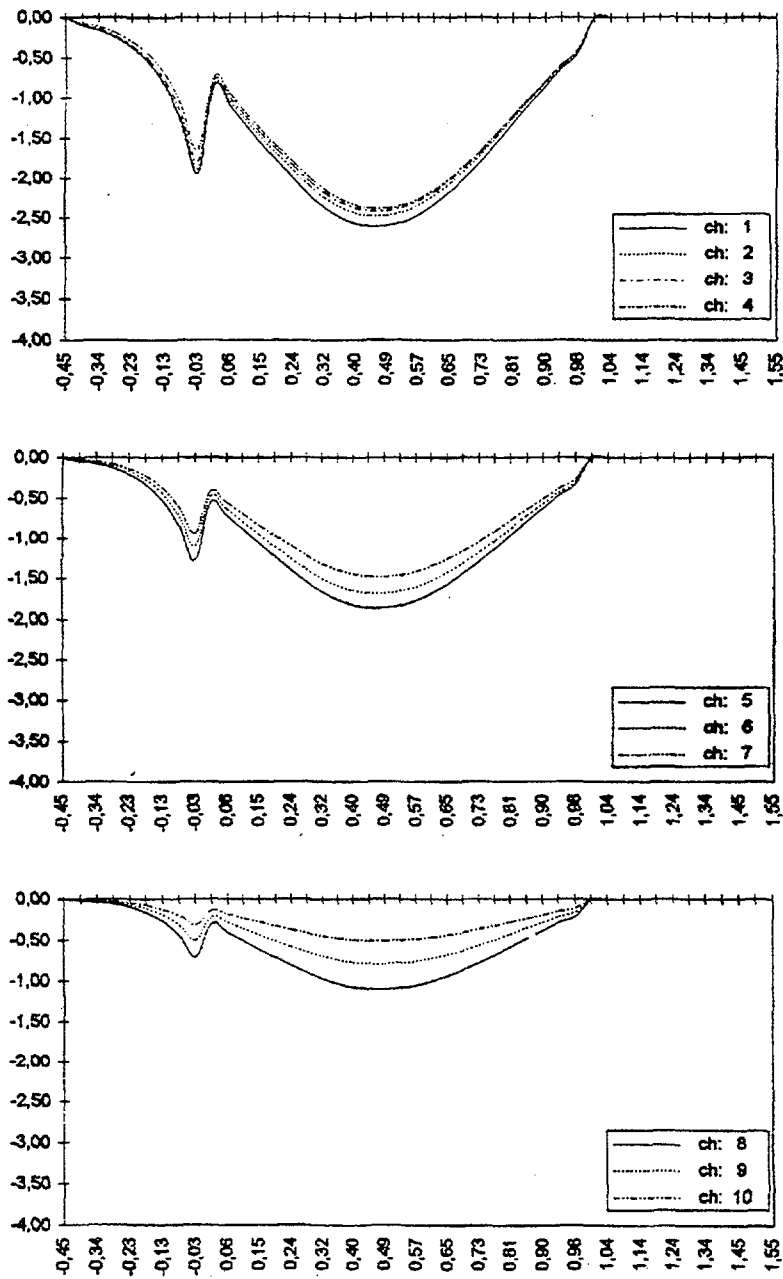


FIG. 1.13. Smeared voided Doppler coefficients (pcm/m) axial distribution per fuel channel for the BN-800 / 1500 MWth benchmark core. (Active core length normalized distance: origin in bottom).

- density effect:
($\delta k/k/\delta\rho/\rho$) = 0.36323
- **Radial expansion:** $\delta H/H = 0$
 - Geometry effect:
 $\delta R/R = +0.025$; $\delta\rho/\rho = 0$ ($\delta k/k/\delta R/R$)_{geo} = 0.14211
 - Net effect:
 $\delta R/R = +0.025$; $\delta\rho/\rho = -0.025$ ($\delta k/k/\delta R/R$)_{net} = -0.59400
 - density effect:
($\delta k/k/\delta\rho/\rho$) = 0.36806

The small relative difference on the density effect value between axial and radial expansion, about 1.3%, is related to a not exact reproduction of the mesh volumes in the two geometry variations.

Material densities coefficients: Density reactivity coefficients for the fuel, sodium, steel, and absorber materials were calculated by first order perturbation theory. The following integral values were obtained:

Fuel: 0.455080; Sodium: 0.044881;
Steel: 0.027123; Absorber: -0.001451.

These values are distributed per zone and channel as in table 1.10, while their distribution per fuel assembly are given respectively in fig's 1.14, 1.15, 1.16 and 1.17. Also the smeared density coefficients rating (pcm/m) axial distribution for each average assembly, of the first 10 (fuel) channels are given in fig's 1.18, 1.19, 1.20 and 1.21 respectively.

TABLE 1.10. DENSITY REACTIVITY COEFFICIENTS DISTRIBUTION PER ZONE AND CHANNEL.

| | Fuel | SS | Na | B ₄ C |
|-------------|-----------|------------|------------|------------------|
| L.E.Z | 1.7994E-1 | -1.3960E-2 | -2.5347E-3 | |
| M.E.Z | 1.3678E-1 | -4.8391E-3 | 5.8701E-4 | |
| H.E.Z | 1.1788E-1 | 5.4562E-3 | 4.4814E-3 | |
| B.A.B | 1.2102E-2 | 8.7071E-3 | 4.0894E-3 | |
| Rd.Blk | 8.3758E-3 | 3.2322E-3 | 1.2992E-3 | |
| Na-Layer | | 6.5788E-3 | 1.7303E-2 | |
| Steel Plugs | | 7.7920E-3 | 7.5293E-4 | |
| C.Rods | | 6.4467E-3 | 1.7476E-2 | -2.6752E-3 |
| Others | | 7.7091E-3 | 1.4268E-3 | 1.2246E-3 |
| Core | 4.5508E-1 | 2.7123E-2 | 4.4881E-2 | -1.4506E-3 |

| | Fuel | | SS | Na | B ₄ C |
|---------|-----------|----------------|-----------|-----------|------------------|
| channel | | $\Delta\%$ (*) | | | |
| 01 | 3.4221E-2 | +25.37 | 8.4460E-4 | 5.1292E-3 | -3.2356E-4 |
| 02 | 4.3671E-2 | +23.26 | 5.2947E-4 | 5.1700E-3 | -4.9638E-4 |
| 03 | 3.6255E-2 | +22.50 | 8.0574E-4 | 4.9792E-3 | -5.0796E-4 |
| 04 | 7.0460E-2 | +20.27 | 2.0967E-3 | 9.9805E-3 | -8.5585E-4 |
| 05 | 7.8371E-2 | +14.23 | 3.6726E-4 | 3.6627E-3 | 3.0233E-4 |
| 06 | 3.0643E-2 | +15.09 | 1.0238E-3 | 1.9006E-3 | 1.2439E-4 |
| 07 | 3.2250E-2 | + 9.35 | 1.1001E-3 | 2.1098E-3 | 1.4054E-4 |
| 08 | 4.4574E-2 | + 4.09 | 2.3014E-3 | 2.8823E-3 | 1.7338E-4 |
| 09 | 5.6819E-2 | + 3.59 | 5.1941E-3 | 4.7191E-3 | 2.3569E-4 |
| 10 | 1.9439E-2 | + 3.06 | 2.8204E-3 | 2.0755E-3 | 8.6233E-5 |
| 11 | 8.3758E-3 | - 9.95 | 3.2454E-3 | 1.3045E-3 | / |
| 12 | 1 | | 6.7939E-3 | 9.6722E-4 | -3.2938E-4 |

(*) $\Delta = (\text{enea-ippe})/\text{ippe}$

Text cont. on page 50.

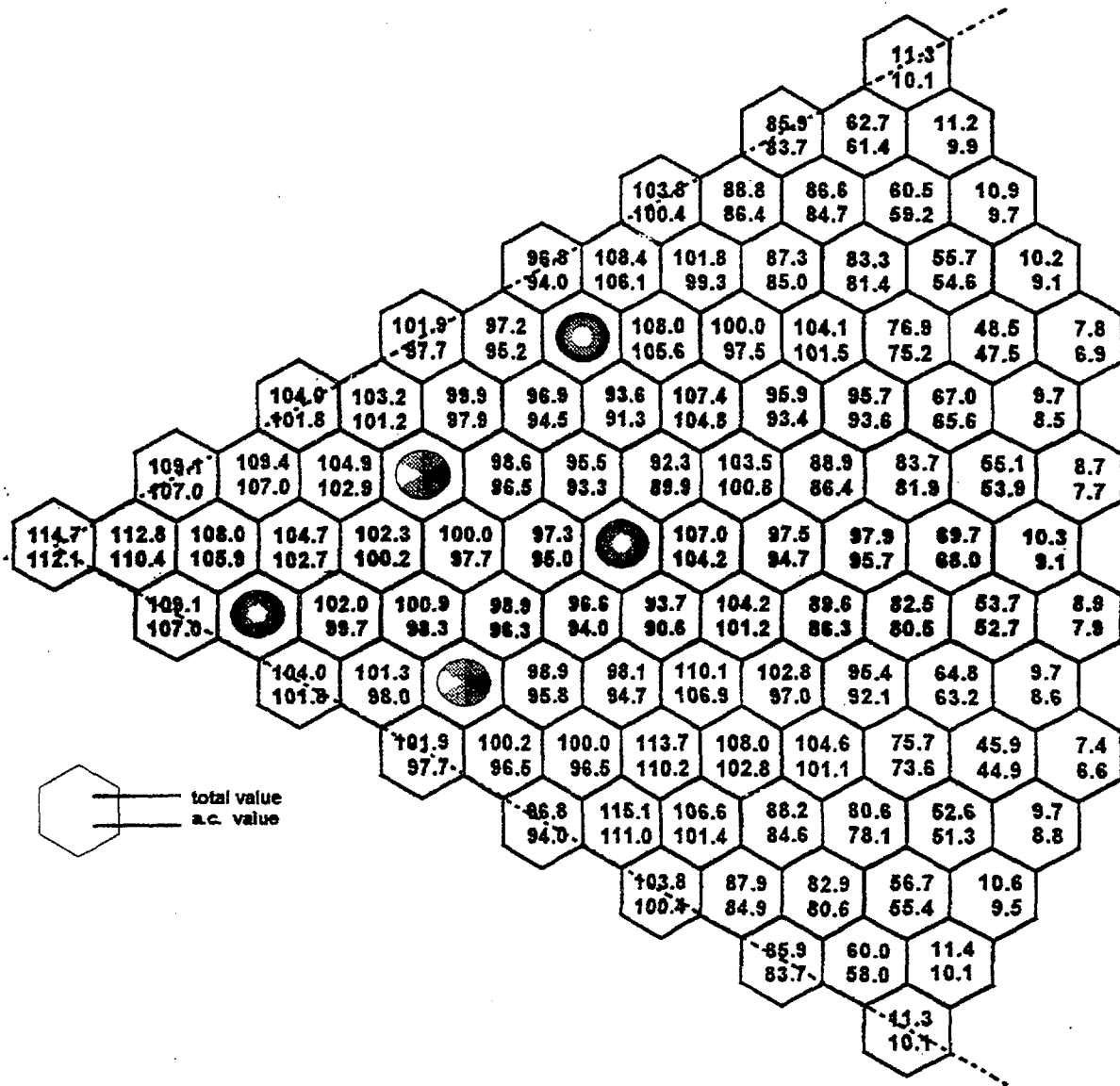


FIG. 1.14. Fuel density coefficients (pcm), total and active core per fuel assembly for the BN-800 / 1500 MWth reactor.

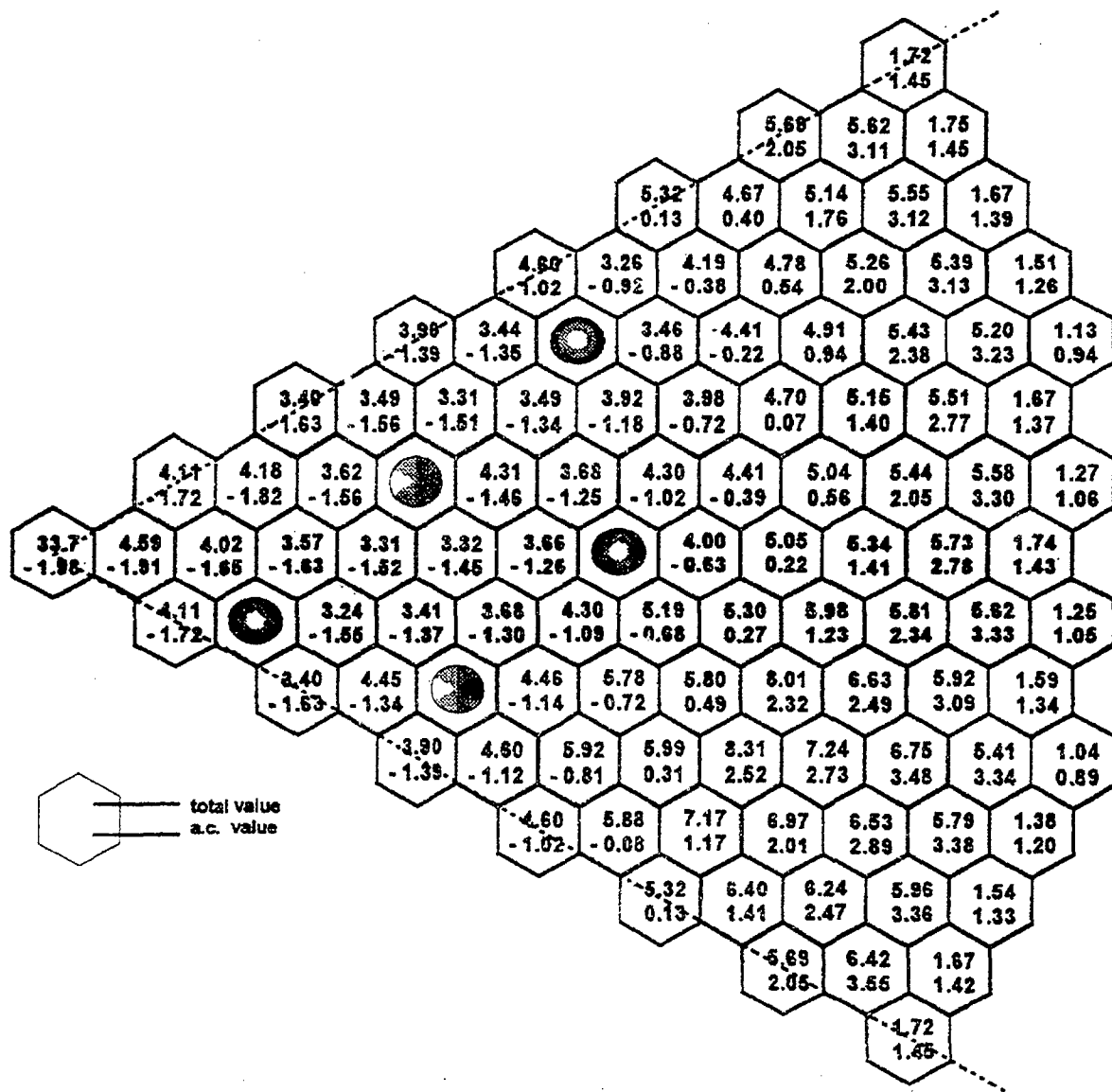


FIG. 1.15. Sodium density coefficients (pcm), total and active core per fuel assembly for the BN-800 / 1500 MWth benchmark core.

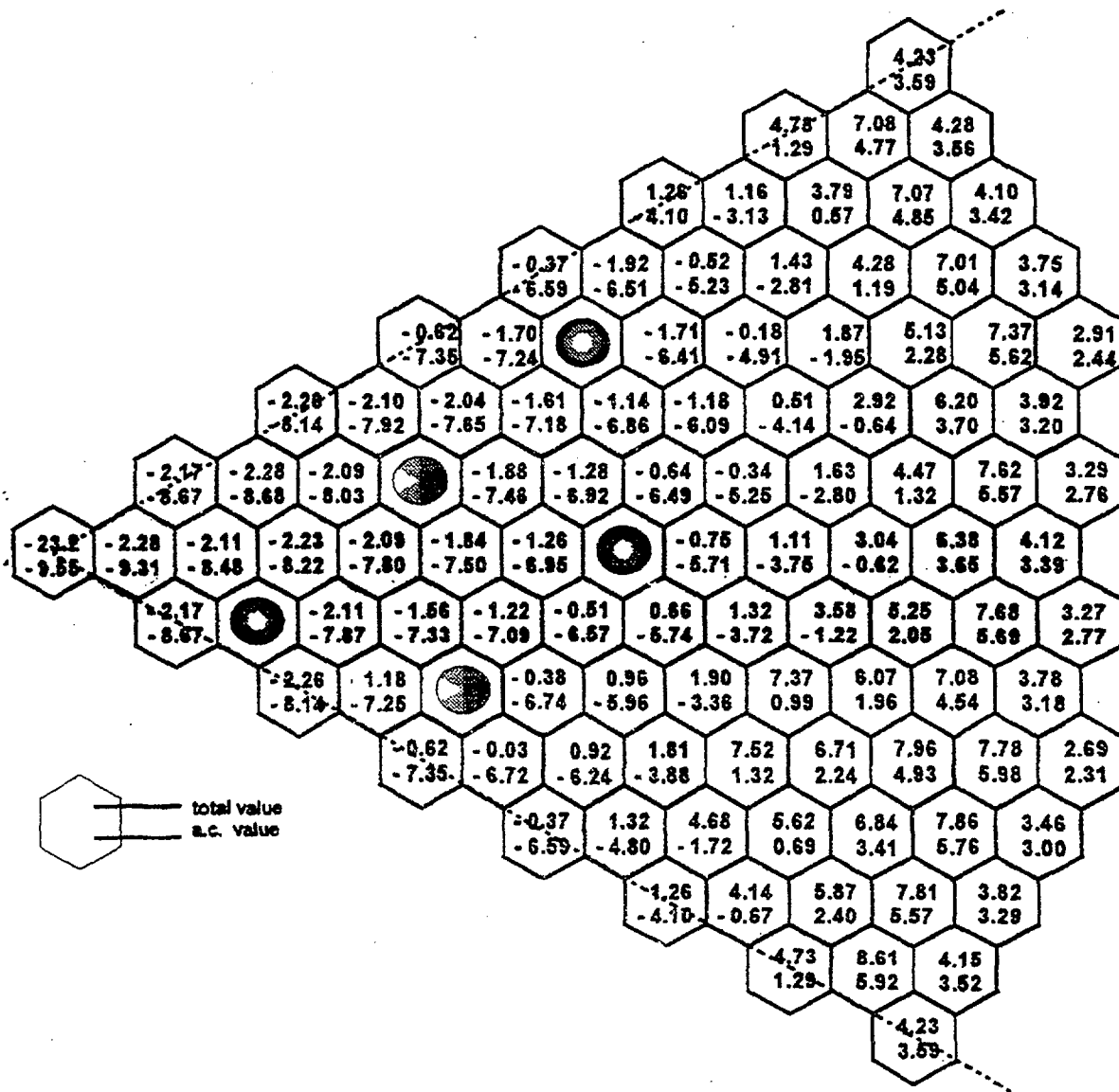


FIG. 1.16. Structural (SS) density coefficients (pcm), total and active core per fuel assembly for the BN-800 / 1500 MWe benchmark core.

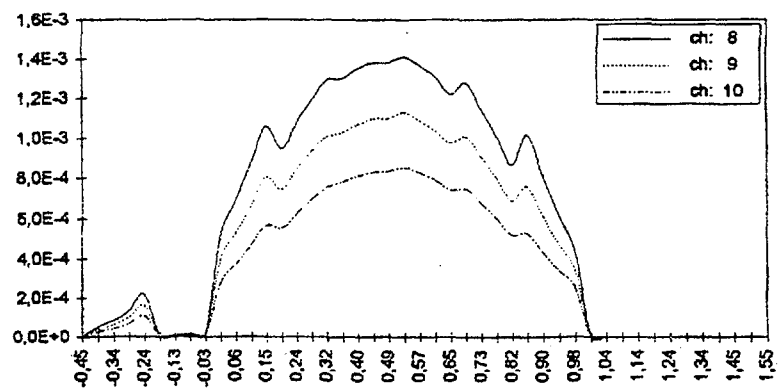
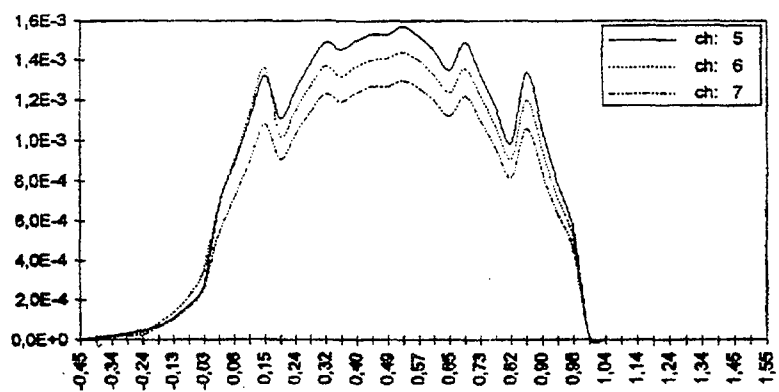
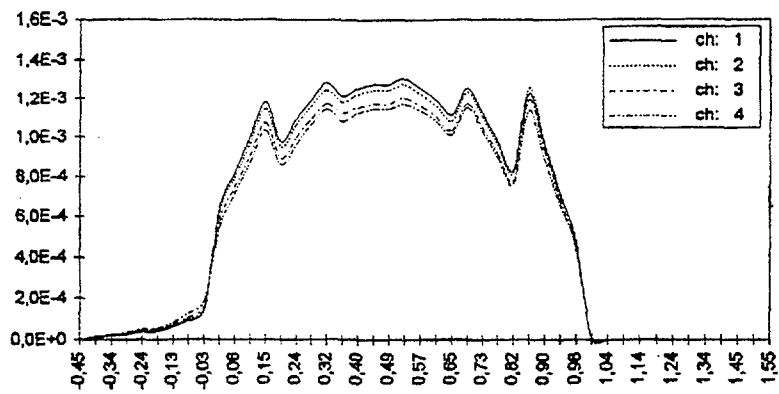


FIG. 1.18. Smeared fuel density coefficients ($\Delta k/k/m$) axial distribution per fuel channel for the BN-800 / 1500 MWth benchmark core.

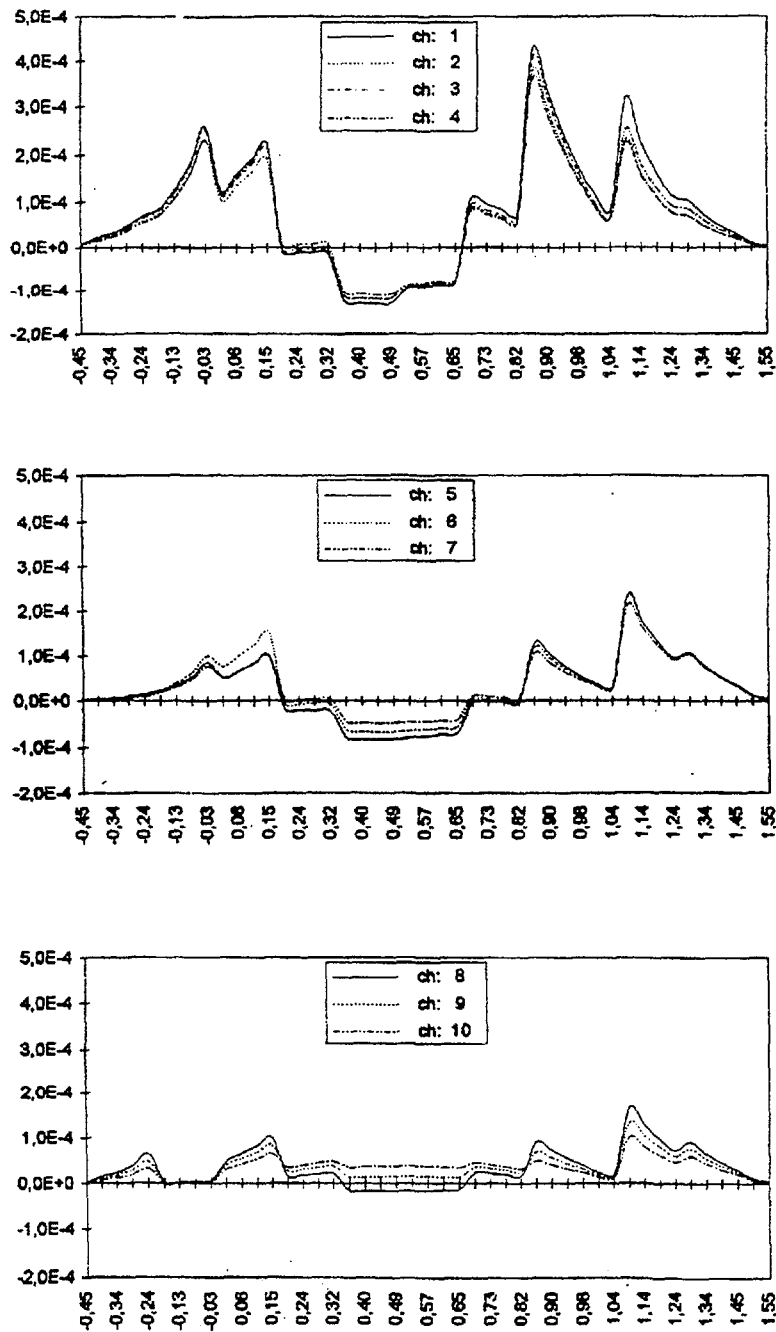


FIG. 1.19. Smeared sodium density coefficients ($\Delta k/k/m$) axial distribution per fuel channel for the BN-800/1500 MWe benchmark core. (Active core length normalized distance; origin in bottom).

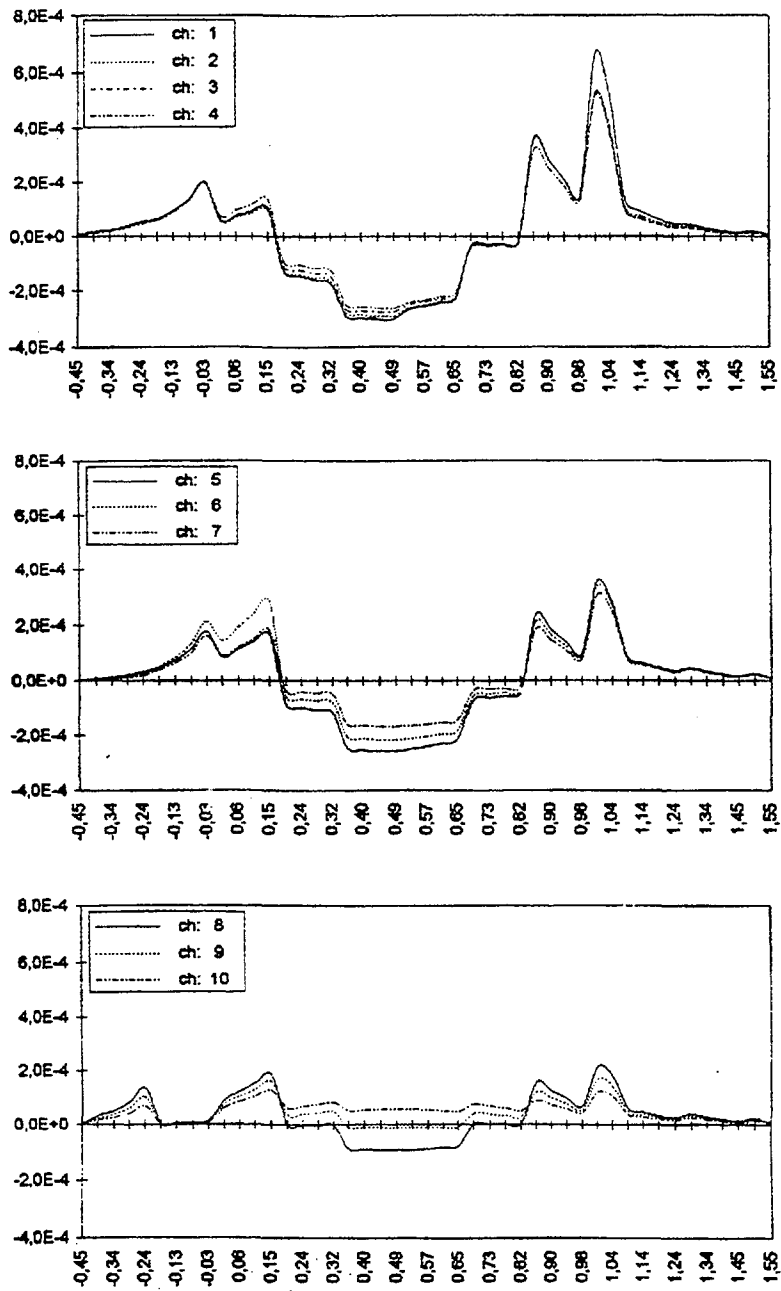


FIG. 1.20. Smeared structure (SS) density coefficients ($\Delta k/k/m$) axial distribution per fuel channel for the BN-800 / 1500 MWe benchmark core. (Active core length normalized distance; origin in bottom).

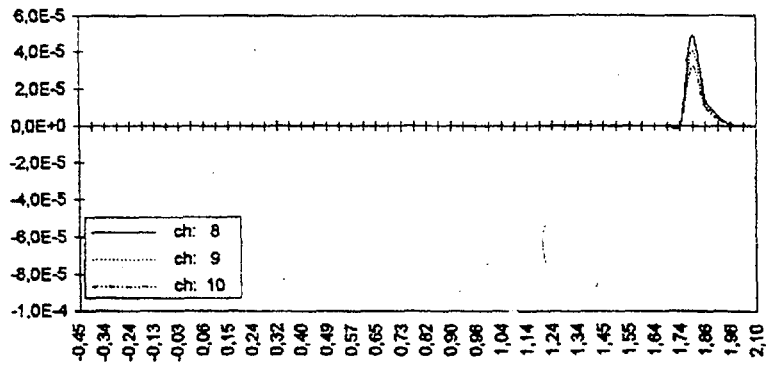
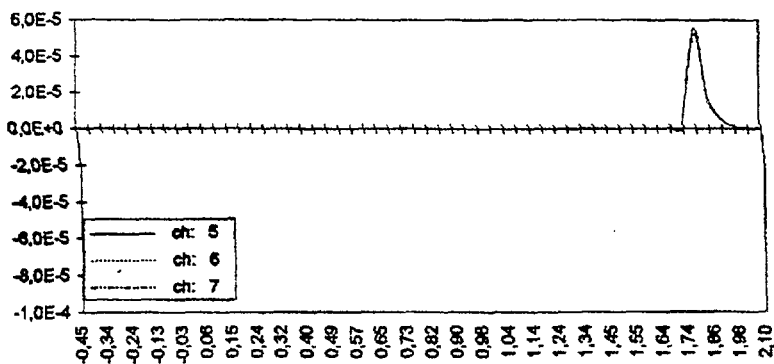
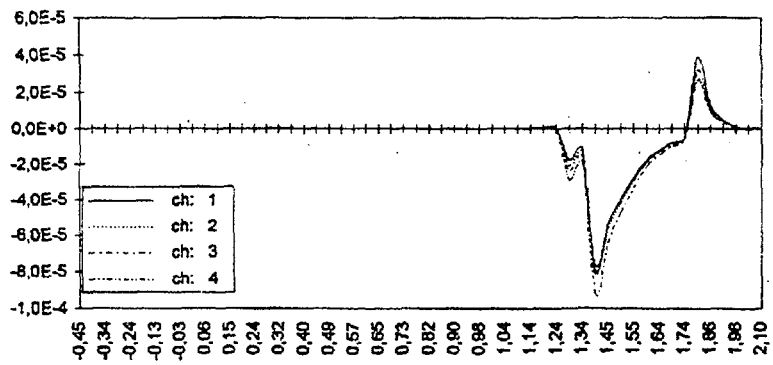


FIG. 1.21. Smeared structure (B_4C) density coefficients ($\Delta k/k/m$) axial distribution per fuel channel for the BN-800 / 1500 MWth benchmark core. (Active core length normalized distance; origin in bottom).

TABLE 1.11. INTEGRAL VALUES FOR NA-VOID COEFF'S $\Delta K/K$, FROM MCNP4A TRANSPORT CALCULATIONS, FOR THE BN-800/1500 MWTH BENCHMARK CORE. ($1\$=3.3769E-3$)

1. 2D(R,Z) Homogeneous model, 1000000 neutron histories

1.A Nominal Configuration (with fission products):

$$\begin{aligned} K_{\text{Ref}} &= 1.00183 \pm 0.00064 \\ K_{\text{void}} &= 1.00215 \pm 0.00067 \\ (\Delta K/K) &= + 0.0946 \$ \pm 0.2744 \$ \end{aligned}$$

1.B Non-Nominal Configuration (without fission products):

$$\begin{aligned} K_{\text{Ref}} &= 1.03801 \pm 0.00067 \\ K_{\text{void}} &= 1.03018 \pm 0.00071 \\ (\Delta K/K) &= - 2.2338 \$ \pm 0.2891 \$ \end{aligned}$$

2. 3D(HEX,Z) Homogeneous model, 1000000 neutron histories

2.A Nominal Configuration (with fission products):

$$\begin{aligned} K_{\text{ref}} &= 1.00323 \pm 0.00074 \\ K_{\text{void}} &= 1.00047 \pm 0.00073 \\ (\Delta K/K) &= - 0.8147 \$ \pm 0.3087 \$ \end{aligned}$$

2.B Non-Nominal Configuration (without fission products):

$$\begin{aligned} K_{\text{Ref}} &= 1.03748 \pm 0.00070 \\ K_{\text{void}} &= 1.02913 \pm 0.00064 \\ (\Delta K/K) &= - 2.3834 \$ \pm 0.2809 \$ \end{aligned}$$

3. 2D(R,Z) Homogeneous model, 2000000 neutron histories

3.A Nominal Configuration (with fission products):

$$\begin{aligned} K_{\text{Ref}} &= 1.00215 \pm 0.00046 \\ K_{\text{void}} &= 1.00230 \pm 0.00045 \\ (\Delta K/K) &= + 0.0443 \$ \pm 0.1906 \$ \end{aligned}$$

3.B Non-Nominal Configuration (without fission products):

$$\begin{aligned} K_{\text{Ref}} &= 1.03810 \pm 0.00048 \\ K_{\text{void}} &= 1.03053 \pm 0.00048 \\ (\Delta K/K) &= - 2.1594 \$ \pm 0.2010 \$ \end{aligned}$$

4. 3P(Hex,Z) Homogeneous model, 2000000 neutron histories

4.A Nominal Configuration (with fission products):

$$\begin{aligned} K_{\text{ref}} &= 1.00299 \pm 0.00048 \\ K_{\text{void}} &= 1.00071 \pm 0.00048 \\ (\Delta K/K) &= - 0.6732 \$ \pm 0.2014 \$ \end{aligned}$$

4.B Non-Nominal Configuration (without fission products):

$$\begin{aligned} K_{\text{ref}} &= 1.03821 \pm 0.00047 \\ K_{\text{void}} &= 1.02955 \pm 0.00047 \\ (\Delta K/K) &= - 2.4701 \$ \pm 0.1968 \$ \end{aligned}$$

About the density coefficients we observe an acceptable difference for the fuel density coefficient: + 13.22%, but not so for the steel. Based on the [1.2] input data for the SS the relative difference is + 57.8%.

Sodium void effect coefficients: Sodium void effect analysis was performed in both diffusion and transport theory. The first one, based on 3D(Triang,Z) geometry, is related to the necessity of a comparison with the IPPE provided results. The second approach, based on 2D(R,Z) and 3D(Hex,Z) geometry with homogeneous cells, is the one to define the reactivity values of the voided zones. A detailed investigation zone by zone based in the second geometry was performed. The voided zones taken into account are the following: three fissile zones, lower axial blanket, radial blanket, sodium layer and pin plugs zones; therefore voiding the whole core means deal with the set of all the previous zones. From the obtained results, given in tab. 1.4, and particularly in the $2 \cdot 10^6$ neutron histories transport approach, we option:

- 2D(R,Z) geometry:

$$k_{\text{Ref}} = 1.00215 \pm 46 \text{ pcm}$$

$$k_{\text{w.c}} = 1.00230 \pm 45 \text{ pcm so: } \Delta k/k = (+ 0.0443 \pm 0.1906)\%$$

- 3D(Hex,Z) geometry:

$$k_{\text{Ref}} = 1.00299 \pm 48 \text{ pcm}$$

$$k_{\text{w.c}} = 1.00071 \pm 48 \text{ pcm so: } \Delta k/k = (- 0.6732 \pm 0.2014)\%$$

These results show that the 2D(R,Z) geometry is inadequate to correctly describe the whole core voiding problem, at least for the configuration with fission products, for the heterogeneous benchmark core. Therefore the single zone values are those of the 3D(Hex,Z) geometry.

In this study the "interaction effect" between single voided fuel zones and voided active core, as well as the active core and sodium layer zones were evaluated. From the results reported in table 1. 12, one can see that the simple sum of the single fuel zone reactivity worths under-estimates the positive actual value of the active core by 5.5%, and the simple sum of the active core and sodium layer zone reactivity worths under-estimates the positive actual value of the whole zone by 11.5%. Finally the simple sum of all the fuel zones and sodium layer zone under-estimates the positive actual value of the created " whole" zone by 33.8%.

To complete the sodium void effect analysis, it was repeated without the lumped fission product in the core, in order to evaluate its influence on the sodium void effect. Eliminating lumped fission products and following the former approach the following results were obtained:

- 2D(R,Z) geometry:

$$k_{\text{Ref}} = 1.03810 \pm 48 \text{ pcm}$$

$$k_{\text{w.c}} = 1.03053 \pm 48 \text{ pcm so: } \Delta k/k = (- 2.1594 \pm 0.2010)\%$$

- 3D(Hex,Z) geometry:

$$k_{\text{Ref}} = 1.03821 \pm 47 \text{ pcm}$$

$$k_{\text{w.c}} = 1.02955 \pm 47 \text{ pcm so: } \Delta k/k = (- 2.4701 \pm 0.1968)\%$$

These results show the strong influence of the fission products evaluated, as large as some 2\$ for the BN-800/1500 MWth benchmark core. Moreover the fission products influences the interaction effect too.

TABLE 1.12. SINGLE ZONE VALUES FOR NA-VOID COEFF'S $\Delta K/K$, IN 3D(HEX,Z)-HOMOG. MODEL & 2-10⁶ HISTORIES, AND "INTERACTION EFFECT" EVALUATION, FROM MCNP4A TRANSPORT CALCULATIONS, FOR THE BN-800/1500 MWTB BENCHMARK CORE.

A. Nominal Configuration (with F.P)

| | |
|--------------------------------------|--|
| $K_{REF} = 1.00299 \pm 0.00048$ | |
| $K_{LEZ} = 1.01193 \pm 0.00048$ | $(\Delta K/K) = + 2.6395 \pm 0.2010$ \$ |
| $K_{MEZ} = 1.00714 \pm 0.00046$ | $(\Delta K/K) = + 1.2253 \pm 0.1969$ \$ |
| $K_{HEZ} = 1.00087 \pm 0.00047$ | $(\Delta K/K) = - 0.6259 \pm 0.1989$ \$ |
| $K_{A.C.} = 1.01460 \pm 0.00045$ | $(\Delta K/K) = + 3.4278 \pm 0.1948$ \$ |
| $K_{LAYER} = 0.99392 \pm 0.00048$ | $(\Delta K/K) = - 2.6779 \pm 0.2010$ \$ |
| $K_{A.C.+LAY} = 1.00586 \pm 0.00044$ | $(\Delta K/K) = + 0.8474 \pm 0.1928$ \$ |
| $K_{PLUGS} = 1.00264 \pm 0.00045$ | $(\Delta K/K) = - 0.1033 \pm 0.1948$ \$ |
| $K_{AX.BLK} = 1.00117 \pm 0.00046$ | $(\Delta K/K) = - 0.5374 \pm 0.1969$ \$ |
| $K_{RD.BLK} = 1.00103 \pm 0.00046$ | $(\Delta K/K) = - 0.5787 \pm 0.1969$ \$ |
| | $\Sigma_{fsl}(\Delta K/K)_{fsl} = + 3.2388 \pm 0.3447$ \$ |
| | $\Sigma_{A.C.&Layer}(\Delta K/K) = + 0.7498 \pm 0.2800$ \$ |
| | $\Sigma_{fsl\&Layer}(\Delta K/K) = + 0.5609 \pm 0.3991$ \$ |

$$\begin{aligned} \%[\Sigma_{fsl}(\Delta K/K)_{fsl} - (\Delta K/K)_{A.C.}] / (\Delta K/K)_{A.C.} &= - 5.5 \\ \%[\Sigma_{A.C.\&Layer}(\Delta K/K) - (\Delta K/K)_{A.C.+LAY}] / (\Delta K/K)_{A.C.+LAY} &= - 11.5 \\ \%[\Sigma_{fsl\&Layer}(\Delta K/K) - (\Delta K/K)_{A.C.+LAY}] / (\Delta K/K)_{A.C.+LAY} &= - 33.8 \end{aligned}$$

B. Not-Nominal Configuration (without F.P)

| | |
|--------------------------------------|---|
| $K_{REF} = 1.003821 \pm 0.00047$ | |
| $K_{LEZ} = 1.04604 \pm 0.00049$ | $(\Delta K/K) = + 2.2334 \pm 0.2011$ \$ |
| $K_{MEZ} = 1.04056 \pm 0.00050$ | $(\Delta K/K) = + 0.6703 \pm 0.2032$ \$ |
| $K_{HEZ} = 1.03594 \pm 0.00048$ | $(\Delta K/K) = - 0.6475 \pm 0.1989$ \$ |
| $K_{A.C.} = 1.04647 \pm 0.00046$ | $(\Delta K/K) = + 2.3560 \pm 0.1948$ \$ |
| $K_{LAYER} = 1.03005 \pm 0.00048$ | $(\Delta K/K) = - 2.3275 \pm 0.1989$ \$ |
| $K_{A.C.+LAY} = 1.03455 \pm 0.00050$ | $(\Delta K/K) = - 1.0439 \pm 0.2032$ \$ |
| $K_{PLUGS} = 1.03949 \pm 0.00050$ | $(\Delta K/K) = + 0.3651 \pm 0.2032$ \$ |
| $K_{AX.BLK} = 1.03689 \pm 0.00046$ | $(\Delta K/K) = - 0.3765 \pm 0.1948$ \$ |
| $K_{RD.BLK} = 1.03669 \pm 0.00051$ | $(\Delta K/K) = - 0.4336 \pm 0.2054$ \$ |
| | $\Sigma_{fsl}(\Delta K/K)_{fsl} = + 2.2562 \pm 0.3483$ \$ |
| | $\Sigma_{A.C.\&Layer}(\Delta K/K) = + 0.0285 \pm 0.2785$ \$ |
| | $\Sigma_{fsl\&Layer}(\Delta K/K) = - 0.0713 \pm 0.4011$ \$ |

$$\begin{aligned} \%[\Sigma_{fsl}(\Delta K/K)_{fsl} - (\Delta K/K)_{A.C.}] / (\Delta K/K)_{A.C.} &= - 4.2 \\ \%[\Sigma_{A.C.\&Layer}(\Delta K/K) - (\Delta K/K)_{A.C.+LAY}] / (\Delta K/K)_{A.C.+LAY} &= - 102.7 \\ \%[\Sigma_{fsl\&Layer}(\Delta K/K) - (\Delta K/K)_{A.C.+LAY}] / (\Delta K/K)_{A.C.+LAY} &= - 93.2 \end{aligned}$$

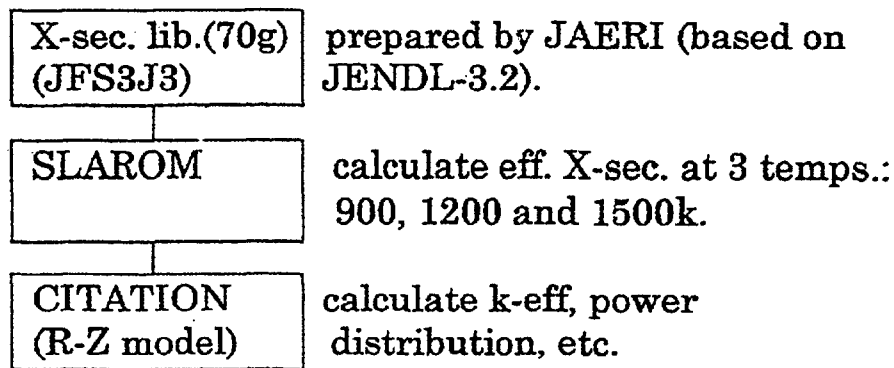
1.3. JAPANESE CALCULATIONS

1.3.1. Introduction

As an input data of the neutronics calculation, the end-of-the- equilibrium cycle (EOEC) core data was used, as provided by the IPPE document[1.2] . The core horizontal cross- section is illustrated in fig.1. 4.

Calculation methods are outlined in Fig.1. 22. Both diffusion and Monte Carlo transport calculations in RZ and HexZ configurations were performed with the latest Japanese nuclear

(a) Diffusion Calculation



(b) Transport Calculation

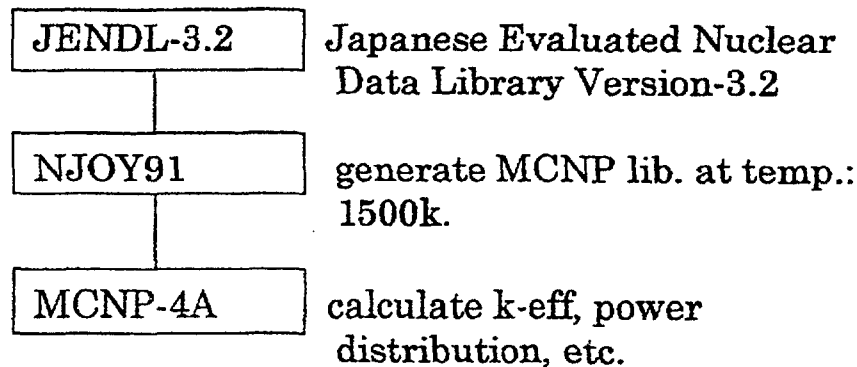


FIG. 1.22. Calculation methods.

data library JENDL-3.2. In diffusion calculations, a seventy group cross-section set JFS3-J3 based on the JENDL3.2 was processed by the SLAROM code to generate the effective cross-sections at the three different temperatures (900, 1200, 1500K) of the core. The CITATION code was used to calculate the keff, power distributions, etc., in the RZ configuration. In the Monte Carlo transport calculation, JENDL3.2 was processed by the NJOY91 code to generate the MCNP cross-section library at the temperature 1500K. The cross-sections of each FP element were not generated in the present calculation. The MCNP-4A code was used to calculate the core characteristics in the RZ and HexZ configurations.

Since the burnup dependent atom density data of each fuel assembly was not provided by the IPPE document, a fuel subassembly batch factor was ignored in both calculations.

1.3.2. Results of calculations

Power distribution: The zone-wise power distributions are shown in tables 1.13 and 1.14, based on the diffusion and transport calculations. No significant difference is seen between the diffusion and transport calculation results for the core configuration in which the above core sodium-layer is flooded.

Doppler coefficient: The calculated zone-wise Doppler coefficients Tdk/dT based on a diffusion theory are shown in table 1.15 for the sodium-unvoided and voided core configurations.

TABLE 1.13. ZONE-WISE POWER DISTRIBUTIONS BASED ON DIFFUSION CALCULATIONS

| | MW | | | |
|------------------|--------|--------|--------|---------------|
| | Upper | Middle | Lower | Total |
| LEZ | 148.50 | 221.50 | 189.78 | 559.5 |
| MEZ | 115.96 | 167.35 | 139.30 | 422.6 |
| HEZ | 114.80 | 160.66 | 131.87 | 407.3 |
| BAB(4) | | | | 50.6 |
| Gas Vol Zone(14) | | | | 1.3 |
| Na-layer(6) | | | | 0.3 |
| Ax Shield(7) | | | | 1.4 |
| Head Zone(17) | | | | 0.02 |
| C Rod(9,11,12) | | | | 2.3 |
| Rad Blkt(5) | | | | 50.7 |
| Others | | | | 3.9 |
| Total | | | | 1500.0 |

Peak power density 551.9 W/cc

Peak linear power 380.8 W/cc

TABLE 1.14. ZONE-WISE POWER DISTRIBUTIONS BASED ON TRANSPORT CALCULATIONS

| | MW | | | |
|------------------|--------|--------|--------|---------------|
| | Upper | Middle | Lower | Total |
| LEZ | 136.56 | 227.71 | 195.15 | 561.4 |
| MEZ | 116.42 | 167.52 | 140.02 | 424.0 |
| HEZ | 115.25 | 160.15 | 132.02 | 407.4 |
| BAB(4) | | | | 49.5 |
| Gas Vol Zone(14) | | | | 1.3 |
| Na-layer(6) | | | | 0.3 |
| Ax Shield(7) | | | | 1.4 |
| Head Zone(17) | | | | 0.03 |
| C Rod(9,11,12) | | | | 2.3 |
| Rad Blkt(5) | | | | 46.1 |
| Others | | | | 6.3 |
| Total | | | | 1500.0 |

TABLE 1.15. CALCULATED ZONE-WISE DOPPLER COEFFICIENTS TDK/DT OR THE SODIUM UNVOIDED AND VOIDED CORE CONFIGURATION

| | $10^{-3}TdK/dT$ | |
|----------|-----------------|---------|
| | Unvoided | Voided* |
| LEZ | 3.401 | 2.221 |
| MEZ | 1.721 | 0.959 |
| HEZ | 0.965 | 0.507 |
| BAB | 0.761 | 0.724 |
| Rad Blkd | 0.424 | 0.353 |

*Voided region: LEZ,MEZ,HEZ,BAB, Rad Blkt, Na-layer, Pin steel plug.

Sodium void reactivity: The calculated whole core sodium void reactivities are shown in tables 1.16 (diffusion Calc.) and 1.17 (Monte Carlo transport Calc.). Since the present MCNP calculations treated no FPs, an additional diffusion calculation in which all the FPs are removed from the core are performed for comparison. Monte Carlo base analysis includes the wrapper heterogeneity effect. The heterogeneous assembly model, which explicitly treats the hexagonal duct and interwrapper sodium, is illustrated in fig. 1.23 in comparison with the homogeneous model.

The results are summarized in fig. 1.24. The void reactivity difference up to a dollar was seen between the 2-D diffusion and Monte Carlo transport calculation results. However, this difference is almost offset by 3-D geometry effect and wrapper heterogeneity effect. The estimated void reactivity will be about -0.9 dollars at the EOEC condition.

TABLE 1.16. CALCULATED WHOLE CORE SODIUM VOID REACTIVITIES (DIFFUSION CALC.)

| (a) Core with Fps | | |
|-------------------|----------|---------------------|
| | k-eff | void reactivity, \$ |
| Unvoided | 1.008329 | |
| 100% voided | 1.004333 | -1.13 |

| (b) Core without Fps | | |
|----------------------|----------|---------------------|
| | k-eff | void reactivity, \$ |
| Unvoided | 1.025336 | |
| Voided | 1.018274 | -1.93 |

TABLE 1.17. CALCULATED WHOLE CORE SODIUM VOID REACTIVITIES (MONTE CARLO TRANSPORT CALC.)

| (a) RZ model (10 ⁶ neutron histories) | | |
|--|-----------------|---------------------|
| | k-eff | void reactivity, \$ |
| Unvoided | 1.02576±0.00048 | |
| Voided | 1.02200±0.00051 | -1.02±0.20 |

| (b) HexZ homogeneous model (4×10 ⁶ neutron histories) | | |
|--|-----------------|---------------------|
| | k-eff | void reactivity, \$ |
| Unvoided | 1.02665±0.00024 | |
| Voided | 1.02140±0.00025 | -1.43±0.10 |

| (c) HexZ heterogeneous model (4×10 ⁶ neutron histories) | | |
|--|-----------------|---------------------|
| | k-eff | void reactivity, \$ |
| Unvoided | 1.02677±0.00024 | |
| Voided | 1.02056±0.00025 | -1.69±0.10 |

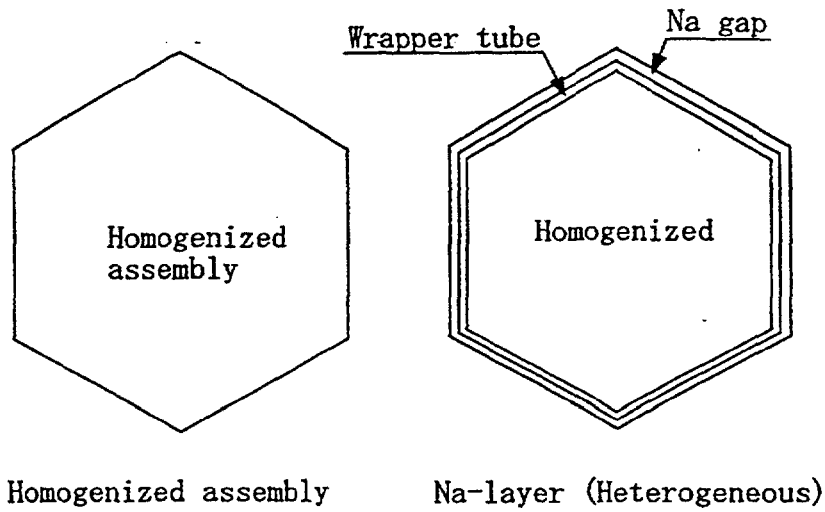


FIG. 1.23. A heterogeneous assembly model in comparison with the homogeneous model.

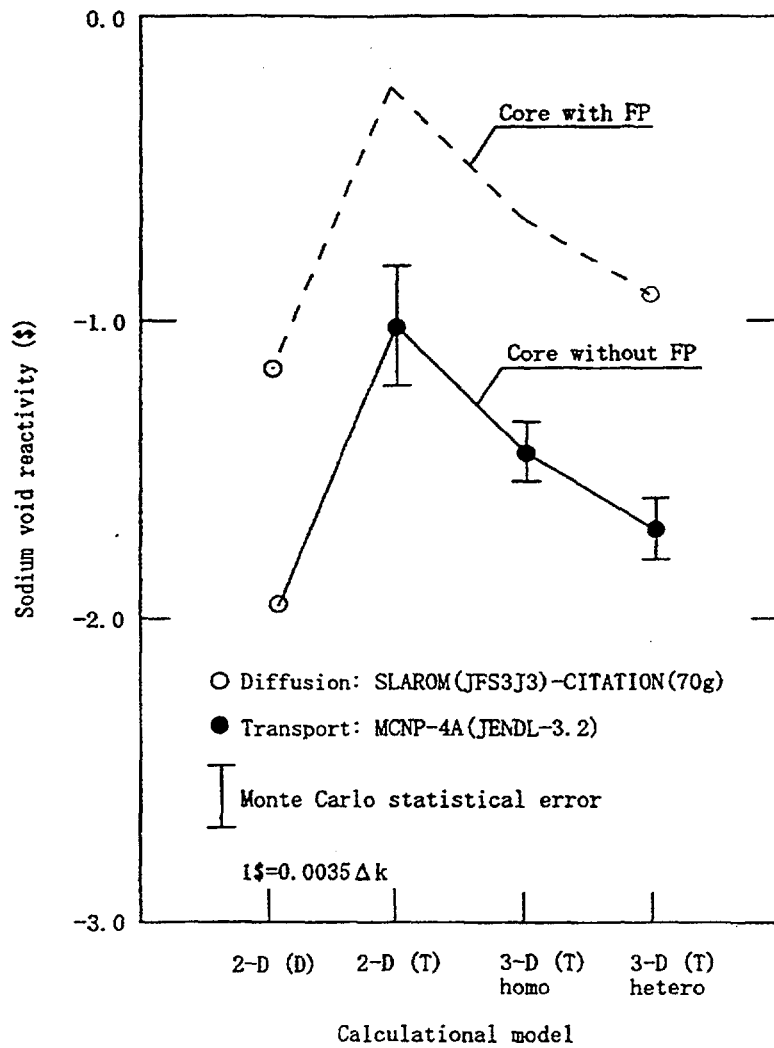


FIG. 1.24 Void reactivity results summary.

1.4. COMPARATIVE ANALYSIS OF NEUTRONICS CALCULATIONS

Criticality parameters: table 1.18 gives K_{eff} values compared with the results obtained by the researchers. ENEA and ERL values are very close to each other. The agreement of IPPE K_{eff} values with results of other researches can be recognized as reasonable.

Power distribution: About the power distribution (table 1.19) a good agreement is observed for the fuel zones, (discrepancies are less than 2% for the integral results and 4.1% for the peak linear power) but not for the absorber and other structural zones. This may be attributed to the capture energy-yield of the B^{10} in the B_4C , as well as to the slowing-down energy-loss evaluation for the Na^{23} in the sodium layer zone.

Kinetics parameters: Satisfactory agreement is observed for kinetics parameters (table 1.20). For example, the differences between the IPPE and ENEA results on integral kinetics parameters are -5.22%, +4.11%, +8.44% for effective delayed neutron fraction, prompt neutron life time and mean decay constant, respectively. The IPPE and ERL values of effective delayed neutron fraction differ from each other by ~1%.

The observed difference in the decay constants of the delay neutron nuclei is mainly caused by the realized method of their averaging on the contributions by the different fissile nuclides:

- averaging on the basis of fission number balance as in the case of averaging of the decay constant values are considered as independent constant factors in the kinetics equation;

TABLE 1.18. EFFECTIVE MULTIPLICATION FACTOR (DIFFUSION THEORY)

| | IPPE | ENEA | ERL (Hitachi) |
|------------------------|----------------------------------|---------|---------------|
| 2D (R,Z) geometry | 1.00445 | 1.00835 | 1.008329 |
| | finite-dif. method, 26 groups | | |
| 2D (R,Z) geometry | 1.006282 | | |
| | synthetic method 26 groups | | |
| 3D (Z-HEX) geometry | 1.006762 | 1.00882 | |
| | 11 groups | | |

TABLE 1.19. POWER DISTRIBUTIONS (DIFFUSION CALCULATIONS)

| | IPPE | ENEA | ERL |
|------------------|--------|--------|--------|
| LEZ | 550.6 | 560.5 | 559.5 |
| MEZ | 419.5 | 421.2 | 422.6 |
| HEZ | 405.9 | 405.9 | 407.3 |
| BAB | 47.5 | 46.8 | 50.6 |
| Gas Voi. Zone | 1.3 | 1.3 | 1.3 |
| Na-layer | 0.3 | 0.7 | 0.3 |
| Ax. Shield | 4.1 | 1.8 | 1.4 |
| Head Zone | 0.1 | 0.03 | 0.02 |
| C. Rods | 5.9 | 2.9 | 2.3 |
| RB | 51.5 | 50.7 | 50.7 |
| Others | 12.4 | 7.9 | 3.9 |
| Total | 1500.0 | 1500.0 | 1500.0 |

TABLE 1.20. NEUTRONICS PARAMETERS.

| IPPE(BNAB Library*) | | | | | | |
|----------------------|-----------------------|-----------------------|-----------------------|-----------------------|-----------------------|-----------------------|
| Group | $\beta_{1\text{eff}}$ | $\beta_{2\text{eff}}$ | $\beta_{3\text{eff}}$ | $\beta_{4\text{eff}}$ | $\beta_{5\text{eff}}$ | $\beta_{6\text{eff}}$ |
| $\Sigma\beta$ | 7.67E-5 | 7.68E-4 | 6.56E-4 | 1.31E-3 | 5.92E-4 | 1.65E-4 |
| β_{eff} | 0.3563E-2 | | | | | |
| L_p , sec | 0.4418E-6 (RADAR) | | | | | |
| λ_i , 1/sec | 0,0128 | 0,0303 | 0,126 | 0,332 | 1,235 | 3,015 |
| IPPE(TATL Library) | | | | | | |
| $\Sigma\beta$ | 8.5343E-5 | 6.7765E-4 | 5.4146E-4 | 1.2906E-3 | 7.5260E-4 | 2.7316E-4 |
| β_{eff} | 3.6208E-3 | | | | | |
| L_p , sec | 4.4776E-7 (RHEIN) | | | | | |
| λ_i , 1/sec | 0.01340 | 0.030781 | 0.11742 | 0.30824 | 1.2418 | 2.9500 |
| ENEA results | | | | | | |
| $\Sigma\beta$ | 8.146E-5 | 6.3114E-4 | 5.1423E-4 | 1.1941E-3 | 7.0349E-4 | 2.5249E-4 |
| β_{eff} | 3.3769E-3 | | | | | |
| L_p , sec | 4.2435E-7 | | | | | |
| λ_i , 1/sec | 0.2920 | 0.030712 | 0.12947 | 0.304082 | 1.2746 | 3.3770 |
| ERL results | | | | | | |
| β_{eff} | 3.5E-3 | | | | | |

*) This results are presented as Input data.

- averaging on the basis of balance of number of fissions with isotope "weight" (proceeding from kinetics equation for the predecessor nuclei content) or with "weight" as in case of ENEA. This difference is caused by the methods of further application of the decay constants in the neutron kinetics equation.

The effect of differences in the results of the conjugate flux and integral values of the fission neutron worth cannot be analyzed on this stage because of the lack of necessary data. Nevertheless the fact of good agreement between the results obtained by the IPPE and ENEA for the same data bases testifies to sufficiently reasonable agreement in the conjugate integral fluxes as well. Some preliminary conclusion on possible coordination in the integral neutron spectra as well can be drawn from the comparison of L_p value showing in addition more hard spectrum in the ENEA analysis.

It is to be noted that the difference in β_{eff} and reactivity coefficients (effect) values presented in the results compared is an argument in favour of results presentation in $\Delta K/K$ terms but not in $\$$ terms. Benchmark calculations of the decay neutron absolute yield (TATRL and BNAB data libraries), carried out earlier in Russia for the point kinetics have shown that BNAB version application gives more pessimistic evaluation of ULOF type accident other things being equal.

Sodium void and density reactivity effects: The program of current works was not aimed at defining SVRE evaluation accuracy, in contrast to [1.11], and therefore the main results on this reactivity effect obtained in Russia were based on the application of diffusion approach, the error being well known. On the base of previous Russian and international experience of experimental and theoretical studies [1.11,1.12] of the SVRE, one can make the following conclusions:

- results of SVRE evaluations, carried out in different countries using various calculation codes based on the same approach and geometry are sufficiently similar;

- diffusion approach gives satisfactory SVRE description for the core and introduces significant error if the sodium is removed from sodium plenum or control rod subassemblies; calculational packages based on kinetics approaches, give higher negative value of the SVRE in the dried zones under consideration (including sodium plenum) as compared to that obtained in the framework of diffusion approach;

- SVRE values obtained in Russia are shifted to positive as compared to those obtained in other countries for all configurations of voided zone, remaining more positive in the core and more negative in the sodium plenum;

- the experiments have elicited the fact that some error compensation of SVRE integral values for the sodium plenum and the core calculated in diffusion approach using BNAB data base library (78 and subsequent versions;) is observed thus bringing the diffusion results nearer to those of the experimental studies.

The attempt to compare single zone values for sodium void reactivities obtained at the IPPE, ENEA and ERL-Hitachi is presented in the table 1. 21. The values reported in the table were calculated using different computational tools with different approaches, nevertheless ENEA and IPPE results are rather close to each other. The most difference is observed for HEZ and "sodium layer + plugs" zones and it is equal to ~20% for both cases. As far as void reactivity for whole reactor is concerned (table 1.22), reasonable agreement is observed between IPPE "Input data ..." and ERL results, ENEA calculations give approximately twice less value of this parameter as compare to the others. One more conclusion which can be made from the data provided is that the IPPE calculations results on of SVRE that were taken as a base for input data for ULOF accident analysis are close to those of most conservative case as long as they give the largest magnitudes of reactivity due to LEZ and MEZ voiding taking into account that sodium boiling initially starts in these zones.

TABLE 1.21. SODIUM VOID REACTIVITY, $\Delta K/K$

| | ENEA | | IPPE | | |
|-----------|----------|-----------|-----------------------------------|-----------|--------------------------------|
| | 3D-Diff. | 3D-Transp | 2D-Diff. (direct calculations) | | 2D-Dif ("Input data...") *) |
| | T | T | T=900°K | T=2100°K | T=1500°K |
| LEZ | - | +0.00891 | +0.00798 | +0.00887 | +0.00955 |
| MEZ | - | +0.00412 | +0.00417 | +0.00467 | +0.00474 |
| HEZ | - | -0.00226 | -0.00196 | -0.00175 | -0.00282 |
| Core | +0.00885 | +0.01158 | +0.01069 | +0.01233 | +0.01150 |
| BAB | -0.00138 | -0.00182 | - | - | -0.00210 |
| Na- layer | -0.01003 | -0.00939 | - | - | -0.01258 |
| +plugs | | | | | |
| Core"+" | -0.00118 | +0.00280 | -0.00328 | -0.000962 | -0.00110 |
| layer | | | | | |
| RB | -0.00122 | -0.00196 | - | - | -0.00160 |

TABLE 1.22. EACTIVITY DUE TO VOIDING WHOLE REACTOR, $\Delta K/K$

| ENEA | IPPE | ERL | HEX, 3D |
|----------|----------------------|----------|---------------------------|
| 3D-Tr. | ("Input data...") *) | 2D-Diff. | 2D Transp. |
| -0.00226 | -0.00481 | -0.00395 | -0.00357 |
| | | | -0.00521 (-0.00591)**) |

*) Combination of direct calculations with 1-st order perturbation calculations.

***) Heterogenous model.

Fuel and steel density coefficients: The comparison of IPPE and ENEA results is carried out in table 1.23. About fuel density coefficient the difference is acceptable: 13%, but not so for steel. It is impossible now to find out the reasons of the discrepancy because of the lack of necessary information.

Doppler reactivity: From the comparison of results obtained by the IPPE, ENEA and ERL-Hitachi (table 1.4, table 1.9 and table 1.15 respectively) the following conclusion can be drawn:

- integral values are rather similar, if the results obtained in Russia using perturbation theory are presented as a sum of Doppler constants for steel and sodium;

- different temperature ranges were used by the IPPE, ENEA and ERL-Hitachi for the Doppler constant evaluation, resulting into interpolation error and in the requirement of statistics increase for narrow temperature ranges when Monte Carlo calculation method is used;

- in cases with sodium, Doppler constant values from IPPE and ENEA are similar (with exception for the radial blanket values), while in the cases without sodium noticeable disagreement between the IPPE and ENEA data is only observed for LEZ, more agreement between IPPE and ENEA data taking place for other zones;

Uniform expansion coefficients: Uniform expansion coefficients calculated by the IPPE and ENEA are compared in table 1.24. Differences between the IPPE and ENEA reactivity coefficients caused by the materials thermal expansion are resulted from both diversity in the material worths (the main reason) and different presentation models of these components : perturbation theory calculation using relationships of the similarity theory at the IPPE, and direct evaluation of linear dimension and content changes at the ENEA. The most uncertainty exists in the model of radial expansion related reactivity coefficient. The ENEA model in which $\delta R/R$ and $\delta \rho/\rho$ values were taken equal, but not proportional to volume, also requires some comments. In general, material expansion related reactivity coefficients presented by the IPPE are in the area of less negative values, i.e. the reactor self-protection under

TABLE 1.23. DENSITY REACTIVITY COEFFICIENTS DISTRIBUTION PER ZONE, $\Delta K/K$

| Material | Fuel | | Steel | |
|----------|--------------------|---------|--------------------|----------|
| | IPPE (Input d.) | ENEA | IPPE (Input d.) | ENEA |
| LEZ | +0.1517 | +0.1799 | | -0.01396 |
| MEZ | +0.1237 | +0.1368 | | -0.00484 |
| HEZ | +0.1151 | +0.1178 | | +0.00546 |
| Reactor | +0.4019 | +0.4551 | +0.01719 | +0.02712 |

TABLE 1.24. REACTIVITY COEFFICIENTS DUE TO CORE THERMAL EXPANSION, $\Delta K/K$
(DIFFUSION APPROACH, 1-ST ORDER PERTURBATION THEORY)

| | Radial expansion | Axial expansion |
|------|------------------|-----------------|
| IPPE | -0.5396 | -0.1082 |
| ENEA | -0.5940 | -0.13804 |

accidental conditions is lower. In order to clarify the reasons for such considerable differences in the material worths, additional more thorough studies are required with the comparison of all the main neutronics functionals. In particular it is necessary to compare the worths of different nuclides (spatial distribution and integral values). Extremely limited information presented does not allow determining the reasons of differences in this phase. In this connection, it can be reasonable to continue analytical studies on the prediction accuracy of reactivity coefficients for the considered BN-800 reactor test model with sodium plenum.

Uncertainties: The comparative analysis of the results showed that reactivity coefficients and other neutronics parameters calculated by different participants differ each others.

This discrepancies are the result of using of different calculational tools (different approaches, different cross section libraries and etc.) and partly the sequence of our insufficient knowledge of the considered phenomena. So as to evaluate the influence of the uncertainties in the neutron-physics parameters on the ULOF accident development it was decided on one of the consultancy meeting to perform the calculations for the set of the parametric cases. For these cases the main neutronics input data should be varied in some definite ranges. As a result of analysis carried out above and after long and intensive discussion among the participants of the work it was proposed to postulate the following uncertainties in using reactivity worth:

- + 15% in Doppler
- + 20% in sodium void worth
- ± 20% in clad worth
- ± 5% in fuel worth

1.5. CONCLUSIONS

1. The core neutronics characteristics of the IPPE core design variant of the BN-800 type reactor with a near-zero void coefficient were evaluated. Three countries - Russia, Italy and Japan - participated in this evaluation with their own theoretical tools. Different approaches and methods (diffusion theory, transport theory, Monte Carlo method) and different cross section libraries (BNAB-78 and - Russia; JEF-1, ENDF/B-5.2 - Italy; JENDL-3.2 - Japan) were used for analysis. Detailed and complete information about all the neutronic parameters related to the ULOF analysis has been obtained.
2. As regards the comparison of the neutronics calculations performed by the participants of this work, the following deductions can be made on the base of the analysis of the results:

Power distributions. A good agreement has been found about fuel power distributions (discrepancies less than 2% for the integral results and 4.1% for the peak linear power).

Kinetics parameters. A satisfactory agreement has also been observed for kinetics parameters. For example, the differences between Russian and Italian calculations of integral kinetics parameters are -5.22%, +4.11%, +8.44% for effective delayed neutron fraction, prompt neutron life time and mean decay constant, respectively.

Doppler reactivity. The integral values are rather close for all participants. In the unvoided cases, Doppler constant values from the IPPE and ENEA are similar (with

exception for the radial blanket values), while in the voided cases noticeable disagreement between the IPPE and ENEA data is only observed for LEZ, more agreement between the IPPE and ENEA data taking place for other zones. The discrepancies in the Doppler coefficients have to be attributed to the different cross-section libraries and to the temperature range ; the last one rules the discrepancy magnitude. Russian and Italian results show that Doppler constant for the reference reactor is not additive value and depends on what reactor parts are voided.

Sodium density and void reactivity effect. In spite of the fact that reactivity calculations were performed using different computational tools with different approaches, the results are rather close to each other. The most difference is observed for HEZ and "sodium layer + plugs" zones and it is equal to ~20% for both cases. As regards void reactivity for whole the reactor, reasonable agreement is observed between IPPE "Input data ..." and ERL results, while ENEA calculations give approximately twice less value of this parameter than others.

The sodium void reactivity effect is not additive character. The simple sum of the void reactivities of the core parts usually underestimates void reactivity of the whole core. Non-additivity is higher when together with the core part, the sodium layer is voided.

The higher-order methods based on the Monte Carlo theory were applied to the void reactivity evaluation. Significant effects of the higher-order methods on the calculated void reactivity results are seen.

The presence of the fission products in the core worsen the sodium void coefficient by about 65-70%, effect being strongly variable and depending on the different zones of the core. Therefore it is important to simulate space distribution of fission products carefully.

3. Finally, regarding the ULOF analysis, the following conclusion can be made. The temperature feedbacks are the most important features of reactor that determine the path of the accident development. It is especially true for sodium void reactivity effect and Doppler effect. As regards the former of the above mentioned effects the scatter for this effect between different researches is the most because of the complexity of the problem. However the calculations made by Russian specialists give the most unfavourable (or very close to that) values of sodium void reactivity effect. The same situation is observed for Doppler effect as well. Therefore as regards reactivity feedbacks the input data prepared by Russia and additional postulate on that radial expansion reactivity effect is negligible gives a very conservative set of the initial data leading to the most severe path of the accident development.
4. Analysis of the results of the comparative neutronics calculations allows making some recommendations for the future:
As long as a significant effects of high order methods on the calculated void reactivity are found out, it can be recommended as one of the topic of future work the calculation of sodium void worth distribution using transport theory (e.g..Sn method) based perturbation code.

Non-additivity of sodium reactivity effect and Doppler effect was shown above. The difference for the former amounts to 30% in total i. e., this difference is similarly large than that originating from the use of different cross-section libraries. So as interaction effect between different core voiding states are not negligibly small the application of

space-time neutronics methods might become necessary for analysis of the severe accidents that can lead to sodium boiling and this task can be characterized as an important field of future activity.

NOMENCLATURE

| | | |
|--------------------------------|--------------------|---|
| H | m | height |
| K_{eff} | | multiplication factor |
| L_p | sec | prompt-neutrons life time: |
| R | m | radius |
| RE | % | reactivity effect |
| $T(\partial K / \partial T)_i$ | | Doppler constant for nuclide «i» |
| $T(0)$ | $^{\circ}\text{K}$ | reference temperature of material |
| $T(\tau)$ | $^{\circ}\text{K}$ | temperature of material for time τ |
| ε | | volume fraction of material |
| ρ^0, ρ^* | $1/\text{cm}^3$ | unperturbed and perturbed nuclear density |
| L^0, L^* | cm | unperturbed and perturbed linear size |
| L_p | sec | prompt-neutrons life time |
| \hat{O}_k, \hat{O}_k^+ | | group neutron flux and ajoint flux |
| i_k, i_k^+ | | group neutron current density and ajoint flux |
| β | | delayed fraction of source neutrons |
| β_{eff} | | effective delayed neutrons fraction |
| λ | sec^{-1} | mean decay constant |
| τ | sec | mean-neutrons life time |
| $\sigma_{\text{trk},i}$ | | transport cross-section of the nuclide «i» for the group «k» |
| $\sigma_{\text{c,f,d,in}}$ | | micro crossections for the reactions: capture fission diffusion inelastic scattering |
| ν_f^i | | fraction of prompt neutron for nuclide «i» |
| χ_k | | fraction of fission neutron in group for the nuclide «k» |
| SVRE | | sodium void RE |

TABLE 1A.1a. NUCLEAR CONCENTRATIONS IN CALCULATIONAL MODEL SUBZONES, 10^{24} NUCL/CM³

| izotopes | Physical sub-zone number | | | | | | | | | |
|----------|--------------------------|------------|------------|------------|------------|------------|------------|------------|------------|------------|
| | 1 | 2 | 3 | 4 | 5 | 6 | 7 | 8 | 9 | 10 |
| U235 | 0.1694E-04 | 0.1694E-04 | 0.1722E-04 | 0.2751E-04 | 0.4387E-04 | 0.0000E+00 | 0.0000E+00 | 0.0000E+00 | 0.0000E+00 | 0.0000E+00 |
| U238 | 0.5518E-02 | 0.5331E-02 | 0.5091E-02 | 0.7757E-02 | 0.1199E-01 | 0.0000E+00 | 0.0000E+00 | 0.0000E+00 | 0.0000E+00 | 0.0000E+00 |
| PU39 | 0.8233E-03 | 0.9228E-03 | 0.1087E-02 | 0.1053E-03 | 0.2264E-03 | 0.0000E+00 | 0.0000E+00 | 0.0000E+00 | 0.0000E+00 | 0.0000E+00 |
| PU40 | 0.3740E-03 | 0.4243E-03 | 0.4988E-03 | 0.2526E-05 | 0.4004E-05 | 0.0000E+00 | 0.0000E+00 | 0.0000E+00 | 0.0000E+00 | 0.0000E+00 |
| PU41 | 0.1265E-03 | 0.1482E-03 | 0.1825E-03 | 0.7811E-07 | 0.7798E-07 | 0.0000E+00 | 0.0000E+00 | 0.0000E+00 | 0.0000E+00 | 0.0000E+00 |
| PU42 | 0.6199E-04 | 0.7070E-04 | 0.8297E-04 | 0.8315E-09 | 0.6940E-09 | 0.0000E+00 | 0.0000E+00 | 0.0000E+00 | 0.0000E+00 | 0.0000E+00 |
| FP39 | 0.3090E-03 | 0.3164E-03 | 0.2706E-03 | 0.1698E-04 | 0.3335E-04 | 0.0000E+00 | 0.0000E+00 | 0.0000E+00 | 0.0000E+00 | 0.0000E+00 |
| O | 0.1446E-01 | 0.1446E-01 | 0.1446E-01 | 0.1582E-01 | 0.2460E-01 | 0.0000E+00 | 0.0000E+00 | 0.0000E+00 | 0.0000E+00 | 0.0000E+00 |
| NA | 0.8630E-02 | 0.8630E-02 | 0.8630E-02 | 0.8630E-02 | 0.5420E-02 | 0.1938E-01 | 0.7190E-02 | 0.6190E-02 | 0.2096E-01 | 0.1197E-01 |
| FE | 0.1284E-01 | 0.1284E-01 | 0.1284E-01 | 0.1284E-01 | 0.1015E-01 | 0.5990E-02 | 0.9920E-02 | 0.9100E-02 | 0.4300E-02 | 0.9980E-02 |
| CR | 0.2830E-02 | 0.2830E-02 | 0.2830E-02 | 0.2830E-02 | 0.2230E-02 | 0.1030E-02 | 0.2060E-02 | 0.1950E-02 | 0.1060E-02 | 0.2400E-02 |
| NI | 0.1510E-02 | 0.1510E-02 | 0.1510E-02 | 0.1510E-02 | 0.1060E-02 | 0.1700E-04 | 0.8700E-03 | 0.9260E-03 | 0.6420E-03 | 0.1510E-02 |
| MO | 0.2480E-03 | 0.2480E-03 | 0.2480E-03 | 0.2480E-03 | 0.1620E-03 | 0.6500E-04 | 0.1700E-03 | 0.1650E-03 | 0.1080E-03 | 0.2330E-03 |
| NB | 0.6300E-04 | 0.6300E-04 | 0.6300E-04 | 0.6300E-04 | 0.4100E-04 | 0.1900E-04 | 0.4400E-04 | 0.4200E-04 | 0.0000E+00 | 0.3100E-04 |
| B-10 | 0.0000E+00 | 0.0000E+00 | 0.0000E+00 | 0.0000E+00 | 0.0000E+00 | 0.0000E+00 | 0.7890E-02 | 0.7890E-02 | 0.1000E-07 | 0.1069E-01 |
| B-11 | 0.0000E+00 | 0.0000E+00 | 0.0000E+00 | 0.0000E+00 | 0.0000E+00 | 0.0000E+00 | 0.3200E-01 | 0.3200E-01 | 0.1000E-07 | 0.1212E-01 |
| C | 0.0000E+00 | 0.0000E+00 | 0.0000E+00 | 0.0000E+00 | 0.0000E+00 | 0.0000E+00 | 0.9960E-02 | 0.9960E-02 | 0.1000E-07 | 0.5707E-02 |

TABLE 1A. 1b. NUCLEAR CONCENTRATIONS IN CALCULATIONAL MODEL SUBZONES, 10^{24} NUCL/CM³ (cont'd.)

| izotopes | 11 | 12 | 13 | 14 | 15 | 16 | 17 | 18 | 19 | 20 |
|----------|------------|------------|------------|------------|------------|------------|------------|------------|------------|------------|
| U235 | 0.0000E+00 | 0.1694E-04 | 0.1694E-04 | 0.1722E-04 |
| U238 | 0.0000E+00 | 0.5518E-02 | 0.5331E-02 | 0.5091E-02 |
| PU39 | 0.0000E+00 | 0.8233E-03 | 0.9228E-03 | 0.1087E-02 |
| PU40 | 0.0000E+00 | 0.3740E-03 | 0.4243E-03 | 0.4988E-03 |
| PU41 | 0.0000E+00 | 0.1265E-03 | 0.1482E-03 | 0.1825E-03 |
| PU42 | 0.0000E+00 | 0.6199E-04 | 0.7070E-04 | 0.8297E-04 |
| FP39 | 0.0000E+00 | 0.3090E-03 | 0.3164E-03 | 0.2706E-03 |
| O | 0.0000E+00 | 0.1446E-01 | 0.1446E-01 | 0.1446E-01 |
| NA | 0.1197E-01 | 0.1197E-01 | 0.8630E-02 | 0.8630E-02 | 0.6450E-02 | 0.1480E-01 | 0.1830E-01 | 0.8630E-02 | 0.8630E-02 | 0.8630E-02 |
| FE | 0.9980E-02 | 0.9980E-02 | 0.3537E-01 | 0.1284E-01 | 0.4658E-01 | 0.1940E-01 | 0.1110E-01 | 0.1284E-01 | 0.1284E-01 | 0.1284E-01 |
| CR | 0.2400E-02 | 0.2400E-02 | 0.7820E-02 | 0.2830E-02 | 0.7770E-02 | 0.5460E-02 | 0.3120E-02 | 0.2830E-02 | 0.2830E-02 | 0.2830E-02 |
| NI | 0.1510E-02 | 0.1510E-02 | 0.4170E-02 | 0.1510E-02 | 0.1320E-03 | 0.3950E-02 | 0.2260E-02 | 0.1510E-02 | 0.1510E-02 | 0.1510E-02 |
| MO | 0.2330E-03 | 0.2330E-03 | 0.6850E-03 | 0.2480E-03 | 0.5010E-03 | 0.3080E-03 | 0.1760E-03 | 0.2480E-03 | 0.2480E-03 | 0.2480E-03 |
| NB | 0.3100E-04 | 0.3100E-04 | 0.1740E-03 | 0.6300E-04 | 0.1460E-03 | 0.0000E+00 | 0.0000E+00 | 0.6300E-04 | 0.6300E-04 | 0.6300E-04 |
| B-10 | 0.1380E-01 | 0.2180E-01 | 0.0000E+00 |
| B-11 | 0.9180E-02 | 0.1900E-02 | 0.0000E+00 |
| C | 0.5750E-02 | 0.5920E-02 | 0.0000E+00 |
| | 21 | 22 | 23 | 24 | | | | | | |
| U235 | 0.1694E-04 | 0.1694E-04 | 0.1722E-04 | 0.0000E+00 | | | | | | |
| U238 | 0.5518E-02 | 0.5331E-02 | 0.5091E-02 | 0.0000E+00 | | | | | | |
| PU39 | 0.8233E-03 | 0.9228E-03 | 0.1087E-02 | 0.0000E+00 | | | | | | |
| PU40 | 0.3740E-03 | 0.4243E-03 | 0.4988E-03 | 0.0000E+00 | | | | | | |
| PU41 | 0.1265E-03 | 0.1482E-03 | 0.1825E-03 | 0.0000E+00 | | | | | | |
| PU42 | 0.6199E-04 | 0.7070E-04 | 0.8297E-04 | 0.0000E+00 | | | | | | |
| FP39 | 0.3090E-03 | 0.3164E-03 | 0.2706E-03 | 0.0000E+00 | | | | | | |
| O | 0.1446E-01 | 0.1446E-01 | 0.1446E-01 | 0.0000E+00 | | | | | | |
| NA | 0.8630E-02 | 0.8630E-02 | 0.8630E-02 | 0.8630E-02 | | | | | | |
| FE | 0.1284E-01 | 0.1284E-01 | 0.1284E-01 | 0.2080E-01 | | | | | | |
| CR | 0.2830E-02 | 0.2830E-02 | 0.2830E-02 | 0.4740E-02 | | | | | | |
| NI | 0.1510E-02 | 0.1510E-02 | 0.1510E-02 | 0.2500E-02 | | | | | | |
| MO | 0.2480E-03 | 0.2480E-03 | 0.2480E-03 | 0.4350E-03 | | | | | | |
| NB | 0.6300E-04 | 0.6300E-04 | 0.6300E-04 | 0.0000E+00 | | | | | | |
| B-10 | 0.0000E+00 | 0.0000E+00 | 0.0000E+00 | 0.0000E+00 | | | | | | |
| B-11 | 0.0000E+00 | 0.0000E+00 | 0.0000E+00 | 0.0000E+00 | | | | | | |
| C | 0.0000E+00 | 0.0000E+00 | 0.0000E+00 | 0.0000E+00 | | | | | | |

TABLE 1A2. SODIUM VOID REACTIVITY COEFFICIENTS, $\Delta K/K$

| k_i | LEZ | | | | MEZ | | | | HEZ | | BR | RS+Stor |
|-------|----------|----------|----------|----------|----------|----------|----------|----------|----------|----------|----------|----------|
| | 1 | 2 | 3 | 4 | 5 | 6 | 7 | 8 | 9 | 10 | 11 | 12 |
| 2 | -5.47E-7 | -6.71E-7 | -4.97E-7 | -8.14E-7 | -6.03E-7 | -2.03E-7 | -2.13E-7 | -2.35E-7 | -2.85E-7 | -1.01E-7 | -1.75E-7 | -3.21E-7 |
| 3 | -1.60E-5 | -2.42E-5 | -2.31E-5 | -4.23E-5 | -3.19E-5 | -1.06E-5 | -1.14E-5 | -1.28E-5 | -1.55E-5 | -5.21E-6 | -8.33E-6 | -9.91E-6 |
| 4 | -1.15E-4 | -1.43E-4 | -1.26E-4 | -3.01E-4 | -3.90E-4 | -1.67E-4 | -1.95E-4 | -2.45E-4 | -3.19E-4 | -1.08E-4 | -1.21E-4 | -7.09E-5 |
| 5 | 1.15E-5 | 1.72E-5 | 1.16E-5 | -3.30E-6 | -6.35E-5 | -4.13E-5 | -5.69E-5 | -9.77E-5 | -1.89E-4 | -8.97E-5 | -6.68E-5 | -4.55E-5 |
| 6 | 9.62E-5 | 1.25E-4 | 1.01E-4 | 1.76E-4 | 1.15E-4 | 2.38E-5 | 1.05E-5 | -3.58E-5 | -1.60E-4 | -1.01E-4 | -9.09E-5 | -5.96E-5 |
| 7 | 1.96E-4 | 2.53E-4 | 2.08E-4 | 3.92E-4 | 3.29E-4 | 1.02E-4 | 9.13E-5 | 3.84E-5 | -1.26E-4 | -1.15E-4 | -1.18E-4 | -7.51E-5 |
| 8 | 2.67E-4 | 3.44E-4 | 2.85E-4 | 5.50E-4 | 4.84E-4 | 1.59E-4 | 1.50E-4 | 9.23E-5 | -1.02E-4 | -1.26E-4 | -1.37E-4 | -8.63E-5 |
| 9 | 3.15E-4 | 4.08E-4 | 3.40E-4 | 6.62E-4 | 5.96E-4 | 2.00E-4 | 1.93E-4 | 1.31E-4 | -8.50E-5 | -1.35E-4 | -1.52E-4 | -9.50E-5 |
| 10 | 3.27E-4 | 4.23E-4 | 3.54E-4 | 6.93E-4 | 6.30E-4 | 2.13E-4 | 2.07E-4 | 1.44E-4 | -8.12E-5 | -1.39E-4 | -1.58E-4 | -9.89E-5 |
| 11 | 2.98E-4 | 3.87E-4 | 3.24E-4 | 6.37E-4 | 5.80E-4 | 1.96E-4 | 1.89E-4 | 1.28E-4 | -9.06E-5 | -1.38E-4 | -1.55E-4 | -9.78E-5 |
| 12 | 2.41E-4 | 3.14E-4 | 2.63E-4 | 5.18E-4 | 4.69E-4 | 1.57E-4 | 1.49E-4 | 9.15E-5 | -1.09E-4 | -1.33E-4 | -1.45E-4 | -9.25E-5 |
| 13 | 1.49E-4 | 1.94E-4 | 1.63E-4 | 3.19E-4 | 2.78E-4 | 8.83E-5 | 7.95E-5 | 2.88E-5 | -1.37E-4 | -1.22E-4 | -1.25E-4 | -8.15E-5 |
| 14 | 5.87E-5 | 7.67E-5 | 6.05E-5 | 1.23E-4 | 8.65E-5 | 1.86E-5 | 8.08E-6 | -3.51E-5 | -1.63E-4 | -1.09E-4 | -1.03E-4 | -6.90E-5 |
| 15 | -4.58E-5 | -6.26E-5 | -4.91E-5 | -1.06E-4 | -1.47E-4 | -6.66E-5 | -8.00E-5 | -1.15E-4 | -1.92E-4 | -8.76E-5 | -7.24E-5 | -5.17E-5 |
| 16 | -1.43E-4 | -1.99E-4 | -1.78E-4 | -3.29E-4 | -3.23E-4 | -1.29E-4 | -1.45E-4 | -1.79E-4 | -2.17E-4 | -6.55E-5 | -4.33E-5 | -3.75E-5 |
| 17 | -7.42E-5 | -1.00E-4 | -8.92E-5 | -1.68E-4 | -1.39E-4 | -5.52E-5 | -6.47E-5 | -8.29E-5 | -1.11E-4 | -3.30E-5 | -1.69E-5 | -1.87E-5 |
| 18 | -6.57E-4 | -7.82E-4 | -6.13E-4 | -1.40E-3 | -1.50E-3 | -6.13E-4 | -7.20E-4 | -9.17E-4 | -1.30E-3 | -5.00E-4 | -7.28E-5 | -3.65E-5 |
| 19 | -1.24E-4 | -1.26E-4 | -1.06E-4 | -2.79E-4 | -3.72E-4 | -1.61E-4 | -1.93E-4 | -2.52E-4 | -3.79E-4 | -1.60E-4 | -2.02E-5 | -9.74E-6 |
| 20 | -2.33E-5 | -2.12E-5 | -1.86E-5 | -5.69E-5 | -9.39E-5 | -4.37E-5 | -5.35E-5 | -7.07E-5 | -1.07E-4 | -4.56E-5 | -7.57E-6 | -3.86E-6 |
| 21 | 3.27E-7 | 4.56E-7 | 3.79E-7 | 8.64E-7 | 4.08E-7 | 1.15E-7 | 1.11E-7 | 1.13E-7 | 1.46E-7 | -1.07E-8 | -5.55E-8 | -8.39E-7 |
| 22 | 2.87E-8 | 3.81E-8 | 3.22E-8 | 6.76E-8 | 7.40E-8 | 3.04E-8 | 3.47E-8 | 4.20E-8 | 5.03E-8 | 6.55E-9 | -2.26E-8 | -1.86E-7 |
| 23 | 4.81E-9 | 6.47E-9 | 5.60E-9 | 1.24E-8 | 1.38E-8 | 5.89E-9 | 6.70E-9 | 7.77E-9 | 8.30E-9 | 1.62E-9 | -1.82E-9 | -2.19E-8 |
| 24 | 1.00E-9 | 1.38E-9 | 1.27E-9 | 2.87E-9 | 3.19E-9 | 1.36E-9 | 1.59E-9 | 1.98E-9 | 2.72E-9 | 1.01E-9 | 1.71E-9 | 8.29E-10 |

TABLE 1A3. DOPPLER REACTIVITY COEFFICIENTS, $\Delta K/K$

| k\i | LEZ | | | | | MEZ | | | HEZ | | BR |
|-----|------------|------------|------------|------------|------------|------------|------------|------------|------------|------------|------------|
| | 1 | 2 | 3 | 4 | 5 | 6 | 7 | 8 | 9 | 10 | 11 |
| 3 | 0.0000E-00 |
| 4 | 0.5631E-04 | 0.7929E-04 | 0.6686E-04 | 0.1305E-03 | 0.8904E-04 | 0.3696E-04 | 0.4483E-04 | 0.2837E-04 | 0.4568E-04 | 0.2139E-04 | 0.9543E-04 |
| 5 | 0.2888E-04 | 0.4084E-04 | 0.3640E-04 | 0.7458E-04 | 0.4058E-04 | 0.1684E-04 | 0.2043E-04 | 0.1237E-04 | 0.1991E-04 | 0.9326E-05 | 0.1600E-04 |
| 6 | 0.3542E-04 | 0.5026E-04 | 0.4531E-04 | 0.9336E-04 | 0.5085E-04 | 0.2110E-04 | 0.2560E-04 | 0.1565E-04 | 0.2520E-04 | 0.1180E-04 | 0.2024E-04 |
| 7 | 0.4285E-04 | 0.6088E-04 | 0.5537E-04 | 0.1148E-03 | 0.6325E-04 | 0.2625E-04 | 0.3185E-04 | 0.1966E-04 | 0.3165E-04 | 0.1482E-04 | 0.2543E-04 |
| 8 | 0.4946E-04 | 0.7034E-04 | 0.6435E-04 | 0.1339E-03 | 0.7466E-04 | 0.3099E-04 | 0.3759E-04 | 0.2337E-04 | 0.3762E-04 | 0.1762E-04 | 0.3022E-04 |
| 9 | 0.5262E-04 | 0.7491E-04 | 0.6880E-04 | 0.1436E-03 | 0.8019E-04 | 0.3329E-04 | 0.4038E-04 | 0.2225E-04 | 0.3582E-04 | 0.1678E-04 | 0.3373E-04 |
| 10 | 0.5439E-04 | 0.7750E-04 | 0.7135E-04 | 0.1491E-03 | 0.8366E-04 | 0.3472E-04 | 0.4212E-04 | 0.2329E-04 | 0.3750E-04 | 0.1756E-04 | 0.3531E-04 |
| 11 | 0.5291E-04 | 0.7543E-04 | 0.6952E-04 | 0.1454E-03 | 0.8185E-04 | 0.3397E-04 | 0.4121E-04 | 0.2288E-04 | 0.3684E-04 | 0.1725E-04 | 0.3469E-04 |
| 12 | 0.4813E-04 | 0.6859E-04 | 0.6326E-04 | 0.1324E-03 | 0.7485E-04 | 0.3107E-04 | 0.3769E-04 | 0.2105E-04 | 0.3389E-04 | 0.1587E-04 | 0.3192E-04 |
| 13 | 0.3841E-04 | 0.5459E-04 | 0.5038E-04 | 0.1058E-03 | 0.7160E-04 | 0.2972E-04 | 0.3605E-04 | 0.2060E-04 | 0.3316E-04 | 0.1553E-04 | 0.2742E-04 |
| 14 | 0.2919E-04 | 0.4105E-04 | 0.3793E-04 | 0.8035E-04 | 0.5611E-04 | 0.2329E-04 | 0.2825E-04 | 0.1657E-04 | 0.2667E-04 | 0.1249E-04 | 0.2206E-04 |
| 15 | 0.1913E-04 | 0.2584E-04 | 0.2390E-04 | 0.5233E-04 | 0.4102E-04 | 0.1703E-04 | 0.2066E-04 | 0.1293E-04 | 0.2082E-04 | 0.9753E-05 | 0.1722E-04 |
| 16 | 0.9591E-05 | 0.1080E-04 | 0.9740E-05 | 0.2472E-04 | 0.3037E-04 | 0.1261E-04 | 0.1529E-04 | 0.1114E-04 | 0.1793E-04 | 0.8398E-05 | 0.1483E-04 |
| 17 | 0.0000E-00 |
| 18 | 0.0000E-00 |
| 19 | 0.0000E-00 |
| 20 | 0.0000E-00 |
| 21 | 0.0000E-00 |
| 22 | 0.0000E-00 |

TABLE 1A4. REDUCTION FACTOR OF DOPPLER COEFFICIENTS, RDD

| Zone | Sodium density relative to initial state, % | | | | |
|------|---|--------|--------|--------|--------|
| | 100 | 75 | 50 | 25 | 0 |
| LEZ | 1.00 | 0.9084 | 0.8328 | 0.7575 | 0.6354 |
| MEZ | 1.00 | 0.9143 | 0.8299 | 0.7381 | 0.6561 |
| HEZ | 1.00 | 0.9074 | 0.8215 | 0.7664 | 0.7181 |
| BAB | 1.00 | 1.0100 | 0.9257 | 0.8814 | 0.8214 |
| RB | 1.00 | 1.2219 | 1.1801 | 0.9968 | 0.9325 |

TABLE 1A5. AXIAL EXPANSION REACTIVITY COEFFICIENTS, $\Delta K/K/^\circ C$

| k\i | LEZ | | | | | MEZ | | | HEZ | |
|-----|------------|------------|------------|------------|------------|------------|------------|------------|------------|------------|
| | 1 | 2 | 3 | 4 | 5 | 6 | 7 | 8 | 9 | 10 |
| 3 | 0.9001E-06 | 0.3848E-05 | 0.1270E-04 | 0.3782E-04 | 0.4426E-04 | 0.1837E-04 | 0.2229E-04 | 0.2841E-04 | 0.4574E-04 | 0.2141E-04 |
| 4 | 0.1886E-04 | 0.2025E-04 | 0.9717E-05 | 0.9685E-04 | 0.3929E-03 | 0.1631E-03 | 0.1978E-03 | 0.1222E-02 | 0.1967E-02 | 0.9208E-03 |
| 5 | 0.3953E-06 | 0.5034E-05 | 0.1198E-04 | 0.5586E-05 | 0.2261E-03 | 0.9384E-04 | 0.1138E-03 | 0.1480E-02 | 0.2383E-02 | 0.1115E-02 |
| 6 | 0.3734E-05 | 0.1098E-04 | 0.2631E-04 | 0.3966E-04 | 0.2940E-03 | 0.1220E-03 | 0.1480E-03 | 0.2228E-02 | 0.3588E-02 | 0.1680E-02 |
| 7 | 0.8298E-05 | 0.1886E-04 | 0.4401E-04 | 0.8785E-04 | 0.3708E-03 | 0.1539E-03 | 0.1867E-03 | 0.3042E-02 | 0.4898E-02 | 0.2293E-02 |
| 8 | 0.1169E-04 | 0.2574E-04 | 0.6016E-04 | 0.1313E-03 | 0.4375E-03 | 0.1816E-03 | 0.2203E-03 | 0.3728E-02 | 0.6002E-02 | 0.2810E-02 |
| 9 | 0.1372E-04 | 0.3091E-04 | 0.7206E-04 | 0.1625E-03 | 0.4835E-03 | 0.2007E-03 | 0.2435E-03 | 0.4205E-02 | 0.6770E-02 | 0.3169E-02 |
| 10 | 0.1458E-04 | 0.3384E-04 | 0.7790E-04 | 0.1782E-03 | 0.5002E-03 | 0.2076E-03 | 0.2519E-03 | 0.4410E-02 | 0.7100E-02 | 0.3324E-02 |
| 11 | 0.1434E-04 | 0.3407E-04 | 0.7709E-04 | 0.1780E-03 | 0.4826E-03 | 0.2003E-03 | 0.2430E-03 | 0.4315E-02 | 0.6947E-02 | 0.3252E-02 |
| 12 | 0.1299E-04 | 0.3135E-04 | 0.7018E-04 | 0.1634E-03 | 0.4307E-03 | 0.1788E-03 | 0.2169E-03 | 0.3928E-02 | 0.6325E-02 | 0.2961E-02 |
| 13 | 0.1043E-04 | 0.2571E-04 | 0.5860E-04 | 0.1369E-03 | 0.3506E-03 | 0.1455E-03 | 0.1765E-03 | 0.3293E-02 | 0.5301E-02 | 0.2482E-02 |
| 14 | 0.6491E-05 | 0.1738E-04 | 0.4442E-04 | 0.1009E-03 | 0.2540E-03 | 0.1054E-03 | 0.1279E-03 | 0.2479E-02 | 0.3991E-02 | 0.1868E-02 |
| 15 | 0.1504E-05 | 0.7121E-05 | 0.2991E-04 | 0.5929E-04 | 0.1563E-03 | 0.6488E-04 | 0.7870E-04 | 0.1588E-02 | 0.2556E-02 | 0.1197E-02 |
| 16 | 0.5347E-05 | 0.8750E-05 | 0.2410E-04 | 0.5256E-04 | 0.8096E-04 | 0.3360E-04 | 0.4076E-04 | 0.7376E-03 | 0.1188E-02 | 0.5559E-03 |
| 17 | 0.1058E-04 | 0.1341E-04 | 0.1554E-04 | 0.5730E-04 | 0.3095E-04 | 0.1285E-04 | 0.1558E-04 | 0.1525E-03 | 0.2455E-03 | 0.1149E-03 |
| 18 | 0.9990E-05 | 0.7126E-05 | 0.7294E-05 | 0.4891E-04 | 0.2103E-04 | 0.8730E-05 | 0.1059E-04 | 0.5463E-04 | 0.8795E-04 | 0.4117E-04 |
| 19 | 0.6357E-05 | 0.4535E-05 | 0.4641E-05 | 0.3113E-04 | 0.1338E-04 | 0.5556E-05 | 0.6739E-05 | 0.3476E-04 | 0.5597E-04 | 0.2620E-04 |
| 20 | 0.2760E-05 | 0.1966E-05 | 0.2029E-05 | 0.1352E-04 | 0.5802E-05 | 0.2408E-05 | 0.2921E-05 | 0.1520E-04 | 0.2448E-04 | 0.1146E-04 |
| 21 | 0.7209E-07 | 0.4534E-07 | 0.7978E-07 | 0.3702E-06 | 0.1310E-06 | 0.5437E-07 | 0.6596E-07 | 0.6099E-06 | 0.9820E-06 | 0.4597E-06 |
| 22 | 0.2726E-07 | 0.1716E-07 | 0.3047E-07 | 0.1410E-06 | 0.4970E-07 | 0.2063E-07 | 0.2502E-07 | 0.2307E-06 | 0.3714E-06 | 0.1739E-06 |
| 23 | 0.3135E-09 | 0.2166E-09 | 0.7559E-09 | 0.2905E-08 | 0.7871E-09 | 0.3267E-09 | 0.3963E-09 | 0.2686E-08 | 0.4325E-08 | 0.2025E-08 |
| 24 | 0.3344E-10 | 0.1669E-10 | 0.1128E-09 | 0.4918E-09 | 0.1221E-09 | 0.5068E-10 | 0.6147E-10 | 0.2438E-09 | 0.3925E-09 | 0.1837E-09 |

TABLE 1A6. RADIAL EXPANSION REACTIVITY COEFFICIENTS, $\Delta K/K/^\circ C$

| i | 1 | 2 | 3 | 4 | 5 | 6 | 7 |
|---------|------------|------------|------------|------------|------------|------------|------------|
| $K^f i$ | 0.3103E-01 | 0.4315E-01 | 0.4113E-01 | 0.9145E-01 | 0.1074E+00 | 0.4457E-01 | 0.5406E-01 |
| i | 8 | 9 | 10 | 11 | 12 | | |
| $K^f i$ | 0.5808E-01 | 0.9351E-01 | 0.4378E-01 | 0.1876E-01 | 0.5705E-02 | | |

TABLE 1A7. STEEL DISPLACEMENT REACTIVITY COEFFICIENTS, $\Delta K/K$.

| k_j | LEZ | | | MEZ | | | HEX | | | BR | RS=Stor | |
|-------|----------|----------|----------|----------|----------|----------|----------|----------|----------|----------|----------|----------|
| | 1 | 2 | 3 | 4 | 5 | 6 | 7 | 8 | 9 | 10 | 11 | 12 |
| 2 | -1.37E-6 | -1.67E-6 | -2.02E-6 | -2.02E-6 | -1.50E-6 | -5.08E-7 | -5.35E-7 | -5.94E-7 | -7.32E-7 | -2.61E-7 | -4.60E-7 | -6.28E-7 |
| 3 | -1.94E-5 | -3.11E-5 | -3.13E-5 | -5.91E-5 | -4.59E-5 | -1.55E-5 | -1.67E-5 | -1.91E-5 | -2.38E-5 | -8.18E-6 | -1.38E-5 | -1.68E-5 |
| 4 | -1.79E-4 | -2.19E-4 | -1.93E-4 | -4.71E-4 | -8.23E-4 | -2.88E-4 | -3.11E-4 | -3.89E-4 | 5.10E-4 | -1.74E-4 | -2.07E-4 | -2.91E-4 |
| 5 | 8.00E-5 | 1.08E-4 | 8.43E-5 | 1.20E-4 | 1.54E-5 | -2.25E-5 | -4.28E-5 | -1.00E-4 | -2.42E-4 | -1.29E-4 | -1.22E-4 | -1.89E-4 |
| 6 | 2.50E-4 | 3.25E-4 | 2.64E-4 | 4.79E-4 | 3.72E-4 | 1.09E-4 | 9.48E-5 | 3.29E-5 | -1.58E-4 | -1.37E-4 | -1.64E-4 | -2.47E-4 |
| 7 | 4.48E-4 | 5.78E-4 | 4.78E-4 | 9.05E-4 | 7.92E-4 | 2.63E-4 | 2.57E-4 | 1.90E-4 | -6.04E-5 | -1.48E-4 | -2.10E-4 | -3.12E-4 |
| 8 | 5.85E-4 | 7.58E-4 | 6.28E-4 | 1.21E-3 | 1.01E-3 | 3.76E-4 | 3.75E-4 | 3.04E-4 | 9.46E-6 | -1.57E-4 | -2.44E-4 | -3.59E-4 |
| 9 | 6.80E-4 | 8.83E-4 | 7.35E-4 | 1.43E-3 | 1.31E-3 | 4.57E-4 | 4.61E-4 | 3.87E-4 | 5.91E-5 | -1.65E-4 | -2.70E-4 | -3.98E-4 |
| 10 | 7.04E-4 | 9.15E-4 | 7.64E-4 | 1.53E-3 | 1.38E-3 | 4.84E-4 | 4.89E-4 | 4.15E-4 | 7.45E-5 | -1.69E-4 | -2.81E-4 | -4.13E-4 |
| 11 | 6.50E-4 | 8.46E-4 | 7.08E-4 | 1.39E-3 | 1.29E-3 | 4.52E-4 | 4.57E-4 | 3.84E-4 | 5.40E-4 | -1.89E-4 | -2.78E-4 | -4.08E-4 |
| 12 | 5.41E-4 | 7.04E-4 | 5.09E-4 | 1.16E-3 | 1.08E-3 | 3.77E-4 | 3.79E-4 | 3.11E-4 | 8.44E-6 | -1.66E-4 | -2.58E-4 | -3.85E-4 |
| 13 | 3.59E-4 | 4.68E-4 | 3.92E-4 | 7.75E-4 | 7.12E-4 | 2.45E-4 | 2.43E-4 | 1.82E-4 | -8.73E-5 | -1.56E-4 | -2.23E-4 | -3.39E-4 |
| 14 | 1.79E-4 | 2.30E-4 | 1.94E-4 | 3.85E-4 | 3.40E-4 | 1.10E-4 | 1.03E-4 | 5.09E-5 | -1.40E-4 | -1.43E-4 | -1.84E-4 | -2.88E-4 |
| 15 | -3.75E-5 | -6.34E-5 | -4.89E-5 | -8.77E-5 | -1.17E-4 | -5.53E-5 | -6.85E-5 | -1.12E-4 | -2.24E-4 | -1.19E-4 | -1.29E-4 | -2.15E-4 |
| 16 | -2.37E-4 | -3.49E-4 | -3.16E-4 | -5.42E-4 | -4.56E-4 | -1.72E-4 | -1.91E-4 | -2.32E-4 | -2.84E-4 | -5.88E-5 | -7.68E-5 | -1.57E-4 |
| 17 | -2.84E-4 | -3.95E-4 | -3.49E-4 | -6.35E-4 | -4.83E-4 | -1.72E-4 | -1.98E-4 | -2.15E-4 | -3.38E-4 | -1.02E-4 | -4.37E-5 | -7.86E-5 |
| 18 | -1.32E-4 | -1.62E-4 | -1.28E-4 | -2.84E-4 | -2.85E-4 | -9.77E-5 | -1.12E-4 | -1.41E-4 | -2.03E-4 | -5.06E-5 | -7.58E-5 | -1.54E-4 |
| 19 | -2.70E-5 | -2.89E-5 | -2.42E-5 | -6.15E-5 | -7.30E-5 | -2.92E-5 | -3.42E-5 | -4.40E-5 | -8.61E-5 | -2.83E-5 | -2.26E-5 | -4.08E-5 |
| 20 | -6.49E-6 | -6.47E-6 | -5.57E-6 | -1.58E-5 | -2.34E-5 | -1.04E-5 | -1.25E-5 | -1.81E-5 | -2.38E-5 | -9.81E-6 | -1.05E-5 | -1.61E-5 |
| 21 | -6.99E-8 | -3.52E-8 | -4.06E-8 | -2.34E-7 | -4.73E-7 | -2.28E-7 | -2.73E-7 | -3.40E-7 | -4.46E-7 | -2.39E-7 | -3.77E-7 | -3.54E-6 |
| 22 | 5.59E-9 | 9.58E-9 | 7.11E-9 | 1.04E-8 | 1.22E-8 | 5.18E-9 | 5.95E-9 | 7.16E-9 | 3.89E-9 | -1.42E-8 | -3.74E-8 | -3.78E-7 |
| 23 | 1.20E-10 | 4.74E-10 | 2.86E-10 | -7.9E-11 | -5.1E-10 | 2.48E-11 | 8.0E-11 | 2.81E-11 | -8.2E-10 | -1.03E-9 | -4.85E-9 | -2.06E-8 |
| 24 | 4.58E-10 | 6.63E-10 | 5.91E-10 | 1.25E-9 | 1.40E-9 | 6.73E-10 | 8.51E-10 | 1.18E-9 | 1.87E-9 | 7.72E-10 | 1.37E-9 | 3.02E-10 |

TABLE 1A8. FUEL DISPLACEMENT REACTIVITY COEFFICIENTS, $\Delta K/K$

| k\i | LEZ | | | | | MEZ | | | HEZ | | | BR | R.shield |
|-----|-------------|-------------|-------------|-------------|-------------|-------------|-------------|-------------|-------------|-------------|-------------|-------------|----------|
| | 1 | 2 | 3 | 4 | 5 | 6 | 7 | 8 | 9 | 10 | 11 | 12 | |
| 2 | 0.0000E+00 | |
| 3 | 0.0000E+00 | |
| 4 | 0.1791E-03 | 0.2732E-03 | 0.2040E-03 | 0.1098E-03 | -0.4320E-03 | -0.2587E-03 | 0.3328E-03 | -0.4655E-03 | -0.6716E-03 | -0.2458E-03 | -0.2725E-03 | 0.1312E-04 | |
| 5 | -0.1641E-02 | -0.2123E-02 | -0.1756E-02 | -0.3408E-02 | -0.3766E-02 | -0.1431E-02 | -0.1566E-02 | -0.2165E-02 | -0.2680E-02 | -0.8911E-03 | -0.4164E-03 | -0.1714E-04 | |
| 6 | -0.1963E-02 | -0.2541E-02 | -0.2104E-02 | -0.4108E-02 | -0.4669E-02 | -0.1789E-02 | -0.1967E-02 | -0.2802E-02 | -0.3535E-02 | -0.1198E-02 | -0.5787E-03 | -0.2686E-04 | |
| 7 | -0.2364E-02 | -0.3059E-02 | -0.2538E-02 | -0.4980E-02 | -0.5795E-02 | -0.2234E-02 | -0.2466E-02 | -0.3592E-02 | -0.4589E-02 | -0.1577E-02 | -0.7617E-03 | -0.3744E-04 | |
| 8 | -0.2663E-02 | -0.3446E-02 | -0.2863E-02 | -0.5637E-02 | -0.6646E-02 | -0.2572E-02 | -0.2844E-02 | -0.4189E-02 | -0.5387E-02 | -0.1863E-02 | -0.8936E-03 | -0.4490E-04 | |
| 9 | -0.2887E-02 | -0.3737E-02 | -0.3111E-02 | -0.6143E-02 | -0.7304E-02 | -0.2834E-02 | -0.3140E-02 | -0.4653E-02 | -0.6008E-02 | -0.2086E-02 | -0.9941E-03 | -0.5048E-04 | |
| 10 | -0.2968E-02 | -0.3844E-02 | -0.3205E-02 | -0.6343E-02 | -0.7567E-02 | -0.2941E-02 | -0.3261E-02 | -0.4842E-02 | -0.6264E-02 | -0.2178E-02 | -0.1035E-02 | -0.5272E-04 | |
| 11 | -0.2897E-02 | -0.3755E-02 | -0.3135E-02 | -0.6217E-02 | -0.7414E-02 | -0.2884E-02 | -0.3199E-02 | -0.4743E-02 | -0.6137E-02 | -0.2134E-02 | -0.1016E-02 | -0.5158E-04 | |
| 12 | -0.2709E-02 | -0.3515E-02 | -0.2938E-02 | -0.5834E-02 | -0.6926E-02 | -0.2695E-02 | -0.2990E-02 | -0.4411E-02 | -0.5700E-02 | -0.1979E-02 | -0.9466E-03 | -0.4767E-04 | |
| 13 | -0.2373E-02 | -0.3084E-02 | -0.2582E-02 | -0.5127E-02 | -0.6022E-02 | -0.2341E-02 | -0.2595E-02 | -0.3788E-02 | -0.4874E-02 | -0.1686E-02 | -0.8108E-03 | -0.4010E-04 | |
| 14 | -0.2027E-02 | -0.2642E-02 | -0.2213E-02 | -0.4390E-02 | -0.5076E-02 | -0.1970E-02 | -0.2181E-02 | -0.3132E-02 | -0.4001E-02 | -0.1375E-02 | -0.6592E-03 | -0.3179E-04 | |
| 15 | -0.1608E-02 | -0.2115E-02 | -0.1768E-02 | -0.3491E-02 | -0.3914E-02 | -0.1510E-02 | -0.1667E-02 | -0.2319E-02 | -0.2906E-02 | -0.9792E-03 | -0.4471E-03 | -0.2082E-04 | |
| 16 | -0.1375E-02 | -0.1841E-02 | -0.1586E-02 | -0.3019E-02 | -0.3076E-02 | -0.1166E-02 | -0.1283E-02 | -0.1721E-02 | -0.2095E-02 | -0.6700E-03 | -0.2496E-03 | -0.1251E-04 | |
| 17 | 0.0000E+00 | -0.5314E-04 | -0.5396E-05 | |
| 18 | 0.0000E+00 | -0.1058E-03 | -0.1007E-04 | |
| 19 | 0.0000E+00 | -0.3403E-04 | -0.2771E-05 | |
| 20 | 0.0000E+00 | -0.2518E-04 | -0.1080E-05 | |
| 21 | 0.0000E+00 | -0.1278E-05 | -0.9239E-07 | |
| 22 | 0.0000E+00 | -0.1040E-06 | -0.9637E-08 | |
| 23 | 0.0000E+00 | |
| 24 | 0.0000E+00 | |

REFERENCES TO CHAPTER 1

- [1.1] MATVEEV V.I., et al., Physical Grounds for Further Improvement of Fast Sodium Reactor Safety. (Proc. of the International Fast Reactor Safety Meeting, Snowbird, Utah, USA, 1990), Vol.11. Snowbird, Utah, (1990).
- [1.2] EC/IAEA Benchmark, Input Data. Obninsk Russia- (1995).
- [1.3] BARANOV O.V., ZHUKOV A.V., KOROBENIKOV V.V., POPOV E.D. Application of various codes for calculation of the BN-600 type reactor secondary circuit activity, in "Radiological safety and NPP protection", issue 2, Moscow, Energoatomizdat, (1987).
- [1.4] REICHE CHR. und a., Reaktor-Code-System RHEIN für ESER-Computer. Zfk-558 ÀW, Berlin, DDR. (1989).
- [1.5] KISLITSYNA F.A. et al, Adaptation of TRIGEX code for EC type computer, IPPE preprint N1919, (1988).
- [1.6] ABAGYAN L.P. et al, On taking resonance interlock into account when evaluating sodium reactivity coefficient of fast reactor (Bulletin of the information center on nuclear data, issue 3, Moscow, (1966).
- [1.7] OLOV V. et al, Kernenergie, Heft, Berlin, DDR,(1969), .112-118.
- [1.8] SHIKHOV S.B., TROYANSKI V.B., Nuclear Reactors Theory, v.2, Gas-kinetics theory, Moscow, Energoatomizdat, (1983).
- [1.9] GLINATSI G., BN-800 Neutronic Analysis 3-rd Consultancy Meeting on BN-800 Reactor Vienna, December 11-13, (1995).
- [1.10] FOWLER T.B., VONDY D.R., G.V.GUNNIGHAM, Cunnigham Nuclear Reactor Core Analysis Code: Citation ORNL-TM-2596, Rev.2 July (1971)
- [1.11] G. GLINATSI, BN-800/1500 MWth Core Updated Results 4-th Consultancy Meeting on BN-800 Reactor. Brussels, June 25-27, (1996).
- [1.12] BRIESMEISTER J., MCNP A General Monte Carlo Code N-Particle Transport Code, Version 4A La-12625. November (1993).
- [1.13] INTERNATIONAL ATOMIC AGENCY, Evaluation of benchmark calculations on a fast power reactor core with near zero sodium void effect (final report). \ IAEA-TECDOC-731 (1994).
- [1.14] CHEBESKOV A.N., Evaluation of sodium void reactivity on the BN-800 fast reactor design. Vol.2,(Proc. Int.Conf. «PHUSOR-96», Sept. 1996)

Chapter 2

EVALUATION OF STEADY STATE CALCULATIONS OF THE FUEL PIN BEHAVIOUR DURING POWER OPERATION IN A BN-800 LIKE REACTOR CORE

2.1 INTRODUCTION

Within the framework of the IAEA/EC comparative exercise for an evaluation of consequences of a severe accident in a BN-800 like reactor core with a near zero void coefficient, steady state calculations have been performed to study the thermal-mechanical behaviour of the fuel pin design for the three batch equilibrium cycle operation as foreseen by the project. Six countries participated in the exercise, namely Russia, France, UK, India, Germany and Japan. This summary report compares results of the different contributions to the exercise and identifies areas of modelling where uncertainties of knowledge would need more refined analyses.

2.2 BASIS OF THE CALCULATIONS

2.2.1 Case set-up

Calculations were performed on the basis of input data provided by the Institute of Physics and Power Engineering (IPPE) from Obninsk, Russia [2.1]. The fuel pin design data are given in Table 2.1. The fuel pin height consists of a 0,65 m long lower fission gas plenum followed by a 0,35 m long lower axial breeder zone. Fissile core height amounts to 0,84 m only followed by a 0,05 m long end cap region which acts as an upper axial reflector. Fissile pellets are hollow pellets with chamfered edges.

The cylindrical equivalent fissile core radius amounts to 1.1869 m which results in an H/D-ratio of 0.3538. The total thermal power output amounts to 1500 MW_{th} and the total coolant mass flow through the core is 6.027 t/s. With a core inlet temperature of 627.15 K this results in an average coolant heat-up along the core by about 190 K. The coolant pressure difference between the feeding header inlet and the argon gas plenum amounts to 0.59 MPa with a pressure drop along the fuel pin bundle length of 0.302 MPa and along the lower subassembly tail and the pin bundle inlet of 0.11 MPa.

The reactor is designed to operate on a three batch re-loading cycle, with a total residence time for a particular subassembly of 420 equivalent full power days (i.e. 3 cycles, each of length 140 days). The core wide radial power distribution is determined by the three enrichments of the fissile fuel pins which vary from 20.08% in the inner low enrichment zone (LEZ) up to 27.35% in the outer high enrichment zone (HEZ). The local power variation within the different enrichment zones is represented by the definition of representative subassembly groups (SAGs), four groups for the LEZ and three for the MEZ and the HEZ, respectively. Each of the representative SAGs are subdivided into one third portions representing the three batch loading scheme. The radial breeder zone is represented by one characteristic subassembly group with a residence time of 490 days. As consequence of this core representation we simulate the reactor core with 30 SAGs in the fissile core region and one in the radial breeder region. In Table 2.2 the following characteristic data of the case set-up are listed: SAG-number, number of SAs, their residence time, the normalized SA-power, the coolant mass flow per pin, the normalized power to flow ratio, the peak burn-up and the peak clad dose.

The clad material used for the fuel pin design shows nearly no clad swelling up to dose values of about 50 dpa/NRT. At higher dose values a considerable swelling starts which could result in reopening of the fuel clad gap. The threshold value of 50 dpa/NRT is only exceeded in the high power subassembly groups after onset of the third power operation cycle.

In addition IPPE provided experimental data and correlation's to determine the temperature dependence of clad mechanical properties as ultimate tensile strength, yield stress and failure strain. Information on dose and strain rate dependence of these data was however poor though these data are of rather large importance to predict failure conditions under transient fuel pin loading with some precision. For performance of calculations with the SAS4A- code family these experimental data were taken into consideration to modify well evaluated correlation's normally used for the type of clad material in the SAS4A code. Reliability of the correlation's used in SAS4A were qualified by numerous experiments performed within the CABRI project. Adjustment of the SAS4A correlation's to meet experimental data of the BN- 800 clad material was done by varying the strain rate as input parameter. Applying different strain rates led to results of the theoretical prediction which envelops the scatter band of experimental data as provided by IPPE.

TABLE 2.1 PIN SPECIFICATION DATA (293 K)

| | Fissile pins | Breeder pins |
|---------------------------------|---|---|
| Fuel | | |
| inner radius | 0.825 mm | 0.000 mm |
| outer radius | 2.8 mm | 6.5 mm |
| pellet length | 8 mm | 8 mm |
| chamferring | 0.25 x 0.25 mm | 0.25 x 0.25 mm |
| O/M | 1.98 | 2.00 |
| $U^{235} / (U^{235} + U^{238})$ | 0.004 | 0.004 |
| Pu/(U+PU) | 0.2008/0.2317/0.2735 | 0.00 |
| grain diameter | 11 μ m | 11 μ m |
| porosity | 4% total, comprising (guessed) 3% coarse 0.5% fine 0.5% on grain boundaries | 2.4 % total, comprising (guessed) 1.8 % coarse 0.3 % fine 0.3 % on grain boundaries |
| Fuel Stack | | |
| length of stack | 840 mm | 1840 mm |
| Clad | | |
| material | 316 cw-like | 316 cw-like |
| initial cold work strain | 20% | 20% |
| inner radius | 2.9 mm | 6.6 mm |
| outer radius | 3.3 mm | 7.0 mm |
| grain diameter | 8.5 μ m | 8.5 μ m |
| Plenum | | |
| lower plenum volume | $1.770 \times 10^{-5} \text{ m}^3$ | $4.105 \times 10^{-5} \text{ m}^3$ |
| upper plenum volume | $1.149 \times 10^{-6} \text{ m}^3$ | $8.895 \times 10^{-6} \text{ m}^3$ |
| filling gas | 95% He | 95% He |
| filling gas pressure | 0.1 MPa | 0.1 MPa |

TABLE 2.2 CORE CHARACTERIZATION AT EOEC-CONDITIONS ($P_t = 1500 \text{ MW}_{th}$; $Q_t = 6.027 \text{ t/s}$)

| SA-Group | Number of SAs | Residence Time [d] | normalized SA-power | coolant mass flow per pin $10^2[\text{kg/s}]$ | norm. power to flow ratio | peak burn-up at% | peak clad dose dpa/NRT |
|----------|---------------|--------------------|---------------------|---|---------------------------|------------------|------------------------|
| 1/1 | 10 | 141 | 0.990 | 9.808 | 0.979 | 2.8 | 29.8 |
| 1/2 | 11 | 282 | 0.962 | 9.808 | 0.951 | 5.3 | 50.0 |
| 1/3 | 10 | 423 | 0.947 | 9.808 | 0.936 | 7.8 | 72.7 |
| 2/1 | 14 | 141 | 0.970 | 9.572 | 0.982 | 2.7 | 25.3 |
| 2/2 | 14 | 282 | 0.942 | 9.572 | 0.954 | 5.2 | 49.1 |
| 2/3 | 14 | 423 | 0.927 | 9.572 | 0.939 | 7.6 | 71.4 |
| 3/1 | 12 | 141 | 0.959 | 9.476 | 0.981 | 2.7 | 25.2 |
| 3/2 | 12 | 282 | 0.932 | 9.476 | 0.953 | 5.2 | 48.7 |
| 3/3 | 12 | 423 | 0.917 | 9.476 | 0.938 | 7.5 | 70.8 |
| 4/1 | 24 | 141 | 0.947 | 9.346 | 0.982 | 2.6 | 24.8 |
| 4/2 | 24 | 282 | 0.920 | 9.346 | 0.954 | 5.1 | 48.1 |
| 4/3 | 24 | 423 | 0.905 | 9.346 | 0.939 | 7.4 | 69.9 |
| 5/1 | 24 | 141 | 1.000 | 9.711 | 1.000 | 2.6 | 24.8 |
| 5/2 | 24 | 282 | 0.973 | 9.711 | 0.971 | 5.0 | 48.0 |
| 5/3 | 24 | 423 | 0.950 | 9.711 | 0.948 | 7.3 | 69.6 |
| 6/1 | 10 | 141 | 0.945 | 9.646 | 0.950 | 2.4 | 23.5 |
| 6/2 | 10 | 282 | 0.919 | 9.646 | 0.924 | 4.7 | 45.5 |
| 6/3 | 10 | 423 | 0.898 | 9.646 | 0.902 | 6.9 | 65.9 |
| 7/1 | 12 | 141 | 0.894 | 9.457 | 0.917 | 2.3 | 22.2 |
| 7/2 | 12 | 282 | 0.870 | 9.457 | 0.892 | 4.5 | 43.1 |
| 7/3 | 12 | 423 | 0.849 | 9.457 | 0.871 | 6.5 | 62.4 |
| 8/1 | 16 | 141 | 0.934 | 9.487 | 0.954 | 2.6 | 24.8 |
| 8/2 | 16 | 282 | 0.911 | 9.487 | 0.930 | 5.0 | 48.1 |
| 8/3 | 16 | 423 | 0.890 | 9.487 | 0.910 | 7.2 | 69.7 |
| 9/1 | 26 | 141 | 0.781 | 8.767 | 0.863 | 2.1 | 20.7 |
| 9/2 | 26 | 282 | 0.761 | 8.767 | 0.841 | 4.1 | 40.2 |
| 9/3 | 26 | 423 | 0.744 | 8.767 | 0.823 | 6.0 | 58.3 |
| 10/1 | 12 | 141 | 0.618 | 7.035 | 0.851 | 1.7 | 16.4 |
| 10/2 | 12 | 282 | 0.602 | 7.035 | 0.830 | 3.3 | 31.8 |
| 10/3 | 12 | 423 | 0.589 | 7.035 | 0.811 | 4.7 | 46.1 |
| 11 | 84 | 490 | 0.183 | 12.432 | 0.111 | 0.2 | 13.2 |

Tensile properties of the non irradiated clad material

As can be seen in Fig. 2.1 experimental data of the ultimate tensile strength and of the yield stress are available at a temperature range between 20°C up to 800°C. These data show a scattering around average values of about 10 %. Failure strain data for low strain rate show a much more pronounced scattering in the considered temperature domain (see Fig. 2.2).

Tensile properties of the irradiated clad material

Two correlation's were provided for the temperature dependence of the ultimate tensile strength and the yield strength respectively (see Fig. 2.1). They indicate considerable strain hardening especially for low clad temperatures. Failure strain data for the irradiated clad material were not made available.

In the SAS4A code several correlation's are provided for the temperature dependence of the yield strength and the ultimate tensile strength of different clad materials. These correlation's have been deduced from an extensive experimental data base including measurements for irradiated clad material. For part of these experimental campaigns influence of the strain rate on yield strength and ultimate tensile stress has been investigated. When comparing results of the different correlation's with the experimental results provided for the BN-800 clad material it appears that the correlation's

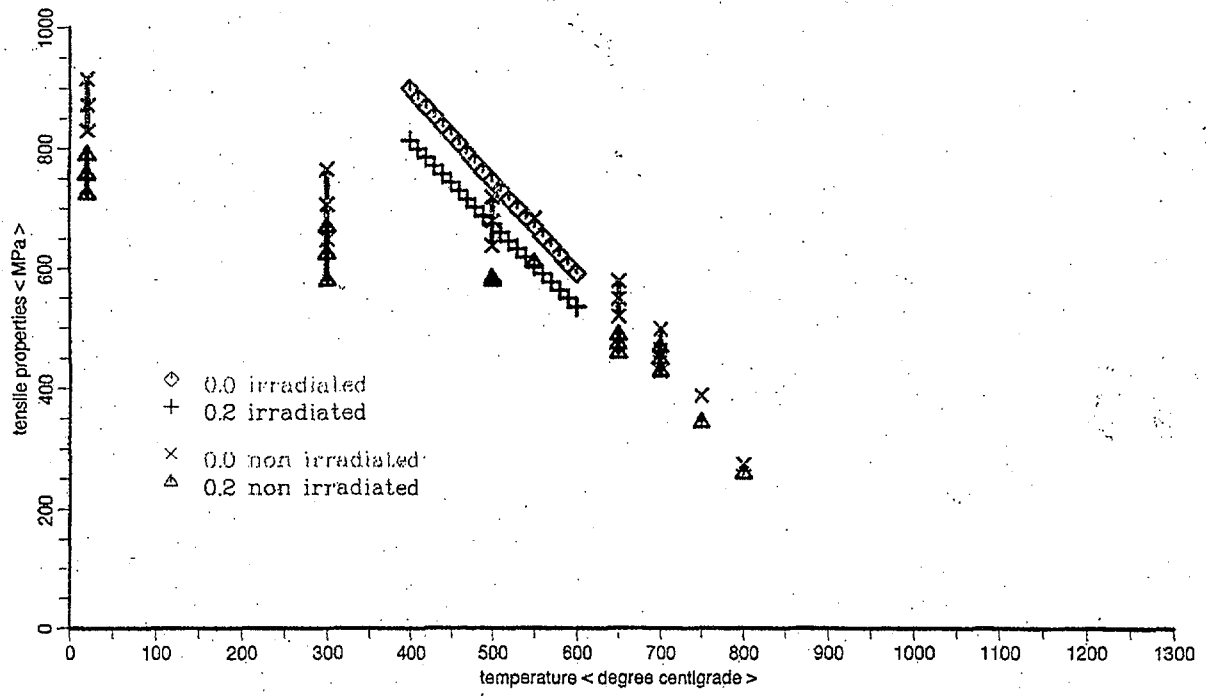


FIG. 2.1. BN-800 tensile properties [MPa] (ultimate tensile strength and yield stress) of irradiated and non-irradiated materials versus temperature [°C].

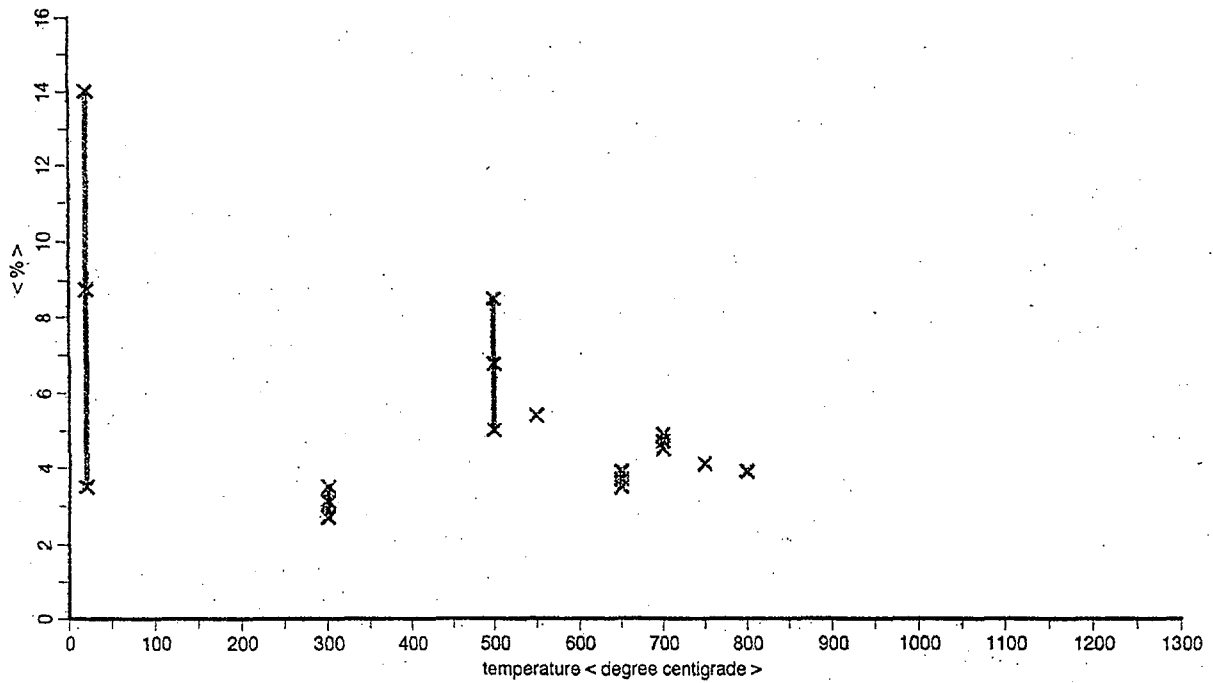


FIG. 2.2. BN-800 failure strain [%] of non-irradiated materials versus temperature [°C].

deduced for the 15/15 Ti stabilised clad material compares best with the provided experimental data of the BN-800 clad material (see Fig. 2.3 and 2.4). Ultimate tensile stress data for high strain rates (10/s) and for low strain rates (10^{-4} /s) bound the scatter band of experimental results of the BN-800 clad material. However, the yield stress data are consistently below measurements for the BN-800 clad material. Failure strain data represent well the average of the scatter band of measurements for the BN-800 clad material when compared to the correlation's used in the SAS4A code (see Fig. 2.5).

Therefore use of the mentioned SAS4A correlation's represent a reasonable approximation of the expected behaviour of the BN-800 clad material. However, some concern was raised whether dose dependence of mechanical clad properties might change compared to the theoretically predicted behaviour when approaching higher dose values. In view of the reported clad swelling behaviour it is expected that failure strain as well as ultimate tensile stress might reduce considerably on the background of knowledge deduced from the behaviour of other clad materials. It is recommended to evaluate this aspect in subsequent analyses campaigns in more depth.

For comparison of the fuel pin states at the end of the three different power operation cycles three positions out of the 10 characteristic subassembly groups were chosen: the highest rated subassembly group of the LEZ i.e. SA group 1/3, the medium rated subassembly group of the MEZ i.e. SA group 6/3 and the lowest rated subassembly group of the LEZ i.e. SA group 10/3. The variation of the linear rating with the residence time was deduced from the input data specification provided by IPPE. This agreed upon procedure resulted in the power history for the three SA groups as listed in Table 3.3. However, it turned out that the total thermal power output did not perfectly match the value of $1500 \text{ MW}_{\text{th}}$ as specified by IPPE. Therefore, two different sets of variations of linear ratings with the residence time were used by the participants: one resulting in a total thermal power output of about $1725 \text{ MW}_{\text{th}}$ (KONDOR, PINCH, GERMINAL) and one resulting in a value of $1525 \text{ MW}_{\text{th}}$ (SAS4A, GERMINAL). The GERMINAL calculations provided results for both cases. In addition it has to be mentioned that this procedure was agreed upon by the participants of the exercise only after some iterations. The contribution by the UK participant is based on a specification of the power dependency with time which corresponds to an initially agreed procedure and therefore is slightly different than the one applied at the end of this exercise by the other participants (see Table 2.3).

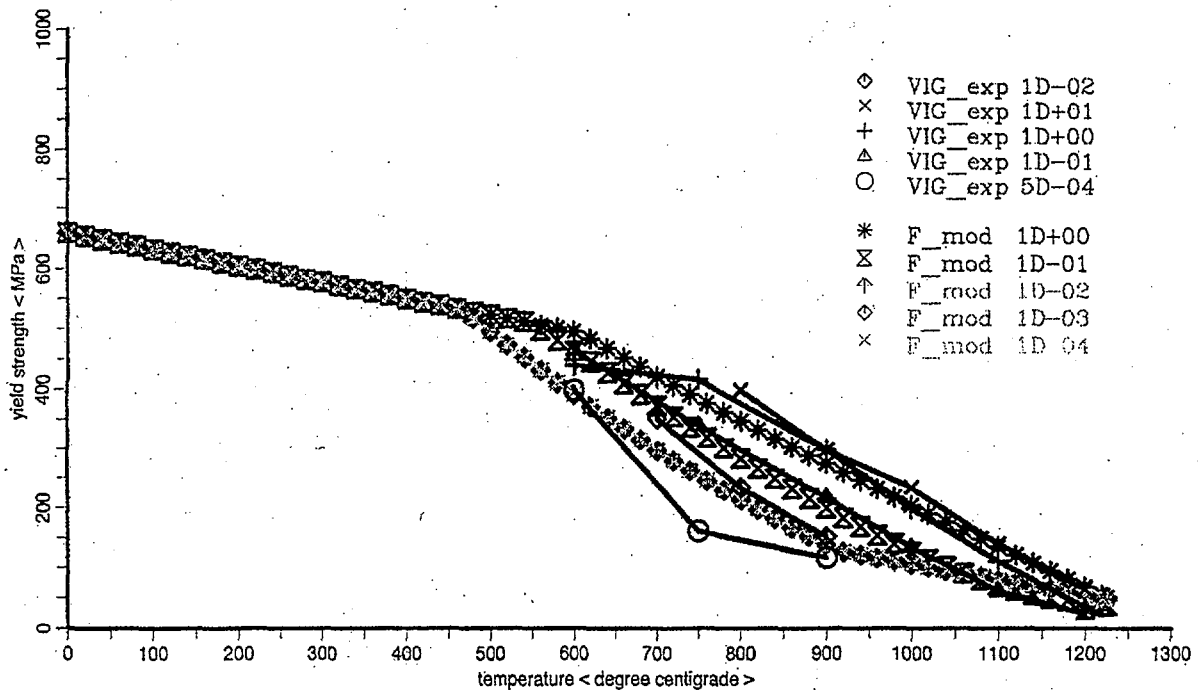


FIG. 2.3. Correlations evaluated in the SAS4A code for validation of the VIGGEN-4 experiments (yield stress).

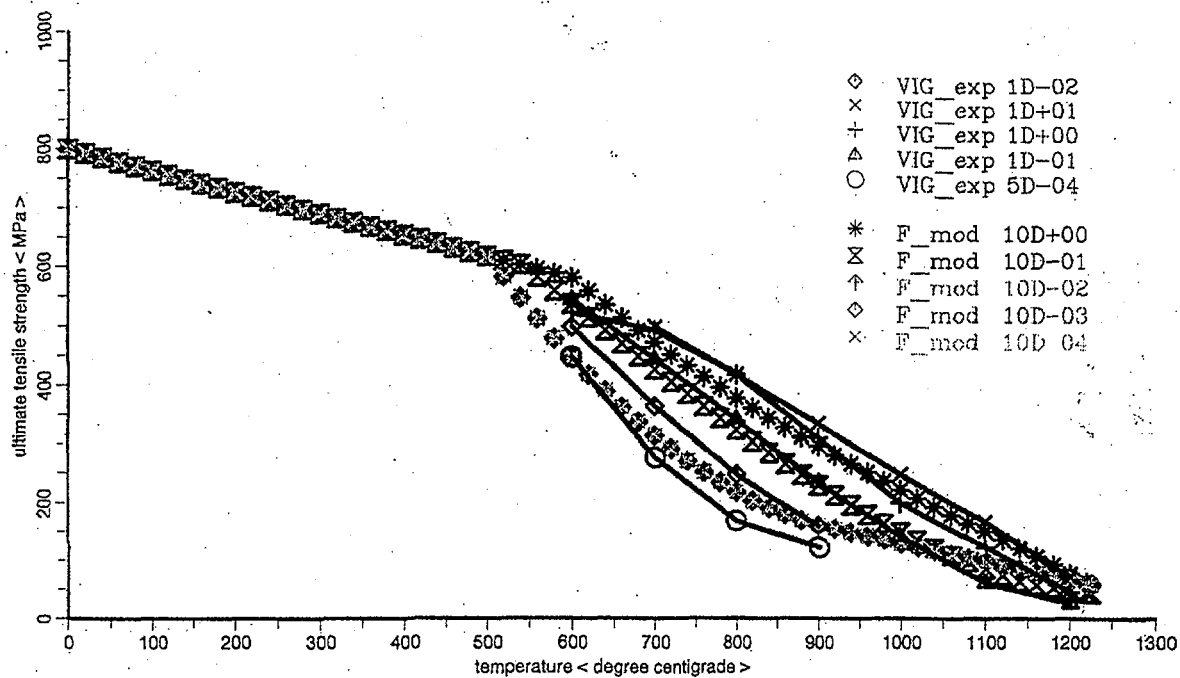


FIG. 2.4. Correlations evaluated in the SAS4A code for validation of the VIGGEN-4 experiments (ultimate tensile strength).

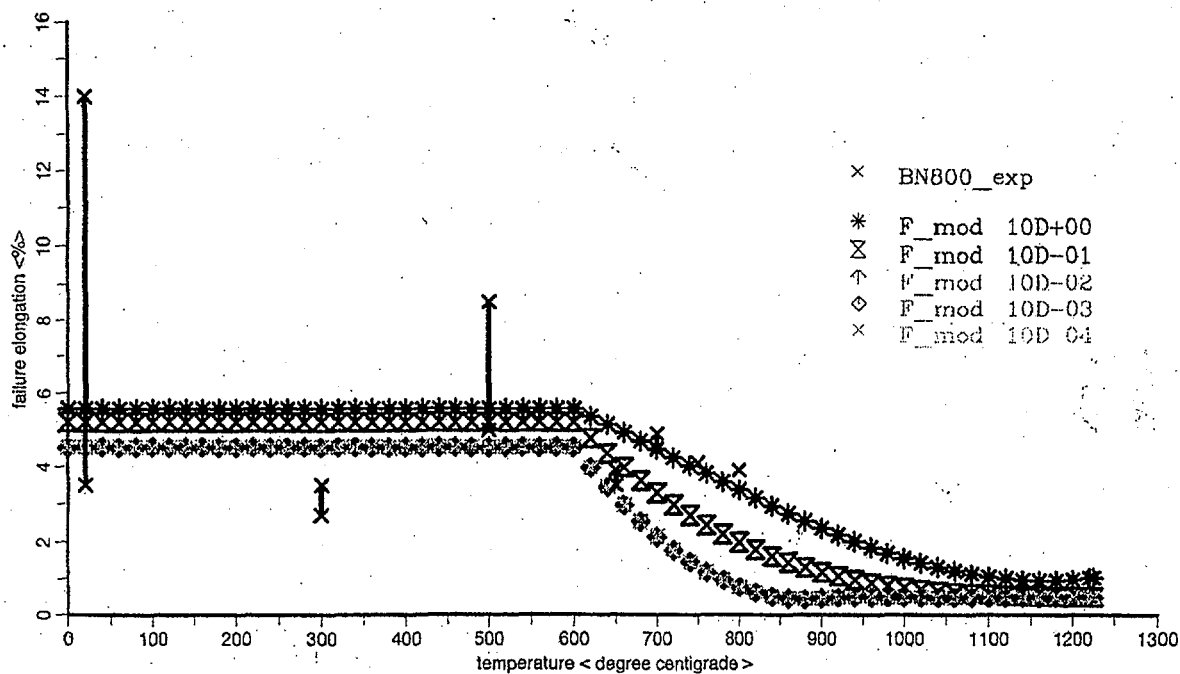


FIG. 2.5. Correlations evaluated in the SAS4A code for validation of the VIGGEN-4 experiments (failure strain).

TABLE 2.3 VARIATION OF PEAK LINEAR RATINGS DURING POWER OPERATION

| Residence time | Cycle | Channel 1/3 [kW/m] | | | Channel 6/3 [kW/m] | | | Channel 10/3 [kW/m] | | |
|-------------------|-------|--------------------|----------------|----------------|--------------------|----------------|----------------|---------------------|----------------|----------------|
| | | I | II | III | I | II | III | I | II | III |
| 1 141 | I | 44.16 40.20 | 42.11 37.96 | 40.25 35.77 | 31.95 33.47 | 35.03 36.62 | 33.43 34.44 | 26.61 24.82 | 25.91 24.04 | 24.46 22.44 |
| 142 282 | II | - 36.24 | 40.20 36.24 | 37.95 33.86 | - 35.00 | 33.47 35.00 | 31.58 32.60 | - 23.03 | 24.82 23.03 | 23.15 21.23 |
| 283 423 | III | | 38.85 35.3 | 36.17 32.26 | - 36.52 | 32.08 33.54 | 29.82 30.80 | - 21.23 | 23.82 22.10 | 21.92 20.08 |

I power history specified in the initial phase of the exercise
(TRAFIC-results)

II power history leading to a total reactor power of 1725 MW_{th}
(KONDOR-, GERMINAL-, PINCH-results)

III power history leading to a total reactor power of 1525 MW_{th}
(GERMINAL SAS4A-results)

2.2.2 Characterization of the applied fuel pin mechanics code packages

Different tools were applied by the participants to this exercise. They will shortly be characterized hereafter and compared with each other.

France applied the computer code GERMINAL 1.2 which is part of the French licensing procedure [2.2]. The code is developed by CEA/DEC to study the fuel pin thermal-mechanical behaviour during steady state and incidental conditions in Fast Breeder Reactors. This version includes the modelling of high burn-up effects on the fission gas release and fuel-clad materials accumulation („joint oxyde gaine“ JOG). This code version has been validated on 29 irradiations corresponding to various experimental conditions: solid and annular pellets, burn-up's from 0 to 20 at%, stoichiometries from 1.90 to 1.999, enrichments between 15 and 30% Pu, different clad materials and so on. GERMINAL 1.2 is a highly sophisticated fuel pin mechanics code package with a broad background of experimental qualification.

The UK applied the latest version of the TRAFIC fuel pin performance code TRAFIC 2.6 [2.3]. The TRAFIC code package is a highly sophisticated fuel pin mechanic code as the GERMINAL 1.2 code. It was developed by AERE Winfrith and continuously validated against a number of irradiation experiments.

Germany applied the SAS4A code package with its parametric fuel pin performance model DEFORM-4C [2.4] developed mainly by Forschungszentrum Karlsruhe on basis of the original approach provided by the Argonne National Laboratory. The code package is validated against 5 irradiation experiments performed within the different CABRI-programmes. These cover solid and annular pellets behaviour of burn-up's from 0 to 12 at% and different clad materials. A parametric approach to simulate the fuel to clad materials behaviour (JOG-materials) is included.

Russia applied their KONDOR code package [2.5] which is a detailed fuel pin performance code developed by IPPE. Qualification of the models is mainly based on results being available in the open literature.

India applied their PINCH code package [2.6] which is a parametric fuel pin performance code developed by IGCAR on the basis of modelling approaches being available in the open literature. Integral validation of the code against irradiation experiments is hardly available.

All code packages applied in this comparative exercise represent the dominant physical processes governing the fuel pins behaviour during irradiation however with a different degree of detail. When trying to characterize the modelling features applied by the different participants in the exercise the following ranking of modelling features could be used:

- D - detailed deterministic model
- P - parametric model approach
- S - simplified model approach

This type of ranking has been used to characterize model features of the different code packages to simulate the solid fission product swelling, the fission gas induced fuel swelling, the JOG-materials behaviour, the fuels thermal behaviour, the fission gas release, the fuels mechanics behaviour, the clad swelling behaviour, the clad mechanics behaviour and the fuel to clad heat transfer. Results of this agreed upon ranking are listed in table 2.4. This overview on model features indicates that the codes used in this comparison cover the whole spectrum of currently available model capabilities ranging from detailed deterministic model approaches realized in codes as GERMINAL and TRAFIC up to simplified parametric approaches as the ones of SAS4A and the PINCH code. The approaches of KONDOR are somewhere in between these two modelling approaches.

TABLE 2.4 OVERVIEW ON MODELLING ASPECTS OF THE APPLIED CODE SYSTEMS

| Code system | TRAFIC | GERMINAL | KONDOR | SAS4A | PINCH |
|-----------------------------------|-------------|------------------|----------------|----------------|----------------|
| Solid fission product swelling | S | S | IPPE law | S, P | IPPE law |
| Fission gas induced fuel swelling | D | D | IPPE law | P | IPPE law |
| JOG-materials behaviour | not applied | D | - | P | - |
| Fuels thermal behaviour | D | D | D | D | D |
| Fission gas release | D | D | P | P | P |
| Fuels mechanics behaviour | D | D | D | S | S |
| Clad swelling law | 15/15 | IPPE | IPPE | IPPE | IPPE |
| Clad mechanics behaviour | D | D | D | S | S |
| Fuel to clad heat transfer | D | D | D | D | S |
| Power operation history | L | T ^{1,2} | T ² | T ¹ | T ² |

D - detailed deterministic model;
P - parametric model;
S - simplified model approach

L - linearized power history (2nd Consultancy)
T - tooth like power history (3rd Consultancy)
¹ scaled to a total power output of 1552 MW_{th}
² scaled to a total power output of 1725 MW_{th}

2.3. SUMMARY OF RESULTS

Individual results provided by the different participants of this exercise are documented in detail in several reports [2.7, 2.8, 2.9, 2.10, 2.11]. In this summary report only a few aspects of the calculated results are compared with each other and are commented. It concentrates on the fuels thermal behaviour with burn-up, the fission gases behaviour and the clad materials behaviour. The individual results obtained at the peak power position are plotted as function of the residence time in the reactor and compared with each other.

2.3.1 Fuels thermal behaviour

The fuels thermal state is characterized by the evolution of inner and outer fuels temperatures at the peak power position and the temperature difference between inner and outer fuel temperatures in the three representative subassembly groups. The respective values are plotted in Fig. 2.1-2.3, 2.4-2.6 and 2.7-2.9.

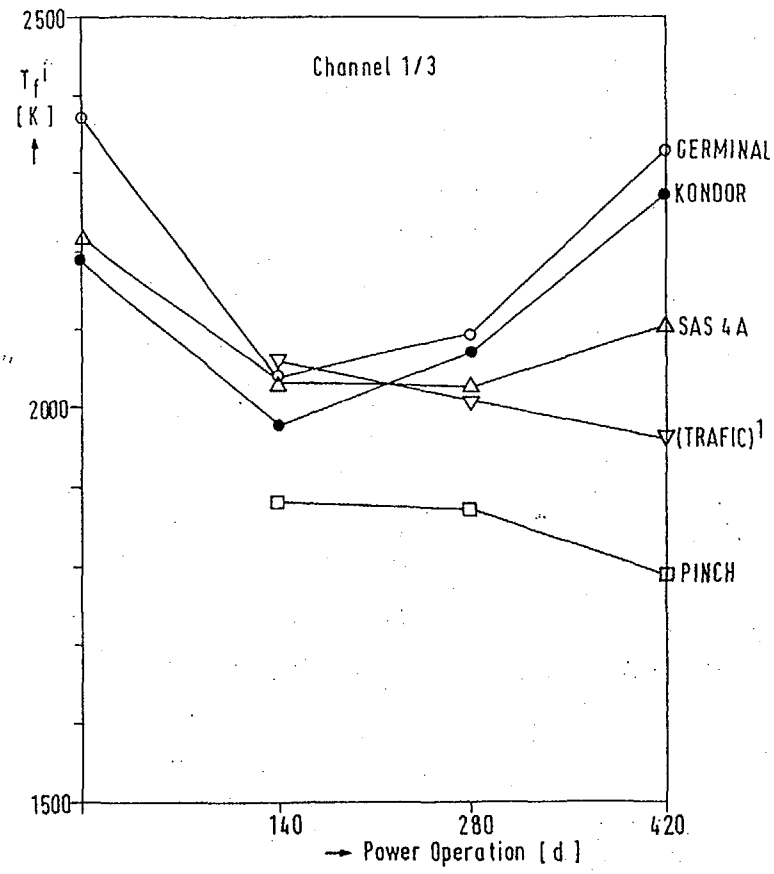
For the high power SAs of channel 1/3 the calculated inner fuel temperatures of GERMINAL, KONDOR and SAS4A are relatively close together decreasing during the first cycle by about 200 to 300 K (see Fig. 2.6). They stay nearly unchanged during the second cycle and increase during the third cycle again but more strongly in the GERMINAL and KONDOR calculations. These differences are related to the fact that gap size variation after onset of clad swelling is calculated differently in the three calculations. The calculated inner fuel temperatures of the PINCH calculation are lower than the ones calculated by the other participants. A more detailed comparison of the TRAFIC results with the other contributions is difficult due to the different power history applied.

The temperature evolution for the medium power SAs of channel 6/3 in the different cycles look similar to the ones of the high power channel 1 (see Fig. 2.7). However, the inner fuel temperature variations are not so pronounced because of the slightly reduced linear ratings and the increase of the linear rating during the cycle length. The linear ratings at the end of the cycles are close to the values obtained at the end of the cycles for the high power SAs. The absolute values of the inner fuel temperatures are therefore quite close together in the GERMINAL, KONDOR and SAS4A calculations. The same holds for the PINCH calculation but the inner fuel temperatures are again considerably lower than the ones calculated by the other participants.

The inner fuels temperature level for the low power SAs of channel 10/3 is considerably lower than the ones of the other two channels considered in this comparative evaluation (see Fig. 2.8): The calculated values of GERMINAL and SAS4A are close together, the ones of KONDOR and PINCH are lower by about 150 to 300 K.

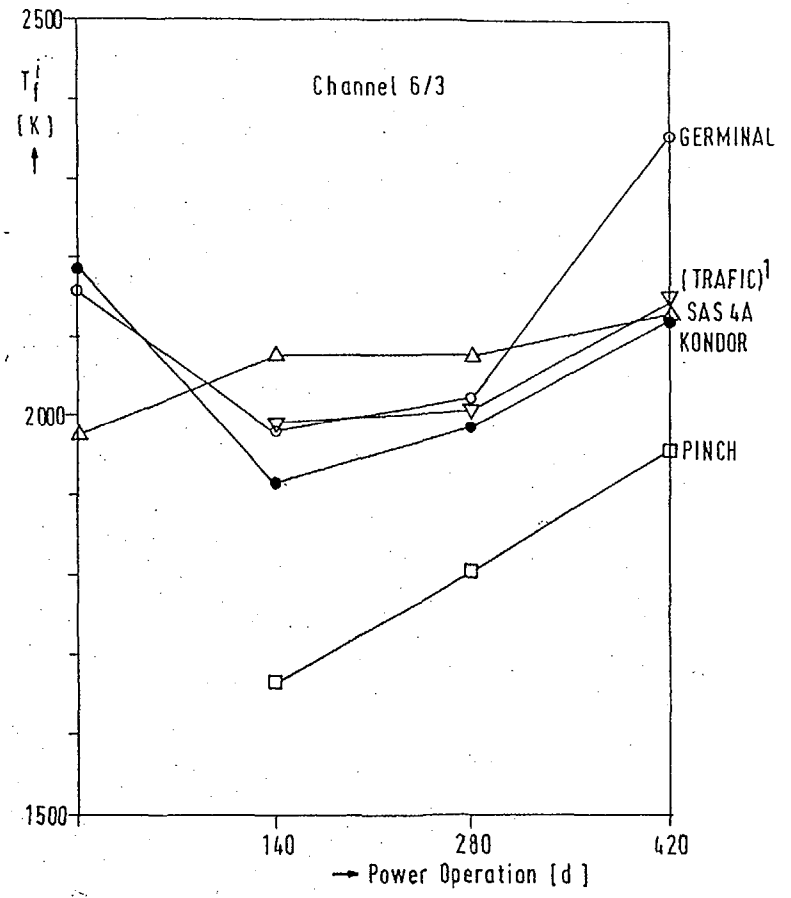
The variation of the outer fuel surface temperatures in the three representative coolant channels during power operation are plotted in Fig. 2.9-2.11. The values as calculated by SAS4A are principally higher than the ones calculated by the other codes because they calculate the effect of JOG-formation and of surface roughness differently what influences the fuel to clad heat transfer coefficient from the very beginning of power operation. In the GERMINAL calculation JOG-formation is assumed to start only after a burn-up value of about 6 at% is exceeded which is consistent with experimental observations.

Common to the calculations is the fact that the fuel surface temperatures stay relatively constant during the first two cycles of the three batch power operation cycles. However, the fuel surface temperatures increase considerably during the third cycle of the power operation in the two high power and medium power coolant channels because clad swelling results in a partial reopening of the fuel to clad gap in the GERMINAL and the KONDOR calculations. Fuel surface temperature increases are more pronounced in the GERMINAL calculation than in the SAS4A calculation because the calculated reopening of the fuel to clad gap is more pronounced in the GERMINAL calculation than in the SAS4A calculation. The effect is not to be seen in the TRAFIC calculation because this



¹ different power history, different clad swelling law

FIG. 2.6. Inner fuel temperature at PPN.



¹ different power history, different clad swelling law

FIG. 2.7. Inner fuel temperature at PPN.

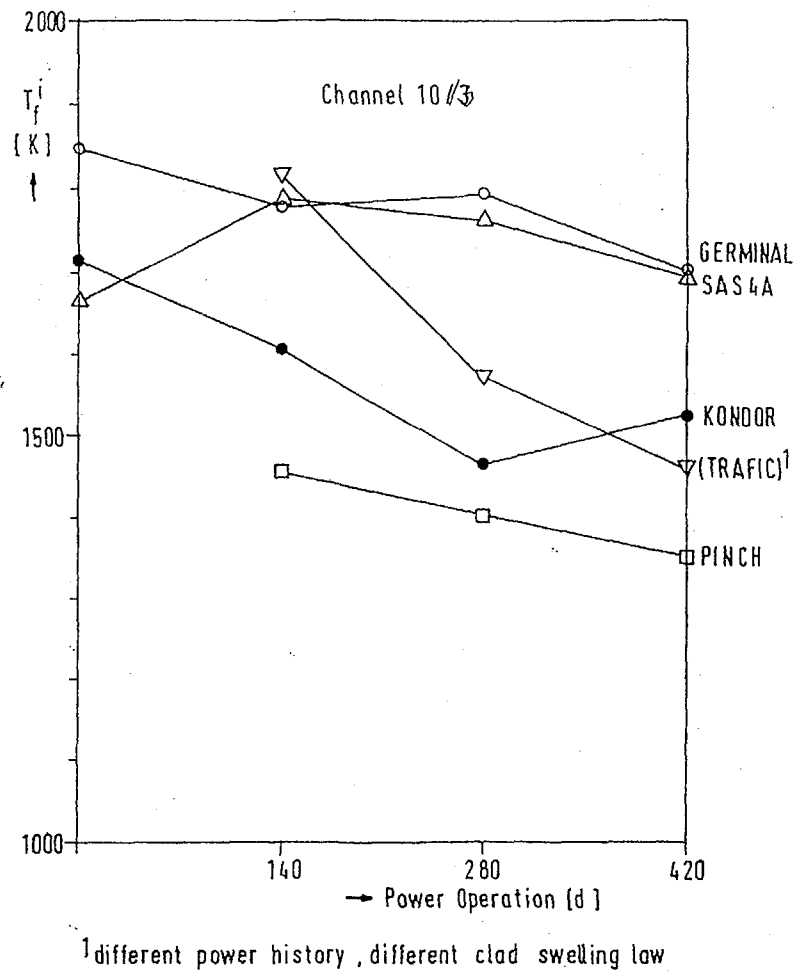


FIG. 2.8. Inner fuel temperature at PPN.

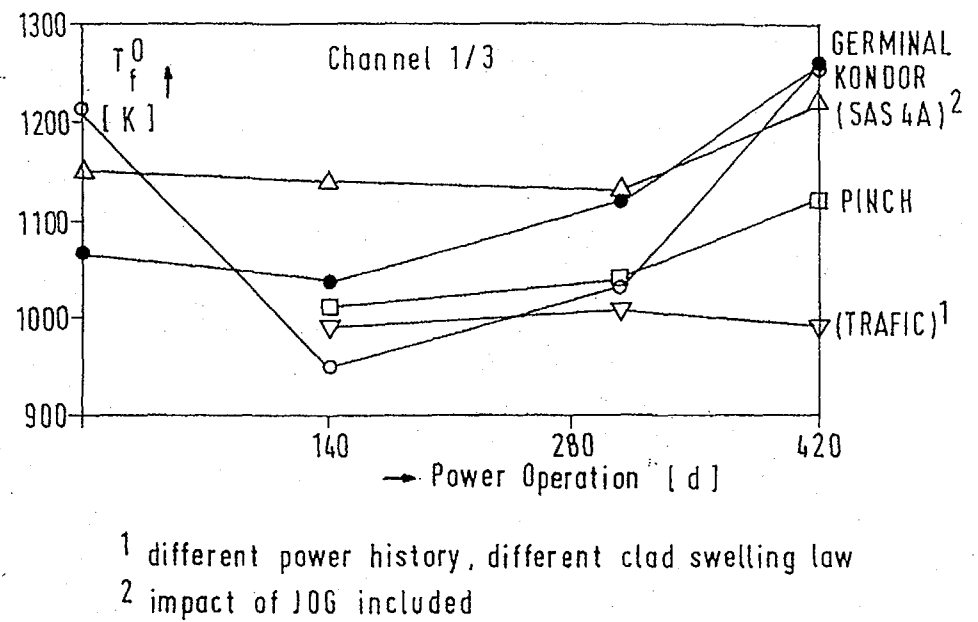
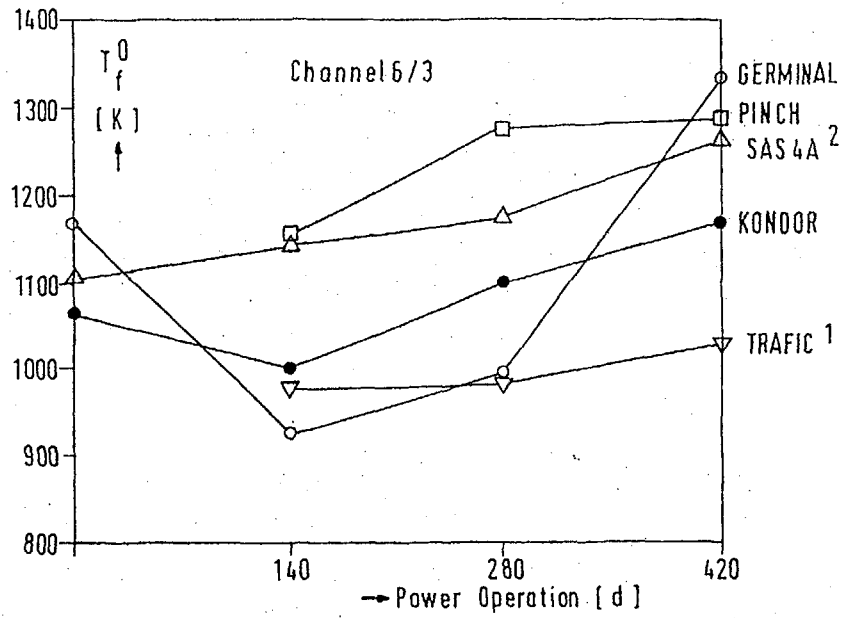
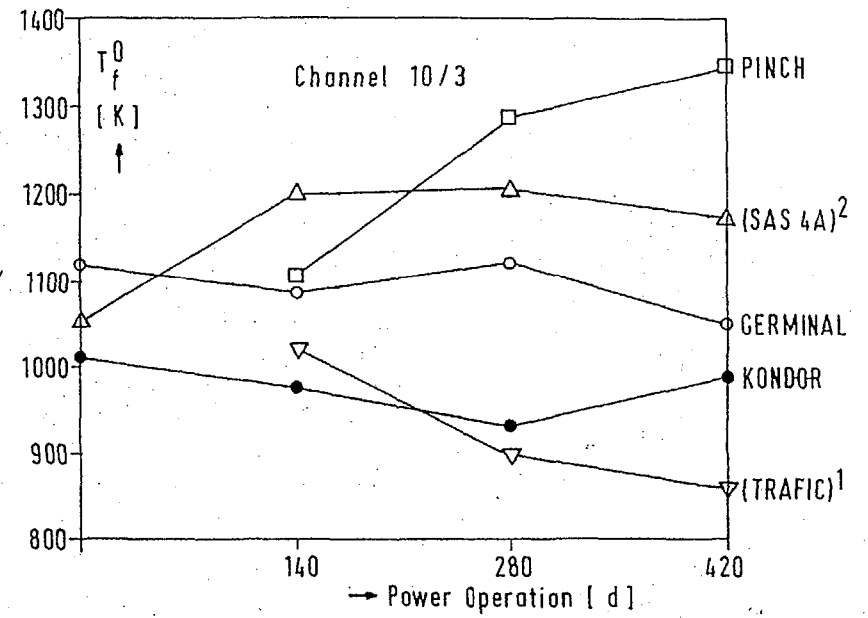


FIG. 2.9. Fuel outer surface temperature at PPN.



1 different power history, different clad swelling law
 2 impact of JOG included

FIG. 2.10. Fuel outer surface temperature.



1 different power history, different clad swelling law
 2 impact of JOG included

FIG. 2.11. Fuel outer surface temperature.

calculation is based on the assumption that a low swelling clad material is used in the design and a slightly different power history is applied. In the results of the PINCH calculation this marked influence of the clad swelling behaviour on the fuel surface temperatures is not represented. The effect does not appear in the results of the low power coolant channel 10/3 because the accumulated dose of the clad material does not exceed the threshold value of the pronounced clad swelling onset.

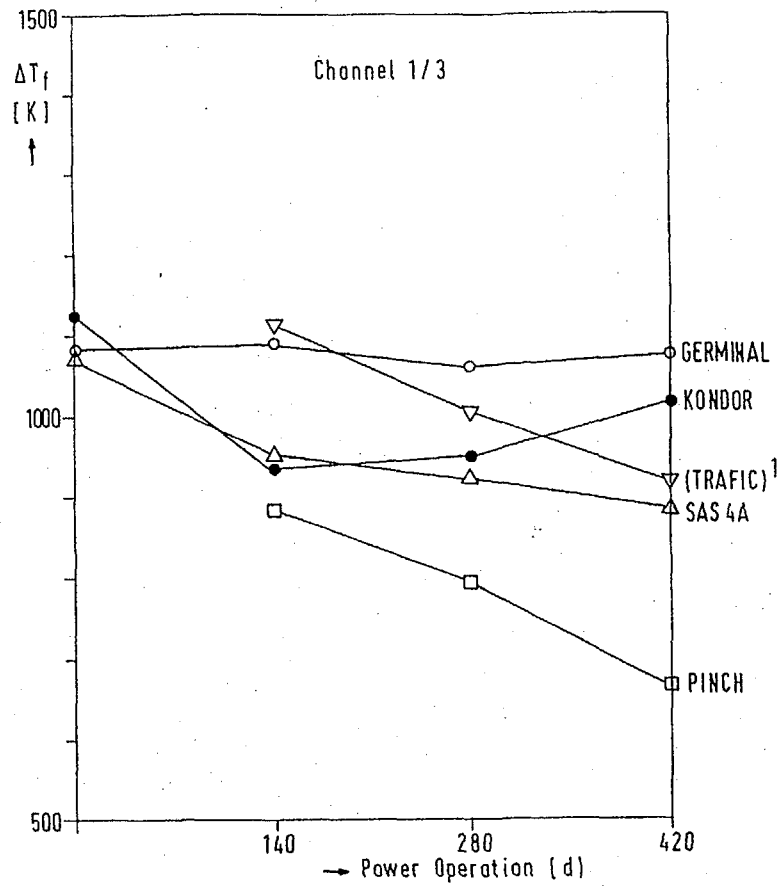
The variation of the fuels temperature difference between the inner and the outer fuel temperatures in the peak power node is plotted in Fig. 2.12-2.14 versus power operation time. This value is an indicator for the impact of transient variation of the radial fuel porosity distribution and thus the fuel conductivity on the radial fuel temperature profiles. These values stay nearly constant in the calculations performed with GERMINAL, KONDOR and SAS4A. However, they decrease continuously in the calculations performed with TRAFIC and PINCH. This behaviour reflects the impact of the difference in the imposed power variation during the cycles operation in case of the TRAFIC calculation but it is clearly indicating that PINCH contains either a coding error or a basic model deficiency because the fuel temperature differences reduce to zero in case of the low power channel 10/3 which is simply wrong. The differences in the calculations amount to about 100 to 150 K with an increasing tendency for the lower power coolant channel 10/3. This reflects the fact that predictive capabilities of the fuel pin behaviour during power operation are less reliable in the low fuel temperature domain than in the high power domain with currently available computer codes. However, if the differences are put into relation to the value of the total fuel temperature difference, the deviation of results could be interpreted as a ± 5 to 10% accuracy of our current predictive capability for the fuel temperature difference along pellet radius. This is felt satisfactory in view of the complexity of the involved physical phenomena and the different complexity of the codes participating in this exercise.

2.3.2 Fuel to clad heat transfer

The variation of the fuel to clad heat transfer coefficients in the peak power node of the three characteristic coolant channels is plotted in Fig. 2.15 to 2.17. The timely variation of the calculated results show rather large differences between the different codes, especially for the first two cycles of the power operation in the high power coolant channels. The SAS4A code calculates the lowest values especially at the beginning of the second cycle of the power operation period. This reflects the fact that closure of the initially open fuel to clad gap takes longer in this calculation than in the GERMINAL or TRAFIC calculations. For subsequent power operation cycles the calculated values come closer to each other considering results of the GERMINAL, KONDOR and SAS4A codes. Due to the different power operation history and the different clad swelling behaviour simulated in the TRAFIC calculation values of the TRAFIC calculation are systematically higher than in the other calculations. Results of the PINCH calculations are systematically higher than the other ones too which seems curious in view of the calculated high fission gas release values (see chapter 2.3.3).

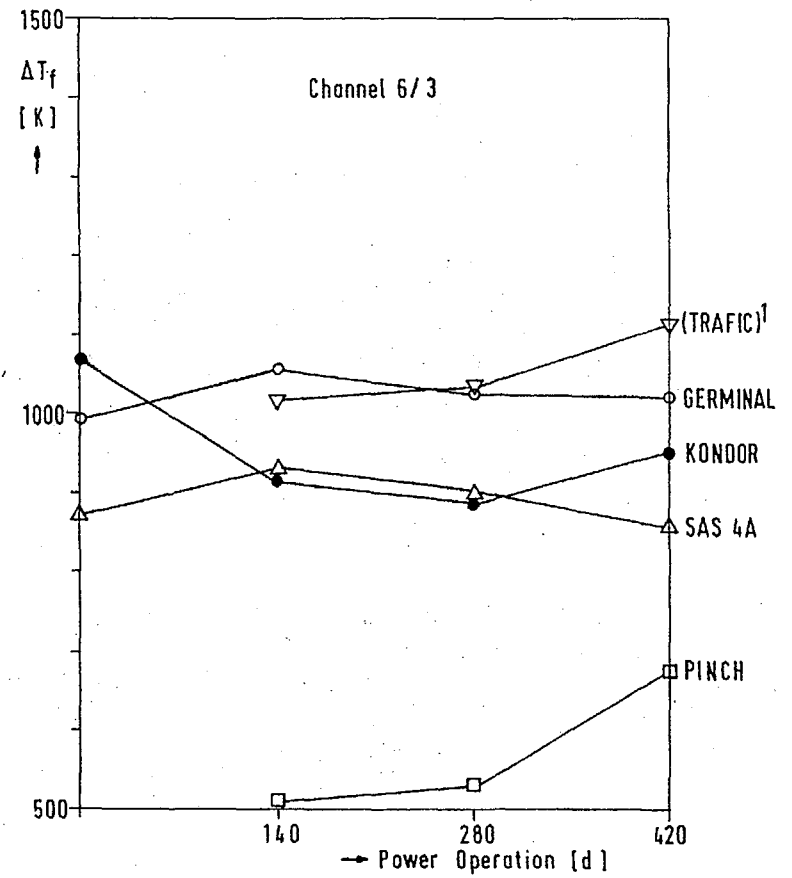
Results for the low power coolant channel of GERMINAL and SAS4A are close together. They show no pronounced dependency on the power operation period due to the fuel to clad width staying open during the whole power operation time period. The respective values of the KONDOR calculation stay considerably above these values. Consequently the calculated fission gas release remain small during the whole low power operation time period. The values calculated by TRAFIC increase systematically with time which is consistent with the applied power operation history and the clad swelling law.

Absolute and relative deviations between the differently calculated fuel to clad heat transfer coefficients are considerably higher than the ones observed for the fuel temperatures. Relative deviations amount to ± 15 to 30 % becoming largest after the first power cycle operation time period. This reflects the fact that different modelling features are used in the codes for the initial phase of fuel swelling at low burn-up values. For higher burn-up values the fuel swelling behaviour comes closer to each other in the different calculations thus reducing the intermediately large differences to values in the order of ± 10 to 15%.



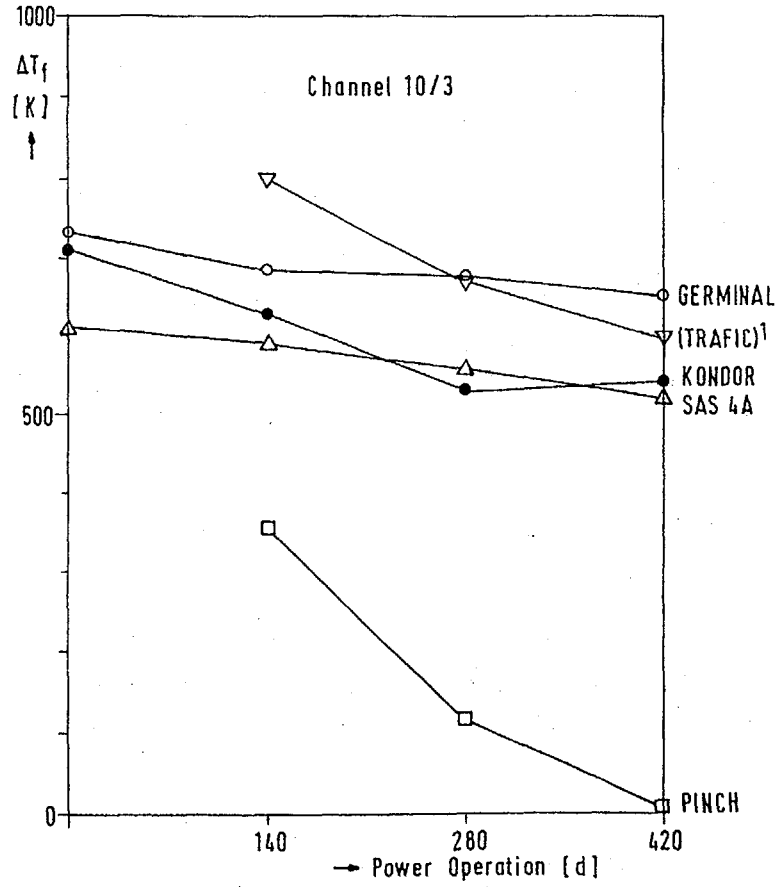
¹ different power history, different clad swelling law

FIG. 2.12. Fuel temperature difference at PPN.



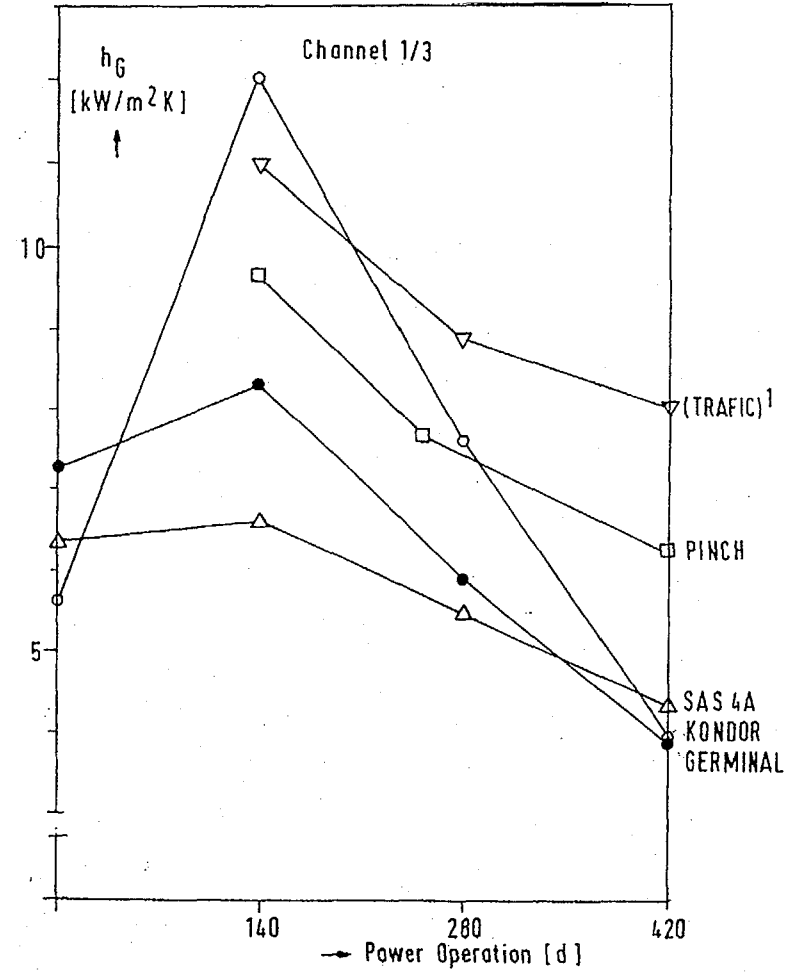
¹ different power history, different clad swelling law

FIG. 2.13. Fuel temperature difference at PPN.



¹ different power history, different clad swelling law

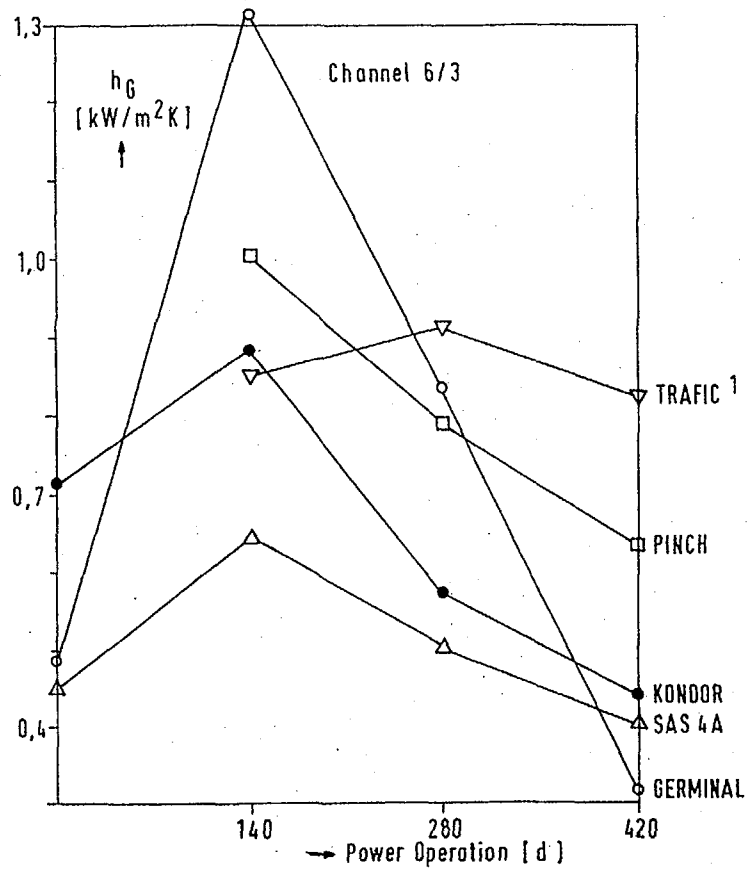
FIG. 2.14. Fuel temperature difference at PPN.



¹ different power history, different clad swelling law

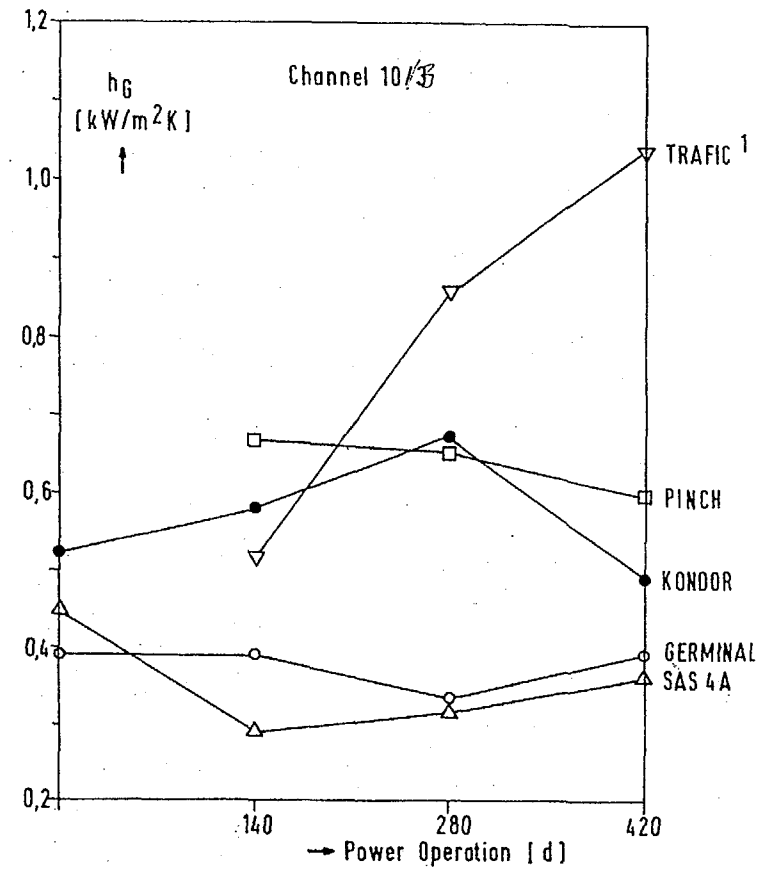
FIG. 2.15. Gap conductance at PPN.

Gap Conductance at PPN



¹ different power history, different clad swelling law

FIG. 2.16. Gap conductance at PPN.



¹ different power history, different clad swelling law

FIG. 2.17. Gap conductance at PPN.

2.3.3 Fission gas release during power operation

The integrated fission gas release fraction as function of the power operation time is plotted in Fig. 2.18 to 2.20 as provided by GERMINAL, TRAFIC, KONDOR and SAS4A. The respective values of the PINCH calculation represent the fission gas release fraction in the peak power node.

Results of the GERMINAL and SAS4A calculations for the representative coolant channel 1/3 are close together for the first two power operation cycles. During the third power operation cycle the calculated incremental increase of the GERMINAL calculation exceeds the one of the SAS4A calculation due to the calculated gap reopening during this third cycle as consequence of the enhanced clad swelling. The fractional fission gas release as calculated by the KONDOR code increases nearly linearly with power operation time. This indicates that modelling of the fission gas release is not deterministically coupled to the actually established fuel temperature level. The results provided by the TRAFIC calculation reflect the differences of the case set-up forming the basis for this calculation with its monotonically varying power versus power operation time and applying a clad swelling law leading to a small clad swelling only. The calculated dependency of the integral fission gas release of the medium power coolant channel 6/3 show a very similar behaviour.

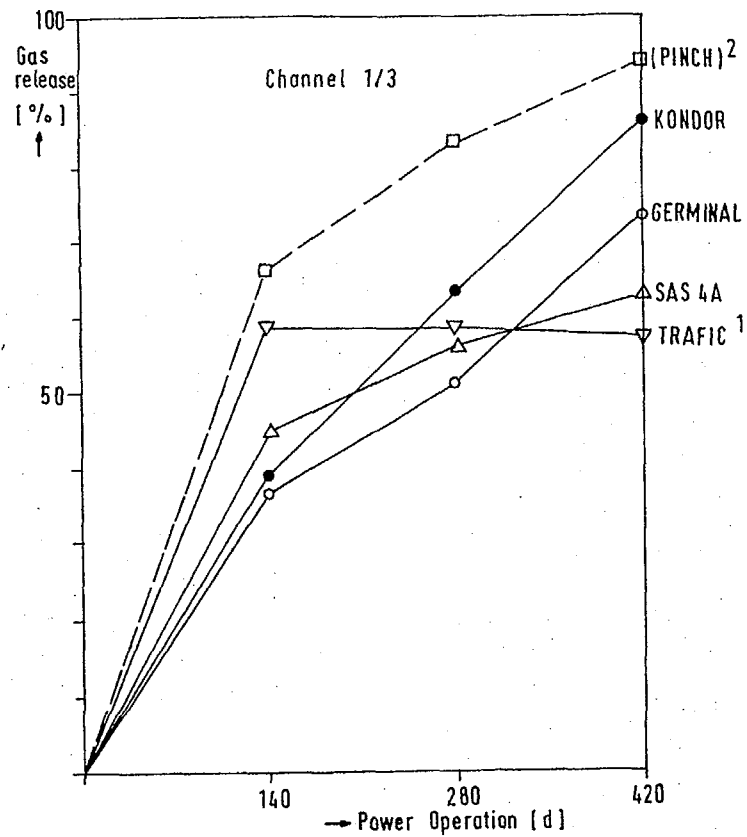
The fractional fission gas release variation with power operation time of the coolant channel 10/3 shows a different behaviour. In the GERMINAL and SAS4A calculation the fractional gas release increases nearly monotonically with power operation time reaching a maximum value of only about 47% after 420 d. The fractional gas release values calculated by the KONDOR code are considerably smaller not exceeding values of 20% during the first two power operation cycles. These values seem to be exceptionally low when compared to the results of the other calculations but they correspond qualitatively to the low fuel temperature levels calculated for this coolant channel.

2.4 CONCLUSIONS AND RECOMMENDATIONS

In the framework of the IAEA/EC comparative exercise for an evaluation of consequences of a severe accident in a BN-800 like reactor core with a near zero void coefficient steady state calculations have been performed to study the thermal-mechanical behaviour of the fuel pin design for the three batch equilibrium cycle operation as foreseen by the project. Five countries participated in this exercise with different code systems: Russia with their KONDOR code package, France with the GERMINAL code, United Kingdom with the TRAFIC code, Germany with the DEFORM-4C code package as part of the SAS4A code and India with the PINCH code package. The different codes applied in this comparative exercise cover the whole spectrum of currently available model capabilities ranging from detailed deterministic model approaches realized in codes as GERMINAL and TRAFIC up to simplified parametric approaches as DEFORM-4C and PINCH, KONDOR being somewhere in between these two modelling approaches.

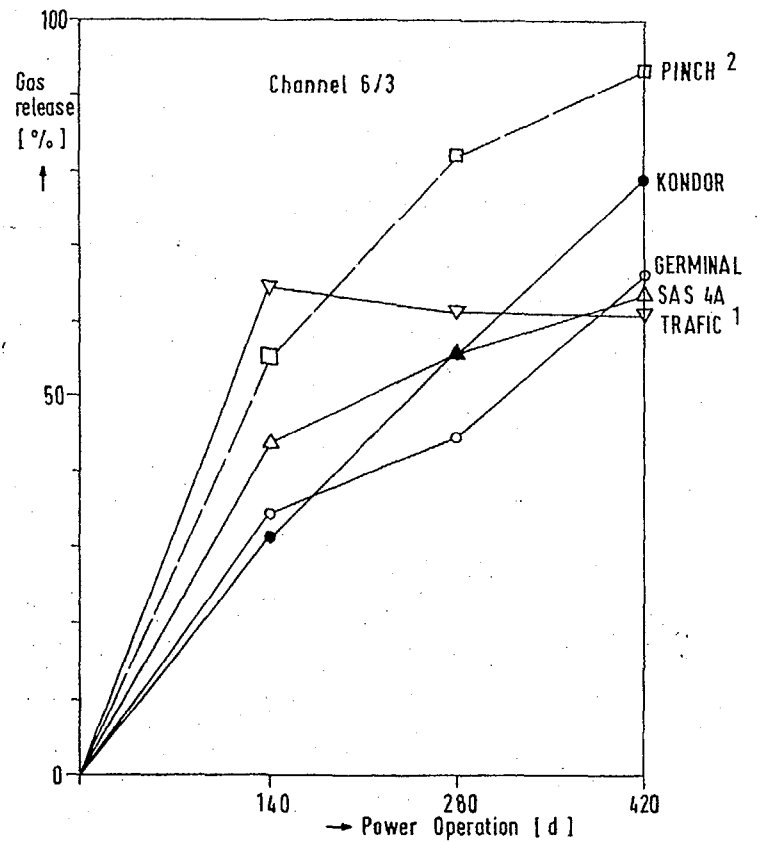
Comparison of results provided by the participants to the exercise leads to the following conclusions:

- Results of the PINCH calculations are partly apart from the ones provided by the other participants. Calculated values of the fractional fission gas releases are unreasonably high when related to the relatively low fuel temperature levels calculated. Other inconsistencies of the results might be related to the consistently too small temperature differences between the inner and outer fuel temperatures. It is felt that partly modelling assumptions are inconsistently chosen. Review and refinement of the chosen approach is strongly recommended.
- Results of the TRAFIC code calculations are difficult to compare to the results of the other participants because differences are mainly determined by the differently simulated power history for the 420 d power operation time and the simulation of a clad which leads to a low clad swelling only even for high doses. However, differences of the results to the ones of the other calculations are clearly explained by the different assumptions taken in the case set-up which were agreed upon at an early stage of the comparative exercise.



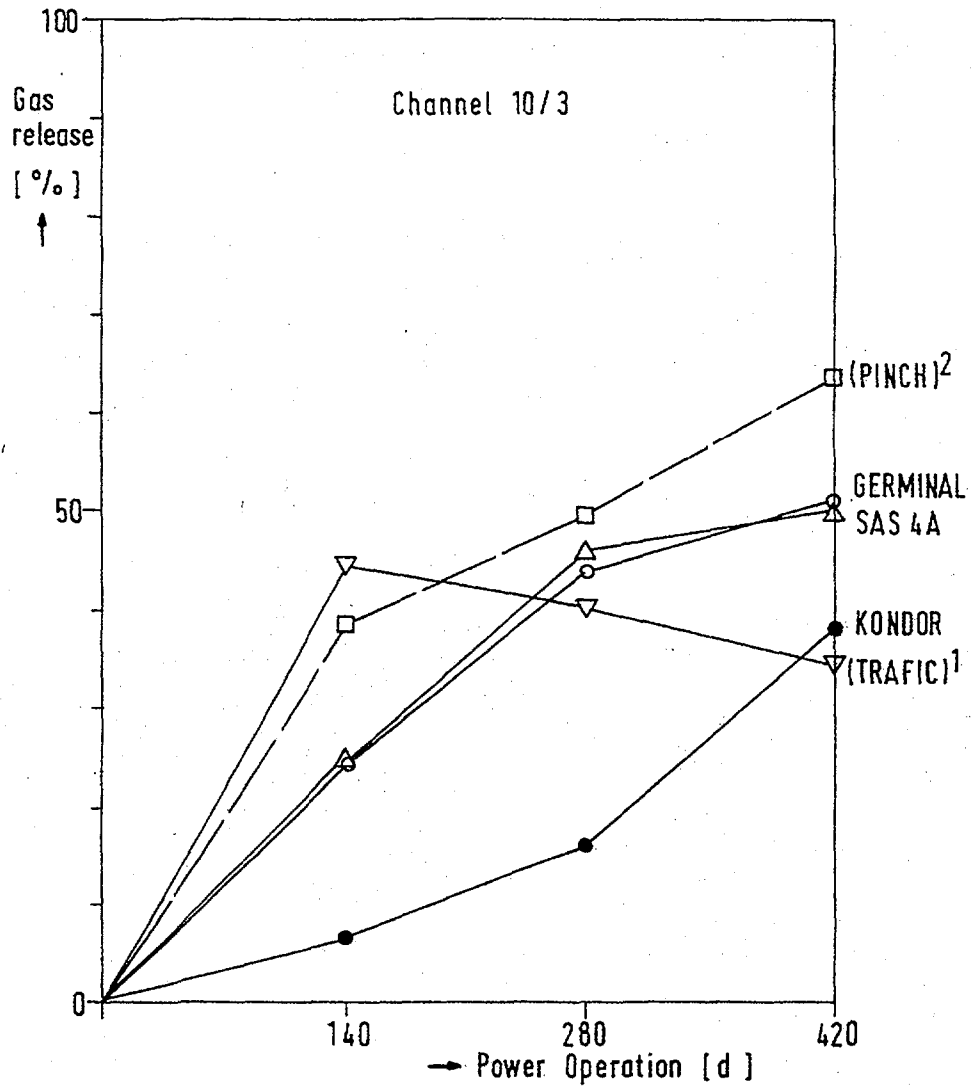
1 different power history, different clad swelling law
 2 values at peak power node

FIG. 2.18. Calculated fission gas release fraction.



1 different power history, different clad swelling law
 2 values at peak power node

FIG. 2.19. Calculated fission gas release fraction.



1 different power history , different clad swelling law
 2 values at peak power node

FIG. 2.20. Calculated fission gas release fraction.

- Results of the KONDOR, GERMINAL and DEFORM-4C calculations are relatively close to each other. However differences in between the calculations become more pronounced when medium burn-up levels of about 5 at% are exceeded. It appears as if more refined modelling approaches need to be developed for the KONDOR code system for an improved description of the fuel pin mechanics behaviour approaching high burn-up levels of 8 to 10 at% and for low linear ratings. Differences between DEFORM-4C and GERMINAL calculations evolve partly from quite different approaches to simulate JOG-formation and its behaviour during power operation. This is a topic of the current research and development activities in this field, which needs more refined analyses and model development and most importantly a broader experimental data base.

For evaluation of the reliability of the provided code predictions about the performance of the BN-800 fuel pins under power operation it would be necessary to compare calculated results with experimental results for the specific BN-800 fuel pins considered in this exercise. This holds especially for results provided on the basis of parametric modelling approaches as the results of DEFORM-4C. Impact of fuel fabrication and clad material properties variation with burn-up can only

be evaluated reliably in view of detailed experimental results. This was not the objective of this comparative exercise. However, it is strongly recommended that results should be compared in more depth with the experimental data base available in Russia from power operation of respective fuel pins in the BN-350 and the BN-600 reactors.

For the purpose of this exercise comparison of the results has shown that the calculated fuel pin states at the end of the equilibrium cycle are rather close together. Therefore transient calculations start from initial conditions sufficiently close to each other so that possible differences in the transient calculations should not be dominated by differences in the steady state fuel pin characterization after power operation. However, differences are to be expected between the transient calculations provided by India, Russia and Japan on the one side and France and Germany on the other side because these two groups of calculations start from a total thermal power output being about 11% apart from each other. This difference results from the fact that the first three calculations normalized the steady state thermal power output to meet the linear ratings as specified in the case set-up provided by IPPE resulting in a total thermal power output of 1725 MW_{th} and the second two calculations normalized the linear ratings to meet the specified total thermal power output of 1500 MW_{th} resulting in about 11% smaller values of the peak linear ratings. It is to be noticed that for the transient calculations France will use as Germany and Japan the SAS4A code.

REFERENCES TO CHAPTER 2

- [2.1] IAEA/EC Benchmark Exercise: Comparative calculations for a severe accident in the IPPE Core Design variant with a near-zero void coefficient of the BN-800 type reactor (Unprotected Loss of Flow Accident, ULOF) - input data specifications - Obninsk, Russia (December 1994 and June 1995 - Updating of the input specifications)
- [2.2] MELIS, J.C., ROCHE, L., PIRON, J.P., TRUFFERT, J., GERMINAL - A computer code for predicting fuel pin behaviour, Journal of Nuclear Materials 188 (1992) 303-307.
- [2.3] MATTHEWS, J.R., The basis of the TRAFIC fuel performance code AERE - R 10818 (rev.) (1984).
- LANEY, A.R., THETFORD, R., TRAFIC 2 - A modified version of the TRAFIC fuel performance code, AERE - R 12210 (1986).
- [2.4] IMKE, U., PORSCHA, B., STRUWE, D., DEFORM-4C - The SAS4A fuel pin performance code for evaluation of the steady state and transient behaviour, Internal FZK Report.
- [2.5] ZABUDKO, L., TRUFANOV, A., KONDOR - the IPPE fuel pin performance code, Internal IPPE Report (1996).
- [2.6] SINGH OM PAL, HARRISH, R., PINCH - The IGCAR fuel pin performance code package, Internal IGCAR Report (1996).
- [2.7] LEMOINE, F., EYRIEY, G., Steady state calculations of a BN-800 type reactor with GERMINAL 1.2, NT SEMAR 95/120.
- LEMOINE, F., EYRIEY, G., New steady state calculations of a BN-800 reactor with GERMINAL 1.2, NT SEMAR 96/69.
- [2.8] MARTIN, D.G., Some TRAFIC calculations of the behaviour of fuel and breeder pins during normal operation of a BN-800 reactor (Issue 1), AEA/CS/16401819/ZJ1644/001 (November 1995).

- [2.9] PORSCHA, B., STRUWE, D., Fuel pin behaviour during power operation of a BN-800 like core design up to end of equilibrium cycle conditions, 4th IAEA Consultancy Meeting, Vienna Austria (December 1996).
- PORSCHA, B., STRUWE, D., Fuel pin behaviour during power operation of a BN-800 like core design up to end of equilibrium cycle conditions, 5th IAEA Consultancy Meeting, Brussels, Belgium (June 1996).
- [2.10] ZABUDKO, L., TRUFANOV, A., Steady state calculations of the behaviour of fuel pins of a BN-800 type reactor with the KONDOR code, 4th IAEA Consultancy Meeting, Brussels, Belgium, (June 1996).
- [2.11] SINGH PAL OM, HARRISH, R., Results of fuel pin characterization and transient calculations for an unprotected loss-of-flow accident in a BN-800 type reactor, 4th IAEA Consultancy Meeting, Brussels, Belgium, (June 1996).

Chapter 3

PREBOILING ANALYSIS OF ULOF ACCIDENTS

3.1. INTRODUCTION

In this chapter the results of transient calculations, upto onset of boiling, of an IAEA/EC benchmark exercise on comparative calculations for unprotected loss of flow (ULOF) accident in BN-800 type reactor with near zero void reactivity, are presented. France, Germany, India, Japan and Russia are participating in this exercise. First, a brief description is given of the code system used by different countries and the modeling aspects that can lead to different predictions are highlighted. Following this, the results are presented in terms of onset of boiling, channel number in which the boiling is initiated first and power and reactivity levels at the onset of boiling. Power and flow profile and different reactivity components as a function of time are also presented.

The preboiling phase calculations were performed by most of the participants for the two cases. In case 1, referred to as **base case**, the radial feedback due to load pad effect is ignored and in case 2, referred to as **parametric case** the feedback is considered. In addition, a set of calculations is also done by considering uncertainties in the core physics parameters like Doppler coefficient and reactivity worths of fuel, clad and the coolant. The calculations have been done for the 31 channel representation of the reactor (30 for core and 1 for radial blanket). FZK Germany also performed many calculations in a 17 channel representation of the core.

In this chapter, first a brief description is given of the computer codes used by different participants and then the results in terms of onset of boiling, channel number in which the boiling is initiated first and power and reactivity levels at the onset of boiling and their time profile are presented for base case as well as parametric case. This is followed by the results of uncertainties in core physics parameters.

3.2. COMPUTER CODES USED

IPPE Russia

The IPPE used the GRIF-SM code for the transient calculations [3.1]. The GRIF-SM code performs the solution of non-stationary equations of neutronics, hydrodynamics and heat transfer. The code is suitable to investigate the whole core accident like ULOF and Unprotected Transient Over Power (UTOP) requiring simulation of the whole reactor and flow blockage accident in a single subassembly. The reactor power is calculated using point kinetics model with 6 groups of delayed neutrons. Reactivity feedbacks from thermal expansion of sodium and boiling, axial and radial expansion of the core as a whole, fuel and clad material density changes, expansion of absorber rods and its drives and Doppler effect are accounted. Sodium boiling is described by slip model of two phase flow; the friction factors and slip ratio being defined by Lockhart and Martinelli correlation. The phenomena like heat transfer in one and two phase flow, forced liquid and vapor sodium flow, boiling of underheated sodium, bubble and film boiling, film dryout when heat flux exceeds critical flux and film condensation are considered. Two dimensional temperature distributions is also calculated for subassembly wrapper which is important for correct simulation of sodium vapor condensation in top part of the core subassemblies. Inter wrapper sodium boiling is simulated

in 2D model. Fuel and clad melting is calculated and latent heat of melting is accounted for. The equations are solved numerically by the method of iterations. Equations involving space derivative are numerically integrated on computational grid with variable steps. The code for single phase calculations has been checked on a number of standard problems of hydrodynamics of incompressible flow requiring calculations of 2D or 3D distributions of velocity. The sodium boiling subroutine is validated against experiments conducted in KFK Germany. The gap conductance during transient is taken to be the same as that existed during steady state.

IPSN France, FZK Germany and PNC Japan

IPSN France, FZK Germany and PNC Japan have been using the version of the SAS4A code [3.2] improved by the respective individual organizations. SAS4A code was originally developed at ANL and is the next generation of the SAS3D code 3.3. It is validated through inpile safety experiments such as TREAT and CABRI. SAS4A code is a multichannel code; one channel being represented by one pin. The primary and secondary coolant loops are also modeled. The boiling model is a 1D, multibubble boiling model similar to SAS3D; its main new feature being a variable coolant flow cross section treatment which allows consistent coupling with the pin mechanics and clad motion models. Major improvements made in the code by France, Germany and Japan are in the areas of fuel pin mechanics module, pre and post failure in-pin fuel motion, reformulation of the two phase sodium flow, introduction of a new fission gas mass transfer model as well as JOG model and a new formulation of a chunk jamming model.

IPSN France and FZK Germany used a version of SAS4A, namely, SAS4A. REF96 [3.4, 3.5]. This code version introduces the newest state of the knowledge into the discussion of the BN-800 analysis. Representation of the BN-800 subassemblies is detailed. The primary and secondary loops are simulated using the scaled-down LSPB-PRIMAR4 representation. The calculations are performed with a basically modified two-phase flow model and balance of force model to determine axial fuel pin expansion.

PNC Japan used a variant of the SAS4A code for the transient calculations [3.6] which is close to the one used by Germany and France especially prior to the onset of boiling. The code used the JOG model with the input provided by IPPE. Interwrapper sodium void effect is considered.

The gap conductance during transient is calculated deterministically by the codes from the three countries.

IGCAR India

IGCAR, India used the PINCHTRAN code for the transient calculations. One subassembly is represented by one pin and all the subassemblies in a ring are represented by one subassembly. The code employs the point kinetics for power calculations and calculates the reactivity feedback effects due to fuel, clad and coolant expansion including core boundary movements and sodium boiling, fuel melting and slumping, steel vaporization, control rod drive expansion and grid plate expansion. Lumped model of heat transfer is used in calculating the fuel, clad and coolant temperatures. Central line temperature of fuel is calculated by assuming the steady state temperature profile in the fuel pellet and subsequently it is used in

calculating the fuel melt fraction. Sodium boiling model used is similar to the one used in ANL developed code, SAS1A [3.7]. Vapor condensation in the above core structure and flow reversal are not modeled. Fuel pin mechanics calculations during the transient are not performed but the clad temperature limits and fuel melt fraction limits are used as criteria for fuel pin failure. The code in its previous form [3.8] has been validated against the European LOFA benchmark problem [3.9] and SEFOR transient [3.10]. The gap conductance during transient is taken to be the same as that existed during steady state.

3.3. RESULTS

The following flowcoast down rule is employed by all the participants [1].

$$\begin{aligned}
 W_1 &= 5.5 / (t+5.5) && \text{for } 0 < t < 49.5 \\
 W_1 &= (120-t)/705 && \text{for } 49.5 < t < 120 \\
 W_1 &= 0 && \text{for } t > 120
 \end{aligned}$$

where W_1 is the normalised pump rotation speed and the time, t is expressed in seconds. Results of the analysis are presented below. Results are interpreted keeping in view that initial steady state temperatures are different in all the cases, gap conductance remains constant during the transient in Russian and Indian studies while it is time dependent in SAS4A based calculations. Further, fuel axial expansion is determined based on balance of force model in SAS4A based calculations while it is constant and free expansion in the case of Russian and Indian studies. Also the initial power is 1525 MWt for French, German, Indian and Russian studies and 1725 MWt in Japanese studies.

The important design and reactivity parameters of the reactor are given in the appendix for ready reference.

3.3.1. Base case

All the computer codes predict the initiation of boiling in the core and therefore establish that the negative feedback from the sodium plenum is not sufficient to prevent the onset of boiling. All the computer codes also predict uniformly that boiling is initiated first in channel number 5/1 (first channel of medium enrichment zone with 140 fpd operated fuel pins) which has the highest power to flow ratio.

Time of onset of boiling, channel in which the boiling takes place first, normalised power, net reactivity and reactivity feedbacks from, axial fuel expansion and Doppler effect at the time of onset of boiling predicted by different codes are compared in Table 3.1. It can be seen that the time of onset of boiling is predicted between 16.72 s and 19.01 s; the maximum deviation being 14%. The approaches that consider transient fuel pin mechanics and the transiently varying gap conductance (French, German and Japanese studies) predict initiation of boiling between 18.93 and 19.01 s. Russian and Indian predictions are 16.72 and 17.60 s respectively.

Power at the time of onset of boiling predicted by the various codes lies in the range of 0.63 to 0.71 times the nominal power. Again it is seen that German, French and Japanese

predictions are close to each other and Russian and Indian predictions are close to each other. The French and Japanese predictions are almost identical. It can also be observed that in the present design of BN-800 reactor with near zero sodium void coefficient of reactivity, the power at the time of onset of boiling is in the range of 60 to 70 % of the nominal power, where as for the conventional design core the power level is much higher [3.11]. Thus in the new design, the fuel pin failure is delayed as compared to the conventional design.

Table 3.1: Results at Onset of Boiling (Base Case)

| Parameter | Germany | France | Japan | Russia | India |
|--------------------------------------|---------|--------|---------|--------|--------|
| Time (s) | 17.96 | 18.93 | 18.96 | 16.72 | 17.60 |
| Channel No. | 5/1 | 5/1 | 5/1 | 5/1 | 5/1 |
| Axial position from core bottom (cm) | 84 - 90 | 95 | 87 - 94 | 85 | 84 |
| Normalised Power | 0.66 | 0.63 | 0.63 | 0.71 | 0.71 |
| Net Reactivity (\$) | -0.170 | -0.183 | -0.183 | -0.135 | -0.147 |
| Doppler Reactivity (\$) | 0.026 | -0.005 | -0.004 | +0.039 | +0.027 |
| Fuel Axial Expansion Reactivity (\$) | -0.003 | +0.015 | +0.014 | +0.017 | +0.020 |
| Sodium Reactivity (\$) | -0.207 | -0.205 | -0.205 | -0.188 | -0.223 |

The net reactivity at the onset of boiling is predicted between -0.135 \$ and -0.183 \$. Again the predictions based on modified SAS4A code, are closer to each other and the Russian and Indian predictions are close to each other. Predictions of reactivity feedbacks from sodium expansion is in the range of -0.188 \$ and -0.223 \$. The predictions of Japan and France are very close to each other. Russian studies predict the lowest reactivity from the sodium. The contribution of the Doppler and fuel axial expansion is relatively small.

The comparison of time variation of flow and power and net reactivity upto onset of boiling is depicted in Figs. 3.1 and 3.2 respectively. The flow variation has been depicted up to the earliest onset of boiling only. The variation of various reactivity components (sodium expansion, Doppler and fuel axial expansion) upto onset of boiling is shown in Figs. 3 to 5 respectively. In this case, Doppler reactivity is positive at the onset of boiling in the German, Russian and Indian calculations. The reactivity is negative initially and attains positive value before onset of boiling. The French and Japanese values of Doppler reactivity are negative throughout the preboiling state and are almost identical. However, the fuel axial expansion reactivity feedback is positive at the onset of boiling in all the cases except the German one where it is negative throughout. The Russian and Indian results are closer together and the French and Japanese results are almost identical. The closeness of predictions by IPPE and IGCAR and the SAS4A based results is also reflected in Figs.3.1 and 3.2 and is probably because IPPE and IGCAR use constant gap conductance model while FZK, IPSN and PNC use transiently varying gap conductance during the transient. The differences in the predictions

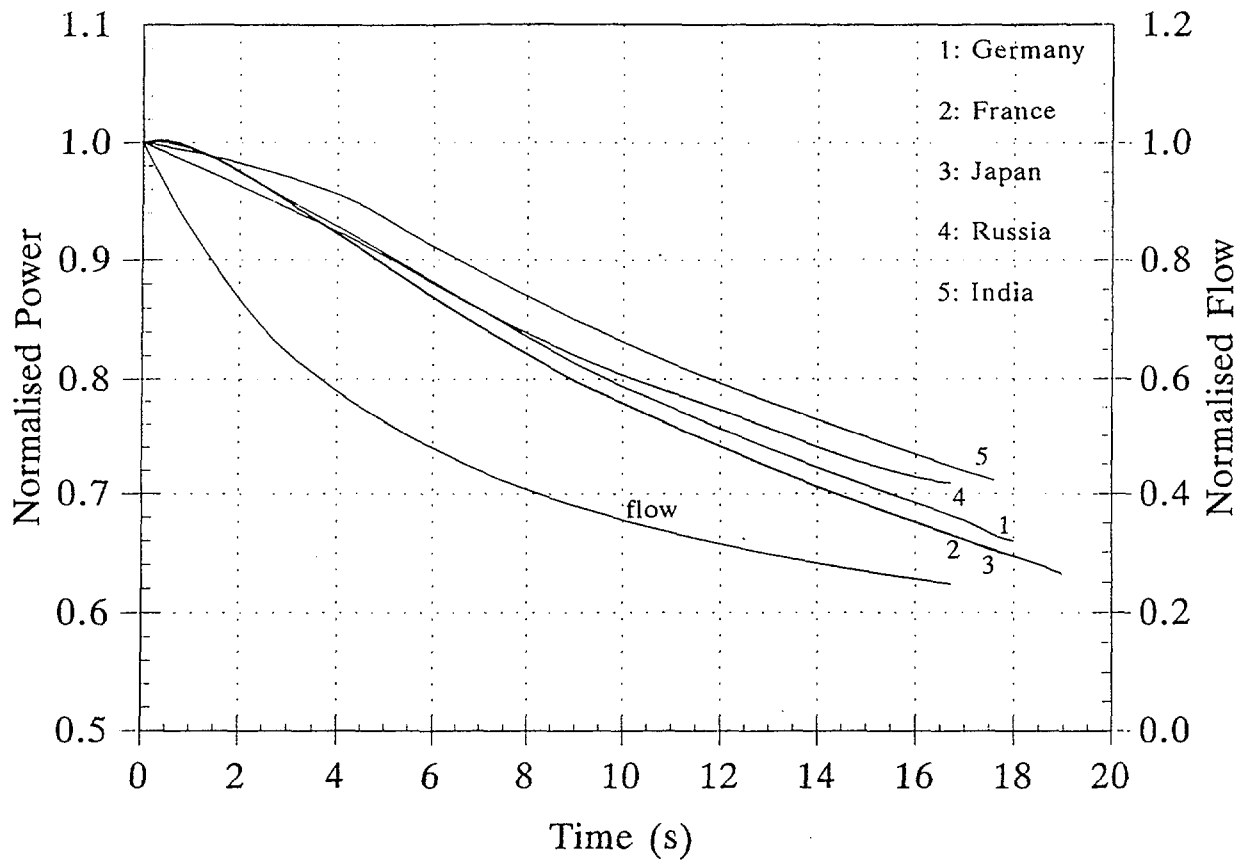


FIG. 3.1. Power (base case).

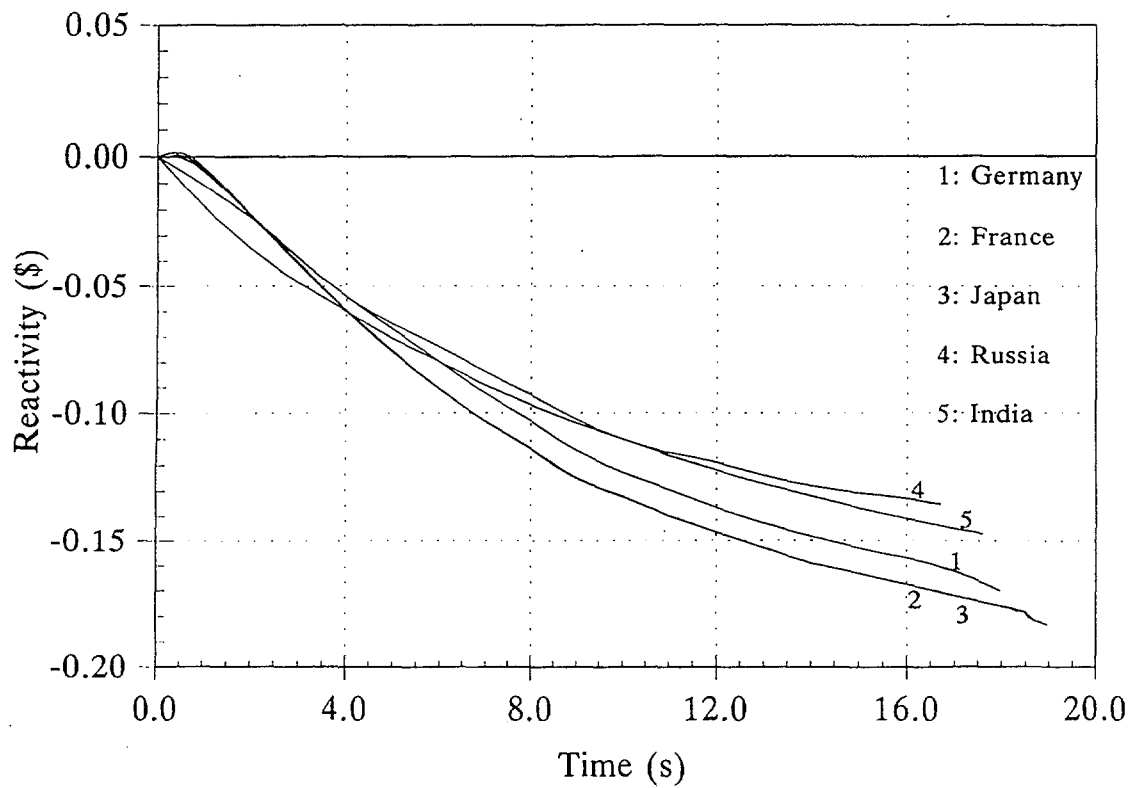


FIG. 3.2. Net reactivity (base case).

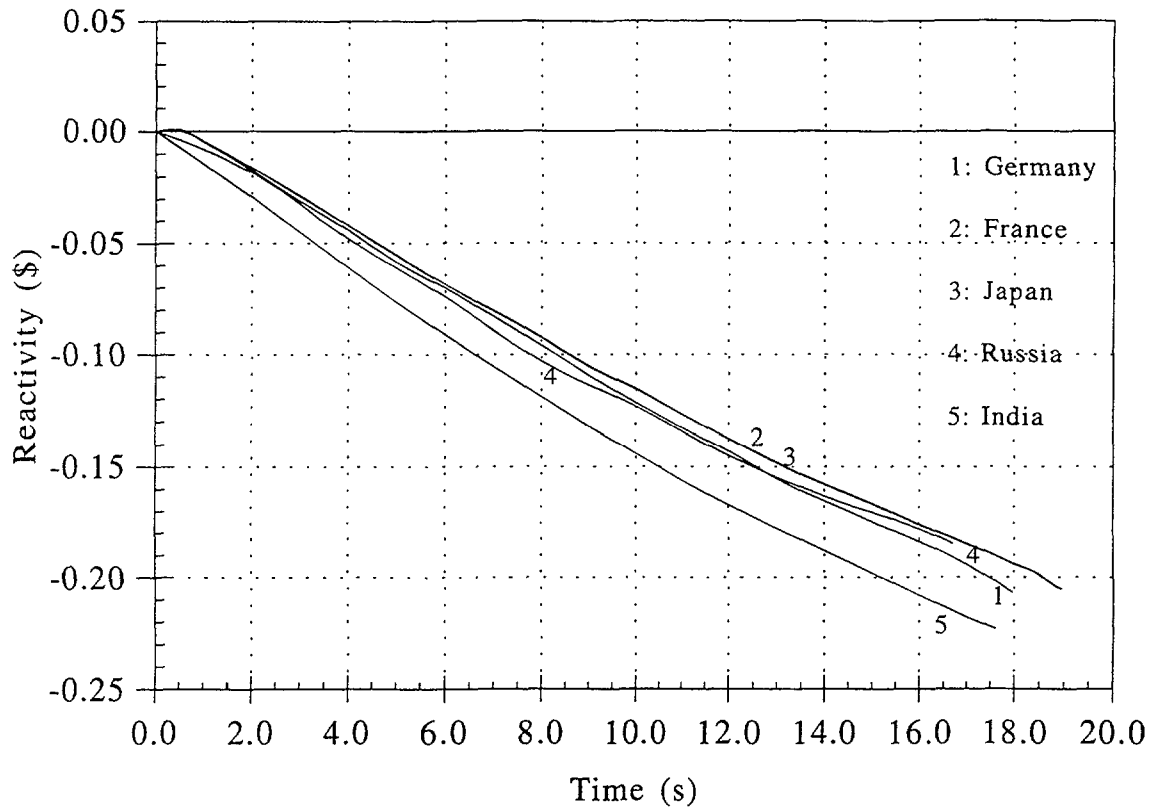


FIG. 3.3. Sodium reactivity (base case).

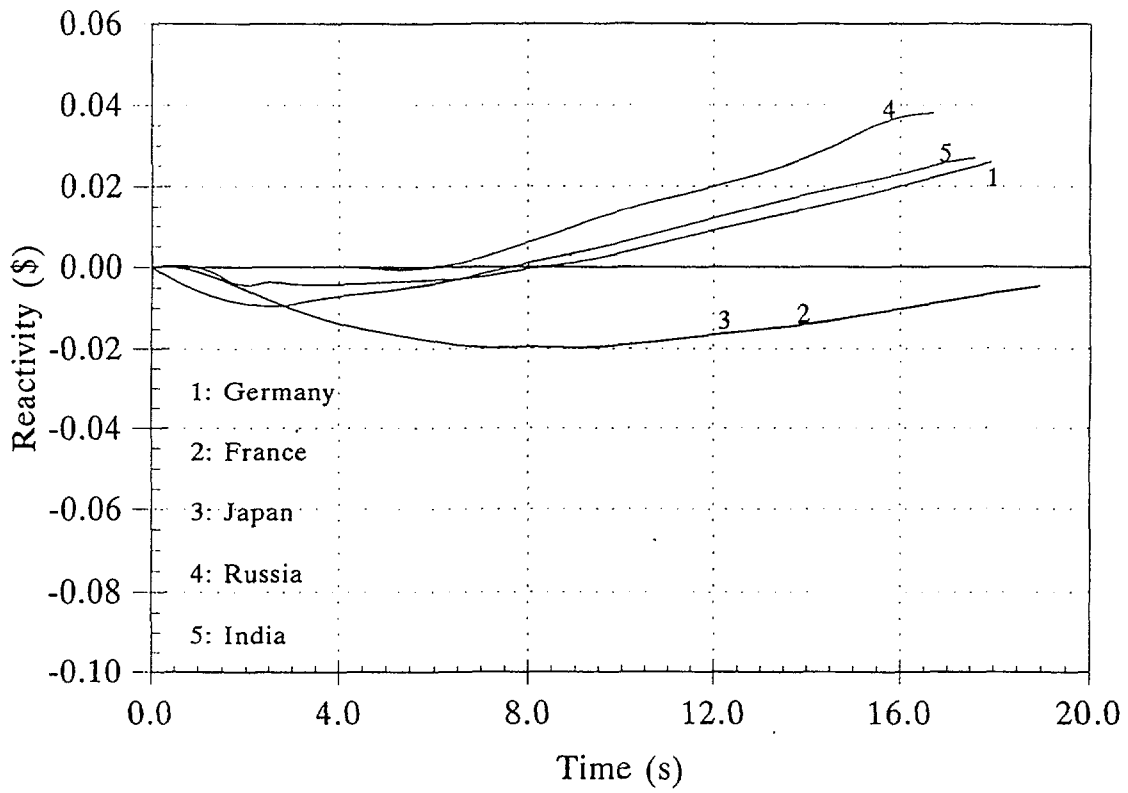


FIG. 3.4. Doppler reactivity (base case).

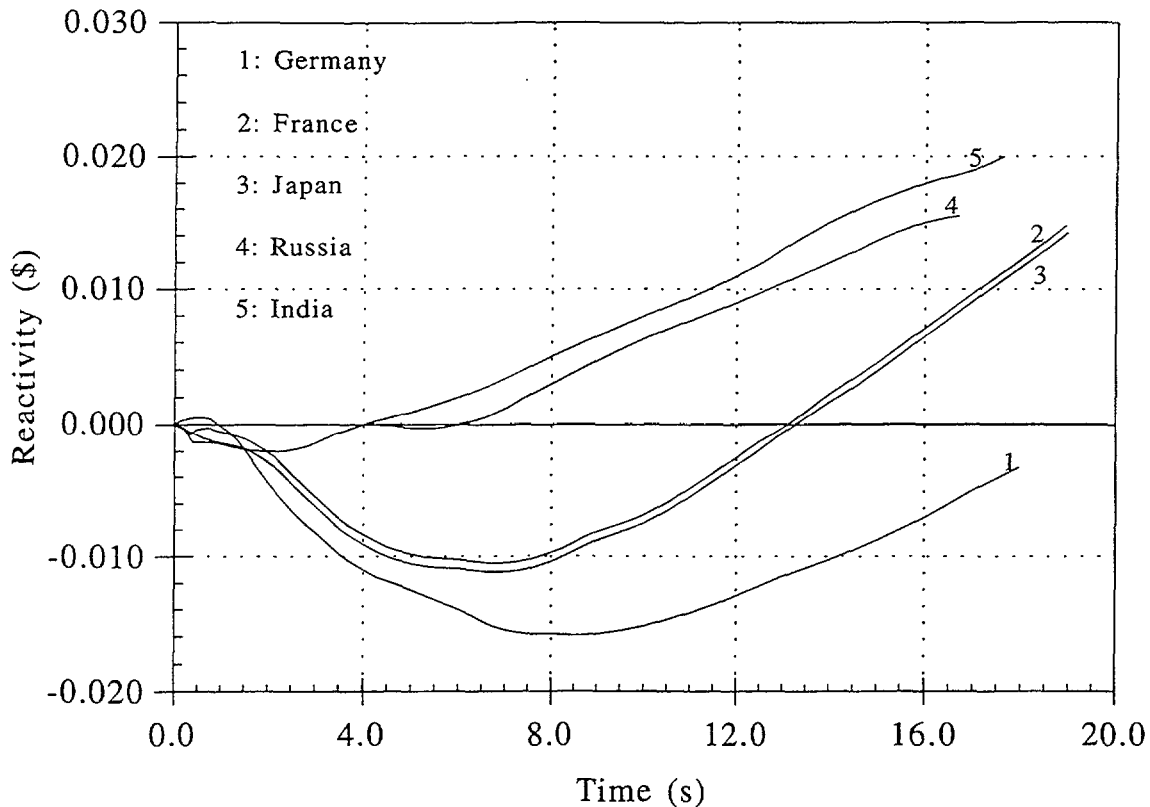


FIG. 3.5. Fuel axial expansion reactivity (base case).

of sodium reactivity feedback is also due to different space discretisation scheme used by different organizations. The fuel axial expansion feedback is small and the differences in the predictions arise from different models used for fuel expansion.

FZK Germany also did many calculations in 17 channel representation of the core and reflector. The predictions of the parameters in 17 channel representation is close to the predictions of the 31 channel representation. The results presented in this section are taken from Ref. [3.4, 3.11-3.16].

3.3.2. Parametric case

In this case additional negative feedback from the load pad radial expansion is accounted for. The load pad reactivity is calculated by the participants using the reactivity coefficients and the associated time constants as provided by IPPE Russia. Results from FZK, PNC, IPPE and IGCAR are available in this study. FZK performed these calculations with 17 channel representation of the core and blanket. The ULOF results of Germany are taken from Ref.[3.4].

In this case also, the codes predict the initiation of boiling inspite of the radial reactivity feedback. However, the onset of boiling is delayed. The initiation of boiling is delayed considerably from 16.72 to 18.96 s in the base case to 28.88 to 33.16 s in the parametric case. As in the base case, all the codes predict the first boiling in channel 13 (5/1) where power to flow ratio is maximum.

The normalised power is considerably lower as compared to the base case as it should be expected. It is in the range of 0.39 to 0.45.

Due to the sodium plenum being heated up, the sodium void reactivity is large and negative as in the base case. However, the dominant reactivity in this case is the load pad reactivity. There is a fair agreement in the calculation of this reactivity effect as can be expected due to the calculation methodology being the same.

Doppler and axial feedbacks are positive at the time of onset of boiling. However, these feedbacks are slightly negative at the beginning. These cross over to positive values at roughly the boiling onset in the SAS4A series of codes for base case, but the crossover is relatively earlier in the parametric case. The crossover to positive values is predicted earlier, in base case as well as parametric case by the Russian and Indian codes. The results in terms of time, channel number, normalised power and reactivity components at the boiling onset are given in Table 3.2. The time profile of these parameters is depicted in Figs. 3.6-3.11. As observed in the base case, SAS4A code based results are close to each other and the Russian and Indian results fall together.

Table 3.2: Results at Onset of Boiling (Parametric Case)

| Parameters | Germany | France | Japan. | Russia | India |
|--------------------------------------|---------|--------|---------|--------|--------|
| Time (s) | 28.88 | - | 33.16 | 31.4 | 32.29 |
| Channel No. | 5/1 | - | 5/1 | 5/1 | 5/1 |
| Axial position from core bottom (cm) | 84 - 91 | - | 87 - 94 | - | 84 |
| Normalised Power | 0.43 | - | 0.39 | 0.44 | 0.39 |
| Net reactivity (\$) | -0.295 | - | -0.299 | -0.244 | -0.278 |
| Doppler reactivity (\$) | +0.183 | - | +0.153 | +0.292 | +0.263 |
| Fuel axial expansion reactivity (\$) | +0.174 | - | +0.220 | +0.100 | +0.100 |
| Sodium Reactivity (\$) | -0.223 | - | -0.230 | -0.203 | -0.219 |
| Radial Core Expn. Reactivity (\$) | -0.418 | - | -0.432 | -0.432 | -0.454 |

IPPE Russia, in one set of calculations assumed reactivity feedback from control rod drive mechanism expansion which is negative. The onset of boiling is delayed from 31.4 s to 36.4 s. The feedback is not enough to prevent the onset of boiling.

3.3.3. Uncertainties in core physics data

A set of calculations have been carried out to check the sensitivity of the results to the uncertainties in core physics parameters. PNC, IPPE and IGCAR participated in this exercise. Japan and India assumed the uncertainties in the core physics parameters as: +5% in fuel, +20% in steel, -20% in sodium expansion and +15% in Doppler effect (case 1). This is to maximise the positive reactivity feedback and minimise the negative reactivity feedback (conservative case). The results indicate that the onset of boiling is advanced by 0.4 and 1.0 s respectively. In addition, India made one more set of calculations with uncertainties in core

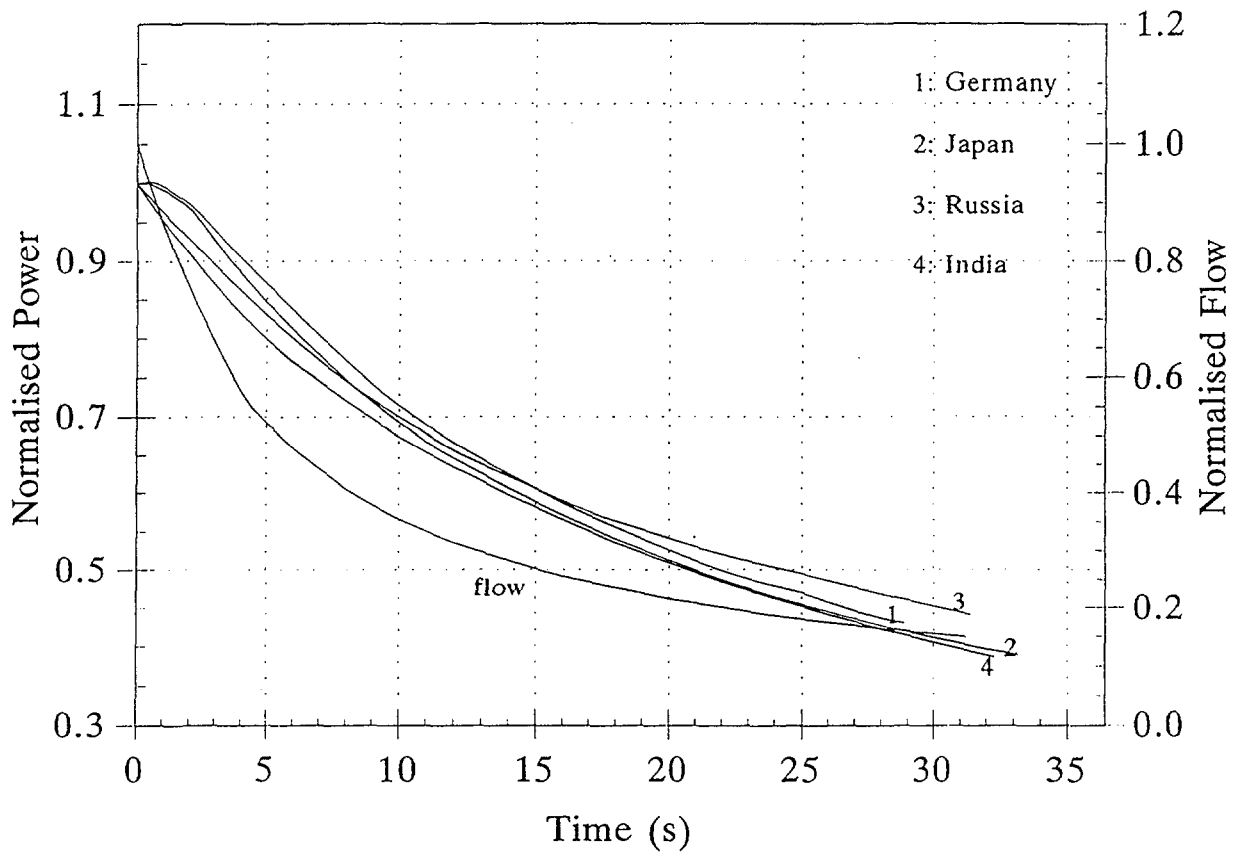


FIG. 3.6. Power (parametric case).

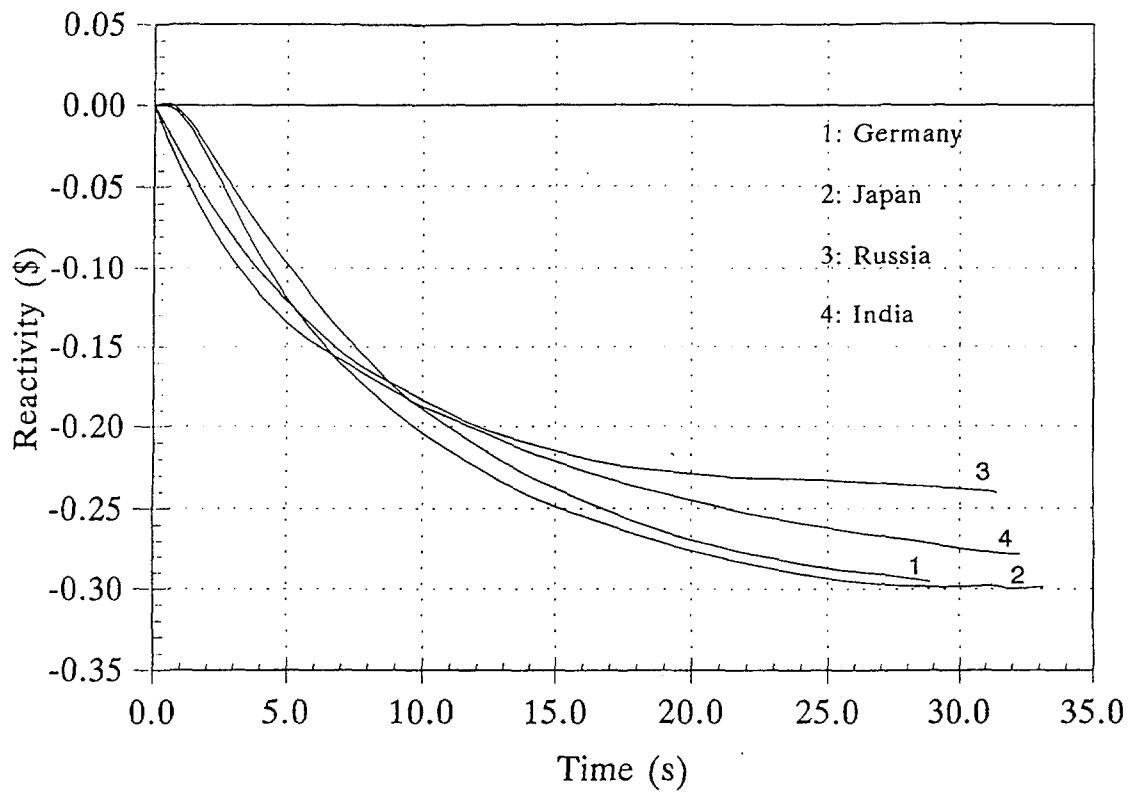


FIG. 3.7. Net reactivity (parametric case).

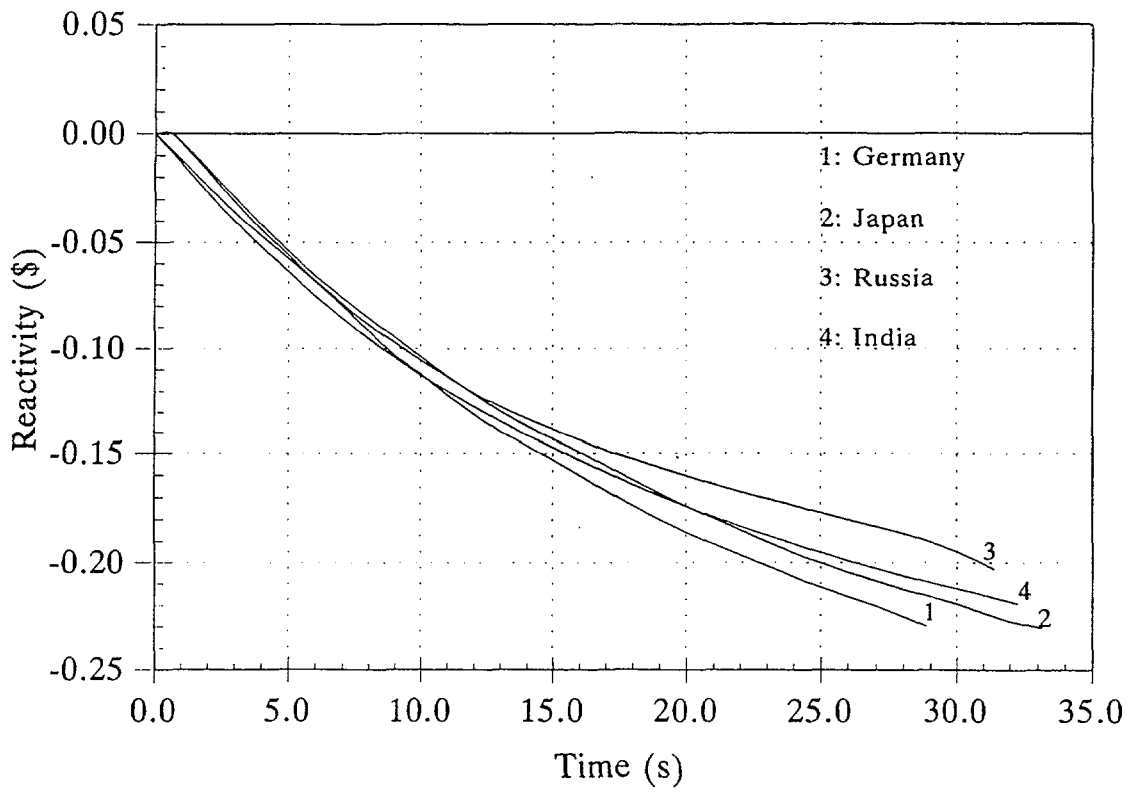


FIG. 3.8. Sodium reactivity (parametric case).

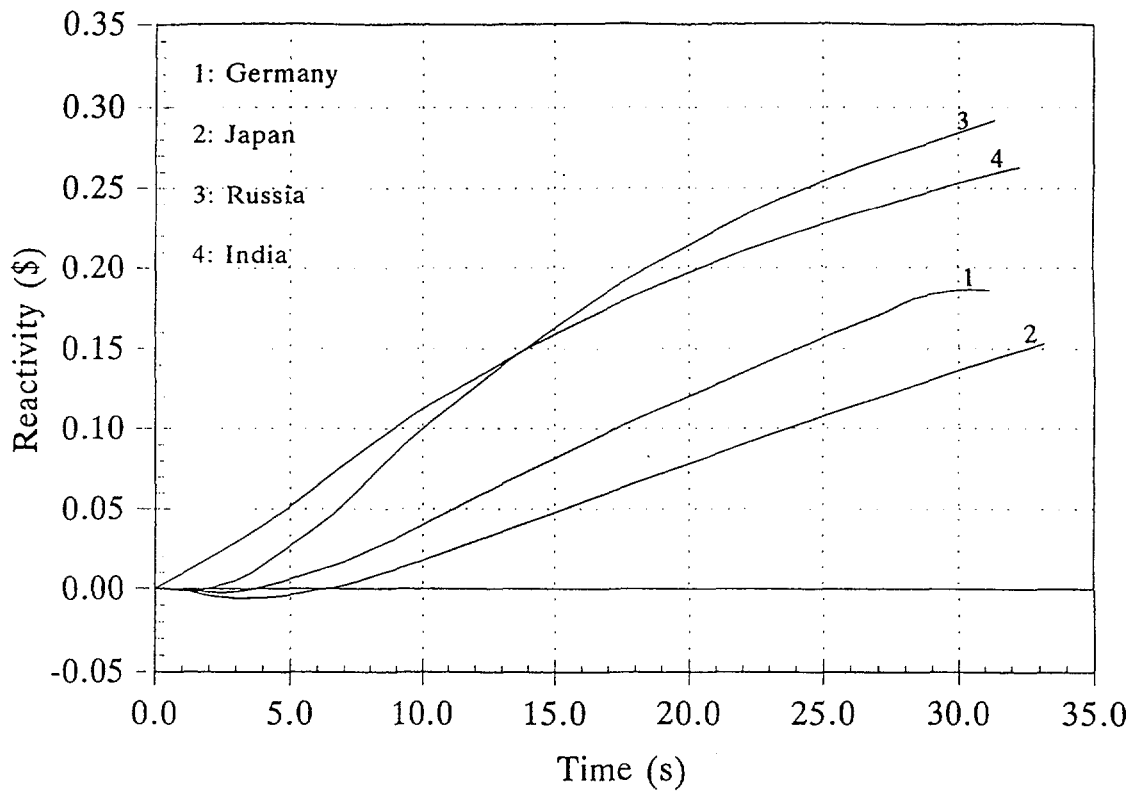


FIG. 3.9. Doppler reactivity (parametric case).

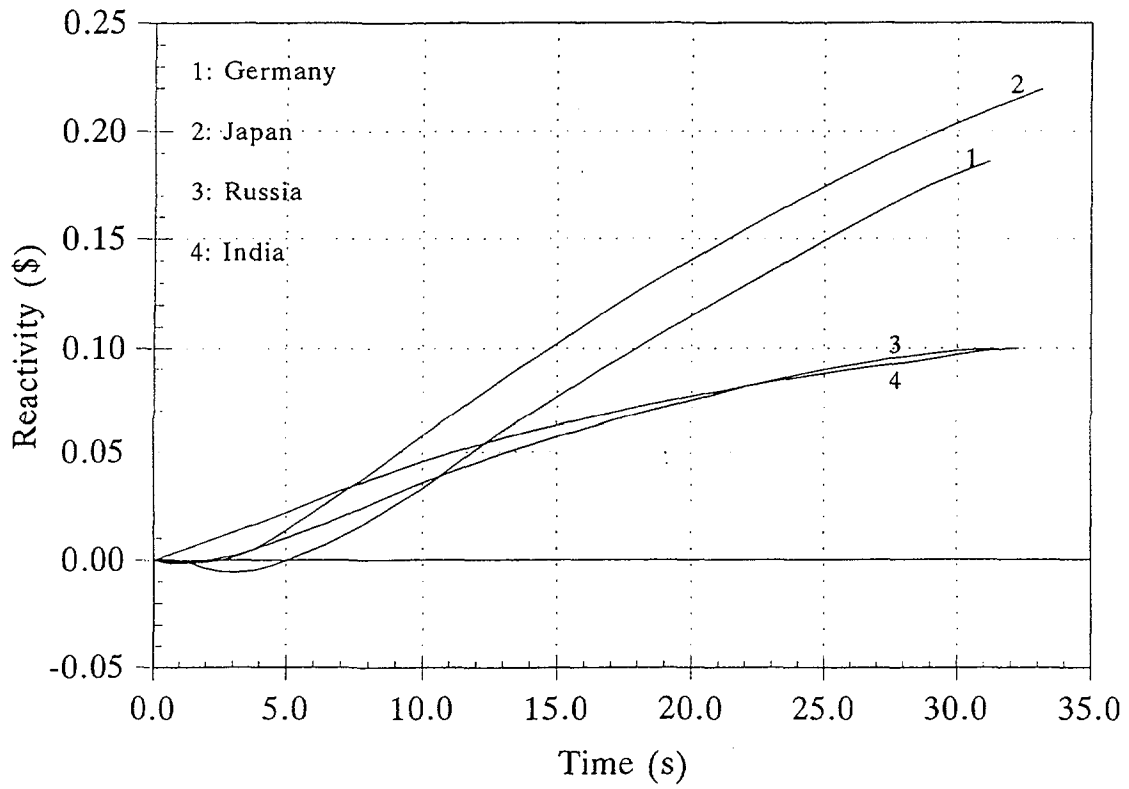


FIG. 3.10. Axial reactivity (parametric case).

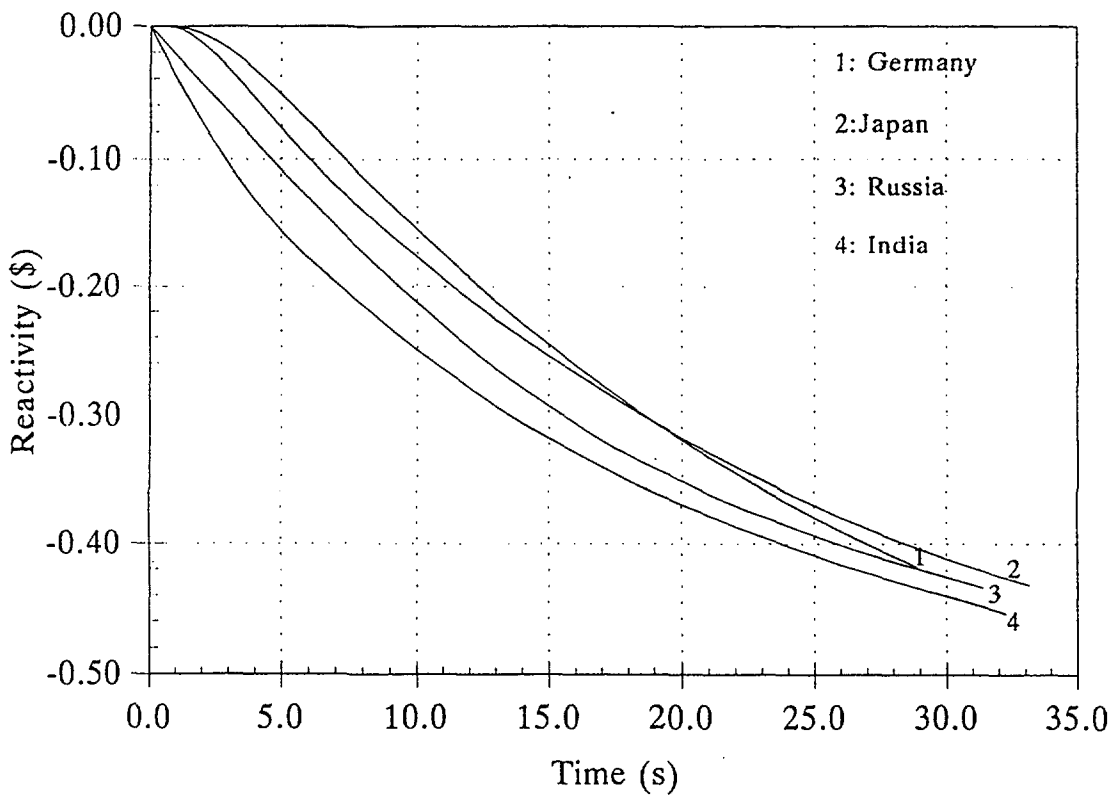


FIG. 3.11. Radial core expansion reactivity (parametric case).

physics parameters as: +5% in fuel, +20% in steel, +20% in sodium and +15% in Doppler effect (case 2). This case being optimistic with respect to sodium void reactivity feedback shows that the onset of boiling is delayed by 0.75 s because of increased negative feedback from sodium plenum. Russian results obtained by considering an increase by 15% in Doppler coefficient (case 3) shows that the onset of boiling is advanced by a fraction of a second and when steel worths are increased by 20% (case 4), the onset of boiling is delayed by fraction of a second. By and large, it is concluded that the uncertainties in core physics parameters do not lead to much changes in the results.

3.4. CONCLUSIONS

The following conclusions can be drawn from the study.

- ◆ All the codes predict the onset of boiling and therefore establish that the negative feedback from the sodium plenum is not sufficient to prevent the onset of boiling. However, the sodium plenum reactivity feedback is influential in delaying the onset of boiling. The power at this time is also low (63-71% times the nominal power) and net reactivity is negative which are favorable to the reactor safety.
- ◆ All the codes predict uniformly that onset of boiling takes place in the 5/1 channel (first channel of medium enrichment zone with 140 fpd operated fuel pins) where the power to flow ratio is maximum.
- ◆ The prediction of the time of onset of boiling by different codes compares well within 14%.
- ◆ Study indicates that the results are not very sensitive to the uncertainties in the core physics parameters.
- ◆ It is observed that SAS4A based results fall close to each other (Japanese and French results are almost identical) and IPPE and IGCAR results fall close to each other. This is mainly because SAS4A based calculations use transiently varying fuel to clad heat transfer coefficient while IPPE and IGCAR use constant gap heat transfer coefficients. The differences in predictions of sodium reactivity feedback is also due to different space discretisation scheme followed in different codes. Doppler and fuel axial expansion reactivity feedbacks are of smaller magnitude and hence the scatter in predictions can be expected. Fuel axial expansion feedback is also dependent whether one follows the balance of force model (as followed by IPSN, FZK and PNC) or free axial expansion of the fuel (as followed by IPPE and IGCAR). Radial expansion feedback is dependent on the precision of calculations of the temperature of sodium and upper core structure.

REFERENCES TO CHAPTER 3

- [3.1] I. Chvetsov, I. Kuznetsov and A. Volkov, "GRIF-SM- A Computer Code for the Analysis of the Severe Beyond Design Basis Accidents in Sodium Cooled Reactors", Proc. Int. Top. Meeting on Sodium Cooled fast Reactor Safety, Obninsk, Russia, Oct. 3-7, 1994.

- [3.2] A. M. Tentner, et al, "The SAS4A LMFBR Whole Core Accident Analysis Code" Proc. Int. Mtg. Fast Reactor safety, pp 989-998, Knoxville, TN (1985).
- [3.3] J.E. Cahalan and D. R. Ferguson, "A preliminary User's Guide to Version 1.0 of the SAS3D LMFBR Accident Analysis Code" ANL RAS Division, (1977).
- [3.4] D. Struwe, B. Porsha, W. Pfrang and H. Eigenewe, "Results of ULOF Analyses for a BN-800 like Reactor With a Near Zero Void Worth Core Design", 5th consultancy meeting on "IAEA/EC Comparative Calculations for Severe Accident (ULOF) in BN-800 Reactor" held in Vienna, Austria, Dec 4-6,1996.
- [3.5] C. Rongier and J. M. Frizonnet, "Preliminary SAS4A Calculations", 5th consultancy meeting on "IAEA/EC Comparative Calculations for Severe Accident (ULOF) in BN-800 Reactor" held in Vienna, Austria, Dec 4-6,1996.
- [3.6] H. Niwa and K. Nemura, "A study of ULOF Sequences in BN-800 type 1500 MWth Reactor With SAS4A at PNC", 5th consultancy meeting on "IAEA/EC Comparative Calculations for Severe Accident (ULOF) in BN-800 Reactor" held in Vienna, Austria, Dec 4-6,1996.
- [3.7] J. C. Carter et al. "SAS1A - A Computer Code for the Analysis of Fast Reactor Power and Flow Transients" ANL-7607, 1970.
- [3.8] Om Pal Singh, P.B. Rao and R.S. Singh, "Accident Analysis Work at Indira Gandhi Centre for Atomic Research and Some Interesting Results for a Small and Medium Sized Fast Reactor" Symposium on Science & Technology of Fast Reactor Safety, BNES, London, 1986.
- [3.9] P. Royal et al., "Comparative Analysis of Hypothetical LOFA in LMFBR using Different Computer Programmes for a Common Benchmark Problem", EUR-6318E, 1979.
- [3.10] L.D.Noble et al., "SEFOR Core 1 Test Results to 20 MWt" GEAP- 13702, 1971.
- [3.11] D. Struwe, I. Kuznetsov, J. M. Frizonnet, G. Holford and G.V. Goethem, "Synthesis of Transient Calculations for a BN-800 Type Benchmark Exercise of an Unprotected Loss of Flow Accident" Proc. Int. Top. Meeting on Sodium Cooled Fast Reactor Safety, Obninsk, Russian Federation, Oct. 3-7,1994. and 8th Consultancy meeting held at IPPE, Obninsk, Russian Federation, June 2-6, 1998.
- [3.12] J. M. Frizonnet and C. Rongier, "New SAS4A Calculations (ULOF) (Ref96.R1.mod)" 8th consultancy meeting on "IAEA/EC Comparative Calculations for Severe Accident (ULOF) in BN-800 Reactor held at IPPE, Obninsk, Russian Federation, June 2-6, 1998.
- [3.13] H. Niwa and K. Nemura, " New Results of ULOF in a BN-800 Type Core -Base Case and parametric Case With SAS4A at PNC", 8th consultancy meeting on "IAEA/EC Comparative Calculations for Severe Accident (ULOF) in BN-800 Reactor" held at IPPE Obninsk, Russian Federation, June 2-6, 1998.

- [3.14] IPPE: "EC/IAEA Benchmark/Comparative Calculations for a Severe ULOF Accident in the IPPE Core Design Variant With a Near Zero Void Coefficient of the BN 800 Type Reactor", 5th Consultancy meeting on "IAEA/EC Comparative Calculations for Severe Accident (ULOF) in BN-800 Reactor" held in Vienna, Austria, Dec 4-6,1996.
- [3.15] D. Struwe, B. Porscha and W. Pfrang, "Results of ULOF analysis for a BN-800-like Reactor With a Near Zero Void worth Core Design", 8th Consultancy Meeting on "IAEA/EC Comparative Calculations for Severe Accident (ULOF) in BN-800 Type Reactor", held at IPPE Obninsk, Russian Federation, June 2-6, 1998.
- [3.16] R. Harish and Om Pal Singh, "A Study of Unprotected Loss of Flow Accident in BN-800 Like Reactor Beyond Onset of Boiling", 8th Consultancy Meeting on "IAEA/EC Comparative Calculations for Severe Accident (ULOF) in BN-800 Type Reactor", held at IPPE Obninsk, Russian Federation, June 2-6, 1998.

APPENDIX

A. Some of the Important Design Data of BN-800 Reactor

| | Core | Blanket |
|---------------------------------------|--------------------------|-------------------------|
| Power (MWt) | 1376.09 | 60.54 |
| Core Height (cm) | 84 | 84 |
| Fuel Pellet Radius (cm) | 0.28 | 0.65 |
| Fuel Pellet Central Hole Radius (cm) | 0.0825 | - |
| Clad inner surface radius (cm) | 0.29 | 0.66 |
| Clad outer surface radius (cm) | 0.33 | 0.70 |
| Lower plenum length (cm) | 67 | 30 |
| Lower plenum volume (m ³) | 1.77 x 10 ⁻⁵ | 4.11x 10 ⁻⁵ |
| Upper plenum length (cm) | 4.35 | 6.50 |
| Upper plenum volume (m ³) | 1.149 x 10 ⁻⁶ | 8.90 x 10 ⁻⁶ |
| Filling gas | 95% He & 5% air | 95% He & 5% |
| Filling gas pressure (MPa) | 0.1 | 0.1 |

B. Reactivity Parameters

(i) Reactivity worth of fuel, steel & sodium

| Material | Reactivity worth (pcm) | |
|----------|------------------------|---------|
| | Core | Total |
| Sodium | 1150 | - 1318 |
| Steel | 3424 | + 1753 |
| Fuel | - 39471 | - 40584 |

(ii) Reactor Kinetics Parameters

| Parameters | Value |
|--|--------|
| Delayed neutron fraction (pcm) | 356.3 |
| Prompt neutron lifetime (μs) | 0.44 |
| Wet Doppler coefficient, T dk/dT (pcm) | -617 |
| Dry Doppler coefficient, T dk/dT (pcm) | -401 |
| Temperature reactivity coefficients (pcm/°C) | -1.842 |
| Power reactivity coefficient (pcm/MWt) | -0.404 |

**NEXT PAGE(S)
left BLANK**

Chapter 4

BOILING AND POST FAILURE ANALYSIS RESULTS OF ULOF ACCIDENTS

This chapter describes the boiling and post-failure analyses of ULOF-accidents in a BN-800 type core design. The chapter consists of three sections, which are (1) boiling and post-failure phase transients, (2) core configuration at the end of the initiating phase, and (3) conclusions.

4.1. BOILING AND POST-FAILURE PHASE TRANSIENTS

Analytical codes

Boiling phase calculations are continued following those of the pre-boiling phase by each code of the participants (see Chapter 3). The code used are:

| | |
|--------------|-----------------------------------|
| IPSN /France | : SAS4A Ref.96. V1.15, |
| FZK /Germany | : SAS4A Ref.96.rel 1.0 Mod.FZK |
| IGCAR /India | : PINCHTRAN, |
| PNC /Japan | : SAS4A Ref.96.rel 1 Mod.PNC, and |
| IPPE /Russia | : GRIF-SM. |

Regarding the PINCHTRAN and the GRIF-SM, the characteristics of each code are already explained in Chapter 3.

SAS4A code family is used by the participants from France, Germany and Japan. The code version used by these three participants are based on the identical version, SAS4A Ref.96 release 1, but each participant performed some modifications independently in order to apply to this reactor. The French participant introduced mechanical properties of 15/15 Ti stabilized cladding and improved the sodium EOS in the post failure module. The German participant modified and improved the fuel pin mechanics model and two-phase boiling model in order to cope with the boiling behaviour at low-power level. The Japanese participant improved the treatment of clad motion by means of switching over from clad motion model to material motion model and thus extended the applicability of the model.

Void and steel worth of the core

Table 4.1 shows the void worth of each core region and steel worth in the fissile region of this reactor. It can be understood from this table that the positive void worth of the core region (+4.5 \$) is almost similar to that of a typical MOX-fueled core of this size, but the strong negative void worth in the upper sodium layer (-3.3 \$) makes total reactivity zero or negative (-0.6 \$). It is also indicated that displacement of the steel from the fissile region introduces positive reactivity effect (+5.2 \$). When molten clad moves from the fissile region to the upper sodium layer or lower blanket region, a significant positive reactivity effect is expected because reflector effect of the steel at the core edge is superimposed to the steel displacement reactivity effect.

Analytical cases and conditions

As a basis of the present comparative exercise, two cases are investigated in this phase similarly to the pre-boiling phase transient (see Chapter 3).

TABLE 4.1. VOID AND STEEL WORTH IN BN-800 TYPE CORE

| region | void worth [\$] | displacement of steel [\$] |
|-------------------------------|-----------------|----------------------------|
| positive worth region | +4.5 | --- |
| fissile region | +2.7 | +5.2 |
| upper sodium layer region | -3.3 | --- |
| fissile reg. + up. sod. layer | -0.6 | --- |

Base Case: radial expansion reactivity effect is neglected, and

Parametric Case: radial expansion reactivity effect is fully considered based on the IPPE's proposal.

Nominal reactivity coefficients are used for Doppler, sodium void, fuel axial expansion, clad motion and fuel motion in both cases.

Evaluation of these cases were complemented by analyses of consequences of an early blowout of fission gases from the upper fission gas plenum to the coolant channel by Japan. As it turned out that this effect does not modify the integral event sequence drastically it was agreed to neglect this effect in most of the analyses. However, it is thought reasonable and necessary to re-evaluate the case when more reliable results are to be provided or if it would come to licensing of the reactor design.

Thermal expansion of the control rod drive line (CRDL) leads to negative reactivity insertion. However, because its time constant of the expansion is not verified in the present reactor conditions, it is considered to be overly optimistic to superpose the 100% of CRDL expansion effect on the 100% of radial core expansion effect. Therefore it was concluded that the assumption of the CRDL expansion is beyond the domain of this comparative exercise. It is needed to be reviewed if more rapidly developing consequences of CRDL expansion could be demonstrated.

4.1.1. Base case results

Outline

All the codes predict onset of coolant boiling and dryout of the cladding in Base Case. Furthermore the SAS4A code family reaches the phenomena of molten cladding motion, fuel breakup and its motion. The calculated results by each participant are summarised in Table 4.2. Coolant boiling is onset in Channel* 13 (the hottest subassembly group located in MEZ) at about 17 to 19 s into transient. Table 4.3 shows the order and timing of the boiling onset in the earliest five channels. Following the boiling onset in the first channel (Ch. 13), it is predicted in Channels 1, 4, 7, and 10 within 2 seconds in all the codes.

* Channel (Ch.) : a group of subassemblies with similar design parameters such as power, coolant flow, and burnup.

TABLE 4.2. SUMMARY OF THE ULOF CALCULATION (BASE CASE)

| Parameters \ Participant | France | Germany | India | Japan | Russia |
|--|---|-------------------|-------------------|-------------------|------------------------------------|
| BOILING ONSET | | | | | |
| 1st Ch. time [s] | 13 (5/1) 18.93 | 13 (5/1) 17.95 | 13 (5/1) 17.60 | 13 (5/1) 18.96 | 13 (5/1) 16.72 |
| DRYOUT | | | | | |
| time after LOF (time after B.O. [s]) | 21.57 (+2.64) | 20.20 (+2.32) | 64.0 (+47.4) | 21.44 (+2.48) | 18.80 (+2.08) |
| axial position from BFC [cm] | 65 - 72 | 64 - 71 | 84 | 65 - 72 | 63 - 70 |
| CORE STATE AT THE FIRST CLAD MELTING | | | | | |
| time after LOF (time after B.O. [s]) | 23.98 (+5.05) | 23.33 (+5.38) | 68.0 (+51.4) | 23.68 (+4.72) | 19.44 (+2.72) |
| Channel No. | 13 (5/1) | 13 (5/1) | 13 (5/1) | 13 (5/1) | 13 (5/1) |
| Normalized Power | 0.61 | 0.46 | 0.64 | 0.55 | 0.69 |
| Net Reactivity [\$] | -0.062 | -0.440 | +0.325 | -0.187 | -0.051 |
| Doppler Reactivity [\$] | +0.035 | +0.089 | +0.095 | +0.042 | +0.088 |
| Fuel Axial Expansion Reac. [\$] | +0.079 | +0.069 | +0.057 | +0.086 | +0.040 |
| Clad Axial Expansion Reac. [\$] | +0.010 | +0.016 | +0.057 | +0.008 | |
| Sodium Reactivity [\$] | -0.186 | -0.614 | +0.281 | -0.323 | -0.177 |
| CORE STATE AT THE FIRST FUEL MOTION | | | | | |
| time after LOF (time after B.O. [s]) | (model limit. reached before fuel motion start) | 28.33 (+10.38) | 69.08 (+52.48) | 30.68 (+11.72) | (calculation stop at clad melting) |
| Channel No. | | 13 (5/1) | 13 (5/1) | 13 (5/1) | |
| Normalized Power | | 1.62 | 32 | 24 | |
| Net Reactivity [\$] | | +0.326 | +0.912 | +0.952 | |
| Doppler Reactivity [\$] | | -0.251 | -1.050 | -0.304 | |
| Fuel Axial Expansion Reac. [\$] | | -0.121 | -0.813 | -0.378 | |
| Sodium Reactivity [\$] | | +0.353 | +3.051 | +0.407 | |
| Clad Motion Reactivity [\$] | | +0.248 | --- | +1.142 | |
| CORE STATE AT THE END OF THE CALCULATION | | | | | |
| time [s] | 29.095 | 30.283 | 69.123 | 31.300 | 19.44(*1) |
| Normalized Power | 1.24 | 1.25 | 62 | 1.6 | 0.687 |
| Net Reactivity [\$] | +0.471 | +0.161 | +0.891 | +0.070 | -0.051 |
| Doppler Reactivity [\$] | -0.071 | -0.359 | -1.118 | -0.438 | -0.088 |
| Fuel Axial Expansion Reac. [\$] | -0.055 | -0.098 | -1.805 | -0.422 | +0.040 |
| Clad Axial Expansion Reac. [\$] | +0.041 | +0.166 | +0.131 | +0.097 | |
| Sodium Reactivity [\$] | +0.074 | -0.544 | +3.265 | -0.587 | -0.177 |
| Fuel Motion Reactivity [\$] | 0 | -0.1 | 0.788 | -0.666 | 0 |
| Clad Motion Reactivity [\$] | +0.481 | +1.14 | 0 | +2.086 | 0 |
| Core Average Fuel Tem. [K] | | | | 2611 | |
| MAXIMUM NET REACTIVITY IN THE CALCULATION AFTER BOILING ONSET | | | | | |
| Max. Net Reactivity [\$] | +0.482 | +0.754 | +1.030 | +0.961 | |
| time [s] | 29.03 | 27.725 | 69.122 | 30.670 | |
| Normalized Power [Po] | 1.23 | 3.09 | 95 | 22.8 | |
| Major Component | steel motion | steel motion | void | steel motion | |
| MAXIMUM POWER IN THE CALCULATION AFTER BOILING ONSET | | | | | |
| Max. power [Po] | 1.24 | 3.31 | | 24.9 | |
| time [s] | 29.095 | 27.875 | | 30.673 | |
| Net Reactivity [\$] | +0.471 | +0.728 | | +0.956 | |

TABLE 4.3. ORDER OF BOILING ONSET UP TO THE 5TH CHANNEL
(ULOF BASE CASE)

| Order of B.O. | France | Germany | India | Japan | Russia |
|---------------------|-------------------|-------------------|-------------------|-------------------|-----------------------|
| 1st Ch. time [s] | 13 (5/1) 18.93 | 13 (5/1) 17.95 | 13 (5/1) 17.60 | 13 (5/1) 18.96 | 13 (5/1) 16.6 |
| 2nd Ch. time [s] | 1 (1/1) 19.73 | 1 (1/1) 18.64 | 4 (2/1) 18.26 | 1 (1/1) 19.76 | B.O. in Chs. 1/1, |
| 3rd Ch. time [s] | 4 (2/1) 19.82 | 4 (2/1) 18.78 | 10 (4/1) 18.36 | 4 (2/1) 19.85 | 2/1, 3/1, and 4/1 |
| 4th Ch. time [s] | 7 (3/1) 19.95 | 7 (3/1) 18.92 | 7 (3/1) 18.37 | 7 (3/1) 19.99 | occurs at 17.2 [s] |
| 5th Ch. time [s] | 10 (4/1) 20.05 | 10 (4/1) 19.01 | 1 (1/1) 18.43 | 10 (4/1) 20.09 | |

Dryout of the cladding occurs at 2.1 - 2.6 s after boiling onset in most codes (see Table 4.2). The axial position of dryout initiation is at about 80 % of the fissile length. The sodium boiling model in the PINCHTRAN code is based on the formulations similar to ANL code SAS1A which is thought to be too simple and insufficient. Consequently the results of the boiling transients with PINCHTRAN code are very slow compared with those of the other codes.

Clad melting is predicted to occur at about 3 to 5 s after boiling onset except for PINCHTRAN code. The power level is 0.5 to 0.7 Po (Po : nominal power) and the net reactivity is sub-critical (-0.1 to -0.4 \$).

The calculation with the GRIF-SM is terminated at 19.4 s (2.7 s after boiling onset) because clad melting is predicted and the phenomena after clad melting are not yet modeled in the code.

After a few seconds from clad melting onset, molten steel starts to move mainly upward. This steel motion introduces positive reactivity and causes a mild power transient. The calculation by French participant stops at 4s after clad motion onset because model limitation is reached. Just after this power transient caused by cladding motion, a fuel breakup and motion is predicted in the calculations by German and Japanese participants. The core state at the fuel breakup/motion onset is shown in Table 4.2. The net reactivity becomes positive and the power level exceeds the nominal value (1 Po).

The core state at the end of the calculation and the maximum net reactivity and power in the calculation are summarized in Table 4.2. It is clear that the power transient is very mild mainly due to the negative reactivity effect in the upper sodium layer, but removal of the molten steel from the core region leads to a positive reactivity insertion and it drives power increase resulting in fuel breakup. It is commonly concluded based on the present results that the accident enters into the transition phase.

(2) Transient behaviour of the reactivity and power in the boiling phase up to fuel pin breakup

Figures 4.1 (1) - (5) show the results of the reactivity and power transient behaviour in the boiling phase calculated by each participant and the order of boiling onset upto the 5th Channel is shown in Table 4.3. The general tendency which could be perceived from these figures is summarized in Table 4.4. An oscillation of the net reactivity is repeated a few times and the final positive reactivity insertion due to steel motion at +8 to +10 s after boiling onset causes a mild power increase leading to fuel breakup.

Voiding zone extension in Ch.13

Figures 4.2. (1) - (3) show the extension behaviour of the voiding zone in Ch.13 calculated by Germany, Japan and Russia respectively. All the figures show a common behaviour that the voiding region extends upward more rapidly, nevertheless the lower interface enters into the fissile region without delay. The lower interface of the voiding zone passes the core mid-plane at about 2 s after the boiling onset in these figures.

Figures 4.2. (1) and (3) also show the sodium void reactivity of Ch.13 itself together with the voiding zone extension. Both the figure show that the sodium void reactivity decreases to about - 0.2 \$ at 1.8 s after boiling onset as the upper interface enters into the upper sodium plenum region. Then the lower interface enters into the fissile region without delay and the sodium void reactivity of this channel is compensated with the positive void reactivity at the fissile zone. It reaches the saturation value, i.e. +0.07 \$ at 4.4 s after boiling onset.

The voiding behaviour of the other channels are similar to that of Ch.13 as shown in Fig. 4.2, therefore the increase of the sodium reactivity and the net reactivity during +2 to +6 s after boiling onset, which is described in Table 4.4, is caused by extension of the lower interface into the fissile region in the following boiling channels (see Table 4.3 too).

Figure 4.2. (3) also shows the extension behaviour of the dryout zone. It is clear that the lower interface of the dryout zone follows the lower interface of the voiding zone extension within 1 s of delay in the middle part of the fissile region because the linear power density is higher there.

General behaviour of the void reactivity insertion due to boiling extension over the core

Figure 4.3 shows the transient behaviour of the sodium void reactivity of each channel (Base Case, Japan). It can be observed from this Figure that the void reactivity in every Channel decreases first but it increases within a few seconds and approaches to a saturated value which corresponds to a fully voided channel condition of each coolant channel. The saturated value is positive in the low enrichment zone (LEZ) (Ch.1 to Ch.12) and half of the medium enrichment zone (MEZ) (Ch 13 to Ch.15). On the other hand, this value is nearly zero or negative in the rest of MEZ (Ch.16 to Ch.21) and high enrichment zone (Ch.22 to Ch.30). Because boiling onset occurs earlier in the hotter channels i.e. LEZ and MEZ (high-powered Channel such as Ch. 13 or Ch. 1), this incoherent boiling behaviour reveals first the characteristics of positive (non-negative) void worth of the core, even though the total void worth of the core is nearly zero or slightly negative as described in Table 4.1.

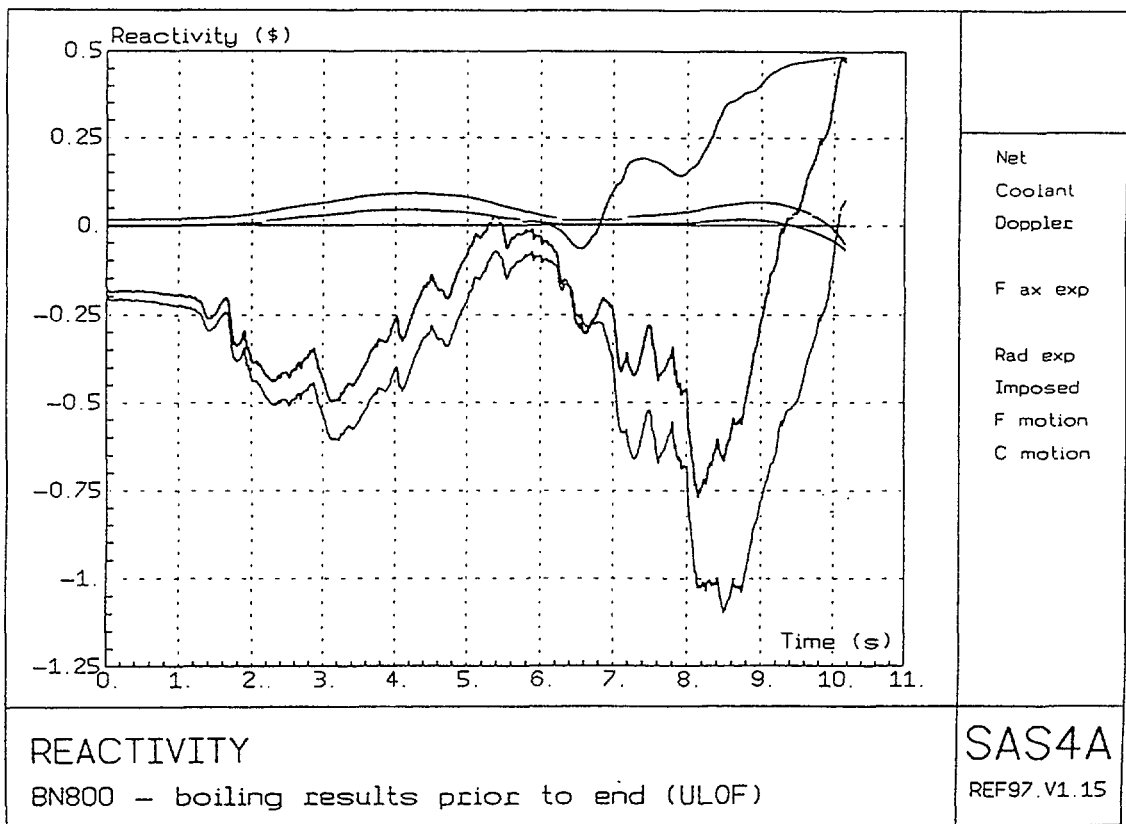
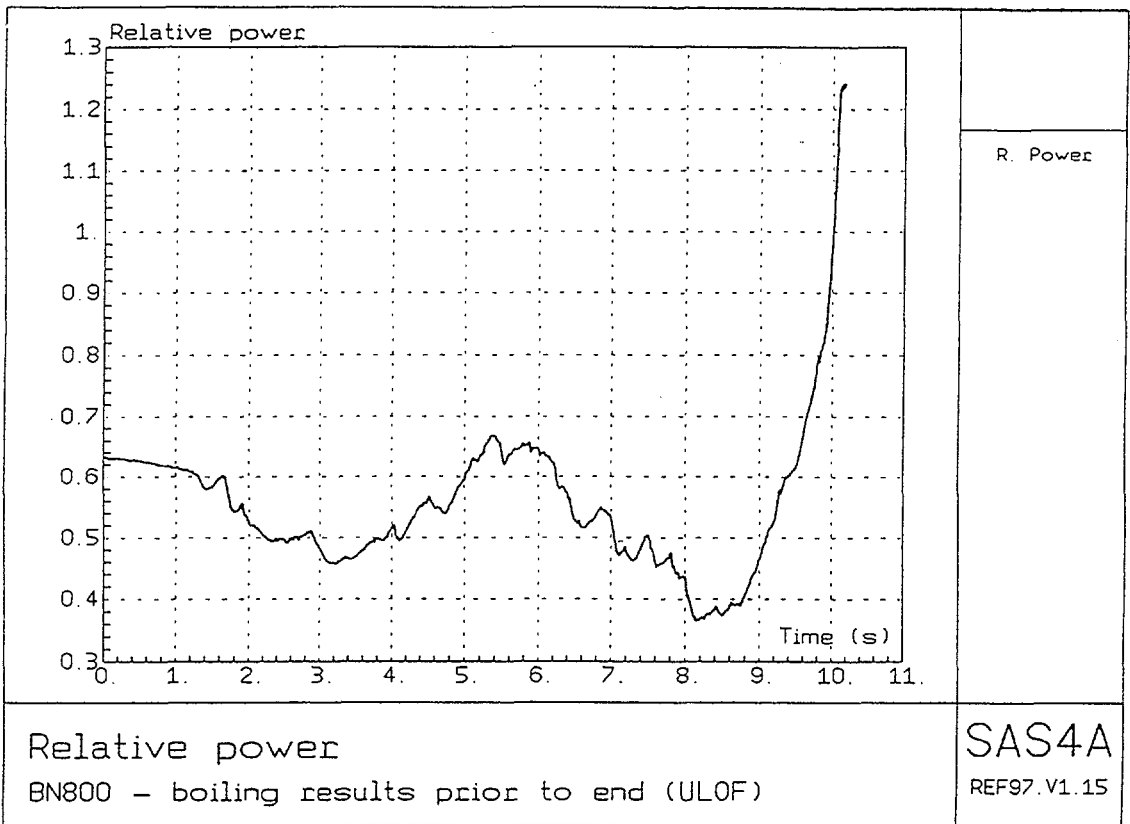
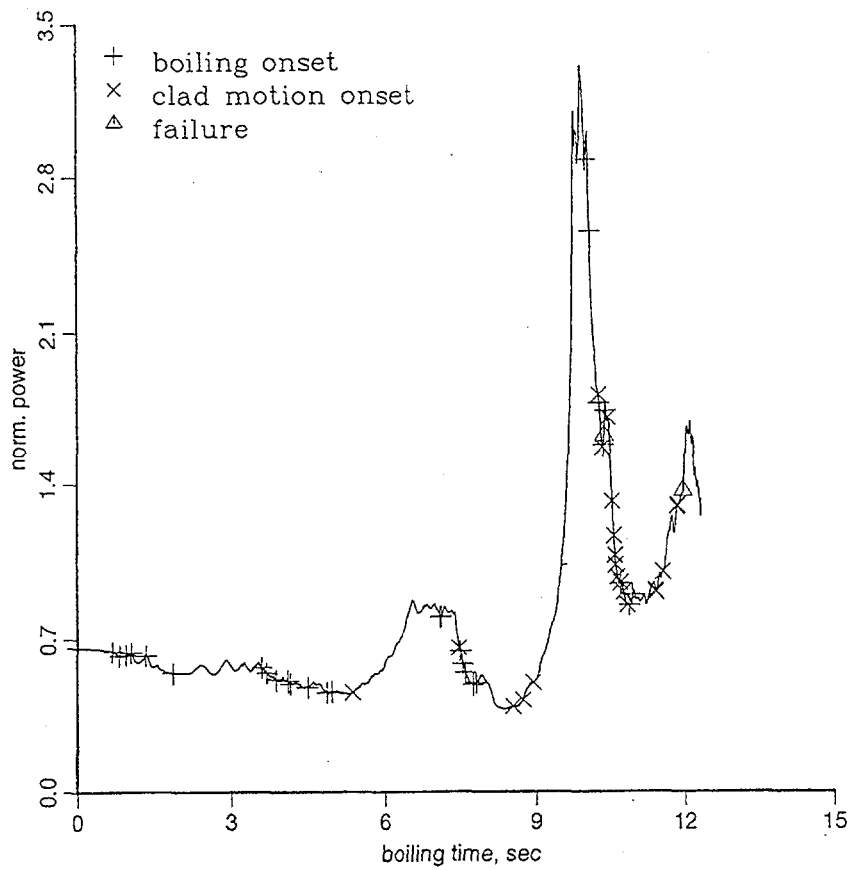
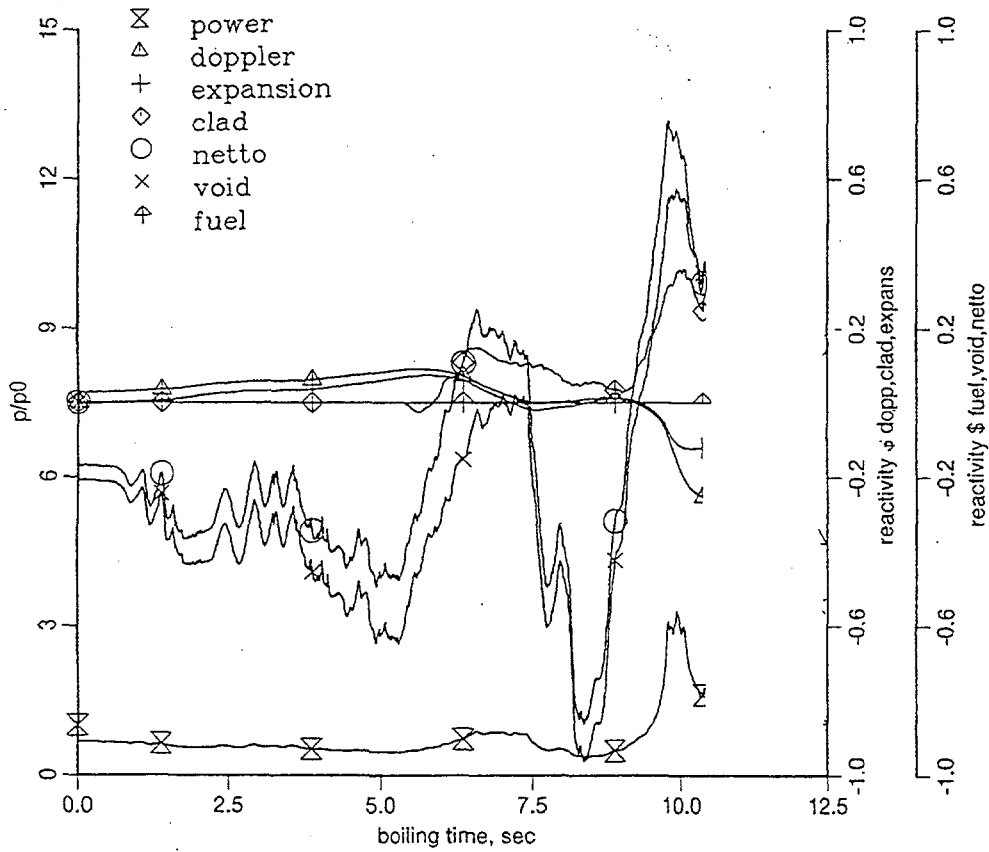


FIG. 4.1. Power and reactivity behavior after boiling onset (ULOF BASE CASE)
(1) France

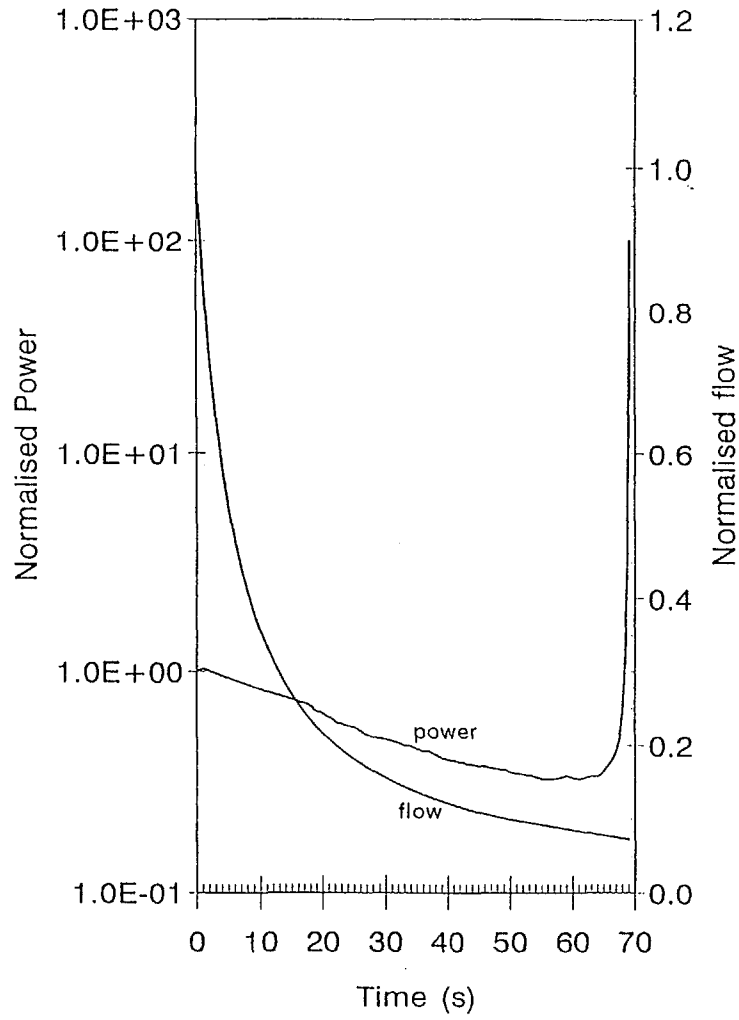


BN800 31 Channel 11.05.1998

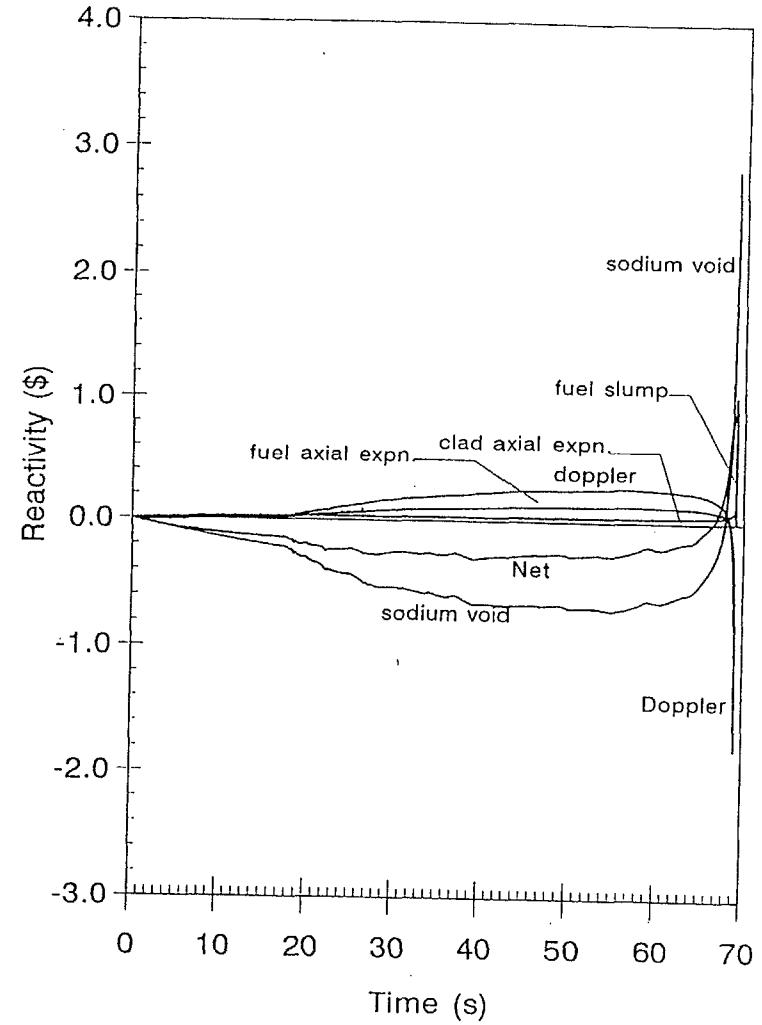


BN800 31 Channel 11.05.1998

FIG. 4.1. Power and reactivity behavior after boiling onset (ULOF BASE CASE)
 (2) Germany



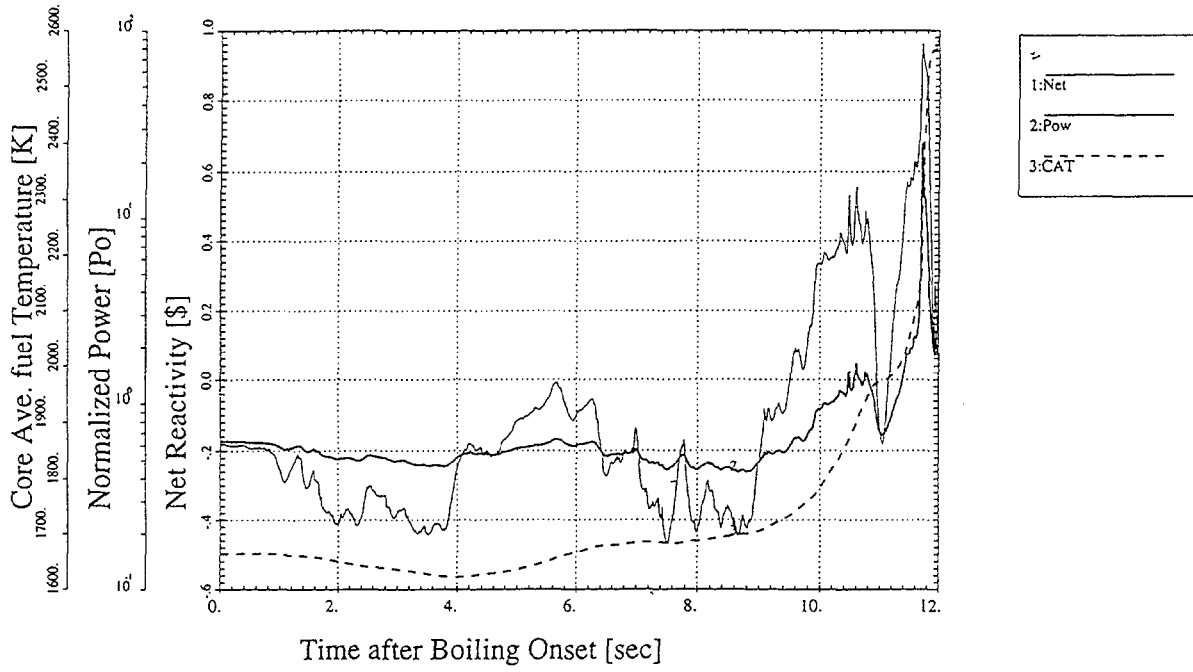
Power and Flow for ULOF (Base Case)



Reactivity for ULOF (Base Case)

FIG. 4.1. Power and reactivity behavior after boiling onset (ULOF BASE CASE)
(3) India

s4a.r96r1.bn



s4a.r96r1.bn

1:Net 2:Dop 3:FD 4:Void 5:FM 6:CM 7:RAD

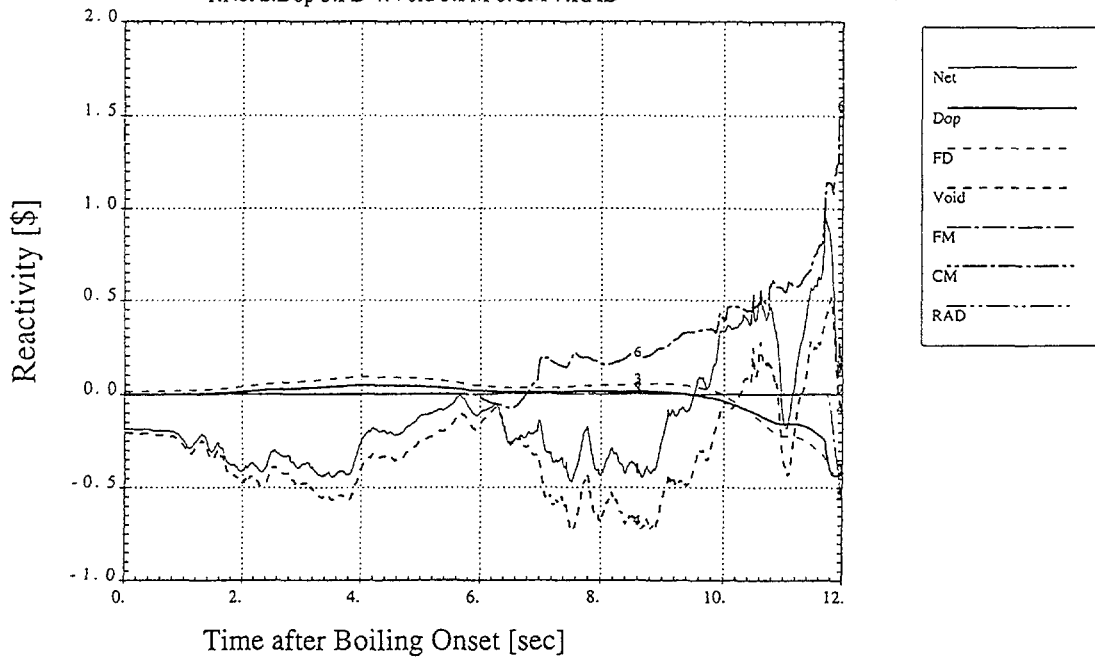
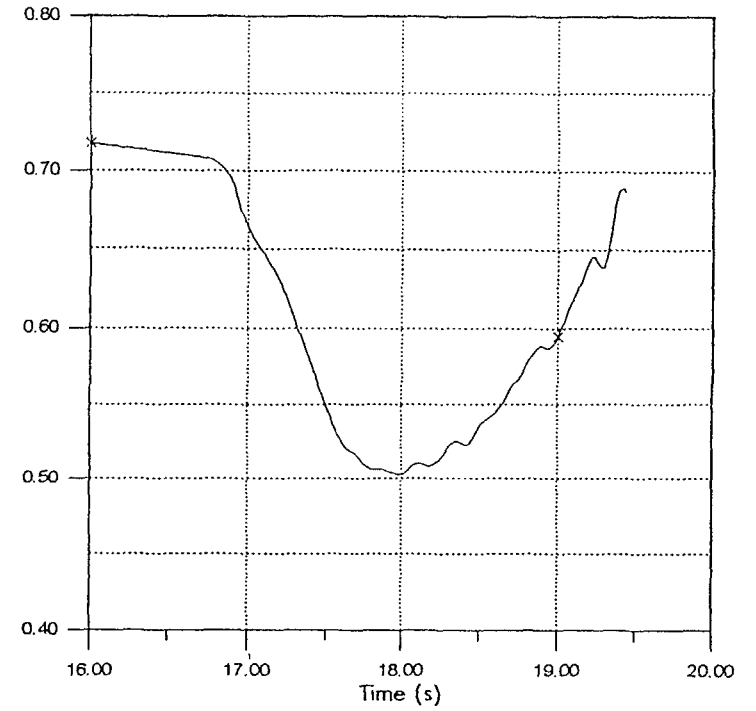
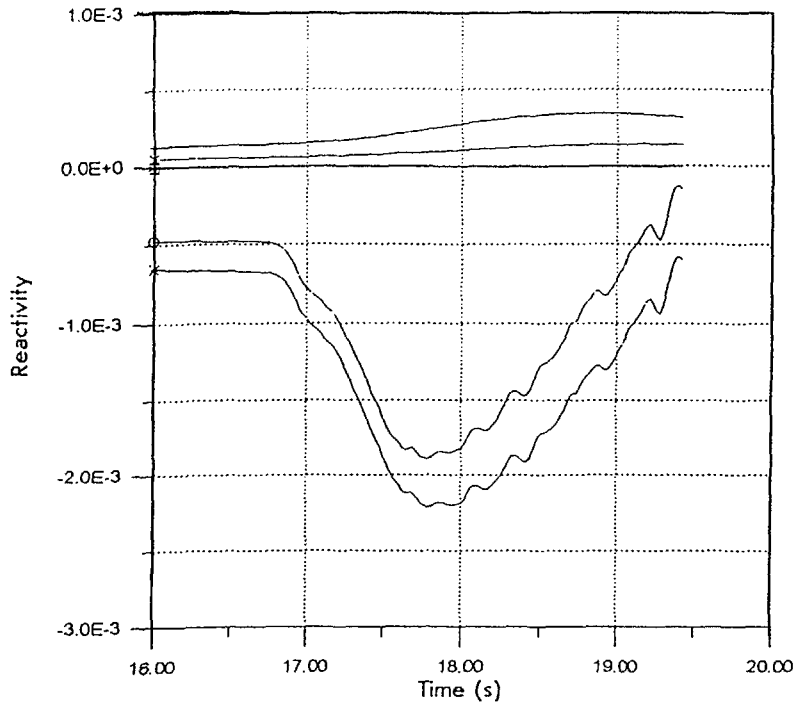


FIG. 4.1. Power and reactivity behavior after boiling onset (ULOF BASE CASE)
(4) Japan



- +— Doppler reactivity
- X— Axial expansion reactivity
- *— Sodium reactivity
- ◇— Radial expansion reactivity
- Control rods drivers expansion reactivity
- ▣— Control rods expansion reactivity
- Net reactivity

Reactivity versus time

Relative reactor power.

FIG. 4.1. Power and reactivity behavior after boiling onset (ULOF BASE CASE)
(5) Russia

TABLE 4.4 TRANSIENT BEHAVIOUR AFTER BOILING ONSET UP TO FUEL BREAKUP

| time after boiling onset | observation |
|--------------------------|---|
| 1) +0 - +2 s | net reactivity decreasing to -0.4 ~ -0.5 \$ due to negative void reactivity insertion, power decreasing to 0.4 ~ 0.5 Po |
| 2) +2 ~ +6 s | net reactivity increasing to 0 \$ due to positive void reactivity insertion, power increasing to 0.6 ~ 0.7 Po |
| 3) +6 ~ +8 s | decreasing of sodium reactivity but increasing of steel motion reactivity, totally decreasing of net reactivity to -0.7 \$ and power decreasing to 0.4 Po |
| 4) +8 ~ +10 s | increasing of net reactivity to positive value due to positive reactivity of void and steel motion, and power exceeding 1.0 Po |

Steel motion behaviour

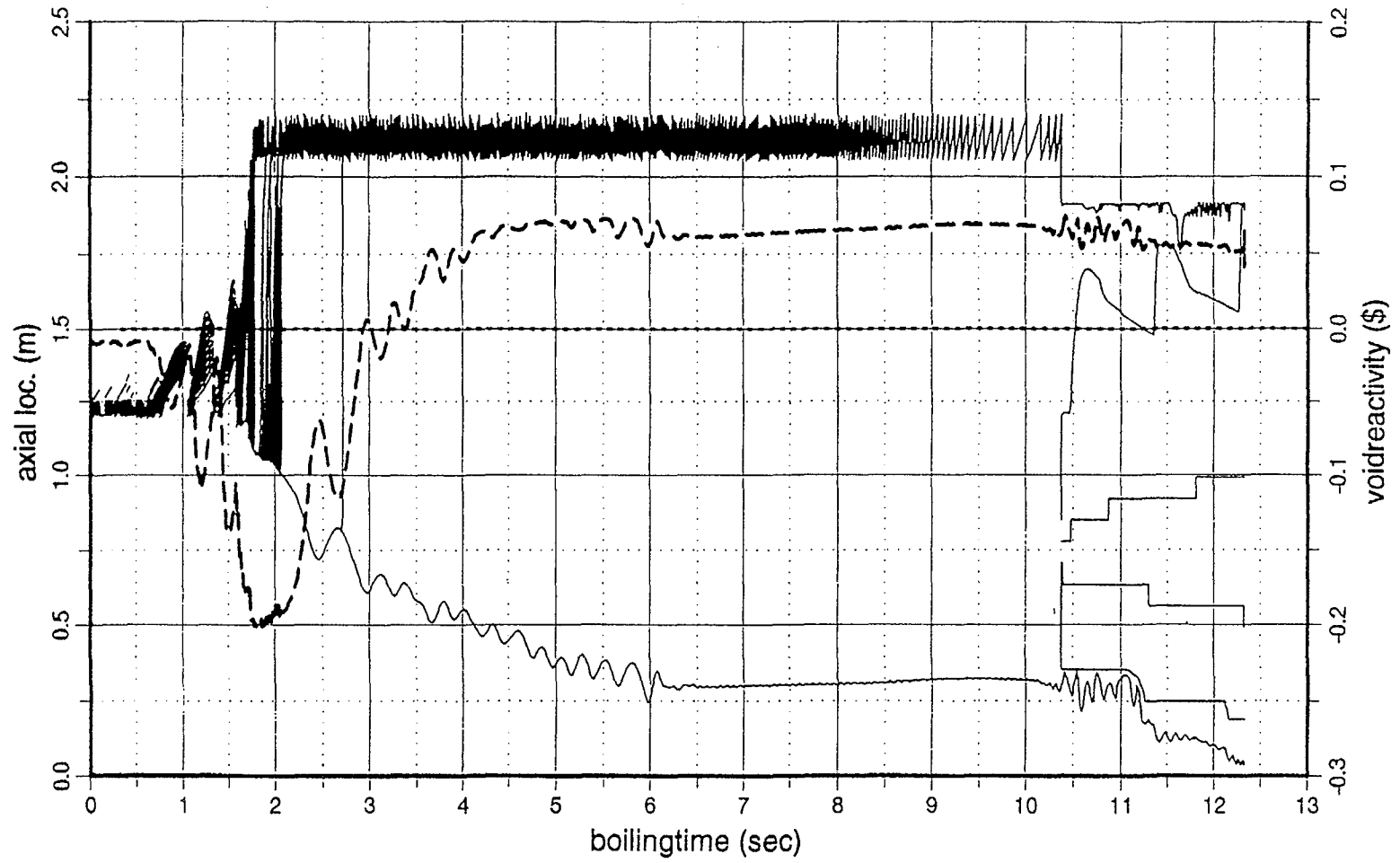
Figures 4.1 (1), (2), and (4) include the power and reactivity behaviour after steel motion onset. It is read from these figures that steel motion begins at 5 to 6 s after boiling onset, and the steel motion reactivity gradually increases up to 0.5 \$ at 10 s after boiling onset. Figures 4.4 (1) and (2) show the steel motion reactivity of each channel. Its behaviour of Ch. 13 is similar between the results from France and Japan up to 0.2 \$ at 10 s after boiling onset, but the results from Japan, Fig. 4.4 (2), shows a further increase up to 0.4 \$ in Ch. 13 at 11 - 12 s. This is because the switching over of the calculation models from the clad motion model (CLAP) to a general material motion model (LEVITATE).

Molten steel motion behaviour calculated by Japanese participant is presented in detail in Fig. 4.5. This shows that the initial motion of the molten steel goes downward to the core mid-plane (see Fig. 4.5 (1)) and this motion results in several cents of negative reactivity insertion. Steel crust is formed on the cladding at the lower part of the fissile zone (see Fig. 4.5 (2)). After about 1 s after clad motion onset, molten steel reaches at the top node of the fuel (see (3)), then the calculation model is switched from the clad motion model to a general material motion model. Molten steel moves upward up to the reflector zone and forms some crust on the reflector surface ((4) ~ (6)). This upward steel motion leads to positive reactivity insertion and, together with the void reactivity insertion, it causes a power increasing of 25 Po and net reactivity reaching 0.961 \$ at 30.67 s (Fig. 4.1 (4)).

Fuel motion behaviour

Just after the power increase due to the positive reactivity insertion of the steel motion together with the voiding extension, a fuel breakup and motion is predicted at 28 to 31 s in the calculation of SAS4A by Germany and Japan (Table 4.2). Figures 4.6 (1) and (2) show the power and reactivity behaviour after fuel motion initiation.

Fuel motion behaviour is presented in detail in Fig. 4.7 (Japan). The fuel and steel moves mainly upward direction because of the sodium vapor flow (see Fig. 4.7 (2) ~ (5)), but most of them remains within the fissile zone (see (6) ~ (8)). The wrapper wall structure is



BN800/31Ch. ichan= 13 boiling onset= 17.955 sec

FIG. 4.2. Extension behavior of the voiding zone (ULOF BASE CASE, Ch. 13)
(1) Germany

SAS4A r96r1.bn

CH.13

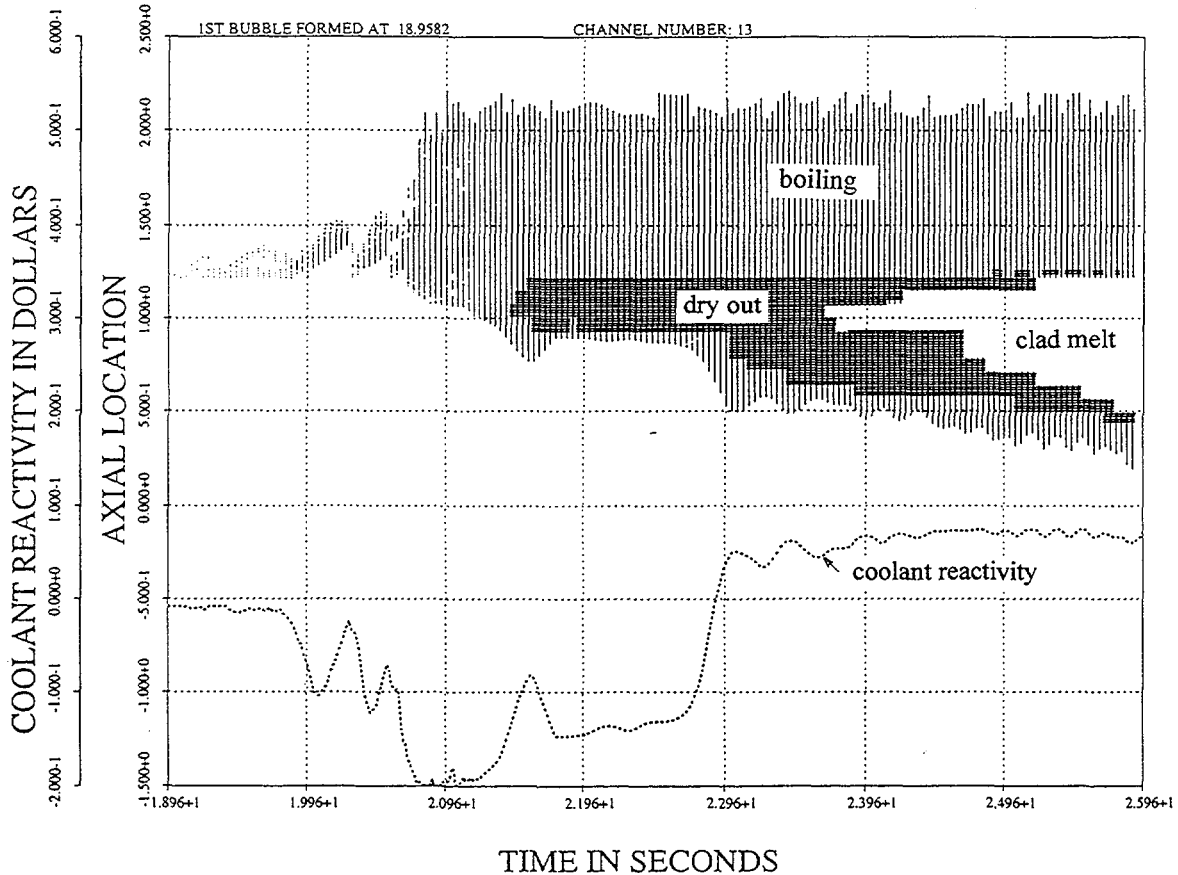
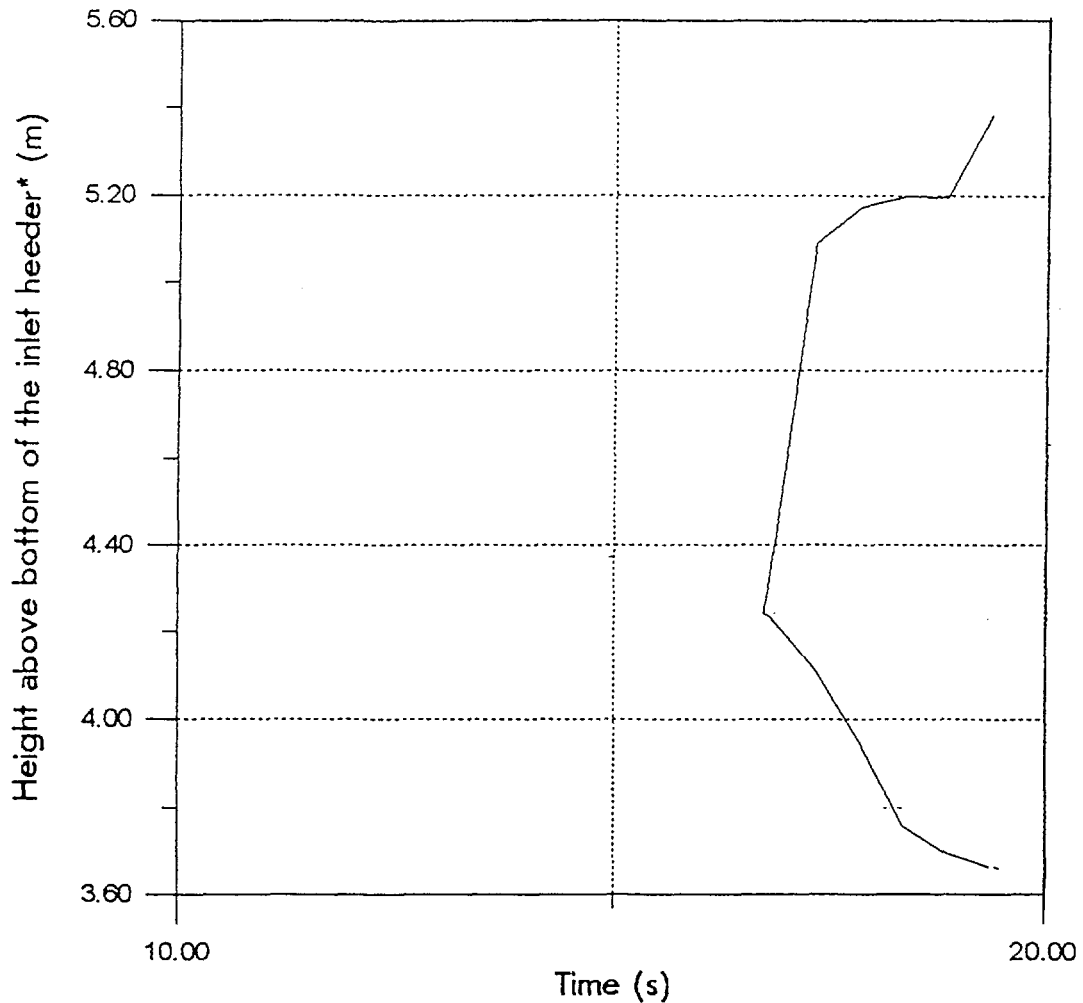


FIG. 4.2. Extension behavior of the voiding zone (ULOF BASE CASE, Ch. 13) (2) Japan

ablated by the molten fuel and steel in the coolant channel and dispersed mainly upward together with the molten fuel. This displacement of the wrapper tube steel also gives an additional positive reactivity effect. A half of the wrapper wall thickness is ablated at 31.36 s (see Fig. 4.7 (8), 0.7 s after fuel breakup). This situation is judged to be one of the model limitations of SAS4A because the wrapper tube strength is lost and a radial material motion could occur soon. The power level is higher than 1 Po and the net reactivity stays around delayed critical. Consequently entering the transition phase is inevitable but very slowly because the fuel stays mainly in the fissile region and fuel escape from the core region is not sufficient to lead the core to the permanent shut down.

The result from Germany (Fig. 4.6 (1)) shows that a very mild power transient occurs at 27.7 - 27.9 s up to 3.3 Po due to positive reactivity effect of both the steel motion and the voiding evolution. The switching over of the calculation models from the clad motion model to a general material motion model is not taken into account. Nevertheless, this power increase is sufficient to cause fuel breakup in Ch.13 at 28.33s. Fuel dispersal is not significant compared with Fig. 4.6 (2) (Japan) because the preceding power increase is much milder, and thus the fuel reactivity stays around the original level (see Fig. 4.6 (1)). Model limitation (wrapper wall melting and initiation of the radial material motion) is also reached at 2 s into fuel breakup. The power level is around 1 Po and the net reactivity is about 0.2 \$.



Channel 5: Boiling front.

*) The height of the fissile zone is 4.24 m.

FIG. 4.2. Extension Behavior of the Voiding Zone (ULOF BASE CASE, Ch.13)
(3) Russia

It is indicated based on the results that the transient behaviour of the initiating phase in this type of core becomes very mild compared with that of the conventional design core. Prompt critical will not be exceeded. These are attributed to the characteristics of the reduced void worth in this core design. Moreover, it is also clarified that steel motion reactivity plays an important role to drive the net reactivity and power increase in the initiating phase instead of the positive void reactivity in a conventional core design.

4.1.2. Parametric case results

Parametric Case was investigated by the participants from Germany, India, Japan and Russia.

Outline

The event progression in Parametric Case is similar to that in Base Case except for the time scale which is prolonged due to full consideration of the radial core expansion effect. The calculated results by each participant are summarised in Table 4.5.

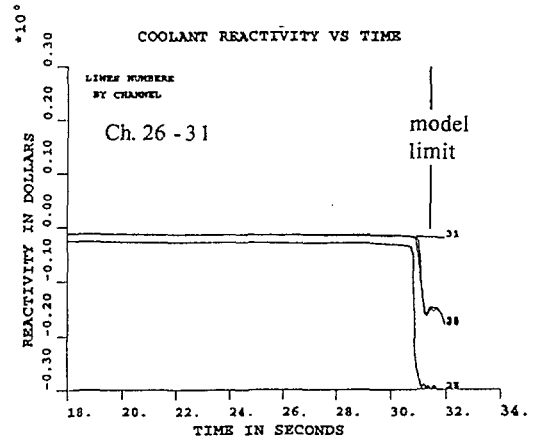
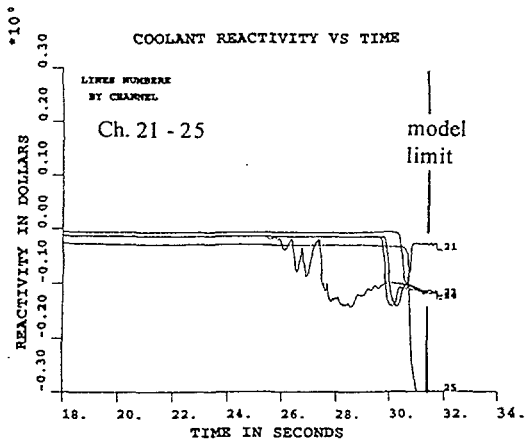
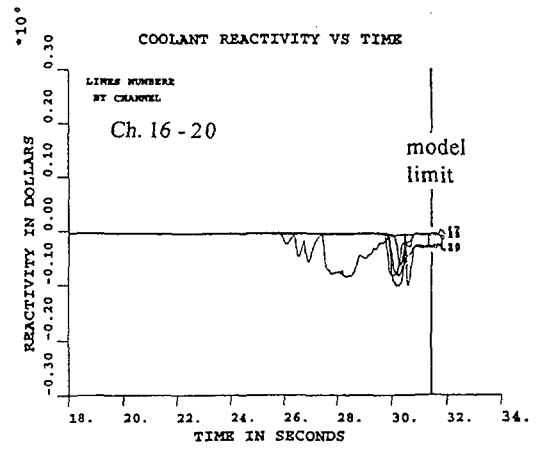
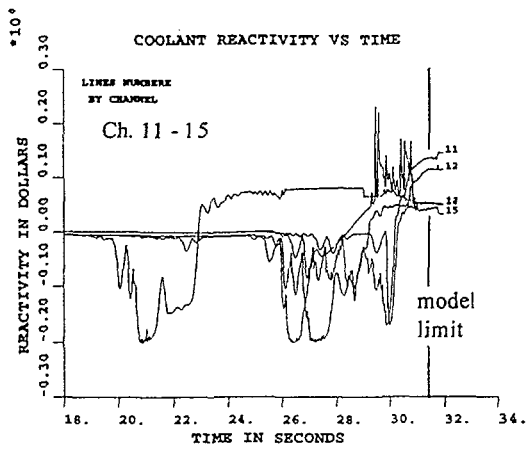
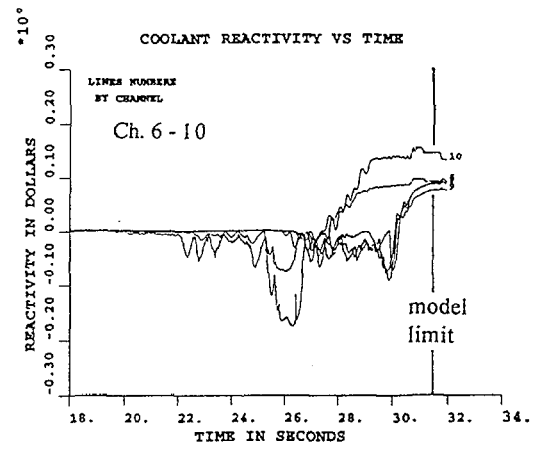
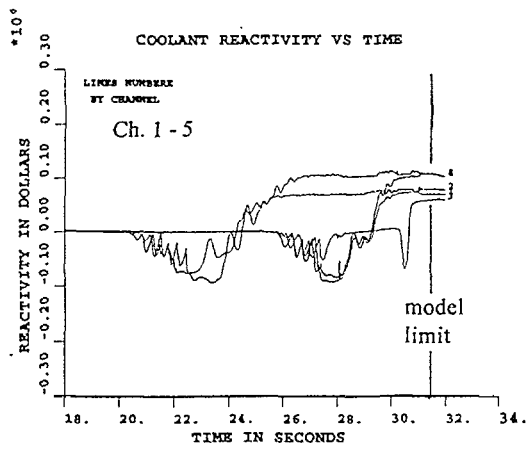


FIG. 4.3. Sodium void reactivity of each channel (ULOF BASE CASE, Japan)

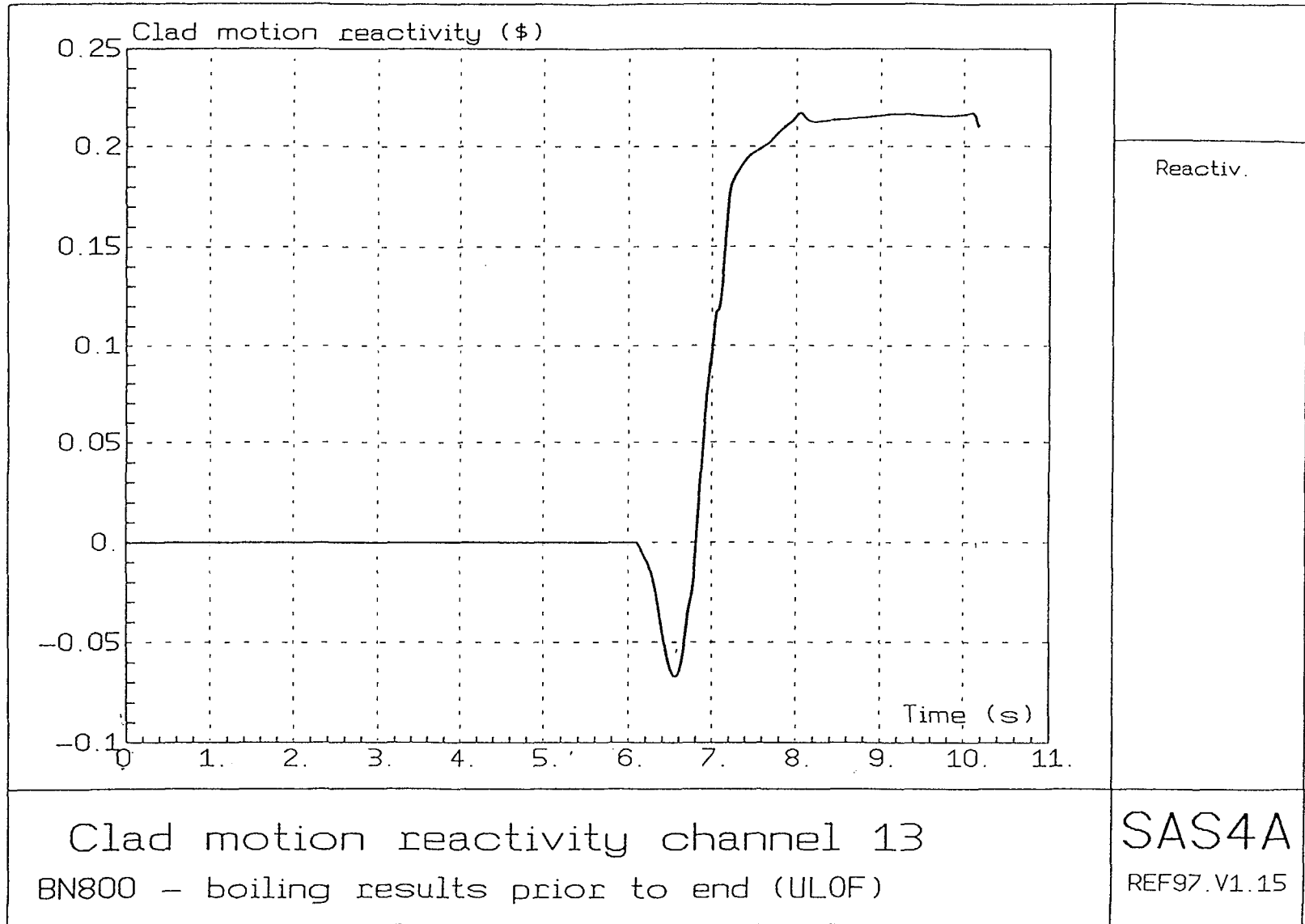


FIG. 4.4. Steel motion reactivity (ULOF BASE CASE) (1) France

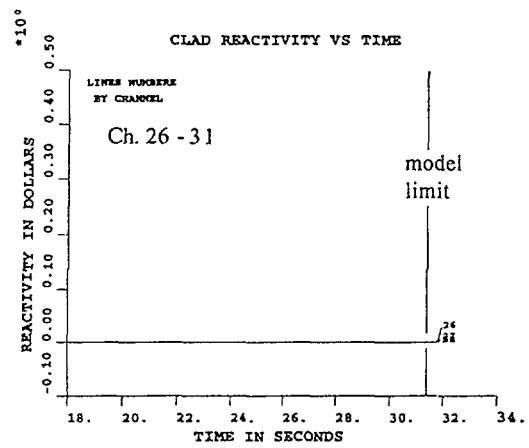
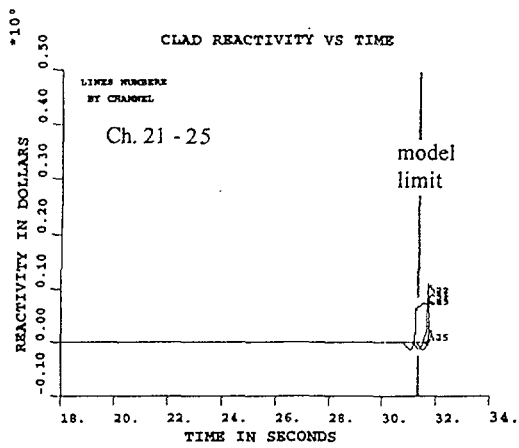
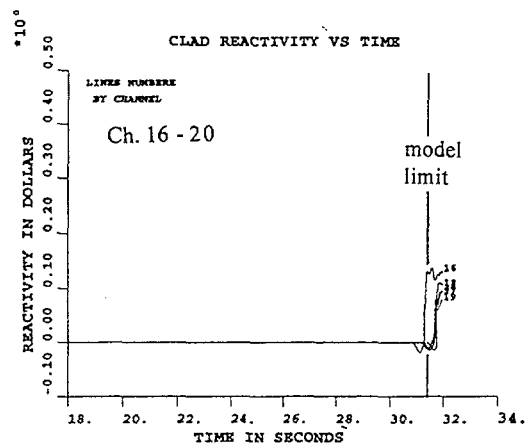
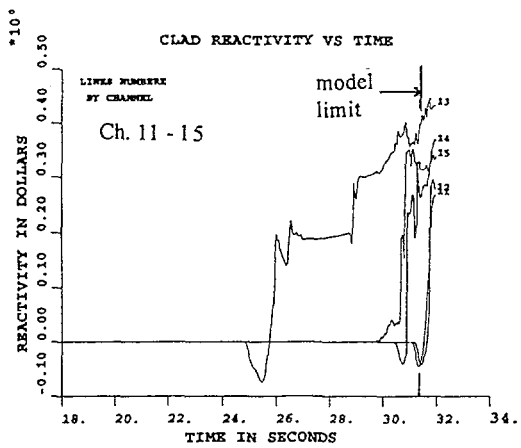
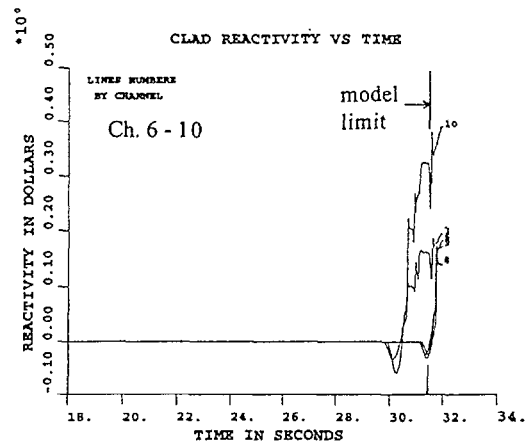
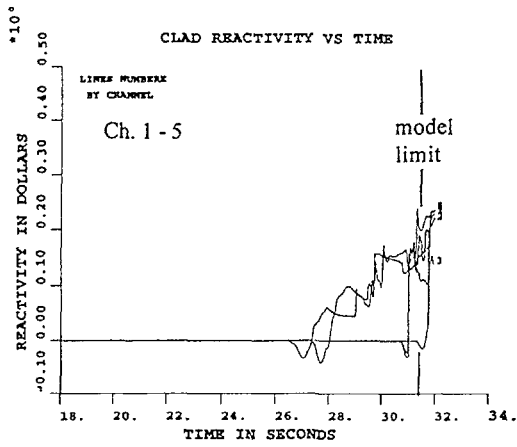


FIG. 4.4. Steel motion reactivity (ULOF BASE CASE) (2) Japan

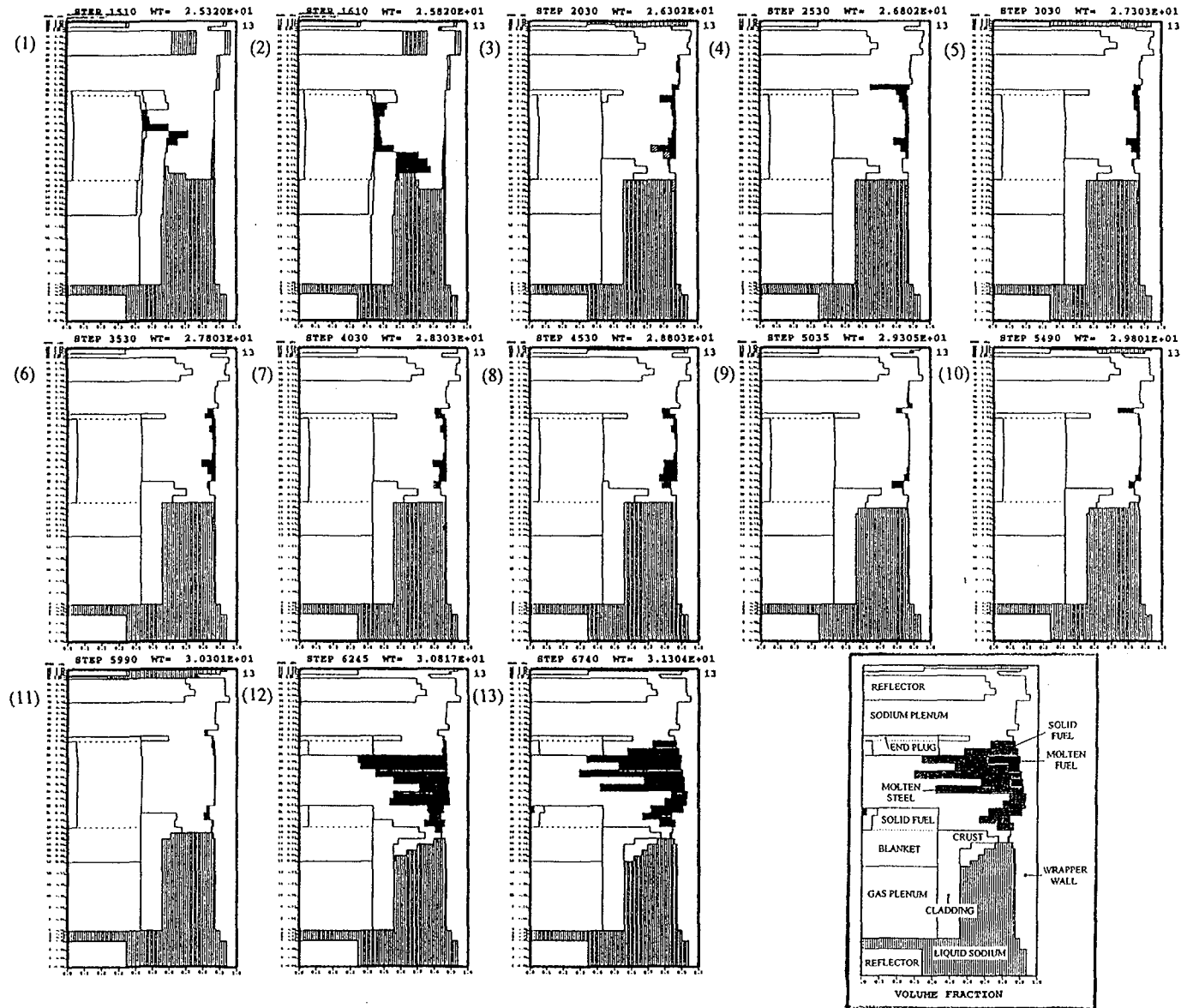
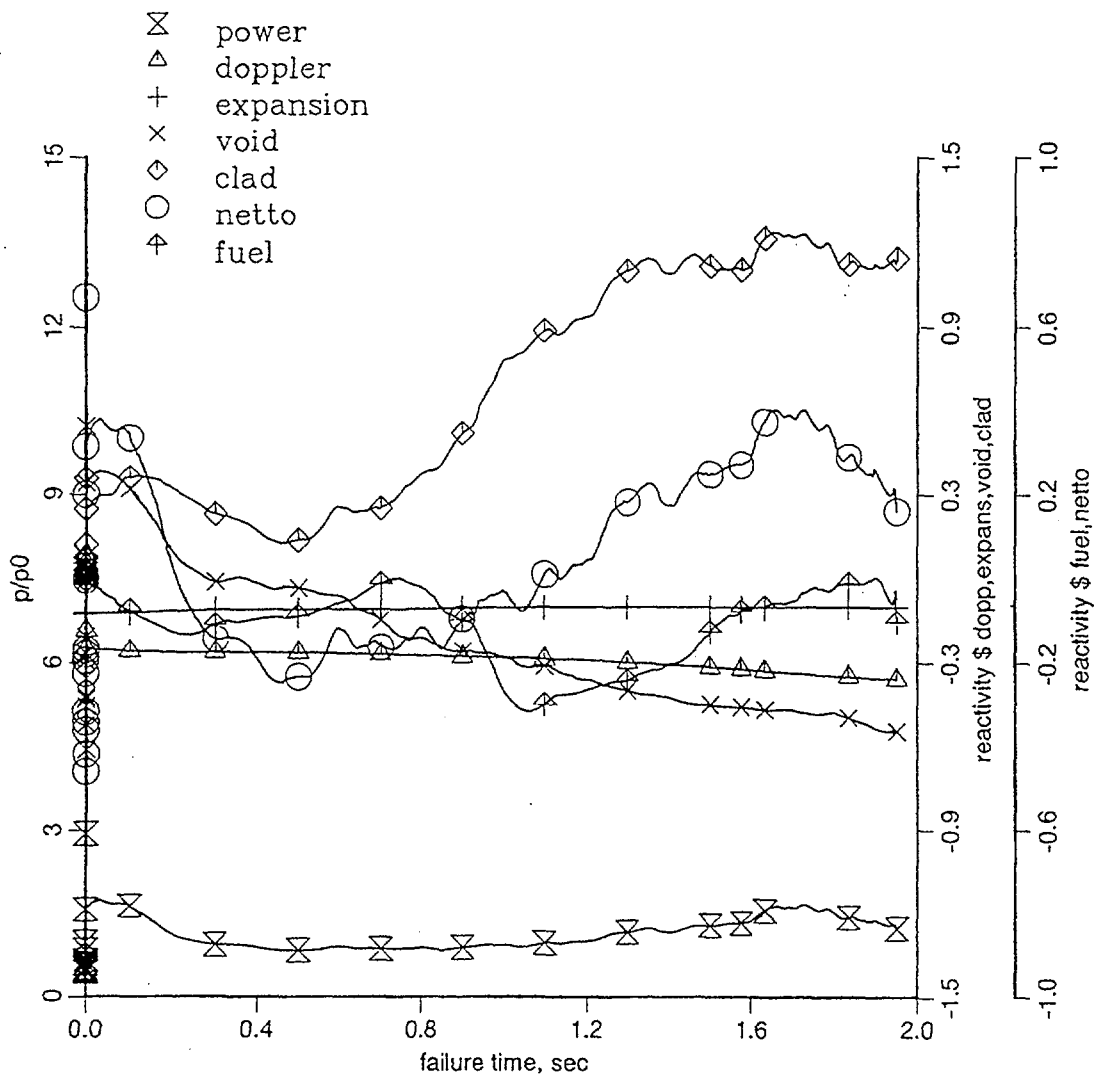


FIG. 4.5. Steel motion behaviour (ULOF BASE CASE, Ch. 13, Japan)

All the codes predict boiling onset in Parametric Case, too. The first coolant boiling occurs in Ch. 13 as well as in Base Case but the time is at about 29 to 33 s into transient which is almost double (see Table 4.5). Dryout of the cladding is predicted in Parametric Case by all the participants. Table 4.5 summarizes the timing and axial position of dryout in Ch. 13. Dryout occurs at 5 s after boiling onset in the result from Russia and 13 - 17 s by Germany and Japan. The axial position of dryout is higher than 90 % of the fissile length and this is higher than that of Base Case because of the slower extension of the voiding zone.

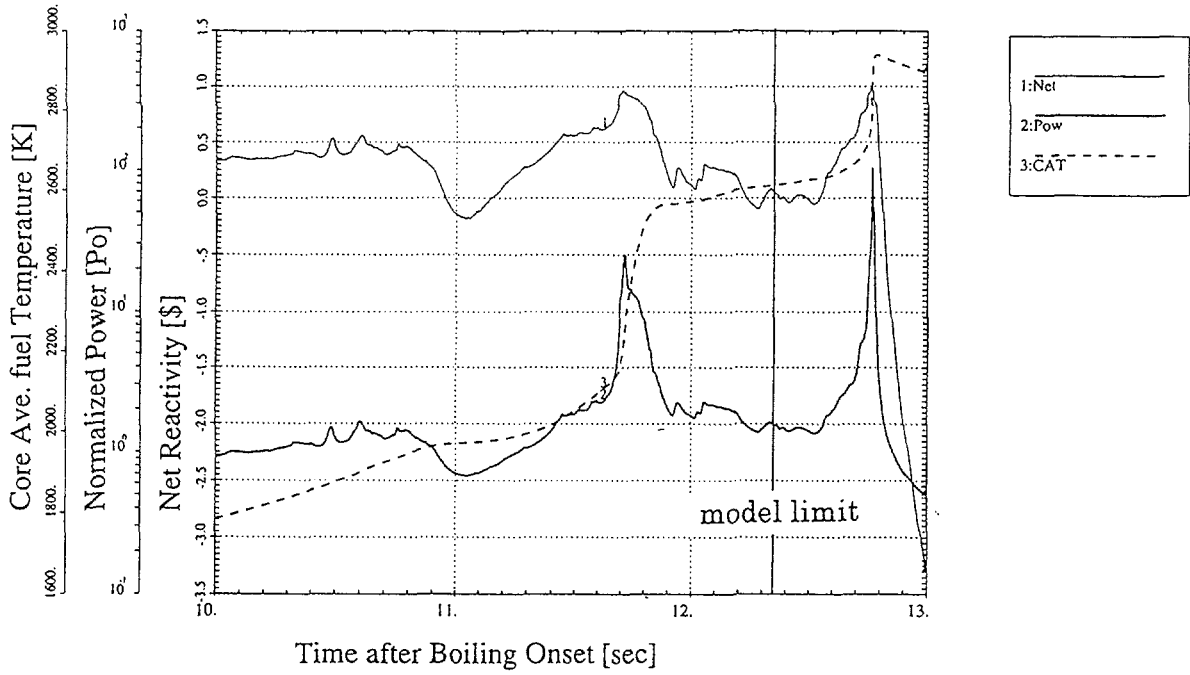
It is concluded based on the presented results that clad melting occurs in Parametric Case, too. The results of clad melting and following phenomena are presented from Germany and Japan (see Table 4.5). Clad melting is predicted to occur at about 20 - 23 s after boiling onset. The power level at this time is about 0.3 of the nominal power and the net reactivity is negative (-0.2 to -0.5 \$). These values are smaller than those in Base Case (-0.1 to -0.2 \$), because radial core expansion reactivity reaches about -0.5 \$ in both the cases.



BN800 31 Channel 11.05.1998

FIG. 4.6. Power and reactivity behavior after fuel motion (ULOF BASE CASE)
(1) Germany

s4a.r96r1.bn



s4a.r96r1.bn

1:Net 2:Dop 3:FD 4:Void 5:FM 6:CM 7:RAD

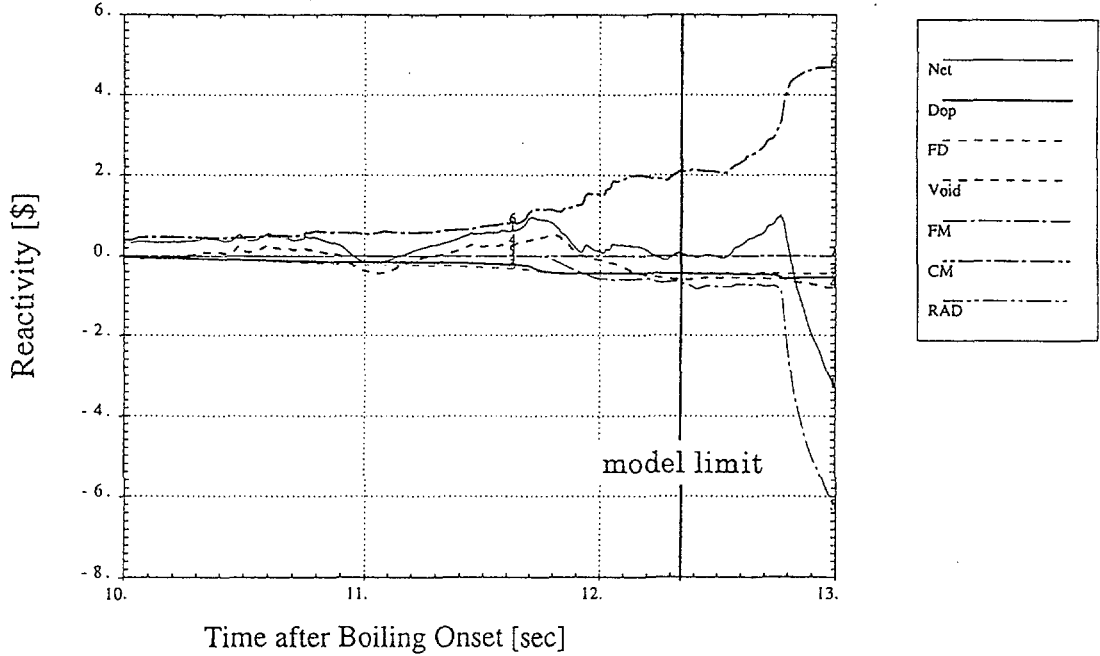


FIG. 4.6. Power and reactivity behavior after fuel motion (ULOF BASE CASE)
(2) Japan

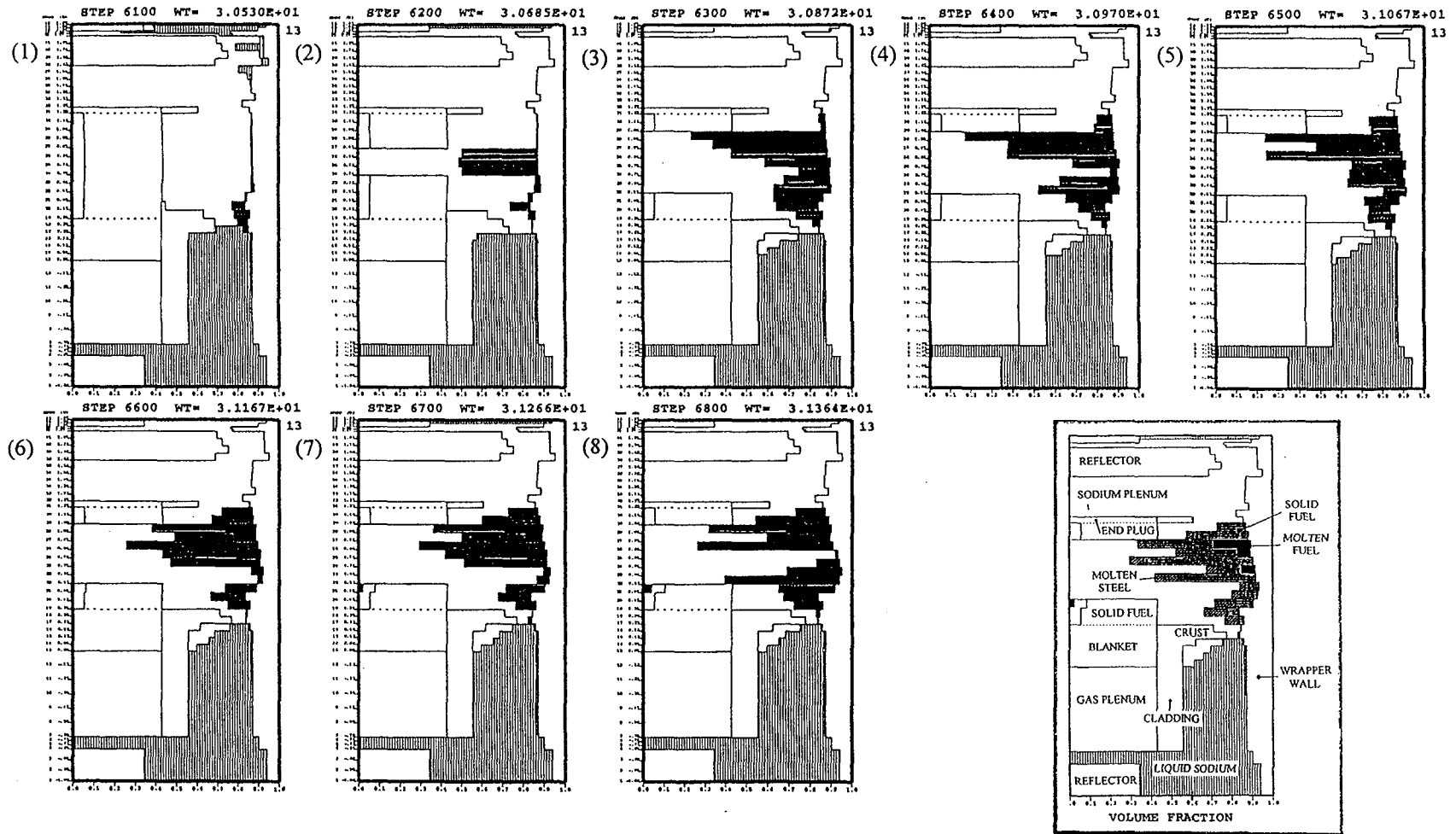


FIG. 4.7. Fuel motion behaviour (ULOF BASE CASE, Ch. 13, Japan)

TABLE 4.5. SUMMARY OF THE ULOF CALCULATION (PARAMETRIC CASE)

| Parameters \ Participant | Germany | India | Japan | Russia |
|--|-------------------|-----------------------------|-----------------------|-----------------------------|
| BOILING ONSET | | | | |
| 1st Ch. | 13 (5/1) | 13 (5/1) | 13 (5/1) | 13 (5/1) |
| time [s] | 28.88 | 32.29 | 33.16 | 31.4 |
| DRYOUT | | | | |
| time after LOF (time after B.O. [s]) | 42.13 (+13.25) | (dryout predicted) | 50.57 (+17.41) | 36.5 (+5.1) |
| axial position from BFC [cm] | 78 - 85 | | 72 - 79 | 77 - 84 |
| CORE STATE AT THE FIRST CLAD MELTING | | | | |
| time after LOF (time after B.O. [s]) | 49.05 (+20.17) | (clad melting predicted) | 55.9 (+22.73) | (clad melting predicted) |
| Channel No. | 13 (5/1) | | 13 (5/1) | |
| Normalized Power | 0.27 | | 0.32 | |
| Net Reactivity [\$] | -0.529 | | -0.161 | |
| Doppler Reactivity [\$] | +0.288 | | +0.239 | |
| Fuel Axial Expansion Reac. [\$] | +0.270 | | +0.291 | |
| Clad Axial Expansion Reac. [\$] | -0.008 | | -0.011 | |
| Sodium Reactivity [\$] | -0.569 | | -0.186 | |
| Radial Core Exp. Reac. [\$] | -0.510 | | -0.491 | |
| CORE STATE AT THE FIRST FUEL MOTION | | | | |
| time after LOF (time after B.O. [s]) | 61.42 (+32.54) | (calculations stop at | 80.46 (*) (* after | (calculations stop at |
| Channel No. | 13 (5/1) | onset of | model | clad melting) |
| Normalized Power | 0.88 | fuel melting) | limitation | |
| Net Reactivity [\$] | +0.227 | | reached) | |
| Doppler Reactivity [\$] | -0.162 | | | |
| Fuel Axial Expansion Reac. [\$] | -0.011 | | | |
| Sodium Reactivity [\$] | +0.485 | | | |
| Clad Motion Reactivity [\$] | -0.536 | | | |
| Radial Core Exp. Reac. [\$] | +0.354 | | | |
| CORE STATE AT THE END OF THE CALCULATION | | | | |
| time [s] | 62.11 | | 77.5 | (calculations |
| Normalized Power | 0.9 | | 0.26 | stop at |
| Net Reactivity [\$] | +0.264 | | -0.914 | clad melting) |
| Doppler Reactivity [\$] | -0.193 | | -0.014 | |
| Fuel Axial Expansion Reactivity | -0.007 | | -0.003 | |
| Sodium Reactivity [\$] | +0.083 | | -1.164 | |
| Radial Core Expansion Reactivity | -0.542 | | -0.440 | |
| Fuel Motion Reactivity [\$] | -0.084 | | -- | |
| Clad Motion Reactivity [\$] | +0.35 | | +0.670 | |
| Core Average Fuel Tem. [K] | N.A. | | 1795 | |
| MAXIMUM NET REACTIVITY IN THE CALCULATION AFTER BOILING ONSET | | | | |
| Max. Net Reactivity [\$] | +0.710 | | +0.541 | |
| time [s] | 60.205 | | 76.233 | |
| Normalized Power [Po] | 1.675 | | 0.976 | |
| Major Component | Steel motion | | steel motion | |
| MAXIMUM POWER IN THE CALCULATION AFTER BOILING ONSET | | | | |
| Max. power [Po] | 1.896 | | 0.976 | |
| time [s] | 60.655 | | 76.233 | |
| Net Reactivity [\$] | +0.641 | | +0.541 | |

Steel motion is also predicted in the results from Germany and Japan. Because the steel motion leads to positive reactivity insertion, net reactivity and power increase furthermore. Fuel breakup is predicted at 61 s during a very mild power increase in the results from Germany (~2 Po). The results from Japan shows fuel breakup at 80 s into transient, but it is later than model limitation is reached (wrapper wall melt-through) at 77.5 s.

The core state at the end of the calculation and the maximum net reactivity and power in the calculation are summarized in Table 4.5. It is observed that the power transient is milder than Base Case due to radial core expansion effect in addition to the negative reactivity worth in the upper sodium layer. However removal of the molten steel from the core region also leads to a positive reactivity insertion and it drives a mild power increase resulting in fuel breakup. It is concluded based on the present results that the accident enters into the transition phase even if the radial core expansion effect is fully considered.

Transient behaviour of the reactivity and power in the boiling phase

Figures 4.8 (1) - (3) show the reactivity and power transient behaviour in the boiling phase of the Parametric Case by the participant from Germany, Japan and Russia. It is clear from the Figures that the transient behaviour becomes milder compared with the Base Case due to consideration of the core radial expansion feedback which is approximately -0.4 \$ at boiling onset and reaches -0.5 \$ during boiling phase. Although the deviation of the results among the codes becomes somehow notable, the general tendency seems to be similar to that of the Base Case except for the enlarged time scale.

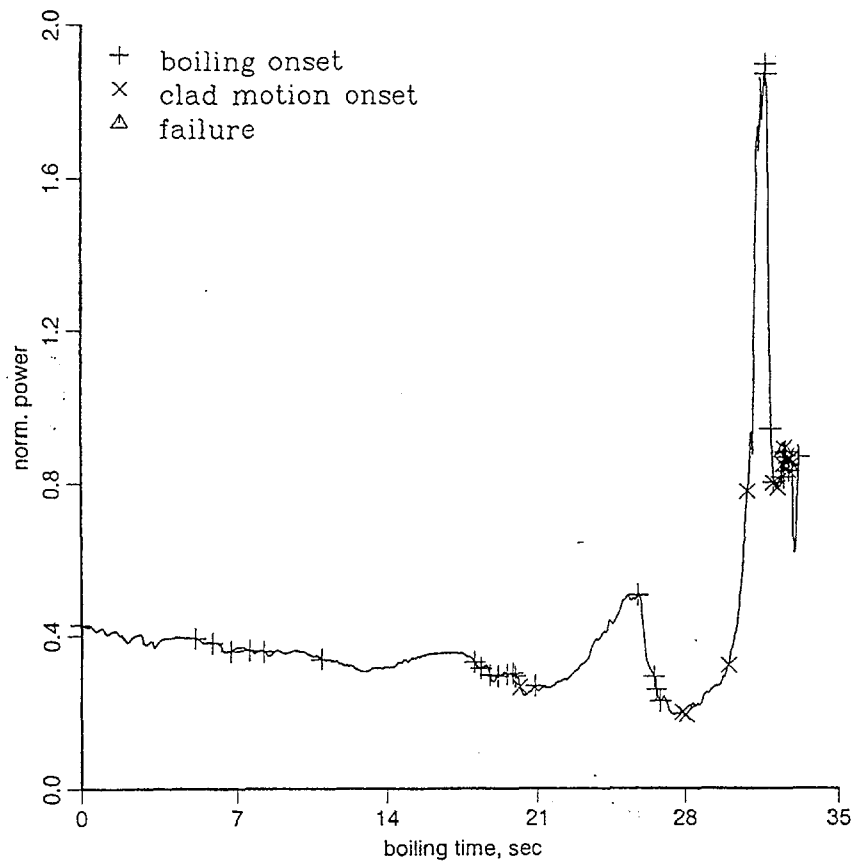
After boiling onset at about 28 to 33 s under 0.4 of the normalized power, voiding zone extension introduces negative reactivity first and then positive values later. This basic behaviour of the void reactivity insertion from each channel causes an oscillatory behaviour of the total void reactivity. Clad melting is predicted at 49 to 56 s (SAS4A code family) and results in molten clad motion. This positive reactivity causes a mild power transient and leads to fuel breakup.

Extension of the voiding region in Ch.13

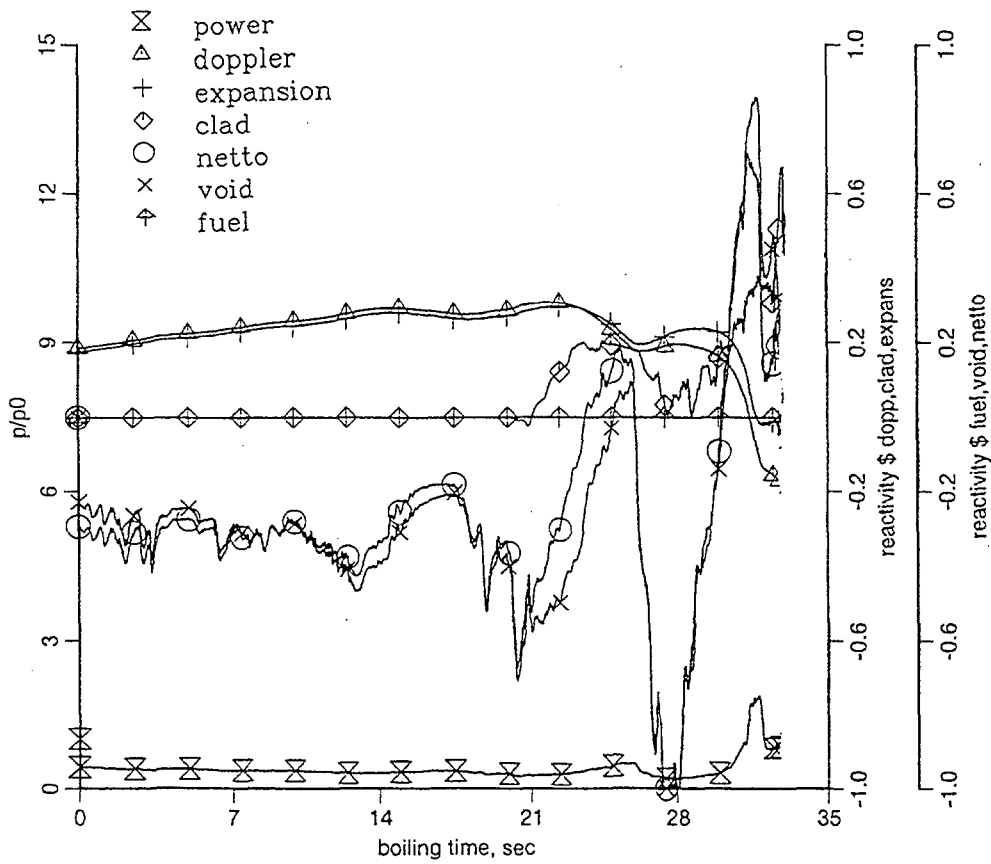
Figure 4.9 (1) - (3) show the calculated results by Germany, Japan and Russia of the extension behaviour of the voiding zone in Ch. 13 for the Parametric Case. In Fig. 4.9 (3) the voiding zone extends as similar as that in the Base Case. But on the other side in Fig. 4.9 (1) and (2) the voiding is reduced within several seconds and it appears again. This cycle continues for 12 to 13 s and then a typical extension of the voiding zone is observed. After the lower interface entering into the fissile region, the phenomena become similar to those of the Base case.

Figure 4.9 (2) also shows the extension behaviour of the dryout zone. The general tendency is similar to that observed in Fig. 4.2 (2) except that the axial position of the initial dryout onset is higher in Parametric Case.

Void reactivity behaviour of each Channel is presented in Fig. 4.10 (Japan). It is shown that, prior to voiding zone extension which is characterized by reaching the saturation of the void reactivity, negative reactivity insertion is repeated due to bubble generation/disappearance in the upper sodium layer.



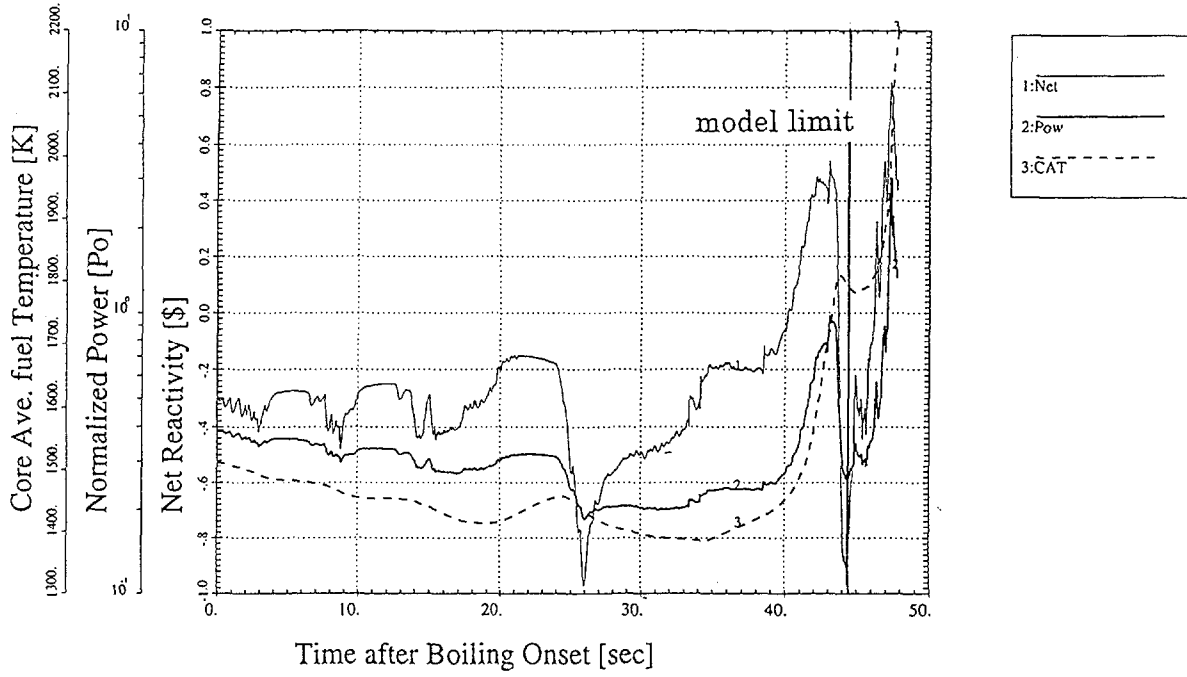
BN800 31 Channel RE 15.05.98



BN800 31 Channel RE 15.05.98

FIG. 4.8. Power and reactivity behavior (ULOF PARAMETRIC CASE) (1) Germany

s4a.r96r1.bn



s4a.r96r1.bn

1:Net 2:Dop 3:FD 4:Void 5:FM 6:CM 7:RAD

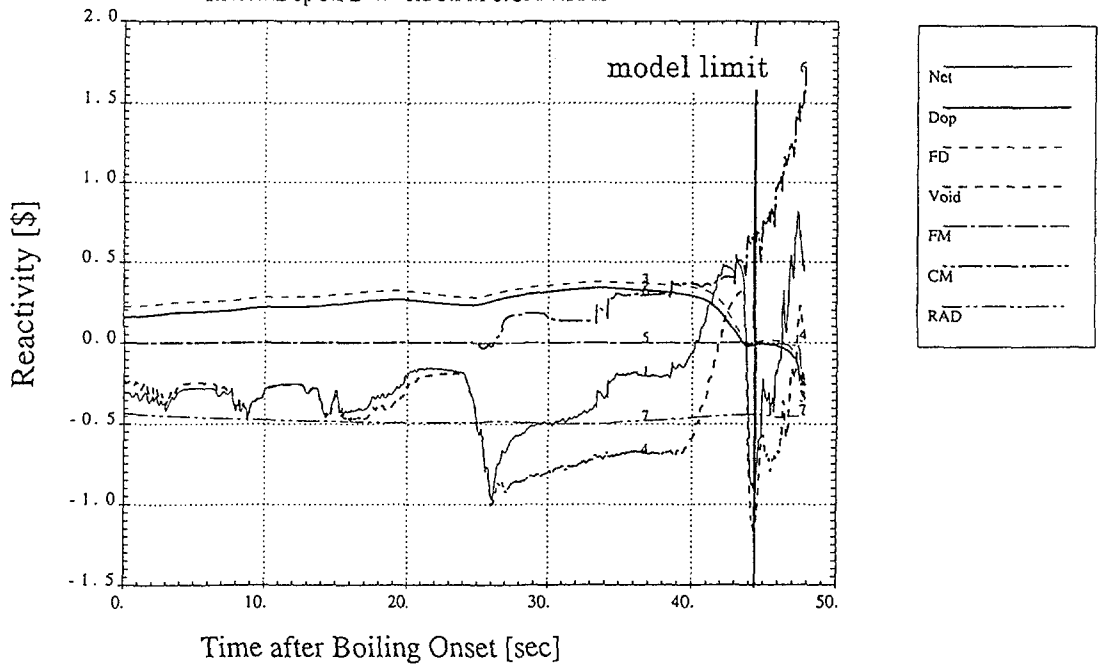
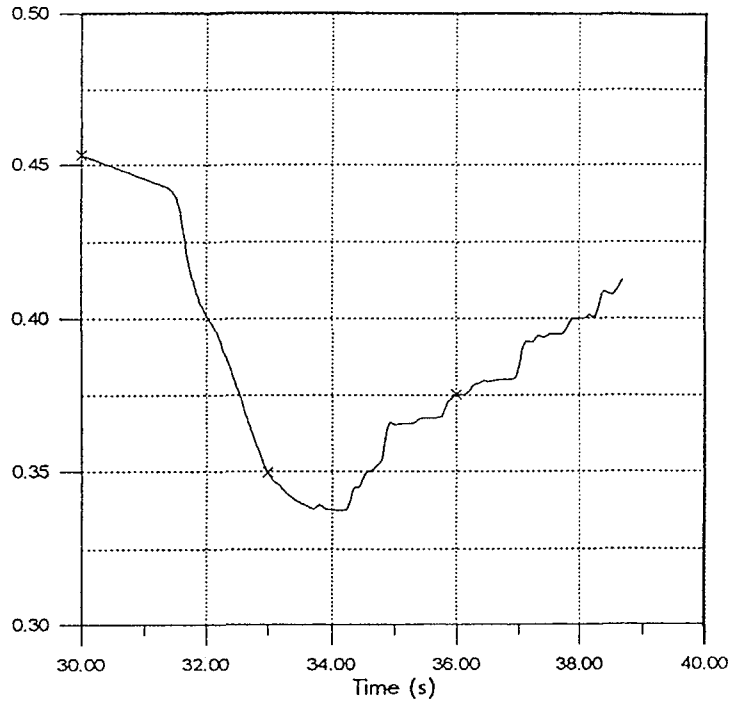
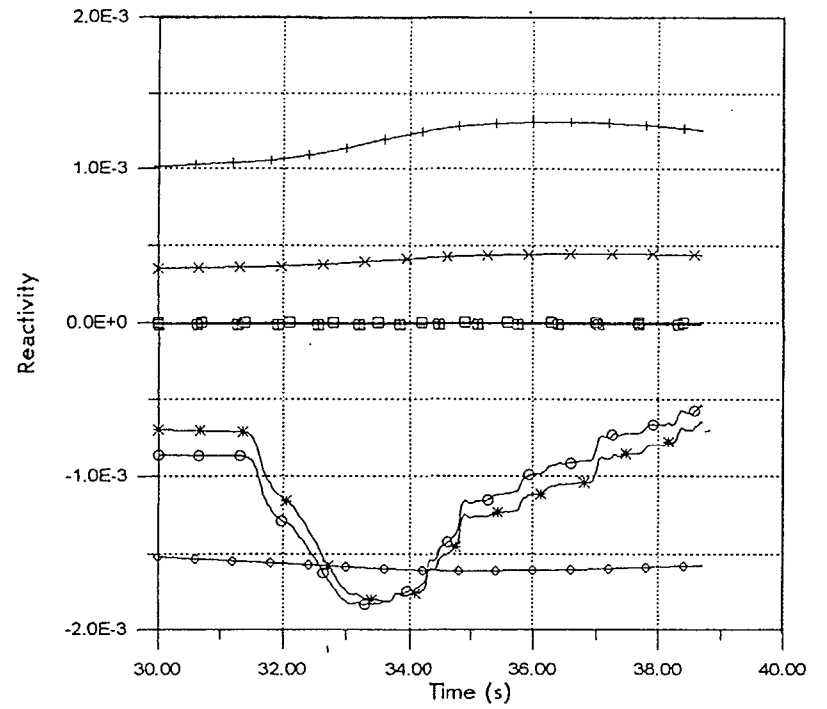


FIG. 4.8. Power and reactivity behavior (ULOF PARAMETRIC CASE) (2) Japan



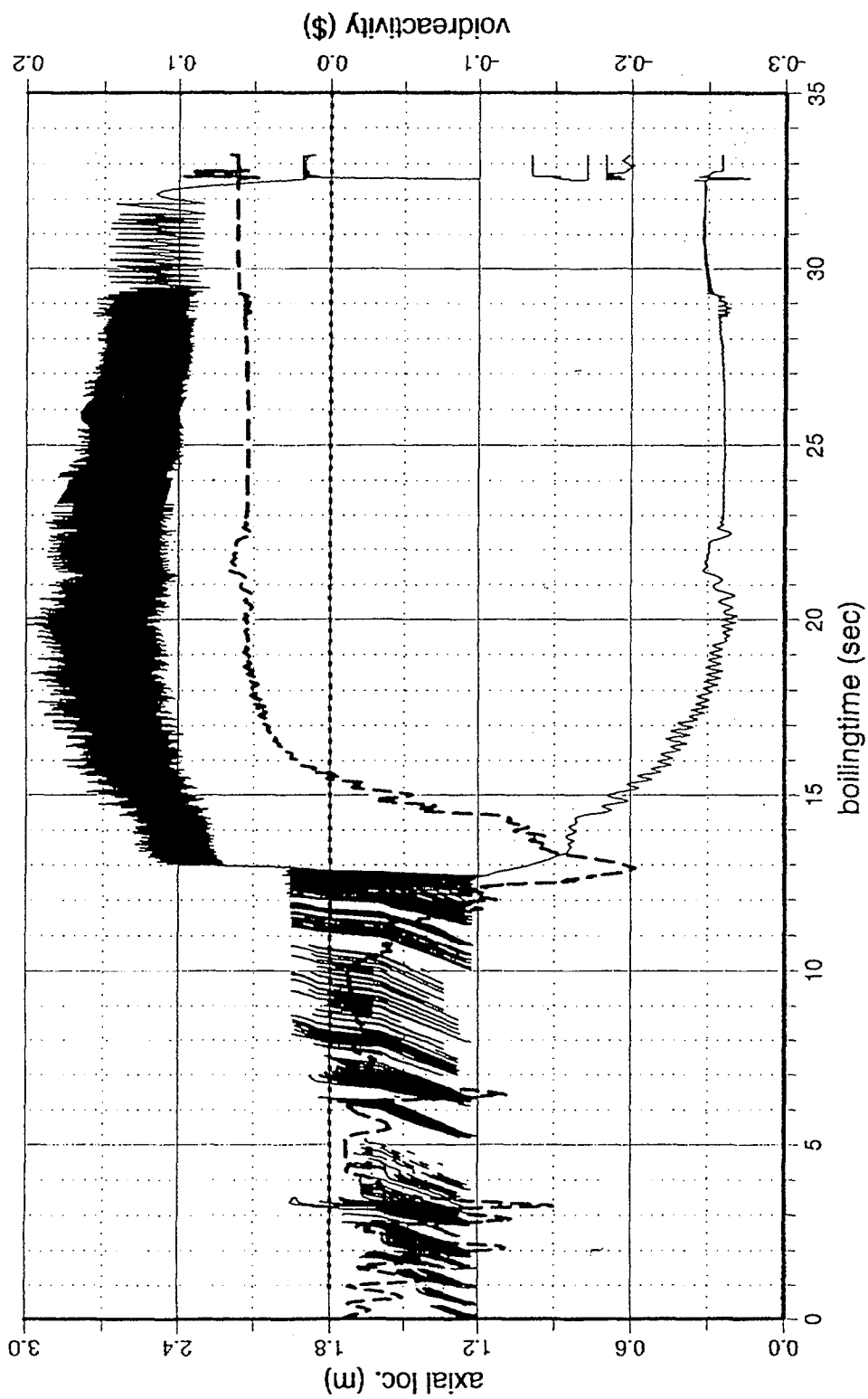
Relative reactor power.



- +— Doppler reactivity
- x— Axial expansion reactivity
- *— Sodium reactivity
- ◇— Radial expansion reactivity
- Control rods drivers expansion reactivity
- Control rods expansion reactivity
- Net reactivity

Reactivity versus time.

FIG. 4.8. Power and reactivity behavior (ULOF PARAMETRIC CASE) (3) Russia



BN800/31Ch. ichan= 13 boiling onset= 28.880 sec

FIG. 4.9. Extension behavior of the voiding zone (ULOF PARAMETRIC CASE, Ch. 13)
 (1) Germany

Steel and fuel motion behaviour

Based on the results from Japan, Fig. 4.8 (2) shows that steel motion begins at 25 s after boiling onset. Steel motion reactivity and detailed material motion behaviour is presented in Figs. 4.11 and 4.12 respectively. At first the molten steel drains down (see Fig. 4.12 (2)) and form a steel crust at the lower end of the fissile column (Fig. 4.12 (3) - (5)). Some steel is driven upward and form a crust on the wrapper wall and the reflector surface (Fig. 4.12 (6) - (8)). This behaviour is similar to that of Base Case (Fig. 4.5). A model limitation is reached at 77.5 s (Fig. 4.12 (9); wrapper wall melt through). During this transient, the maximum net reactivity is +0.541 \$ and the maximum power is 0.98 Po at 76.233 s (see Fig. 4.13 (2)). Although the net reactivity decreases at 44 s due to boiling onset in several Channels with their initial negative void reactivity insertion, net reactivity increases again due to continuous steel motion and voiding zone extension into the fissile zone.

The result from Germany (Fig. 4.8 (1)) shows that a mild power transient occurs at 60.2 - 60.7 s reaching 1.9 Po and +0.710 \$ (see also Table 4.5) which is driven by reactivity insertion due to voiding zone extension and steel motion. This power increase causes fuel breakup in Ch. 13 at 61.42 s. Negative reactivity effect due to fuel dispersal is not remarkable because the energy injection rate is low (see Fig. 4.13 (1)). Therefore the net reactivity

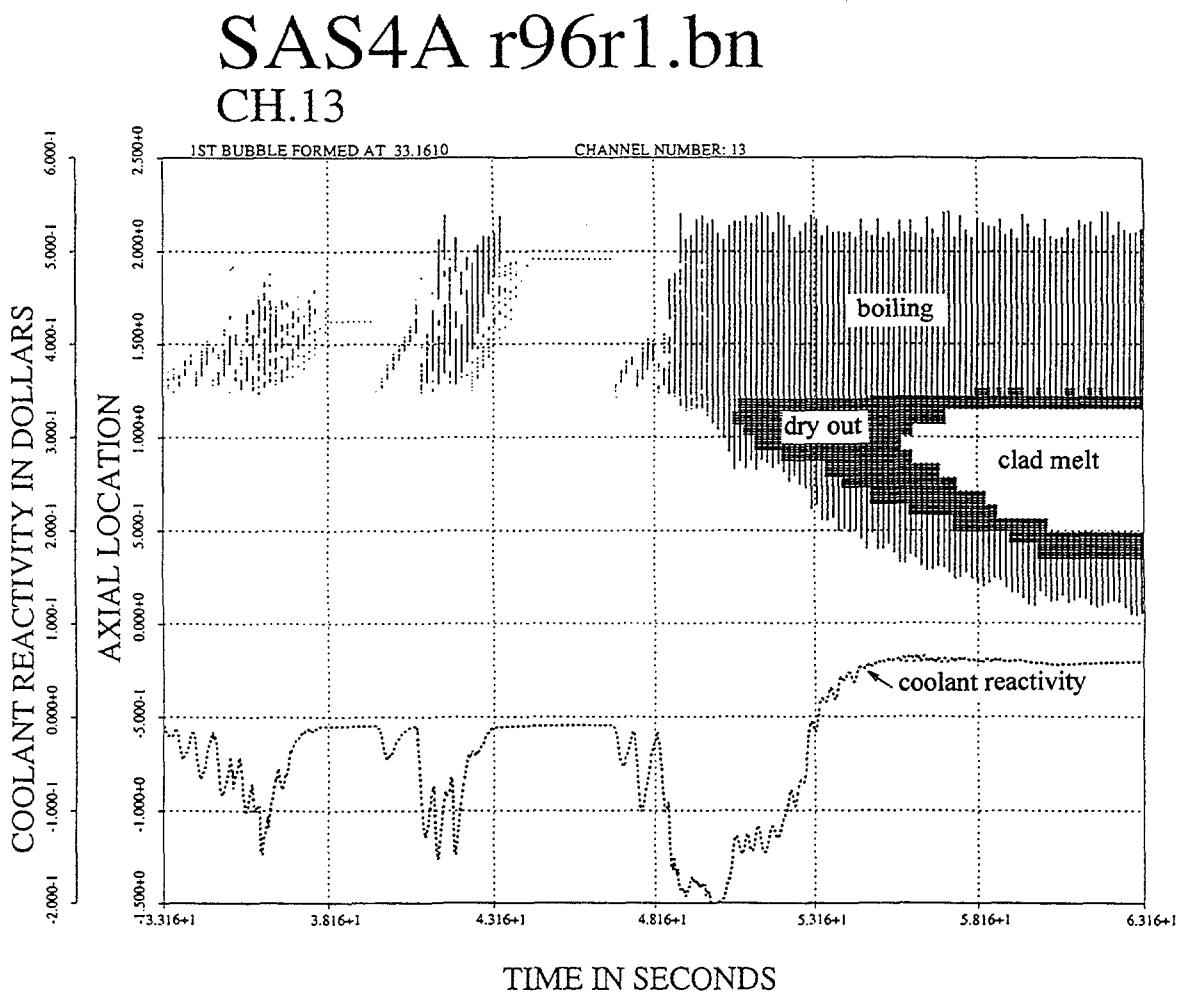
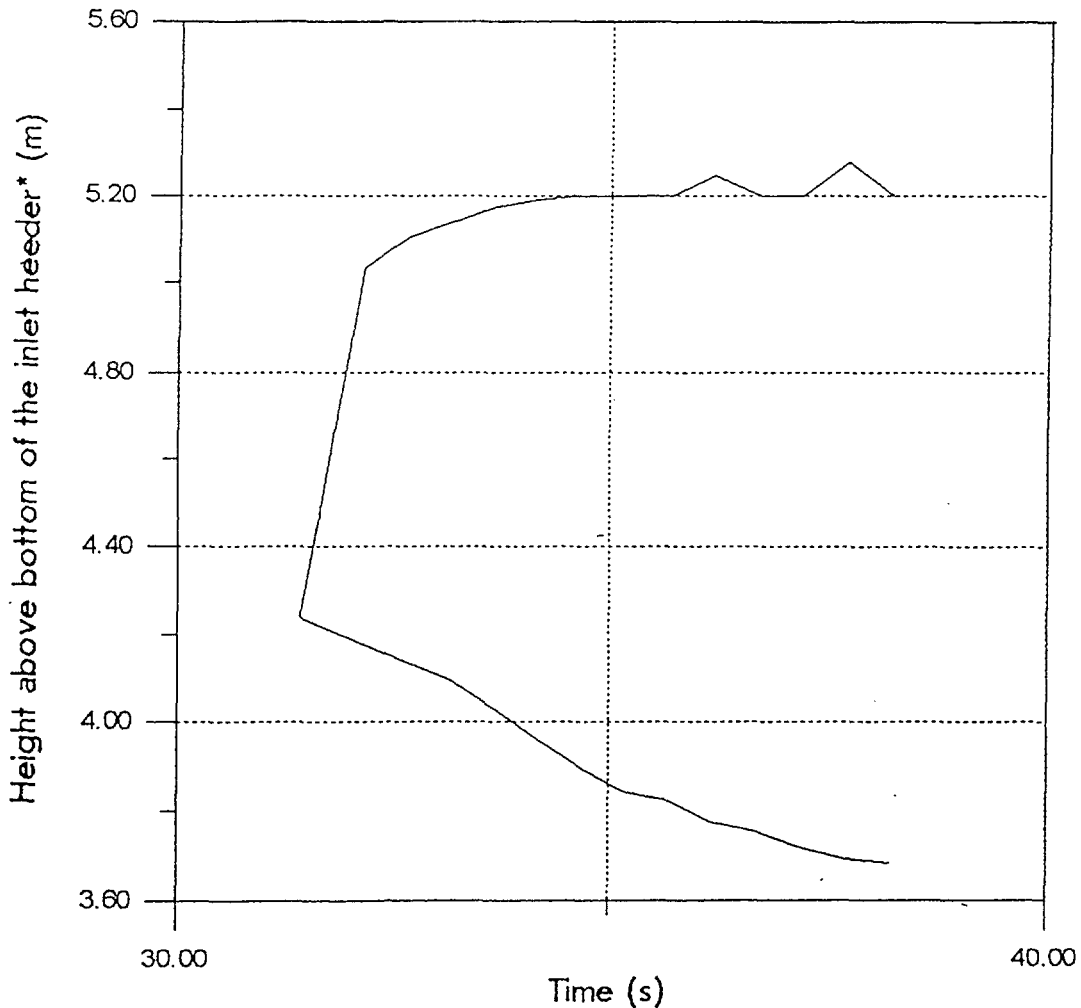


FIG. 4.9. Extension behavior of the voiding zone (ULOF PARAMETRIC CASE, Ch. 13)
(2) Japan



Channel 5: Boiling front.

*) The height of the fissile zone is 4.24 m.

FIG. 4.9. Extension behavior of the voiding zone (ULOF PARAMETRIC CASE, Ch. 13)
(3) Russia

begins to increase again due to steel motion reactivity insertion. Model limitation is also reached at 0.7 s into fuel breakup. The power level is around 1 Po and the net reactivity is about 0.3 \$.

It is shown that the transient behaviour of Parametric Case is much milder than that of Base Case due to consideration of the radial core expansion effect. However displacement of the molten steel from the core region to the upper or lower region of the core also leads to a positive reactivity insertion and it drives a mild power increase resulting in fuel breakup. It is concluded based on the present results that the accident enters into the transition phase even if the radial core expansion effect is fully considered.

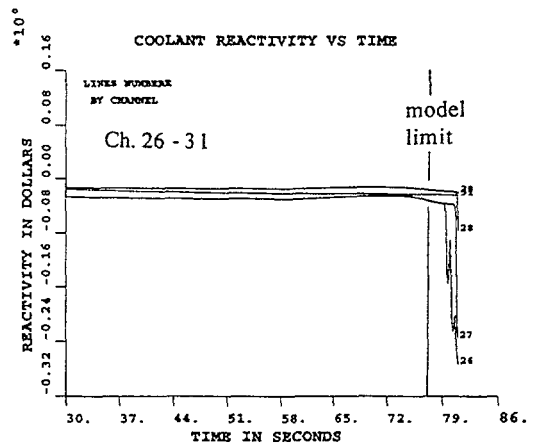
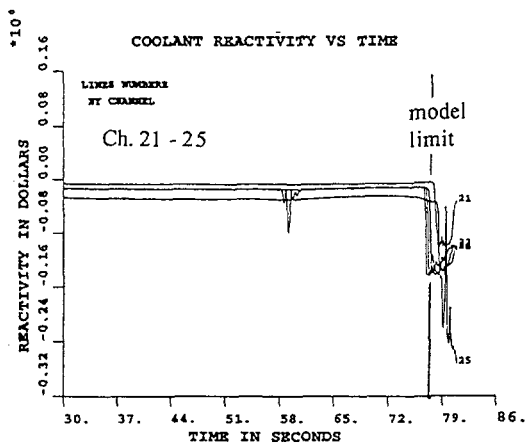
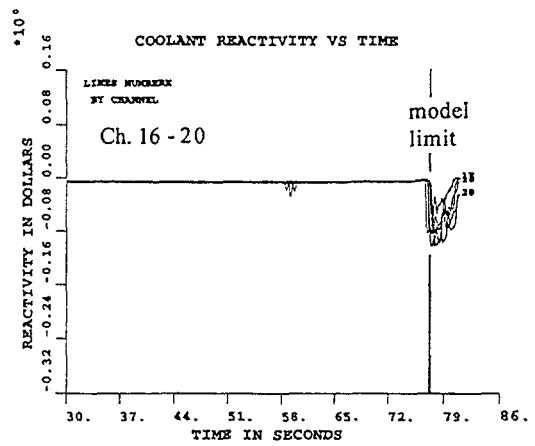
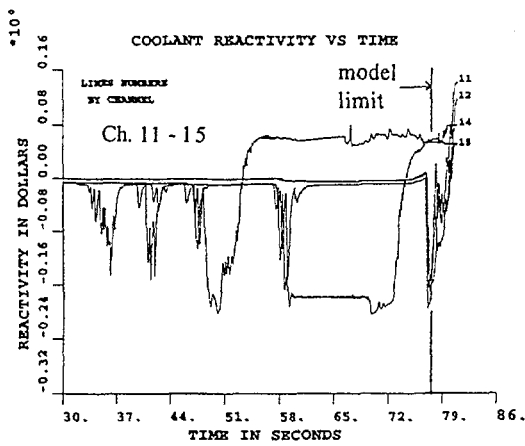
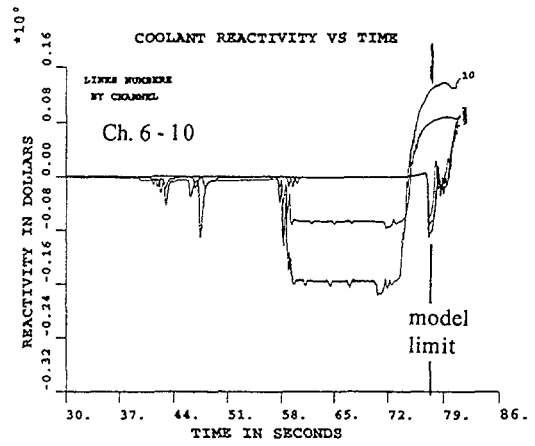
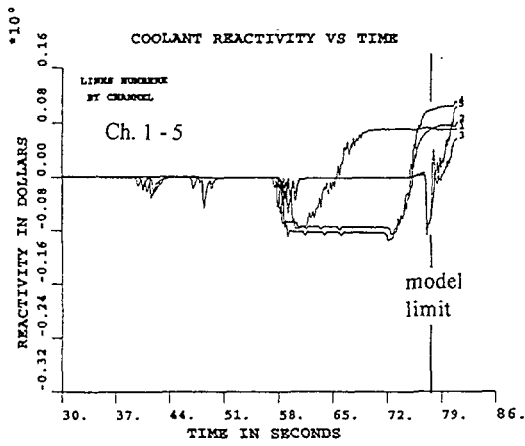


FIG. 4.10. Sodium void reactivity of each channel (ULOF PARAMETRIC CASE, Japan)

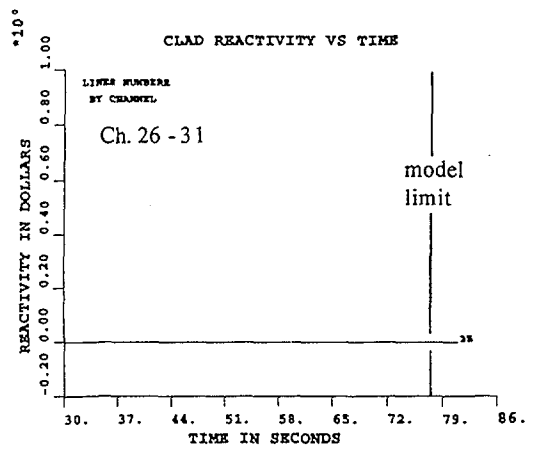
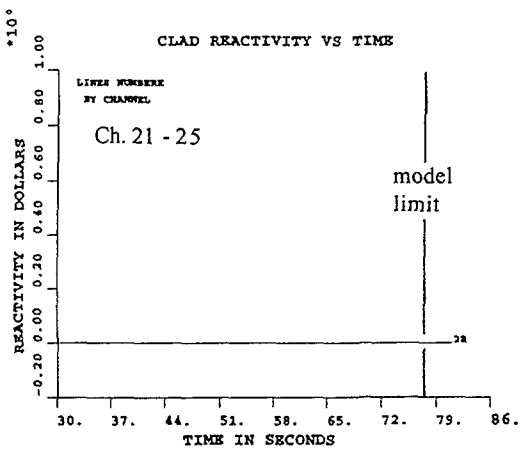
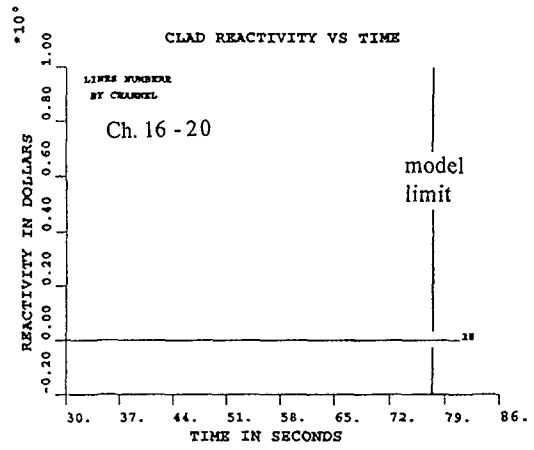
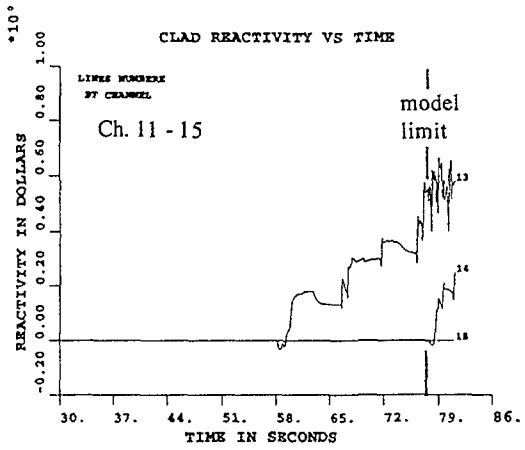
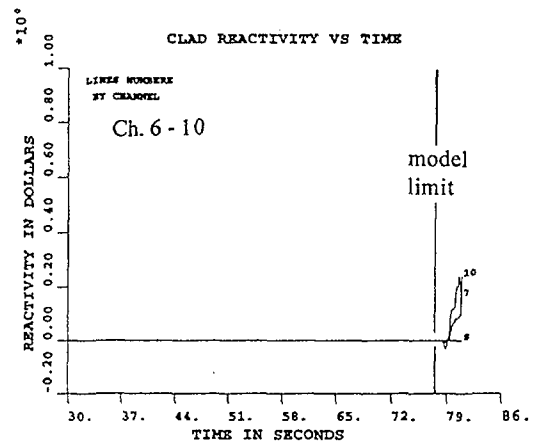
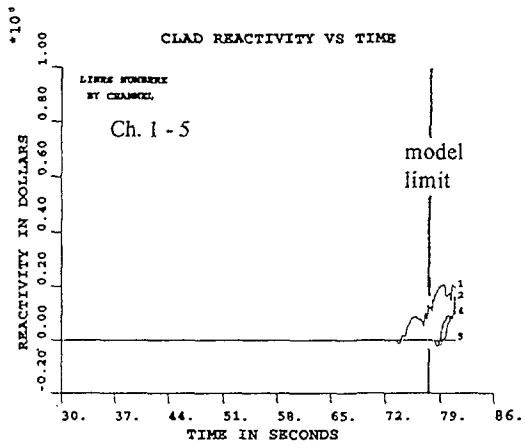


FIG. 4.11. Steel motion reactivity (ULOF PARAMETRIC CASE, Japan)

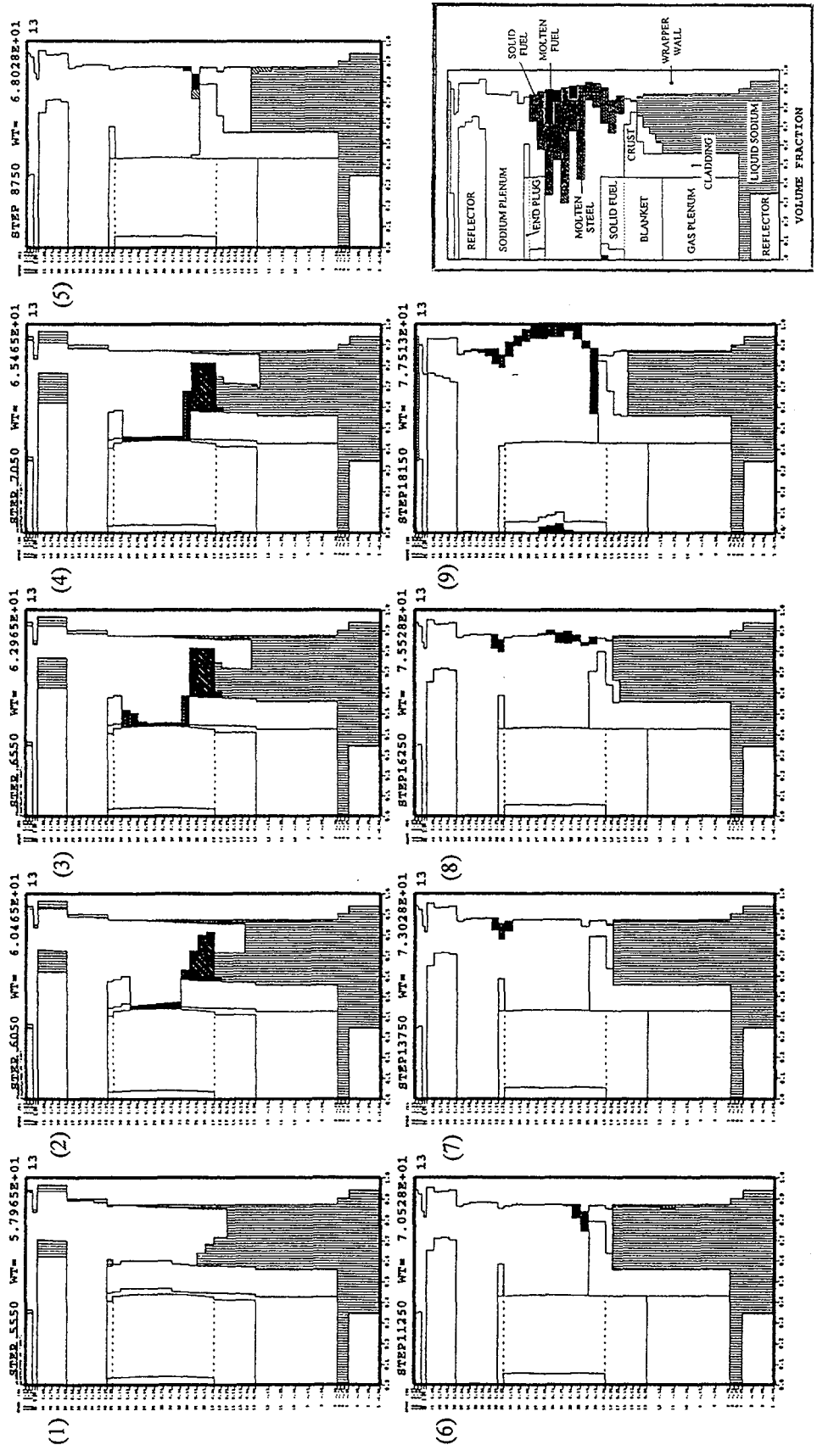
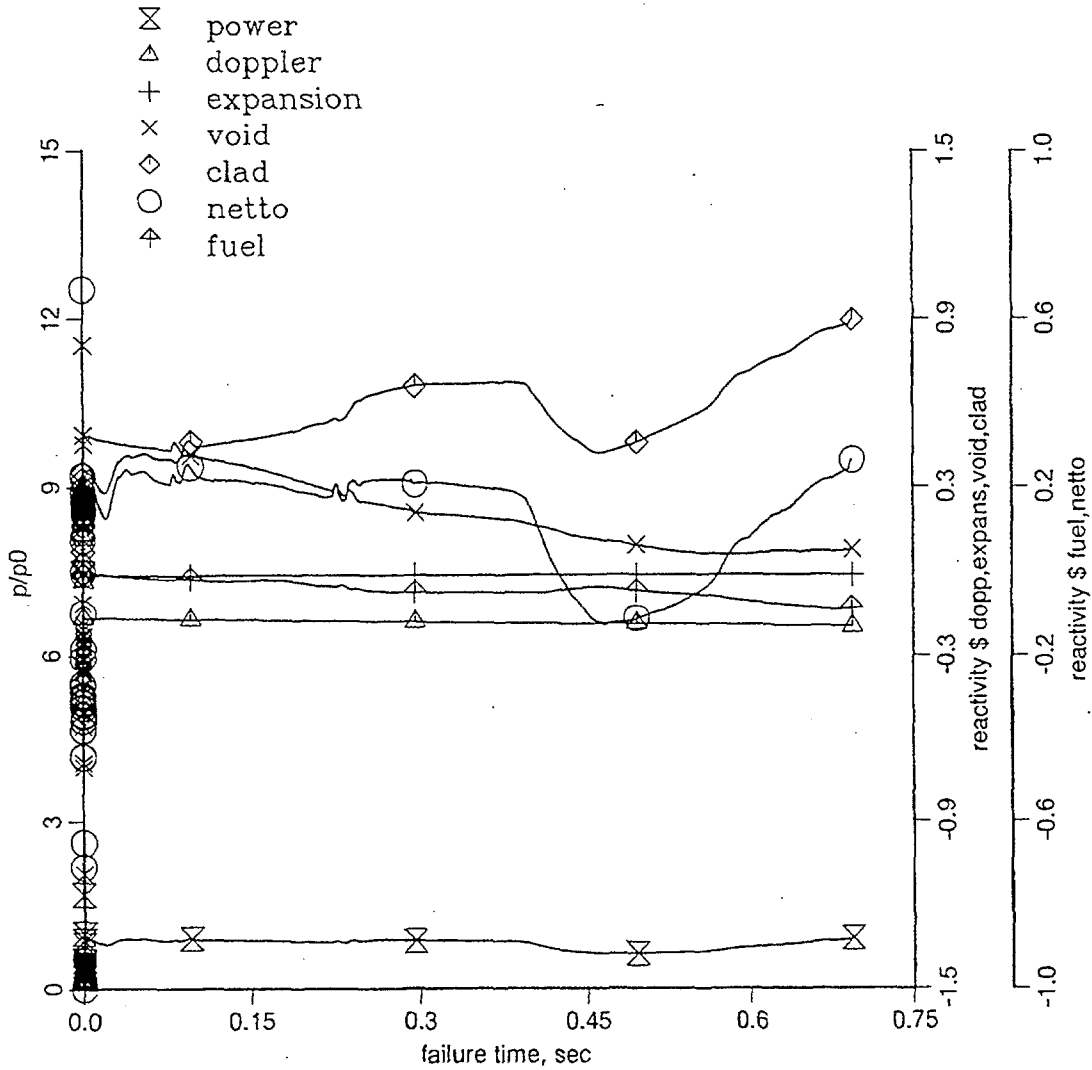


FIG. 4.12. Steel motion behaviour (ULOF PARAMETRIC CASE, Ch. 13, Japan)

Additional parametric case

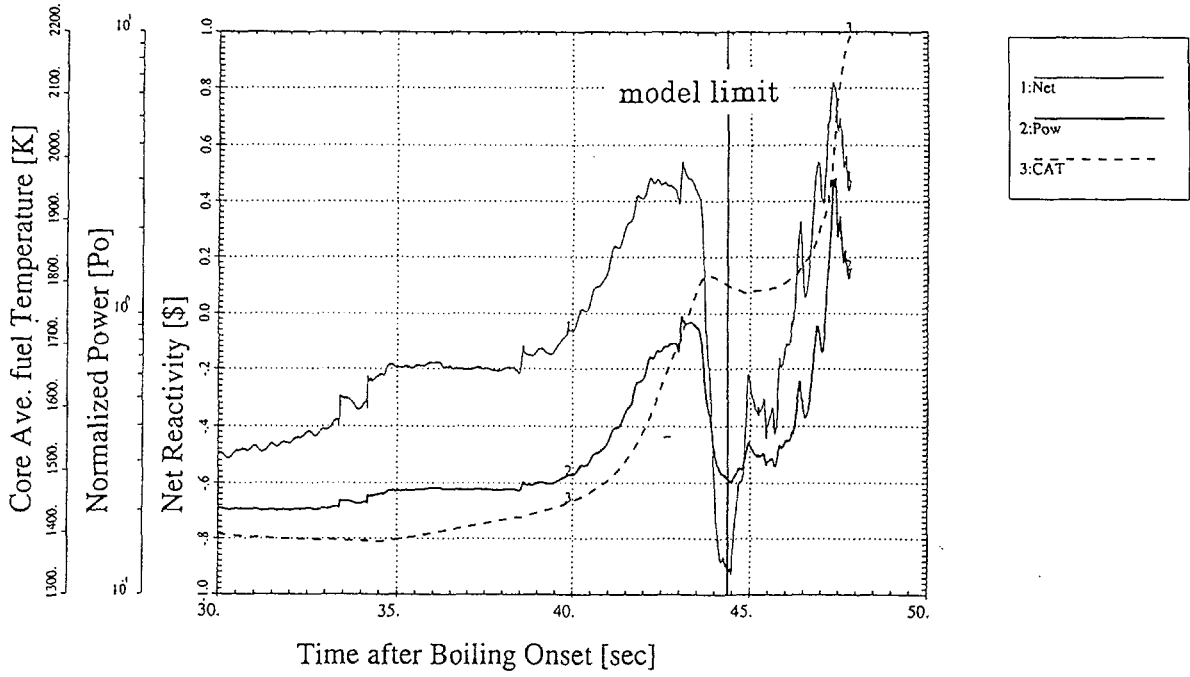
The effect of the superposition of the negative reactivities due to CRDL expansion and radial core expansion has been investigated in detail in a case with GRIF-SM code, though this case is beyond the domain of this comparative exercise. It shows significant mitigation of the event progression up to 100 s into transient such as nearly stable boiling continues without cladding dryout, while the increase of the inlet sodium temperature does not yet occur during this time period. It is pointed out that the influence of the transient variation of the fuel to clad heat transfer on the boiling and dryout behaviour should be evaluated, and also that the effect of inlet temperature increase should be analysed carefully.



BN800 31 Channel RE 15.05.98

FIG. 4.13. Power and reactivity behavior (ULOF PARAMETRIC CASE)
(1) Germany (after fuel motion)

s4a.r96r1.bn



s4a.r96r1.bn

1:Net 2:Dop 3:FD 4:Void 5:FM 6:CM 7:RAD

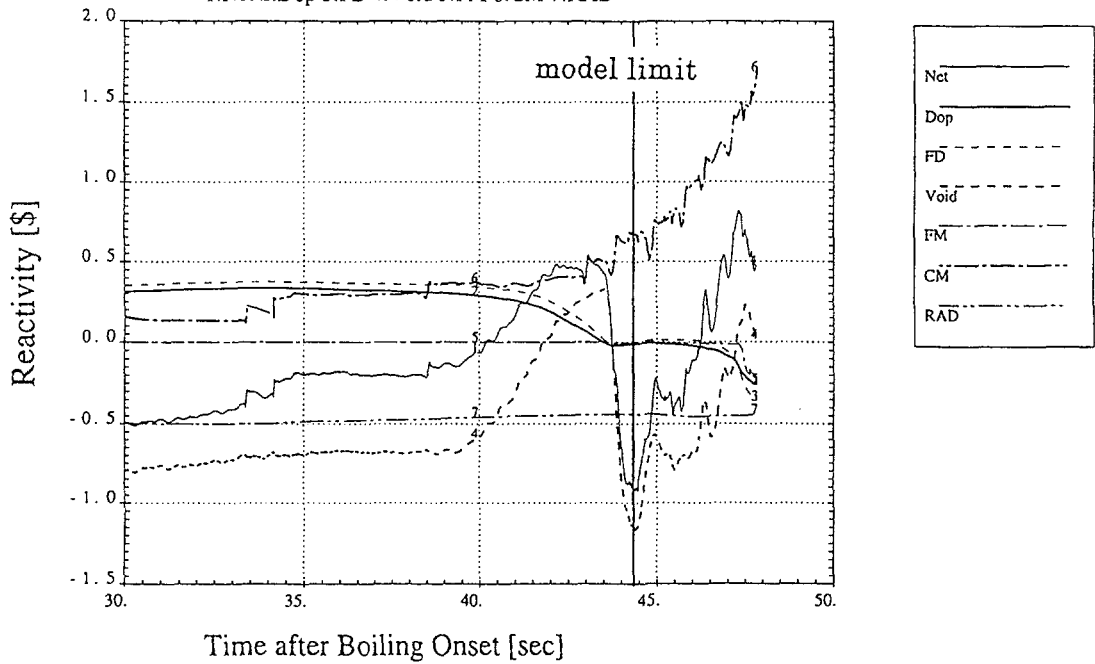


FIG. 4.13. Power and reactivity behavior (ULOF PARAMETRIC CASE)
(2) Japan (later phase)

4.2. CORE CONFIGURATION AT THE END OF THE INITIATING PHASE

The core configuration at the end of the calculation is shown in Figs. 4.14 and 4.15 for the Base Case and the Parametric Case respectively.

In the results of the Base Case from France (Fig. 4.14 (1)), sodium boiling is predicted in about half of the core subassemblies at the end of calculation (29.095 s). Steel motion is also predicted in some channels.

In Figure 4.14 (2) (Germany), coolant boiling is observed in most of the channels and fuel breakup occurs in Ch. 13 and Ch. 1. Because fuel in these channels still remains within the fissile region a permanent reactor shutdown is never attained at this moment. Therefore the accident will enter into the transition phase although the progression might be very mild.

In the Base Case of Japan (Fig. 4.14 (3)) in which the calculation is proceeded up to 31.3 s, all the channels are voided and thus the void reactivity is already saturated at about -0.6 \$ (note the consistency with the value in Table 4.1). Clad melting is predicted in almost all the channels, and fuel breakup is predicted in Ch. 13 (24 SAs), Ch. 1 (10 SAs) and Ch. 4 (14 SAs). Because the melt-through of the wrapper tube occurs at the time of model limitation, this situation could be thought as the end of the initiating phase. Because the steel motion reactivity is still increasing and the core average temperature is high (exceeding 2600 , see Fig. 4.6 (2)), it can be concluded that the accident will enter into the transition phase with containing practically solid fuel within the original fissile region.

In the Parametric Case results from Japan (Fig. 4.15 (2)), at the time of model limitation, the region of the boiling zone does not spread so widely yet compared with the Base Case. Nevertheless, because the steel motion reactivity is increasing, it can be foreseen that a further power increase could occur. Figure 4.13 (2) shows an increase of power and the core average fuel temperature which is driven by steel motion reactivity insertion, though it is after model limitation is reached. Judging from these results, it can be concluded that the accident will also enter into the transition phase.

Termination of the ULOF transient is only possible if fissile core material is efficiently removed from the original core region. At the end of the initiating phase relocation paths are difficult to become accessible and material relocation is rather limited as long as the fuel stays practically solid as indicated in the results. Therefore a mild progression to the transition phase is foreseen in these analytical cases.

Within this exercise no analyses were performed for the transition phase. It is hardly possible to predict the behaviour of the core design during this phase. Most probably it is characterised by a slowly progressing core melt-down interrupted by multiple recriticality events. Whether these might lead to mechanical loading of the heated-up structures of the primary system cannot be predicted without detailed analyses. Thermal and mechanical loading of structures of the primary system can only be determined by analyses of the transition phase and post-accident material relocation/heat removal phase. In this sense it is not yet demonstrated that this innovative core design leads only to benign consequences in terms of thermal and mechanical loading of structures of the primary system.

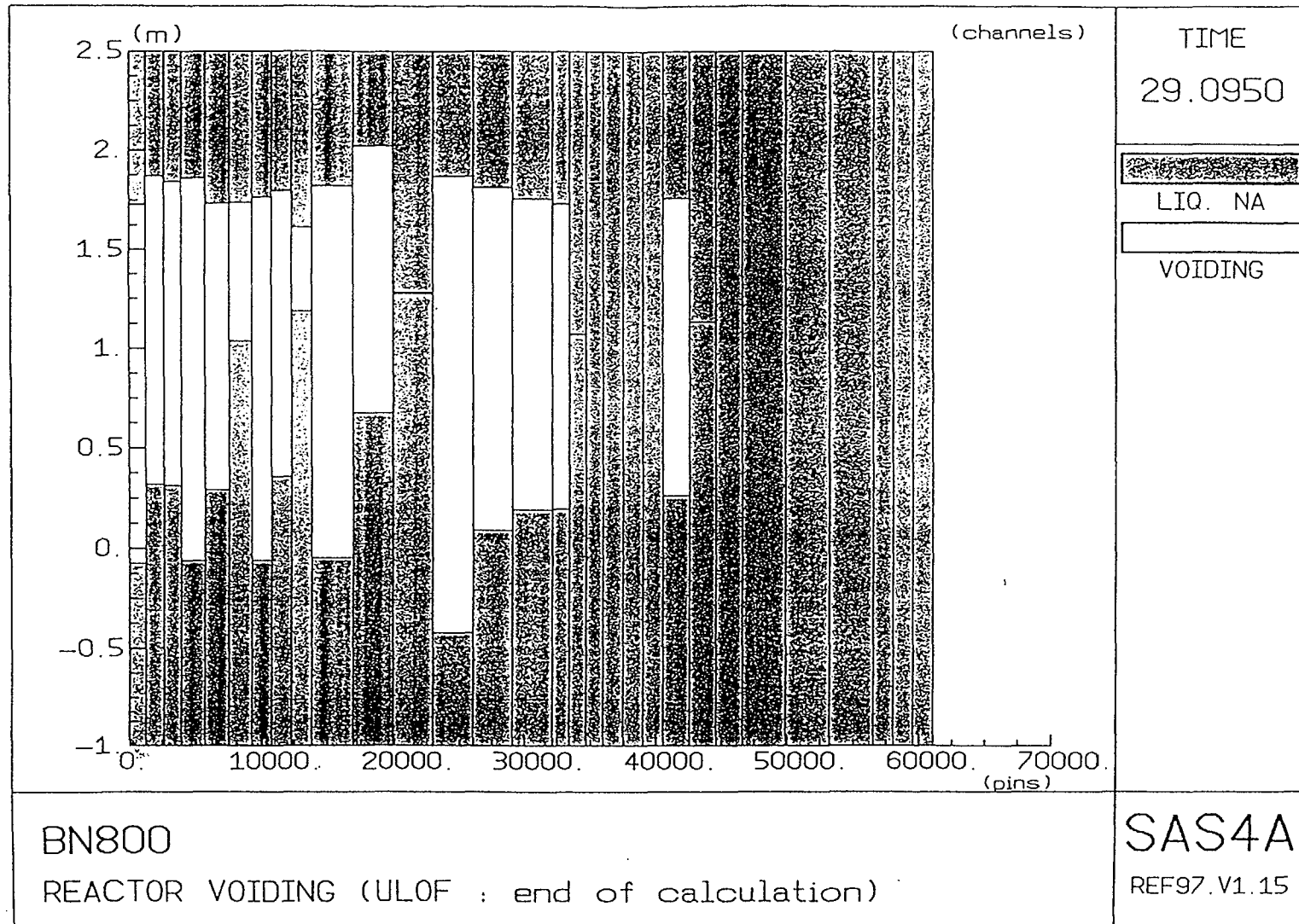


FIG. 4.14. Core configuration at the end of the initiating phase (ULOF BASE CASE)
(1) France

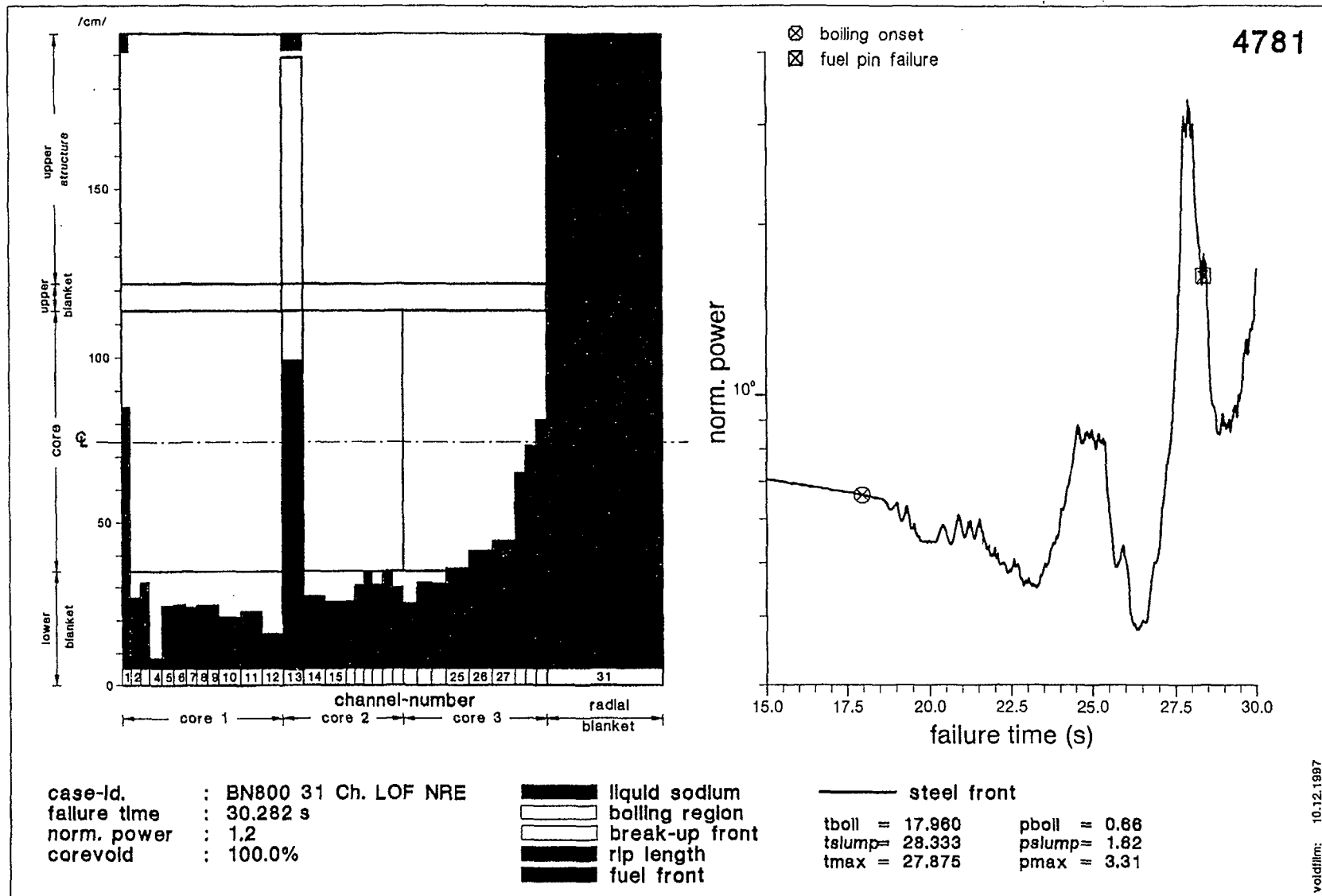
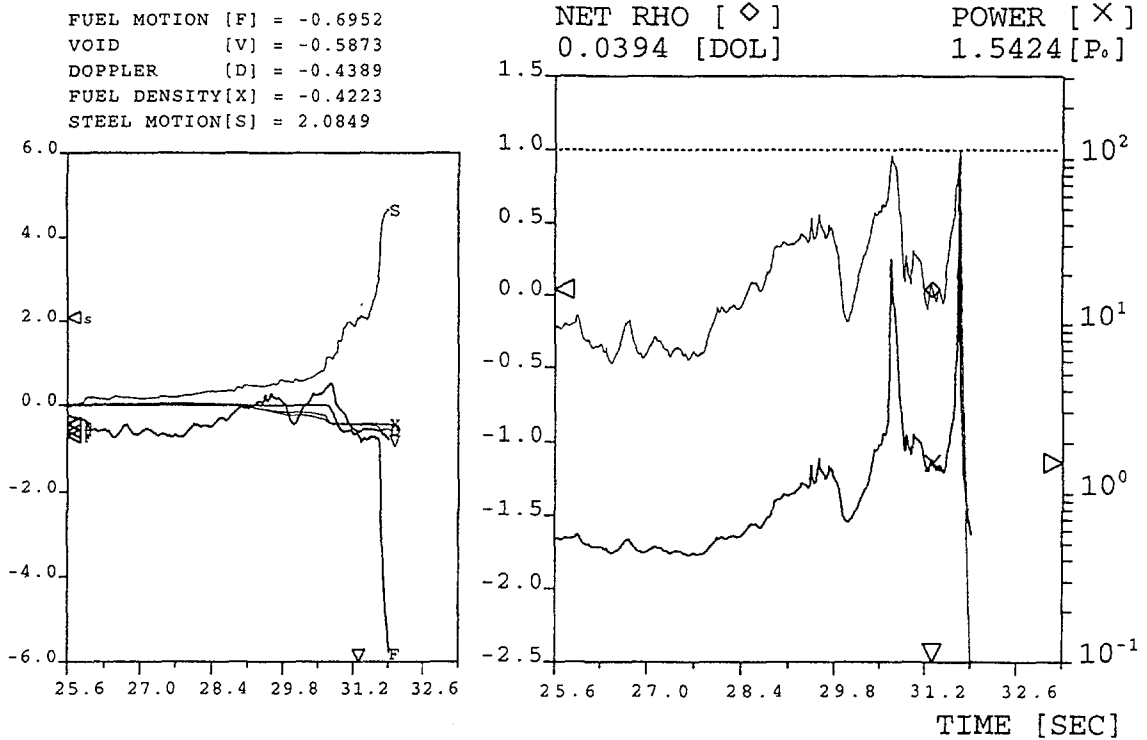
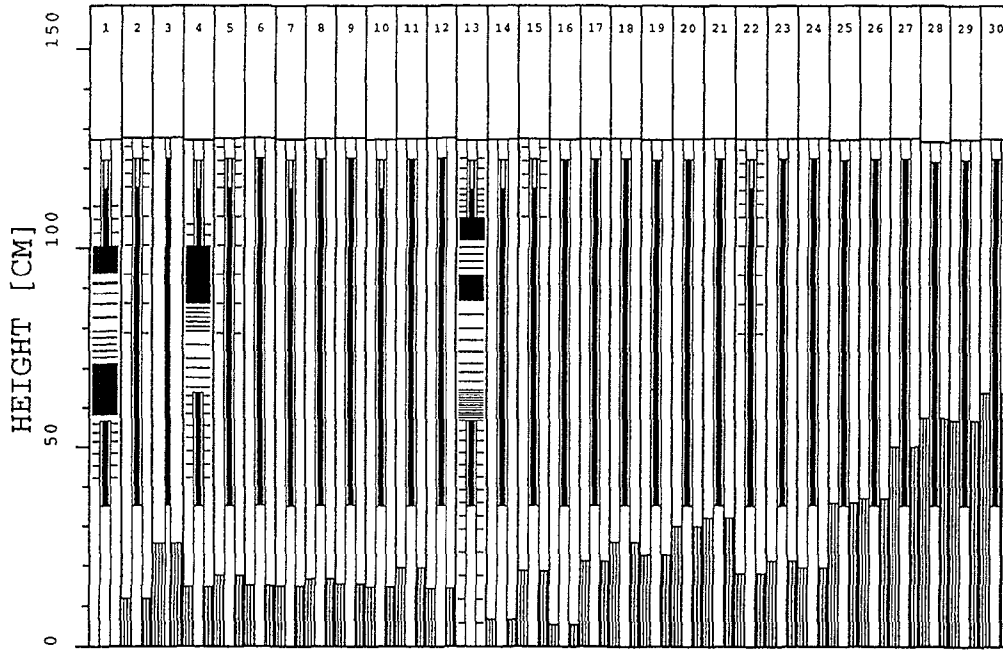


FIG. 4.14. Core configuration at the end of the initiating phase (ULOF BASE CASE)
 (2) Germany

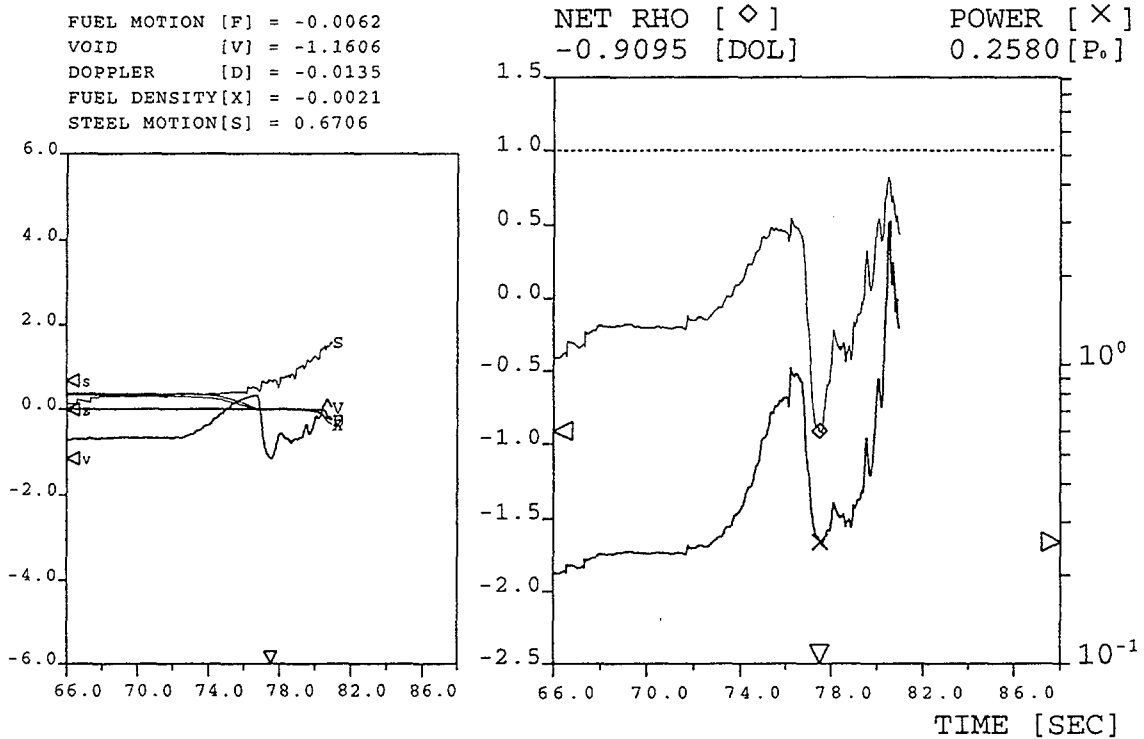
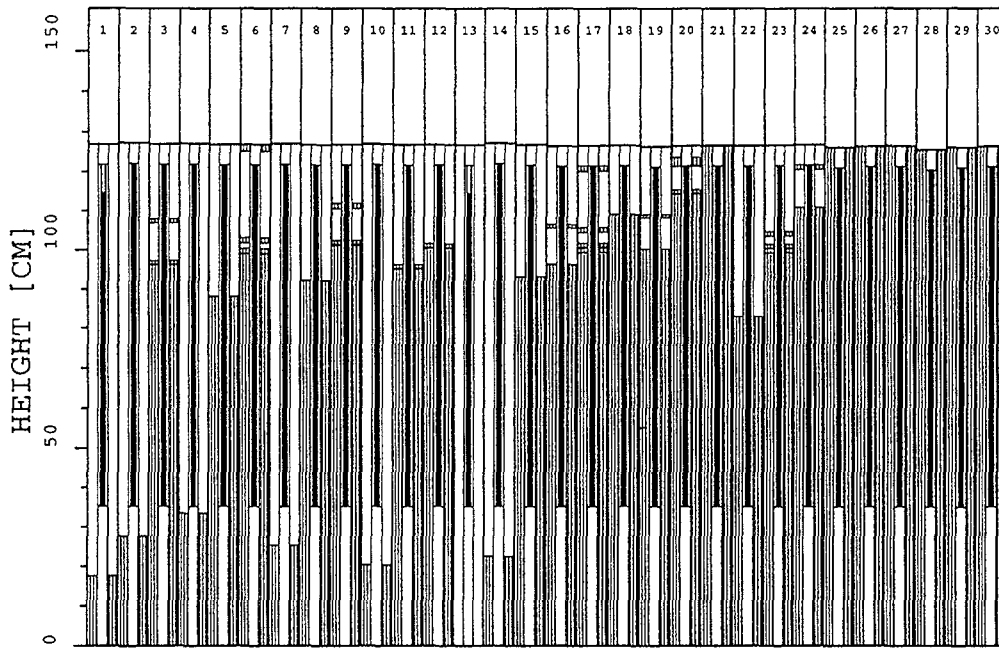
STEP = 6800
 TIME = 31.3153 [SEC]
 NUMBER BY CHANNEL



SAS-CHANNEL STATUS / NET REACTIVITY VS. TIME

FIG. 4.14. Core configuration at the end of the initiating phase (ULOF BASE CASE)
 (3) Japan

STEP = 18200
 TIME = 77.5140 [SEC]
 NUMBER BY CHANNEL



SAS-CHANNEL STATUS / NET REACTIVITY VS. TIME

FIG. 4.15. Core configuration at the end of the initiating phase
 (ULOF PARAMETRIC CASE, Japan)

4.3. CONCLUSIONS

The negative reactivity feedback contribution due to the voiding of the upper sodium layer is a quite efficient measure to mitigate the impact of the positive reactivity feedback contribution when the coolant along fissile core height becomes heated up and subsequently voided.

As consequence of the ULOF the power becomes considerably reduced and is nearly stabilized at a low value after boiling onset. However, this power reduction is not sufficient to prevent clad dryout and clad melting to occur in several channels. This hold for both the Base Case and Parametric Case.

In the subassemblies where clad relocation is calculated blockages of the coolant channels at the upper fissile core end and more massive ones at the lower fissile core end are calculated to become established in a few seconds. Clad relocation results in a considerable positive reactivity feedback.

Several seconds after clad relocation onset fuel breakup occurs in the hotter subassemblies due to the net reactivity increase upon clad relocation. However dispersed fuel remains within the original core region and thus the permanent shut down of the reactor is hardly attained within the presented calculation results.

Termination of the ULOF transient is only possible if fissile core material is efficiently removed from the original core region. At the end of the initiating phase relocation paths are difficult to become accessible and material relocation is rather limited as long as the fuel stays practically solid.

The ULOF transient is not at all finished at the end of the calculated results of the participants. Establishment of long-term coolability of the partially disrupted core is not to be expected neither in the Base Case nor in the Parametric Case. A quite complicated transition phase will follow where material relocation phenomena will deviate considerably from the quasi-one-dimensional behaviour in the initiating phase due to an expected early wrapper wall melting.

It is hardly possible to predict the behaviour of the core design during transition phase. Most probably it is characterised by a slowly progressing core melt-down interrupted by multiple recriticality events. Whether these might lead to mechanical loading of the heated-up structures of the primary system cannot be predicted without detailed analyses.

Results of the comparative exercise does not allow yet to conclude that ULOF-transients in a BN-800 type reactor core design leads only to benign consequences in terms of the thermal and mechanical loading of structures of the primary system. However the results have shown that the upper sodium layer is a quite efficient design measure to prevent the net reactivity to approach or exceed prompt criticality in the initiating phase of a ULOF-transient.

Thermal and mechanical loading of structures of the primary system can only be determined by analyses of the transition phase and post-accident material-relocation/heat-removal phase. In this sense it is not yet demonstrated that this innovative core design leads to less severe consequences of core disruptive accidents when compared with conventional core designs.

Conclusions from this comparative exercise hold for the as-specified case set-up. They need to be reviewed when some of the design features change or when more detailed evaluations lead to different input data. It is thought that there are possibilities for improvement of the analyses and/or for optimization, especially when a more realistic core design would be considered. However, the comparative exercise has shown as well that consequences of these type of modifications need to be analysed carefully and in detail on a case to case basis. The use of more sophisticated theoretical models might be helpful to improve the reliability of results.

**NEXT PAGE(S)
left BLANK**

Chapter 5

TRANSIENT ANALYSIS RESULTS OF UTOP AND UTOP/ULOF ACCIDENTS

5.1. INTRODUCTION

In the framework of the IAEA/EC collaborative project, a comparative exercise have been performed in order to study the consequences of a severe accident in a BN-800 type reactor core with a near zero void coefficient. Two different initiators [unprotected transient overpower (UTOP) as well as unprotected transient overpower driven loss of coolant flow (UTOP/ULOF)] were taken into account for the evaluation of the transient core behaviour under such hypothetical accidents. Two UTOPs simulating a control rod withdrawal were studied: a slow UTOP which simulates a 0.05 \$/s reactivity insertion as well as a fast one whose reactivity insertion corresponds to 0.5 \$/s. Four countries participated in the exercise : Russia, France, Germany and India.

This chapter compares the results of the different contributions to the exercise and identifies the complementary studies which appear to be necessary in order to describe until the very end of the accident, the behaviour of the core.

5.2. BASIS OF THE CALCULATIONS

5.2.1. Case set-up

Calculations were performed on the basis of input data provided by the Institute of Physics and Power Engineering (IPPE) from Obninsk, Russia [5.1]. On this basis, the neutronic data were evaluated [5.2] as well as the steady state calculations of the fuel pins behaviour during power operation [5.3]. The core is characterised by an upper sodium layer which significantly reduces the sodium void coefficient of the core. The reactor is supposed to operate using a three batch management scheme. At the end of equilibrium cycle (EOEC) the burnups of the pins reached 140, 280 and 420 effective full power days and the postulated accident is supposed to occur.

Two UTOPs simulated a control rod withdrawal were analysed : a slow one which simulates a 0.05 \$/s reactivity insertion and a fast one whose reactivity insertion corresponds to 0.5 \$/s. It is to be noticed that the total reactivity added is restricted to a maximum value of 3.9 \$.

Then a UTOP-ULOF simulating an unauthorised withdrawal of six compensator rods from the core accompanied by the failure of all scram system absorber rods was analysed. This accident leads to a first reactivity ramp insertion (0.05 \$/s for 10 s) and to an additional one (0.05 \$/s for 100 s) when the power reaches 1.15 nominal, associated one second later to a coolant mass-flow reduction down to 25 % nominal flow.

Russia, France, Germany and India performed calculations which were finalised and presented during eight consultancy meetings. This chapter mainly synthetised the update presentation of each country [5.4, 5.5, 5.6, 5.7, 5.8, 5.9]. In all the base case calculations, the reactivity effect due to hypothetical radial core expansion is not taken into account. The detailed input data of these calculations can be found in [5.1, 5.2, 5.3].

5.2.2. Codes applied

Different tools were used by the participants to the exercise.

Germany and France applied the SAS-4A code. This code was originally developed by ANL [5.10] and was during the last years significantly improved on the basis of an international collaboration (France, Japan, Germany). The main improvements concern the multibubbles boiling model, the fuel pin mechanics module as well as the particle jamming model. As improvement of the code is a continuous process, it must be noticed that France and Germany applied slightly different variants of a common agreed reference version of the code. The SAS-4A code is a multichannels code, each channel is represented by one pin. The phenomena which are expected to occur in UTOP and ULOF accidents are sodium boiling, fuel melting, fuel pin break-up, mechanical clad failure, clad melting, clad motion, post-failure fuel and clad motions and relocations, fuel coolant interaction. The accident sequence can be evaluated until the melting of the hexcan. At that time of the accident, the one dimensional approach of the SAS-4A code is not sufficient to be extended to radial molten material relocation which can affect the whole core. The SAS-4A code is validated against experiments performed in the frame of the different TREAT and CABRI programmes. All the SAS-4A calculations were performed using input data set provided by FZK and the balance of force option for the evaluation of fuel and clad expansions.

The clad material properties of the BN-800 reactor distributed by IPPE, have been evaluated by FZK. It was noted that these data showed some uncertainties, especially no strain rate dependencies, higher ultimate tensile strengths and yield stresses for irradiated than for non-irradiated material, and a large scattering for failure strains, where measurements are only available for non irradiated material. Although the experimental data are partially taken into account in the SAS-4A code (15/15 Ti-stabilised steel), they were compared with those given by FZK modified modelling for steel material properties. As a conclusion from the comparison of the experimental data of BN-800 and the well evaluated data for 15/15 Ti-stabilised steel, calculations for the BN-800 safety analysis with the material properties of a 15/15 Ti-stabilised steel were performed by FZK with a high and a low strain rate to bound the scatter band of the experimental data of ultimate tensile strength. Yield strength data are consequently below measured values, but the difference between the experimental yield stress and ultimate tensile strength was kept constant. Failure strain data represent well the average of the scatter band of measurements for BN-800, taking into account that failure strains for irradiated material are lower than those for non-irradiated material.

On the contrary, IPSN takes the SAS-4A original 15/15 Ti-stabilised steel data using a low strain rate dependency (10^{-2} s^{-1}) for the UTOP analysis and a high strain rate dependency ($1. \text{ s}^{-1}$) for the UTOP/ULOF analysis.

Russia (IPPE) applied the GRIF-SM code [5.11] to investigate the UTOP accident. Sodium boiling is calculated using a slip model. Interwrapper sodium boiling is simulated in 2D model. Fuel and clad melting are calculated but the code can only be applied until fuel pin failure conditions based on a local fuel melt fraction (50 %). At that time, the present limit of applicability of the code is reached

For the UTOP-ULOF analysis, the clad motion modelling CANDLE was coupled to the GRIF-SM code and thus the calculation is allowed to be continued until significant molten steel relocation and occurrence of fuel melting.

India (IGCAR) run the calculations using his own developed PINCHTRAN code which is a modified version of the PREDIS code [5.12]. It was validated using European loss of flow benchmark. Sodium boiling without flow reversal effects and fuel melting are modelled. Fuel pin failure can be assessed by two different criteria, the first one being a local fuel melt fraction (50 %) and a second one is based on damage parameters deduced from experiments performed in the TREAT reactor. No post-failure modelling allows to continue the calculation.

5.3. TRANSIENT RESULTS FOR THE FAST UTOP (0.5 \$/S)

The fast UTOP (0.5 \$/s) simulates a fast control rod withdrawal. It is recalled that the total reactivity inserted is restricted to a maximum value of 3.9 \$ which is reached 7.8 s after the beginning of the reactivity insertion.

The scenarios of the accident, as calculated by FZK and IPSN using the SAS-4A code are very similar. Nevertheless, they slightly differ due to the fact that FZK uses his own evolution of the pin mechanics module (DEFORM-4C) which induces a different axial fuel pin extension and thus a different associated reactivity feedback. FZK also starts the transient calculations from different EOEC conditions and performs a different failure analysis taking into account more appropriately IPPE modified mechanical properties of the irradiated cladding [5.13].

The scenarios of the accident, as calculated by IGCAR and IPPE do not differ from the SAS-4A one until the first pin failure onset. The failure time is estimated very roughly on basis of a molten fuel fraction (50 % - IPPE - IGCAR) or of an improved manner based on a damage parameter criterion of Bars (IGCAR). Unfortunately no post failure calculations were performed by IPPE and only a very simple modelling in the PINCHTRAN code allows to end the accident sequence.

Tables 5.1, 5.2 and 5.3 summarized the results at boiling onset and the failure conditions found by the different participants to the exercise.

TABLE 5.1. BN-800 FAST UTOP (0.5 \$/s) RESULTS AT BOILING ONSET

| | SAS-4A | | GRIF-SM | PINCHTRAN | |
|-------------------|-----------|-------|---------|-----------|---------------------|
| | FZK (1) | IPSN | IPPE | IGCAR | |
| | BASE CASE | | | | PARAMETRIC CASE (2) |
| Boiling onset (s) | 4.116 | 4.270 | 4.125 | 3.57 | NO |
| Channel number | 5/1 | 5/1 | 4/1 | 5/1 | |
| Relative power | 8.15 | 6.41 | 7.4 | | |
| Net reactivity | 0.64 | 0.55 | | | |

TABLE 5.2. BN-800 FAST UTOP (0.5 \$/s) RESULTS AT FIRST FAILURE TIME

| | SAS-4A | | GRIF-SM | PINCHTRAN | | |
|--------------------------|-----------|------|---------|-----------|---------------------|---------|
| | FZK (1) | IPSN | IPPE | IGCAR | | |
| | BASE CASE | | | | PARAMETRIC CASE (2) | |
| Failure time (s) | 4.645 | 5.25 | 4.5 (3) | 3.3 (4) | 4.35 (3) | 5.0 (3) |
| Channel number | 5/1 | 5/1 | 8/3 | 1/1 | 5/3 | 5/3 |
| Relative power | 2.24 | 5.13 | | | 3.84 | 3.59 |
| Net reactivity (\$) | -0.38 | 0.45 | | | 0.43 | 0.40 |
| Failure location (%) | 83 | 62. | - | 71. | 58. | 58. |
| Molten fuel fraction (%) | 52 | 65. | | | 50. | 50. |
| Clad plastic strain (%) | 0.6 | 0.5 | | | - | - |

- (1) updated EOEC - conditions
- (2) with radial core expansion feedback
- (3) based on 50 % fuel melt fraction
- (4) based on damage parameter criterion of Bars

TABLE 5.3. BN-800 FAST UTOP (0.5 \$/s) RESULTS AT FIRST FAILURE TIME

| | SAS-4A | | GRIF-SM | PINCHTRAN | |
|---------------------------|-----------|-------|---------|---------------------|---------|
| | FZK (1) | IPSN | IPPE | IGCAR | |
| | BASE CASE | | | PARAMETRIC CASE (2) | |
| Failure time (s) | 4.65 | 5.25 | 4.5 (3) | 4.35 (3) | 5.0 (3) |
| Net reactivity (\$) | -0.38 | 0.45 | 0.52 | 0.43 | 0.40 |
| Doppler (\$) | -0.915 | -0.93 | | -0.92 | -1.0 |
| Fuel axial expansion (\$) | -0.741 | -0.66 | | -0.56 | -0.61 |
| Clad axial expansion (\$) | 0.088 | 0.10 | | 0.03 | 0.03 |
| Sodium (\$) | -1.135 | -0.69 | | -0.12 | -0.15 |
| External reactivity (\$) | 2.322 | 2.62 | | 2.17 | 2.50 |

Linked to slightly different reactivity feedbacks, boiling is reached at 4.125s in the IPPE calculation, at 3.57 s in the IGCAR base case calculation and at 4.27s in the IPSN calculation. At 5.0 s boiling is not reached in the IGCAR parametric calculation which takes into account the radial core expansion feedback (table 5.1).

During the two first seconds of the reactivity ramp insertion, the net reactivity and thus the relative power increase (figure 5.1a). Then, the net reactivity is rapidly stabilised and the

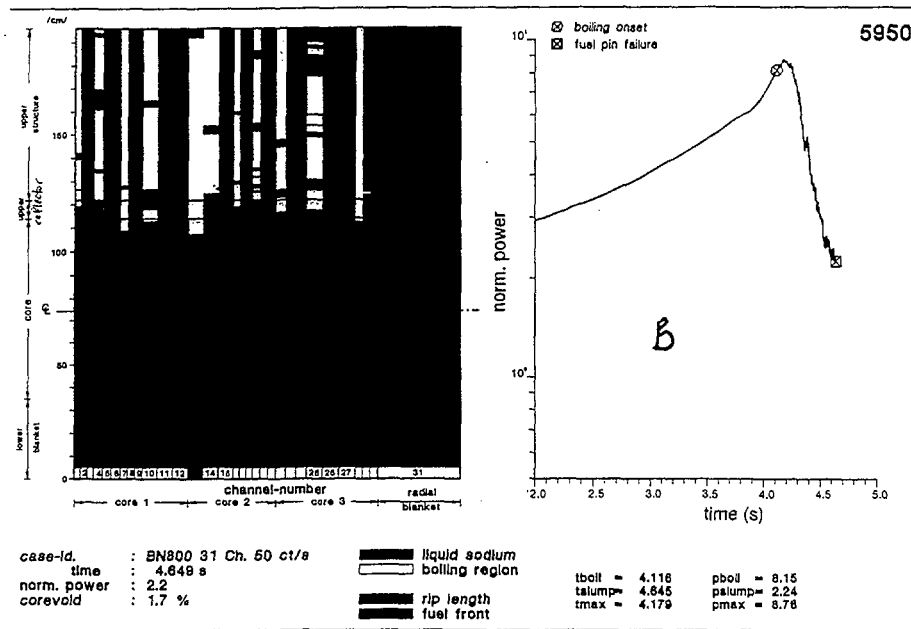
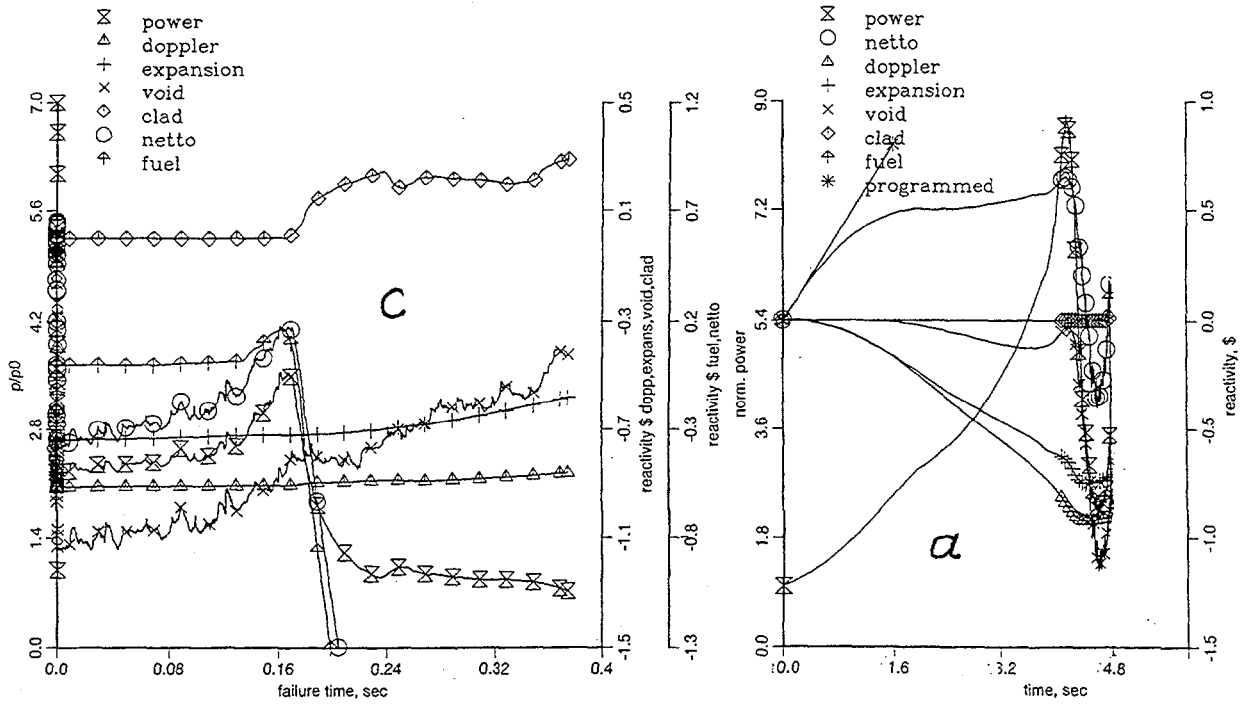


FIG. 5.1. Fast UTOP, reactivity and power behavior, core configuration (Germany)

imposed reactivity ramp is mainly counterbalanced by the Doppler effect and by the axial fuel expansion feedback. The negative reactivity effect due to the sodium heating also play a role. A quasi-linear power ramp is initiated in all the calculations. In the SAS-4A calculation performed by FZK, sodium boiling is reached at 4.116 s in channel 5/1 at the top of the core.

In the SAS-4A calculations, boiling is calculated to extend radially over about half of the core. Nevertheless, the voiding of the sodium processes in a slightly different way in the FZK and IPSN calculations due to a lower power reached at boiling onset in the IPSN calculation. In the FZK calculation, the boiling phase prior to failure is very short (0.53 s). Boiling extends radially in 18 channels and upwards in the upper sodium layer and in the upper structure zone (figure 5.1b) leading to a decrease of the sodium reactivity, of the net reactivity and thus of the power.

In the IPSN calculation, the boiling phase prior to failure is significantly longer (0.98 s). Boiling extends radially in 16 channels. During the beginning of the boiling phase, boiling extends also upwards leading to a decrease of the sodium reactivity and of the net reactivity and thus of the relative power (figure 5.2) but 0.7 s after boiling initiation, voiding extends downwards towards the center of the core in the channel 5/1 leading to an increase of the voiding reactivity in this channel and thus of the net reactivity and of the power. This phenomenon is amplified due to a similar behaviour of the voiding in the highest power channels.

The IPPE boiling results are very similar to the FZK results. The boiling phase prior to failure is very short (0.38 s) and leads to a decrease of the relative power. It is also to be noticed that fuel melting is calculated to occur prior to sodium boiling in channel 5/1 at 2.857 s.

In the IPSN calculation, four channels fail (channel 5/1 at 5.25 s). The first mechanical clad failure occurs at 62 % core height when the clad strain reaches 0.5 % and the molten fuel fraction 65 %.

In the FZK calculation, two channels fail (channel 5/1 at 4.645 s). The first mechanical clad failure occurs at 83 % core height when the clad strain reaches 0.6 %.

Based on a 50 % fuel melt fraction criterion, clad failure is predicted to occur at 4.5 s in channel 8/3 by IPPE and at 4.35 s in channel 5/3 by IGCAR. These results indicate that the evaluations of the failure times by IPPE and IGCAR are very consistent (tables 5.2 and 5.3).

Based on damage parameter criterion of Bars, failure is predicted to occur prior to sodium boiling at 3.3 s by IGCAR. It was noticed that in accordance with the SAS-4A results, using this failure criteria shifts the failure location in the upper part of the core.

Post-failure SAS-4A results obtained by IPSN indicate that during the first 15 ms following the first failure, limited fuel accumulation near core mid-plane leads to an increase of the fuel reactivity and thus of the net reactivity (figure 5.3) and of the relative power which reaches 6. Later significant fuel dispersal leads the fuel reactivity, net reactivity and power decrease. At the end of the transient (5.6s), hexcan melting is calculated in channel 5/1 so that the limitation of the use of the SAS-4A code is reached. At that time, the relative power is 0.77.

Post-failure SAS-4A results obtained by FZK are rather similar (figures 5.1c and 5.4), but due to a higher failure location, fuel relocation initiates a rapid shut-down of the reactor. Nevertheless, average fuel temperature at core mid-plane reaches 3538K in channel 5/1.

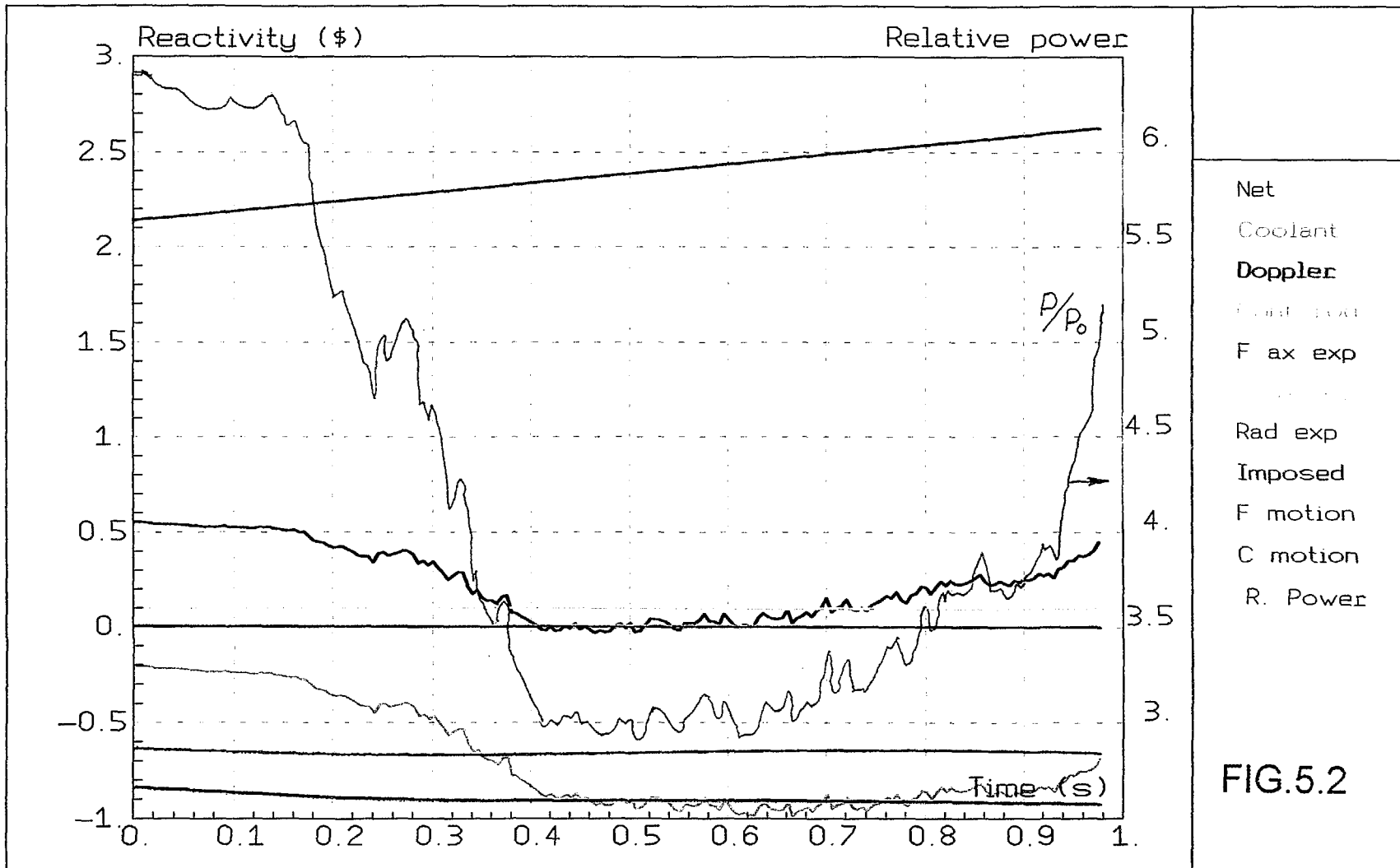


FIG.5.2

REACTIVITY

RELATIVE POWER

SAS4A

BN800 - boiling results prior to failure (UTOP 0.5 \$/s)

REF97.V1.15

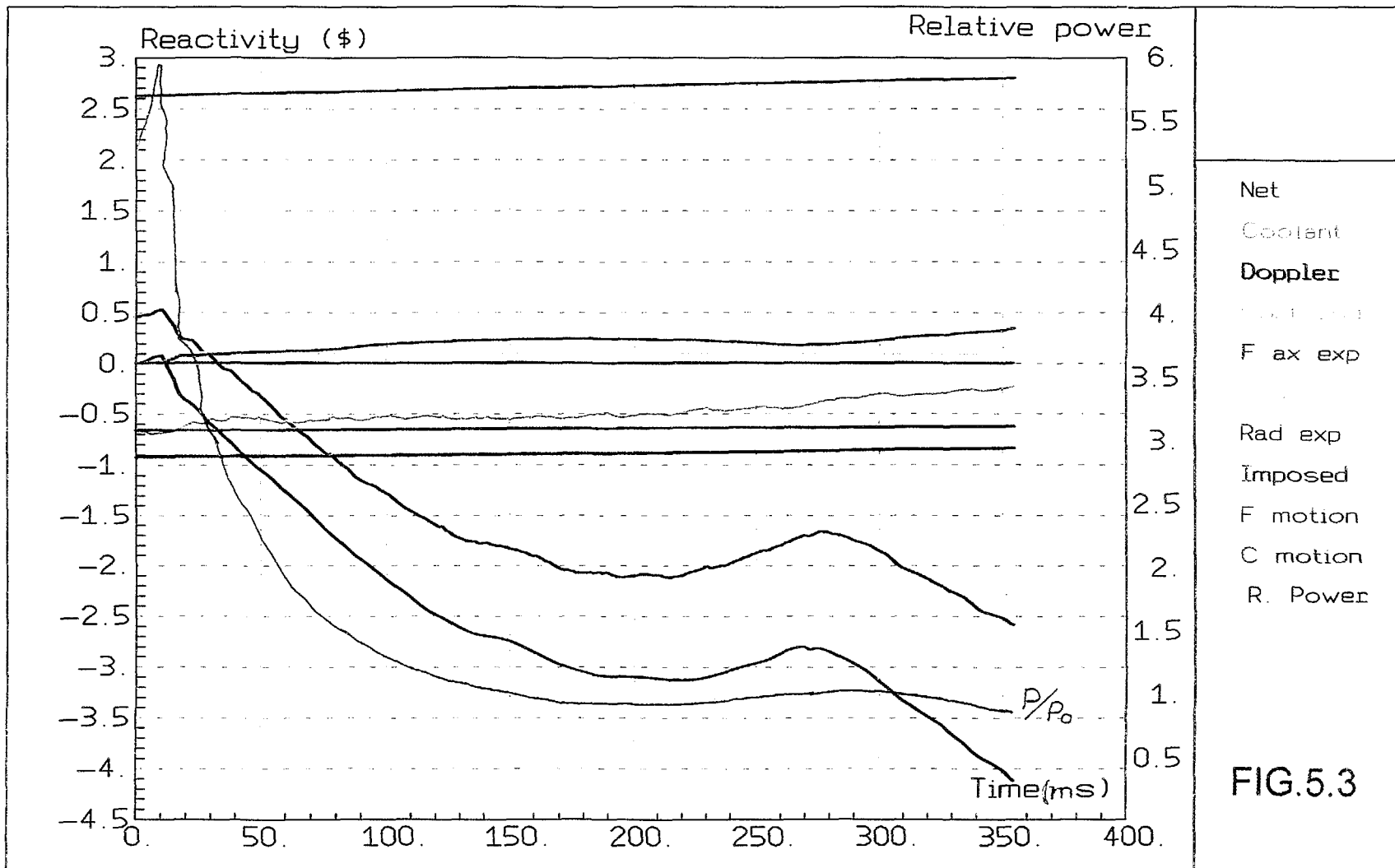


FIG.5.3

REACTIVITY

RELATIVE POWER

SAS4A

BN800 - postfailure results (UTOP 0.5 \$/s)

REF97.V1.15

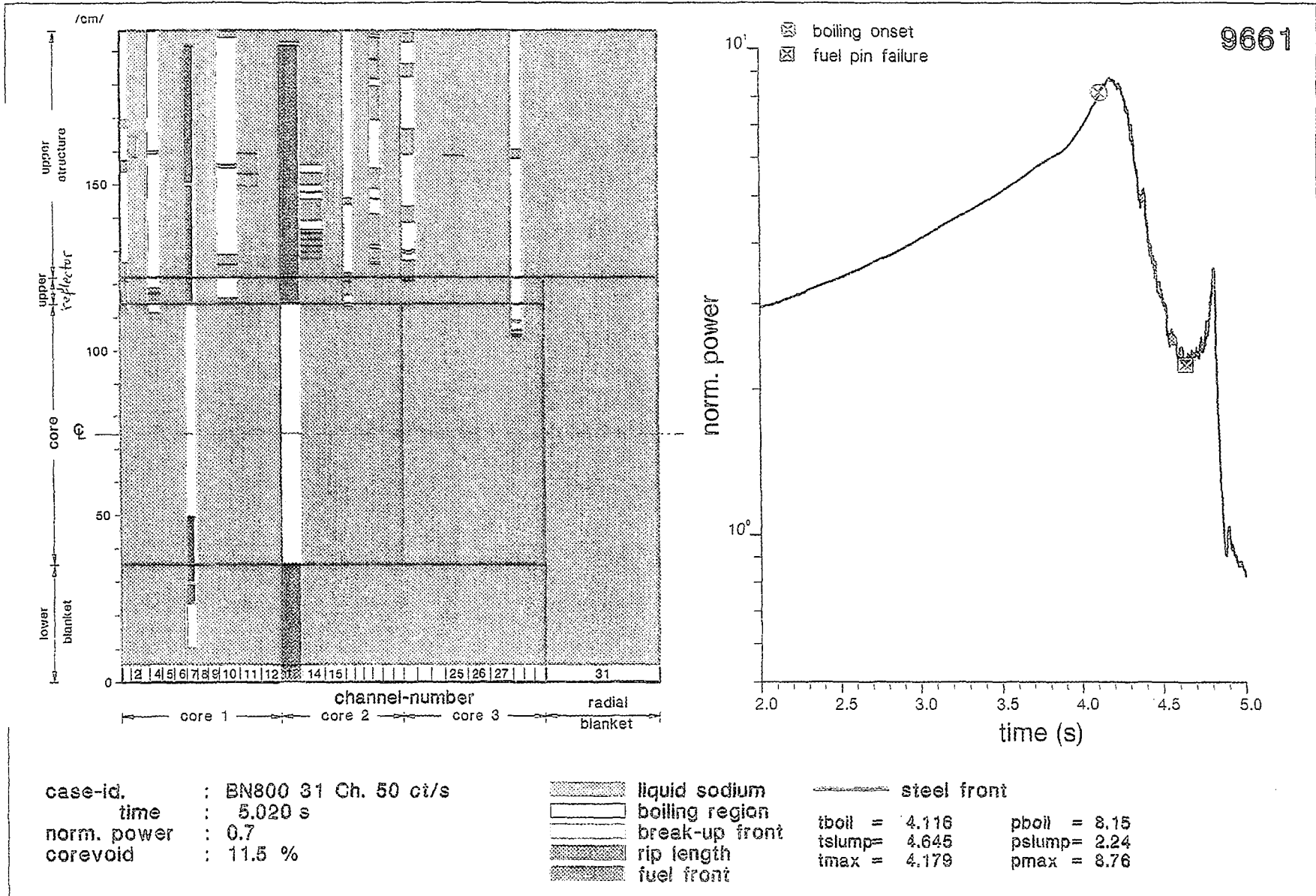


FIG. 5.4. Fast UTOP, post failure, core configuration (Germany)

In the IGCAR calculations, a fuel coolant interaction drives the fuel in the region outside the core at a velocity of 7 m/s giving a rapid negative reactivity insertion rate of - 5 \$/s shutting down the reactor. It is clear that the post-failure modelling of the PINCHTRAN code needs improvement. In particular, no compensating effect due to sodium voiding is taken into account.

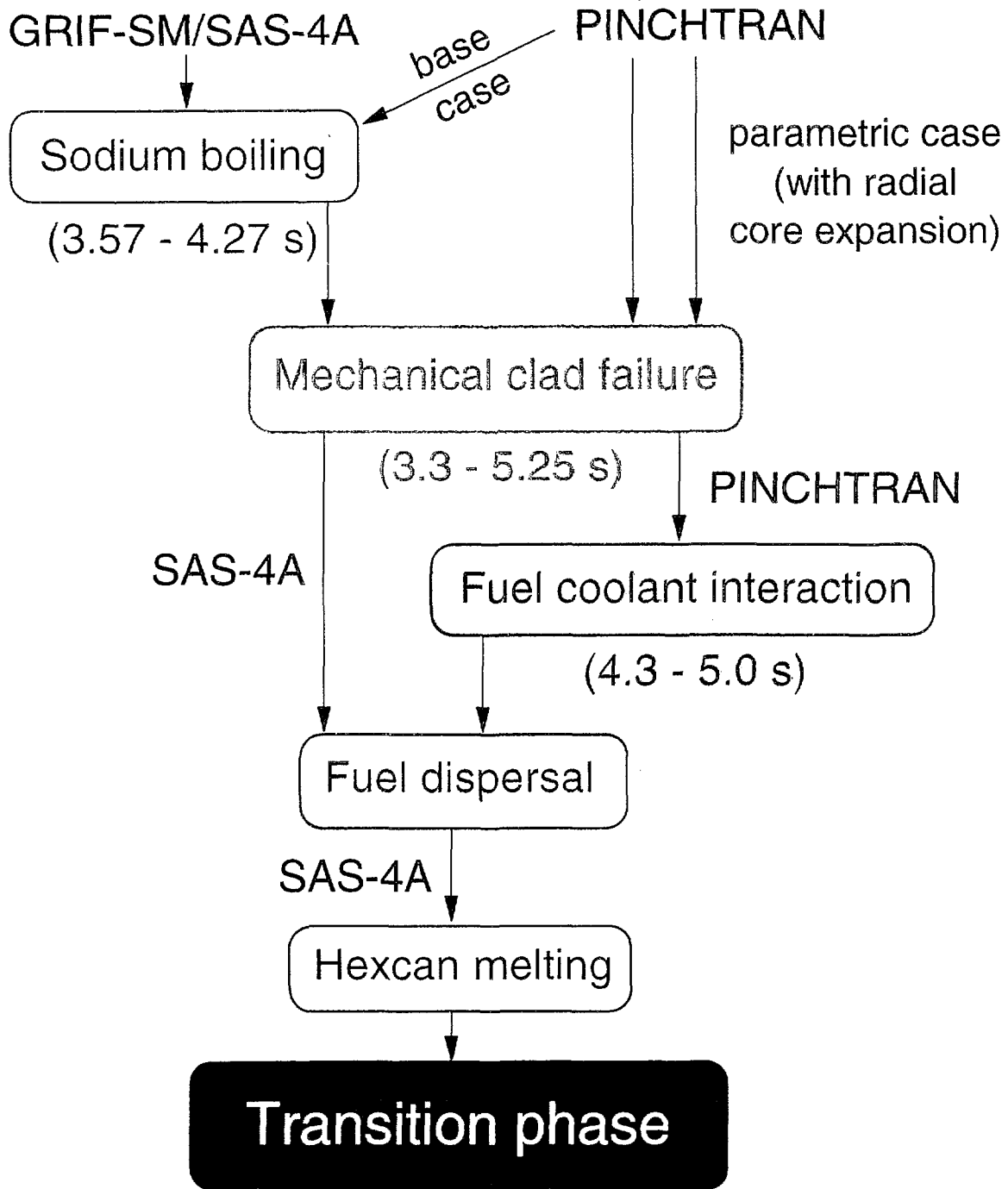
IGCAR performed a parametric calculation taking into account radial core expansion feedback. In spite of a significant negative reactivity effect, the scenario of the accident is not very much affected and pin failure cannot be avoided. Based on a 50 % fuel melt fraction criterion, failure onset is delayed by only 0.65 s (failure at 5.0 s).

FZK performed a parametric calculation using a low strain rate dependency of the ultimate tensile strength of the clad. Strong influence on the results were evidenced due mainly to the dependency of the post-failure calculations with regard to the failure axial location.

On basis of all the fast UTOP calculations performed by all the participants to this exercise, it can be concluded that :

- a clear scenario of the accident can be found in all the calculations (appendix 5.1) : negative reactivity feedback of the BN-800 type core are not enough efficient to prevent, in case of a rapid reactivity ramp insertion (0.5 \$/s), the increase of the power which in most of the calculations leads to sodium boiling and in all cases to clad failures,
- a rapid axial fuel relocation is the dominant phenomenon which shuts down the reactor,
- fuel axial expansion feedback needs to be carefully evaluated due to the impact on the accident,
- the results are strongly dependent on the reliability of the calculated failure time and more importantly of the failure location; calculations depend on the reliability of assumptions of the dose and strain rate dependencies of the clad material properties ; the data base for these assumptions should be strengthened to defend the provided results ; thus it is strongly recommended to evaluate experimentally the strain rate and temperature dependencies of the mechanical properties of the irradiated BN-800 clad material up to dose values of 70 - 100 dpa NRT,
- taking into account the negative reactivity due to the hypothetical radial core expansion cannot avoid the pin failure,
- the lack of deterministic clad failure analysis as well as the lack of post-failure modelling in the GRIF-SM code of IPPE is a strong limitation of the use of this code,
- the post-failure modelling in the PINCHTRAN code of IGCAR needs significant improvements,
- at the end of the reactor shutdown, due to the fuel relocation, hexcan melting and partial blockage formation in the concerned subassembly groups, high fuel enthalpies as well as the coolant heat-up hardly allow long-term in-place coolability of the partially restructured core configuration.

ACCIDENT SCENARIO



5.4. TRANSIENT RESULTS FOR THE SLOW UTOP (0.05 \$/S)

The slow UTOP (0.05 \$/s) simulates a slow control rod withdrawal. It is recalled that the total reactivity inserted is restricted to a maximum value of 3.9 \$ which is reached 78 s after the beginning of the reactivity insertion.

As for the fast UTOP calculations, FZK uses his own evolutions of the pin mechanics module (DEFORM-4C). This induces when compared to the IPSN results, a different axial fuel pin extension and thus a different associated reactivity feedback. FZK also starts the transient calculations from different EOEC conditions and performs a different failure analysis taking into account more appropriately IPPE modified mechanical properties of the irradiated cladding [5.13]. This leads to two scenarios which differ slightly. But, as the reactivity ramp rate due to the UTOP is ten times lower than for the fast UTOP, the accident processes slower than in the fast UTOP accident. In this case, contrary to all the other calculations, sodium boiling is reached only in the IPSN calculation.

The scenarios of the accident, as calculated by IGCAR and IPPE do not differ from the SAS-4A one obtained by FZK until the first pin failure onset. The failure time is estimated very roughly on the basis of a molten fuel fraction of 50 %. Unfortunately, as for the fast UTOP case, no post failure calculations were performed by IPPE and only a very simple modelling in the PINCHTRAN code allows to end the accident sequence.

Tables 5.4, 5.5 and 5.6 summarized the results at boiling onset and the failure conditions found by the different participants to the exercise. Some transient characteristics are presented at the relevant figures.

During the ten first seconds of the reactivity ramp insertion, the net reactivity and thus the relative power increase (figure 5.5). Then, the net reactivity is stabilised and the imposed reactivity is mainly counter-balanced by the Doppler effect and the axial fuel expansion feedback. From the negative reactivity effect due to the sodium heating also play a role. A quasi-linear power ramp is initiated in all the calculations.

TABLE 5.4. BN-800 SLOW UTOP (0.05 \$/s) RESULTS AT BOILING ONSET

| | SAS-4A | | GRIF-SM | PINCHTRAN | |
|-------------------|-----------|--------|---------|---------------------|----|
| | FZK (1) | IPSN | IPPE | IGCAR | |
| | BASE CASE | | | PARAMETRIC CASE (2) | |
| Boiling onset (s) | NO | 37.876 | NO | NO | NO |
| Channel number | | 5/1 | | | |
| Relative power | | 3.29 | | | |
| Net reactivity | | 0.18 | | | |

(1) updated EOEC - conditions

(2) with radial core expansion feedback

(3) based on 50 % fuel melt fraction

TABLE 5.5. BN-800 SLOW UTOP (0.05 \$/s) RESULTS AT FIRST FAILURE TIME

| | SAS-4A | | GRIF-SM | PINCHTRAN | | |
|--------------------------|-----------|--------|----------|-----------|---------------------|----------|
| | FZK (1) | IPSN | IPPE | IGCAR | | |
| | BASE CASE | | | | PARAMETRIC CASE (2) | |
| Failure time (s) | 35.966 | 41.095 | 33.3 (3) | 36.75 (3) | 39.9 (4) | 43.3 (3) |
| Channel number | 5/2 | 5/1 | 8/3 | 5/3 | 2/1 | 5/3 |
| Relative power | 3.13 | 3.11 | | 2.50 | - | 2.48 |
| Net reactivity | 0.172 | 0.12 | | 0.14 | - | 0.12 |
| Failure location (%) | 67 | 79. | | 58. | 92. | 58. |
| Molten fuel fraction (%) | 65. | 55. | | 50. | - | 50. |
| Clad plastic strain (%) | 1.7 | 0.5 | | - | - | - |

TABLE 5.6. BN-800 SLOW UTOP (0.05 \$/s) RESULTS AT FIRST FAILURE TIME

| | SAS-4A | | GRIF-SM | PINCHTRAN | | |
|---|-----------|--------|----------|-----------|---------------------|----------|
| | FZK (1) | IPSN | IPPE | IGCAR | | |
| | BASE CASE | | | | PARAMETRIC CASE (2) | |
| Failure time (s) | 35.966 | 41.095 | 33.3 (3) | 36.75 (3) | 39.9 (4) | 43.3 (3) |
| Time interval between failure and boiling onset (s) | | 3.219 | | - | - | - |
| Net reactivity (\$) | 0.172 | 0.12 | 0.18 | 0.14 | - | 0.12 |
| Doppler (\$) | -0.906 | -0.98 | | -1.0 | - | -1.02 |
| Fuel axial expansion (\$) | -0.810 | -0.73 | | -0.53 | - | -0.54 |
| Clad axial expansion (\$) | 0.086 | 0.10 | | 0.03 | - | 0.03 |
| Sodium (\$) | 0.004 | -0.32 | | -0.16 | - | -0.16 |
| External reactivity (\$) | 1.798 | 2.05 | | 1.83 | - | 2.16 |

- (1) updated EOEC - conditions
- (2) with radial core expansion feedback
- (3) based on 50 % fuel melt fraction
- (4) based on damage parameter criterion of Bars.

In the SAS-4A calculation performed by IPSN, fuel melting is predicted to occur in channel 5/1 at 19.14 s and sodium boiling is reached in the same channel at 37.876 s (table 5.4). Boiling extends radially in 9 channels. During the beginning of the boiling phase, boiling extends also upwards leading to a decrease of the sodium reactivity and of the net reactivity (figure 5.6) and thus of the relative power, but 3 s after boiling initiation, voiding extends downwards towards the center of the core in the channel 5/1 leading to an increase of the voiding reactivity in this channel and thus of the net reactivity and of the power.

In the IPSN calculation, only one channel fails (5/1) at 41.095 s, 3.2 s after first boiling onset. Figure 5.7a shows the voiding pattern of the core at onset of pin failure. The mechanical clad failure occurs at 79 % core height when clad strain reaches 0.5 % and molten fuel fraction 55 %.

In the FZK calculation, only channel 5/2 fails at 35.966 s (figure 5.7b). The mechanical clad failure occurs at 67 % core height when the clad strain reaches 1.7 %. When compared to the IPSN calculation, this result reflects the consequences of the lower sodium temperature.

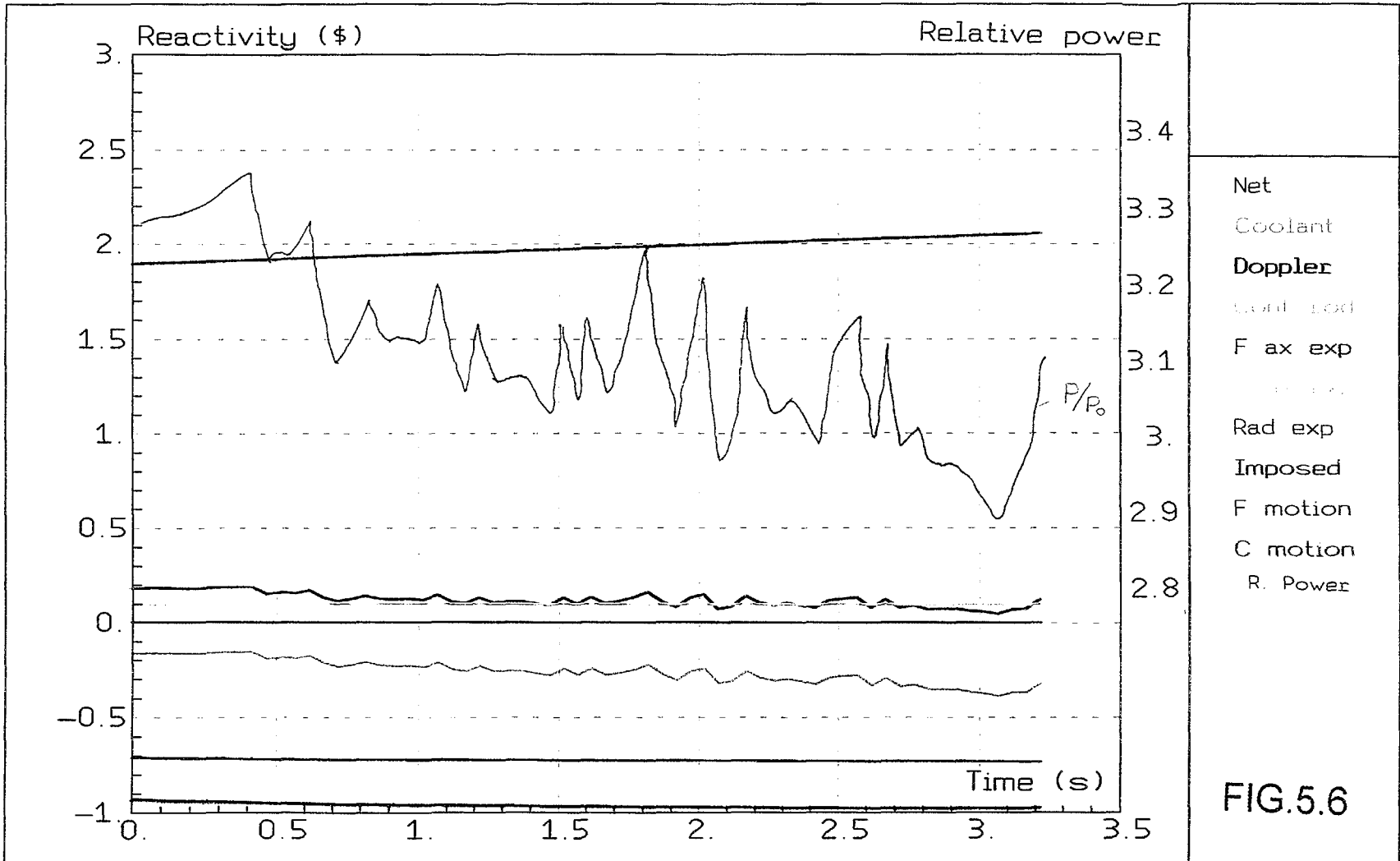
Based on a 50 % fuel melt fraction criterion, clad failure is predicted to occur at 33.3 s in channel 8/3 by IPPE. Using the same criterion, IGCAR predicted the clad failure in channel 5/3 at 36.75 s. Based on damage parameter criterion of Bars, IGCAR obtained a clad failure at 39.9 s in channel 2/1.

Post-failure SAS-4A results obtained by IPSN indicate that during the first 10 ms following the failure, limited fuel motion leads to an increase of the fuel reactivity and thus of the net reactivity and of the relative power (figure 5.8) which reaches 3.35. Later, significant axial fuel dispersal in channel 5/1 leads the fuel reactivity, net reactivity and power decrease. At 41.726 s hexcan melting is calculated in channel 5/1. Thus the limit of applicability of the one dimensional material motion, multi-channels SAS-4A is reached. At that time the relative power is 0.6.

After the failure, SAS-4A results obtained by FZK indicates an increase of the void reactivity and thus of the net reactivity and of the power (figure 5.9). This is a consequence of the fuel-coolant interaction. Then, the fuel reactivity increases slightly until 160 ms after failure time. Only 170 ms after failure time, significant fuel and clad dispersals occur and initiate a rapid shut down of the reactor. In this accident sequence, only the channel 5/2 fails. The average fuel temperature at core mid-plane reaches 3287 K.

In the IGCAR calculations, as for the fast UTOP case, a fuel coolant interaction drives the fuel in the region outside the core at 7 m/s giving a rapid negative reactivity insertion rate of - 5 \$/s shutting down the reactor. It is clear that the post-failure modelling of the PINCHTRAN code needs improvement. In particular, no compensating effect due to sodium voiding is taken into account.

IGCAR performed again a parametric calculation taking into account the radial core expansion feedback. Pin failure cannot be avoided and, based on a 50 % fuel melt fraction, is delayed by 3.4 s (failure at 43.3 s).



Net
Coolant
Doppler
Cond. load
F. ax exp
F. motion
C. motion
R. Power

FIG.5.6

REACTIVITY

RELATIVE POWER

SAS4A

BN800 - boiling results prior to failure (UTOP 0.05 \$/s)

REF97.V1.15

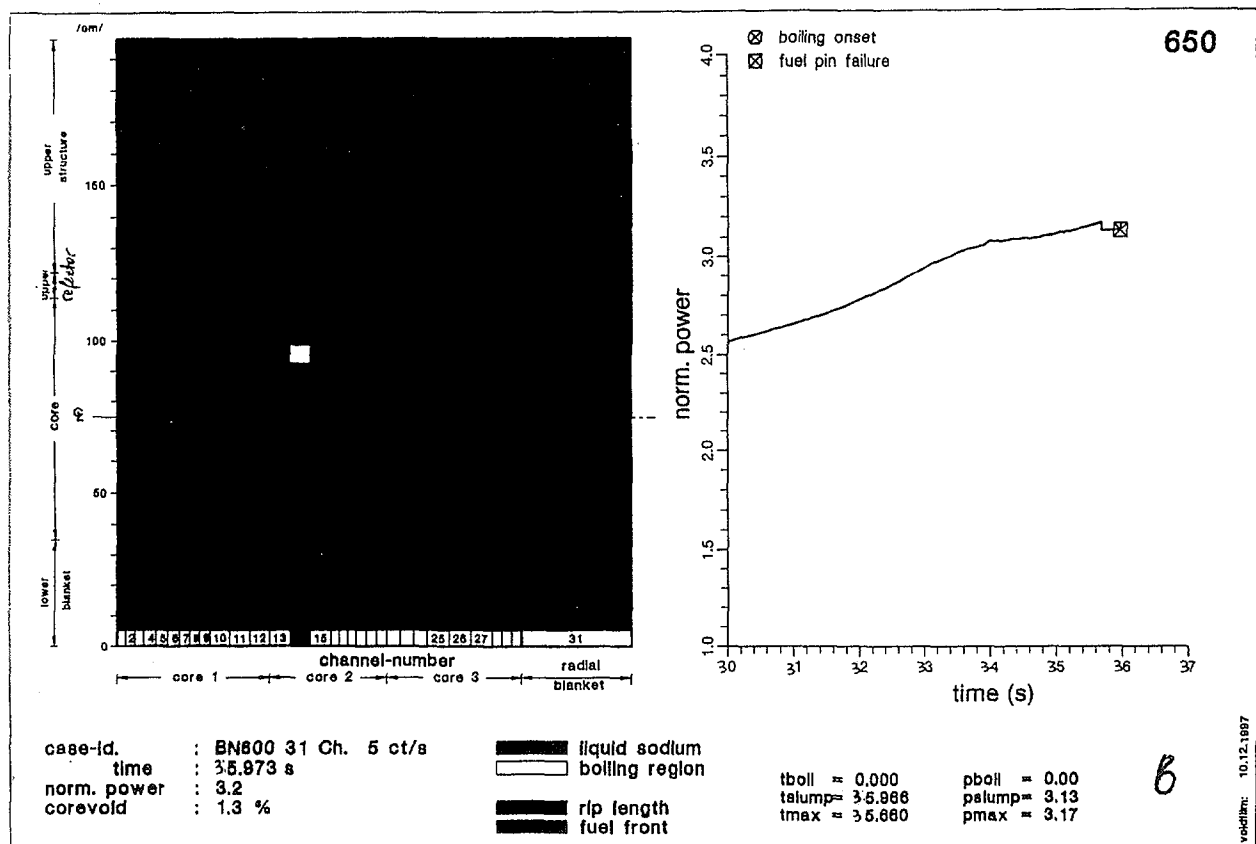
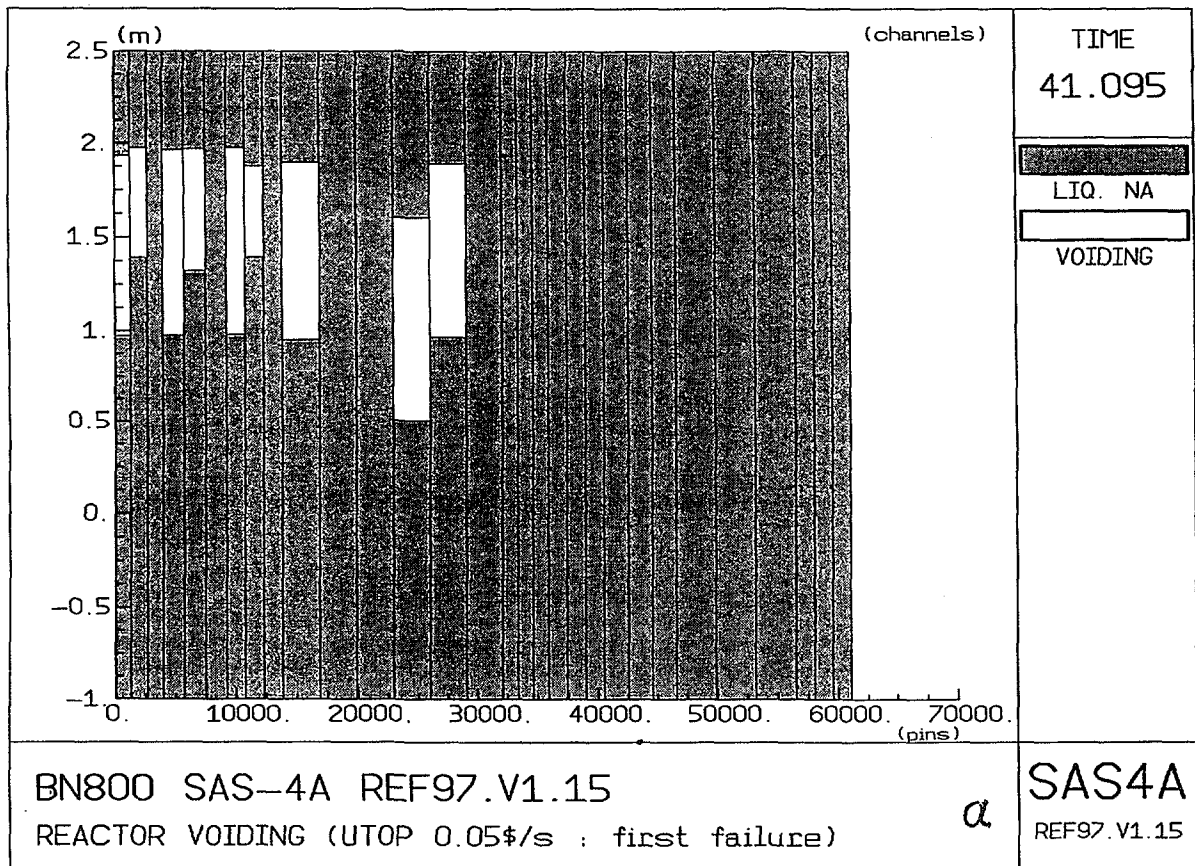
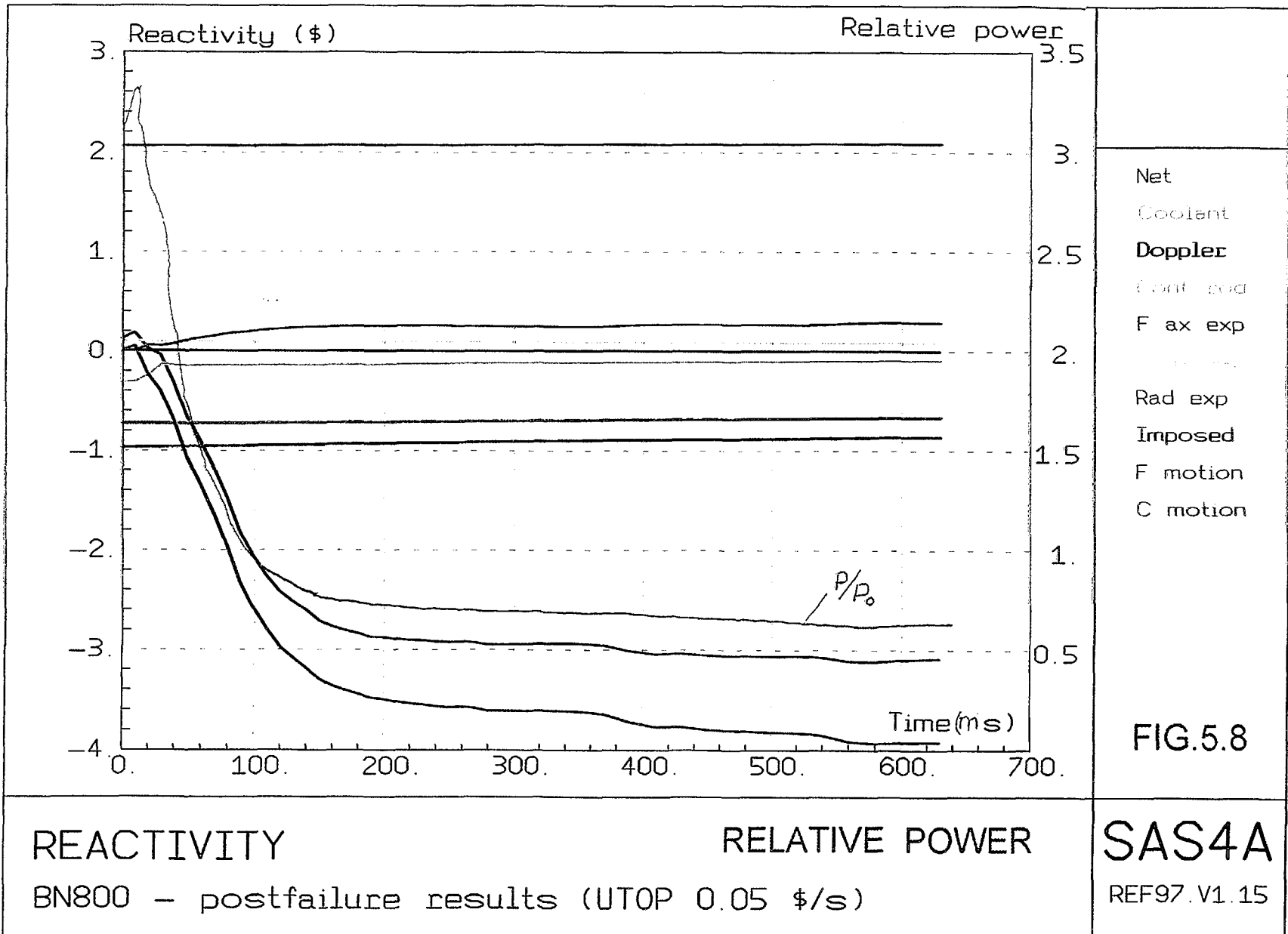


Fig.5.7. Slow UTOP, voiding phase. Core configuration [France(a), Germany (b)]



REACTIVITY

RELATIVE POWER

BN800 - postfailure results (UTOP 0.05 \$/s)

SAS4A

REF97.V1.15

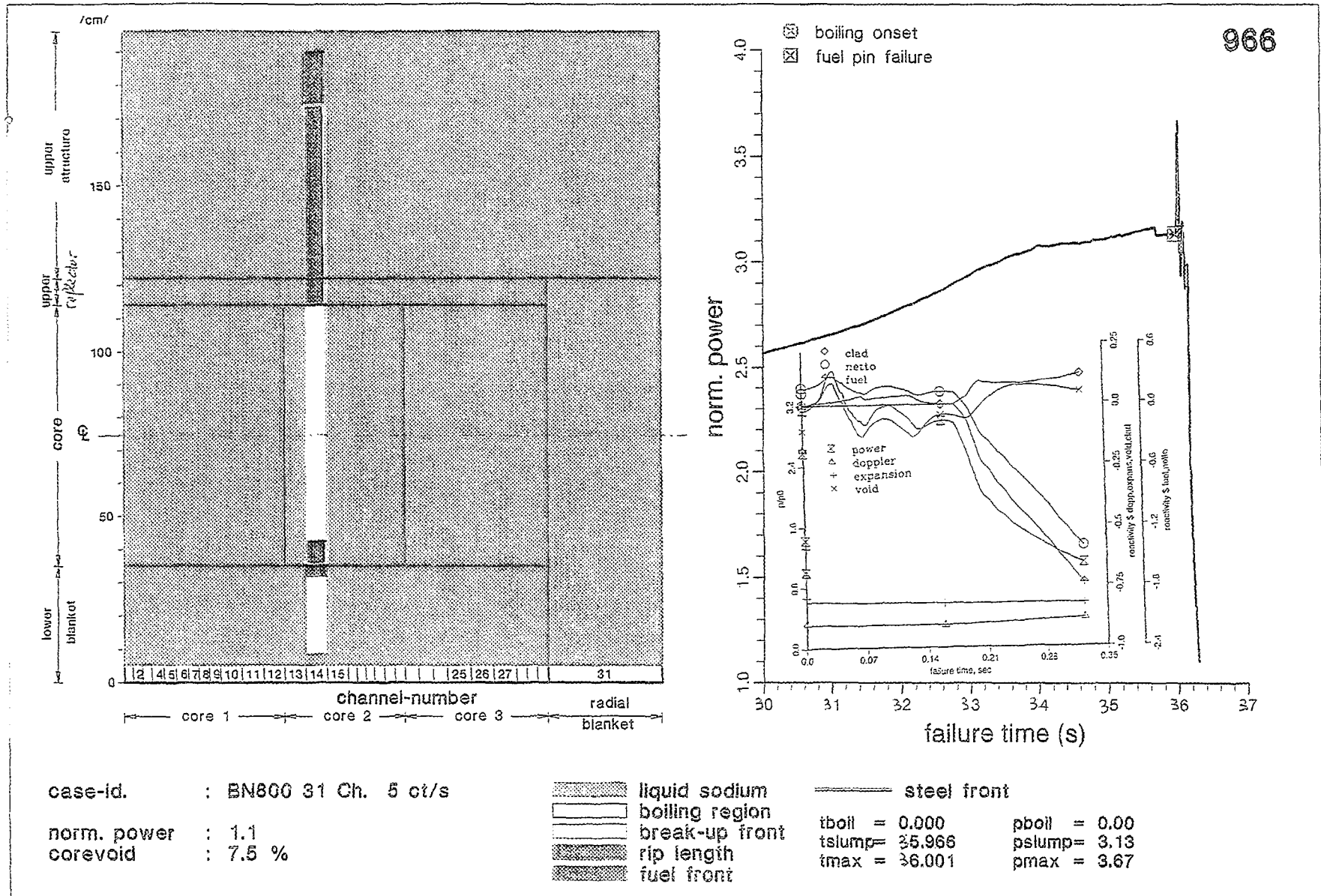


Fig.5.9. Slow UTOP, post failure. Reactivity and power behaviour, core configuration (Germany)

On basis of all the slow UTOP calculations performed by all the participants to this exercise, it can be concluded that :

- a clear scenario of the accident can be found in most of the calculations (appendix 5.2) : negative reactivity feedback of the BN-800 type core are not enough efficient to prevent, in case of a slow reactivity ramp insertion (0.05 β /s), the increase of the power which leads in all cases to clad failure in one channel,
- a rapid axial fuel relocation is the dominant phenomenon which shuts down the reactor,
- SAS-4A calculation performed by IPSN is the only one which leads to sodium boiling prior to clad failure ; thus, pin mechanics and the associated calculated fuel axial expansion feedback need to be carefully evaluated due to their impact on the kinetics of the accident,
- at the end of the reactor shutdown due to the fuel relocation in one subassembly group, hexcan melting and partial blockage formation in the concerned subassembly group results in a configuration which can hardly be cooled in-place on a long-time scale ; the accident most probably will enter into a slow core melt down with a progressive core destruction by a thermally induced subassembly to subassembly propagation.

Similarly to the fast UTOP analysis, it can be added that :

- realistic clad mechanical properties need to be taken into account due to their impact on the time and location of the failure which affects the post-failure results,
- the lack of deterministic clad failure analysis as well as the lack of post-failure modelling in the GRIF-SM code of IPPE is a strong limitation of the use of this code,
- the post-failure modelling in the PINCHTRAN code of IGCAR needs significant improvements.

5.5. TRANSIENT RESULTS FOR THE UTOP-ULOF ACCIDENT

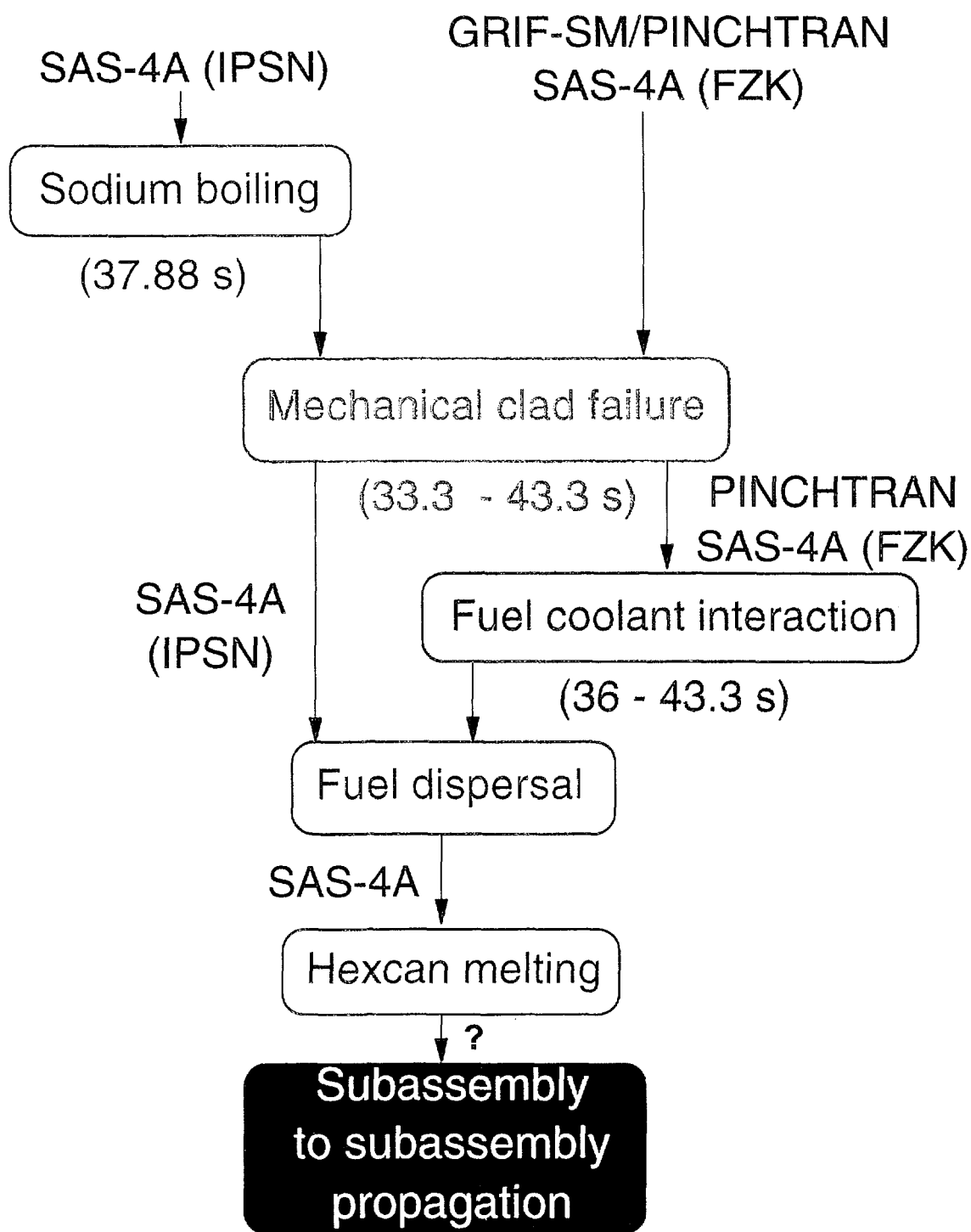
The UTOP-ULOF accident studied in this paragraph simulates an unauthorised withdrawal of six compensator rods from the core accompanied by the failure of all scram system absorber rods.

The scenarios of this accident assumes the following sequence of accidental events :

- wrong phase alternation on sections of the first source of reserve power supply of absorber rods,
- loss of power supply of rod drives from the first main source,
- failure of interlock preventory transfer of rods group to the first reserve source with wrong phase alternation,
- transfer of power supply of absorber rods group to the first source,
- withdrawal of one control rod from the core caused by the wrong power supply of its drive,
- formation of scram signal when the reactor power is increased by 15 % (two sets of devices with « two out of three » logic in each set),
- upwards movements of six compensator rods, supplied from the first reserve source,

ACCIDENT SCENARIO

(slower)



- de-energization of primary and secondary pumps after appearance of scram signal and their further low speed operation (25 % of rated value),
- failure of all other absorber rods which should be inserted into the core (9 safety rods, 6 compensation rods, 1 control rod, 3 passive safety rods).

For the calculation, this accident leads to the following scenario :

- first reactivity ramp insertion : 0.05 \$/s for 10 s,
- when the power reaches 1.15 times nominal, an additional reactivity ramp is inserted : 0.05 \$/s for 100 s,
- one second later, a coolant mass flow reduction is initiated down to 25 % nominal flow ; before flow stabilisation, the rotation speed w of the pump is assumed to decrease with the time t according with the following law :

$$w = \frac{5.5}{t + 5.5}$$

A very coherent scenario is calculated by all the participants to the exercise.

Preboiling calculations

Due to the reactivity ramp initiation (0.05 \$/s) figure 5.10), the net reactivity and thus the relative power increase.

The power reaches 1.15 times nominal at 1.97 s in the IGCAR calculation (figure 5.11), at 3 s in the IPPE and IPSN calculations (figures 5.12, 5.10) and at 3.2 s in the FZK calculation (figure 5.12).

When the power reaches 1.15 times nominal, an additional reactivity ramp is initiated (0.05 \$/s, figures 5.11). It leads to a more rapid net reactivity increase (figures 5.10, 5.12) and power increase.

One second later, the loss of flow is initiated. Until 10 s (end of the first reactivity ramp rate), axial fuel expansion feedback, Doppler effect and additional negative coolant reactivity due to sodium heating have a tendency to stabilise the net reactivity (figures 5.10, 5.12) and thus limits the power increase rate.

After 10 s, in the IPSN, FZK and IPPE calculations, due to the end of the first reactivity ramp the net reactivity and thus the power (figures 5.10, 5.12) decrease.

Boiling calculations

Boiling onset is reached, in channel 5/1 in the upper sodium layer above the core at 9.8 s in the IGCAR calculation, at 10.25 s in the IPSN calculation, at 10.74 s in the IPPE calculation and at 11.11 s in the FZK calculation (table 5.7). Nevertheless, the agreement on the boiling onsets obtained by IPPE and IGCAR with regard to those obtained in the SAS-4A calculations (IPSN and FZK) is a consequence of an overestimation of the Doppler effect in the GRIF-SM-CANDLE and PINCHTRAN codes due to the use of a low and

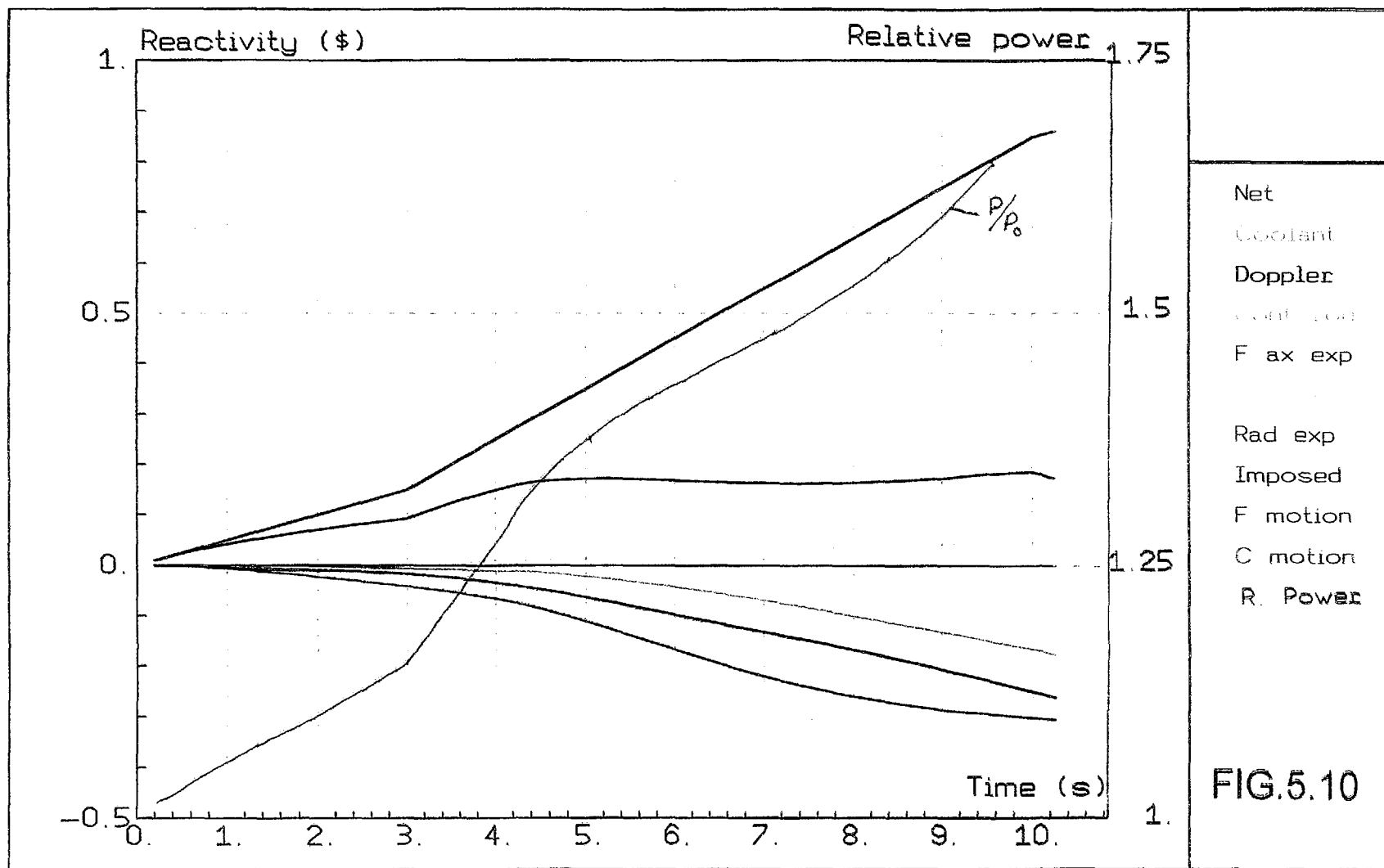


FIG.5.10

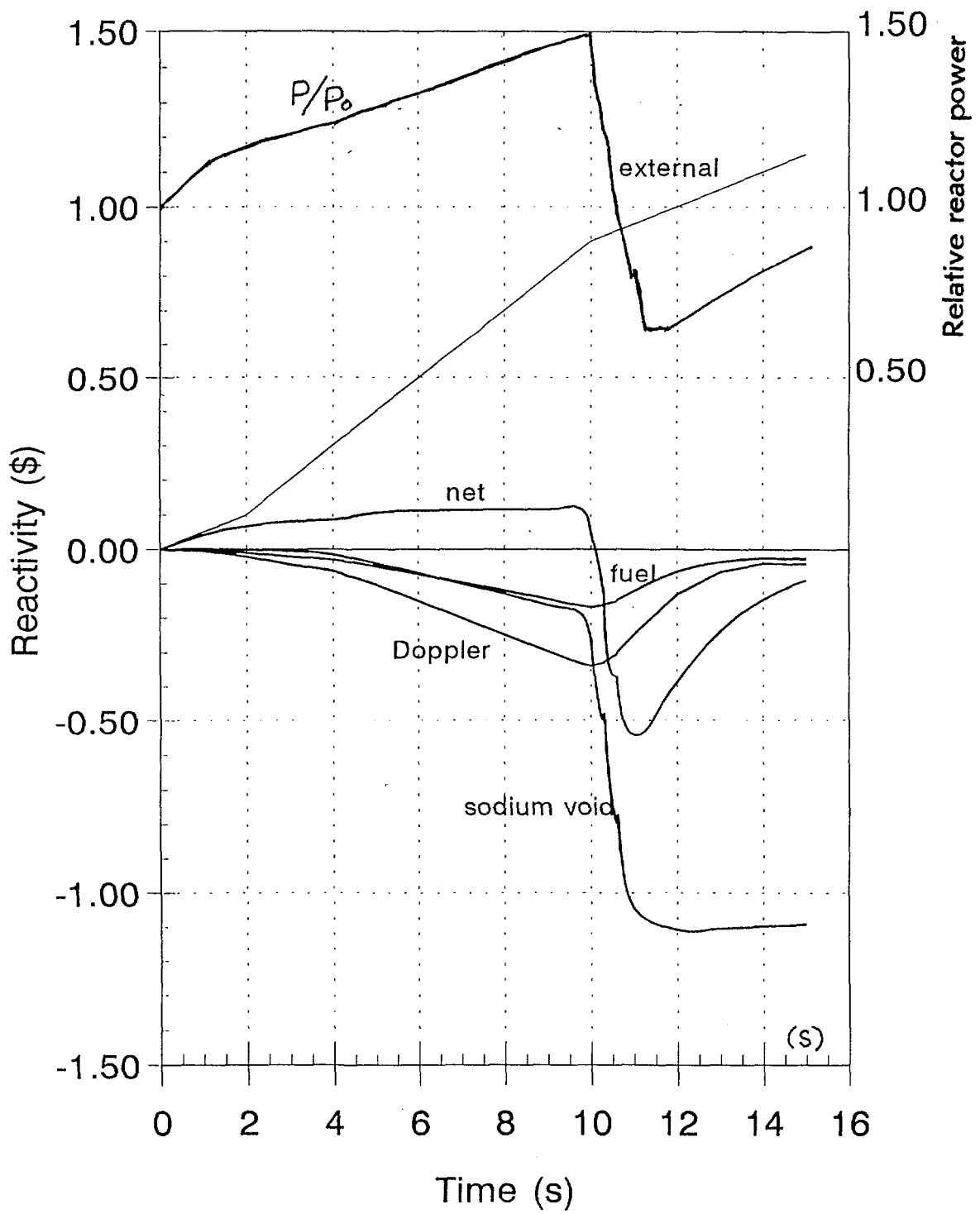
REACTIVITY

RELATIVE POWER

SAS4A

BN800 - preboiling results (ULOF-UTOP)

REF97.V1.15



UTOP/ULOF (Without Radial Feedback)

Fig.5.11. Preboiling phase, reactivity and power behaviour (India)

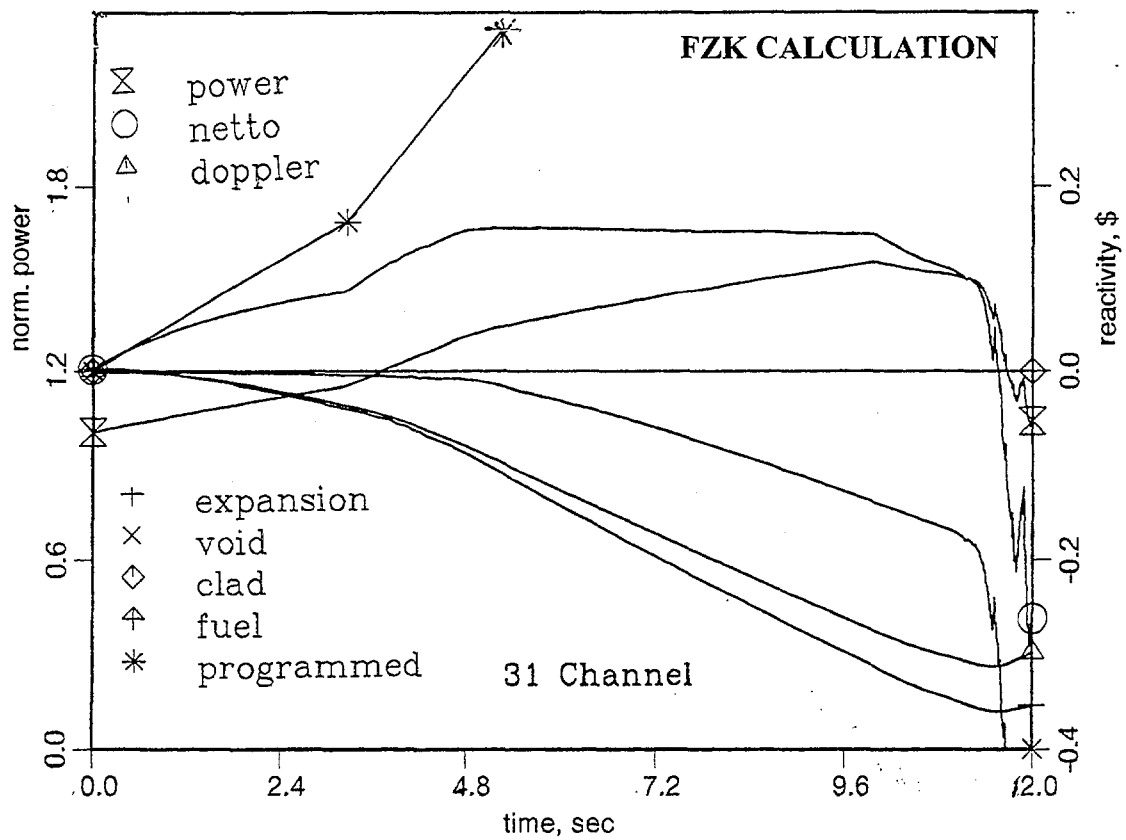
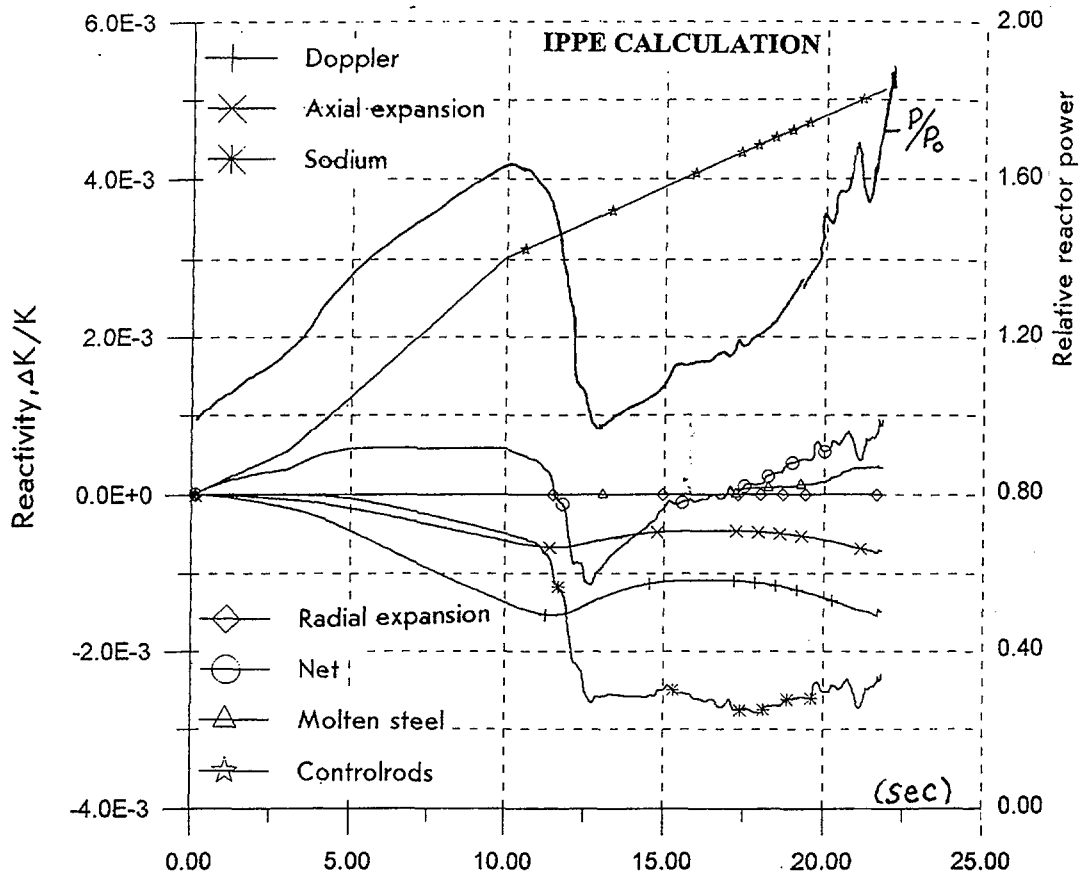


Fig.5.12. UTOP/ULOF, preboiling phase, reactivity and power behaviour

constant fuel to clad gap conductance compensated by an underestimation of the fuel axial expansion reactivity feedback due to a less refined modellisation of this transient effect in these codes (table 5.7).

Voiding calculations

The voiding calculations differ significantly depending on the degree of refinements in the different codes.

Using a simplified approach, the PINCHTRAN calculation performed by IGCAR leads to a significant voiding of the upper sodium layer without core voiding. Thus, the sodium void reactivity decreases strongly by about 1 \$ (figure 5.11) leading to a significant decreases of the net reactivity and of the power. Nevertheless, the calculation was stopped too early because a constant sodium void reactivity is reached during the last four seconds of the calculation inducing, due to the continuation of the reactivity ramp, an increase of both net reactivity. Without any doubt the accident will continue but a lack of modelling (pin break-up, clad and fuel motions and relocations) does not allow a continuation of the calculation of the accident.

The voiding calculations performed by IPPE lead only to a partial voiding of the core which is counter-balanced by the upper sodium layer voiding (figure 5.12). Modelling needs refinements as it can be observed in the results that, during the last ten seconds of the calculation, nearly constant sodium reactivity is obtained in spite of an increase of the power. This is contradictory with the use of a constant fuel clad heat transfer coefficient and leads to avoid the voiding propagation downwards towards the core where the void reactivity effect is positive. This can only be partially explained by the clad rewetting modelling which does not allow sodium vaporisation to occur. It is also to be noticed that no significant clad temperature increase rate after cladding dry-out is calculated indicating that the clad-sodium heat transfer coefficient after dry-out must be improved.

TABLE 5.7. BN-800 UTOP-ULOF (base case) RESULTS AT BOILING ONSET

| | SAS-4A | | GRIF-SM-CANDLE | PINCHTRAN |
|---------------------------|---------|-------|----------------|-----------|
| | FZK (1) | IPSN | IPPE | IGCAR |
| Boiling onset (s) | 11.11 | 10.25 | 10.74 | 9.8 |
| Relative power | 1.50 | 1.68 | 1.62 | 1.45 |
| Net reactivity (\$) | 0.102 | 0.17 | 0.13 | 0.1 |
| Doppler (\$) | -0.306 | -0.26 | -0.42 | -0.35 |
| Fuel axial expansion (\$) | -0.351 | -0.30 | | -0.15 |
| Clad axial expansion (\$) | 0.043 | 0.05 | | - |
| Sodium (\$) | -0.177 | -0.18 | -0.16 | -0.18 |
| External reactivity (\$) | 0.893 | 0.86 | 0.88 | 0.9 |

The calculations performed by IPSN and FZK using the SAS-4A code are very similar and lead to the following scenario. During the first second of the boiling phase, voiding extends radially in the high power channels in the upper sodium layer leading to a decrease of the sodium voiding reactivity (figures 5.13 and 5.13a) and thus to the net reactivity and of the power. Then, voiding extends axially in the higher power channels downwards towards the center of the core in the high power channels : this leads for about 1.5 s to an increase of the sodium voiding reactivity and thus of the net reactivity and of the power. Extensive sodium layer voiding leads then to decrease the sodium voiding reactivity but downwards voiding extension in lower power channels leads finally to reactivity and power increase. 25 channels and 28 channels are predicted to boil respectively in the IPSN and FZK calculation. It must be noticed that this oscillatory behaviour of the sodium voiding reactivity and thus of the net reactivity and power is similar to the one calculated in the ULOF scenario with the SAS-4A code but the sequence is faster due to the superposition of the reactivity ramps. *It can be noticed also that this voiding behaviour is even more complex due to the inlet plenum pressure increase consecutive to the extensive downwards voiding propagation in the high power channels (figure 5.14) which leads the boiling in lower power channels to disappear (figures 5.15).*

Clad motion

In the SAS-4A calculations performed by IPSN and FZK, clad motion is predicted to occur respectively 2.26 s and 2.09 s after boiling onset (table 5.8). The status of the voiding as calculated by IPSN using the SAS-4A code is plotted in figure 5.16.

In the GRIF-SM-CANDLE calculation performed by IPPE (table 5.8), the time interval between clad motion and sodium boiling is much larger (5.11 s). This is a consequence of the too low and constant fuel to clad heat transfer coefficient as well as the too high clad melting temperature (1500°C) used in the GRIF-SM-CANDLE calculation and also of the too low sodium voiding reactivity which is linked to the lack of downwards voiding propagation and which leads to a too low net reactivity and power (table 5.8).

In the SAS-4A calculations performed by IPSN and FZK, clad motion is predicted to occur respectively in 5 channels and 14 channels. After a limited reactivity effect during the first half second of the motion, a significant positive reactivity ramp rate due to clad motion outside the center of the core towards the fissile ends is superposed to the positive sodium void reactivity effect (figures 5.13). This leads to a significant increase of the power (figures 5.13a).

The same scenario is calculated by IPPE using the GRIF-SM-CANDLE code (figure 5.12) but in this calculation clad relocation occurs only upwards. It is to be noticed that during the whole boiling phase of the accident, in spite of a significant power increase and of fuel melting reached 20 s after accident initiation, no significant Doppler and fuel axial expansion reactivity feedbacks are calculated which indicated a need of modelling improvements. A lack of modelling after fuel melting is evidenced.

It is to be noticed that during this stage of the accident, massive core voiding as well as significant axial steel relocation are predicted to occur.

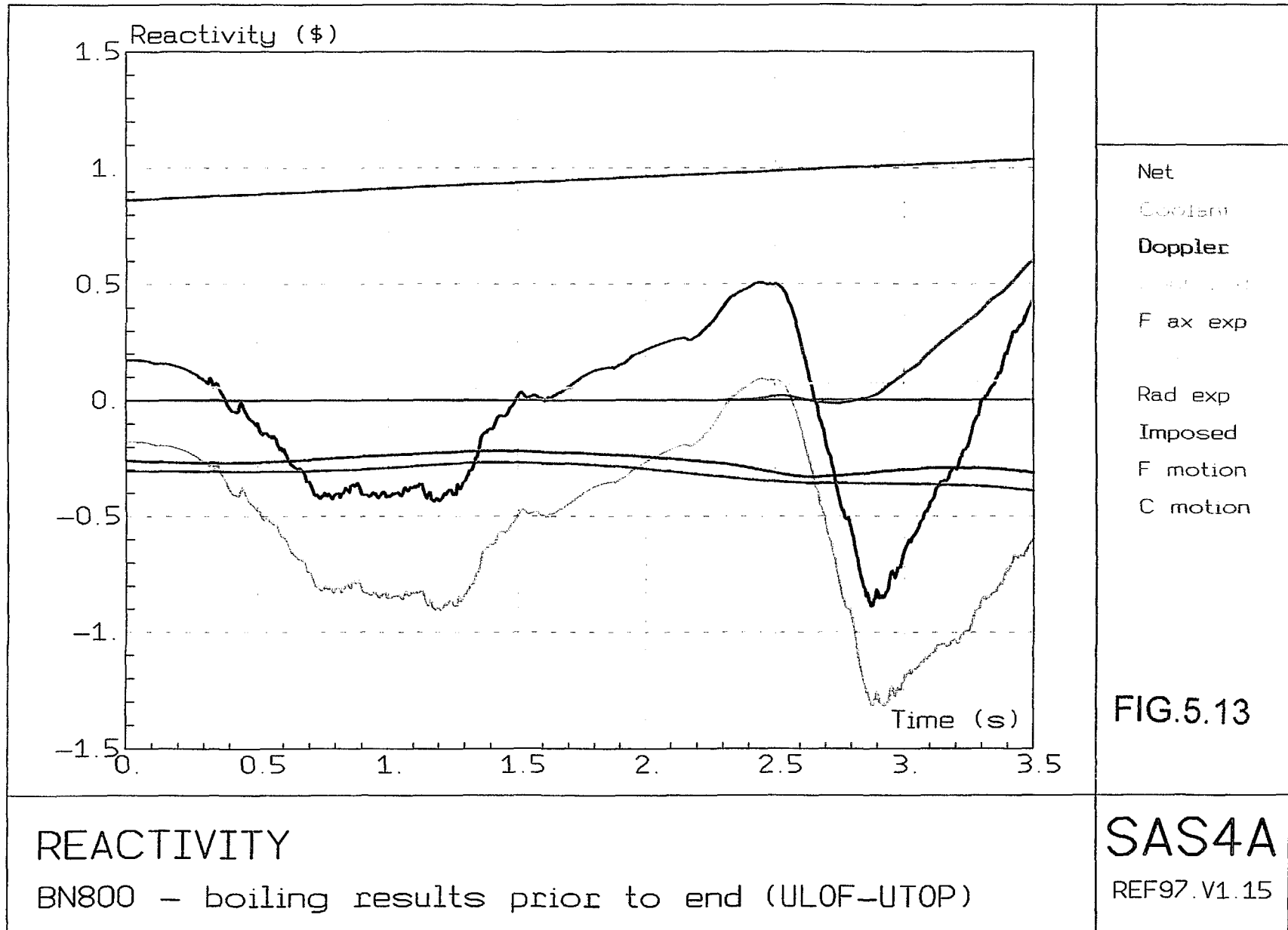


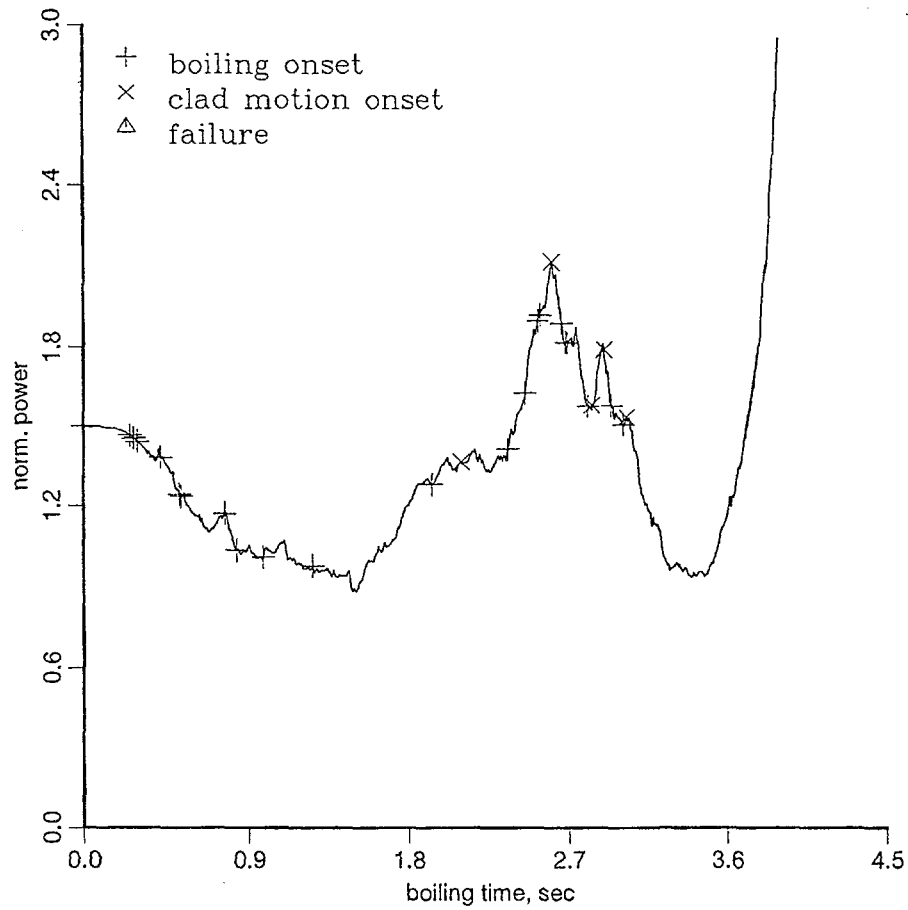
FIG.5.13

REACTIVITY

BN800 - boiling results prior to end (ULOF-UTOP)

SAS4A

REF97.V1.15



BN800 31 Channel 0.05\$/s 14.05.1998

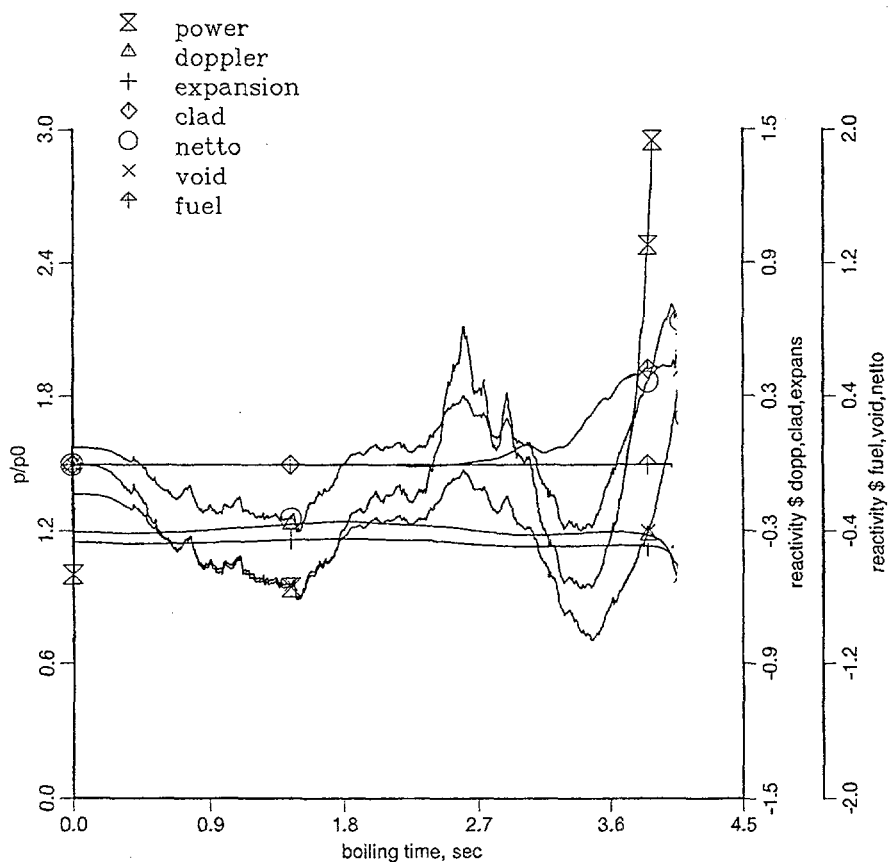


Fig. 5.13a. Slow UTOP/ULOF. Power and reactivity behaviour (Germany)

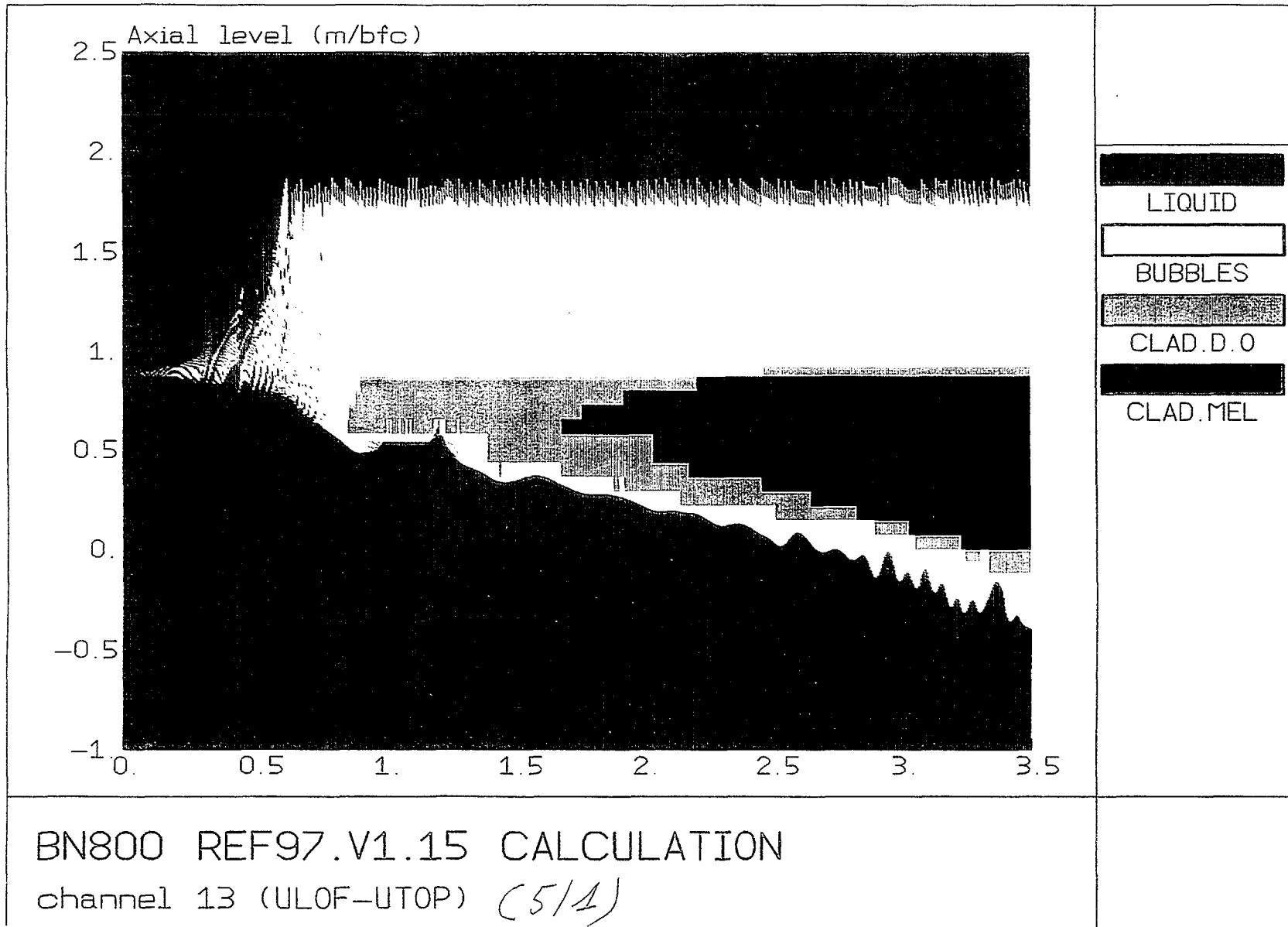
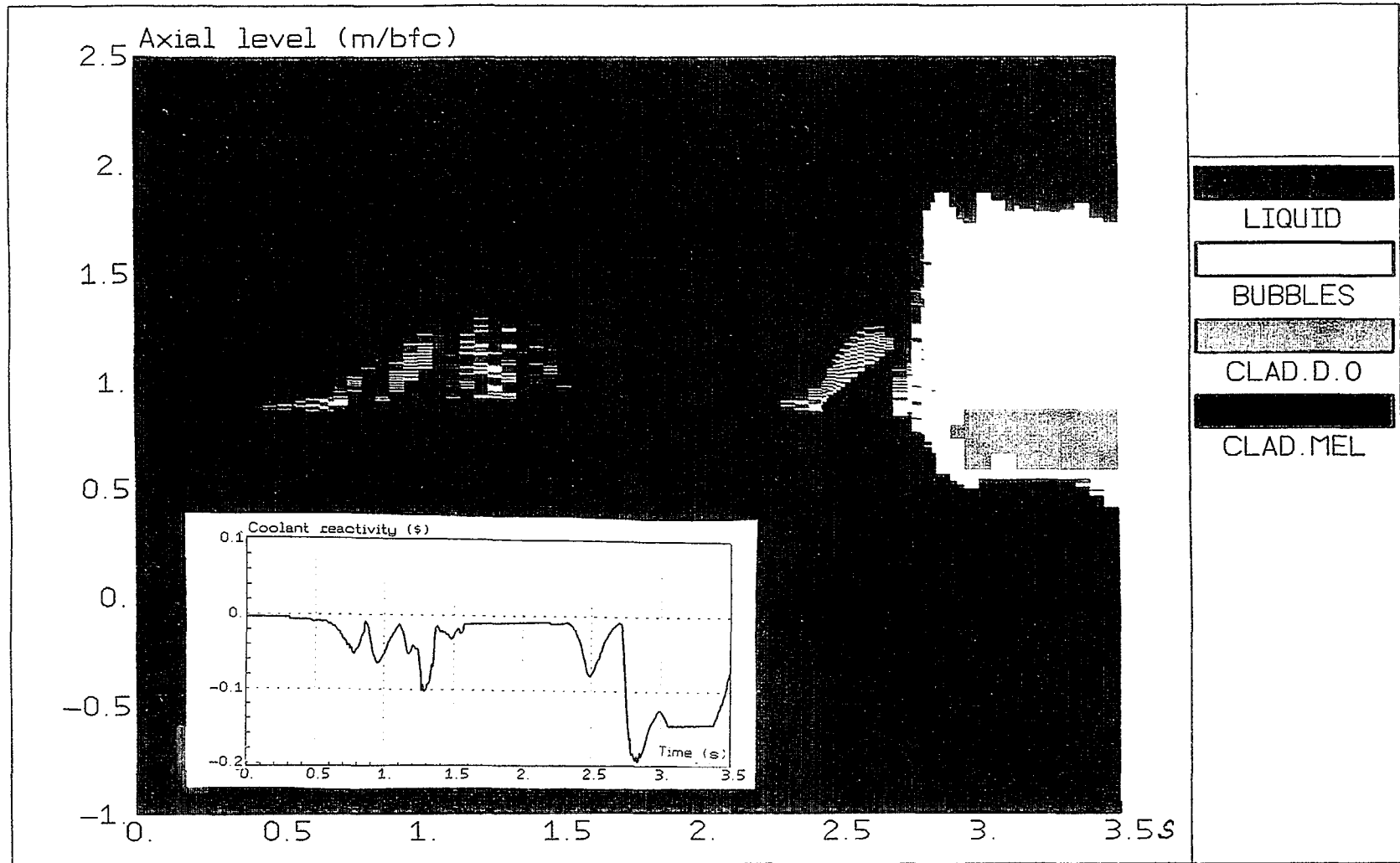


Fig.5.14. Voiding propagation, channel configuration (France)



BN800 REF97.V1.15 CALCULATION

channel 14 (ULOF-UTOP) (5/2)

Fig.5.15. Voiding propagation, channel configuration (France)

TABLE 5.8. BN-800 UTOP-ULOF (base case) RESULTS AT CLAD MOTION ONSET

| | SAS-4A | | GRIF-SM-CANDLE |
|---|---------|--------|----------------|
| | FZK (1) | IPSN | IPPE |
| Clad motion onset (s) | 13.2 | 12.51 | 15.85 |
| Time interval between clad motion and boiling onset (s) | 2.09 | 2.26 | 5.11 |
| Relative power | 1.37 | 1.99 | 1.14 |
| Net reactivity (\$) | 0.108 | 0.34 | - 0.31 |
| Doppler (\$) | -0.267 | - 0.27 | |
| Fuel axial expansion (\$) | -0.341 | - 0.33 | |
| Clad axial expansion (\$) | 0.052 | 0.06 | |
| Sodium (\$) | -0.334 | - 0.10 | - 0.72 |
| External reactivity (\$) | 0.998 | 0.98 | 1.14 |

(1) updated EOEC - conditions

Steel blockage

In the SAS-4A calculation performed by IPSN, upper steel blockages in the upper pin plugs zone are predicted to occur 3.50 s after first boiling onset. Thus the limit of applicability of the SAS-4A code is reached. It is to be noticed that, at the end of the calculation, the net reactivity ramp rate reaches 2.2 \$/s, the net reactivity reaches 0.43 \$ and the relative power 2.29. This means that very rapidly fuel pin break-up is expected to occur.

GRIF-SM-CANDLE calculation indicated also a significant clad relocation in the upper part of the core.

Fuel pin break-up

In the SAS-4A calculation performed by FZK, fuel pin break-up occurs (table 5.9) and is followed by fuel dispersal. Nevertheless, the increase of the void reactivity and of the steel reactivity only allow a significant decrease of the net reactivity and of the power 55 ms after the first fuel pin break-up time. It is to be noticed that fuel pin break-ups are calculated to occur in 16 channels.

The main results at the end of the calculations are compared in table 5.10. Figure 5.16 shows the voiding pattern calculated using the SAS-4A code by IPSN and figure 5.17 clearly indicates the status of the core as calculated by FZK using the SAS-4A code.

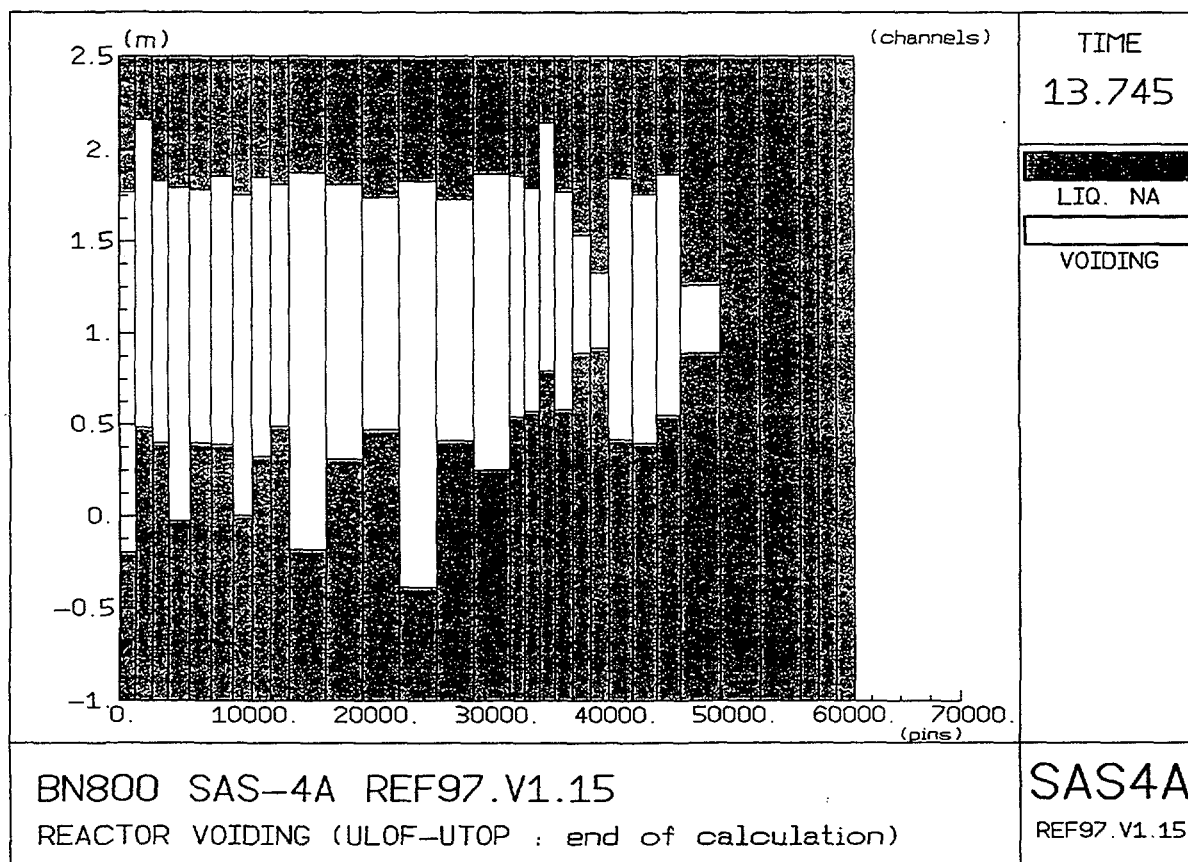
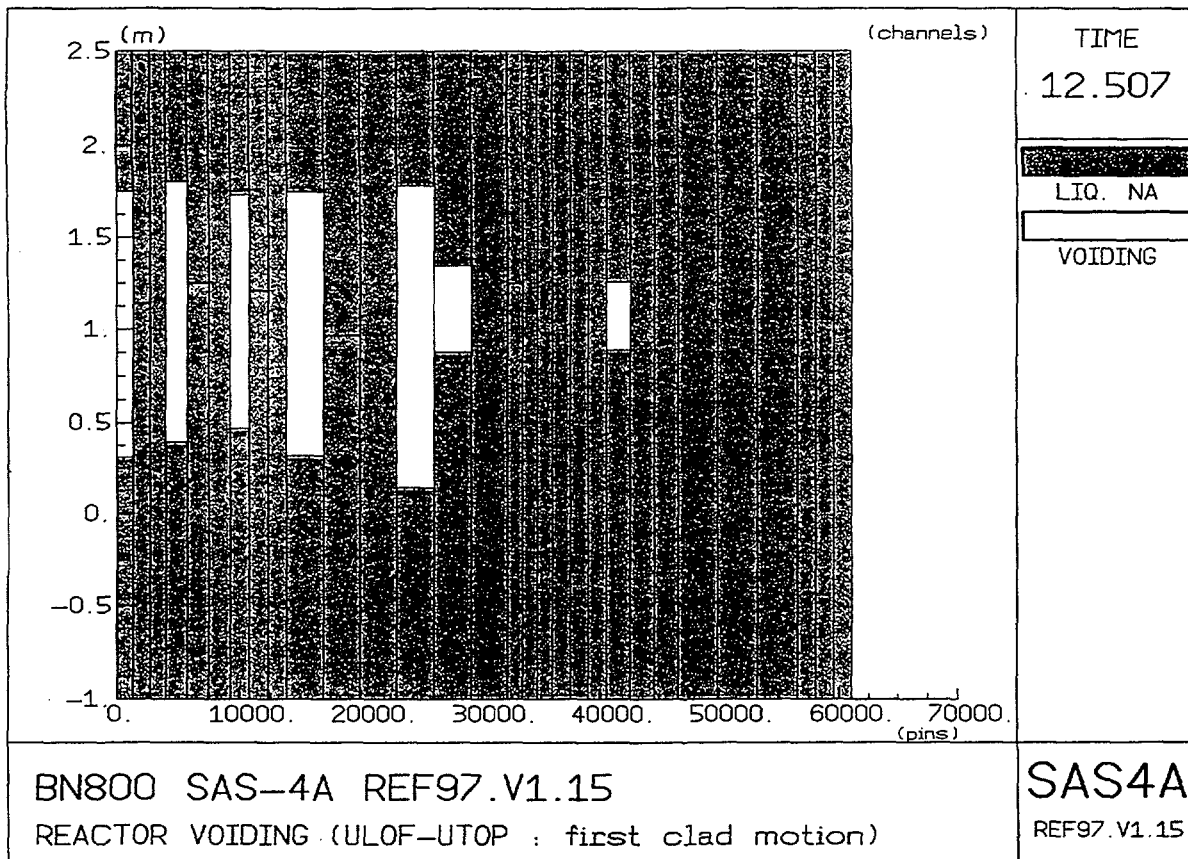


Fig.5.16. UTOP/ULOF, voiding. Core configuration (France)

TABLE 5.9. BN-800 UTOP-ULOF RESULTS AT FAILURE TIME

| | SAS-4A | |
|--|---------------------|-----------|
| | IPSN | FZK (1) |
| | Parametric case (2) | Base case |
| Failure time (s) | 14.322 | 15.12 |
| Time interval between failure time and boiling onset (s) | 4.072 | 4.014 |
| Relative power | 13.1 | 30.84 |
| Net reactivity (\$) | 0.877 | 0.95 |
| Doppler (\$) | - 0.42 | -0.44 |
| Fuel axial expansion (\$) | - 0.48 - | -0.42 |
| Clad axial expansion (\$) | 0.12 | 0.09 |
| Sodium (\$) | 0.59 | 0.20 |
| Fuel motion (\$) | 0. | 0. |
| Clad motion (\$) | 0. | 0.43 |
| External reactivity (\$) | 1.07 | 1.05 |

TABLE 5.10. BN-800 UTOP-ULOF RESULTS AT THE END OF THE CALCULATION

| | SAS-4A | | | GRIF-SM-CANDLE |
|--|----------------------------|---------------------------|-------------------------|----------------|
| | IPSN | FZK (1) | IPPE | |
| | PARAMETRIC CASE (2) | BASE CASE | | |
| End of calculation (s) | 14.946 (hexcan melting) | 13.74 (steel blockage) | 15.22 (coding error) | 20.64 |
| Time interval between end of calculation and boiling onset (s) | 4.696 | 3.50 | 4.11 | 9.9 |
| Relative power | 0.30 | 2.29 | 3.34 | 1.65 |
| Net reactivity (\$) | - 7.09 | 0.43 | 0.27 | 0.21 |
| Doppler (\$) | - 0.53 | - 0.31 | -0.53 | - 0.40 |
| Fuel axial expansion (\$) | - 0.74 | - 0.39 | -0.81 | |
| Clad axial expansion (\$) | 0.15 | 0.09 | 0.11 | |
| Sodium (\$) | - 0.41 | - 0.60 | 0.668 | - 0.68 |
| Fuel motion (\$) | - 9.33 | | -1.26 | 0. |
| Clad motion (\$) | 2.67 | 0.60 | +1.0 | 0.08 |
| External reactivity (\$) | 1.10 | 1.04 | 1.10 | 1.38 |

(1) updated EOEC - conditions

(2) without clad motion prior to fuel pin break-up

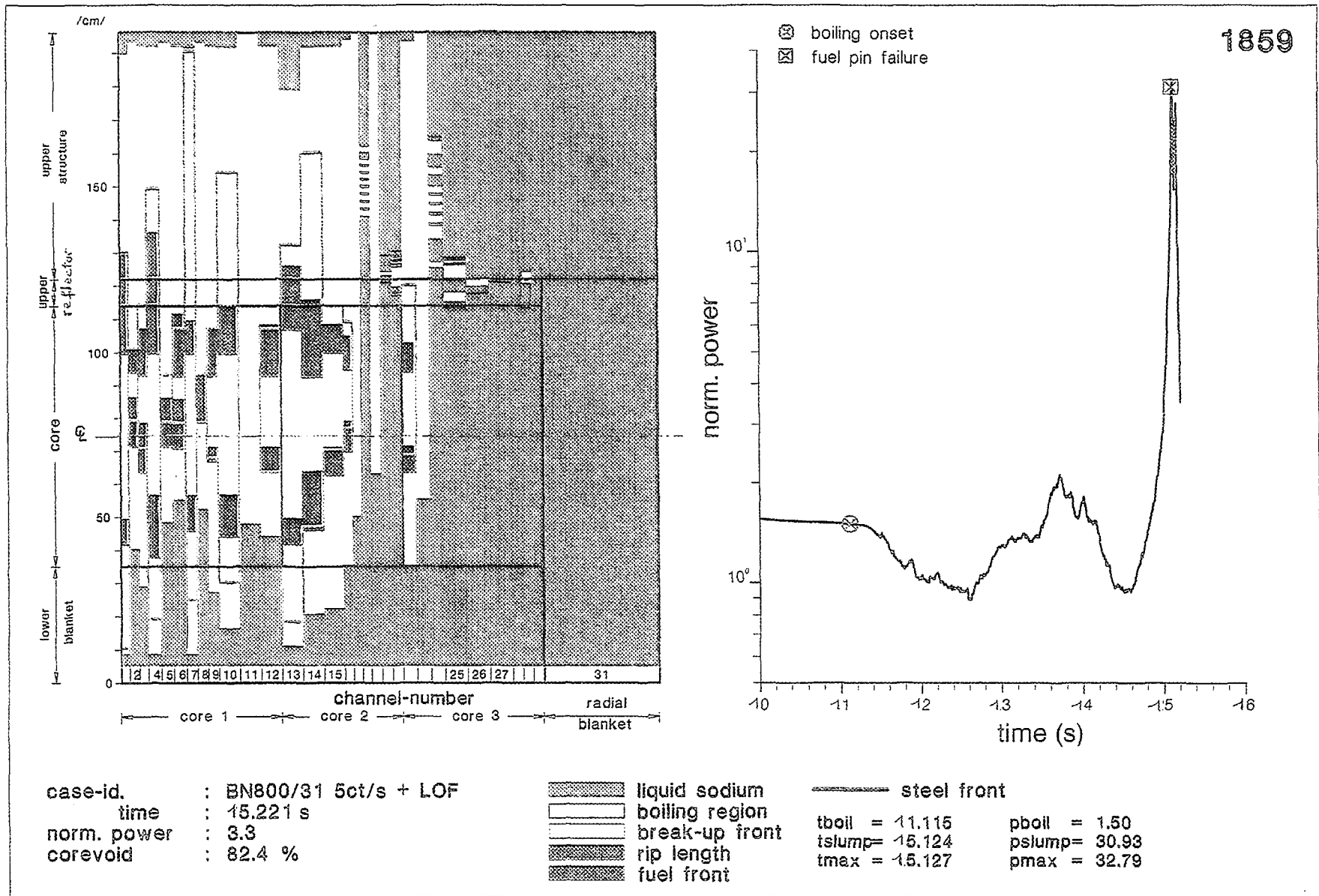


Fig.5.17. ULOF/UTOP. Core configuration (Germany)

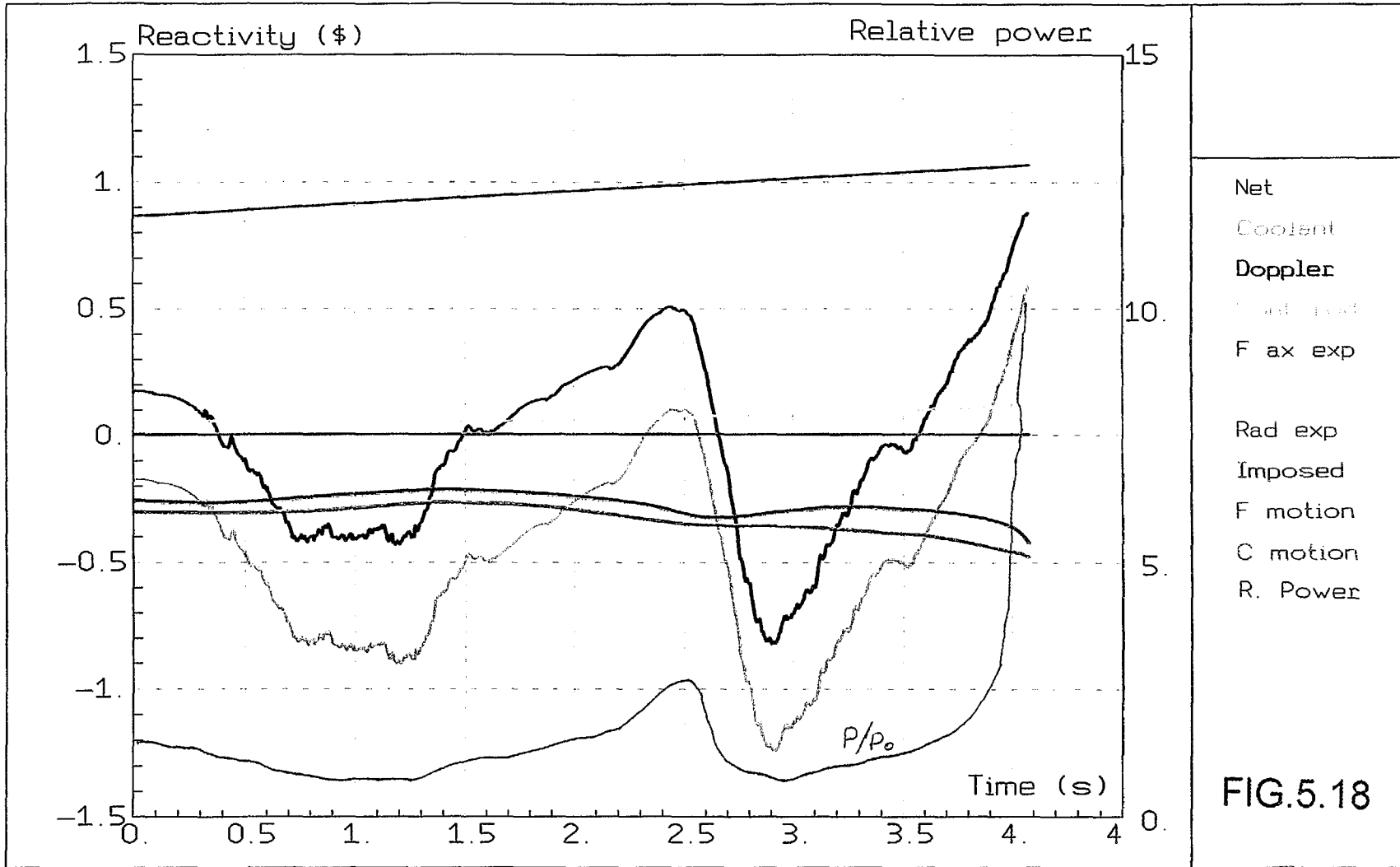
Parametric calculation

In order to avoid the limitation of the SAS-4A code due to steel blockage and to try to get some results at the end of the accident scenario, IPSN performed a parametric calculation switching off the clad motion calculation. A more extended sodium voiding is calculated (30 channels) leading to a large sodium voiding reactivity increase and thus net reactivity increase and power increase (figure 5.18). First fuel melting is reached in channel 5/1, 13.89 s after accident initiation. First fuel pin break-up occurs in channel 5/1 at 14.32 s (4.07 s after the first boiling onset). At that time, the relative power reaches 13.1 (table 5.9).

Extended fuel pin break-ups occur mainly at core mid-plane in 22 channels. During the first 30 ms after the first fuel pin break-up, reactivity increases mainly due to steel relocation effect and thus a power peak of 230 times nominal is triggered (figure 5.19). Later, extended fuel dispersal out of the core leads the reactivity decrease and thus shuts down the reactor. Hexcan melting is predicted to occur in channel 5/1 at 14.95 s (4.8 s after first boiling onset). At that time, the relative power is 0.3 and the limit of applicability of the one dimensional material relocation modelling of the SAS-4A code is reached. The main results at the end of the calculation are compared with the results of the other calculations in table 5.10.

On basis of all the UTOP-ULOF calculations performed by all the participants to this exercise, it can be concluded that :

- a clear scenario of the accident can be found in all the calculations (appendix 5.3) : negative reactivity feedback of the BN-800 type core are not enough efficient to prevent in case of a UTOP-ULOF accident, the increase of the power which leads to sodium boiling in the upper sodium layer in all the calculations,
- the limitation of the modelling in the PINCHTRAN code avoids the downward voiding extension towards core mid-plane where sodium voiding reactivity feedback is positive and the calculation of the end of the accident sequence ; modelling improvements of the PINCHTRAN code are needed,
- the limitation of the modelling in the GRIF-SM-CANDLE code underestimates significantly the downward voiding extension towards core mid-plane ; modelling improvements of the GRIF-SM-CANDLE code are also needed, especially with regard to heat transfer coefficients between fuel and clad and between clad and sodium as well as clad rewetting after boiling onset,
- the SAS-4A calculations clearly show the propagation of radial voiding in the upper sodium layer and indicate that downwards voiding cannot be avoided ; this leads to net reactivity and thus to power oscillations ; increase of inlet plenum pressure due to core voiding pressurisation contributes also to sodium vapour condensation in some channels,
- the clad melting is predicted by the SAS-4A and GRIF-SM-CANDLE codes ; clad melting temperature has to be decreased in the GRIF-SM-CANDLE code,
- the steel relocation is calculated by the SAS-4A and GRIF-SM-CANDLE codes but this later code, due to an underestimation of the downward sodium voiding, predicts only an upward steel motion ; this steel relocation, enhanced in the SAS-4A code by further downward sodium voiding, lead to an increase of the net reactivity and of the power,



REACTIVITY

RELATIVE POWER

SAS4A

BN800 - boiling results prior to failure (ULOF-UTOP without clad motion)

REF97.V1.15

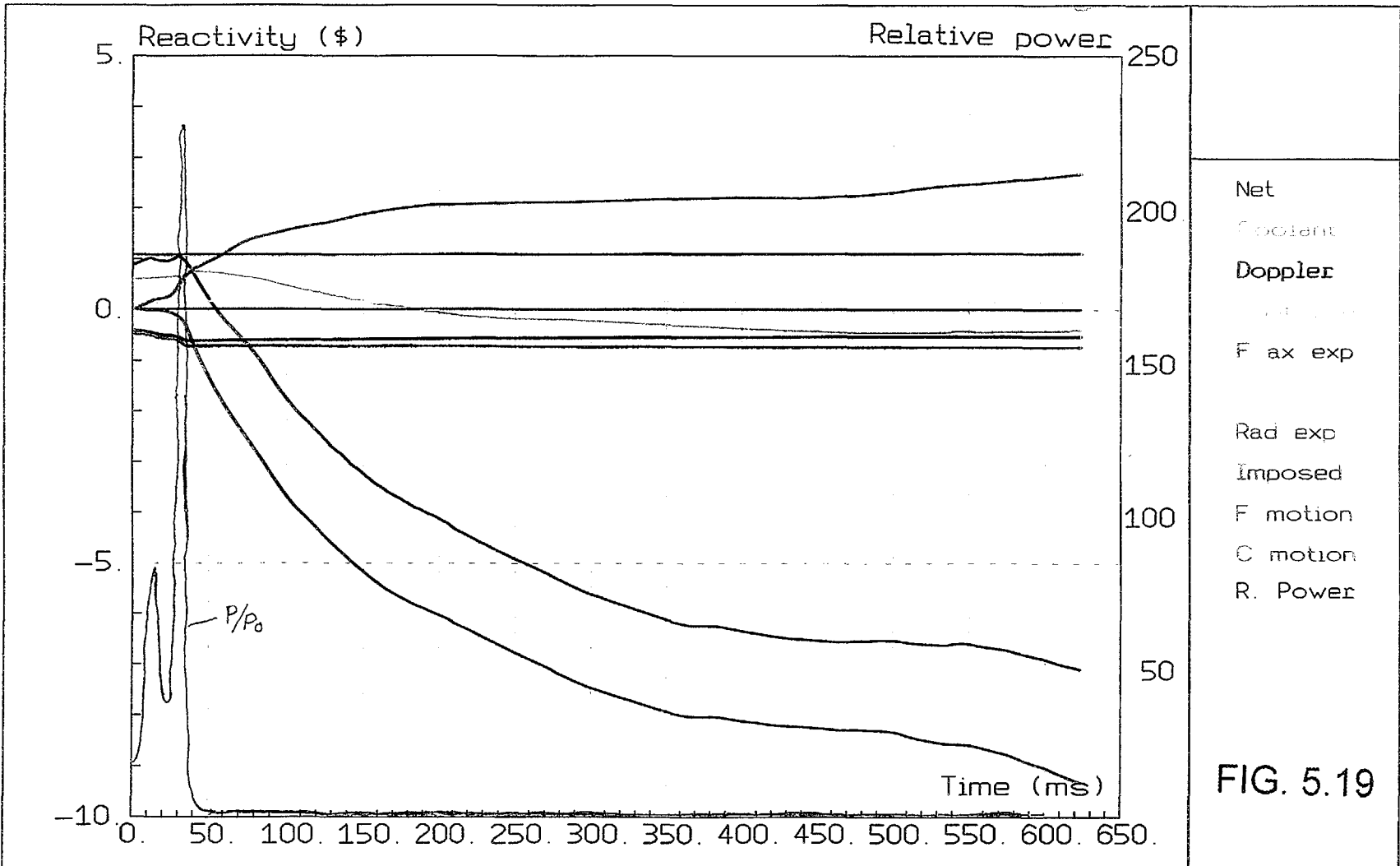


FIG. 5.19

REACTIVITY

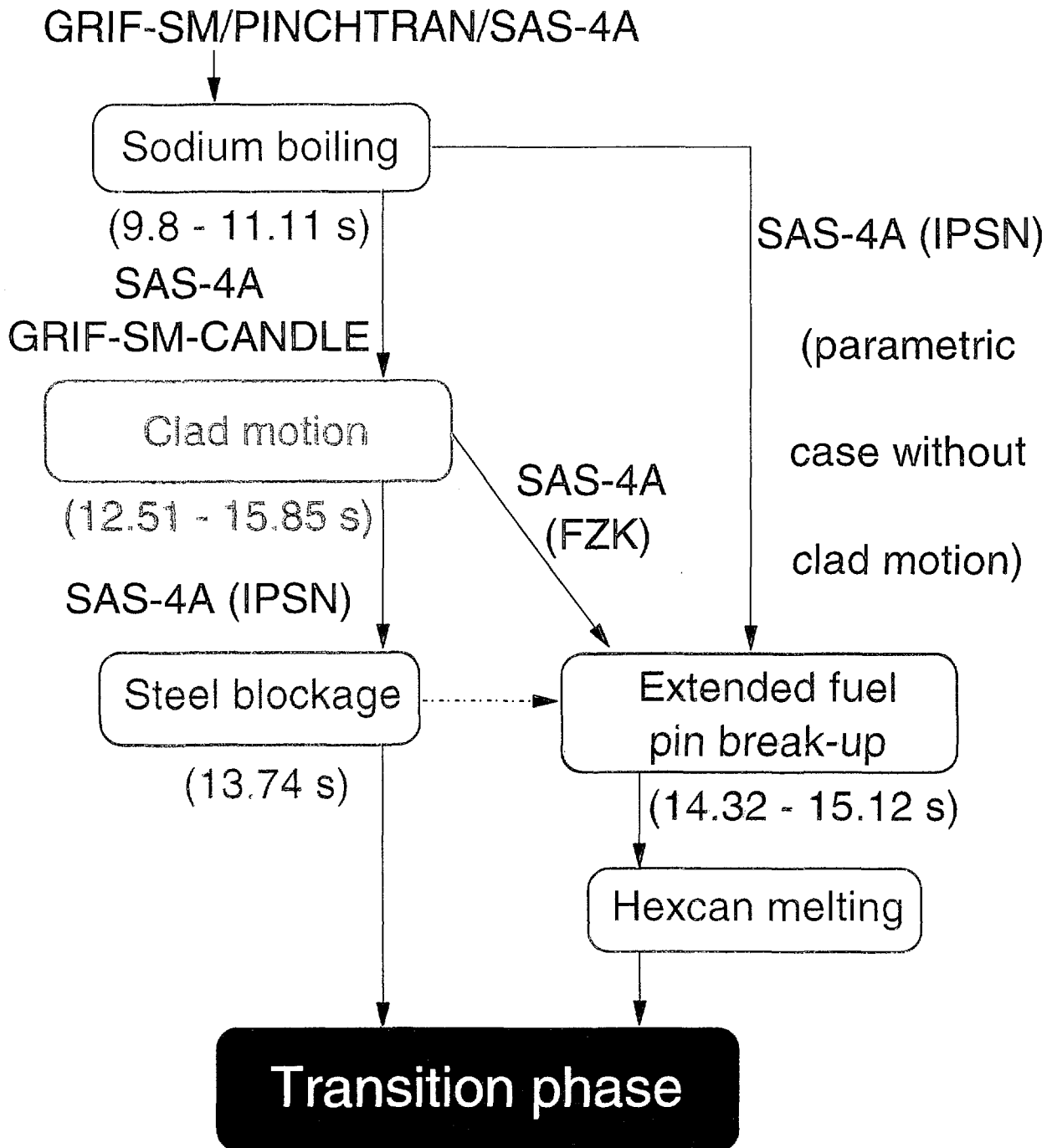
RELATIVE POWER

SAS4A

BN800 - postfailure results (ULOF-UTOP without clad motion)

REF97.V1.15

ACCIDENT SCENARIO



- the fuel melting is calculated ; modelling improvement of the GRIF-SM-CANDLE code after fuel melting is needed,
- in spite of steel blockage which is the limit of applicability of the SAS-4A code, extended fuel pin break-up is anticipated in the SAS-4A (IPSN) base case calculation and is calculated in the SAS-4A (FZK) calculation as well as in a parametric study performed by IPSN, which neglected the clad relocation ; in this later case, hexcan melting is calculated and thus the limit of applicability of the SAS-4A code is also reached,
- the integrity of a large part of the fuel pins and of the hexcans cannot be maintained.

5.6. CONCLUSIONS AND RECOMMENDATIONS

Different initiators (fast UTOP, slow UTOP, UTOP-ULOF) which are postulated in the BN-800 type reactor HCDA were investigated using the SAS-4A code by IPSN and FZK, the GRIF-SM-CANDLE code by IPPE and the PINCHTRAN code by IGCAR.

The fast reactivity ramp rate (0.5 \$/s) accident initiator leads to sodium boiling in a large part of the core. Then mechanical clad failures are calculated to occur in the high power group of subassemblies in the time interval 3.3 s - 5.25 s after accident initiation. The subsequently calculated fuel axial relocation initiates a rapid shut-down of the reactor. Hexcan melting is calculated to occur in the same group of subassemblies less than half a second after mechanical clad failure. Partial blockage formation, hexcan melting, high fuel enthalpies and the heated-up coolant hardly allows long-term in-place coolability of the partially destroyed core configuration. A more or less rapid core melt-down is to be expected. The recriticality issue needs to be analysed carefully.

The slow reactivity ramp rate (0.05 \$/s) accident initiator leads to mechanical clad failures in one subassembly group. In one calculation, they are preceded by sodium boiling in limited high power group of subassemblies. Due to the slower reactivity ramp rate, the accident evolves slower than for the fast UTOP and mechanical clad failures are calculated to occur in the time interval 33.3 s - 41.1 s after accident initiation. The subsequent calculated fuel axial relocation initiates a rapid shut-down of the reactor. Hexcan melting is calculated to occur in the high power group of subassemblies about half a second after mechanical clad failure. Partial blockage formation, hexcan melting, high fuel enthalpies and the heated-up coolant hardly allows, as for the fast UTOP, long-term in-place coolability of the partially destroyed core configuration.

The UTOP-ULOF accident initiator, initiates coolant boiling first at the level of the upper sodium layer in the time interval 9.8 s - 11.11 s after accident initiation. Negative reactivity feedback due to the initial voiding of the upper sodium layer mitigates efficiently the positive reactivity feedback due to the beginning of the voiding of the core. The events sequence is almost similar but more rapid than the one calculated, using the same hypothesis, for the ULOF accident initiator [5.6, 5.14]. However, the power level stays higher due to the superimposed external reactivity ramp rate. Thus a very large propagation of the voiding radially as well as downwards towards the center of the core cannot be avoided. Clad melting and relocation towards the axial limits of the core are calculated. Steel blockages, and fuel melting are predicted. In the FZK base case as well as in the IPSN parametric case, fuel pin break-ups are calculated on a large extension of the core. In this latter case, due to the steel axial relocation, a significant power pulse is triggered but fuel relocation shuts down rapidly the reactor.

From the modelling point of view, in spite of a significant improvement of the GRIF-SM code which was coupled to the clad motion modelling CANDLER, extension of the modelling in the PINCHTRAN and GRIF-SM-CANDLER code are urgently needed in order to calculate as with the SAS-4A code the whole sequence of the primary excursion. This holds especially for a mechanistic modelling of mechanical clad failure and fuel pin break-up taking into account appropriately the mechanical properties of the involved cladding, as well as post-failure modelling.

From a neutronic point of view, at high temperature, it was shown that the Doppler effect is significantly lower and the fuel worth higher than the values used in these calculations. These effects are still to be studied.

The results of the calculations are strongly dependent on the reliability of the calculated failure time and more importantly of the failure location. It is strongly recommended to evaluate experimentally strain-rate and temperature dependencies of the mechanical properties of the irradiated BN-800 clad material up to dose values of 70 - 100 dpa NRT.

It is also obvious that the as calculated accidental scenarios need to be analysed beyond this study. The transition phase which is anticipated to follow these accidental scenarios must be assessed in details.

REFERENCES TO CHAPTER 5

- [5.1] IAEA/EC Benchmark Exercise : comparative calculations for a severe accident in the IPPE core design variant with a near zero void coefficient of the BN-800 type reactor - input data specifications - Obninsk, Russia (December 1994 and June 1995 Updating of the input specifications).
- [5.2] I.Burjevski, A.Chebeskov, A.Danilichev, G.Glinatsis, K.Kawashima, V.Stogov. Synthesis of neutronics calculation for the IPPE core design variant of the BN-800 type reactor with a near zero void reactivity coefficient.
- [5.3] D.Struwe, B.Porscha. Evaluation of steady state calculations of the fuel pin behaviour during power operation in a BN-800 like reactor core.
- [5.4] I. Chvetsov, I.Kuznetsov, A.Volkov. EC/IAEA comparative calculations - ULOF, UTOP and ULOF/UTOP accidents (preliminary results). 6th IAEA Consultancy meeting - 29 June - 2 July, 1997, Brussels.
- [5.5] I.Chvetsov, I.Kuznetsov, A.Volkov. Results of ULOF + UTOP accidents for BN-800 like reactor with a near zero void core design. 7th Consultancy meeting - 11-12 December 1997, Vienna.
- [5.6] J.M.Frizonnet, C.Rongier. IAEA/EC Comparative calculation for severe accident in BN-800 type reactor. SAS-4A calculations. 8th IAEA Consultancy meeting - 2-5 June, 1998, Obninsk.

- [5.7] D.Struwe, B.Porscha, W.Pfrang. Results of UTOP-analyses for a BN-800 like reactor with a near zero void worth core design (revision 3). 8th IAEA Consultancy meeting 2-5 June, 1998, Obninsk.
- [5.8] R. Harish and Om Pal Singh (UTOPs calculations). Analysis of unprotected transient overpower and loss of flow accidents in BN-800 like reactor. 6th IAEA Consultancy meeting 30 June-3 July 1997, Brussels.
- [5.9] R.Harish and Om Pal Singh (UTOP/ULOF calculations). Analysis of unprotected transient overpower and loss of flow accidents in BN-800 like reactor. 7th IAEA Consultancy meeting 11-12 December 1997, Vienna.
- [5.10] The SAS-4A LMFBR accident analysis code system. ANL Report.
- [5.11] I.Chvetsov, I.Kuznetsov and A.Volkov. GRIF-SM - The computer code for the analysis of the severe beyond design basis accidents in sodium cooled reactors. Proc. Int. Top. meeting on sodium cooled fast reactor safety, Obninsk, Russia, Oct. 3-7, 1994.
- [5.12] Om Pal Singh, P.B.Rao and R.S.Singh. Accident analysis work at Indira Gandhi Center for Atomic Research and some interesting results for a small and medium size fast reactor. Symposium on science and technology of fast reactor safety, BNES, London 1986.
- [5.13] B. Porscha, D. Struwe. Evaluation of the BN-800 clad material properties. 7th IAEA Consultancy meeting 11-12 December 1997, Vienna.
- [5.14] D. Struwe, B. Porscha, W. Pfrang. Results of ULOF-analyses for a BN-800 like reactor with a near zero void worth core design (revision 3). 8th IAEA Consultancy meeting 2-5 June, 1998, Obninsk.

Chapter 6

PHYSICS PARAMETERS OF PARTIALLY DESTROYED CORE CONFIGURATION

6.1. CALCULATION MODEL AND ANALYSIS METHODS

In the process of the core destruction accompanied by boiling out of considerable amount of sodium and relocation of molten materials, reactor neutronics changes take place. This is the basis for the use of combined analysis of dynamics of the core neutronic and thermohydraulic conditions. Such combined analysis is quite tedious. In this connection, decomposition methods assuming neutronics analysis for several core conditions are widely used. This approach being clearly evident makes it possible to easily identify factors having maximum effect on the process dynamics. It is assumed that detailed analysis should be made for all neutronic processes on each considered specific stage of the accident. Obviously the choice of specific states of the core between which reactivity coefficients can be assumed constant or approximated by some simple relationships, is the main problem.

The comparison of reactivity effects will be carried out for two conditions of the BN-800 reactor: initial state and final condition in accident with reactor heated up, sodium removed from the core and steel relocated to the top and the bottom of the core. For neutronic analysis the reactor calculational model in R,Z-geometry was prepared. The calculation model is given in Fig. 6.1. The consecutive transition to the final condition is carried out on the following stages:

- heating up of the core from 1500°K up to 2100°K;
- boiling out of sodium from LEZ and MEZ SAs (inter-wrapper sodium and sodium in the control rods channels remains in liquid phase);
- melting of pin clad, removal of steel from the core (SA wrapper is kept intact);
- formation within SA wrapper «plugs» of molten steel at the top and the bottom of the core.

For possible interpolations of total changing of reactivity of material intermediate stages of the core perturbation were also considered:

- 25,50 and 75% of sodium removed from the core (LEZ+MEZ+HEZ+pin plugs+sodium plenum);
- 25,50 and 75% of steel removed (LEZ+MEZ+HEZ);
- 50% of steel and sodium removed (LEZ+MEZ+HEZ).

Preliminarily approved assumptions were used for the development of the calculation model. It was assumed for the final state that only sodium vapours are present within the core (100-80% of the coolant volume according to Fig.6.1. data) at 1300°C in LEZ and MEZ and at 800°C in HEZ. Vapour density values of 0.03443 and 0.04233 g/cm³ were assumed taking into account presence of sodium residues (0-20%) making homogeneous mixture at ~1150°C. Inter-wrapper sodium temperature was kept below 900°K. Fuel temperature was ~2200°K. There were no changes of the fuel phase condition. Steel plugs on the upper and lower core boundaries were rather thick, blocking the total cross section area of the SA. Molten steel of the fuel element claddings were redistributed within the core volume as follows: 25% and 75% of steel is located respectively at the level of fuel element ends and on the core/lower blanket boundary, with 50 mm steel melt penetration to the lower blanket. Configuration and the main input parameters of the reactor, core composition and nuclide contents in different physical zones are given in the homogeneous representation in [1.1, 1.2]. In order to have the

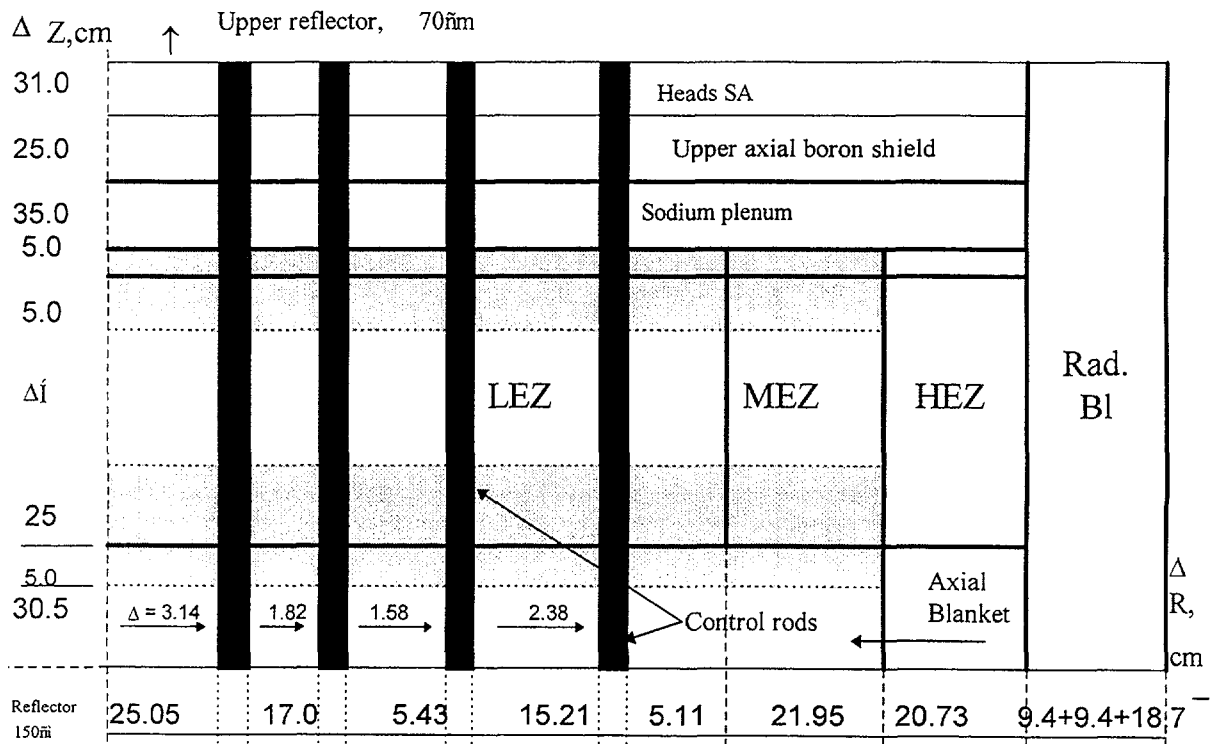
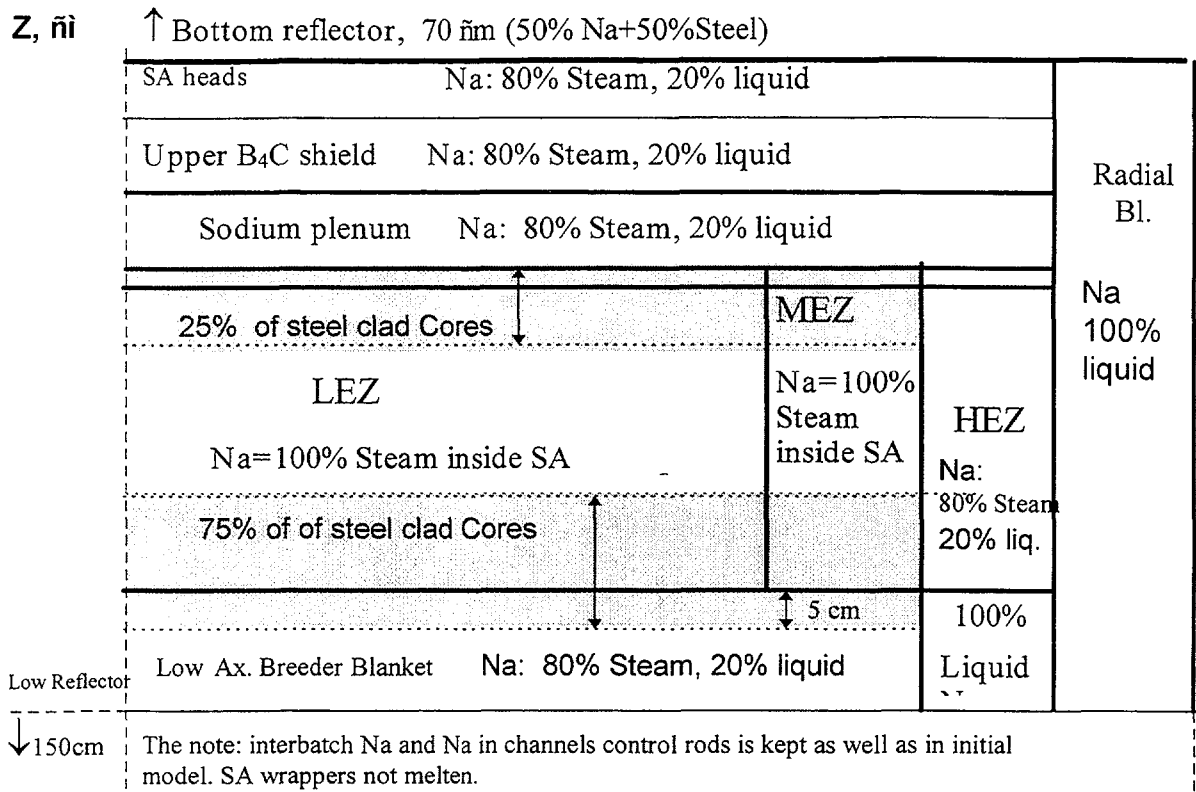


FIG. 6.1. R, Z-model of the reactor with partial destruction of the core.

possibility for approval of the calculation results presented below contents of the main nuclides steel and sodium are given in the Table 6.1-6.3 for the disturbed condition. Fuel:

Core thermal expansion is taken into account.

$$RO = RO_0(H_{hot}/H_{cold}) = RO_0 \cdot 86.7/86.1 = 0.99308 RO_0 \text{ for the core.}$$

In LAB and RB concentration change caused by thermal expansion is not taken into account. All fission products are assumed to be kept within the fuel.

The following values of thermal expansion coefficients were used:

$$\alpha_{fuel} = 11 \cdot 10^{-6} \text{ 1/}^\circ\text{C}, \quad \alpha_{steel} = 18 \cdot 10^{-6} \text{ 1/}^\circ\text{C}, \quad \beta_{Na} \approx 0.0002783 \text{ 1/}^\circ\text{C}$$

TABLE 6.1. TEMPERATURES AND DENSITIES OF MATERIALS IN ZONES ACCORDING TO FIG 6.1.

| Zones | T _{fuel} | T _{steel} | T _{Na} | ρ _{steel} | ρ _{Na liquid} | ρ _{Na vapour} |
|----------------------------|-------------------|--------------------|-----------------|--------------------|------------------------|------------------------|
| LAB | 1150 | 1150 | 1150 | 7.55 | 0.7427 | 0.04233 |
| LEZ | 2200 | 1500 | 1300 | 7.55 | 0 | 0.03443 |
| LEZ + «steel-plugs» | 2200 | 1500 | 800 | 7.55 | 0 | 0 |
| Sodium plenum | - | 1150 | 1150 | 7.55 | 0.7427 | 0.04233 |
| B ₄ C reflector | - | 1150 | 1150 | 7.55 | 0.7427 | 0.04233 |
| SA heads | - | 1150 | 1150 | 7.55 | 0.7427 | 0.04233 |
| LAB _{HEZ} | 1150 | 750 | 700 | 7.55 | 0.92 | 0 |
| HEZ | 1800 | 800 | 800 | 7.55 | 0.825 | 0.04233 |
| RB | 900 | 750 | 750 | 7.55 | 0.825 | 0 |
| Fuel element ends | - | 1500 | - | 7.55 | 0 | 0 |

Note: [ρ] = g/cm³; [T] = °C. 900°C inter wrapper sodium temperature and 1500°K SA wrapper temperature at 7.55 g/cm³ steel density were assumed for the analysis (for the initial option steel density of 7.67 g/cm³ was taken at 600°C).

TABLE 6.2. MATERIAL CONCENTRATION VALUES FOR DISTURBED CORE REGIONS

| Steel (7.67 g/cm ³ initial density) | Wrapper (initial) | «Steel-plugs» | Fuel element ends | Inside SA (initial) |
|--|-------------------|-----------------------|-----------------------|---------------------|
| ε _{steel} | | 0.4155 (inside SA) | 0.8067 (inside SA) | |
| FE | 5.99e-3 | 0.026644 | 0.046091 | 6.85e-3 |
| CR | 1.03e-3 | 0.006457 | 0.011567 | 1.80e-3 |
| NI | 1.7e-5 | 0.004518 | 0.00874 | 1.493e-3 |
| MO | 6.50e-5 | 0.0006168 | 0.0011363 | 1.83e-4 |
| NB | 1.9e-5 | 0.0001517 | 0.0002766 | 4.40e-5 |
| Steel (7.55 g/cm ³ density) | Wrapper (initial) | «Steel-plugs» | Fuel element ends | Inside SA (initial) |
| ε | | 0.4155 (inside SA) | 0.8067 (inside SA) | |
| FE | 5.8963e-3 | 0.02623 | 0.04537 | 6.743e-3 |
| CR | 1.0139e-3 | 0.006356 | 0.01138 | 1.772e-3 |
| NI | 1.6734e-5 | 0.004447 | 0.008603 | 1.47e-3 |
| MO | 6.398e-5 | 0.0006071 | 0.001118 | 1.801e-4 |
| NB | 1.87e-5 | 0.0001494 | 0.0002733 | 4.331e-5 |

Note: Steel concentration in radial blanket and radial reflector was taken the same as in the initial option.

TABLE 6.3. SODIUM CONCENTRATIONS

| Zone | Interbath sodium | LEZ | MEZ | HEZ | Sodium plenum | Ax.Blanket LEZ and MEZ | Ax.Blanket HEZ |
|---|------------------|------------|------------|-----------|---------------|------------------------|----------------|
| $\gamma, \text{g/cm}^3$ | 0.8575 | 0.03443 | 0.04233 | 0.04233 | 0.04233 | 0.04233 | 0.8575 |
| Condition | liquid | 100% steam | 100% steam | 80% steam | 80% steam | 0.002714 | |
| $\text{RO} \cdot 10^{22}, \text{nucl/cm}^3$ | 0.2402 | 0.2656 | 0.2714 | 0.3868 | 0.5135 | 0.2714 | 0.863 |

Note: Sodium density value of 0.8575 g/cm^3 was assumed for the initial case, the same value being taken for inter wrapper sodium (for the inter wrapper gap: $\text{RO}_{\text{Na}} = 0.002402 \cdot 10^{24} \text{ nuclei/cm}^3$).

| | |
|--------------------------------|--|
| UAB | $\text{RO} = 0.00342 \cdot 10^{24}, \text{nucl/cm}^3$ |
| «Steel-plugs» | $\text{RO} = 0.002402 \cdot 10^{24}, \text{nucl/cm}^3$ |
| RB | $\text{RO} = 0.005214 \cdot 10^{24}, \text{nucl/cm}^3$ |
| Fuel element ends (outside SA) | $\text{RO} = 0.02402 \cdot 10^{24}, \text{nucl/cm}^3$ |
| SA heads | $\text{RO} = 0.003893 \cdot 10^{24}, \text{nucl/cm}^3$ |

Diffusion method in a standard 26 group approximation was used for the initial condition when calculating reactivity coefficients. Space distribution of the reactivity coefficients were obtained using first order disturbance theory (their integral values were normalised to the relative direct calculation results). This methodology is justified by both quite acceptable accuracy of diffusion calculation and comparability to the similar results obtained by the time of design licensing. Disturbed core condition under consideration is characterised by rather strong perturbations, such as sodium dry-out, removal of fuel element cladding steel, etc.) For these conditions diffusion approximation may have considerable error. In this connection, results presented below realise the following approximations:

RHEIN (26 groups diffusion theory, R-Z, homogeneous media, Fig. 6.2),

TWODANT (26 groups transport theory, R-Z, homogeneous media, Fig1.1)

Comparison of kinetic (TWODANT) and diffusion (RHEIN) approximation in calculation of temperature reactivity coefficient components was made within the framework of the code package developed for evaluation of required functionals using disturbance theory. Flux and worth functions values calculated by TWODANT code and integrated with respect to angle were transferred to the unit of reactivity coefficient evaluation using disturbance theory in the standard diffusion code.

MCNP (Monte-Carlo, GEZ-Z, heterogeneous media)

Heterogeneous representation of the wrapper, fuel elements and claddings is given for all axial sections of the SA (see Fig.6.3). DLC-105(6) data base (see Table 6.4) was used for the analysis made using MCNP4A code. About two million stories were played in the calculations made on the basis of MCNP4A code.

Three main directions were taken for studies:

- estimation of reactivity effects and change of reactivity of materials using traditional (diffusion) methods;
- definition of possible error of diffusion approach;
- studies on acceptability of transfer of material worths obtained for the initial reactor condition to the disturbed condition.

6.2. INTEGRAL REACTIVITY EFFECTS

The main integral neutronic characteristics of both initial and final reactor states are presented in Table 6.5 (diffusion approximation).

Preliminary evaluations of K_{eff} changes were made for transition phase which is between initial core state and different damage phases at different neutron spectrum temperatures (see Tables 6.6). Reactivity change obtained by different evaluation methods is given in Table 6.7.

Further calculations of different core destruction phases were made for 2100°K temperature of the neutron spectrum, which is one of the reference temperatures in the BNAB nuclear data base taken for Doppler effect calculation. Adoption of higher nuclide

dZ

| | | | | | | | | | | | | | | | |
|------|----|----|----|----|----|----|----|----|----|----|----|----|----|----|----|
| | 15 | 15 | 15 | 15 | 15 | 15 | 15 | 15 | 15 | 15 | 15 | 15 | 15 | 15 | 15 |
| | 13 | 9 | 13 | 9 | 13 | 9 | 13 | 9 | 13 | 13 | 13 | 13 | 13 | 13 | 15 |
| 25.1 | 4 | 9 | 4 | 9 | 4 | 9 | 4 | 9 | 4 | 4 | 4 | 4 | 14 | 8 | 15 |
| 5.0 | 19 | 9 | 19 | 9 | 19 | 9 | 19 | 9 | 19 | 20 | 21 | 4 | 14 | 8 | 15 |
| 25.0 | 17 | 9 | 17 | 9 | 17 | 9 | 17 | 9 | 17 | 18 | 3 | 5 | 14 | 8 | 15 |
| | 1 | 9 | 1 | 9 | 1 | 9 | 1 | 9 | 1 | 2 | 3 | 5 | 14 | 8 | 15 |
| ↑ | 1 | 9 | 1 | 9 | 1 | 9 | 1 | 9 | 1 | 2 | 3 | 5 | 14 | 8 | 15 |
| 5.67 | 1 | 9 | 1 | 9 | 1 | 9 | 1 | 9 | 1 | 2 | 3 | 5 | 14 | 8 | 15 |
| ↓ | 1 | 9 | 1 | 9 | 1 | 9 | 1 | 9 | 1 | 2 | 3 | 5 | 14 | 8 | 15 |
| | 1 | 9 | 1 | 9 | 1 | 9 | 1 | 9 | 1 | 2 | 3 | 5 | 14 | 8 | 15 |
| | 1 | 9 | 1 | 9 | 1 | 9 | 1 | 9 | 1 | 2 | 3 | 5 | 14 | 8 | 15 |
| | 1 | 9 | 1 | 9 | 1 | 9 | 1 | 9 | 1 | 2 | 3 | 5 | 14 | 8 | 15 |
| | 1 | 9 | 1 | 9 | 1 | 9 | 1 | 9 | 1 | 2 | 3 | 5 | 14 | 8 | 15 |
| | 1 | 9 | 1 | 9 | 1 | 9 | 1 | 9 | 1 | 2 | 3 | 5 | 14 | 8 | 15 |
| | 1 | 9 | 1 | 9 | 1 | 9 | 1 | 9 | 1 | 2 | 3 | 5 | 14 | 8 | 15 |
| 5.0 | 17 | 9 | 17 | 9 | 17 | 9 | 17 | 9 | 17 | 18 | 3 | 5 | 14 | 8 | 15 |
| 5.0 | 22 | 11 | 22 | 12 | 22 | 12 | 22 | 11 | 22 | 22 | 10 | 5 | 14 | 8 | 15 |
| 35.0 | 6 | 11 | 6 | 12 | 6 | 12 | 6 | 11 | 6 | 6 | 6 | 5 | 14 | 8 | 15 |
| 25.0 | 7 | 11 | 7 | 12 | 7 | 12 | 7 | 11 | 7 | 7 | 7 | 5 | 14 | 8 | 15 |
| 31.0 | 16 | 11 | 16 | 12 | 16 | 12 | 16 | 11 | 16 | 16 | 16 | 16 | 16 | 16 | 15 |
| 70.0 | 15 | 15 | 15 | 15 | 15 | 15 | 15 | 15 | 15 | 15 | 15 | 15 | 15 | 15 | 15 |

DR

↓

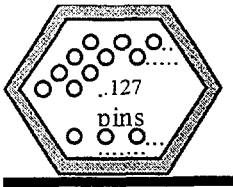
DR=26.05 3.14 17.0 1.82 5.43 1.58 15.21 2.38 5.11 21.95 20.73 9.44 9.40 18.7 70.

Number of isotopes 17, number of physical zones 21.

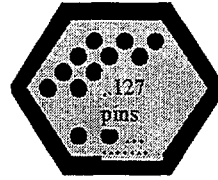
$H_{core}=86.7$ cm - 2200°K ($H_{core}=86.1$ cm T=1500°K)

Zone 1 - LEZ, Zone 2 - MEZ, Zone 3 - HEZ, Zone 4 - axial blanket, Zone 5 - radial blanket, Zone 6+7 - Sodium plenum, Zone 22 - pin plugs, Zone 17,19 - steel-«plugs».

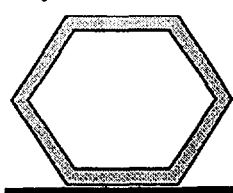
FIG. 6.2. Calculation diagram of the reactor in R,Z geometry (upwards) for the code RHEIN (diffusion approach)



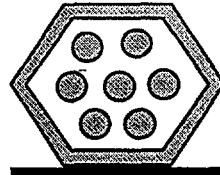
MOX fuel, depleted uranium dioxide and gas plenum SA section. Heterogeneous patterns of SA wrapper, fuel elements (gas plenums) and claddings are represented. Lower axial blanket and fuel element ends are represented in a similar way



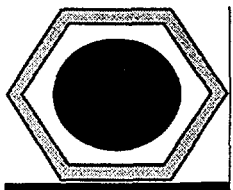
Plugs formed from cladding steel melt in SA. Heterogeneous patterns of SA wrapper, fuel elements and cladding are represented



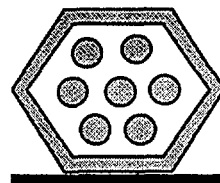
Sodium plenum section of SA. Heterogeneous patterns of SA wrappers are represented



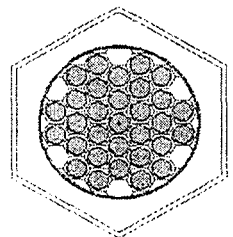
Subassembly of the inner row of steel shielding. Subassembly of radial boron shielding. Wrapper and steel elements are separated.



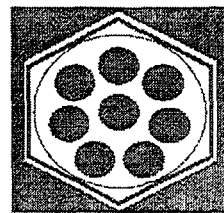
Subassembly of the second row of steel shielding. Wrapper and steel rod are separated



Control rod subassembly. Heterogeneous patterns of SA wrapper, control rod sleeve, absorber elements and fuel element claddings are given



Safety rod subassembly. Heterogeneous representation of SA wrapper, control rod sleeve, absorber rods and their claddings is given



Shim rod subassembly. Heterogeneous representation of SA wrapper, control rod sleeve, absorber rods and their claddings is given

Inter wrapper sodium is separated in all SA. Homogeneous description is used for the rest of reactor areas

FIG. 6.3. Heterogeneous SA representation for the Monte-Carlo calculations (MCNP code).

temperatures for calculations means going beyond the framework of standard data base BNAB, and this may result in significant errors in Doppler broadenings extrapolation. In this connection, forced limitation of the neutron spectrum temperature ($\leq 2100^\circ\text{K}$) was introduced in the standard computer codes used for these calculations.

Additional analysis was made on the effect of thickness and density of «steel plugs» formed in the upper and lower core sections on the system reactivity (Table 6.8 and Fig.6.4).

In order to make interpolation of the final changes of material related reactivity additional intermediate stages were introduced in the main chosen core disturbance options: (a) removal of 50% of sodium, (b) removal of 50% of steel, and (c) removal of both 50% of steel and 50% of sodium (Table 6.9-6.11). Criticality change caused by such sequential change of concentrations when removing material from the core is presented in Fig.6.5.

TABLE 6.4. CROSS SECTION REFERENCE (MCNP).

| Nuclides | Name in catalogue | Date | File | Source |
|-------------------|-------------------|----------|--------|-----------|
| B ¹⁰ | 5010.50c | 79/09/10 | rmccs | endf/b-v |
| B ¹¹ | 5011.55c | 30781 | rmccs | endf/b-v |
| C | 6000.50c | 79/07/31 | rmccs | endf/b-v |
| O | 8016.50c | 05/14/81 | rmccs | endf/b-v |
| Na | 11023.50c | 79/06/21 | endf5p | endf/b-v |
| Cr | 24000.50c | 79/06/21 | rmccs | endf/b-v |
| Mg | 25055.50c | 79/06/21 | endf5u | endf/b-v |
| Fe | 26000.55c | 10/21/82 | rmccs | group t-2 |
| Ni | 28000.50c | 79/06/21 | rmccs | endf/b-v |
| Nb | 41093.50c | 79/08/02 | endf5p | endf/b-v |
| Mo | 42000.50c | 79/08/01 | endf5u | endf/b-v |
| Îñîñîñîñ | 50120.35c | | rmccs | endl-85 |
| U ²³⁵ | 92235.50c | 79/09/12 | rmccs | endf/b-v |
| U ²³⁸ | 92238.50c | 79/09/13 | rmccs | endf/b-v |
| Pu ²³⁹ | 94239.55c | 02/21/85 | rmccs | group t-2 |
| Pu ²⁴⁰ | 94240.50c | 79/09/13 | rmccs | endf/b-v |
| Pu ²⁴¹ | 94241.50c | 79/08/30 | endf5p | endf/b-v |
| Pu ²⁴² | 94242.50c | 79/09/06 | endf5p | endf/b-v |

TABLE 6.5. BASIC NEUTRONIC CHARACTERISTICS OF BN-800 TYPE REACTOR

| | Initial condition | Final condition |
|---|-------------------|-----------------|
| K _{eff} | 1.0066007 | 1.0238916 |
| Reactivity, (% ΔK/K) | - | 2.3751 |
| Reactivity of materials in the CORE | | |
| - Fuel | 0.3957 | 0.4095 |
| - Sodium (for 10 ²⁴ nukl/cm ³) | 0.0285 | 0.0244 |
| - Steel | -0.03625 | -0.0206 |
| Doppler-constant, 10 ⁻² for 900-1500°K | | |
| - Fuel | -0.573 | -0.437 |
| - Steel | -0.012 | -0.003 |
| TCR from radial expansion, (1/degree) | -0.1306E-4 | -0.147E-4 |
| TCR from axial expansion, (1/degree) | -0.1715E-5 | -0.183E-5 |
| β _{eff} | 0.00362 | 0.00364 |

Preliminary analysis of Tables 6.7 and 6.8 shows that the maximum influence on the reactivity change is made by formation of the plugs on the upper core boundary, resulting in decrease of neutron leakage. Neutron leakage decrease on the lower core boundary caused by the increasing thickness of the steel layer becomes competitive with the steel related absorption. Reactivity values are given taking into account sodium vapour porosity of the plugs (Table 6.8 and Fig. 6.4), while reactivity value obtained by the Monte-Carlo method taking into account fuel element heterogeneity effect is given in Table 6.6. It can be seen that using transport theory gives ~9% increase of K_{eff} as compared to the results obtained by diffusion theory. The effect of sodium removal is insignificant.

Thus, formation of thick «steel plugs» in the upper core section (reducing neutron leak) has maximum influence on the reactivity. In the lower section of the core plug thickness increase makes the neutron leak decrease compete with absorption in steel. Removal of over

TABLE 6.6. CHANGE K_{eff} WHEN TURNING TO DISTURBED CONDITION (COMPARISON OF DIFFERENT METHODS OF APPROACH)

| Condition | Diffusion approach | Transport approach (S8) | Monte-Carlo (MCNP) |
|--|--------------------|-------------------------|---|
| Initial condition, 1500°K | 1.0066007 | 1.014882 | 1.01648 ± 0.00040 ^{a)} 1.01663 ± 0.00030 ^{b)} 1.01385 ± 0.00031 ^{c)} |
| Heating up to 2100°K | 0.9995832 | 1.007755 | 1.00955 ± 0.00043 ^{a)} 1.00956 ± 0.00030 ^{b)} |
| Removal of sodium (2100°K) from SA | 0.9992928 | 1.007969 | 1 1.01327 ± 0.00027 ^{b)} 1.01236 ± 0.00035 ^{c)} |
| Removal of sodium (2100°K) from SA+interwrapper Na | 0.9987202 | | 1.010327 ± 0.00027 ^{**)} |
| Removal of steel of clad (2100°K) | 1.0238333 | 1.028355 | 1.04196 ± 0.00034 ^{c)} |
| Final condition (2100°K) (formation steel-«plugs») | 1.0238916 | 1.028416 | 1.02045 ± 0.00055 ^{a)} 1.02057 ± 0.00032 ^{b)} |
| Final condition (3500°K) | | | 1.02114 ± 0.00034 ^{b)} 1.02049 ± 0.00032 ^{c)} |

a) 10^6 history

b) $2 \cdot 10^6$ history

c) $\sim 3 \cdot 10^6$ history

TABLE 6.7. REACTIVITY CHANGE OBTAINED BY DIFFERENT EVALUATION METHODS.

| Condition of the core | Reactivity, % $\Delta K/K$ | | |
|--|----------------------------|-------------------------|----------------------------------|
| | Diffusion approach | Transport approach (S8) | Monte-Carlo ^{c)} (MCNP) |
| Heating up to 2100°K | -0.6974 | -0.6968 | -0.635057 ± 0.0417 ^{b)} |
| Removing Na from SA | -0.029 | +0.2107 | -0.145170 ± 0.0461 |
| Removing of steel of clad | +2.3695 | +1.988 | +0.308008 ± 0.0438 |
| Final condition (2100°K) (formation steel-«plugs») | +2.3751 | +1.993 | +2.66095 ± 0.0447 |

b) $2 \cdot 10^6$ history

c) $\sim 3 \cdot 10^6$ history

Note: Reactivity was counted out from the source condition at 2100°K.

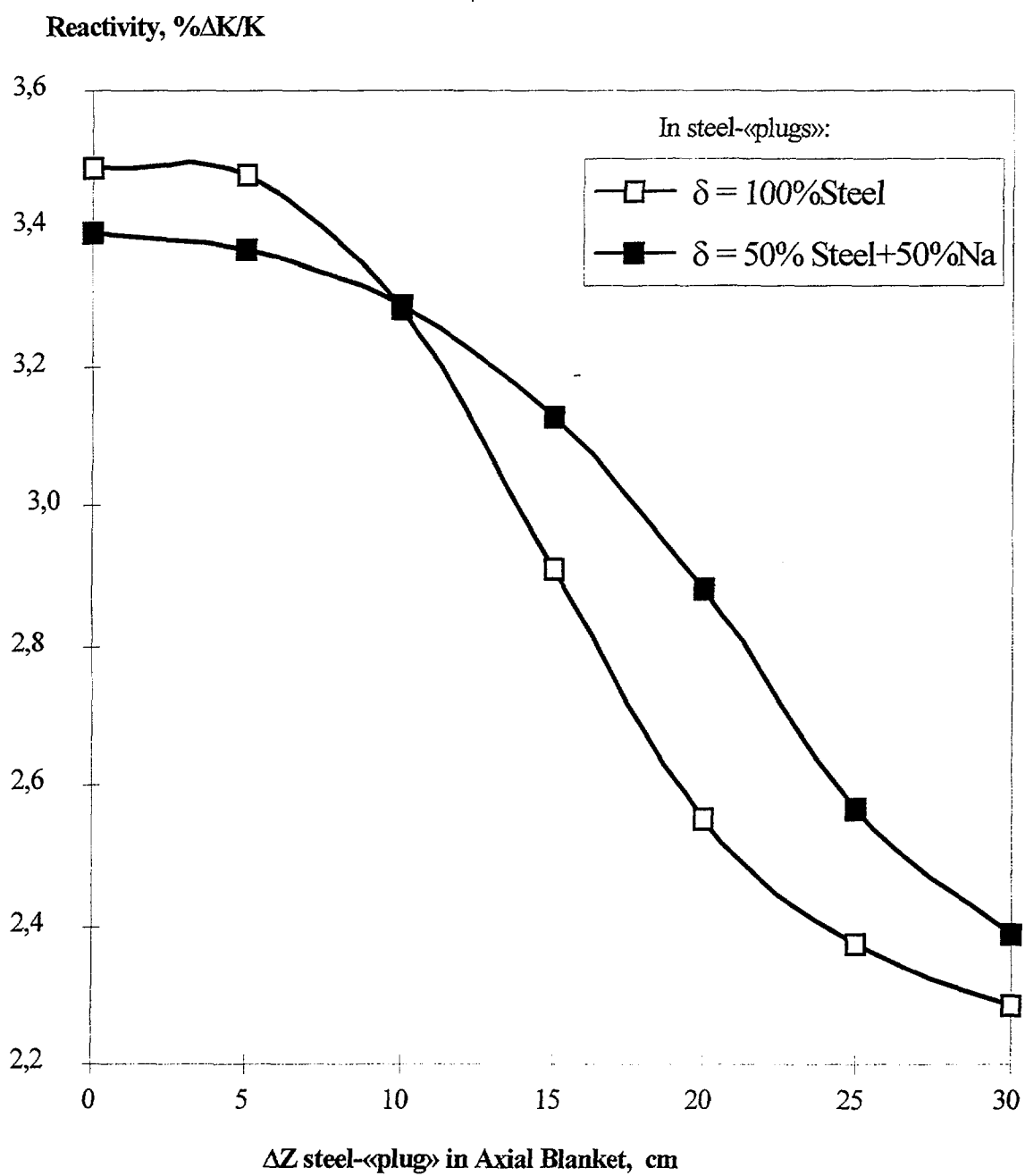


FIG.6.4. Reactivity as function of thickness and density of steel-«plug» in clearance between pins the SA

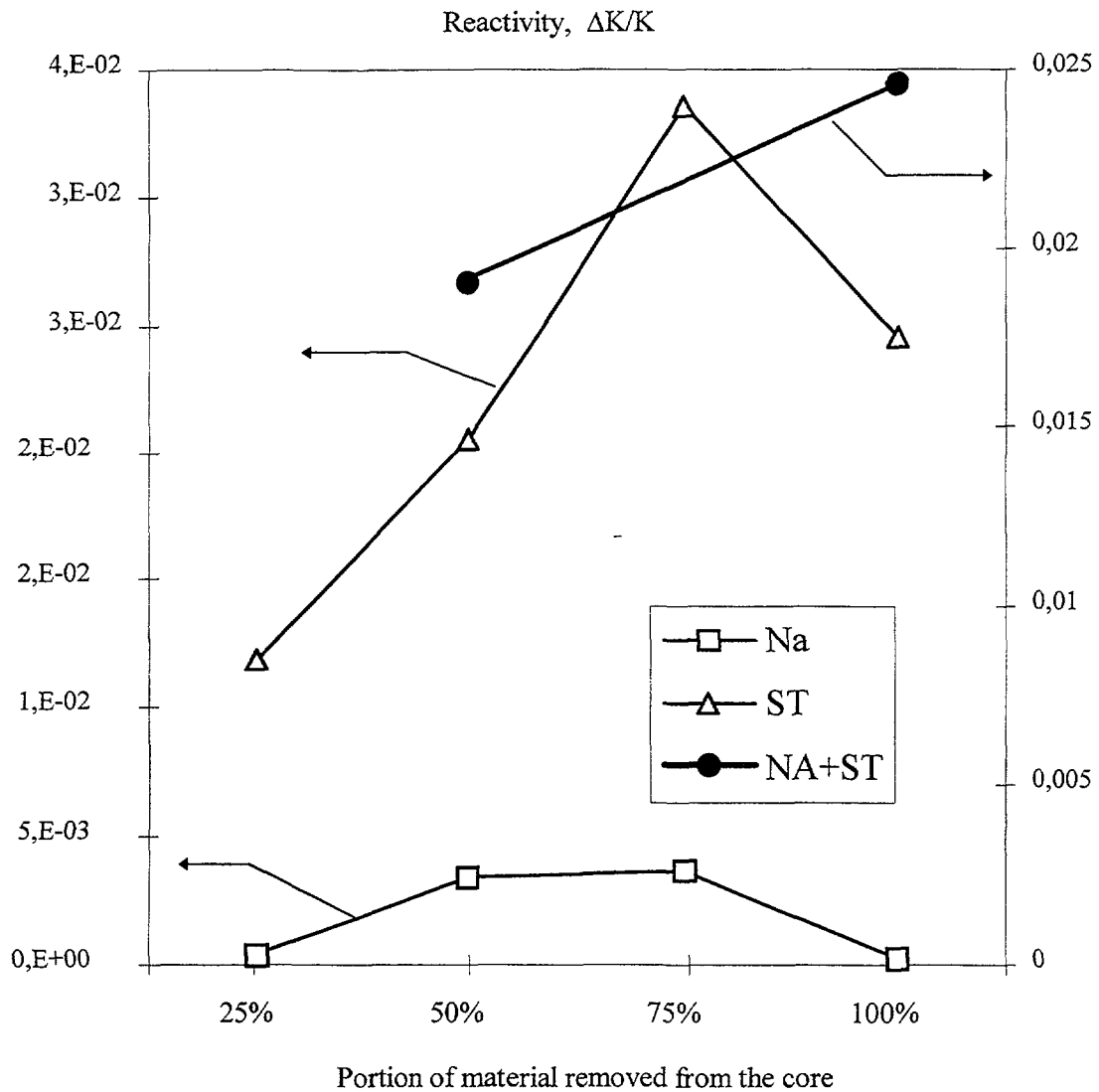


FIG.6.5. Changing of reactivity when removing material from the core (diffusion approach at 2100°K)

50% of sodium and steel leads to significant disturbances of material reactivity in the upper and lower core sections. Disturbances varying over radial and axial coordinates are different for different physical zones. Disturbances of the reactivity profile depend on type and amount of removed disturbing material. These effects are determined by the deformations of neutron spectrum, arising as a result of the removal of efficient moderators, namely sodium and steel (steel removal in addition favours decrease of the neutron absorption in the core).

The most change (in % of initial value) of material worth takes place on the core/LAB and core/gas plenum boundaries, as well as in the end sections of the fuel elements. However, in these sections worth are insignificant (for instance, the sign of sodium worth is changed in these sections).

Resulting change of worth is formed basically by the core itself (sodium plenum contributes to the sodium worth change).

Intermediate states of the core considered are characterised by rather strong disturbances, occurring in the core (SA drying out, fuel element cladding steel removal, etc.), including those taking place on the interfaces of sections having different physical properties (formation of steel plugs in the upper and lower sections of the core). In these calculation models diffusion approach used for evaluation of reactivity coefficients may produce significant errors. Even for nondisturbed medium diffusion approach has significant error on the core/sodium plenum boundary.

Preliminary calculation results obtained for the core mid plane in LEZ centre and in the middle points of radii of MEZ and HEZ plane (thickness of calculated layer $\Delta H \sim 13$ cm) show that neutron spectra in the mid plane do not differ much for diffusion and transport solutions with the same data base versions and data processing methods.

If the result obtained in transport approximation using TWODANT code (S_2) is taken as a reference, then diffusion calculation results deviation from these reference values in spectrum characteristics does not exceed 10-15%. This error can be considered quite acceptable for the standard engineering calculations in diffusion approximation. Reactivity effects having maximum influence on the accident process dynamics, namely sodium density and Doppler effects have spectrum distribution with its maximum in different energy ranges (see Fig.6.6). Therefore, group flux values obtained would not result in significant errors in Doppler and sodium density reactivity effects, as compared to the reference calculation (using TWODANT code). Diffusion calculation results can be used for the further analysis.

6.3. DOPPLER EFFECT

Table 6.12 gives the following relationships for Doppler constant values obtained for different accident stages by disturbance theory:

$$T \frac{\partial K}{\partial T} = \frac{1}{\ln(T/T_0)} \frac{K_{eff}(T) - K_{eff}(T_0)}{K_{eff}(T)K_{eff}(T_0)}$$

Because of uncertainties of Doppler effect calculations made using standard codes for the temperatures over 2100°K accuracy of effect description for the accident conditions using initial state parameters cannot be considered sufficient. In this connection it is proposed to use only Doppler constant value obtained at $\sim 2100^\circ\text{K}$. In this case Doppler effect vs. steel amount in the core relationship can be introduced, as it was made for taking into account sodium amount changing. Such relationship using parameters of the initial state is as follows:

$$\rho_D = \sum_i \sum_n K_{D,i,n}(T_{i,n}) * \left[\overline{K_{D,i,n}} + \Delta \overline{K_{Na,i,n}} \frac{\rho_{Na,i,n} - \rho_{Na,i,n}^0}{\rho_{Na,i,n}^0} + \Delta \overline{K_{St,i,n}} \frac{\rho_{St,i,n} - \rho_{St,i,n}^0}{\rho_{St,i,n}^0} \right]$$

For the sake of further extrapolation of Doppler constant as a function of temperature it is reasonable to use its values for several temperature ranges (see, for instance, Fig.6.7).

6.4. REACTIVITY OF MATERIALS (2100°K)

6.4.1. Sodium integrals of reactivity and space distribution

Deformation of group flux spectra and worth caused by change of the reactor condition in the energy range typical for both Doppler effect and SVRE is rather small (at least for the central layer of ~ 20 cm thickness) -see Fig.6.8.

Text cont. on page 214.

TABLE 6.8. CHANGE \hat{E}_{EFF} WITH FORMATION STEEL-PLUGS (WITHOUT POROSITY ON SODIUM). 26-GROUP DIFFUSION APPROACH. 2100°K.

| Condition of the core | K_{eff} | $\Delta K/K, \%$ (with respect to initial condition 2100°K) | |
|---|-----------|---|--------|
| | | 0 | 50% |
| Steel-«plugs» porosity (filled with sodium steam) | | 0 | 50% |
| Initial (2100°K) | 0.9995832 | - | |
| Absence of steel-«plugs» | 1.0238333 | 2.3695 | |
| Absence of steel-«plugs» + Na in core | 1.0212960 | 2.1269 | |
| Absence of steel-«plugs» + Na in core and sodium plenum | 1.0208940 | 2.0883 | |
| Steel-«plugs» only in bottom axial blanket (5 cm) | 1.0243884 | 2.4225 | |
| Steel-«plugs» only in pin plugs | 1.0309405 | 3.0430 | |
| Steel-«plugs» in pin plugs and top end face of the core (5 cm) | 1.0352030 | 3.4423 | |
| Steel-«plugs» in bottom Ax.Blanket (5 cm), in pin plugs and in the top of the core (5 cm) | 1.0356972 | 3.4869 | |
| Steel-«plugs» in bottom Ax.Blanket (5 cm), in pin plugs and in the top of the core (5 cm), bottom (5 cm) | 1.0355792 | 3.4774 | 3.3692 |
| Steel-«plugs» in bottom Ax.Blanket (5 cm), in pin plugs and in the top of the core (5 cm), bottom (10 cm) | 1.0334889 | 3.2821 | 3.2911 |
| Steel-«plugs» in bottom Ax.Blanket (5 cm), in pin plugs and in the top of the core (5 cm), bottom (15 cm) | 1.0295405 | 2.911 | 3.1278 |
| Steel-«plugs» in bottom Ax.Blanket (5 cm), in pin plugs and in the top of the core (5 cm), bottom (20 cm) | 1.0257536 | 2.5524 | 2.8832 |
| Steel-«plugs» in bottom Ax.Blanket (5 cm), in pin plugs and in the top of the core (5 cm), bottom (25 cm) | 1.0238916 | 2.3751 | 2.5655 |
| Steel-«plugs» in bottom Ax.Blanket (5 cm), in pin plugs and in the top of the core (5 cm), bottom (25 cm) + NA: | | | |
| - in sodium plenum | | | |
| - in core | 1.0247213 | 2.4542 | |
| - in core and sodium plenum | 1.0131058 | 1.3352 | |
| | 1.0166751 | 1.6449 | |

TABLE 6.9. AXIAL DISTRIBUTION OF SODIUM REACTIVITY INTEGRATED OVER LEZ RADIUS WHEN DISTURBING REACTOR ON CONCENTRATIONS OF SODIUM AND STEELS (2100°K, DIFFUSION APPROACH), $\Delta K/K$

| Na | LEZ (removed sodium and steel, %) | | | | | | | |
|-------------|-----------------------------------|-----------|-----------|-----------|-----------|-----------|-----------|-----------------|
| | Initial Condition | 25%Na | 50%Na | 75%Na | 25%St | 59%st | 75%St | 50%Na+ 50%St |
| Ax.BI | 2,22E-04 | 1,86E-04 | 1,63E-04 | 1,86E-04 | 2,03E-04 | 2,72E-04 | 2,53E-04 | 1,92E-04 |
| ↑ | 4,74E-05 | 2,62E-05 | 3,28E-05 | 1,81E-05 | 5,70E-05 | 1,21E-04 | 1,45E-04 | 7,07E-05 |
| | -4,01E-04 | -3,41E-04 | -2,27E-04 | -1,20E-04 | -4,22E-04 | -3,87E-04 | -4,02E-04 | -2,21E-04 |
| | -8,20E-04 | -6,83E-04 | -4,64E-04 | -2,43E-04 | -8,65E-04 | -8,41E-04 | -8,83E-04 | -4,76E-04 |
| | -1,17E-03 | -9,69E-04 | -6,59E-04 | -3,42E-04 | -1,24E-03 | -1,21E-03 | -1,27E-03 | -6,81E-04 |
| C | -1,41E-03 | -1,15E-03 | -7,81E-04 | -4,02E-04 | -1,48E-03 | -1,45E-03 | -1,52E-03 | -8,04E-04 |
| O | -1,48E-03 | -1,21E-03 | -8,09E-04 | -4,13E-04 | -1,55E-03 | -1,52E-03 | -1,59E-03 | -8,27E-04 |
| R | -1,38E-03 | -1,12E-03 | -7,38E-04 | -3,72E-04 | -1,44E-03 | -1,41E-03 | -1,47E-03 | -7,47E-04 |
| E | -1,12E-03 | -9,01E-04 | -5,79E-04 | -2,86E-04 | -1,17E-03 | -1,13E-03 | -1,17E-03 | -5,73E-04 |
| | -7,44E-04 | -5,88E-04 | -3,54E-04 | -1,67E-04 | -7,75E-04 | -7,24E-04 | -7,44E-04 | -3,29E-04 |
| | -3,06E-04 | -2,27E-04 | -9,67E-05 | -3,15E-05 | -3,11E-04 | -2,47E-04 | -2,35E-04 | -4,73E-05 |
| | 1,25E-04 | 1,30E-04 | 1,54E-04 | 1,01E-04 | 1,53E-04 | 2,34E-04 | 2,87E-04 | 2,34E-04 |
| | 5,11E-04 | 4,50E-04 | 3,81E-04 | 2,20E-04 | 5,74E-04 | 6,80E-04 | 7,79E-04 | 4,95E-04 |
| Pin plugs | 5,95E-04 | 6,66E-04 | 4,24E-04 | 9,10E-04 | 6,40E-04 | 7,04E-04 | 7,66E-04 | 4,99E-04 |
| Sod. Pl. | 2,53E-03 | 2,49E-03 | 2,33E-03 | 1,60E-03 | 2,74E-03 | 3,03E-03 | 3,34E-03 | 2,80E-03 |
| $\Sigma(Z)$ | -4,73E-03 | -3,16E-03 | -1,11E-03 | 7,74E-04 | -4,82E-03 | -3,81E-03 | -3,64E-03 | -2,85E-04 |

TABLE 6.9. (CONTINUED). AXIAL DISTRIBUTION OF SODIUM REACTIVITY INTEGRATED OVER MEZ RADIUS WHEN DISTURBING REACTOR ON CONCENTRATIONS OF SODIUM AND STEELS (2100°K, DIFFUSION APPROACH), $\Delta K/K$

| Na | MEZ (removed sodium and steel, %) | | | | | | | |
|-----------|-----------------------------------|-----------|-----------|-----------|-----------|-----------|-----------|-----------------|
| | Initial Condition | 25%Na | 50%Na | 75%Na | 25%St | 59%st | 75%St | 50%Na+ 50%St |
| Ax.BI | 3,35E-04 | 3,27E-04 | 2,18E-04 | 3,55E-04 | 3,34E-04 | 3,75E-04 | 3,76E-04 | 2,42E-04 |
| ↑ | 2,10E-04 | 1,59E-04 | 1,24E-04 | 6,03E-05 | 2,14E-04 | 2,43E-04 | 2,53E-04 | 1,41E-04 |
| | -1,07E-04 | -9,55E-05 | -5,46E-05 | -3,04E-05 | -1,12E-04 | -8,76E-05 | -8,81E-05 | -4,48E-05 |
| | -3,84E-04 | -3,17E-04 | -2,06E-04 | -1,07E-04 | -3,95E-04 | -3,65E-04 | -3,72E-04 | -1,98E-04 |
| | -6,19E-04 | -5,04E-04 | -3,33E-04 | -1,69E-04 | -6,34E-04 | -5,98E-04 | -6,08E-04 | -3,23E-04 |
| C | -7,78E-04 | -6,28E-04 | -4,14E-04 | -2,08E-04 | -7,94E-04 | -7,51E-04 | -7,62E-04 | -4,01E-04 |
| O | -8,37E-04 | -6,70E-04 | -4,39E-04 | -2,18E-04 | -8,52E-04 | -8,05E-04 | -8,15E-04 | -4,22E-04 |
| R | -7,87E-04 | -6,26E-04 | -4,02E-04 | -1,97E-04 | -8,00E-04 | -7,52E-04 | -7,60E-04 | -3,83E-04 |
| E | -6,36E-04 | -4,99E-04 | -3,10E-04 | -1,48E-04 | -6,45E-04 | -5,99E-04 | -6,04E-04 | -2,89E-04 |
| | -4,04E-04 | -3,09E-04 | -1,76E-04 | -7,81E-05 | -4,09E-04 | -3,66E-04 | -3,65E-04 | -1,51E-04 |
| | -1,24E-04 | -8,09E-05 | -1,59E-05 | 4,13E-06 | -1,22E-04 | -8,34E-05 | -7,37E-05 | 1,27E-05 |
| | 1,67E-04 | 1,55E-04 | 1,48E-04 | 8,78E-05 | 1,79E-04 | 2,16E-04 | 2,37E-04 | 1,83E-04 |
| ↓ | 4,33E-04 | 3,69E-04 | 2,95E-04 | 1,63E-04 | 4,57E-04 | 4,96E-04 | 5,32E-04 | 3,42E-04 |
| Pin plugs | 3,43E-04 | 3,86E-04 | 2,34E-04 | 5,22E-04 | 3,63E-04 | 3,91E-04 | 4,19E-04 | 2,70E-04 |
| Sod. Pl. | 1,95E-03 | 1,79E-03 | 1,55E-03 | 1,00E-03 | 2,08E-03 | 2,27E-03 | 2,46E-03 | 1,82E-03 |
| Σ | -1,19E-03 | -4,83E-04 | 2,99E-04 | 1,12E-03 | -1,08E-03 | -3,67E-04 | -1,19E-04 | 8,92E-04 |

TABLE 6.9. (CONTINUED). AXIAL DISTRIBUTION OF SODIUM REACTIVITY INTEGRATED OVER HEZ RADIUS WHEN DISTURBING REACTOR ON CONCENTRATIONS OF SODIUM AND STEELS (2100°K, DIFFUSION APPROACH), $\Delta K/K$

| NA | HEZ (removed sodium and steel, %) | | | | | | | |
|-----------|-----------------------------------|----------|----------|----------|-----------|-----------|-----------|-----------------|
| | Initial Condition | 25%Na | 50%Na | 75%Na | 25%St | 59%st | 75%St | 50%Na+ 50%St |
| Ax.BI | 3,47E-04 | 3,53E-04 | 2,28E-04 | 3,97E-04 | 2,69E-04 | 3,08E-04 | 3,41E-04 | 2,60E-04 |
| ↑ | 3,72E-04 | 3,02E-04 | 2,25E-04 | 1,20E-04 | 1,90E-04 | 2,23E-04 | 2,41E-04 | 2,84E-04 |
| ↑ | 2,50E-04 | 1,99E-04 | 1,49E-04 | 7,85E-05 | 1,22E-04 | 1,51E-04 | 1,59E-04 | 1,83E-04 |
| ↑ | 1,80E-04 | 1,39E-04 | 1,06E-04 | 5,50E-05 | 7,46E-05 | 1,02E-04 | 1,04E-04 | 1,29E-04 |
| ↑ | 1,18E-04 | 8,67E-05 | 6,94E-05 | 3,56E-05 | 5,47E-05 | 8,19E-05 | 8,13E-05 | 8,49E-05 |
| C | 7,53E-05 | 5,09E-05 | 4,49E-05 | 2,29E-05 | 6,39E-05 | 9,17E-05 | 9,27E-05 | 5,63E-05 |
| O | 5,68E-05 | 3,64E-05 | 3,58E-05 | 1,86E-05 | 9,97E-05 | 1,29E-04 | 1,35E-04 | 4,63E-05 |
| R | 6,50E-05 | 4,47E-05 | 4,29E-05 | 2,31E-05 | 1,56E-04 | 1,87E-04 | 2,01E-04 | 5,51E-05 |
| E | 9,77E-05 | 7,37E-05 | 6,45E-05 | 3,52E-05 | 2,23E-04 | 2,57E-04 | 2,82E-04 | 8,08E-05 |
| ↓ | 1,49E-04 | 1,18E-04 | 9,63E-05 | 5,25E-05 | 2,91E-04 | 3,29E-04 | 3,65E-04 | 1,19E-04 |
| ↓ | 2,09E-04 | 1,70E-04 | 1,33E-04 | 7,20E-05 | 3,52E-04 | 3,95E-04 | 4,43E-04 | 1,62E-04 |
| ↓ | 2,70E-04 | 2,21E-04 | 1,67E-04 | 9,01E-05 | 2,77E-04 | 3,00E-04 | 3,26E-04 | 2,05E-04 |
| ↓ | 3,25E-04 | 2,66E-04 | 1,96E-04 | 1,05E-04 | 1,84E-03 | 2,02E-03 | 2,21E-03 | 2,41E-04 |
| Pin plugs | 2,60E-04 | 2,67E-04 | 1,54E-04 | 2,95E-04 | 1,81E-05 | 2,00E-05 | 2,21E-05 | 1,81E-04 |
| Sod. Pl. | 1,72E-03 | 1,58E-03 | 1,39E-03 | 9,12E-04 | -4,06E-09 | -4,24E-09 | -4,58E-09 | 1,66E-03 |
| Σ | 4,53E-03 | 3,96E-03 | 3,17E-03 | 2,39E-03 | 1,13E-03 | 1,21E-03 | 1,28E-03 | 3,82E-03 |

TABLE 6.10. AXIAL DISTRIBUTION OF STEEL REACTIVITY INTEGRATED OVER LEZ RADIUS WHEN DISTURBING REACTOR ON CONCENTRATIONS OF SODIUM AND STEELS (2100°K, DIFFUSION APPROACH), $\Delta K/K$

| Steel | LEZ (removed sodium and steel, %) | | | | | | | |
|-----------|-----------------------------------|-----------|-----------|-----------|-----------|-----------|-----------|-------------|
| | Initial Condition | 25%Na | 50%Na | 75%Na | 25%St | 59%st | 75%St | 50%Na+50%St |
| Ax.BI | 4,20E-04 | 4,22E-04 | 6,06E-04 | 4,54E-04 | 4,31E-04 | 4,71E-04 | 4,74E-04 | 6,68E-04 |
| ↑ | -3,13E-04 | -3,14E-04 | -2,79E-04 | -3,09E-04 | -2,40E-04 | -1,22E-04 | -5,84E-05 | -9,78E-05 |
| | -1,37E-03 | -1,42E-03 | -1,44E-03 | -1,51E-03 | -1,11E-03 | -7,25E-04 | -3,89E-04 | -7,65E-04 |
| | -2,39E-03 | -2,47E-03 | -2,53E-03 | -2,64E-03 | -1,94E-03 | -1,29E-03 | -6,97E-04 | -1,37E-03 |
| | -3,24E-03 | -3,35E-03 | -3,41E-03 | -3,53E-03 | -2,62E-03 | -1,76E-03 | -9,46E-04 | -1,85E-03 |
| C | -3,79E-03 | -3,90E-03 | -3,96E-03 | -4,07E-03 | -3,07E-03 | -2,05E-03 | -1,10E-03 | -2,13E-03 |
| O | -3,96E-03 | -4,06E-03 | -4,08E-03 | -4,17E-03 | -3,20E-03 | -2,13E-03 | -1,14E-03 | -2,18E-03 |
| R | -3,72E-03 | -3,79E-03 | -3,76E-03 | -3,80E-03 | -3,00E-03 | -1,99E-03 | -1,06E-03 | -1,99E-03 |
| E | -3,10E-03 | -3,13E-03 | -3,04E-03 | -3,02E-03 | -2,49E-03 | -1,64E-03 | -8,72E-04 | -1,58E-03 |
| ↓ | -2,17E-03 | -2,15E-03 | -2,00E-03 | -1,92E-03 | -1,74E-03 | -1,12E-03 | -5,88E-04 | -9,93E-04 |
| | -1,08E-03 | -1,01E-03 | -7,95E-04 | -6,55E-04 | -8,43E-04 | -4,98E-04 | -2,47E-04 | -3,06E-04 |
| | 4,39E-05 | 1,62E-04 | 4,20E-04 | 6,13E-04 | 8,32E-05 | 1,49E-04 | 1,13E-04 | 4,00E-04 |
| | 1,10E-03 | 1,26E-03 | 1,55E-03 | 1,79E-03 | 9,61E-04 | 7,71E-04 | 4,64E-04 | 1,07E-03 |
| Pin plugs | 1,94E-03 | 2,14E-03 | 2,47E-03 | 2,79E-03 | 2,08E-03 | 2,28E-03 | 2,48E-03 | 2,93E-03 |
| Sod. Pl. | 1,14E-03 | 1,38E-03 | 1,77E-03 | 2,11E-03 | 1,23E-03 | 1,36E-03 | 1,49E-03 | 2,12E-03 |
| Σ | -2,04E-02 | -2,02E-02 | -1,84E-02 | -1,79E-02 | -1,54E-02 | -8,23E-03 | -2,03E-03 | -6,01E-03 |

TABLE 6.10. (CONTINUED). AXIAL DISTRIBUTION OF STEEL REACTIVITY INTEGRATED OVER MEZ RADIUS WHEN DISTURBING REACTOR ON CONCENTRATIONS OF SODIUM AND STEELS (2100°K, DIFFUSION APPROACH), $\Delta K/K$

| Steel | MEZ (removed sodium and steel, %) | | | | | | | | |
|-----------|-----------------------------------|-----------|-----------|-----------|-----------|-----------|-----------|-------------|-----------|
| | Initial Condition | 25%Na | 50%Na | 75%Na | 25%St | 59%st | 75%St | 50%Na+50%St | |
| Ax.BI | 6,70E-04 | 6,88E-04 | 8,40E-04 | 7,53E-04 | 6,90E-04 | 7,28E-04 | 7,49E-04 | 9,10E-04 | |
| ↑ | 1,67E-04 | 1,72E-04 | 2,27E-04 | 1,87E-04 | 1,34E-04 | 1,11E-04 | 6,11E-05 | 1,45E-04 | |
| | -5,72E-04 | -5,88E-04 | -5,70E-04 | -6,13E-04 | -4,49E-04 | -2,76E-04 | -1,42E-04 | -2,77E-04 | |
| | -1,25E-03 | -1,27E-03 | -1,27E-03 | -1,32E-03 | -9,77E-04 | -6,21E-04 | -3,22E-04 | -6,38E-04 | |
| | -1,81E-03 | -1,85E-03 | -1,85E-03 | -1,89E-03 | -1,42E-03 | -9,07E-04 | -4,71E-04 | -9,30E-04 | |
| | C | -2,19E-03 | -2,23E-03 | -2,21E-03 | -2,25E-03 | -1,71E-03 | -1,10E-03 | -5,68E-04 | -1,11E-03 |
| | O | -2,33E-03 | -2,36E-03 | -2,32E-03 | -2,34E-03 | -1,82E-03 | -1,16E-03 | -6,02E-04 | -1,16E-03 |
| | R | -2,21E-03 | -2,22E-03 | -2,16E-03 | -2,15E-03 | -1,73E-03 | -1,10E-03 | -5,66E-04 | -1,07E-03 |
| | E | -1,85E-03 | -1,83E-03 | -1,74E-03 | -1,70E-03 | -1,44E-03 | -9,06E-04 | -4,66E-04 | -8,47E-04 |
| | | -1,29E-03 | -1,25E-03 | -1,13E-03 | -1,05E-03 | -9,99E-04 | -6,17E-04 | -3,14E-04 | -5,23E-04 |
| | | -6,11E-04 | -5,43E-04 | -3,94E-04 | -2,92E-04 | -4,64E-04 | -2,65E-04 | -1,28E-04 | -1,35E-04 |
| | 9,63E-05 | 1,91E-04 | 3,65E-04 | 4,94E-04 | 9,61E-05 | 1,06E-04 | 6,88E-05 | 2,72E-04 | |
| | 7,37E-04 | 8,61E-04 | 1,06E-03 | 1,22E-03 | 6,08E-04 | 4,47E-04 | 2,51E-04 | 6,55E-04 | |
| Pin plugs | 9,26E-04 | 1,08E-03 | 1,26E-03 | 1,51E-03 | 9,81E-04 | 1,05E-03 | 1,12E-03 | 1,47E-03 | |
| Sod. Pl. | 7,87E-04 | 9,27E-04 | 1,12E-03 | 1,29E-03 | 8,38E-04 | 9,07E-04 | 9,80E-04 | 1,32E-03 | |
| Σ | -1,07E-02 | -1,02E-02 | -8,73E-03 | -8,15E-03 | -7,63E-03 | -3,57E-03 | -3,14E-04 | -1,89E-03 | |

TABLE 6.10. (CONTINUED). AXIAL DISTRIBUTION OF STEEL REACTIVITY INTEGRATED OVER HEZ RADIUS WHEN DISTURBING REACTOR ON CONCENTRATIONS OF SODIUM AND STEELS (2100°K, DIFFUSION APPROACH), $\Delta K/K$

| Steel | HEZ (removed sodium and steel, %) | | | | | | | | |
|-----------|-----------------------------------|-----------|-----------|-----------|-----------|-----------|-----------|-------------|-----------|
| | Initial Condition | 25%Na | 50%Na | 75%Na | 25%St | 59%st | 75%St | 50%Na+50%St | |
| Ax.BI | 6,95E-04 | 7,23E-04 | 8,78E-04 | 8,15E-04 | 7,27E-04 | 7,80E-04 | 8,28E-04 | 9,94E-04 | |
| ↑ | 5,89E-04 | 6,35E-04 | 7,09E-04 | 7,62E-04 | 5,11E-04 | 4,03E-04 | 2,44E-04 | 4,91E-04 | |
| | 2,80E-04 | 3,03E-04 | 3,44E-04 | 3,72E-04 | 2,49E-04 | 2,11E-04 | 1,30E-04 | 2,54E-04 | |
| | 6,14E-05 | 7,27E-05 | 1,02E-04 | 1,13E-04 | 6,87E-05 | 8,57E-05 | 5,77E-05 | 1,08E-04 | |
| | -1,25E-04 | -1,22E-04 | -9,94E-05 | -9,72E-05 | -8,35E-05 | -1,82E-05 | -1,14E-06 | -8,64E-06 | |
| C | -2,53E-04 | -2,53E-04 | -2,32E-04 | -2,32E-04 | -1,88E-04 | -8,84E-05 | -4,05E-05 | -8,37E-05 | |
| O | -3,07E-04 | -3,05E-04 | -2,80E-04 | -2,76E-04 | -2,30E-04 | -1,17E-04 | -5,62E-05 | -1,09E-04 | |
| R | -2,79E-04 | -2,72E-04 | -2,38E-04 | -2,24E-04 | -2,08E-04 | -1,01E-04 | -4,73E-05 | -8,41E-05 | |
| ↓ | E | -1,77E-04 | -1,60E-04 | -1,16E-04 | -8,86E-05 | -1,25E-04 | -4,50E-05 | -1,57E-05 | -1,35E-05 |
| | -1,76E-05 | 9,98E-06 | 6,62E-05 | 1,08E-04 | 4,62E-06 | 4,24E-05 | 3,34E-05 | 9,09E-05 | |
| | 1,73E-04 | 2,12E-04 | 2,78E-04 | 3,35E-04 | 1,60E-04 | 1,47E-04 | 9,26E-05 | 2,13E-04 | |
| | 3,66E-04 | 4,16E-04 | 4,89E-04 | 5,59E-04 | 3,18E-04 | 2,55E-04 | 1,53E-04 | 3,36E-04 | |
| Pin plugs | 5,34E-04 | 5,96E-04 | 6,78E-04 | 7,59E-04 | 4,55E-04 | 3,47E-04 | 2,06E-04 | 4,45E-04 | |
| Sod. Pl. | 6,59E-04 | 7,08E-04 | 7,94E-04 | 8,36E-04 | 7,04E-04 | 7,58E-04 | 8,27E-04 | 9,43E-04 | |
| Σ | 6,61E-04 | 7,87E-04 | 9,74E-04 | 1,15E-03 | 7,07E-04 | 7,71E-04 | 8,42E-04 | 1,16E-03 | |
| | 2,87E-03 | 3,36E-03 | 4,37E-03 | 4,89E-03 | 3,08E-03 | 3,44E-03 | 3,26E-03 | 4,76E-03 | |

TABLE 6.11. AXIAL DISTRIBUTION OF FUEL REACTIVITY INTEGRATED OVER MEZ RADIUS WHEN DISTURBING REACTOR ON CONCENTRATIONS OF SODIUM AND STEELS (2100°K, DIFFUSION APPROACH), $\Delta K/K$

| FUEL | LEZ (removed sodium and steel, %) | | | | | | | |
|-----------|-----------------------------------|-----------|-----------|-----------|-----------|-----------|-----------|-------------|
| | Initial Condition | 25%Na | 50%Na | 75%Na | 25%St | 59%st | 75%St | 50%Na+50%St |
| Ax.BI | -2,12E-03 | -2,16E-03 | -1,96E-03 | -2,36E-03 | -2,20E-03 | -2,39E-03 | -2,47E-03 | -2,15E-03 |
| ↑ | 1,09E-02 | 1,15E-02 | 1,23E-02 | 1,30E-02 | 1,14E-02 | 1,20E-02 | 1,26E-02 | 1,35E-02 |
| | 1,17E-02 | 1,22E-02 | 1,28E-02 | 1,34E-02 | 1,20E-02 | 1,22E-02 | 1,25E-02 | 1,34E-02 |
| | 1,38E-02 | 1,43E-02 | 1,49E-02 | 1,54E-02 | 1,39E-02 | 1,39E-02 | 1,40E-02 | 1,50E-02 |
| | 1,55E-02 | 1,60E-02 | 1,65E-02 | 1,70E-02 | 1,55E-02 | 1,53E-02 | 1,52E-02 | 1,62E-02 |
| C | 1,66E-02 | 1,70E-02 | 1,75E-02 | 1,79E-02 | 1,65E-02 | 1,62E-02 | 1,59E-02 | 1,70E-02 |
| O | 1,70E-02 | 1,73E-02 | 1,77E-02 | 1,80E-02 | 1,68E-02 | 1,64E-02 | 1,61E-02 | 1,71E-02 |
| R | 1,65E-02 | 1,68E-02 | 1,72E-02 | 1,74E-02 | 1,64E-02 | 1,60E-02 | 1,58E-02 | 1,66E-02 |
| E | 1,52E-02 | 1,56E-02 | 1,58E-02 | 1,61E-02 | 1,52E-02 | 1,50E-02 | 1,49E-02 | 1,56E-02 |
| ↓ | 1,34E-02 | 1,37E-02 | 1,40E-02 | 1,42E-02 | 1,35E-02 | 1,35E-02 | 1,36E-02 | 1,41E-02 |
| | 1,13E-02 | 1,16E-02 | 1,18E-02 | 1,21E-02 | 1,15E-02 | 1,17E-02 | 1,21E-02 | 1,24E-02 |
| | 9,08E-03 | 9,37E-03 | 9,66E-03 | 9,99E-03 | 9,51E-03 | 9,95E-03 | 1,05E-02 | 1,07E-02 |
| | 7,25E-03 | 7,54E-03 | 7,86E-03 | 8,24E-03 | 7,79E-03 | 8,42E-03 | 9,17E-03 | 9,28E-03 |
| Pin plugs | 0,00E+00 | 0,00E+00 | 0,00E+00 | 0,00E+00 | 0,00E+00 | 0,00E+00 | 0,00E+00 | 0,00E+00 |
| Sod. Pl. | 0,00E+00 | 0,00E+00 | 0,00E+00 | 0,00E+00 | 0,00E+00 | 0,00E+00 | 0,00E+00 | 0,00E+00 |
| Σ | 1,56E-01 | 1,61E-01 | 1,66E-01 | 1,70E-01 | 1,58E-01 | 1,58E-01 | 1,60E-01 | 1,69E-01 |

TABLE 6.11 (CONTINUED). AXIAL DISTRIBUTION OF FUEL REACTIVITY INTEGRATED OVER MEZ RADIUS WHEN DISTURBING REACTOR ON CONCENTRATIONS OF SODIUM AND STEELS (2100°K, DIFFUSION APPROACH), $\Delta K/K$

| FUEL | MEZ (removed sodium and steel, %) | | | | | | | |
|-----------|-----------------------------------|----------|----------|----------|-----------|-----------|-----------|-------------|
| | Initial Condition | 25%Na | 50%Na | 75%Na | 25%St | 59%st | 75%St | 50%Na+50%St |
| Ax.BI | -1,86E-05 | 8,24E-06 | 2,69E-04 | 4,62E-05 | -7,27E-06 | -2,84E-05 | -1,35E-05 | 3,03E-04 |
| ↑ | 7,95E-03 | 8,31E-03 | 8,72E-03 | 9,20E-03 | 8,17E-03 | 8,34E-03 | 8,63E-03 | 9,23E-03 |
| | 8,86E-03 | 9,16E-03 | 9,48E-03 | 9,86E-03 | 8,90E-03 | 8,85E-03 | 8,92E-03 | 9,54E-03 |
| | 1,07E-02 | 1,10E-02 | 1,13E-02 | 1,16E-02 | 1,06E-02 | 1,03E-02 | 1,02E-02 | 1,09E-02 |
| | 1,23E-02 | 1,25E-02 | 1,27E-02 | 1,30E-02 | 1,20E-02 | 1,16E-02 | 1,13E-02 | 1,20E-02 |
| C | 1,34E-02 | 1,35E-02 | 1,37E-02 | 1,38E-02 | 1,30E-02 | 1,24E-02 | 1,20E-02 | 1,27E-02 |
| O | 1,37E-02 | 1,39E-02 | 1,39E-02 | 1,40E-02 | 1,33E-02 | 1,26E-02 | 1,22E-02 | 1,29E-02 |
| R | 1,34E-02 | 1,35E-02 | 1,35E-02 | 1,36E-02 | 1,30E-02 | 1,23E-02 | 1,19E-02 | 1,25E-02 |
| E | 1,24E-02 | 1,24E-02 | 1,24E-02 | 1,25E-02 | 1,21E-02 | 1,15E-02 | 1,12E-02 | 1,16E-02 |
| | 1,08E-02 | 1,09E-02 | 1,08E-02 | 1,09E-02 | 1,06E-02 | 1,02E-02 | 1,01E-02 | 1,04E-02 |
| | 8,89E-03 | 8,97E-03 | 8,97E-03 | 9,06E-03 | 8,87E-03 | 8,72E-03 | 8,74E-03 | 8,94E-03 |
| | 6,94E-03 | 7,05E-03 | 7,10E-03 | 7,25E-03 | 7,07E-03 | 7,13E-03 | 7,33E-03 | 7,45E-03 |
| | 5,24E-03 | 5,39E-03 | 5,52E-03 | 5,72E-03 | 5,48E-03 | 5,70E-03 | 6,04E-03 | 6,15E-03 |
| Pin plugs | 0,00E+00 | 0,00E+00 | 0,00E+00 | 0,00E+00 | 0,00E+00 | 0,00E+00 | 0,00E+00 | 0,00E+00 |
| Sod. Pl. | 0,00E+00 | 0,00E+00 | 0,00E+00 | 0,00E+00 | 0,00E+00 | 0,00E+00 | 0,00E+00 | 0,00E+00 |
| Σ | 1,25E-01 | 1,27E-01 | 1,28E-01 | 1,30E-01 | 1,23E-01 | 1,20E-01 | 1,19E-01 | 1,25E-01 |

TABLE 6.11. (CONTINUED). AXIAL DISTRIBUTION OF FUEL REACTIVITY INTEGRATED OVER HEZ RADIUS WHEN DISTURBING REACTOR ON CONCENTRATIONS OF SODIUM AND STEELS (2100°K, DIFFUSION APPROACH), $\Delta K/K$

| FUEL | HEZ (removed sodium and steel, %) | | | | | | | |
|-----------|-----------------------------------|----------|----------|----------|----------|----------|----------|-------------|
| | Initial Condition | 25%Na | 50%Na | 75%Na | 25%St | 59%st | 75%St | 50%Na+50%St |
| Ax.BI | 6,60E-04 | 7,10E-04 | 9,97E-04 | 8,35E-04 | 7,02E-04 | 7,43E-04 | 8,06E-04 | 1,14E-03 |
| ↑ | 6,46E-03 | 6,83E-03 | 7,24E-03 | 7,80E-03 | 6,78E-03 | 7,14E-03 | 7,66E-03 | 8,14E-03 |
| | 7,63E-03 | 7,97E-03 | 8,33E-03 | 8,80E-03 | 7,82E-03 | 7,98E-03 | 8,30E-03 | 8,82E-03 |
| | 9,57E-03 | 9,90E-03 | 1,02E-02 | 1,07E-02 | 9,65E-03 | 9,64E-03 | 9,83E-03 | 1,04E-02 |
| | 1,12E-02 | 1,15E-02 | 1,18E-02 | 1,22E-02 | 1,12E-02 | 1,10E-02 | 1,11E-02 | 1,18E-02 |
| C | 1,23E-02 | 1,26E-02 | 1,29E-02 | 1,32E-02 | 1,22E-02 | 1,20E-02 | 1,19E-02 | 1,26E-02 |
| O | 1,28E-02 | 1,30E-02 | 1,32E-02 | 1,35E-02 | 1,26E-02 | 1,23E-02 | 1,22E-02 | 1,28E-02 |
| R | 1,25E-02 | 1,27E-02 | 1,28E-02 | 1,30E-02 | 1,23E-02 | 1,20E-02 | 1,20E-02 | 1,24E-02 |
| E | 1,14E-02 | 1,16E-02 | 1,17E-02 | 1,18E-02 | 1,14E-02 | 1,11E-02 | 1,11E-02 | 1,15E-02 |
| ↓ | 9,86E-03 | 9,99E-03 | 1,00E-02 | 1,01E-02 | 9,88E-03 | 9,75E-03 | 9,85E-03 | 1,00E-02 |
| | 7,93E-03 | 8,04E-03 | 8,05E-03 | 8,16E-03 | 8,04E-03 | 8,06E-03 | 8,28E-03 | 8,31E-03 |
| | 5,92E-03 | 6,02E-03 | 6,03E-03 | 6,14E-03 | 6,12E-03 | 6,27E-03 | 6,60E-03 | 6,52E-03 |
| | 4,13E-03 | 4,22E-03 | 4,25E-03 | 4,37E-03 | 4,37E-03 | 4,62E-03 | 5,02E-03 | 4,88E-03 |
| Pin plugs | 0,00E+00 | 0,00E+00 | 0,00E+00 | 0,00E+00 | 0,00E+00 | 0,00E+00 | 0,00E+00 | 0,00E+00 |
| Sod. Pl. | 0,00E+00 | 0,00E+00 | 0,00E+00 | 0,00E+00 | 0,00E+00 | 0,00E+00 | 0,00E+00 | 0,00E+00 |
| Σ | 1,12E-01 | 1,15E-01 | 1,17E-01 | 1,21E-01 | 1,13E-01 | 1,13E-01 | 1,15E-01 | 1,19E-01 |

TABLE 6.12. DOPLER-CONSTANT IN VARIOUS PHYSICAL REACTORS ZONES, $T(\partial K / \partial T)$ 10^{-2} (DIFFUSION-APPROACH).

| Condition | Zone | 1500-2100°K | | 2100-3500°K | |
|--|--------|-------------|------------|-------------|-----------|
| | | Steel | Fuel | Steel | Fuel |
| Initial condition (900-1500°) | LEZ | -3.42E-02 | -2.96E-01 | | |
| | MEZ | -1.83E-02 | -1.40E-01 | | |
| | HEZ | -1.08E-02 | -7.36E-02 | | |
| | Ax.Bl | -4.26E-03 | -7.88E-02 | | |
| | Rad.Bl | -1.33E-03 | 4.11E-02 | | |
| → Heating up 1500-2100°K | LEZ | -0.0334 | -0.291 | -1.40E-02 | -1.27E-01 |
| | MEZ | -0.0175 | -0.138 | -7.43E-03 | -5.89E-03 |
| | HEZ | -0.0100 | -0.0695 | -4.33E-03 | -3.07E-02 |
| | Ax.Bl | -0.0026 | -0.0437 | -9.30E-04 | -1.52E-02 |
| | Rad.Bl | -0.00122 | -0.0369 | -4.84E-04 | -1.47E-02 |
| Sodium «boiling» | LEZ | -2.93E-02 | -2.46E-01 | -1.61E-05 | -7.15E-06 |
| | MEZ | -1.39E-02 | -1.06E-01 | -5.41E-06 | -2.04E-06 |
| | HEZ | -8.73E-03 | -5.78E-02 | -2.93E-06 | -1.16E-06 |
| | Ax.Bl | -2.76E-03 | -4.65E-02 | -5.32E-06 | -1.04E-05 |
| | Rad.Bl | -1.20E-03 | -3.51E-02 | -6.55E-07 | -4.36E-07 |
| Removal of steel of clad | LEZ | -1.18E-02 | -2.04E-01 | -1.88E-05 | -8.14E-06 |
| | MEZ | -5.45E-03 | -8.97E-02 | -6.04E-06 | -2.28E-06 |
| | HEZ | -8.19E-03 | -5.46E-02 | -3.22E-06 | -1.27E-06 |
| | Ax.Bl | -3.05E-03 | -5.13E-02 | -6.01E-06 | -1.17E-05 |
| | Rad.Bl | -1.17E-03 | -3.41E-02 | -7.14E-07 | -4.76E-07 |
| Final condition: Formation steel-«plugs» | LEZ | -3.07E-04 | -1.96E-01 | -8.37E-06 | -3.75E-06 |
| | MEZ | -1.48E-02 | -0.862E-01 | -2.81E-06 | -1.09E-06 |
| | HEZ | -8.04E-03 | -5.07E-02 | -1.59E-06 | -6.28E-07 |
| | Ax.Bl | | | -2.72E-06 | -5.40E-06 |
| | Rad.Bl | | | -3.74E-06 | -2.66E-06 |

Since the product of group spectra F^*F^+ appears in the calculation of material worth using disturbance theory, the conclusion on small changes of reactivity characteristics for all areas may turn inexact.

If sodium or both sodium and steel are removed from the upper and lower ends of the core differences of neutronic characteristics on the boundaries with the sodium plenum and lower blanket are getting larger. In this case diffusion approach based calculation can bring error in sodium worth as large as 20% and more. On the other hand, in these areas sodium worth is sufficiently low as compared to that of the core.

Table 6.13 gives integral sodium worth after reactor core reflooding with sodium in final state (diffusion approach). Results of calculations of sodium worth, made using different methods are presented in Figs. 6.9-6.17 and Tables 6.14-6.15.

Sodium and steel removal gives an increase to the positive sodium worth itself, thus decreasing the area of positive SVRE values. Maximum variations is observed at the core top and core bottom. The effect of sodium and steel removal is additive in the central part of the core. The use of the input sodium worth for the disturbed core conditions gives conservative estimation. In case of steel plugs the accuracy of calculation of disturbance area periphery should be regarded carefully. Obviously, it would be difficult in this case to make the simplified correlation between material worth for nondisturbed and final states.

Change of axial distribution of sodium worth:

$\delta RE_{Na}(z) = \frac{RE_{Na}^*(z) - RE_{Na}^0(z)}{RE_{Na}^0(z)}$ is given for the numbers of layers according to the calculation consequence, shown in Fig. 6.13 (transport approximation).

Taking into account transport corrections in sodium worth for the upper core region and sodium plenum is important on the stage preceding sodium boiling, i.e. when there exists rather strong factor of deformation with time of axial sodium temperature profile. On the other hand, these corrections play insignificant role under disturbed conditions considered at practically constant sodium temperatures over the height. In general, results of diffusion calculations of space distribution of the sodium temperatures can be used.

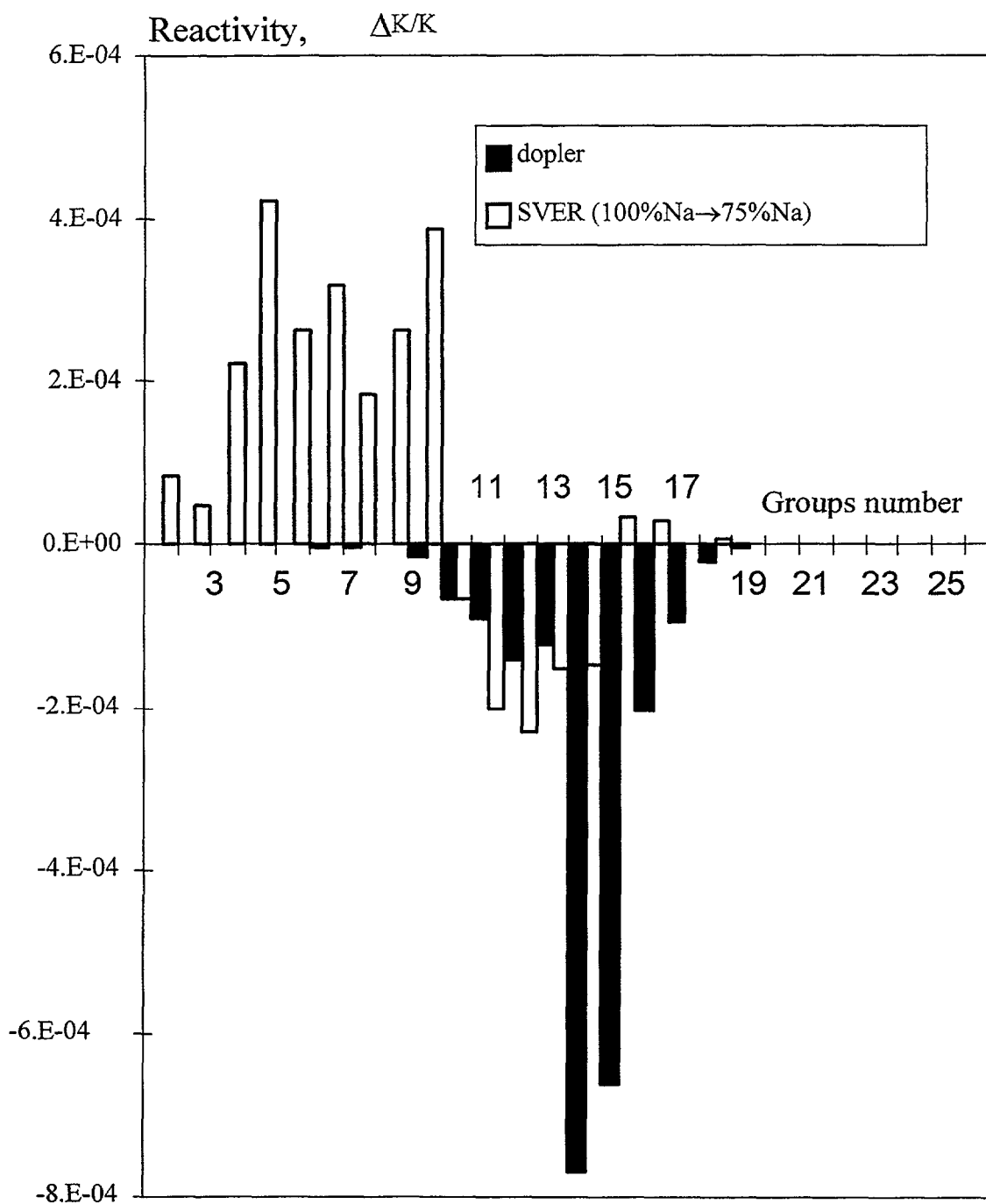


FIG. 6.6. Doppler effect and SVRE spectral representation

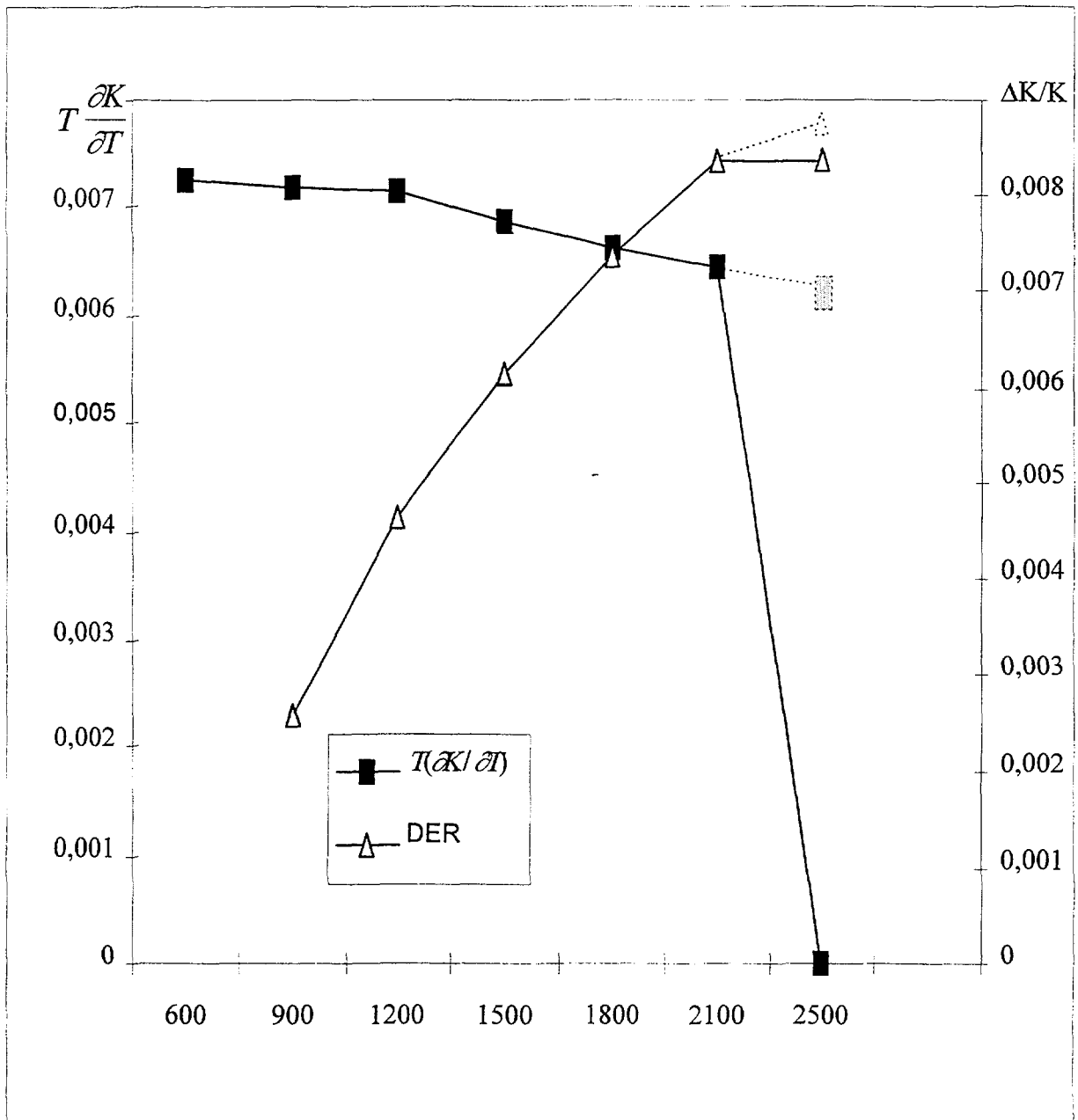


FIG. 6.7. Doppler constant $T \frac{\partial K}{\partial T}$ in various ranges of temperatures

6.4.2. Steel worth

Steel worth integrated over physical zones are given for different conditions of reactor in Table 6.16 (diffusion approach). Spatial distributions of steel worth is presented in Figs.6.18-6.21.

Reactivity effect caused by steel relocation is determined mainly by its concentration change in the areas of disturbance. Change of capture on the steel nuclei is insignificant (Fig.6.22-6.23 and Table 6.17). Contributions to the reactivity effect made by upper and lower plugs have different signs. Upper plugs result in decrease of neutron leakage from the core (positive reactivity effect), while in the lower plugs capture increase exceeds neutron leakage decrease (negative effect) - see Fig.6-18-6.20. Net reactivity caused by the steel relocation is $\sim 3\% \Delta K/K$.

Text cont. on page 228.

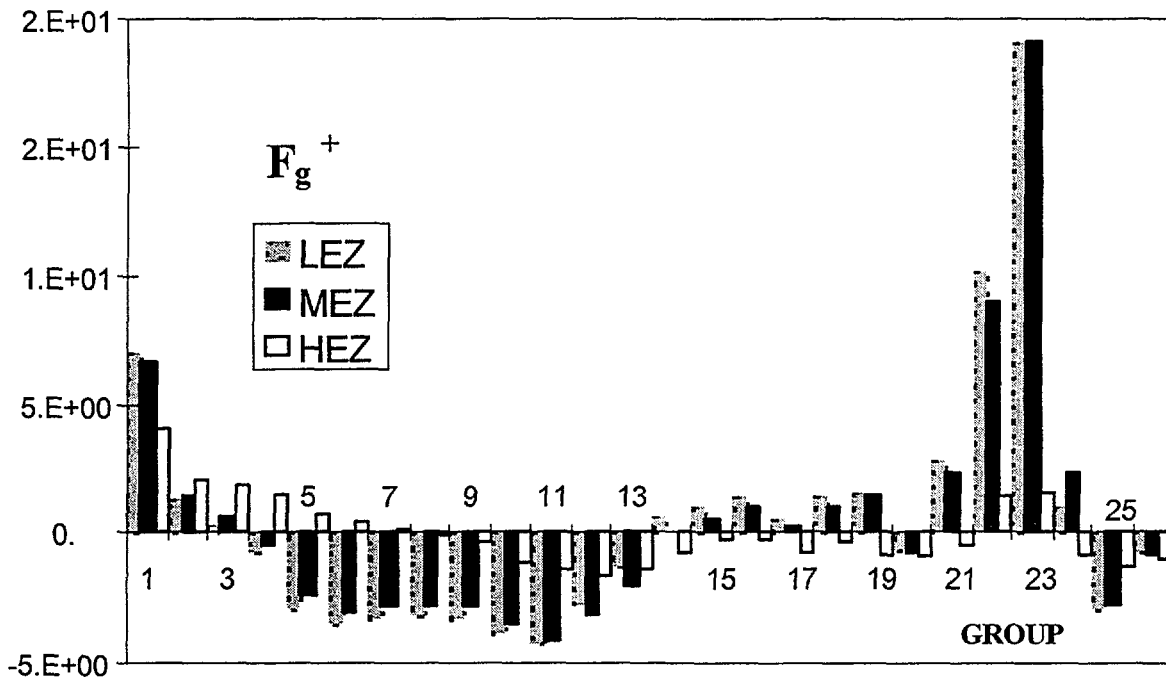
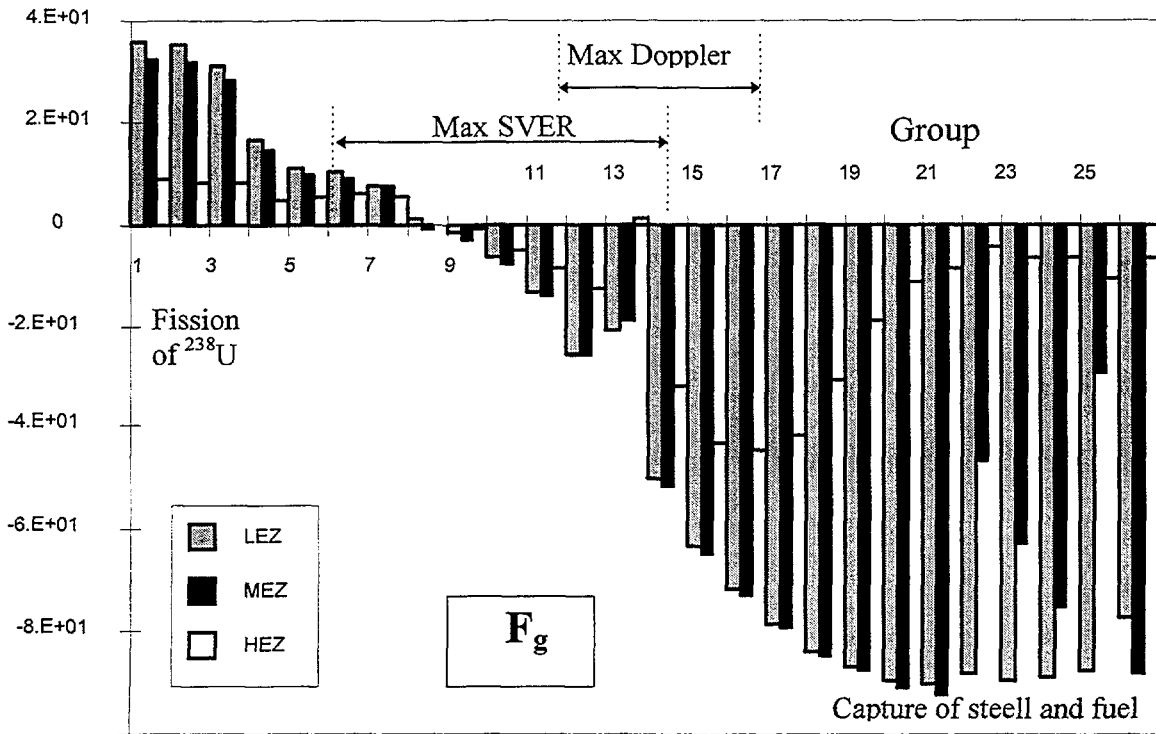


FIG.6.8. Changes of group spectra of a neutrons flux (F_g) and group spectra of the adjoin flux (F_g^+) with transition from the initial condition to a condition with removed sodium and steel of environments for centers LEZ, MEZ and HEZ, (%).

TABLE 6.13. INTEGRAL SODIUM WORTH AFTER REACTOR CORE REFLOODING WITH SODIUM IN THE FINAL CTATE (2100°K,) ΔK/K.

| Zone | DIFFUSION APROACH | | | | | |
|---------------|-------------------|-----------|----------|--|-----------|----------|
| | Initial Condition | | | Final condition (Formation steel-«plugs») | | |
| | LEZ | MEZ | HEZ | LEZ | MEZ | HEZ |
| Axial Blanket | 1,89E-04 | 3,20E-04 | 3,39E-04 | 2,33E-04 | 3,60E-04 | 3,92E-04 |
| CORE | -6,65E-03 | -3,73E-03 | 2,37E-03 | -6,86E-03 | -3,00E-03 | 2,08E-03 |
| Sod.plenum | 2,55E-03 | 1,95E-03 | 1,71E-03 | 3,36E-03 | 2,36E-03 | 1,88E-03 |
| Total | -3,91E-03 | -1,47E-03 | 4,44E-03 | -3,27E-03 | -2,78E-04 | 4,37E-03 |
| Reaktor | | -9,40E-04 | | | 8,22E-04 | |

TABLE 6.14. INTEGRAL OF SODIUM REACTIVITY (10²⁴ NUCLEI) IN ZONES. 2100°K, ΔK/K

| Initial Condition | TRANSPORT APPROACH (TWO DANT CODE) | | | |
|-------------------|------------------------------------|------------|----------|----------|
| | Total in zone | LEZ | MEZ | HEZ |
| Axial Blanket | 0.313 | 1.36E-01 | 1.03E-01 | 7.44E-02 |
| Core | 0.461 | -1.95E-01 | 3.76E-02 | 6.18E-01 |
| Pin plugs | 1.90E-01 | | | |
| Sodium plenum | 0.339 | 1.81E-01 | 1.19E-01 | 9.90E-02 |
| Rad.banket | 0.269 | | | |
| Na=0 | | | | |
| Axial Blanket | 0.418 | 1.84E-1 | 1.38E-01 | 9.55E-02 |
| CORE | 0.817 | -0.925E-1 | 1.53E-01 | 7.56E-01 |
| Pin plugs | 0.308 | | | |
| Sodium plenum | 1.17 | 6.08E-01 | 3.04E-01 | 2.59E-01 |
| Rad.banket | 0.305 | | | |
| Na+Steel=0 | | | | |
| Axial Blanket | 0.487 | 2.23E-01 | 1.62E-01 | 1.02E-01 |
| CORE | 1.04 | 2.71E-2 | 2.74E-01 | 7.35E-01 |
| Pin plugs | 0.378 | | | |
| Sodium plenum | 1.43 | 7.64E-01 | 3.74E-01 | 2.91E-01 |
| Rad.banket | 0.296 | | | |
| Final | | | | |
| Axial Blanket | 0.174 | 4,53E-02 | 6,41E-02 | 6,50E-02 |
| CORE | 0.759 | -1,586E-01 | 1,37E-01 | 7,81E-01 |
| Pin plugs | 0.272 | 1,25E-01 | 6,66E-02 | 8,04E-02 |
| Sodium plenum | 1,15 | 5,99E-01 | 2,68E-01 | 2,80E-01 |
| Rad.banket | 0.282 | | | |

TABLE 6.15. COMPLETE EFFICIENCY SODIUM IN REACTOR AND SODIUM DENSITY COMPONENTS OF TEMPERATURE REACTIVITY COEFFICIENT

| | Na worth, (Δ K/K) | TCR-Na, (ΔK/K) /degree | δTCR-NA, (%) |
|---|----------------------|---------------------------|-----------------|
| Initial condition | 2.85E-02 | -7.93E-06 | - |
| Variant with Na = 0 in SA | 2.51E-02 | -6.98E-06 | -12 |
| Removal of Na and steel (Na + St = 0) | 2.62E-02 | -7.29E-06 | -8.1 |
| Final condition (Formation steel-«plugs») | 2.447E-02 | -6.81E-06 | -14.1 |

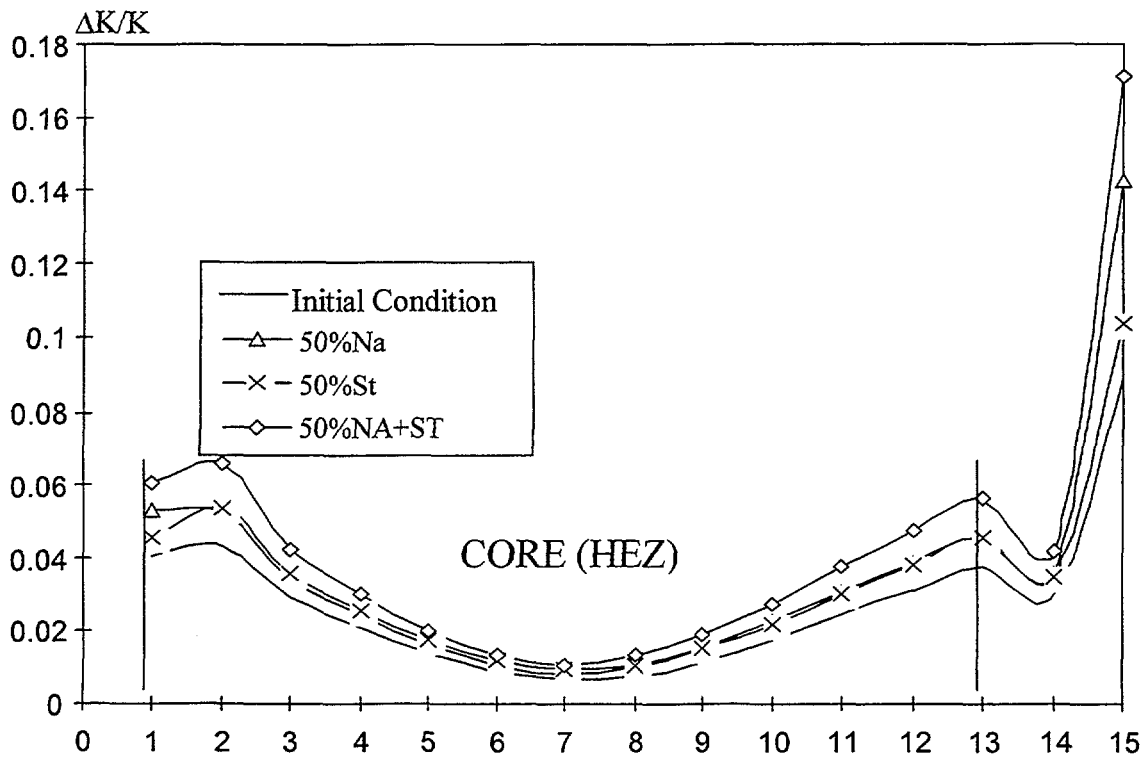
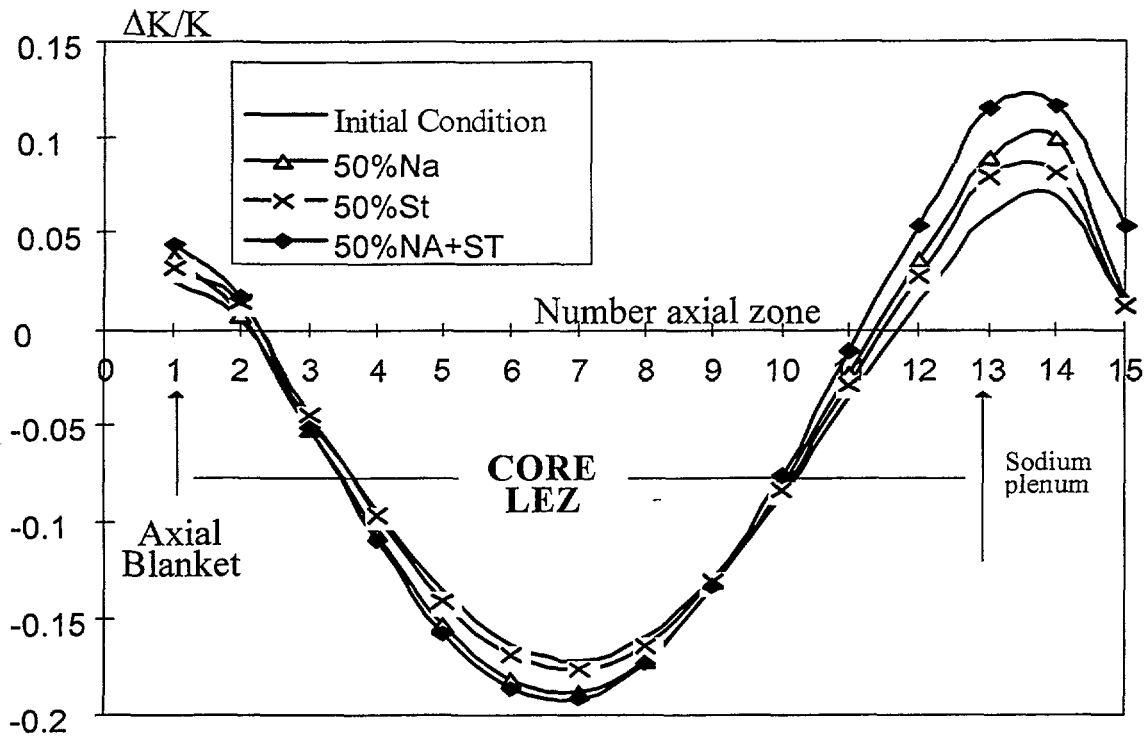


FIG.6.9. Axial distribution of efficiency sodium with concentration 10^{24} nucl./cm³ integrated on the LEZ and HEZ square (diffusion approach)

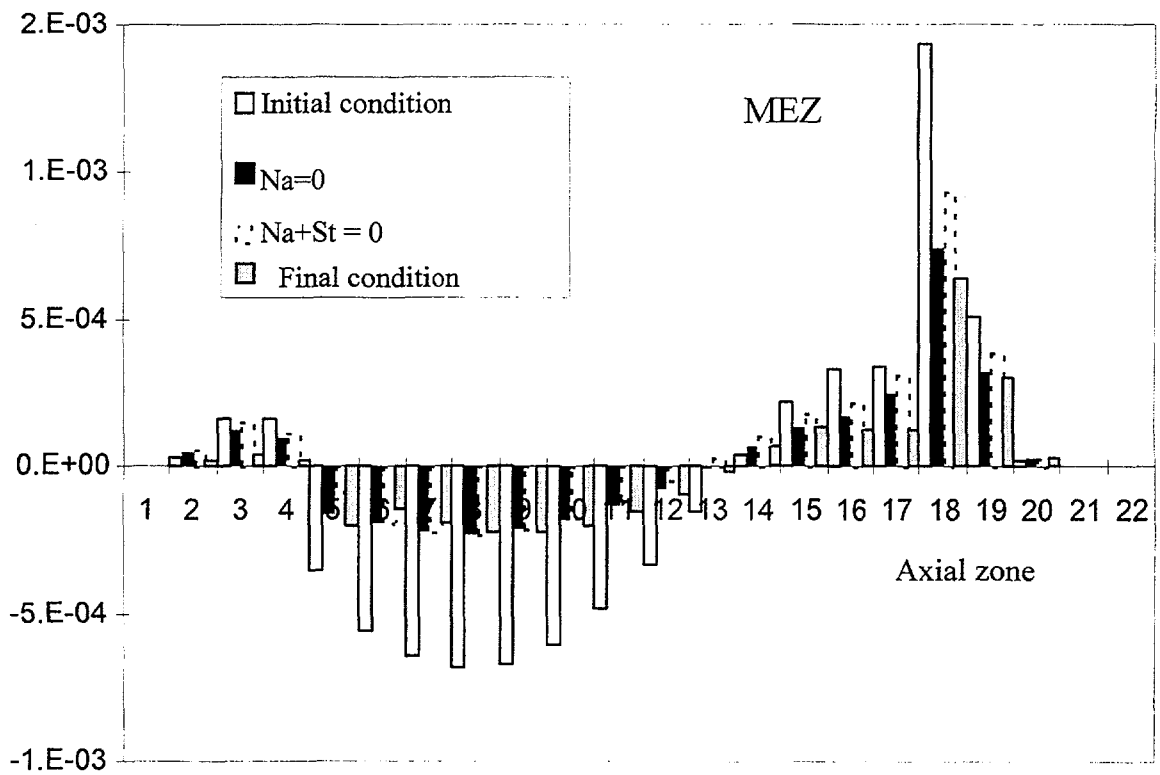
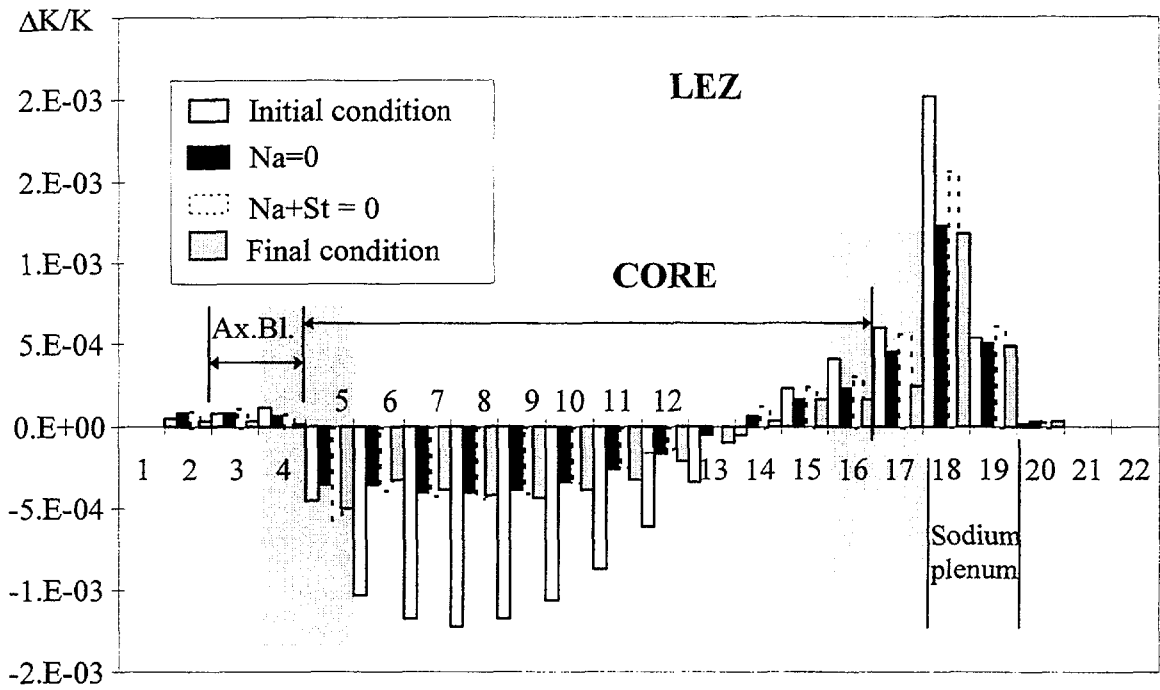


FIG.6.10. Axial distribution of integral sodium worth in Lez and MEZ taking into account sodium concentration change in zones. (2100°K, diffusion approach)

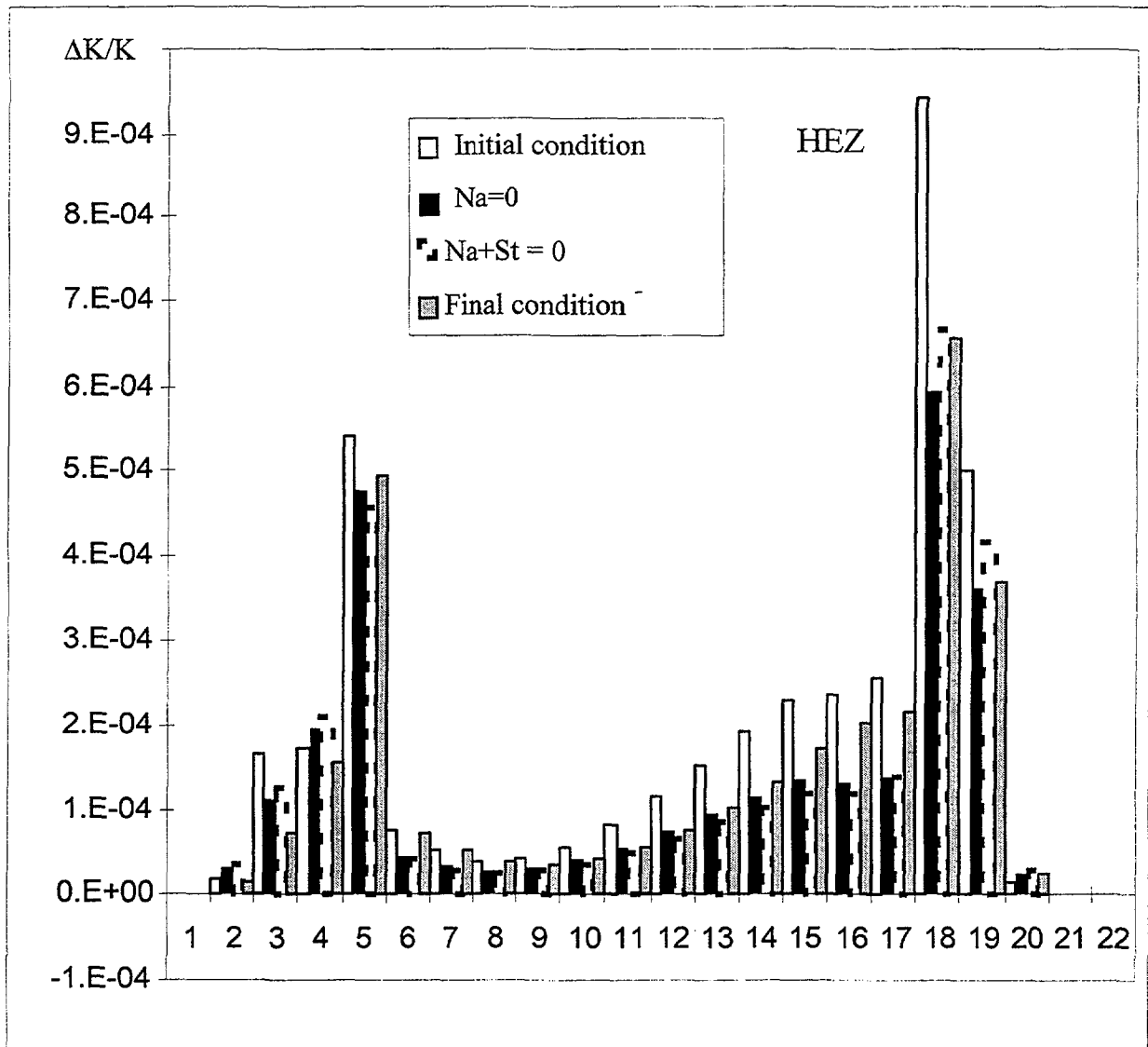
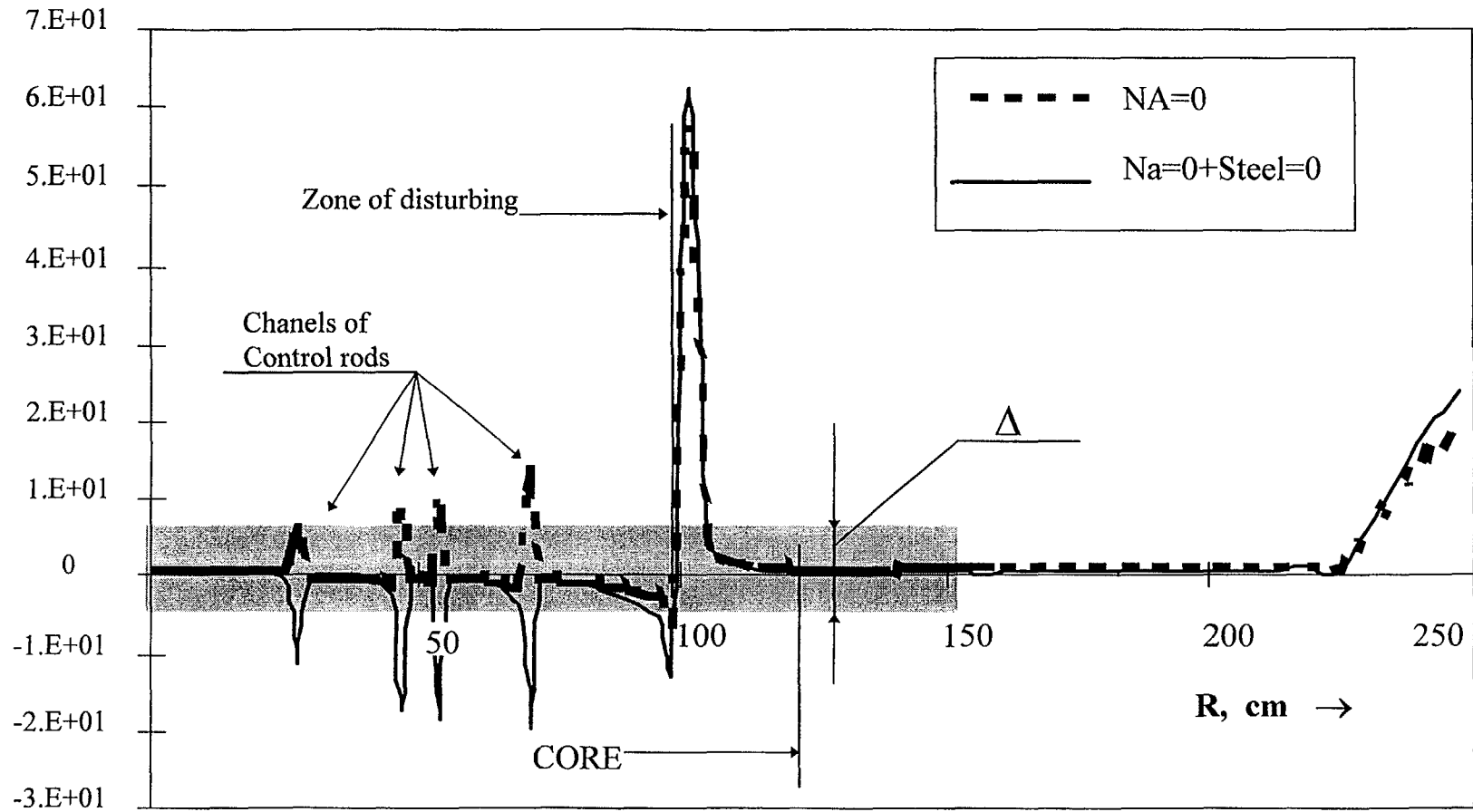


FIG.6.11. Axial distribution of integral sodium worth in HEZ taking into account sodium concentration change in zones. (2100°K, diffusion approach)



6.12 Change of radial distribution in a central plane of the core of sodium efficiency (1 m^3 , 10^{24} nuclei) in % in relation to the initial condition (Transport approach - S_8)

$$\Delta_R = \max \left\{ \frac{RE_{Na}^{diff}(r) - RE_{Na}^{transp}(r)}{RE_{Na}^{transp}(r)} \right\} - \text{For a central layer by thickness } 10 \text{ cm}$$

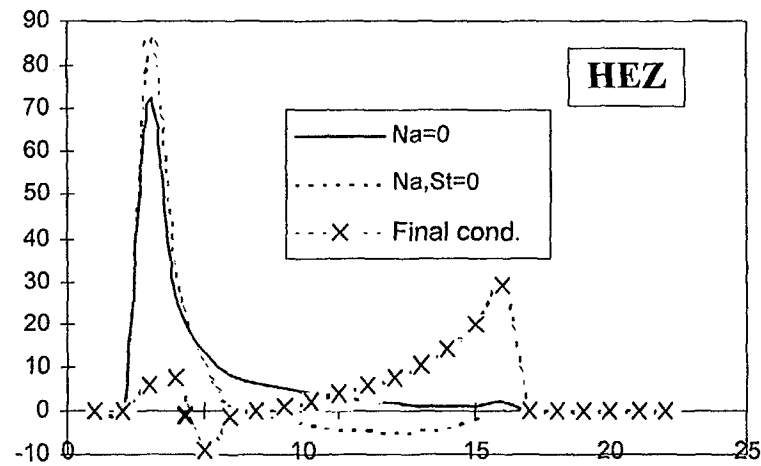
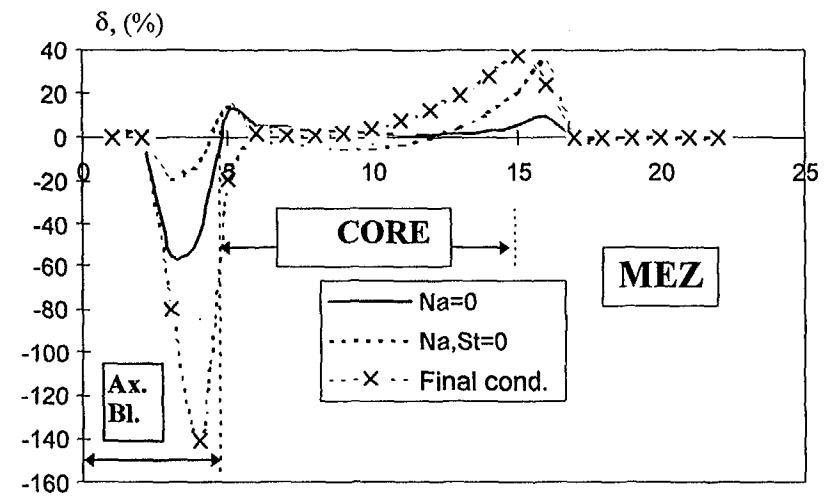
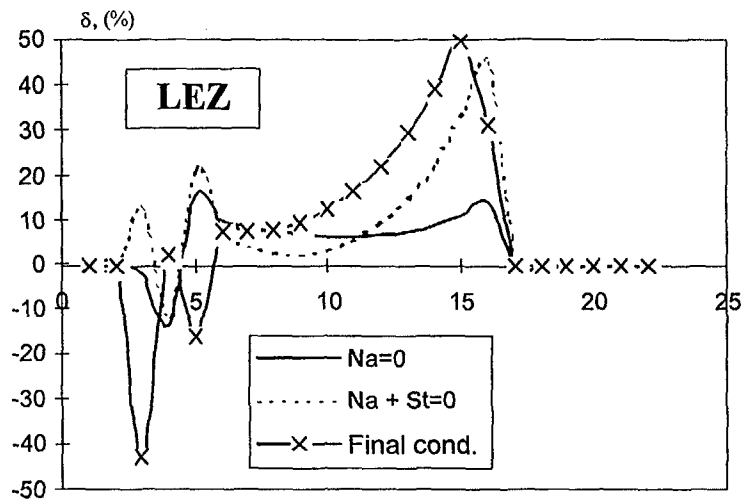


Fig.6.13 . Change of axial distribution of efficiency sodium as $\delta RE_{Na}(z) = \frac{RE_{Na}^+(z) - RE_{Na}^0(z)}{RE_{Na}^0(z)}, (\%)$ (TWODANT calculations)

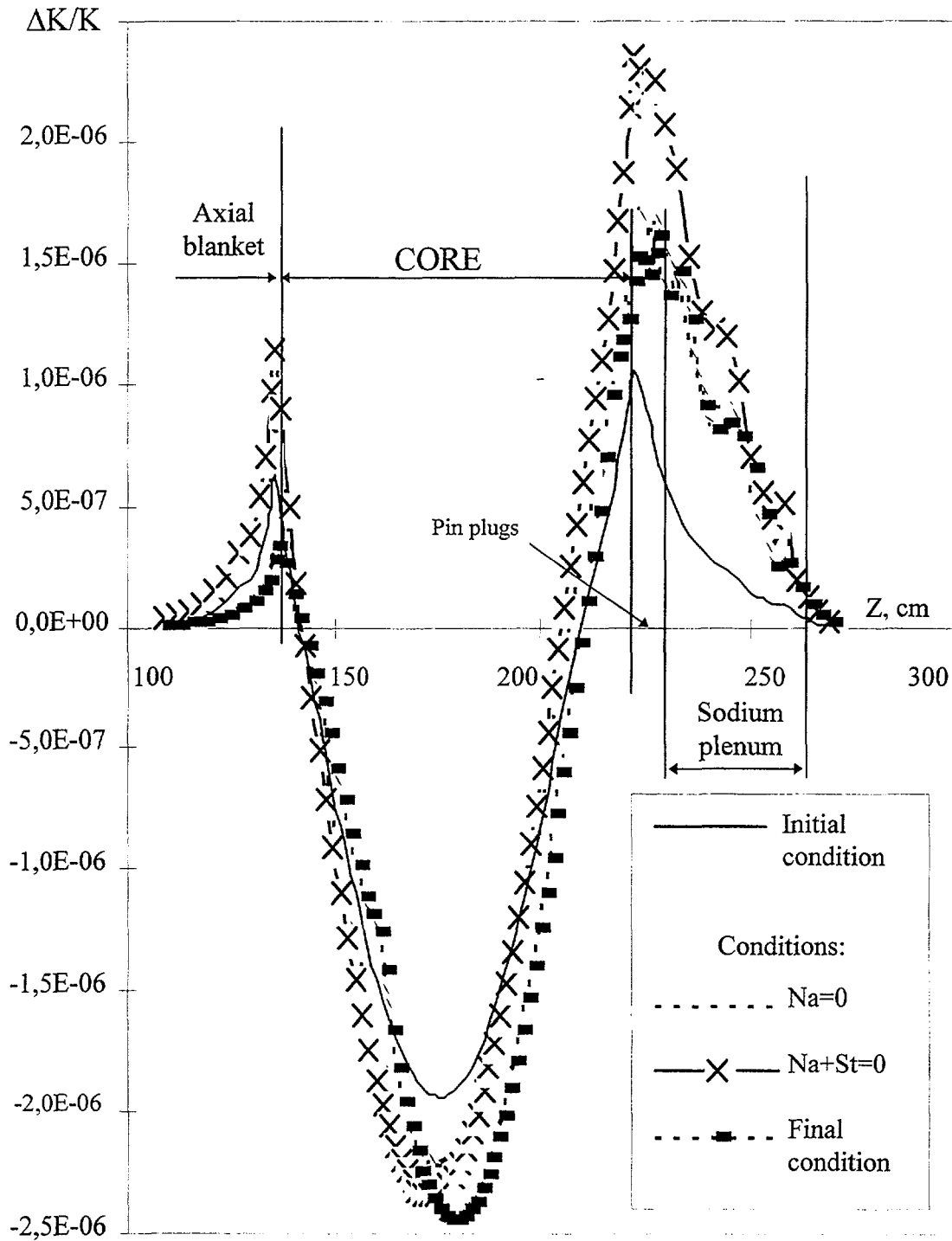


FIG.6.14. Distribution of worth of 1 cm^3 of sodium (10^{24} nuclei) over the core height in LEZ central area (transport approach - TWODANT code)

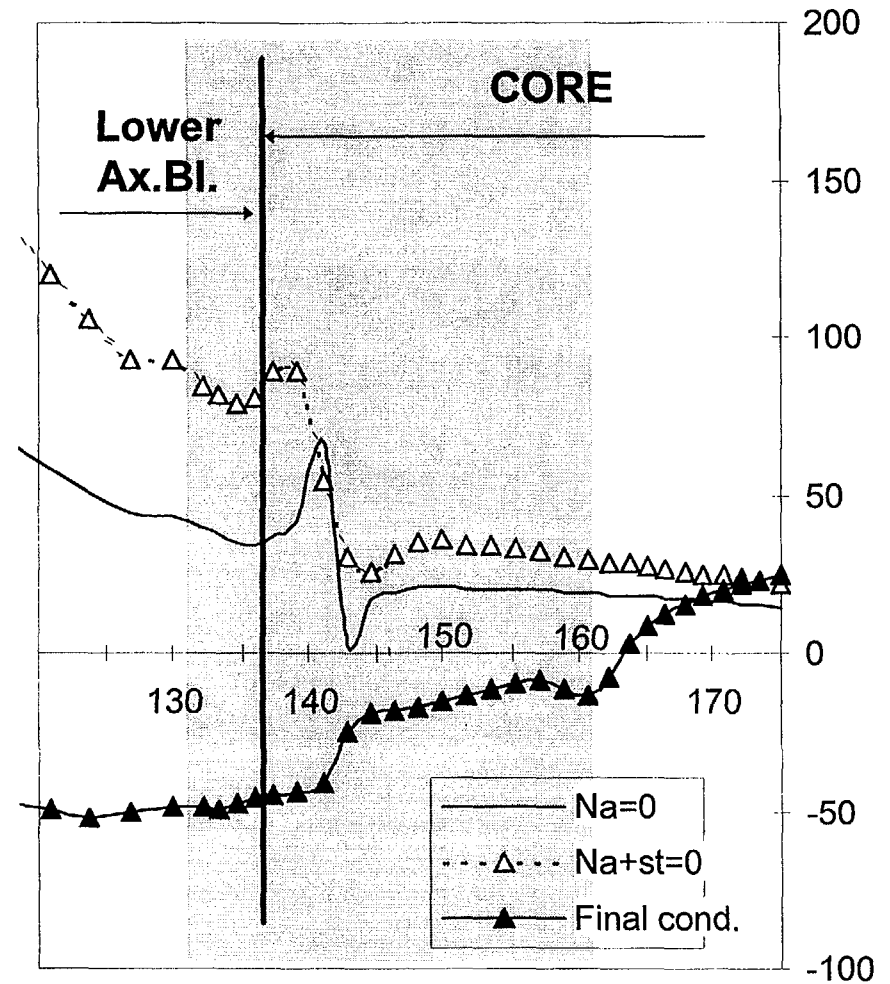
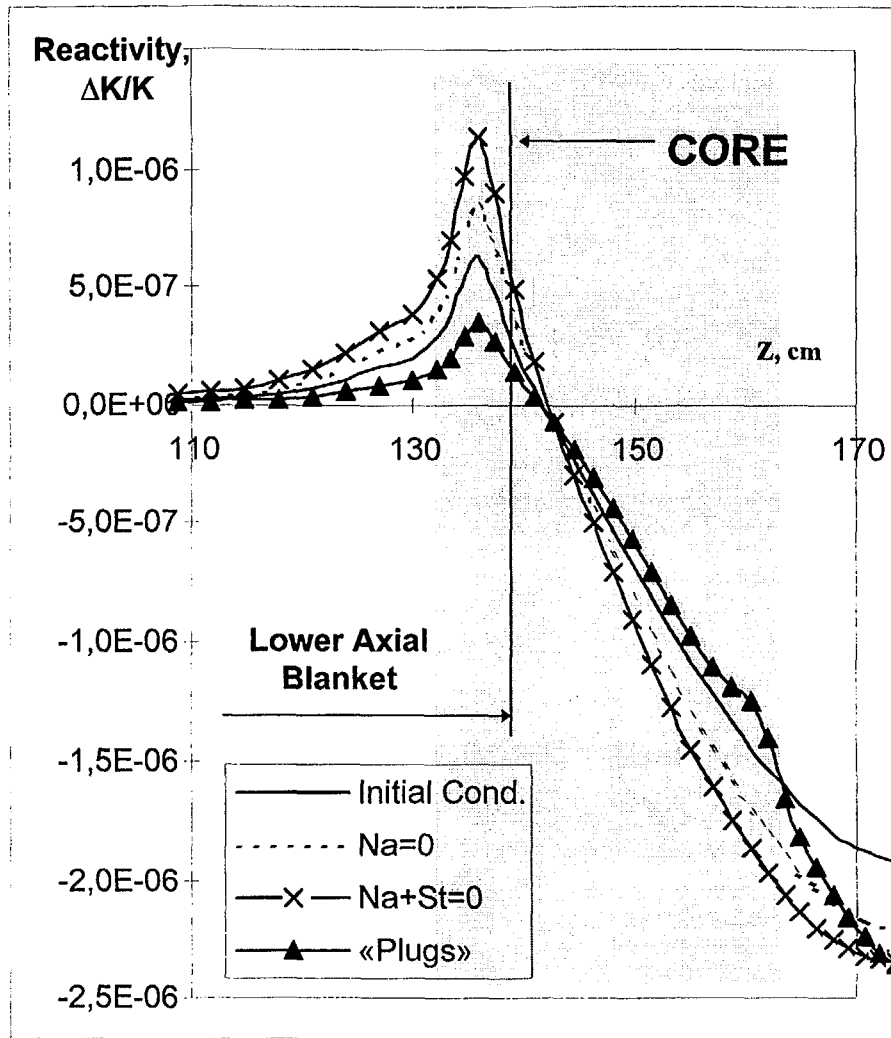


FIG.6.15. Axial distribution of worth of $1 \text{ cm}^3 \text{ Na}$ (with concentration 10^{24} nucl.) and its change in % of the initial value in the area of location of lower steel-«plugs» for different conditions of the core (2100°K , transport approach)

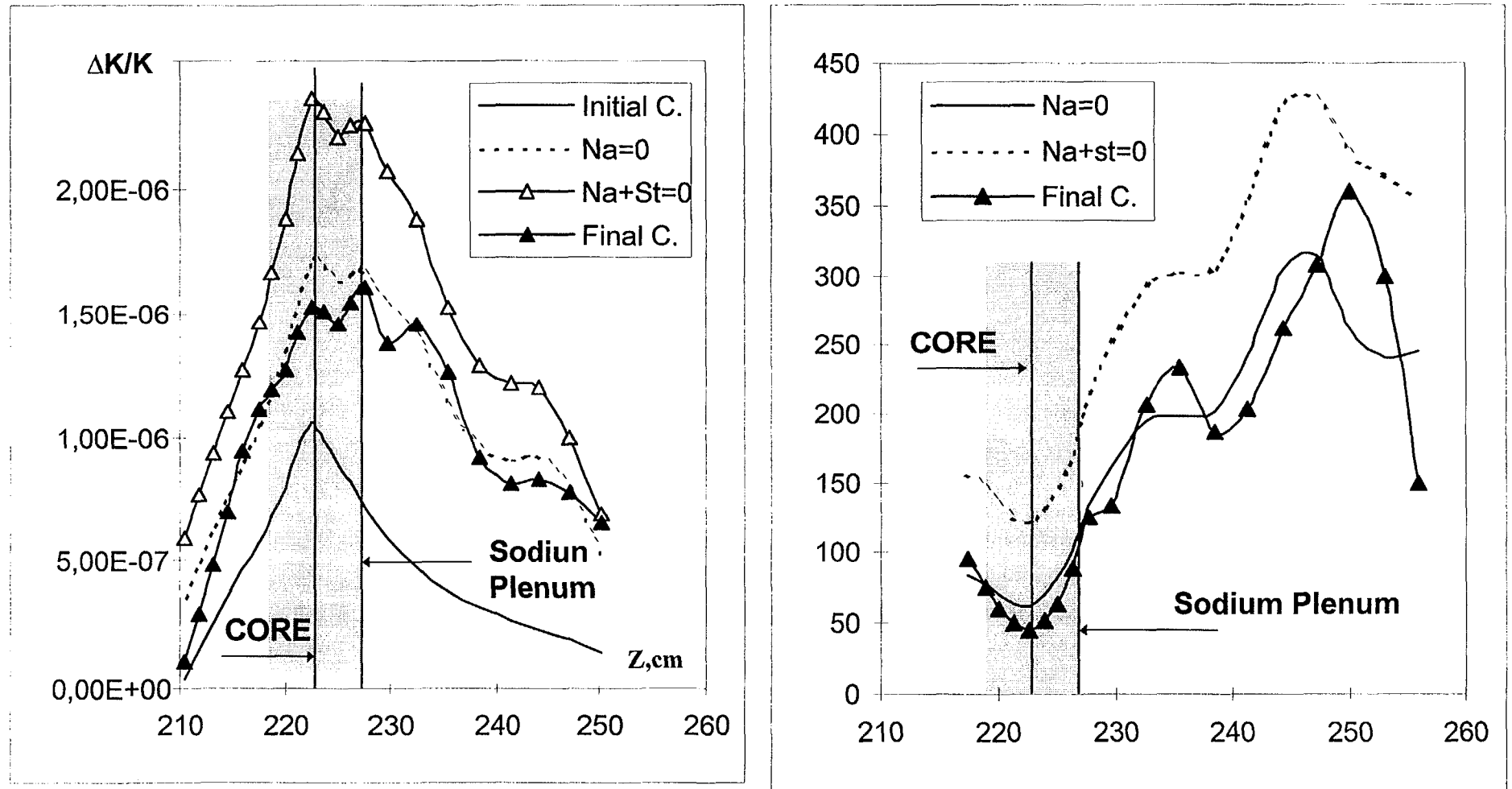


FIG.6.16. Axial distribution of worth of $1 \text{ cm}^3 \text{ Na}$ (with concentration 10^{24} nucl.) and its change in % of the initial value in the area of location of top steel-«plugs» for different conditions of the core (2100°K , transport approach)

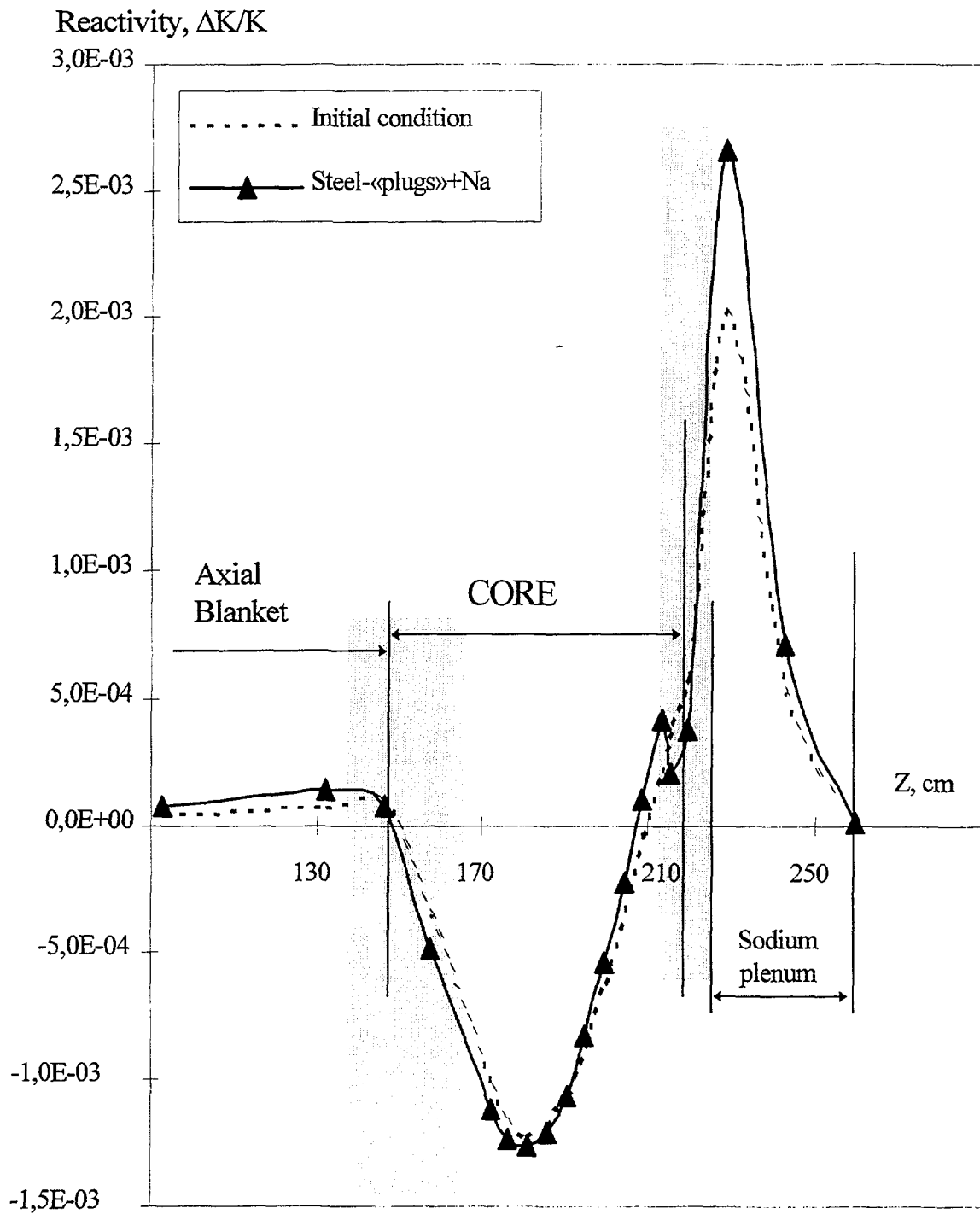


FIG.6.17. Axial distribution of integral sodium worth in LEZ after its bringing back to the core under final condition (2100°K, diffusion approach)

TABLE 6.16. STEEL WORTH INTEGRATED OVER PHYSICAL ZONES, $\Delta K/K$ (2100°K, DIFFUSION APPROACH).

| Zone | Condition | | | |
|---------------|-----------|-----------|-----------|-------------|
| | Initial | Na=0 | Na+St=0 | St.-«plugs» |
| LEZ | | | | |
| Ax. Blanket | 4,08E-04 | 6,37E-04 | 7,51E-04 | 3,13E-04 |
| CORE | -2,46E-02 | -2,30E-02 | -8,33E-03 | -1,70E-02 |
| Pin plugs | 1,88E-03 | 2,76E-03 | 3,50E-03 | 5,57E-03 |
| Sodium plenum | 1,10E-03 | 2,10E-03 | 2,68E-03 | 2,01E-03 |
| TOTAL | -2,12E-02 | -1,75E-02 | -1,30E-03 | -9,11E-03 |
| MEZ | | | | |
| Ax. Blanket | 6,50E-04 | 8,95E-04 | 1,08E-03 | 5,06E-04 |
| CORE | -1,35E-02 | -1,15E-02 | -3,52E-03 | -7,58E-03 |
| Pin plugs | 8,92E-04 | 1,44E-03 | 1,85E-03 | 2,66E-03 |
| Sodium plenum | 7,57E-04 | 1,28E-03 | 1,58E-03 | 1,13E-03 |
| TOTAL | -1,11E-02 | -7,85E-03 | 1,05E-03 | -3,28E-03 |
| HEZ | | | | |
| Ax. Blanket | 6,70E-04 | 8,60E-04 | 9,31E-04 | 6,09E-04 |
| CORE | 6,84E-04 | 1,86E-03 | 1,58E-03 | 2,95E-03 |
| Pin plugs | 6,34E-04 | 8,02E-04 | 8,05E-04 | 1,27E-03 |
| Sodium plenum | 6,33E-04 | 1,12E-03 | 1,27E-03 | 1,20E-03 |
| TOTAL | 2,62E-03 | 4,67E-03 | 4,62E-03 | 6,03E-03 |

TABLE 6.17. INTEGRALS OF NUMBERS OF CAPTURES ON IRON IN ZONES

| Nc- FE | Initial cond. | NA+ST=0 | Formation steel-«plugs» |
|--------------|---------------|----------|-------------------------|
| Total in LEZ | 4,07E-07 | 2,17E-07 | 3,79E-07 |
| Total in MEZ | 3,31E-07 | 1,69E-07 | 2,95E-07 |

6.4.3. Fuel worth

Integral fuel worth in reactor zones obtained using different approaches are given in Table 6.18 and Fig.6.24, spatial distribution being presented in Fig.6.25-6.30.

Within the core, fuel worth difference between diffusion and transport calculation is insignificant, thus allowing to use diffusion calculation results. Fuel worth change is insignificant just for the types of disturbances considered, however these are quite different from the initial state worth. New worth values should be used for description of molten fuel relocation. Using data obtained for initial, undisturbed state, would result in lower reactivity effects, i.e. in the more pessimistic estimations. In this case LEZ would give highest error (Fig.6.24).

6.5. REACTIVITY EFFECTS CAUSED BY MATERIAL EXPANSION

Table 6.19 gives comparison of integral values of reactivity coefficients caused by thermal expansion of the core materials (calculation based on disturbance theory, transport approach, 2100°K). Thereby, use of reactivity feedback component obtained for the initial condition gives more pessimistic evaluation in the emergency process description because of the thermal expansion of material.

TABLE 6.18. INTEGRAL WORTH OF FUEL, $\Delta K/K$ (2100°K).

| Zone | Approach | Condition | | | |
|-----------------|-----------|-----------|-----------|------------|-----------|
| | | Initial | Na=0 | Na+Steel=0 | «Plugs» |
| LEZ | Diffusion | 1.5533E-1 | 1.7115E-1 | 1.7578E-1 | 1.6959E-1 |
| | Transport | 1,57E-01 | 1,72E-01 | 1,77E-01 | 1,70E-01 |
| MEZ | Diffusion | 1.2374E-1 | 1.3061E-1 | 1.3007E-1 | 1.2587E-1 |
| | Transport | 1,24E-01 | 1,30E-01 | 1,29E-01 | 1,25E-01 |
| HEZ | Diffusion | 1.1167E-1 | 1.1894E-1 | 1.1282E-1 | 1.1399E-1 |
| | Transport | 1,11E-01 | 1,18E-01 | 1,11E-01 | 1,13E-01 |
| Rad/Bl. | Diffusion | 8.7592E-3 | 9.352E-3 | 9.5670E-3 | 9.4997E-3 |
| Ax/Bl. LEZ | Diffusion | -1.30E-3 | -1.27E-3 | -1.46E-3 | -7.42E-4 |
| | Transport | -1,98E-03 | -1,87E-03 | -2,07E-03 | -1,47E-03 |
| Ax/Bl. MEZ | Diffusion | -2.90E-5 | 1.94E-4 | 2.87E-4 | -6.00E-5 |
| | Transport | 1,93E-05 | 4,04E-04 | 6,24E-04 | -2,09E-04 |
| Ax/Bl. HEZ | Diffusion | 3.14E-4 | 5.39E-4 | 5.82E-4 | 3.33E-4 |
| | Transport | 6,55E-04 | 9,62E-04 | 1,02E-03 | 6,93E-04 |
| Σ Ax/Bl. | Diffusion | -1.01E-3 | -5.38E-4 | -5.87E-4 | -4.69E-4 |
| | Transport | -1,30E-3 | -5,00E-4 | -4,26E-4 | -9,86E-4 |

6.6. NEUTRON KINETICS FUNCTIONALS

Tables 6.20 and 6.21 give neutron kinetics parameters obtained for sequential change of the core states (data, obtained using flux and worth evaluated by TWODANT code are also presented for the initial undisturbed state). Analysis results show that neutron kinetics parameters changes are insignificant when changing over from one state to another, and hence values obtained for undisturbed core state can be used.

TABLE 6.19. REACTIVITY EFFECTS FROM EXPANSION OF MATERIALS (TRANSPORT APPROACH, 2100°K)

| | | Condition | | | |
|---|-----------------------|------------|------------|------------|-------------------|
| | | Initial | Na=0 | Na+St=0 | Steel- «plugs» |
| R-Leakage (δK_1) | | 0.077935 | 0.084048 | 0.087183 | 0.0830861 |
| Z Leakage (δK_2) | | 0.12618 | 0.14571 | 0.15496 | 0.14833 |
| δK_3 | | 0.26936 | 0.29117 | 0.29617 | 0.288515 |
| TCR (1/degree) | from radial expansion | -.13065E-4 | -.14622E-4 | -.15268E-4 | -.14699E-4 |
| TCR (1/degree) | from axial expansion | -.17146E-5 | -.1849E-5 | -.1918E-5 | -.18279E-5 |
| Complete reactivity in reactors, ($\Delta K/K$) | sodium | .28501E-1 | .25074E-1 | .26182E-1 | .24469E-1 |
| Sodium component in TCR (1/degree) | density | -.79324E-5 | -.69788E-5 | -.7287E-5 | -.68103E-5 |

Text cont. on page 241.

TABLE 6.20.EFFECTIVE SHARE OF DELAATED NEUTRONS

| Condition | β_1 | β_2 | β_3 | β_4 | β_5 | β_6 | β_{eff} |
|---|-----------|-----------|-----------|-----------|-----------|-----------|----------------------|
| The initial condition (Diffusion approfch) | 8.5343E-5 | 6.7765E-4 | 5.4146E-4 | 1.2906E-3 | 7.5260E-4 | 2.7316E-4 | 3.6208E-3 |
| The initial condition (Transport approfch) | 8.5010E-5 | 6.7628E-4 | 5.3717E-4 | 1.2760E-3 | 7.4267E-4 | 2.6874E-4 | 3.5859E-3 |
| Heating up to 3500 ^{°E} | 8.4838E-5 | 6.7524E-4 | 5.3600E-4 | 1.2736E-3 | 7.4125E-4 | 2.6821E-4 | 3.5792E-3 |
| Sodium «boiling» | 8.5031E-5 | 6.7639E-4 | 5.4097E-4 | 1.2950E-3 | 7.5670E-4 | 2.7510E-4 | 3.6292E-3 |
| Remjval of steel of pins | 8.5185E-5 | 6.7758E-4 | 5.4946E-4 | 1.3318E-3 | 7.8358E-4 | 2.8717E-4 | 3.7148E-3 |
| The final condition (formation Steel-«plugs») | 8.4897E-5 | 6.7563E-4 | 5.4135E-4 | 1.2983E-3 | 7.5975E-4 | 2.7649E-4 | 3.6364E-3 |

TABLE 6.21. CONSTANT DISINTEGRATION OF NUCLEUSES-PREDECESSORS (1/SEC) AND TIME OF LIFE OF INSTANT NEUTRONS.

| Condition | λ_1 | λ_2 | λ_3 | λ_4 | λ_5 | λ_6 | $L_{i\ddot{a}i} * 10^{-6}$ (sec) |
|---|-------------|-------------|-------------|-------------|-------------|-------------|-------------------------------------|
| The initial condition | 1.3403E-2 | 3.0771E-2 | 1.1733E-1 | 3.0797E-1 | 8.8055E-1 | 2.9481E+0 | 4.3604E-7 |
| Heating up to 3500 ^{°E} | 1.3403E-2 | 3.0771E-2 | 1.1733E-1 | 3.0797E-1 | 8.8055E-1 | 2.9481E+0 | 4.2348E-7 |
| Sodium «boiling» | 1.3406E-2 | 3.0785E-2 | 1.1748E-1 | 3.0845E-1 | 8.8140E-1 | 2.9520E+0 | 3.9613E-7 |
| Remjval of steel of pins | 1.3413E-2 | 3.0804E-2 | 1.1774E-1 | 3.0928E-1 | 8.8285E-1 | 2.9586E+0 | 3.6997E-7 |
| The final condition (formation Steel-«plugs») | 1.3407E-2 | 3.0785E-2 | 1.1751E-1 | 3.0858E-1 | 8.8162E-1 | 2.9531E+0 | 3.7294E-7 |

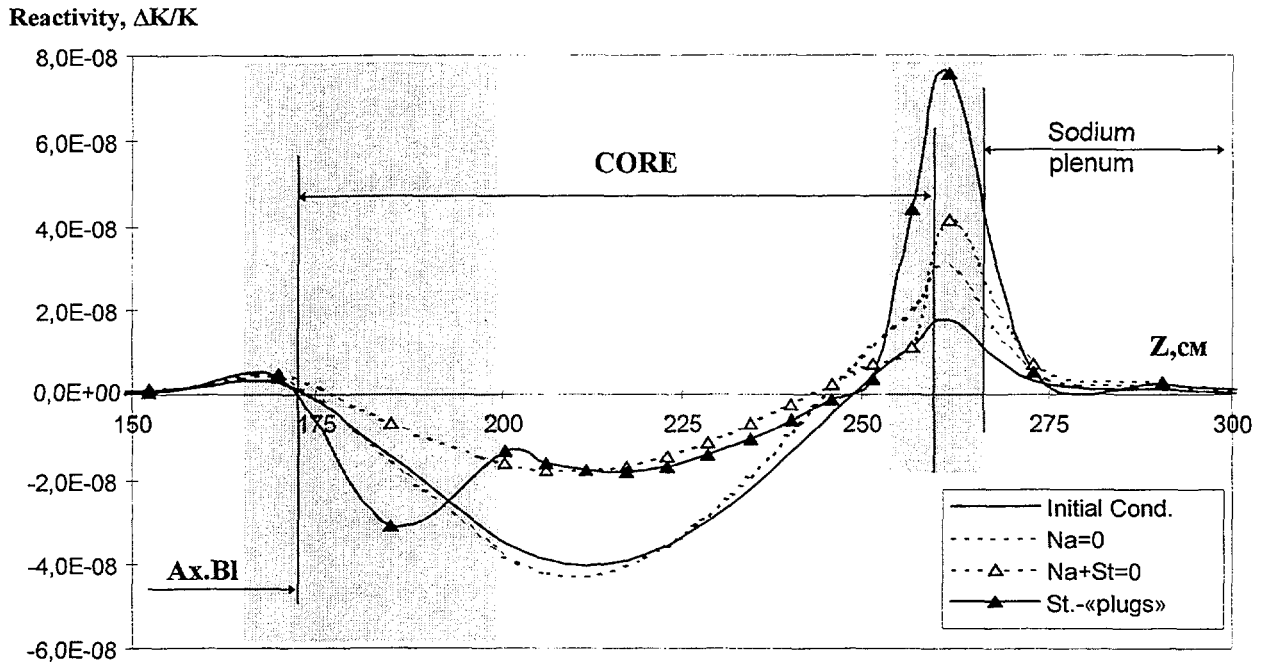


FIG. 6.18. Axial distribution of steel worth under perturbed conditions for the core centre (2100°K diffusion approach)

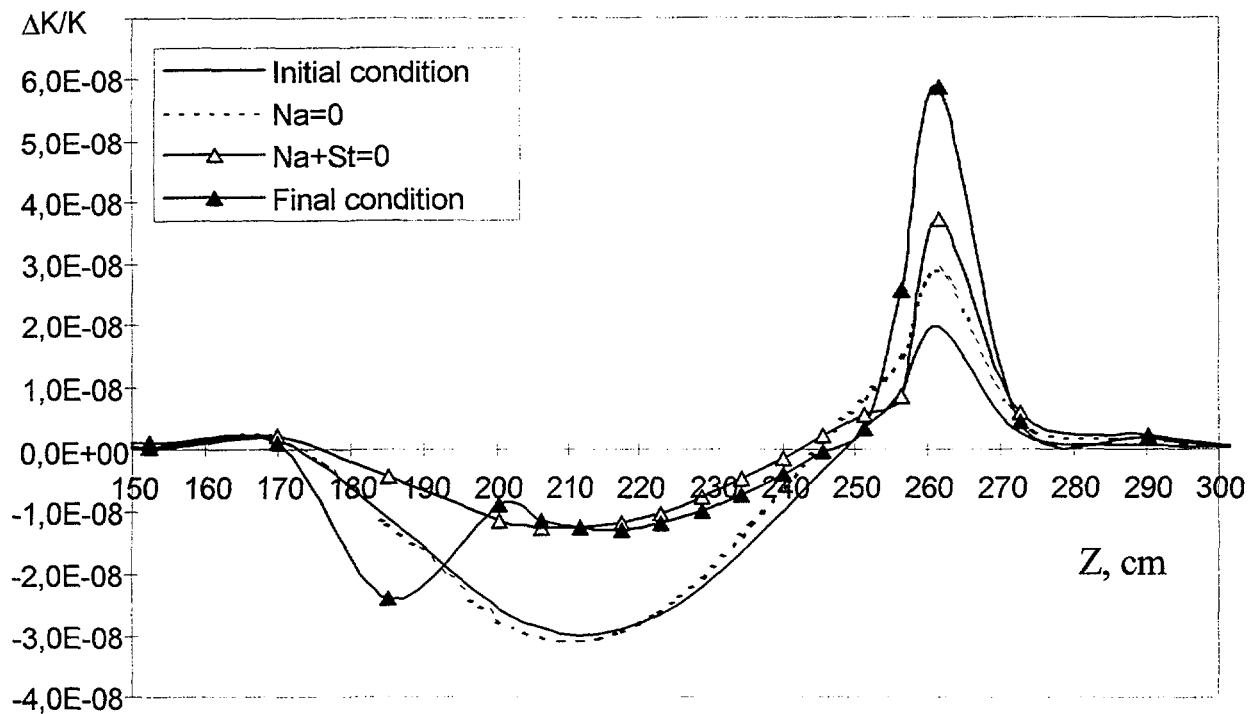


FIG. 6.19. Axial distribution of steel worth integrated over LEZ radius caused by its redistribution in the core under perturbed conditions (2100°K, diffusion approach)

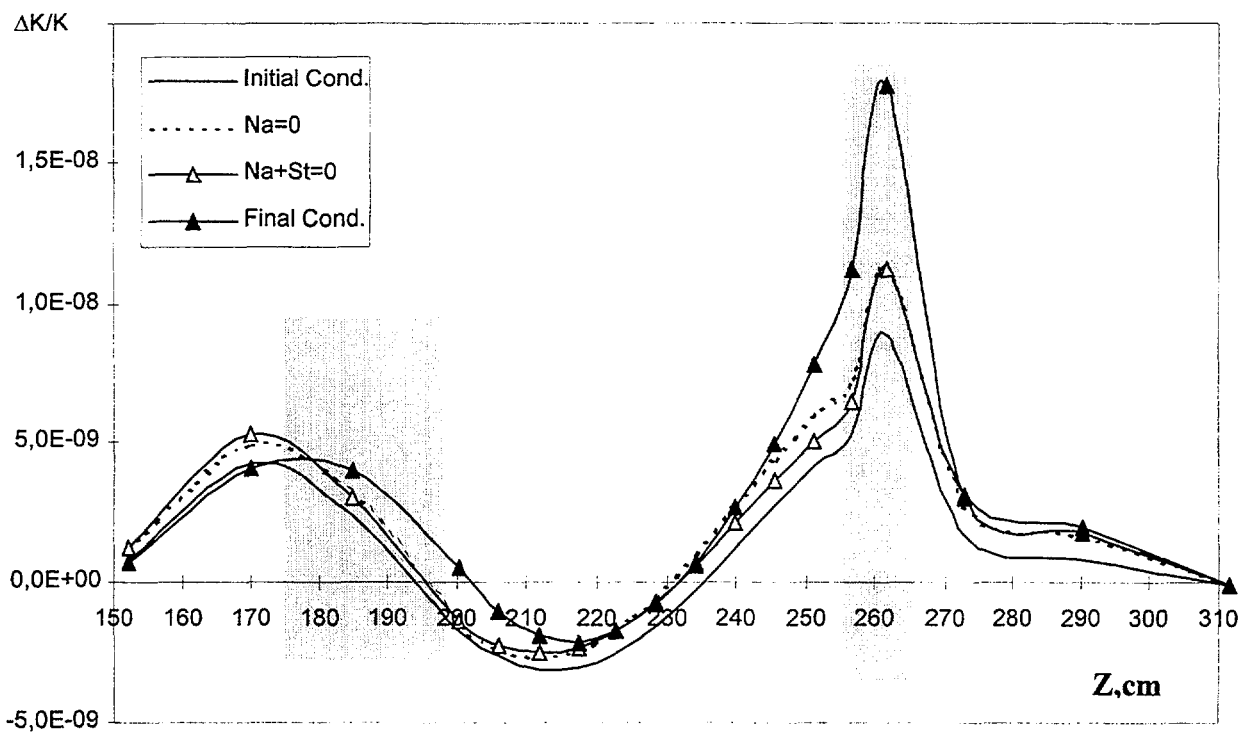
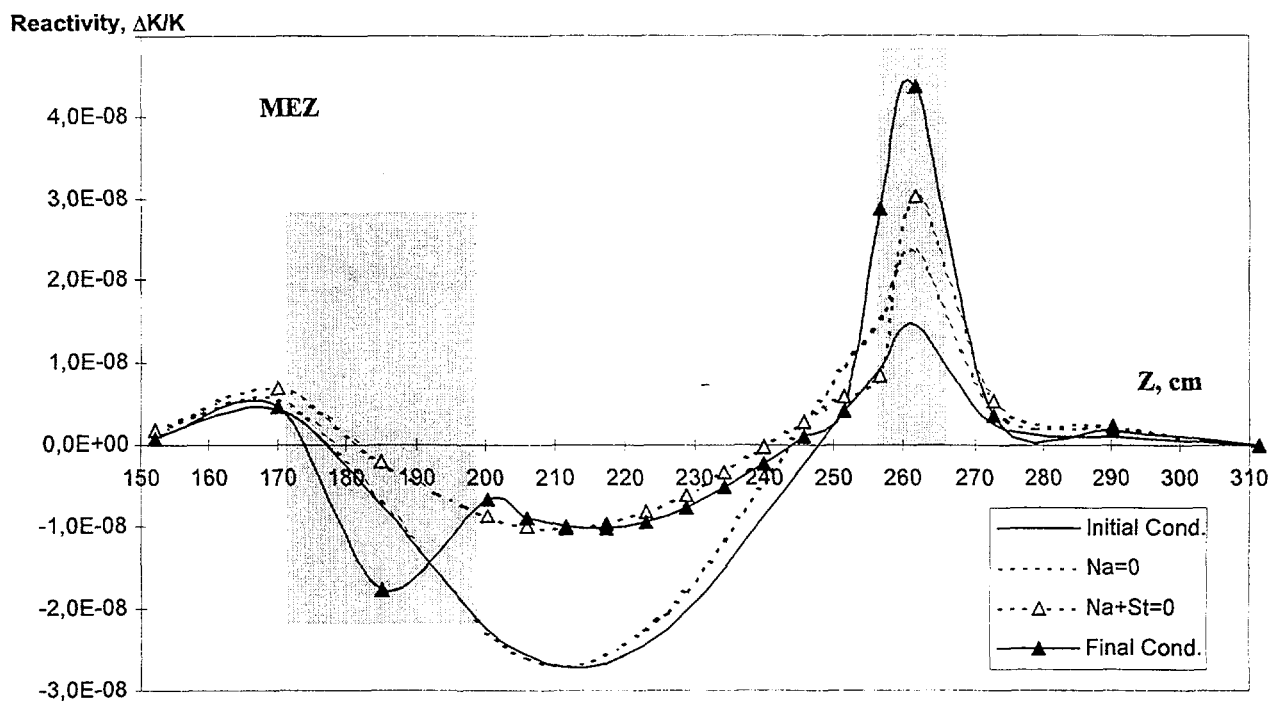


FIG.6.20. Axial distribution of steel worth integrated over MEZ and HEZ radius caused by its redistribution in the core under perturbed conditions (2100°K , diffusion approach)

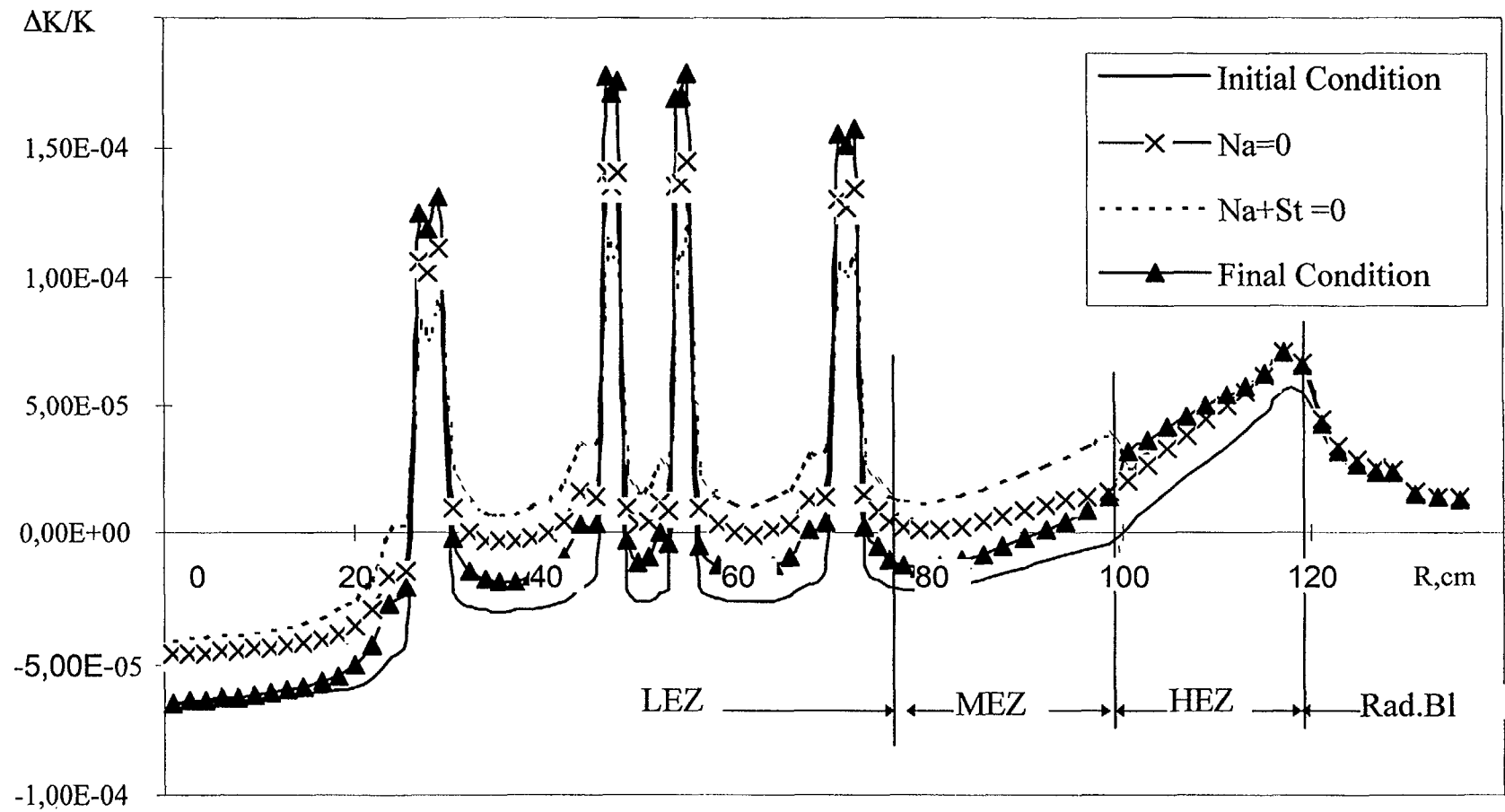


FIG.6.21. Worth of elementary Fe column with cross section of 1 cm^2 and $\Delta Z=H_{\text{core}}$ with 10^{24} nuclei over radius of reactor (transport approach, 2100°K)

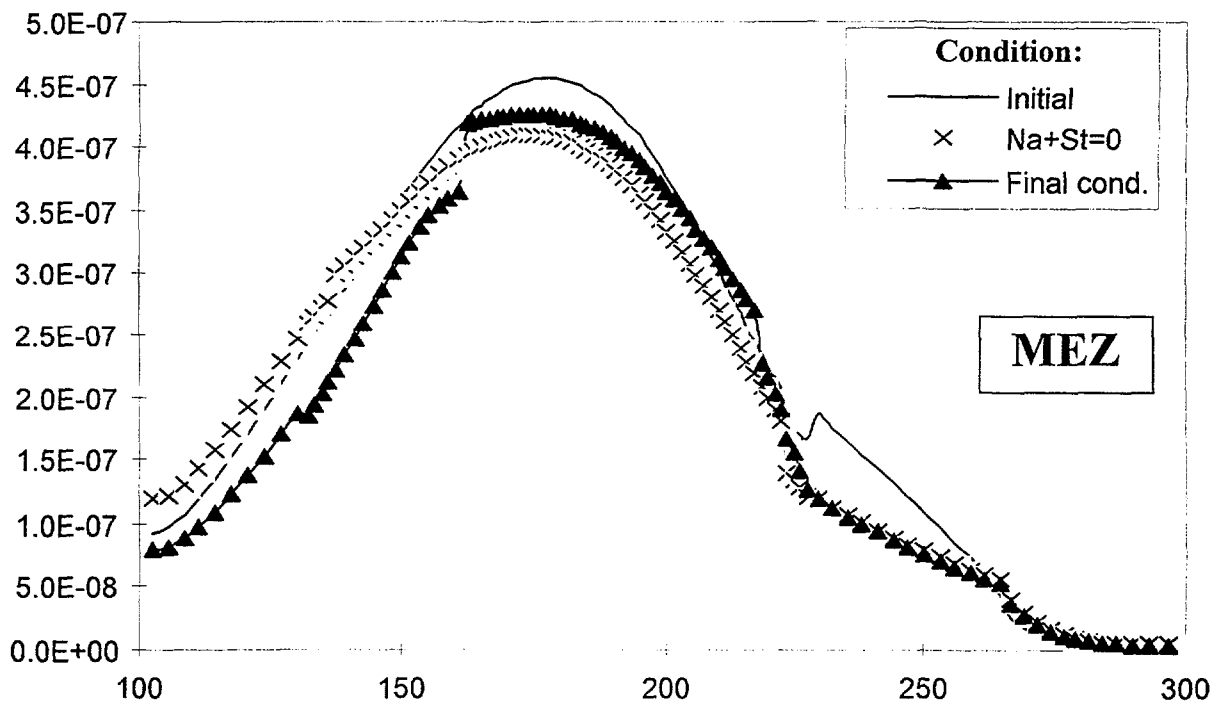
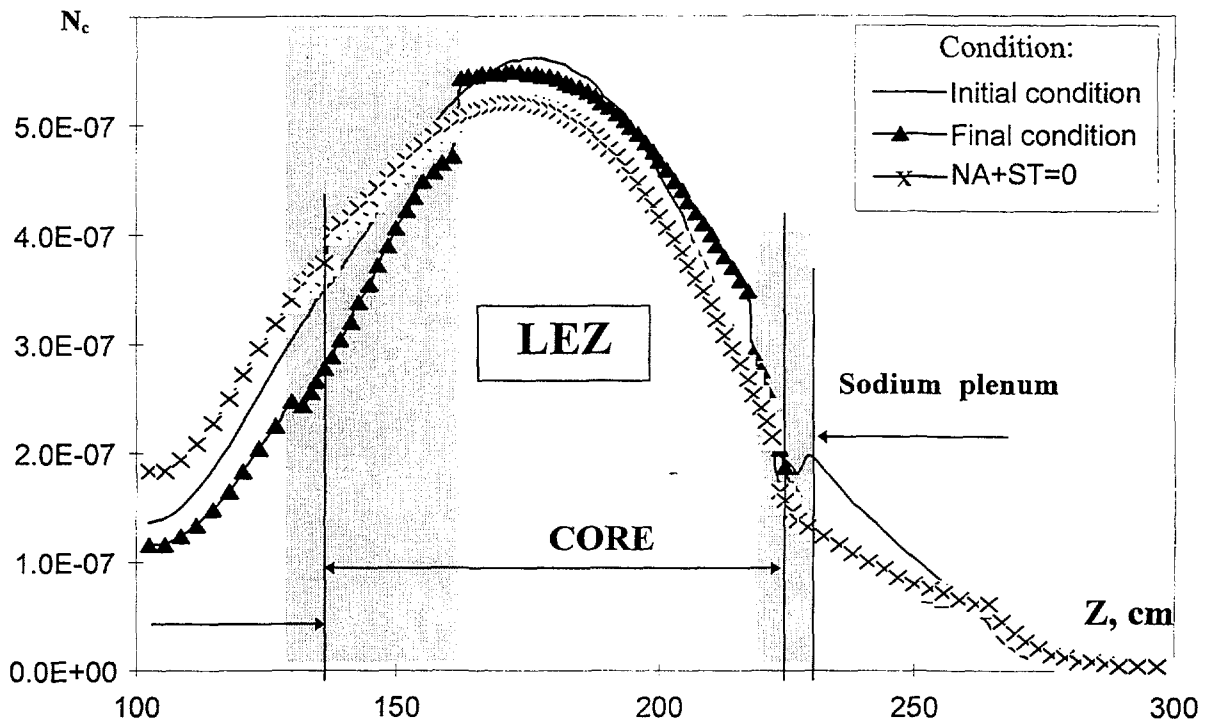


FIG.6.22. Axial distribution of capture number for 10^{24} iron nuclei (normalization on calculated flux)

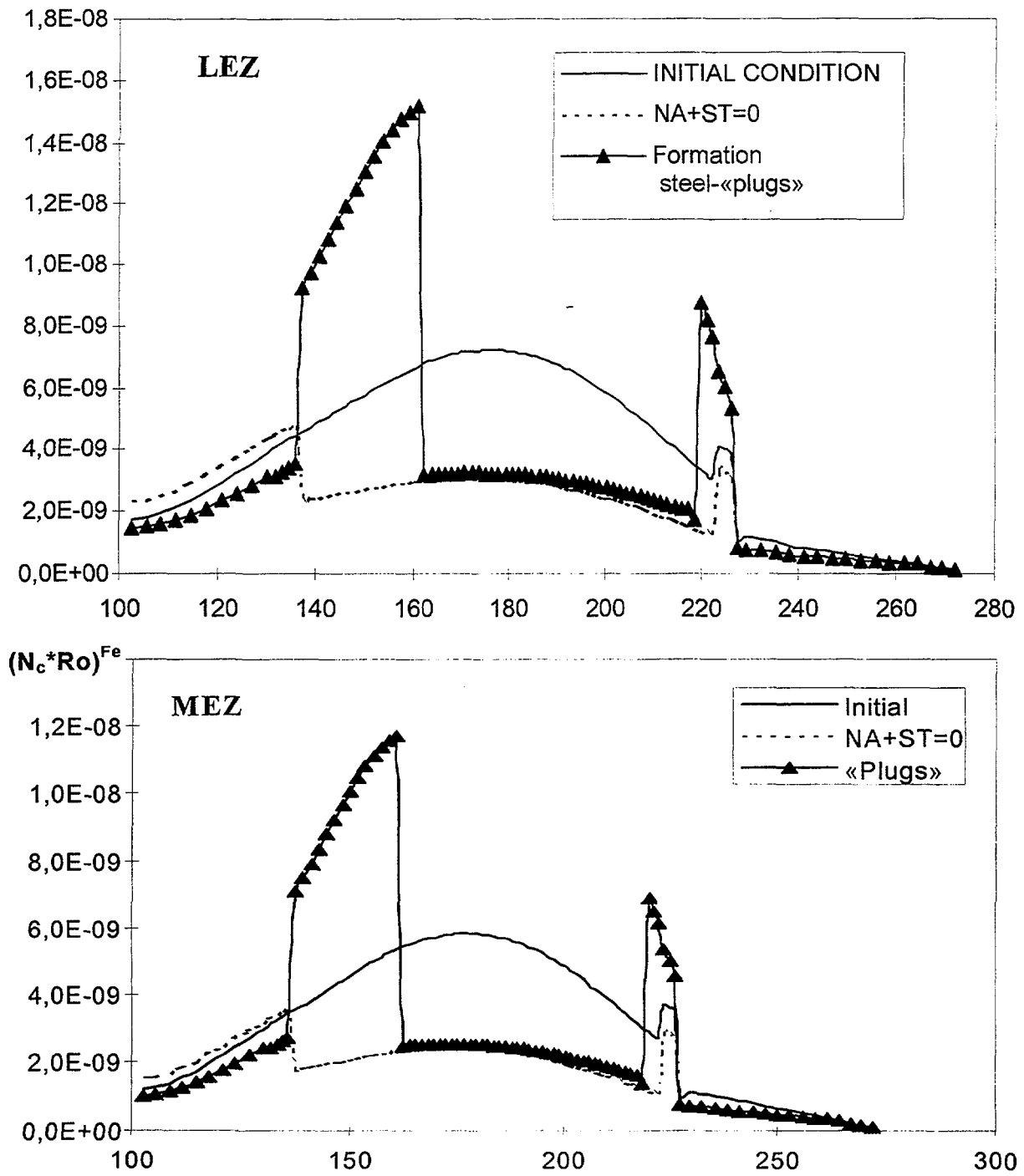


FIG. 6.23. Axial distribution of capture on iron taking into account redistributions of concentration

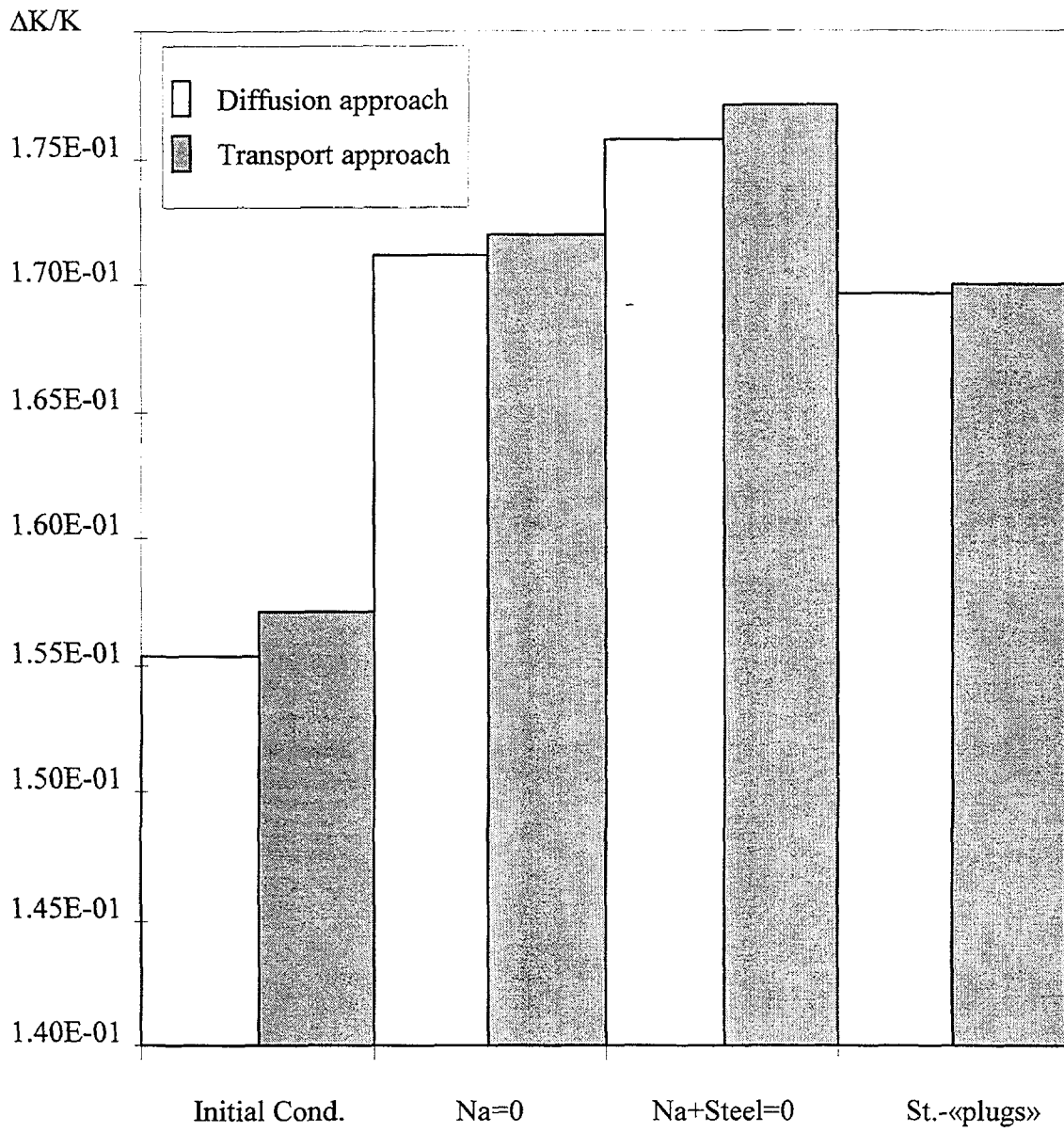


FIG.6.24 Changing of fuel worth in LEZ , $\Delta K/K$

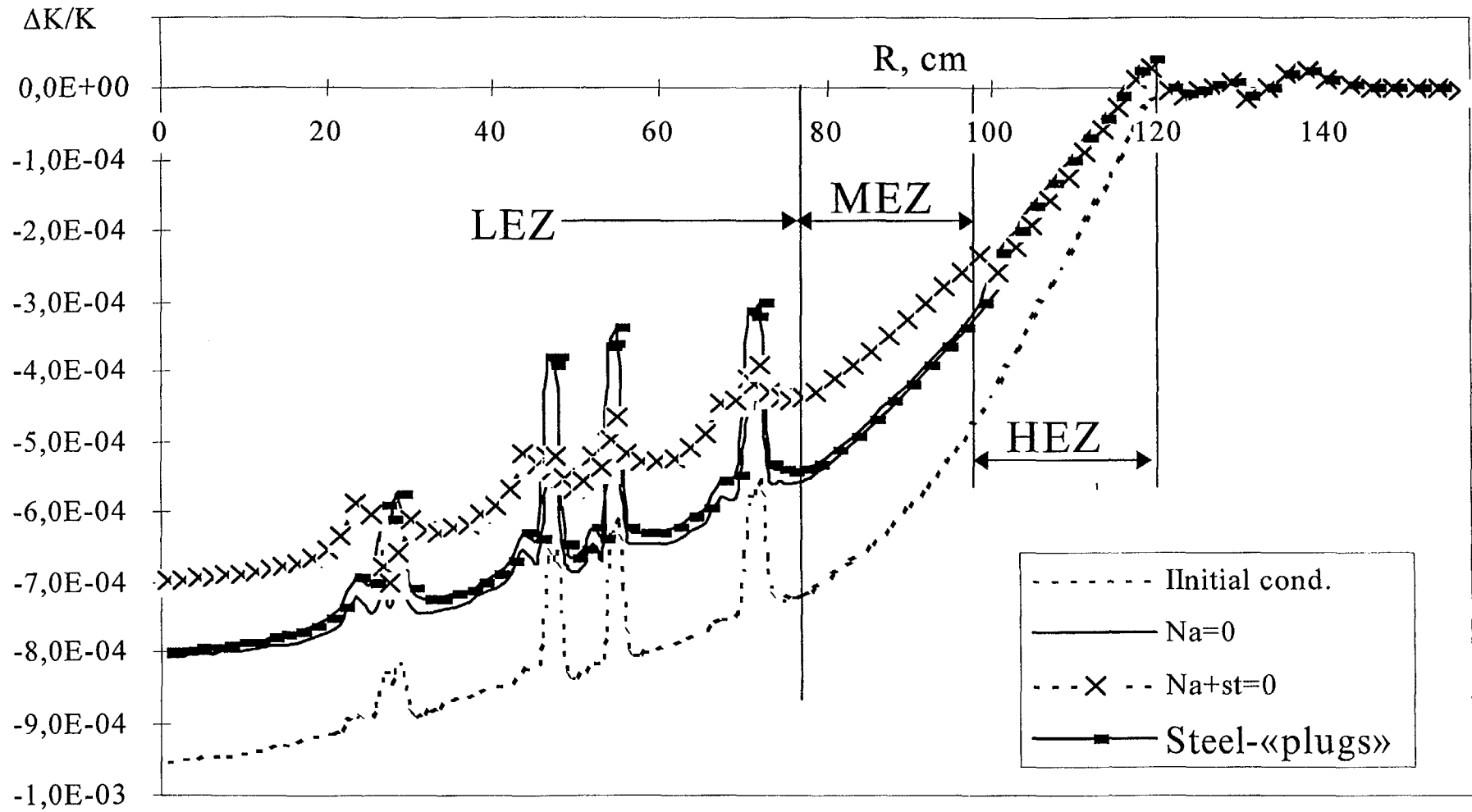


FIG.6.25. Worth of elementary ^{238}U column with cross section of 1cm^2 and $\Delta Z=H_{\text{Core}}$ with 10^{24} nuclei over radius of reactor (transport approach 2100°K)

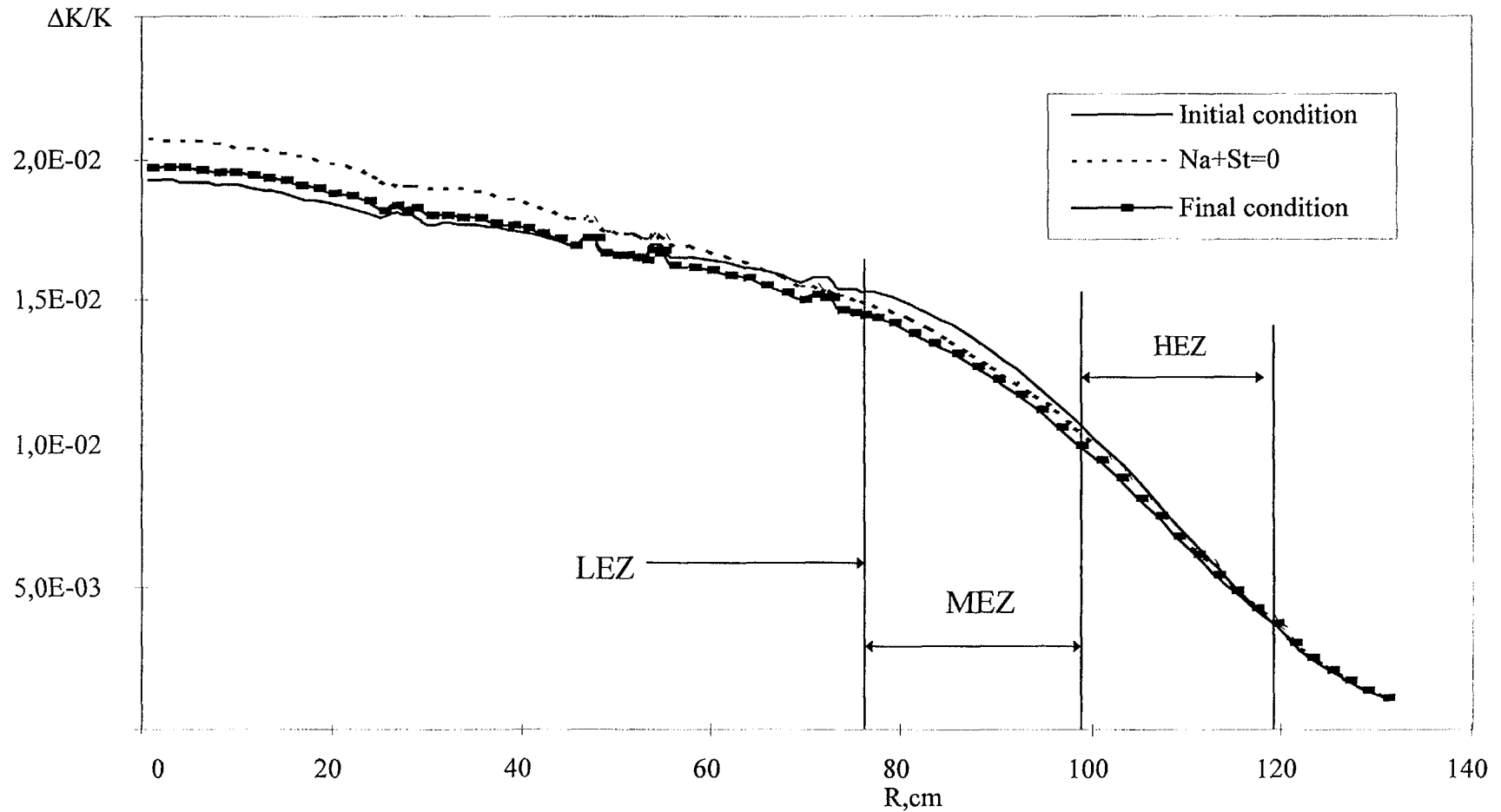


FIG. 6.26. Worth of elementary ^{239}Pu column with cross section of 1cm^2 and $\Delta Z = H_{\text{Core}}$ with 10^{24} nuclei over radius of reactor (transport approach 2100°K)

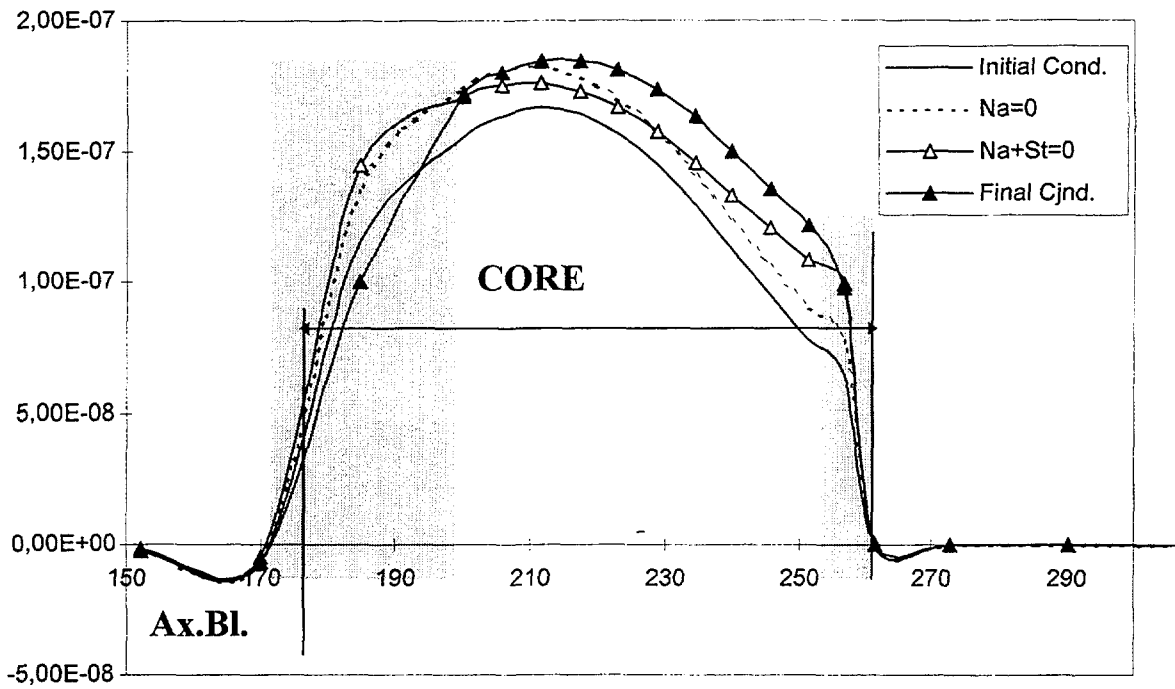


FIG.6.27. Axial distribution of worth of 1 cm^3 fuel composition in the LEZ centre (2100°K , diffusion approach)

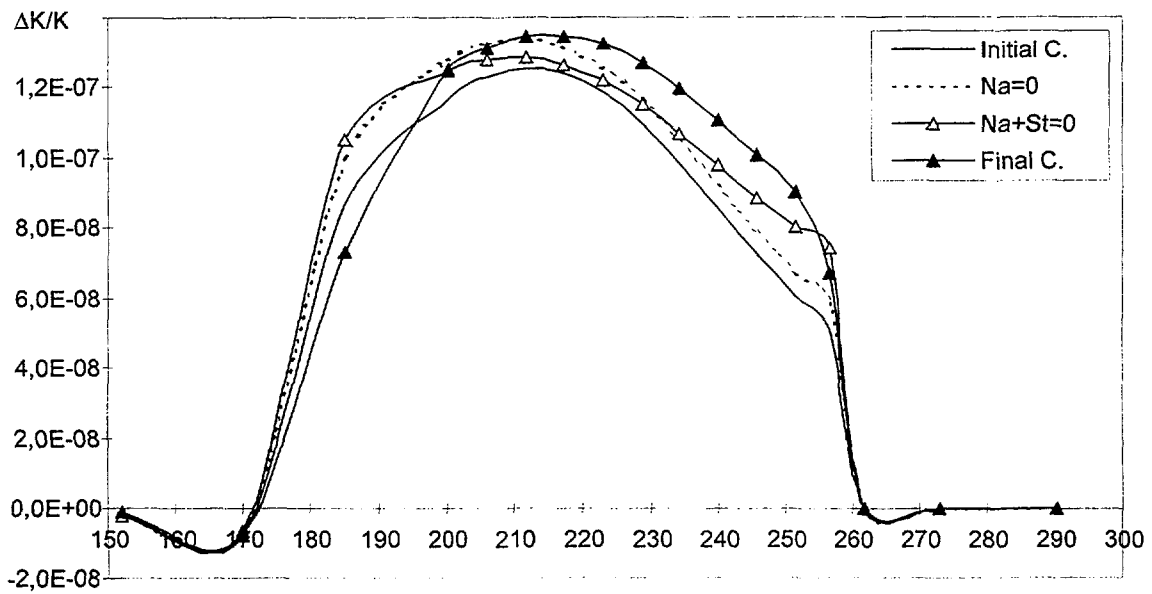


FIG.6.28. Axial distribution of fuel worth integrated over LEZ radius (2100°K , diffusion approach)

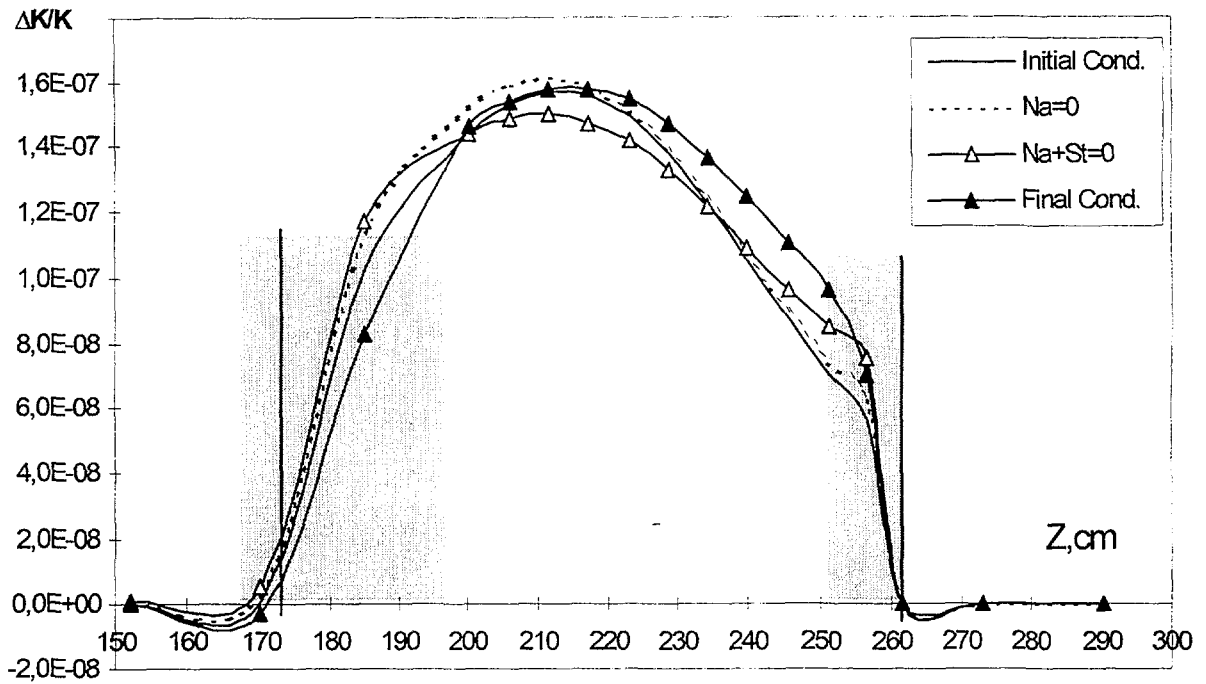


FIG.6.29. Axial distribution of fuel worth integrated over MEZ radius (2100°K, diffusion approach)

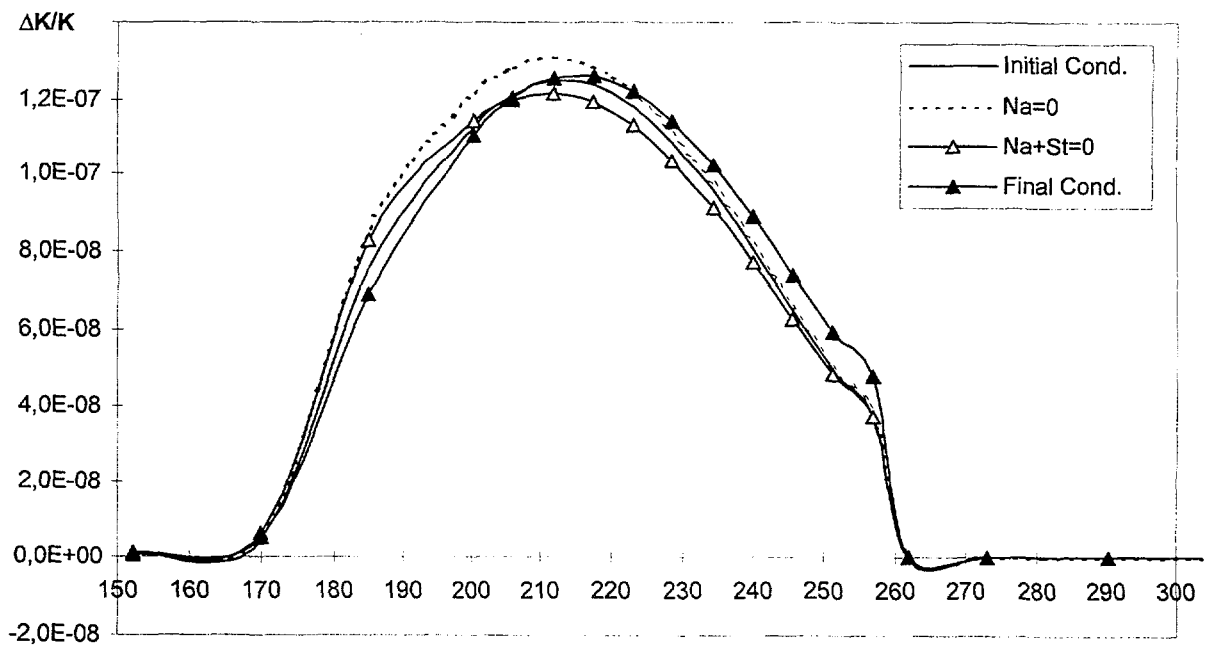


FIG.6.30. Axial distribution of fuel worth integrated over HEZ radius (2100°K, diffusion approach)

6.7. CONCLUSIONS

The detailed analysis neutronic parameters were performed for the sequence of core configurations, simulating the different stages of accident development. Different approaches and codes were used: diffusion theory, transport theory, Monte-Carlo.

The analysis of an accident with partial destruction of large areas of core should be carried out together with neutronics analysis. Use of independent physical analysis has greater presentation on essence of change of neutronic parameters, areas of their maximum influence and change and requirements to methods of analysis. In decomposition approach the number of stages of process approached to real ones should be greater than that considered. The increase of number of considered stages will determine areas of simplified approximation (for example, linear). The application of reactivity obtained for initial condition, for disturbance condition gives for more pessimistic forecasts for the BN-800 reactor. In general for condition of sodium and steel removal from SA internal area it is possible to use multiparametrical approximations for the basic reactivity factors (such as offered earlier). Under considered discrete condition diffusion approach rather precisely describes central area of the core. The largest change of local reactivity factors is observed on borders of zones, where absolute value of material is small. After removal of cladding steel the area positive SVRE values is narrowed, steel removal gives a large positive effect, but the formation steel-«plugs» increases absorption at end faces of the core, partially compensating this effect. With removal of sodium and of part of steel the worth of steel nuclei in a zone of perturbation is increased. The fuel worth practically has not undergone any essential changes for all considered stages. Neutronic characteristics for initial core state describe satisfactory this characteristics during the accident development as concern fuel, steel and sodium efficiency and reactivity feedbacks due to core expansion.

Account for transport corrections in the sodium worth for the upper core area and sodium plenum is important on the process stage preceding sodium boiling, if there is sufficiently strong factor of deformation with time of axial distribution of sodium temperatures. However these corrections are insignificant for the disturbed states considered when there is not practically any sodium temperature axial nonuniformity. In general, results of space distributions of sodium worth obtained from the diffusion calculation can be used.

**NEXT PAGE(S)
left BLANK**

LIST OF PARTICIPATING ORGANIZATIONS AND PARTICIPANTS

Institut de Protection et de Sûreté Nucléaire, France

Frizonnet, J.M.
Lemoine, F.
Rongier, C.

Forschungszentrum, Germany

Struwe, D.
Eigemann, M.
Pfrang, W.
Porscha B.
Zimmermann, W.

Indira Gandhi Centre for Atomic Research, India

Singh, Om Pal
Harish, R.

Centro Ricerche Energie "Ezio Clemental", Italy

Glinantsis, G.

Japan Nuclear Cycle Development Institute, Japan

Niwa, H.
Kanazava, M.
Kawada, K.
Kawashima, K.
Nemura, K.
Takahaski, K.

Institute of Physics and Power Engineering, Russian Federation

Kuznetsov, I.A.
Zabudko, L.
Burjevski, I.
Chebeskov, A.
Chvetsov, Yu.
Danilichev, A.
Volkov, A.
Stogov, V.

AEA Technology, United Kingdom

Martin, D.

International Atomic Energy Agency

Kupitz, J.
Rineiskii, A.

European Commission, Belgium

Van Goethem, G.

Consultants Meetings on "Comparison of calculation method and results for severe accidents in a BN-800 type reactor innovative core design"

5-6 December 1994, IAEA, Vienna
26-28 July 1995, EC, Brussels
11-13 December 1995, IAEA, Vienna
25-28 June 1996, IAEA, Vienna
2-4 December 1996, IAEA, Vienna
30 June -2 July 1997, EC, Brussels
11-12 December 1997, IAEA, Vienna
2-6 June 1998, IPPE, Obninsk, Russian Federation